STUDIES OF CAVE SEDIMENTS

Physical and Chemical Records of Paleoclimate

Revised Edition

Edited by

Ira D. Sasowsky and John Mylroie

Studies of Cave Sediments

Physical and Chemical Records of Paleoclimate

Studies of Cave Sediments

Physical and Chemical Records of Paleoclimate

Revised Edition

Edited by

Ira D. Sasowsky

University of Akron,
Ohio, USA

and

John Mylroie

Mississippi State University,
Mississippi, USA

Springer

A C.I.P. Catalogue record for this book is available from the Library of Congress.

ISBN-13 978-1-4020-5326-9 (HB)
ISBN-13 978-1-4020-5766-3 (e-book)

Published by Springer,
P.O. Box 17, 3300 AA Dordrecht, The Netherlands.

www.springer.com

Cover Illustrations
Insert photo: Stalactites in Poor Farm Cave, Pocohantas County, West Virginia.
Photo by lra D. Sasowsky.
Background photo: Well-developed folia in Browns Room, Devil's Hole, Nevada.
Photo by Alan Riggs.

First published 2004 by Kluwer Academic Publishers / Plenum Publishers, New York
Reprinted with corrections 2007

Printed on acid-free paper

PREFACE

John E. Mylroie and Ira D. Sasowsky*

Caves occupy incongruous positions in both our culture and our science. The oldest records of modern human culture are the vivid cave paintings from southern France and northern Spain, which are in some cases more than 30,000 years old (Chauvet, et al, 1996). Yet, to call someone a "caveman" is to declare them primitive and ignorant. Caves, being cryptic and mysterious, occupied important roles in many cultures. For example, Greece, a country with abundant karst, had the oracle at Delphi and Hades the god of death working from caves. People are both drawn to and mortified by caves. Written records of cave exploration exist from as early as 852 BC (Shaw, 1992). In the decade of the 1920's, which was rich in news events, the second biggest story (as measured by column inches of newsprint) was the entrapment of Floyd Collins in Sand Cave, Kentucky, USA. This was surpassed only by Lindbergh's flight across the Atlantic (Murray and Brucker, 1979).

Cave science also has a long history, with many accounts appearing as early as the sixteenth century (Shaw, 1992; 2000). The term *speleology* has become accepted as the defining term for the scientific study of caves (Moore and Sullivan, 1997), yet the discipline has had difficulty integrating with mainstream sciences. This difficulty has two roots. First, the hidden and arduous nature of most caves means that non-specialists rarely visit them. Second, the bulk of data on caves has come from the recreational caving community, which has cast aspersions on the legitimacy of speleology. Caving for recreation has been considered a fringe activity by society. The journalistic terms "spelunking" and "spelunker", used to describe the activity and the individual, respectively, have emphasized the view that cave explorers are odd people (from personal experience, we can say that a few most certainly are). Those who explore for recreation call themselves "cavers". Over 95% of the cave maps in existence were made by these men and women, who produce them without compensation, for the pure pleasure of creation. And, yet, these maps form the basis for almost all scientific studies within caves. Imagine an analogous situation for the earth sciences, if recreational cartographers drew most of the topographic maps in the world at night, after their day jobs were over.

Some of the criticism of speleology as an immature science has been justified. The difficult, time-consuming and arduous nature of cave exploration has created a lack of

* John E. Mylroie, Dept. of Geology, Mississippi State University, PO Box 2194, Mississippi State, MS 39762 USA, Mylroie@geosci.MsState.edu. Ira D. Sasowsky, Dept. of Geology, University of Akron, Akron, OH 44325-4101 USA, ids@uakron.edu.

manpower in the ranks of cavers and cave scientists. The vast majority of cave scientists around the world began as recreational cavers. Much of the early science done now seems lacking in quality or incomplete. Through time, exploration techniques and technology improved, and concurrently the science of speleology matured. As a result, the science produced has both improved and broadened.

The studies presented in this book concern caves formed by dissolution of soluble bedrock, as an integral part of the production of a karst landscape. This excludes other types of caves (lava tubes, sea caves, talus caves, etc.), which are different, but interesting in their own right. Today, the earth science study of caves falls into two regimes: applied research (land use problems); and basic research (caves as data repositories).

The land use problems in cave and karst areas are legion. These include water quality, flooding, and land subsidence. Such problems have attracted significant governmental (from a regulatory viewpoint) and environmental consultant (from a problem-solving viewpoint) interest. Today, a semi-annual conference on the Engineering and Environmental Impacts of Karst (e.g. Beck and Herring., 2001) draws an international audience to a venue filled with case-histories and technique evaluations.

However, the focus of this book is on the basic quality of caves as data repositories – allowing for the investigation of problems on geologic, not human, timescales. Caves are unique landforms in that they exist within, instead of on, the earth. They create an environment that is predisposed to preservation. As surface landforms age and evolve, the record of their previous condition is destroyed by weathering, and removed by erosion. Not so with caves, where the processes of destruction is greatly delayed, and therefore information is preferentially preserved. Valleys enlarge and deepen as base level lowers, and their former morphology disappears, but in adjacent caves the lowering of base level means the abandonment of conduits and the development of new flow paths deeper down. While active, these cave passages recorded evidence of water flow velocity, water table position, and flow direction in the morphology of their passage walls. In-washed clastic sediment, sometimes inter-layered with chemical precipitates, preserve additional data on active conditions. When abandoned, the cave passages may persist for millions of years. In this setting, they collect additional clastic and chemical deposits that reflect conditions of the environment on the surface above.

The papers in this book have two main stories to tell. One is that retained in the clastic sediments that entered the cave during its active and senescent phases; the chemical precipitates, or speleothems tell the other story. A dominant theme that is carried throughout is the paleoclimatic record that these cave deposits hold.

The initial chapter by Rachel Bosch and Will White describes how clastic sediments enter into caves, how they are transported in conduits, and how they are deposited. This chapter sets the basic framework for the clastic chapters that follow. In chapter 2, Barbara Mahler and her co-authors examine clastic sediments in terms of their water quality implications, from both the inorganic and organic view. Chapter 3, by R. J. Musgrave and J. A. Webb, provides both a case study from Australia, as well as a detailed discussion of paleomagnetic analysis as a geochronological tool in cave sediment studies. Ira Sasowsky and co-authors present in chapter 4 a U.S. case history of clastic sediment deposition and paleomagnetic analysis that provide a measure of the potential rapidity with which cave sediments can collect. Leo Lynch and co-authors present a case study in chapter 5 that shows how sediment provenance can be determined from X-ray diffraction techniques; their results indicate that sediments that were thought to be autogenic were in fact allogenic, with implications for surface contaminant transfer. Chapter 6, by Elizabeth Knapp and co-authors, shows how use of weathering degree, and paleomagnetic analysis in a Virginia, USA cave can be used to determine the timing and climatic

conditions of sediment influx into a cave. Paul Burger, in Chapter 7, describes the use of clastic sediments to determine ice advance and retreat events in the Colorado Rockies, USA, in an area of difficult logistics. The clastic section of the book ends with chapter 8, in which France Šušteršič uses the remnants of caves as found on the surface, and their internal deposits, to look at caves in Slovenia as part of degraded cave systems at the end of their useful life as data repositories.

The second part of the book examines chemical precipitates, or speleothems, as both geochronological tools and paleoclimatic indicators. Chapters 9-11 form a comprehensive resource for scientists interested in the use of speleothems for these indicators, written by people with tremendous experience in the techniques involved. William White, in chapter 9, provides a review of calcite speleothem chemistry and formation, creating the necessary foundation for the later chapters. In chapter 10, Jeff Dorale and co-authors clearly and concisely present an in-depth discussion of the U/Th and related dating techniques as applied to speleothems. Following in chapter 11 is a cautionary presentation by Russ Harmon and co-authors about the use of oxygen isotopes in speleothems for paleoclimatic interpretations. Chapter 12, by Peter Kolesar and Alan Riggs, begins a series of case history studies of speleothems from a variety of sites with an analysis of the depositional environment of the famous Devils Hole calcite. The case histories continue with a series of studies from high altitude or high latitude sites. Cristoph Spötl and co-authors present in chapter 13 an intriguing study of speleothems in a cave in the Austrian Alps that has alternated between ice-cover and ice-free conditions, both in the geologic and the historical record. Chapter 14, by Stein-Erik Lauritzen and Joyce Lundberg, shows how a speleothem from a Norwegian cave at the Arctic Circle reveals the duration and conditions of oxygen isotope stage 11, over 400,000 years ago. Half a world away from Norway, Steven Turgeon and Joyce Lundberg in chapter 15 examined the geochronology and isotope chemistry of speleothems from a cave in Oregon, USA, using growth-rate determinations to carry the speleothem record beyond 500,000 years. In chapter 16, Victor Polyak and Necip Güven present data from caves in the Guadalupe Mountains of New Mexico, USA, where silicates in speleothems were used to show time and temperature conditions needed to mature amorphous silica into trioctahedral smectite and quartz.

Finally, in chapter 17, Donald McFarlane and Joyce Lundberg show how the interplay between speleothems, clastic deposits, and bones can be used to determine aspects of deposition in caves of the West Indies. This concluding chapter brings together many elements presented in earlier chapters to synthesize both a paleoclimatic and paleontological interpretation.

Within this book, we have attempted to present a comprehensive treatment of cave deposits. We are indebted to the patience and skill of the contributing authors. We are also bound to honor and thank the many amateur scientists and cave explorers who have helped cave scientists locate, explore, map and analyze the caves from which important data are collected. We can think of no other scientific discipline where the amateur plays as important a role in the development and advancement of a field.

REFERENCES CITED

Beck, B.F., and Herring, J.G., 2001, Geotechnical and environmental applications of karst geology and hydrology: Lisse, Balkema, 437 p.

Chauvet, J-M., Deschamps, E. B., and Hillaire, C., 1996. Dawn of Art: The Chauvet Cave. Harry N. Abrams, New York, 135 p.

Moore, G. W., and Sullivan, N., 1997. Speleology: Caves and the Cave Environment. Cave Books, St. Louis, 176 p.
Murray, R. K. and Brucker, R. W., 1979. Trapped! G. P. Putnam's and Sons, New York, 335 p.
Shaw, T. R., 1992. History of Cave Science. Sydney Speleological Society, Sydney, 338 p.
Shaw, T. R., 2000. Foreign Travellers in the Slovene Karst 1537-1900.Zalozba ZRC, 244 p.

CONTENTS

LITHOFACIES AND TRANSPORT OF CLASTIC SEDIMENTS IN KARSTIC AQUIFERS

Rachel F. Bosch and William B. White*

1. ABSTRACT

Karst aquifers demand continuous transport of clastic sediments if the conduit system is to remain open. Sediments are injected into the aquifer by sinking surface streams and through sinkholes, vertical shafts, open fractures, and other pathways from the land surface of sufficient aperture to permit gravity- and inwash-driven transport. Much transport of clastic sediments tends to be episodic with sediment loads held in storage until moved by infrequent flood events. Although the overall mix of clastic material depends on material available in the source area, distinctly different facies are recognizable depending on the flow dynamics within the conduit system. The facies are most clearly recognized when the source areas provide a wide variety of particle sizes from clays to boulders. In order of decreasing stream power, one can distinguish (i) diamicton facies: masses of unsorted, unstratified clays through boulders carried as a slurry during high energy flood events, (ii) thalweg facies: coarse gravel to cobble size material, well winnowed, forming armoring on underground streams that moves only during flood flow, (iii) channel facies: usually well sorted and often well stratified silt though gravel carried as bedload at intermediate stream powers, (iv) slackwater facies: mostly clay and silt carried as suspended load and deposited from floodwaters backfilled into the conduit system, (v) backswamp facies: mostly clay derived from the insoluble residue of the limestone, deposited under phreatic conditions with little lateral transport.

2. INTRODUCTION

Caves act as repositories for secondary deposits of many kinds, some locally derived such as breakdown from collapse of cavern roofs, some transported such as sand and silt carried by underground streams, and some the result of chemical deposition in the cavern void space such as calcite and gypsum speleothems. Textbooks on karst hydrology commonly provide descriptions and overall classifications of cave sediments (e.g. Bogli,

*Department of Geosciences, The Pennsylvania State University, University Park, PA 16802.

1980; White, 1988; Ford and Williams, 1989; Gillieson 1996). The classifications are all generally similar although they differ somewhat in detail. The present paper focuses on a specific sub-set of cave sediments: the clastic sediments derived from surface and subsurface weathering and carried into and through the cave system by mainly fluvial processes.

Most of the investigators of clastic sediments in caves have treated them as static deposits, not different in kind from outcrops of sedimentary rock on the land surface. The stratigraphy and petrologic character of the sediments can be described and used to deduce hydraulic history and provenance. This can yield insights into the geomorphic and climatic history of the cave area. Such studies include work by Schmid (1958), Davies and Chao (1959), Frank (1969, 1971, 1972, 1973, 1974), Helwig (1964), Wolfe (1970), Bull (1978, 1981), Milske et al. (1983) and many others.

A somewhat different point of view is to consider the sediments to be an essential part of the hydrology of the ground water basin in which the caves are located. There is, in effect, a flow field of clastic sediments in addition to the flow field of ground water. Investigations from this point of view include the early, comprehensive, and often overlooked monograph of Renault (1968). White and White (1968) drew on fluid mechanics to interpret the mechanism of sediment transport in karst systems. Other descriptions of sediment-bearing cave streams likened them to surface drainage systems with braided streams, point bars, stream meanders, deep V-shaped canyons, and cobble armoring. Jones (1971) referred to these features as the "underground floodplain". Newson (1971) emphasized the importance of flood flows in the transport of clastic materials. Much of the current interest in the hydrology of cave sediments arises because of their role in contaminant transport (Mahler et al., 1999; 2000).

The transport of sediments in conduit systems is episodic with abrupt movements during storm flow and little movement during low flow conditions. In very few cases have investigators been able to directly observe the effects of flood pulses in rearranging clastic sediments. One such observation was made in Cave Springs Cave near Lexington, Virginia (Doehring and Vierbuchen, 1971). Prior to Hurricane Camille in August, 1969, the cave stream carried a sediment load of primarily mud with some well-rounded chert pebbles. After the storm the sediment remaining in the stream bed was predominantly angular to subangular sand and gravel-sized clasts. A terrace composed of sand and gravel was deposited two meters above the normal stream level.

The lithologic characteristics of the clastic sediments reflect the hydraulic conditions that transported them. These characteristics can be described by a sedimentary facies:. Our objective in this paper is to consider the various facies of clastic sediments and the relation of these facies to transport mechanisms and the hydrology of ground water flow in karst

3. CLASTIC SEDIMENTS IN FLUVIOKARST DRAINAGE BASINS

3.1 Inputs of Clastic Sediments to Caves

Karst aquifers receive inputs of sediment from sinking streams and from storm runoff into sinkholes. Runoff from overlying caprock may flush sediment down vertical shafts and so carry fragments of the caprock material deep into the carbonate aquifer. In addition, diffuse infiltration through overlying soils and the epikarst may transmit soils

vertically into the underlying conduit system. All of these materials are commingled to yield the modern day cave sediment piles. As base levels are lowered, entire flow paths in karst are often abandoned resulting in higher elevation, dryer, ancestral cave passages. Once these passages are abandoned, the sediment deposits in them will not be exposed to erosive forces that might rework them. Cave sediments in abandoned passages preserve the final episode of deposition and have been found to span the time scale from the late Pliocene to the Present (Schmidt, 1982)

The sources for clastic sediments in the fluviokarst carbonate aquifers found commonly in the eastern United States are shown in schematic form in Figure 1. This conceptual model is appropriate when a portion of the drainage basin lies on non-carbonate rocks. Drainage basins such as this provide the following sources for clastic sediments.

(i) The clastic load from allogenic surface basins carried into the karst aquifer by sinking streams. The character of these materials depends on the geology and relief of the allogenic drainage basins. In the eastern United States, the rocks underlying allogenic drainage basins are typically shales and sandstones. However, allogenic basins may contribute granitic or basaltic weathering products or indeed any rock material that happens to underlie the allogenic surface stream basins. Influxes of glacial till are common in some basins. Low relief basins may carry only fine silts and clays. High relief allogenic basins may carry loads of pebbles, cobbles and boulders. On those tributaries with no surface overflow routes, any and all clastic materials derived from the allogenic basins will ultimately be carried into the karst aquifer. In the case of sinking streams with no surface overflow routes, simple mass balance arguments demand that transported clastics must be carried through the karst aquifer.

(ii) Soils and regolith from the karst surface flushed into sinkholes by storm runoff. Also carried underground would be glacial tills, volcanic ash, and any other movable material accumulated on the land surface. Sometimes these materials are injected directly into the karst aquifer through the open throat of the sinkhole. In other cases, the sediments are accumulated in the bottom of the sinkhole and then are released abruptly to the subsurface through piping failures. These materials may or may not be distinct from the allogenic sediments depending on the contrast between the regolith on the carbonate rocks compared with the regolith on the non-carbonate rocks of the allogenic catchments.

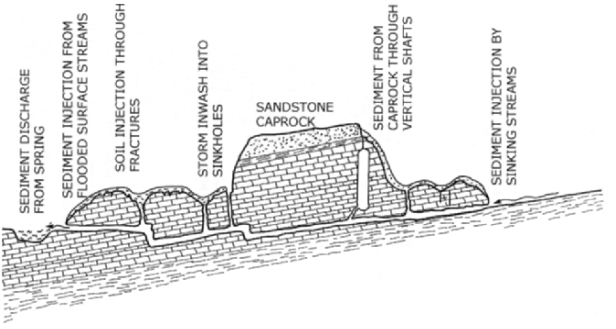

Figure 1. Profile sketch showing various sediment inputs to a fluviokarst aquifer representative of many of the karst areas of the eastern United States.

(iii) A steady flux of soil carried into the aquifer through open fractures at the base of the epikarst. Often there is a continuum of apertures in the fracture system making up the vadose zone of karst aquifers. Larger aperture fractures allow clastic material to descend to the active ground water system. Some of this material is carried into the conduit system where it becomes part of the sediment load.

(iv) Sediment influxes from overlying rock formations. Some aquifers receive input from surface runoff and perched ground water bodies above the vadose zone of the main carbonate aquifer. Examples would be the sandstone and shale capped carbonate aquifers of the Cumberland Plateau and the Mammoth Cave area. Clastic material ranging from clays to sandstone boulders are carried into the underlying conduit system by means of vertical shafts and open fractures in the vadose zone. In many cases these coarse grained materials simply crash down the shaft under the action of gravity without intervention of fluvial processes.

(v) Weathering residuum. Dissolution of the bedrock to form the conduit system will leave behind the insoluble residue in the limestone. This weathering residue includes clays, silts and sands as well as silicified fossil fragments and chert rubble. The insoluble component may make up only a few percent of the carbonate bedrock or it may make up a substantial fraction of the entire rock mass. The weathering residuum will be added to the sediment flux derived from other sources.

(vi) Sediments derived by base-level back-flushing. If the ground water basin discharges to a large surface stream, flooding of the surface stream can flush sediments through the spring orifice back into the karst aquifer. Typically, conduit systems have low gradients so that even modest rises of stage in the surface stream can force water long distances into the aquifer. This is, in effect, an elaborate form of bank storage except that flow reversals carry sediment. Back-flooded sediment depends both on the available source material and on the reversed flow velocity that can be achieved as the flood pulse moves down the surface channel. In Mammoth Cave, back-flooded sediments were found to be fine silts and clays (Hendrickson, 1961). Springer and Kite (1997) found much coarser material in the caves of the Cheat River Gorge in West Virginia.

3.2 Sediment Flux in Karst Drainage Basins

The overall flux of sediment through the karst surface and ground water basin system can be expressed in terms of a sediment budget (Fig. 2). The various fluxes are shown as input terms all balanced against a single output term at the karst spring. Back-flushing from the surface stream is included by the ± sign on the spring sediment discharge. A negative sediment discharge would appear in the budget as a positive increase in storage. It is assumed in this model that no other terms can change sign.

$$S_a + S_i + S_d + S_w \pm S_s = \pm S_f \quad (1)$$

where S_f is the total sediment flux emerging from the karst aquifer, S_a is the sediment carried underground by sinking streams, S_i is the sediment flushed underground by storm

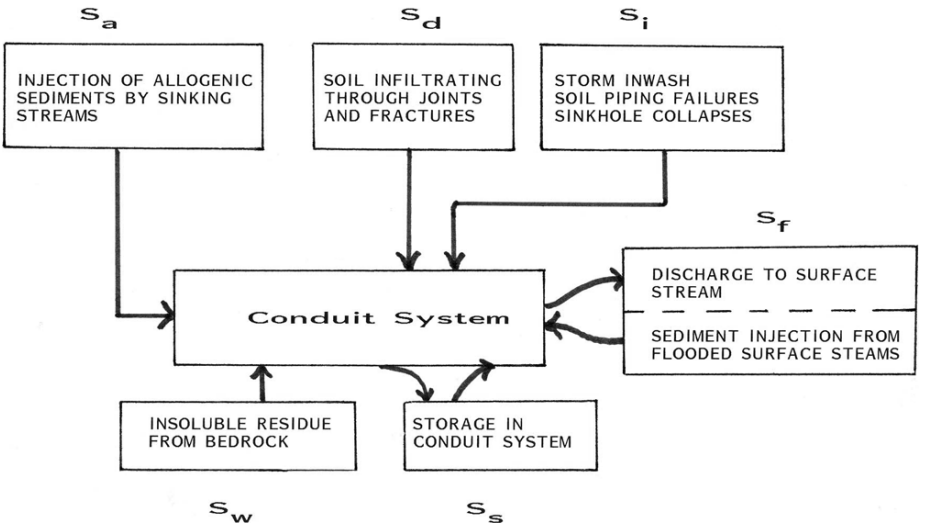

Figure 2. Flow sheet for sediment budget within a karst aquifer.

runoff into sinkholes, S_d is the sediment settling into the conduit system through fractures, S_w is the weathering residuum from dissolution of carbonate rocks and S_s is the quantity of sediment either deposited in storage or removed from storage. Of importance is the storage term. The net storage averaged over long periods of time must satisfy the relation

$$\left[\frac{\partial S_s}{\partial t}\right]_{ave} \leq 0 \tag{2}$$

If the net change of sediment in storage does not satisfy equation (2), the conduit system will ultimately clog up, thus blocking the high capacity ground water flow path, and allogenic recharge will be forced back onto surface routes.

3.3 Importance of Storm Flow

Karst spring hydrographs have a range of responses from those with little or no response to storms to extremely flashy responses with storm flows increased by a factor of 100 over base flows. The flashiness of the response depends on the degree of development of the conduit system and on the fraction of allogenic recharge in the drainage basin. Flashy drainage systems are generally more effective at clastic sediment transport.

Movement of sediments through karst aquifers is episodic with the main movement taking place when pulses of storm water pass through the system. This is the time during which conduits are often under pipe-full conditions so that, with rare exceptions, no observers are present. It will be necessary to relate sediment facies to flood hydrographs rather than to mean or base flow discharge through the conduit system. Ground water basins with a low storm response can move sediment but the sediments will not show the range of structures found in the more flashy basins.

4. FACIES OF CAVE SEDIMENTS

4.1 Previous Systems of Facies Classification

Pickle (1985) examined the sediments in Parker Cave, Kentucky and divided them into a bank facies and a thalweg facies. The thalweg facies was the coarse grained, winnowed material making up the stream bed while the bank facies formed the banks of the stream. Valen et al. (1997) applied the sediment description derived for glacier caves (Eyles, 1983) to cave deposits. This system is more a stratigraphic labeling for the sediments than a facies. Springer and Kite (1997) examined the caves of the Cheat River Canyon in West Virginia. These caves open directly on the river bank and so are subject to the intense flooding of the Cheat. Springer and Kite divided the cave sediments into three main categories: phreatic, vadose, and residual. Each of the phreatic and vadose categories was subdivided into four facies descriptions. Phreatic facies include a diamicton facies, laminated sand facies, silt clay rhythmite facies, and sandy clay loam facies. The vadose facies include gravity deposit facies, travertine facies, overbank facies, and cave stream facies. The Springer and Kite system includes such sediments as breakdown (gravity deposit facies) and various chemical sediments (travertine facies) which are not included in the present discussion. One of the more mechanism-oriented facies classifications is that of Gillieson (1986) who attempted to classify sediments in terms of water flow type and depositional energy. The key parameters are the particle size and the degree of stratification. Gillieson also introduces a diamicton facies for sediments with a range of grain sizes and lack of stratification. The present work is closer to Gillieson's classification.

4.2 Proposed Facies

The various inputs of clastic sediment are commingled in the conduit system. Depending on the transport processes, the sediments are reorganized into distinct facies. The sedimentary facies that were devised based on transport mechanisms are:

Channel Facies
Thalweg Facies
Slackwater Facies
Diamicton Facies
Backswamp Facies

The distinction between the facies is mainly made on particle size and on the degree of sorting as indicated schematically in Figure 3. The actual content of any given sedimentary sequence depends on available source material so the contrast between

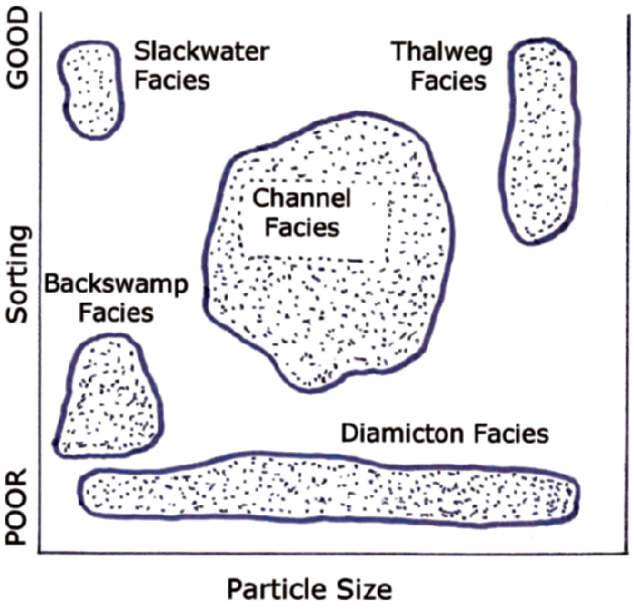

Figure 3. Schematic representation of sediment facies in terms of sorting and particle size.

facies types may be indistinct if a range of source materials is not present. The facies types are sketched in Figure 3 to show the populations as completely distinct in order to locate them on the diagram. For most real sedimentary deposits, the facies types would be less distinct and probably overlap.

4.3 Channel Facies

The channel facies represent sediments that have been sorted or partially sorted by transport along the conduit. They make up the bulk of the clastic sediments found in cave passages. When seen in stratigraphic section, channel facies are found to consist of distinct beds of silts, sands, and gravels. These materials are often well-sorted within a given bed but bed lithology changes rapidly along the stratigraphic section. A typical "stratigraphy" is illustrated with a drawing from Davies and Chao's (1959) report (Fig. 4) The 3-meter passage is filled to the roof with bedded sands and gravels which result from various flow conditions at a time when the passage was an active streamway. Channel facies represent a diverse collection of materials that could easily be subdivided into various subfacies as needed to describe specific sites. Because the detailed characteristics of the sediments depend on both flow regime and source materials, it does not seem useful to make further generic subdivisions of the facies.

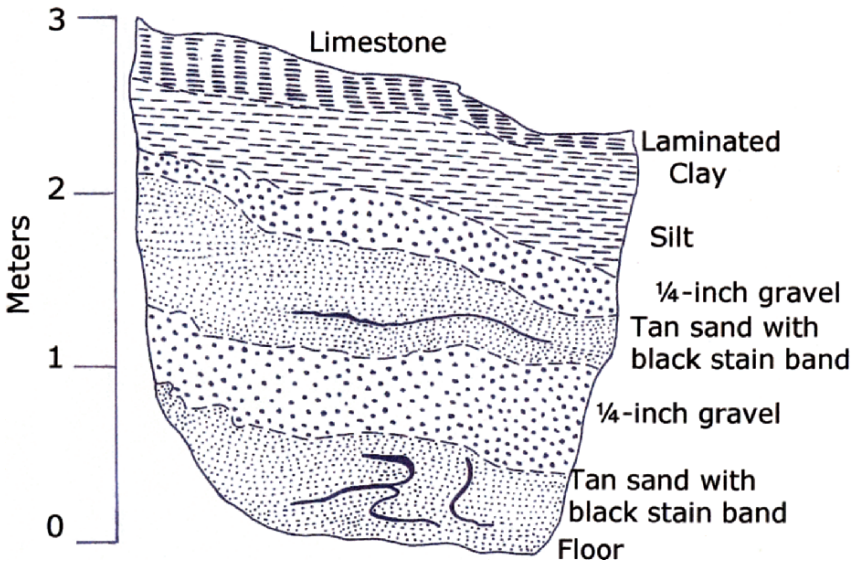

Figure 4. A representative cross-section of channel facies sediment. The Chaperon, a filled side passage on Rose's Pass, Mammoth Cave, Kentucky. From Davies and Chao (1959).

Channel facies sediments are transported mainly as bedload. The varying particle sizes found from bed to bed appear to represent different flow regimes. The ability of any given flow regime to transport sediment is determined by the boundary shear between the moving water and the movable sediment bed. The boundary shear is related to flow velocity through Newton's stress law:

$$\tau = \frac{1}{8}\rho f v^2 \tag{3}$$

where τ is the boundary shear in Nm^{-2}, ρ is the density of the fluid in kgm^{-3}, f is a dimensionless friction factor, and v is the water velocity at the boundary in $msec^{-1}$. The critical boundary shear necessary to move particles of a given size has been determined experimentally for a great variety of particles (Vannoni, 1977). For the particle size range from 0.5 to 100 mm, the data can be fitted approximately by least squares regression to the empirical equation

$$\tau_c = 0.067 D_{50}^{1.08} \tag{4}$$

where τ_c is the critical boundary shear and D_{50} is the average particle size in mm. Because the boundary shear varies as the square of the flow velocity, equations (3) and (4) provide a basis for understanding the winnowing and variation in particle size seen in channel deposits where the material was obtained from the same source area.

4.4 Thalweg Facies

In some caves, active streams have cut through the channel facies to form a secondary stream channel with bed material consisting of gravel, cobbles and boulders. This coarse grained material from which most of the sand and clay has been winnowed out is called the thalweg facies following a suggestion by Pickle (1985). The creation of a thalweg facies requires a flowing stream with a moderate flow velocity even during normal flow conditions. A simple calculation of the required boundary shear for sediment movement illustrates the effectiveness of the winnowing process. To move sand and silt requires a boundary shear of only 0.15 Nm^{-2} whereas moving 30 cm cobbles requires a boundary shear of 165 Nm^{-2} . Moderate flows – annual high flows, not exceptional floods – will provide the boundary shear necessary to strip away sand and silt sized sediment. Only exceptional floods will provide the boundary shear necessary to move cobbles and boulders so these materials tend to accumulate in the stream bed thus forming the thalweg facies.

4.5 Slackwater Facies

The term "slackwater" facies is applied to the sequence of fine-grained clays and silts transported into the conduit system as suspended load. Muddy floodwaters back up into all solution openings including blind side passages. These waters become ponded during which time all or a portion of the suspended load has time to settle out. Settling velocity increases with the square of the particle size according to Stokes law

$$\omega_i = \frac{2(\rho_{s-} \rho)\, g\, d_i^2}{9\,\eta} \qquad (5)$$

where ω_i is the fall velocity of particle i, ρ_s is the density of the sediment particles, ρ is the density of water, g is the acceleration of gravity, d_i is the diameter of particle, i, and η is the viscosity of water. If flood waters are backed up into conduits on the order of one meter in diameter, sand sized particles, even if initially suspended by the flood waters, will deposit within a few meters. Because the fall velocity varies with the square of the particle size, clay and fine silt can be carried distances of hundreds to thousands of meters with a fall of less than the diameter of the conduit. As a result the slackwater facies in most systems is made up of only the smallest particle size material. Slackwater facies can be deposited from suspended load carried in the normal flow direction or from suspended load in water backflooded from surfaced streams.

Slackwater facies are found in most cave deposits, usually as the final layer to be deposited. The slackwater facies appears at the top of the section in Figure 4 as the laminated clay overlying the channel deposits. Even when passages are nearly plugged

with sediment or blocked by breakdown, they can still be flooded with muddy water during periods of high water levels. As a result, casual inspection of undisturbed cave sediments often reveals only the topmost clay layer giving the misleading impression that the entire deposit is composed of fine clay and silt. Slackwater deposits overlying the much coarser sand and gravel of the channel facies may have misled J Harlan Bretz (1942) into thinking that the "red unctuous clays" were much more widespread than they really are. Bretz used the red unctuous clays as supporting evidence for his theory of cave origin by slow-moving, deeply percolating ground water. Reams (1968) devoted much of his Ph.D. dissertation into showing that the red unctuous clays are only a superficial layer over what here is being called a channel facies.

Springer and Kite (1997) used the term "slackwater facies" to describe sediments that backflooded into shallow caves along the Cheat River in West Virginia. With cave entrances opening directly into the river valley, these slackwater sediments have larger particle sizes and also include flotsam that floated into the cave on the flood crest. Otherwise their use of the term is essentially the same as that presented in this paper.

4.6 Diamicton Facies

A diamicton facies was introduced by Gillieson (1986) from his studies of the high relief caves of the New Guinea highlands. Diamictons are unsorted and unbedded sediment masses consisting of a chaotic mixture of all particle sizes from clay to boulders. These are interpreted as debris flows in which the entire sediment mass is entrained and moves as suspended load. Some of these masses may result from extreme floods in otherwise air-filled passages. Some debris flows may take place under water. The diamicton facies is recognized by complete absence of bedding and sorting. Such properties are easier to recognize when a wide range of particle sizes is available in the source area.

Diamicton facies require the most energy for transport of any of the sedimentary facies. They will thus be restricted to high gradient drainage basins. Diamicton facies seem to be uncommon in contemporary drainage basins. Nethertheless, there is much evidence for diamicton facies in old cave deposits suggesting much higher energy flood flows perhaps associated with periglacial climates.

4.7 Backswamp Facies

The term "backswamp facies" is here used to label sedimentary deposits that consist mainly of weathering residue of the bedrock and infiltrate material filtering into the conduit system from overlying soils with little or no lateral transport. The term "backswamp" was chosen because some caves, especially maze caves, tend to function hydrologically much like swamps. Large volumes of water move through them but because of the large total cross-section, velocities are very low. As a result, sediment transport is limited and residual weathering products tend to accumulate with little lateral transport. Depending on the percentage of insoluble residue in the parent bedrock, backswamp facies may occupy a substantial portion of passage cross-sections. Backswamp facies generally consist of clay and fine silt sized material although the deposits may contain chert fragments, silicified fossils, and other insoluble residue extracted from the bedrock.

5. FIELD DOCUMENTATION OF CAVE LITHOFACIES

The sections that follow give specific descriptions of some sites that illustrate the facies concept. Sediment samples were collected, sieved, and weighed to generate particle size distributions. These data are shown on the ϕ scale commonly used in sedimentary petrology. The scale is defined

$$\phi = -\ell g_2 \frac{d}{d_o} \tag{6}$$

where lg_2 = base 2 logarithm (lg_2 x = 3.3219 log x), d = grain size in mm, and d_o = reference particle size = 1 mm.

5.1 Channel Facies

5.1.1 Mammoth Cave: Columbian Avenue

One of the most comprehensive studies of channel facies was undertaken in Columbian Avenue in the Flint Ridge section of Mammoth Cave. Because the results were reported only in a senior thesis (Carwile and Hawkinson, 1968), a summary of some of the key descriptive information is given here. Channel facies sediments consist of interbedded clays, silts, sands, gravels, cobbles and boulders with widely varying distributions of particle sizes and widely varying degrees of sorting. At any particular location in a cave, the clastic sediments often exhibit a distinct sequence of beds. However, the measurements in Columbian Avenue show that these bed sequences cannot be traced for any great distance along cave passages.

Columbian Avenue is an 800 m long elliptical tube that has apparently acted as a cutoff passage draining the higher lying Pohl Avenue to the baselevel Eyeless Fish Trail (Fig. 5). Eyeless Fish Trail lies almost at the pool stage of Green River and floods with even modest rises in Green River. Pohl Avenue floods only when Green River stage exceeds 8 – 10 meters. The upper end of Columbian Avenue is 7 meters above pool stage; the downstream end is at 3.7 meters. Sand and silt sediments fill the passage to depths of as much as three meters.

Carwile and Hawkinson established a series of sections through the entire sediment pile in Columbian Avenue by digging trenches across the passage down to the bedrock floor. They then pressed sections of 5 cm wide x 2 cm deep steel trough against the walls of the pits in order to extract cores of the sediments. From samples of the cores, they determined grain size distributions, analyzed the clay minerals, and constructed stratigraphic columns (Fig. 6). The channel facies are moderately well sorted and well stratified but even in this ideal location – a uniform, low gradient tube with no side passages – the beds cannot be traced from one section to the next. These characteristics seem to be typical of channel facies in general and indeed the variation in bed thickness and bed continuity is mostly more pronounced than it is in the Columbian Avenue examples. A stratigraphic section can be constructed at any particular point along a cave

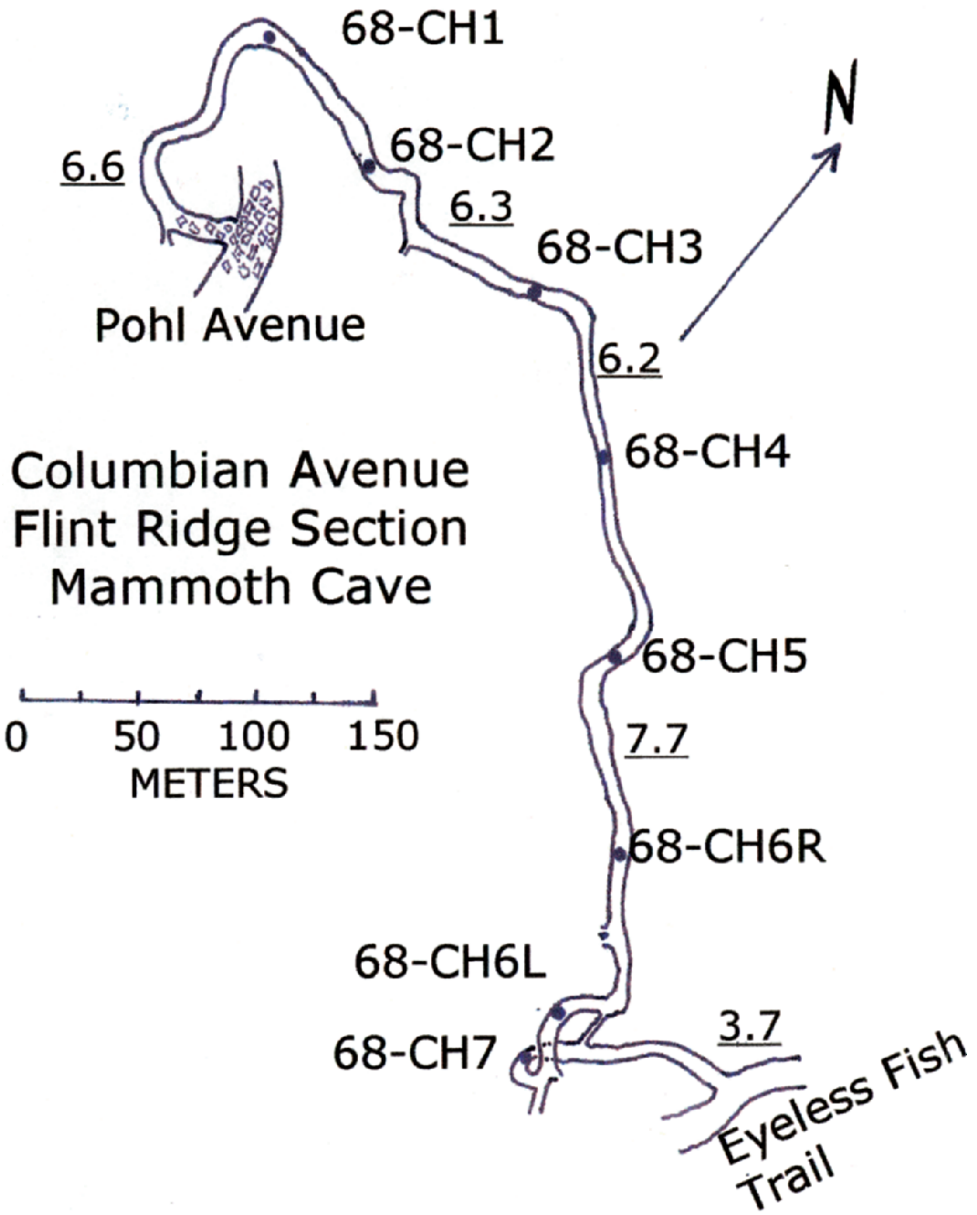

Figure 5. Map of Columbian Avenue, Flint Ridge section of Mammoth Cave showing location of sediment pits. Underlined numbers are elevations in meters above pool stage of Green River. Base map adapted from Brucker and Burns (1964).

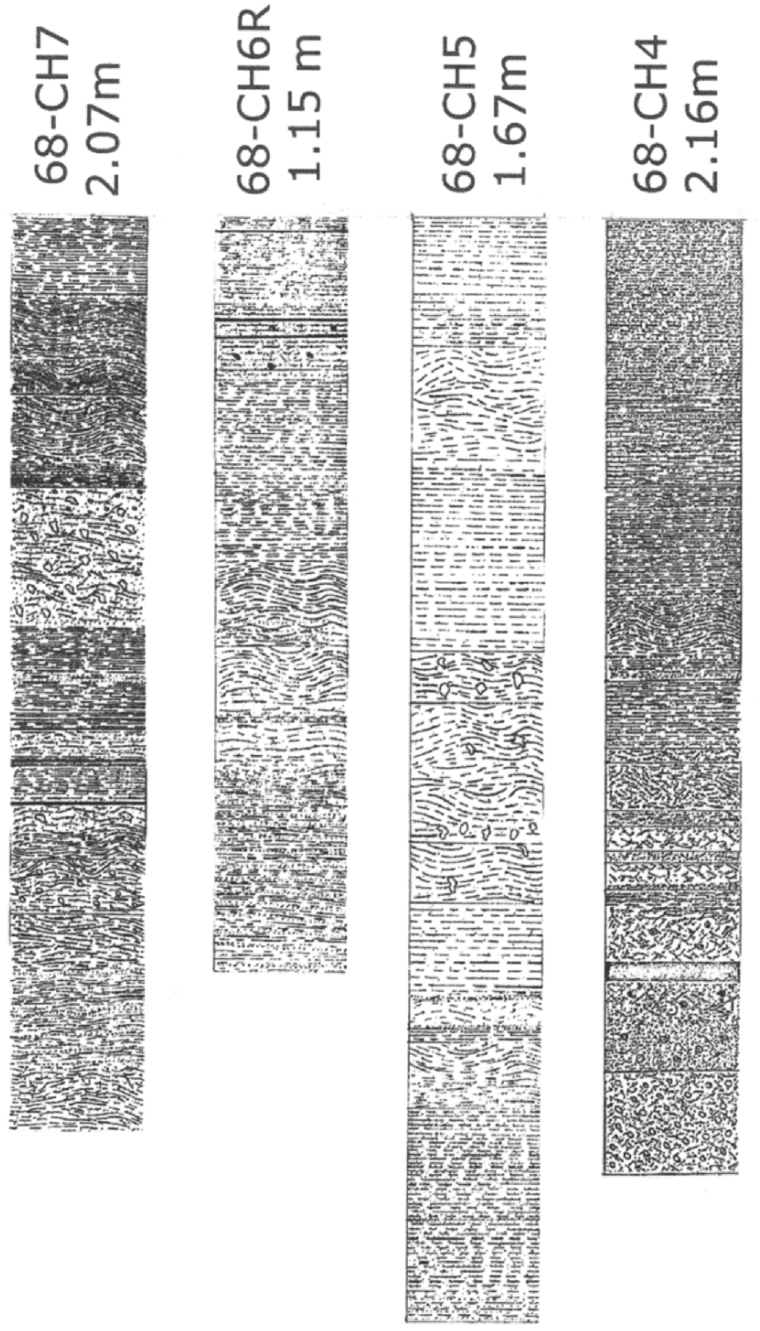

Figure 6. Series of stratigraphic columns along Columbian Avenue, Flint Ridge section of Mammoth Cave Kentucky showing lithologic characteristics of channel facies. Columns are keyed to core locations shown in figure 7. Note the total column thickness; original columns were drawn to two different scales. Original data from Carwile and Hawkinson (1968).

passage, but these sections are not very useful for the interpretation of depositional processes.

5.1.2 Mammoth Cave: Logsdon/Hawkins River

The karst aquifer of which the Mammoth Cave System is a part consists of a well-defined set of ground water basins each of which has multiple inputs and all of which drain ultimately to springs on Green River (Quinlan and Ewers, 1989). One of the largest is the Turnhole Basin. The master trunk draining to the Turnhole Spring has an internal confluence of two very large tributaries known as Hawkins River and Logsdon River. Stream sediments were sampled at several points upstream from the confluence (Fig. 7). These samples were sieved and distribution functions plotted (Fig. 8). Samples taken from the same tributary produced very similar distribution functions. Comparison between the two tributaries shows that the sediments being transported down the two "rivers" are dramatically different in spite of the similar hydrogeologic setting.

Logsdon River has been explored upstream from the confluence for more than seven kilometers. It more or less parallels the escarpment at the southern edge of the Mammoth Cave Plateau and is a master drain for the karst as far northeast as Roppel Cave. It is known to receive recharge from valley drains and vertical shafts and also from the sinking streams and sinkhole inputs on the Sinkhole Plain to the southeast. The Logsdon River sediments are mainly silts and fine sands with 40 – 60% of the material smaller than the smallest sieve size used.

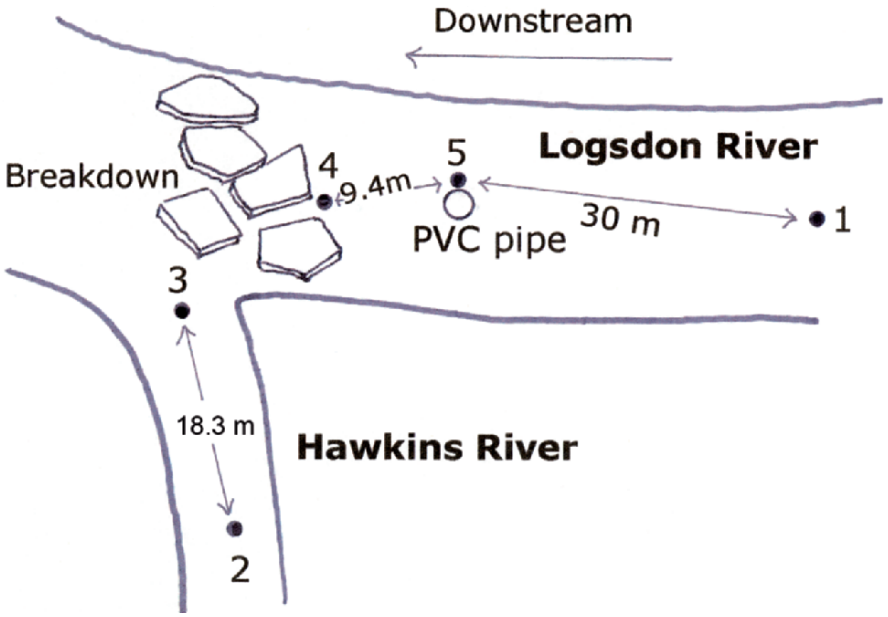

Figure 7. Sketch showing sampling locations at the confluence of Logsdon River and Hawkins River, Mammoth Cave, Kentucky. The PVC pipe is a test well used for hydrologic measurements.

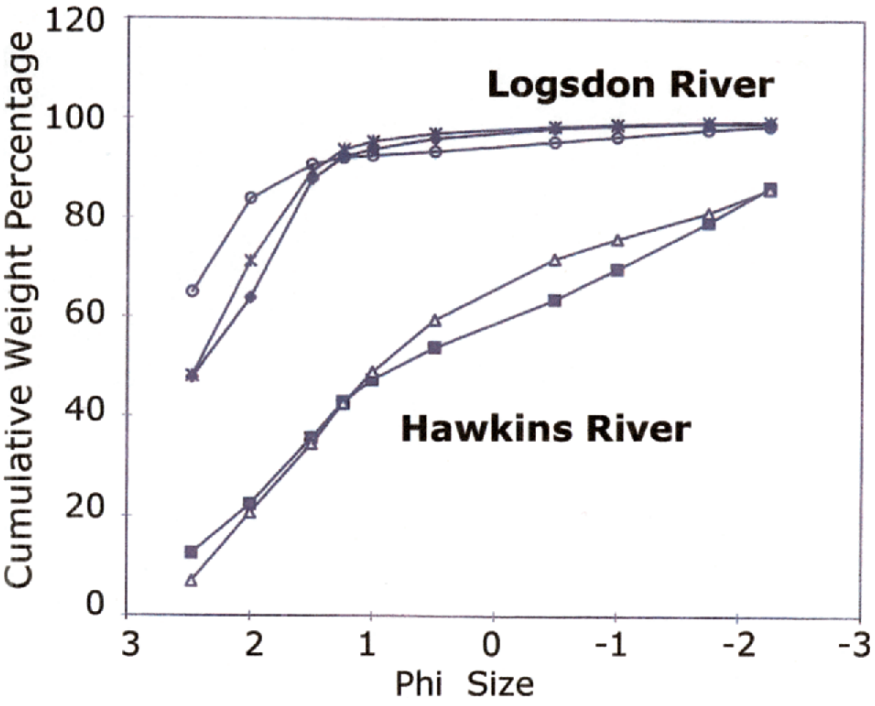

Figure 8. Particle size distribution in Hawkins and Logsdon Rivers. Logsdon River: diamonds = site 1; asterisks = site 5; open circles = site 4. Hawkins River: solid square = site 2; triangles = site 3.

The ultimate source of Hawkins River is not known because the main river sumps a short distance upstream from the confluence. The Hawkins River sediments are more uniformly distributed over the range of silt to gravel with less than 10% of the material smaller than the smallest sieve size used.

The contrast between the two tributaries could be a matter of provenance, a contrast between sediment derived from the Plateau compared to sediment derived from the Sinkhole Plain. It would also be a matter of transport with Hawkins River being the higher energy stream.

5.1.3 Rock Spring

Rock Spring, Centre County, Pennsylvania, is the drain for a 14.2 km^2 ground water basin. The basin is elongate along the trend of the Appalachian folding. Roughly one third of the basin is in folded Ordovician limestones; the remainder is underlain by Orodvician and Silurian shales and sandstones that make up Tussey Mountain which trends northeast-southwest along the trend of the Appalachian folding. More than 50% of

the recharge is mountain runoff that sinks in a series of swallets along the flank of the mountain. The master conduit that feeds the spring is developed parallel to strike and thus parallel to the mountain. Rock Spring has been used as a test site for a variety of karst water investigations. See Jacobson and Langmuir (1974) for a more detailed description.

The conduit that feeds Rock Spring is entirely in the phreatic zone. It has been explored by SCUBA diving for roughly 400 meters. The conduit carries a flux of clastic sediments. The diver reports a lift tube where the flow rises about 4 meters up a slope. Channel facies sediments collected from bottom and top of the lift tube were dried and sieved. The resulting grain size distribution (Fig. 9) reveals little difference between the bottom and the top of the tube. These sediments are being swept down the conduit by pipe flow and quite clearly follow undulations in the pipe.

5.2 Thalweg Facies

5.2.1 Tytoona Cave

Tytoona Cave, Blair County, Pennsylvania provides an example of thalweg facies. Tytoona Cave is a segment of trunk passage carrying an active stream that drains a substantial portion of Sinking Valley (Fig. 10). The cave is subject to flooding. The stream flows in a wide, shallow channel with an armoring of gravel sized sandstone and siltstone derived from the Silurian clastics that make up the ridges bounding Sinking Valley. Surface runoff from the ridges carries the clastic material into the karst drainage system.

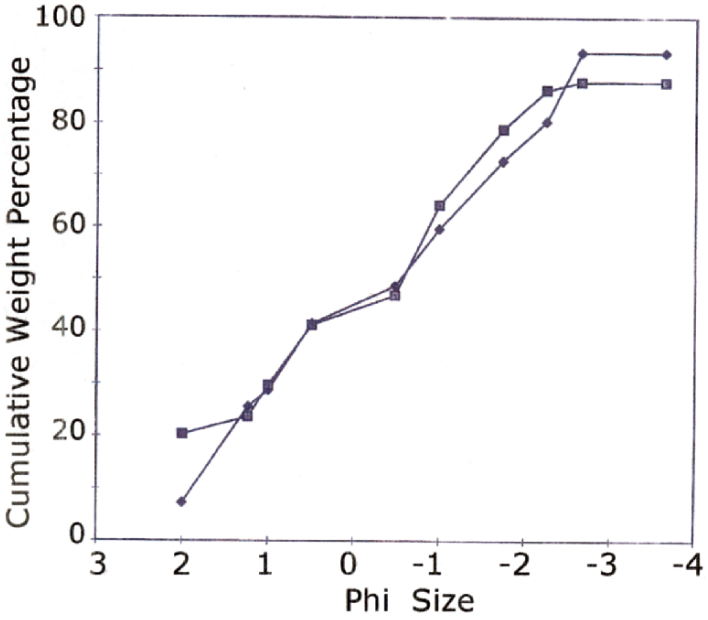

Figure 9. Grain size distribution in feeder conduit of Rock Spring. Diamonds: bottom of lift tube; squares: top of lift tube.

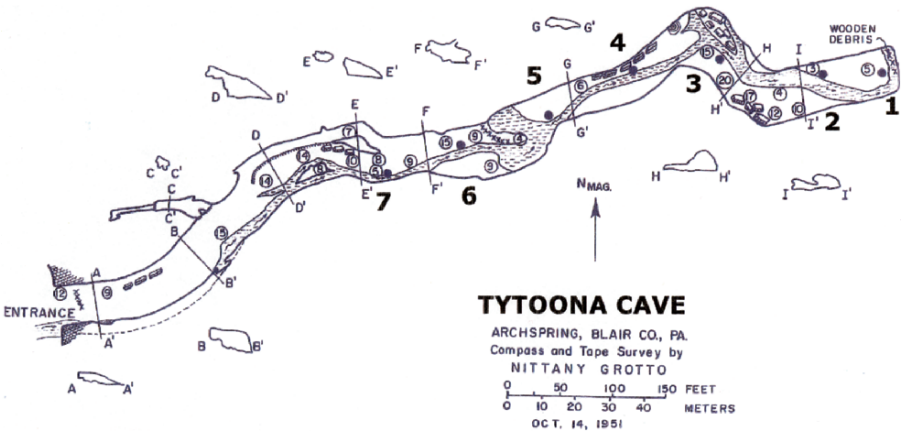

Figure 10. Map of Tytoona Cave, Blair County, Pennsylvania showing sample locations.

The streambed in Tytoona Cave consists of winnowed gravels at the surface. This surface layer is generally about the thickness of the diameter of the largest grain size represented. Near the cave entrance, the largest particles are cobbles and boulders, some as large as 40 cm in diameter. Qualitatively, the armor layer exhibited a fining trend downstream to a largest gravel size of 7 cm just upstream from a pool and low ceiling reach known as the "duckunder". Downstream from the duckunder are gravels with particles as large as 13 cm. These fine downstream to about 2.5 cm just upstream from the terminal sump. Beneath the winnowed cobble layer is a deposit generally consisting of sands mixed with gravels. Grain sizes beneath the winnowed layer are finer than the armor layer and also appear to exhibit a downstream fining trend.

Sediment samples were collected from Tytoona Cave with sampling sites spaced at about 30 m intervals (sample sites are shown by number on Figure 10). Two samples were taken at each site using a shovel. The first sample was taken from the well-winnowed armor layer. The second sample came from directly below the first. These were collected to a depth of about 7.5 cm below the bottom of the first sample. Both sets of samples were dried, sieved, and the particle size distribution plotted (Fig. 11-a,b). The sediments sampled from below the armor layer did indeed show a general downstream fining trend. The winnowed armor layer shows a much narrower distribution of sizes than the underlying material. The thalweg facies consists entirely of coarse (8 – 32 mm) grains. Unfortunately, the accessible segment of Tytoona Cave is only a small fraction of the total conduit so that particle size distributions along the entire drainage channel cannot be determined.

5.2.2 Butler Cave

The Butler Cave-Sinking Creek System, Bath County, Virginia (White and Hess, 1982) is developed with a master trunk passage along the axis of a syncline. Tributary

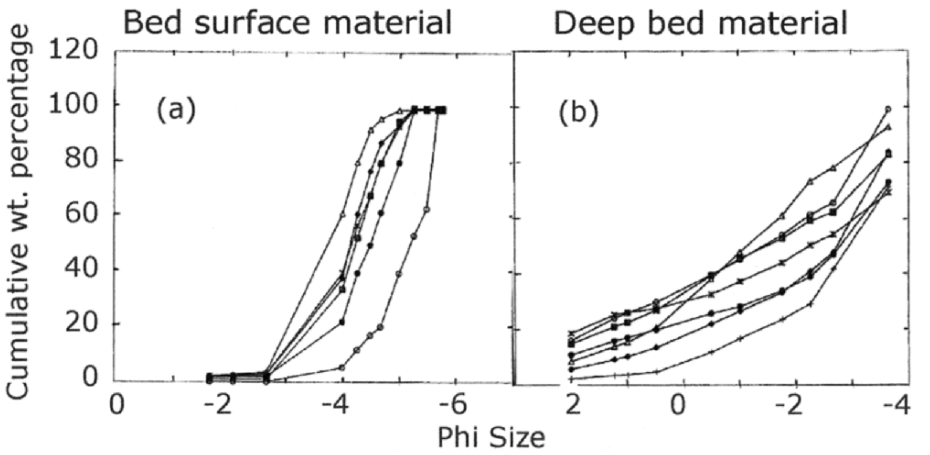

Figure 11. Thalweg facies in Tytoona Cave. (a) Armor layer making up the surface of the stream bed sediments. (b) Sediment lying directly below surface layer. There is both a surface and a subsurface distribution for each sample site. These are keyed to the site numbers shown on figure 10: diamonds = site 1; solid squares = site 2; triangles = site 3; open circles = site 4; asterisks = site 5; solid circles = site 6.

passages are developed along the flank of the syncline. These serve as inlets for clastic sediments flushed down the sides of Jack Mountain into a set of swallets. As a result, the trunk passage contains extensive beds of sand, gravel, and sandstone cobbles. The central portion of the trunk passage presently acts as an overflow channel and carries water only during flood events. Flood flow is injected from the flanks of Jack Mountain at high velocities, and as a result the thalweg facies is very well winnowed with only the coarsest cobble material remaining. The photograph (Fig. 12) was taken in the trunk channel near Sand Canyon (map in White and Hess, 1982) at a location where there are no nearby inlet points. The coarse material is mainly sandstone cobbles which have been carried down the low gradient trunk channel.

5.3 Slackwater Facies

Most caves that contain clastic sediments contain slackwater facies. The slackwater facies material consists of the layer of clay or perhaps clay and silt that makes up the topmost layer of the sediment. Caves subject to flooding collect a layer of slackwater facies every time the cave fills with water.

5.3.1 Mammoth Cave

Mammoth Cave provides excellent exposures of slackwater facies (Fig. 4). At the tops of most sediment piles is a layer, seldom more than a few cm thick, of thinly layer clay and very fine silt. Some of these sedimentary layers are varved, apparently representing an annual cycle of flooding with the rise and fall of the ancestral Green

River. X-ray examination of the material reveals mainly quartz. Clay minerals are a relatively minor component.

5.4 Diamicton Facies

5.4.1 Mystic Cave

Diamicton facies, by their nature, do not lend themselves to direct observation. There may be one example known from anecdotal evidence, that of Mystic Cave, Pendleton County, West Virginia. During the great West Virginia flood of 1985 (Clark et al., 1987) a mass of soil and regolith on the order of 1000 m^3 was torn from a field above one of the cave's entrances and flushed through the cave (J.J. Van Gundy, personal communication). Mystic Cave consists of a single conduit with a small surface stream sinking at one end, flowing through the cave for roughly 1000 meters to emerge at a spring. A tributary stream enters the cave about two-thirds of the distance downstream. The mass of material torn loose during the storm was flushed through the cave as a single debris flow. Later, masses of unsorted clastic material ranging from clays to cobbles were found piled on flowstone and wedged in crevices, very much like the diamicton facies. The characteristic of the diamicton facies is that entire sediment piles are mobilized and move as a single debris flow. In this particular example, the November, 1985 storm was calculated to have a greater than 500 year return period in the Potomac River Valley of Pendleton County. Diamicton facies appear to record rare events in the cave depositional history.

Figure 12. Photo of thalweg facies in Butler Cave main stream channel.

5.4.2 Butler Cave

The Butler Cave - Sinking Creek System, Virginia, USA contains large deposits of what appear to be a diamiction facies, These occur in the tributary caves oriented down the flanks of the syncline (Hess and White, 1982; Chess et al., in preparation). These dip passages have a much steeper gradients than do most cave passages. The upstream ends of the tributaries are along the flanks of Jack Mountains, a quartzite capped ridge that is the source of much of the sediment. Although the updip ends of the passages are now occluded by breakdown and surface weathering material, it appears that the sediment was flushed into the passages from the mountain side. These deposits are plastered into recesses in the passages walls and fill side passages. The sediment is mostly sandtone. There is no evidence of bedding and no sorting. A completely chaotic mix of particle sizes ranges from sandstone clasts 10 to 20 cm across down to fine sand and clays (Fig. 13).

The distribution of sediment masses in the dip slope passages suggest a debris flow that swept down the passage under completely pipe-full conditions. Recesses and side passages served to break the dynamics of the flow and thus trap localized masses of sediment. It is suspected, although not proven, that the initiation and transport of the diamicton flows was related to climatic conditions much wetter than presently occur in this part of Virginia.

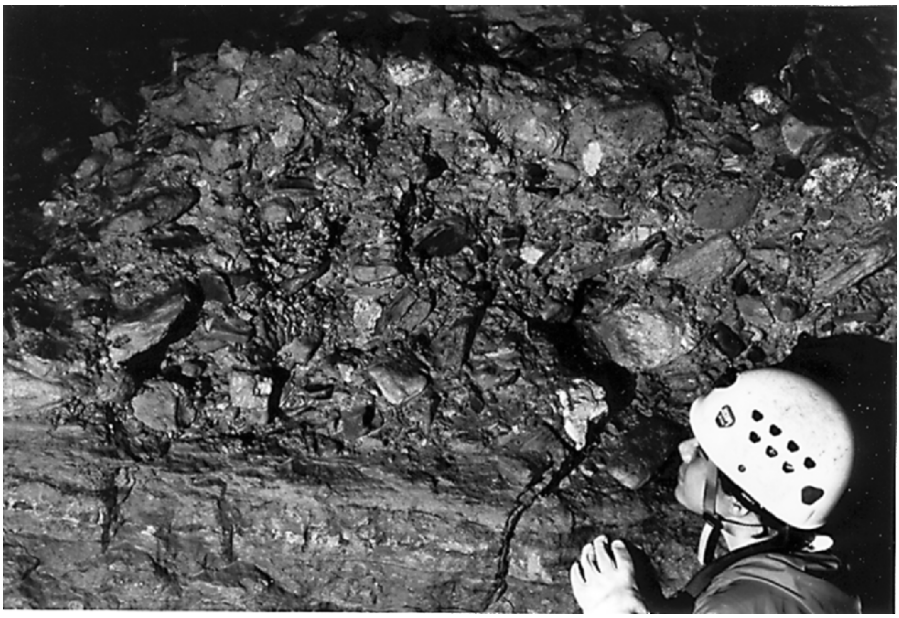

Figure 13. Photo of diamiction facies. Dave's Gallery in Butler Cave.

5.5 Backswamp Facies

5.5.1 Hineman Cave

Clean backswamp facies are difficult to identify because weathering residue from the limestone is difficult to separate from other fine grained clastics. Hineman Cave, Armstrong County, Pennsylvania (White, 1976) may provide an example. Hineman Cave, like other complex maze caves developed in the Pennsylvanian Vanport Limestone, has a low gradient and little evidence for stream flow. The sediment consists of fractions of a meter to more than a meter of wet clay. This material appears to have been derived from the insoluble residue from the limestone with some contribution from overlying fireclays and shales.

6. CONCLUSIONS

Clastic sediments deposited in conduit systems can be conveniently be divided into five facies depending on the mechanism of deposition. The channel facies comprises most observed sediment piles and can be subdivided further depending on the objectives of a particular investigation. Diamicton facies and slackwater facies are deposited from suspended loads. Channel facies and thalweg facies are transported as bedload. The backswamp facies is defined to describe those residual in infiltrated clastic sediments that are deposited in place with little horizontal transport.

ACKNOWLEDGEMENTS

We thank the Superintendent and staff at Mammoth Cave National Park for access to the Logsdon-Hawkins River section of the cave and the Cave Research Foundation for providing necessary maps. These observations were made in cooperation with a long term project of hydrologic and geochemical measurements in this section of the cave conducted by Joe Meiman of the National Park Service and Prof. Christopher G. Groves of Western Kentucky University. Access to the Butler Cave-Sinking Creek System was made available courtesy of the Butler Cave Conservation Society. We thank the National Speleological Society for access to their Tytoona Cave Preserve. We are very grateful to Prof. James J. Van Gundy of Davis and Elkins College for sharing his observations and photographs of the effect of extreme flooding in Mystic Cave. Cave diver Jon Guizar collected the samples from Rock Spring.

REFERENCES

Bogli, A., 1980, *Karst Hydrology and Physical Speleology,* Springer-Verlag, Berlin, 284 p.

Bretz, J H., 1942. Vadose and phreatic features of limestone caverns, *J. Geol.* **50**:675-811

Brucker, R.W. and Burns, D.P., 1964, The Flint Ridge Cave System, Mammoth Cave National Park, Kentucky, Cave Research Foundation, Washington, DC, Folio, 3pp text plus 31 maps.

Bull, P.A., 1978, A study of stream gravels from a cave: Agen Allwedd, Powys, South Wales, *Zeits. Geomorph.* **22**:275-296.

Bull, P.A., 1981, Some fine-grained sedimentation phenomena in caves, *British Geomorph. Res. Grp. J.* **6**:11-22.

Carwile, R.H. and Hawkinson, E.F., 1968, Baselevel sedimentation, Flint Ridge, Kentucky, B.S. Thesis, The Ohio State University, Columbus, OH, 116 pp.

Clark, G.M., Jacobson, R.B., Kite, J.S. and Linton, R.C., 1987, Storm-induced catastrophic flooding in Virginia and West Virginia, November, 1985, Chap. 17 in *Catastropic Flooding*, L. Mayer and D. Nash, eds., Allen & Unwin, Boston, pp. 355-379.

Davies, W.E. and Chao, E.C.T., 1959, Report on the sediments in Mammoth Cave, Kentucky, U.S. Geol. Survey Administrative Rpt. to U.S. Natl. Park Service, 117 p.

Doehring, D.O. and Vierbuchen, R.C., 1971, Cave development during a catastrophic storm in the Great Valley of Virginia, *Science* **174**:1327-1329.

Frank, R., 1969, The clastic sediments of Douglas Cave, Stuart Town, New South Wales, *Helictite* **7**:3-13.

Frank, R., 1971, The clastic sediments of the Wellington Caves, New South Wales, *Helictite* **9**:3-26.

Frank, R.M., 1972 Sedimentary and morphological development of the Borenore Caves, New South Wales, I, *Helictite* **10**:75-91.

Frank, R.M., 1973, Sedimentary and morphological development of the Borenore Caves, New South Wales, II, *Helictite* **11**:27-44.

Frank, R., 1974, Sedimentary development of the Walli Caves, New South Wales, *Helictite* **12**:3-30.

Ford, D.C. and Williams, P.W., 1989, *Karst Geomorphology and Hydrology,* Unwin-Hyman, London, 601 pp.

Gillieson, D., 1986, Cave sedimentation in the New Guinea Highlands, *Earth Surf. Processes Landforms* **11**:533-543.

Gillieson, D., 1996, *Caves. Processes, Development, Management,* Blackwell, Oxford, 324 pp.

Helwig, J.A., 1964, Stratigraphy of detrital fills of Carroll Cave, Camden County, Missouri, *Missouri Speleol.* **6**:1-15.

Hendrickson, G.E., 1971, Sources of water in Styx and Echo Rivers, Mammoth Cave, Kentucky, U.S. Geol. Survey Prof. Paper **424-D**:41-44.

Jacobson, R.L. and Langmuir, D., 1974, Controls on the quality variations of some carbonate spring waters, *J. Hydrol.* **23**:247-265.

Jones, W.K., 1971, Characteristics of the underground floodplain, *Natl. Speleol. Soc. Bull.* **33**:105-114.

Mahler, B.J., Lynch, F.L. and Bennett, P.C., 1999, Mobile sediment in an urbanizing karst aquifer: Implications for contaminant transport, *Environ. Geol.* **39**:25-38.

Mahler, B.J., Personné, J.-C., Lods, G.F. and Drogue, C., 2000, Transport of free and particulate-associated bacteria in karst, *J. Hydrol.* **238**:179-193.

Milske, J.A., Alexander, Jr., E.C., and Lively, R.S., 1983, Clastic sediments in Mystery Cave, Southeastern Minnesota, *Natl. Speleol. Soc. Bull.* **45**:55-75.

Newson, M.D., 1971, A model of subterranean limestone erosion in the British Isles based on hydrology, *Trans. Inst. British Geograph.* **54**:55-70.

Pickle, J.D., 1985, Dynamics of clastic sedimentation and watershed evolution within a low-relief karst drainage basin, Mammoth Cave Region, Kentucky, MS Thesis, University of New Mexico, Albuquerque, 147 pp.

Quinlan, J.F. and Ewers, R.O., 1989, Subsurface drainage in the Mammoth Cave Area, Chap. 3 in *Karst Hydrology – Concepts from the Mammoth Cave Area*, W.B. White and E.L. White, eds., Van Nostrand Reinhold, New York, pp. 65-103.

Reams, M.W., 1968, Cave sediments and geomorphic history of the Ozarks, PhD Thesis, Washington University, St. Louis, MO, .

Renault, P., 1968, Contribution a l'étude des actions mécaniques et sédimentologiques dans la spéléogenèse, *Ann. Spéléol.* **23**:529-574.

Schmid, E., 1958, *Höhlenforschung und Sedimentanalyse,* Schriften des Institutes für Ur- und Frühgeschichte der Schweiz No. 13, 185 pp.

Schmidt, V.A., 1982, Magnetostratigraphy of sediments in Mammoth Cave, Kentucky, *Science* **217**:827-829.

Springer, G.S. and Kite, J.S., 1997, River-derived slackwater sediments in caves along Cheat River, West Virginia, *Geomorph.* **18**:91-100.

Underwood, K.L., 1994, Evaluation of pesticide and nitrate mobility in a conduit-flow dominated karst basin, M.S. Thesis, The Pennsylvania State University, University Park, PA, 204 pp.

White, E.L. and White, W.B., 1968, Dynamics of sediment transport in limestone caves, *Natl. Speleol. Soc. Bull.* **30**:115-129.

White, W.B., 1976, *The caves of Western Pennsylvania,* Pennsylvania Geol. Survey Gen. Geol. Rpt. **67**, 97 pp.

White, W.B. and Hess, J.W., 1982, Geomorphology of Burnsville Cove and the Geology of the Butler Cave – Sinking Creek System, *Natl. Speleol. Soc. Bull.* **44**:67-77.

White, W.B., 1988, *Geomorphology and Hydrology of Karst Terrains,* Oxford, New York, 464 p.

Wolfe, T.E., 1973, Sedimentation in karst drainage basins along the Allegheny Escarpment in southeastern West Virginia, U.S.A, PhD Thesis, McMaster University, Hamilton, Ont., 455 pp.

SEDIMENT AND SEDIMENT-ASSOCIATED CONTAMINANT TRANSPORT THROUGH KARST

Barbara J. Mahler, Jean-Christian Personné, F. Leo Lynch, and Peter C. Van Metre*

1. INTRODUCTION

The unusual characteristics of subterranean flow in karst aquifers allow for the transport of sediment. Karst ground-water systems are created by dissolution of the bedrock matrix coupled with structural and stratigraphic controls. As a result, high flow velocities, large-diameter openings, and turbulent flow, all necessary for the entrainment and transport of particles, are present—at least episodically—in most karst systems. A better understanding of sediment transport in karst is needed to protect these vulnerable systems. Deposition of sediments within the aquifer may decrease aquifer permeability, fill in wells, and cause pumps to seize; their deposition internally or at spring mouths may destroy species habitat; and their presence impairs the esthetic appearance of spring water. Sediment is itself considered a contaminant—the U.S. Environmental Protection Agency (USEPA) (2000) has recently ruled that total maximum daily loads (TMDLs) are required even for stream segments impacted only by high suspended sediment concentrations. Furthermore, mobile sediment in karst may act as a vector for the transport of hydrophobic ("water fearing") contaminants (Ford and Williams, 1989).

Researchers have long remarked on the mobility of sediment in karst (e.g., Bretz, 1942; White and White, 1968; Ford and Williams, 1989). Sediment characteristics have been used as tools to infer hydraulic conditions in conduits during flood flow (Gale, 1984) and to determine sediment source (White, 1977). It is only recently, however, that focus has been shifted to the importance of the sediments themselves and their impact on water quality.

This chapter focuses on the environmental implications of sediments mobilized in response to rain events. Three different aspects are discussed: the role of suspended sediment in bacterial transport, temporal changes in sediment geochemistry, and

* Barbara J. Mahler, U.S. Geological Survey, Austin, Texas, 78754. Jean-Christian Personné, Université Montpellier II, 34095 Montpellier, France. F. Leo Lynch, Mississippi State University, Mississippi State, Mississippi, 39762. Peter C. Van Metre, U.S. Geological Survey, Austin, Texas, 78754.

sampling and analysis of particle-associated hydrophobic contaminants. Presented first are the results of an investigation of the relation between bacterial contamination and suspended sediments in karst, highlighting the importance of surface-water/ground-water interactions at a karst well field in southern France. Second are the results of intensive monitoring of sediment discharging from a karst spring in Austin, Texas, in response to two storm events, during which suspended sediment concentration, mineralogy, and particle size distribution were analyzed. Third is the description of a method to isolate suspended sediment for the direct analysis of sorbed hydrophobic contaminants and the preliminary results of a pilot study designed to determine the effect of urbanization on water quality at a karst spring in Austin, Texas.

2. TRANSPORT OF SEDIMENT-ASSOCIATED BACTERIA IN KARST

Bacteria and other microorganisms (viruses, protozoa) tend to adhere to solid surfaces. In porous media, bacterial transport is attenuated by adhesion of bacteria to the sediment matrix (McCaulou et al., 1995; Bales et al., 1995). In karst aquifers, however, sediment is mobile and thus may act as a vehicle for transport of adsorbed contaminants, including bacteria. Furthermore, karst aquifers display other properties that are highly pertinent to the investigation of bacterial contamination. First, karst aquifers often have a direct and rapid connection between surface water and ground water. Second, karst is highly heterogeneous; wells located only a few meters apart may display very different hydrogeologic behavior, indicating that such wells may have different degrees of vulnerability to microbiological contamination. Third, water quality in karst can vary dramatically over short time periods (e.g., Ryan and Meiman, 1996; Mahler and Lynch, 1999); quarterly, weekly, or even daily sampling may be insufficient to describe contamination events. Episodic contamination is of particular concern in the case of pathogenic microorganisms, where ingestion of even a single microorganism can cause illness.

2.1. Karst Bacteria Field Investigation: Background

A study of storm-event-based bacterial contamination in the Lez Basin in southern France was undertaken to investigate the importance of sediment-mediated bacterial transport in a heterogeneous karst aquifer. The study site (Figure 1), located in southern France 15 km north of the city of Montpellier, is adjacent to a surface stream that receives discharge from a wastewater treatment plant after rainfall. The objectives of the study were to: (1) determine the relation between bacterial contamination of surface water and ground water; and (2) determine the importance of suspended sediment in transporting bacteria. Samples were collected at the monitoring well field from two neighboring wells with contrasting hydraulic conductivities. The wells were sampled for several days immediately following rainfall that was sufficient to cause the surface stream to flow. Samples were analyzed for total suspended solids (TSS) and fecal coliform, generally assumed to be an indicator of fecal contamination and the presence of fecal-born pathogens.

The wells sampled for this study, P7 and P8, are spaced 5 m apart. They are 115-mm in diameter and uncased below the top 50 cm. The annular space at the surface is sealed and encased in concrete. Both wells were drilled to a depth of 57 m with a

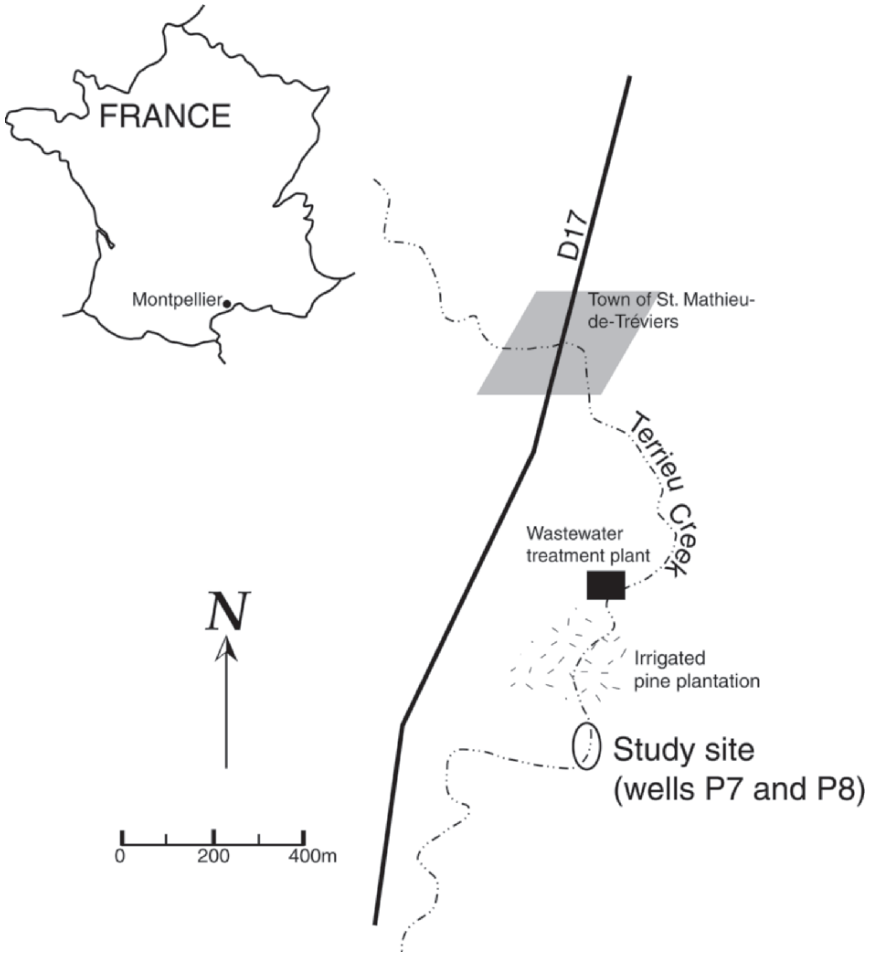

Figure 1. Location of the Terrieu Creek study site.

percussion-drilling rig and without the use of drilling mud. Well P7 is known to intercept a zone of slight fracturing at 40 to 50 m, whereas well P8 intercepts highly-fractured zones at 10 to 12 and 42 to 45 m; water-level changes in the two wells in response to rainfall closely mirror one another (Botton, 1984). The effective hydraulic conductivity of the zone penetrated by P7 is 10^{-7} to 10^{-9} m/s and that of P8 is 10^{-1} to 10^{-3} m/s, as determined by pump test (Drogue, 1974).

The assumed source of fecal coliform contamination is a wastewater treatment plant located 400 m upstream of the well field. Primary-treated wastewater is collected in a basin; during rain storms, the retention basin sometimes overflows and the treated wastewater flows into Terrieu Creek. Previous research by Malard et al. (1994) at this

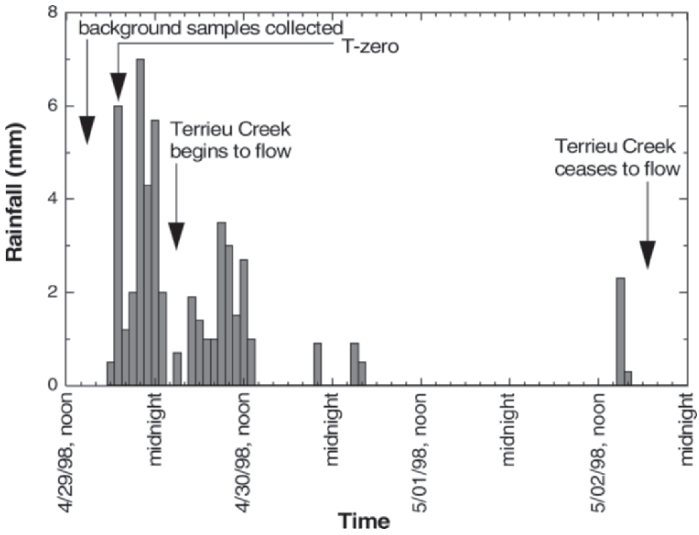

Figure 2. Histogram of rainfall and indication of timing of events.

site demonstrated the relation between the wastewater treatment plant, fecal coliform contamination in Terrieu Creek, and contamination of nearby wells. Primary-treated wastewater is used for irrigation of a pine plantation located between the well field and the treatment plant. There is no known source of bacterial contamination within the confines of the well field.

2.2 Karst Bacteria Field Investigation: Methods

Samples were collected before, during, and after a rainfall of 28 mm spread out over about 18 hours (Figure 2). Prior to the sampled storm event, no rain had fallen for 2 weeks, and the surface stream had not flowed for 4 weeks. Downhole pumps were installed, three well volumes purged, and initial samples collected before rainfall began. Water level was monitored in well P20, located in the same well field as P7 and P8. Piezometric level in P20 is highly correlated to that in P7 and P8 (Botton, 1984). A downhole piston and a downhole diaphragm pump were used to pump the wells at a rate of 5.5 L/min. Once rainfall began, samples were collected from the wells and the surface stream every 3 hours initially, then tapering off after the first 48 hours. Total suspended solids were determined by weight difference after vacuum filtration.

Each sample was split for analysis of the whole (unfiltered) water and analysis of sediment-associated bacteria. Samples for whole-water analysis were sonicated to disaggregate microbial masses and detach bacteria fixed to sediment. Samples for analysis of bacteria associated with suspended sediment were gently agitated and filtered through an 8-μm membrane (for this study the bacteria-sediment conglomerate was operationally defined as having a minimum size of 8 μm to preclude retention of any unadhered bacteria). Sterile distilled water was then passed through the membrane to

rinse the sediment. The membrane was transferred to a flask containing sterile distilled water, which was then sonicated and vortexed.

The whole-water sample and the sample obtained from the treated membrane were analyzed identically to determine the growth and enumeration of the fecal coliform. Based on their probable contamination, at least 2 aliquots of 0.1 to 100 mL of the prepared samples were filtered through a 0.45-μm membrane to filter out all bacteria. The membranes were placed in petri dishes containing TTC + tergitol agar (Diagnostic Pasteur ref. 64454). The dishes were incubated, and then the bacteria were enumerated and expressed as colony forming units (CFU)/100 mL.

2.3. Karst Bacteria Field Investigation: Results

Rainfall at the site sufficient to cause Terrieu Creek to flow resulted in marked temporal changes in TSS and bacterial content in both surface and ground water. Both wells P7 and P8 responded quickly to elevated TSS concentrations and bacteria in Terrieu Creek. Temporal changes in TSS and concentrations of free and sediment-associated bacteria continued over several days.

Water level in well P20 and changes in TSS in wells P7 and P8 and in Terrieu are shown in Figure 3a. Water level rose steadily in the wells for the first 24 hours following rainfall, then dropped gradually over the next 11 days. Concentrations of TSS in Terrieu Creek were highest immediately after the ephemeral creek began to flow, then rapidly decreased over the 24 hours following rainfall. Concentrations of TSS in P7, the low-conductivity well, showed little response to the rain event. (The dramatic increase in TSS in P7 68 hours after the rain event did not have any apparent correlation to any external events; it may have been produced by a sudden unblocking of a clay-filled fracture as water level fell.) In contrast, TSS in P8, the high-conductivity well, increased for the first 11 hours after the rain, then decreased, attaining a TSS similar to that of the creek and lower than that of P7.

Fecal coliform density reached extremely high levels in Terrieu Creek and both wells directly after the creek began to flow and again several days later (Fig. 3b). The first peak in bacteria in Terrieu Creek coincided with the TSS peak in the first flush of streamflow. The second increase occurred when creek flow slowed and the water began to pond, peaking just before the creek ceased to flow. Samples of ponded water were not collected after cessation of flow.

Fecal coliform density in both P7 and P8 increased more than an order of magnitude within 10 hours after flow began in Terrieu Creek. The bacteria then decreased for about 60 hours, before increasing again, peaking 120 hours after rainfall at 30,000 and 25,000 CFU/100 mL, respectively.

Additional information on the relation between the wells and the surface stream can be shown by directly comparing their bacterial densities (Figure 3b). During the initial period of high bacterial densities (about 30 hours after rainfall began), P8 had bacterial densities about an order of magnitude less than those in Terrieu Creek, whereas densities in P7 were intermediate between the two. In contrast, during the second period both wells had bacterial densities of the same order of magnitude as that of the surface water.

A substantial proportion of fecal coliform density was associated with suspended particulates (Figure 4a). The fixed proportion varies over time and shows no temporal pattern, but often represents 50% or more of fecal coliform. In contrast, the ratio between fecal coliform associated with sediment in surface water and ground water does show a

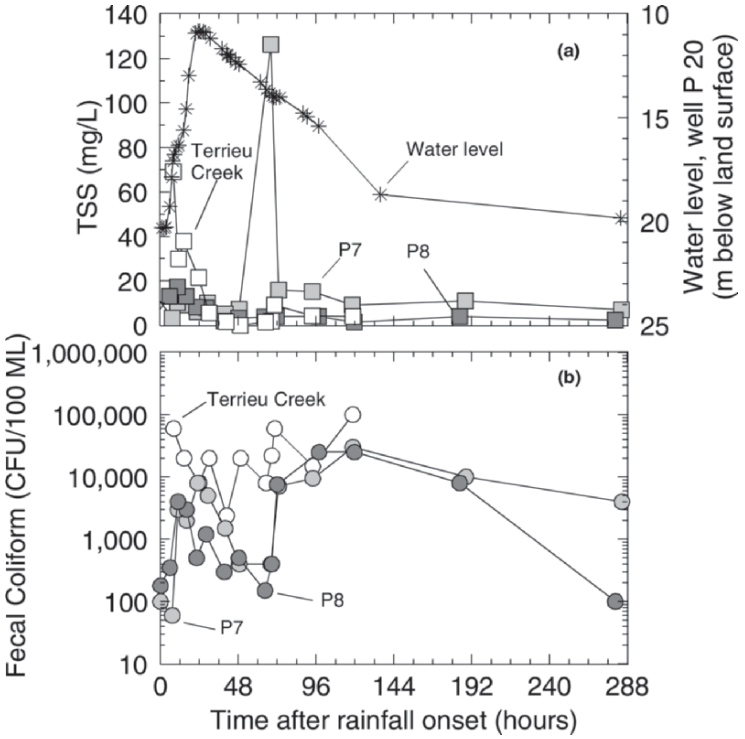

Figure 3. Concentrations of TSS (a) and fecal coliform density (b) in wells P7 and P8 and Terrieu Creek in response to a storm.

temporal pattern (Figure 4b,c), with suspended sediment from both wells initially much less contaminated than that in the surface water. During the latter part of the sampling period, the suspended sediment in both wells, and particularly in the fissured well (P8), had bacterial densities much more similar to that of the surface water.

2.4 Karst Bacteria Field Investigation: Discussion and Implications

Ground-water quality responded virtually immediately (less than 3 hours, the sampling interval) to changes in surface-water quality (Figure 3a,b). The source of the first peak in bacterial densities is most likely the upstream wastewater treatment facility, which overflows into Terrieu Creek after heavy rainfall. The source of the second increase in bacterial densities, which occurred long after overland flow had ceased and when flow in the creek had decreased to a trickle, could not have been the wastewater treatment plant. One possibility is that, given the warm daytime air temperatures (~25°C) and the almost stagnant condition of the water in the creekbed, bacterial populations in the ponding water underwent explosive growth, and infiltrated from the surface water into ground water. Alternatively, it is possible that bacteria were

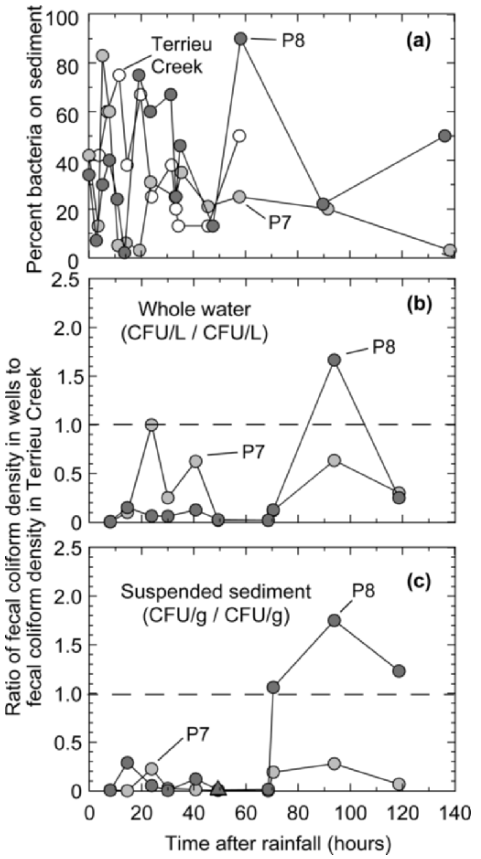

Figure 4. Percent fecal coliform associated with particulates in wells P7 and P8 and Terrieu Creek (a); and comparison of fecal coliform densities in whole water (b) and on suspended sediment (c) in each of the two wells to that in surface water. Ratios are calculated as CFU/L in each well divided by CFU/L in Terrieu Creek for whole water, and CFU/g in each well divided by CFU/g in Terrieu Creek for suspended sediment.

multiplying simultaneously both in the surface water and in the ground water, resulting in similar densities of bacteria in both surface and ground water during this second peak. This hypothesis is supported by the fact that, during the latter portion of the sampling, bacteria densities in well P8, both in whole water and on suspended sediment (Figure 4b,c), were actually greater than those in the surface water. It may be that conditions within the aquifer were more favorable for the growth and/or survival of bacteria than conditions at the surface. A third possibility is that during the early portion of the response to the storm, fecal coliform and sediment stored in small conduits intercepted by the wells were remobilized. Because the sediment would have been in storage since a previous event, the bacterial counts would be expected to be lower because of die-off. However, the travel time from Terrieu Creek to the wells is sufficiently short that the influence of the creek would have been seen long before the second increase in bacterial levels, 60 hours after the onset of rainfall.

Interestingly, well P8, which is situated in a fractured zone and thus might be expected to be more vulnerable to contamination from Terrieu Creek, often had lower fecal coliform densities than well P7, both in whole water and associated with suspended sediment. The differences in bacterial densities between the two wells may reflect varying degrees of dilution of contaminated water and sediment with less-contaminated inputs. One possible explanation is that there are differences in the degree of connection between the epikarstic (subcutaneous) zone and the wells. The epikarstic zone is the upper weathered layer of rock in karst terrain. It has a high permeability that diminishes with depth; during the days immediately following a storm, infiltrated rainwater stored in the epikarstic zone slowly percolates into the subsurface via a few widely spaced master joints (Williams, 1983). If P8 intersects one or more master joints, relatively uncontaminated rain water draining into P8 from the epikarst during the initial portion of the storm would dilute incoming water from the creek, whereas later in the sampling period, after the epikarstic zone had drained, P8 would be more greatly influenced by creek water. Similarly, the difference between the amount of fecal coliform associated with suspended sediment in P8 and Terrieu Creek could be caused by dilution of contaminated sediment from the creek with uncontaminated sediment from the epikarstic zone during the first flush.

The substantial proportion of bacteria attached to a mobile solid phase adds an additional dimension to the prediction of bacterial fate and transport in karst terrain. Bacteria adhered to particulates have the potential to settle out of flow with the particulates and to be later remobilized with the particulates if flow velocity increases. Furthermore, the attachment of bacteria to a solid phase is a function of temperature (McCaulou et al., 1995), ionic strength (Fontes et al., 1991), and pH (Bales et al., 1995). The wide temporal variation of these parameters in karst ground water in response to influxes of surface water should result in the dynamic attachment and detachment of bacteria to particles. Finally, and perhaps most important from a public health perspective, bacteria associated with particulates are both more persistent in nature and more difficult to remove by treatment. They are protected from many of the predators that graze on free-floating bacteria (Harvey et al., 1984); can better resist chemical attack (Rittman, 1993); and may be able to utilize some of the organic materials associated with sediment particles as an energy source. Moreover, common methods of disinfection (chlorination, ozonation, ultraviolet light) are far less effective if the bacteria are entrapped in particulates, particularly those of fecal origin (Schoenen, 1998).

3. CHARACTERISTICS OF SEDIMENT DISCHARGING FROM A KARST SPRING IN RESPONSE TO A STORM

The geochemical characteristics of particulates discharging from a karst spring in response to a storm may be related to sediment source and can affect contaminant transport. Only a few studies, however, have characterized suspended sediment in karst from an environmental standpoint. Ryan and Meiman (1996) investigated temporal changes in bacteria and suspended sediment concentrations in springflow in response to rainfall. They found that fecal coliform and turbidity peaked simultaneously in a karst spring in Kentucky, but they did not attempt to characterize the sediment beyond ascertaining the TSS. Atteia and Kozel (1997) analyzed particle-size distributions in sediment discharging from two karst springs. They found that colloids composed 40% of

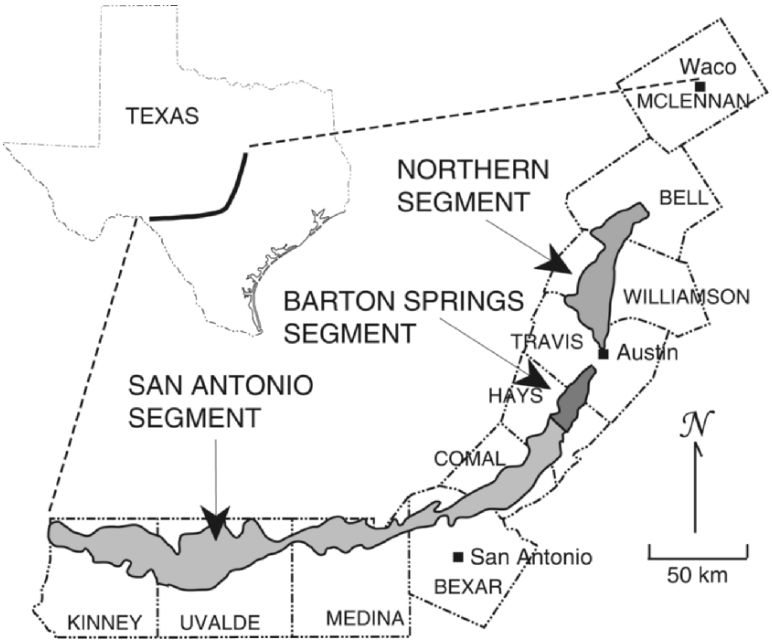

Figure 5. The three segments of the Edwards (Balcones fault zone) aquifer.

the particle surface area, potentially lending them an important role in contaminant transport. Characteristics such as mineralogy, surface area, and organic carbon content—all of which influence the degree to which contaminants adsorb to sediments—have yet to be described.

3.1. Sediment Characteristics Field Investigation: Background

An investigation of temporal variation in geochemical characteristics of suspended sediment in response to a storm was carried out at Barton Springs, the fifth largest spring in Texas (Mahler and Lynch, 1999). Barton Springs is the primary discharge point for the Barton Springs segment of the Edwards aquifer (hereinafter referred to as the Barton Springs aquifer), located in central Texas, one of the most rapidly urbanizing regions in the United States (Figure 5). The aquifer and its watershed are divided into three areas: the contributing zone, the recharge zone, and the confined zone (Figure 6). The contributing zone is not hydrogeologically connected to the aquifer, but surface water originating in this zone ultimately flows, via five main creeks, onto the highly permeable recharge zone. Once over the recharge zone, defined by the area where the highly

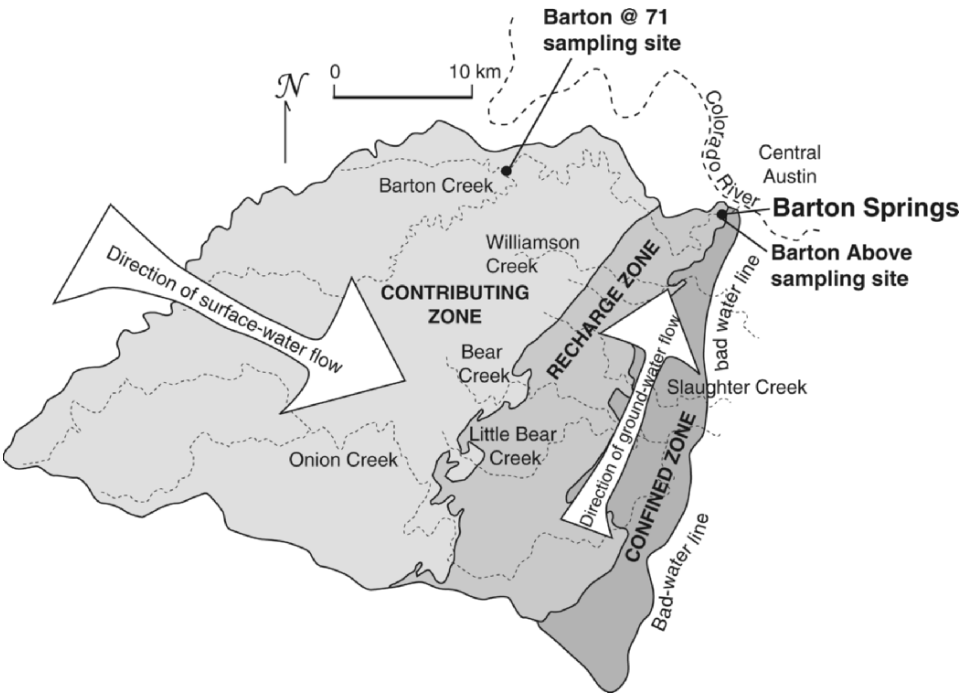

Figure 6. The Barton Springs aquifer and contributing zone and location of sampling sites.

permeable Edwards and Georgetown Limestones outcrop, water infiltrates into the aquifer through sinkholes and fractures in the creekbeds. Slade et al. (1986) estimate that 85% of aquifer recharge occurs in this way, with the remaining 15% occuring through direct infiltration on the uplands. The confined zone is the artesian portion of the aquifer, where the Edwards and Georgetown Limestones are confined by the relatively impermeable Del Rio Clay. Although surface flow across the aquifer's watershed is generally from west to east, ground-water flow is predominantly NNE, and about 90% discharges from Barton Springs. The series of NNE-trending high-angle normal faults comprising the Balcones fault zone are responsible for the structurally controlled direction of subsurface flow (Slade et al., 1986).

The travel time from recharge to discharge is difficult to define, as the distance from the most distal part of the recharge zone to Barton Springs is about 30 km, and recharge occurs through both large and small recharge features in and outside of creekbeds. However, some idea of travel times can be gained from various ground-water traces: a trace carried out during high flow conditions demonstrated that recharge from Williamson Creek discharged from Barton Springs in less than 30 hours (Hauwert et al.,

1998); a second trace showed a travel time from the lower portion of Barton Creek to Barton Springs of 10 hours; in contrast, dye injected into Onion Creek took more than 2 weeks to arrive at Barton Springs (Hauwert et al., in press). Travel time can vary greatly with water level.

Barton Springs is impounded by a dam, creating Barton Springs Pool. Barton Creek, when flowing, is routed around the pool through a bypass. Creek flow does occasionally overwhelm the capacity of the bypass, but this did not occur during the two storms described here. The impoundment of springflow places an artificial head over the springs. When the dam gates are removed, spring discharge (Q) increases as a result of the sudden change in hydraulic gradient.

During the period of investigation, the dam gates were routinely removed once a week and after storm events for pool cleaning. Two separate rating curves, one for use when the pool is full and the second for when the gates are removed, have been developed by the U.S. Geological Survey (USGS) for determining discharge from the spring based on water level in a nearby well. Based on the rating curves, the average discharge from the springs of 1.4 m^3/s increases to 1.9 m^3/s when the pool level is lowered.

The water quality of Barton Springs is important for several reasons. It provides a part of Austin's municipal water supply; it is the sole home of the Barton Springs salamander (*Eurycea sosorum*), listed as an endangered species by the U.S. Fish and Wildlife Service; and it is considered a significant addition to Austin's quality of life and an important tourist attraction.

In general the water quality at Barton Springs is considered "good" (U.S. Fish and Wildlife Service, 1997), but may be declining. Statistically significant increases in conductivity, sulfate, turbidity, and total organic carbon in base flow have been noted (City of Austin, 1999), and soluble pesticides have been detected in both storm discharge and base flow (Mahler and Van Metre, 2000). Analyses of water samples from aquifer wells and small springs have detected petroleum hydrocarbons, pesticides, arsenic, and lead (Hauwert and Vickers, 1994). Reported spills of hazardous materials over the aquifer from 1986 to 1992 included gasoline and diesel fuels, pesticides, trichloroethane, and perchloroethene (U.S. Fish and Wildlife Service, 1997). The sorption of these contaminants onto solid surfaces is a function of the individual contaminant and the organic carbon content, specific surface area, and mineralogy of the solid. Mobile particulates may thus play an important role in the concentration and transport of contaminants through the aquifer.

3.2. Sediment Characteristics Field Investigation: Methods

Hourly grab samples were collected from the mouth of one of the main orifices of Barton Springs for 24 hours following two storm events. Storm 1 occurred toward the end of a period of average rainfall. During this event, a total of 85 mm of rain fell. Storm 2, the first substantial event following storm 1, occurred 6 months later. During this event, 44 mm of rain fell. Prior to storm 1, the dam gates had been removed by pool staff for pool cleaning and were replaced just after the beginning of the storm; the gates were removed by pool staff about 12 hours after rainfall for both storms (Figure 7). The samples were collected in 20-L polyethylene containers, two per sample. One-liter samples were removed for analysis of TSS, which was carried out by weight difference after vacuum filtration. The particles on the filters were examined under a binocular

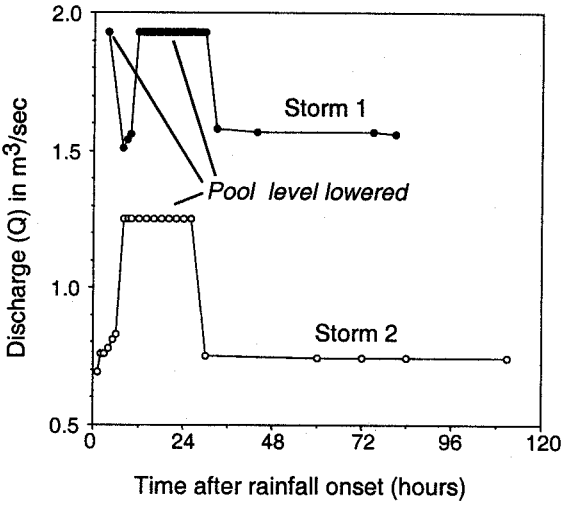

Figure 7. Barton Springs discharge (Q) after storms 1 and 2. Note the increase in Q.

microscope for visual identification. The particulate fraction in the remaining sample was concentrated by in-line centrifugation: sample was pumped at a steady rate of 120 mL/min through a Servall in-line system rotating at 6,000 rpm; the 3.3-minute residence times corresponds to collection of the >0.3-μm fraction, the operational definition of particulate for this study. Particle-size distributions (PSD) were determined by the Coulter Counter system. Mineralogy was analyzed by powder X-ray diffraction with a Siemens D-500 diffractometer, and the data were interpreted as described in Lynch (1997). Turbidity, pH, and specific conductance (SC) were measured *in situ* using a Horiba Model U-10.

3.3. Sediment Characteristics Field Investigation: Results

The response of *Q* to the storm events is difficult to ascertain, as it was obscured by the immediate and dramatic increase caused by removal of the dam gates after the storm events (Figure 7). However, it is clear that the spring hydrographs would have peaked at some time less than 26 hours after rainfall.

Concentrations of TSS began to increase 8 to 9 hours after rainfall began, and peaked at about 12 to 15 hours (Figure 8). The shape of these sedigraphs is similar to those of a typical storm hydrograph, with a steep rising limb and a more gradually-tapering falling limb. The total mass of sediment discharged for storms 1 and 2 was about 805 and 1,013 kg, respectively, based on results of the TSS analysis and *Q*.

Inspection of the particles trapped on the filters revealed numerous fibers in a wide range of colors and lengths. Some fibers were coated with what appeared to be dark brown-black organic matter, and others were ensnared in clumps of inorganic particles and organic matter. Individual pieces of organic matter ranged from a few microns to 50

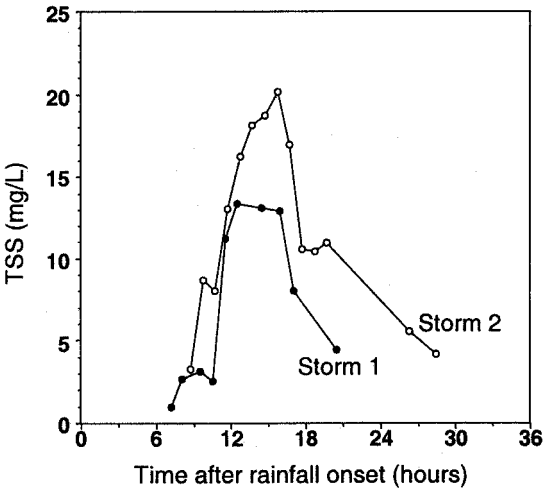

Figure 8. Changes in TSS in response to storms 1 and 2.

μm in diameter. Based on visual inspection, the amount of organic matter seemed to increase with increasing TSS, giving the filter a rich tan color at the peak of the sedigraph. Pieces of quartz, calcite, and dolomite were recognizable on the filters, and other particles 10 to 20 μm in diameter in shades of fuschia-pink, bright green, and turquoise blue were rarer but present.

Temporal changes in mineralogy were somewhat similar between the two storms, but with some differences (Figure 9). For both storms, clay and dolomite were predominant with lesser amounts of quartz and calcite. After both storms, the amount of clay minerals in the samples increased throughout the response to the event. However, at the beginning of the response to storm 2, calcite was present in a proportion equal to that of clay and dolomite before dropping off about 12 hours after rainfall began. The response to storm 2 also showed a marked peak in dolomite coincident with the TSS peak.

The particle-size distribution function (PSDF) is expressed as the number of particles per milliliter of solution per class size (particles ml^{-1} μm^{-1}); a representative PSDF for the storms (as computed for storm 1) is shown in Figure 10. A cubic regression, determined to be the best fit for the data, was used to compute the PSDF at 4 and 10 μm ($N_{4\mu}$ and $N_{10\mu}$) and d_{max}, defined as the particle diameter for which only 10 particles were counted. Changes in these three parameters in response to the storms are shown in Figure 11.

3.4. Sediment Characteristics Field Investigation: Discussion

Visual evidence and timing of sediment peaks indicate that some portion of discharging sediments is allogenic. The colored fibers and organic matter are both clearly allogenic. Sediment samples collected from Barton Springs have an organic

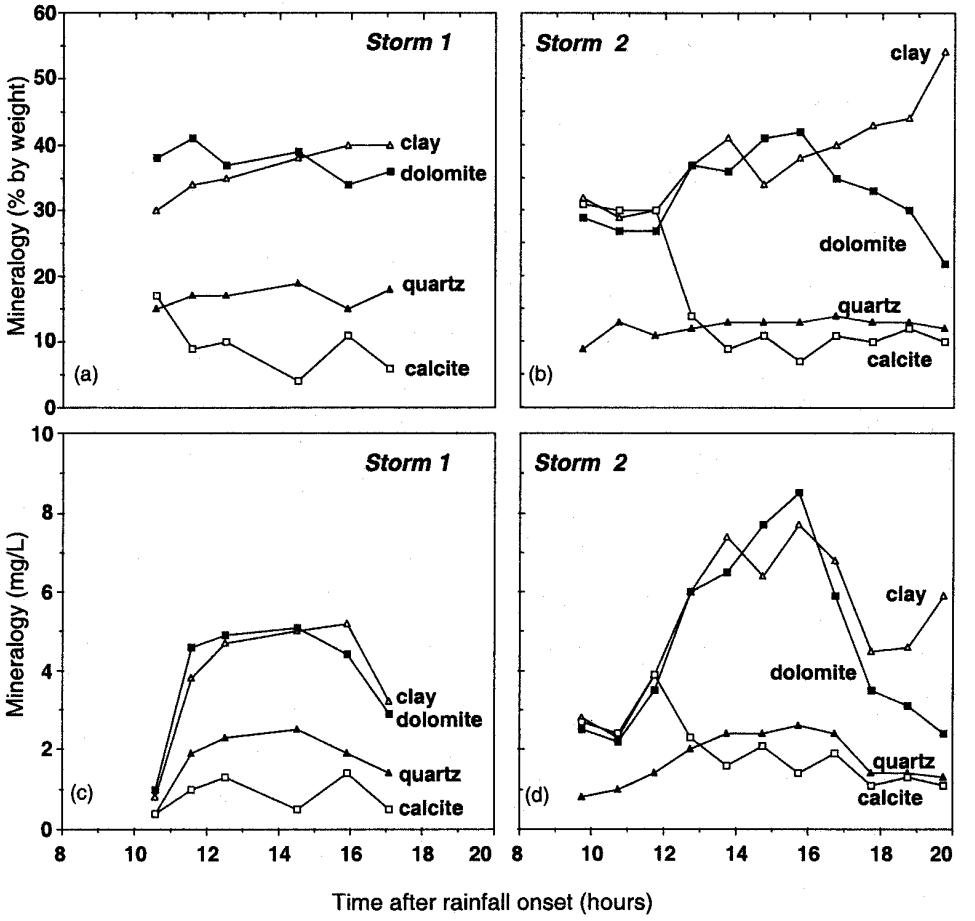

Figure 9. Changes in mineralogy in response to storms 1 and 2 as percent by weight of total sediment (a and b) and as concentration in milligrams per liter of sample (c and d).

carbon content of 1.6 to 2.9% by weight (U.S. Geological Survey, unpublished data), similar to that of surface samples and greater than that of sediment from wells and caves in the recharge zone (Mahler et al., 1999).

Peak concentrations of TSS coincide with changes in specific conductance, indicating flushing of surface water through the aquifer (Mahler and Lynch, 1999) and possibly a surface origin for much of the sediment. Although the removal of the dam gates coincides with increases in TSS during the two storms, the increase cannot be attributed to removal of the gates—note, for example, that although the dam gates were not in place at the beginning of storm 1 (Figure 7), TSS was only 1 mg/L (Figure 8). The gates have been removed dozens of times during routine pool maintenance without resulting in an increase in turbidity, as recorded at 15-minute intervals on a DataSonde installed in the main spring orifice (David Johns, City of Austin, unpublished data).

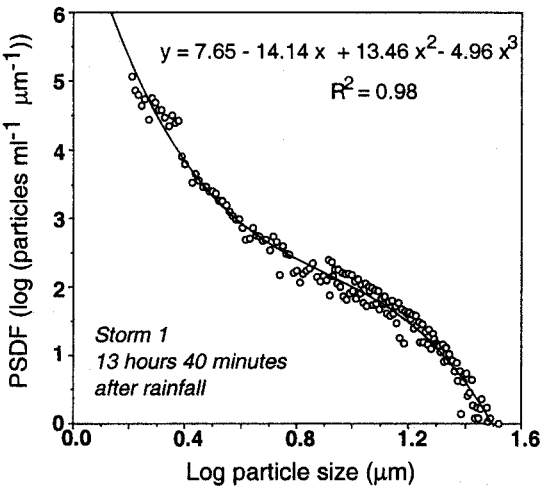

Figure 10. Representative particle-size distribution function (PSDF) for the storms fit with a cubic regression equation.

Furthermore, TSS increased 12 to 24 hours following rainfall even in instances where the pool gates have not been removed (David Johns, City of Austin, unpublished data). Increases in TSS must therefore be caused either by changes in flow conditions at the surface or in the more distal parts of the aquifer unaffected by a change in head at the spring.

Temporal changes in mineralogy indicate a varying contribution of sediment from different sources. The gradual increase in proportions of clay over time was not matched by a gradual decrease in the other three mineralogical constituents over time for either storm. The increase in clay minerals cannot be attributed solely to a hydraulic change causing the small, platy clay minerals to stay in suspension as other minerals drop out, because dolomite both increases and decreases while clay is increasing during storm 2. One hypothesis is that different aquifer compartments are accessed at different stages of the storm surge. Mahler et al. (1999) found statistically significant differences in mineralogy of sediments from the surface, in wells, and in caves in the Barton Springs recharge zone. Surface sediments were calcite rich and may contribute to the initial pulse of sediment discharging from the spring. Furthermore, it is unlikely that the clay and dolomite share the same source, as those compartments found to have a high proportion of dolomite contained little or no clay.

A second and more likely hypothesis to explain the variability in mineralogic composition of the suspended sediment over time stems from mineralogic differences at the surface. The different members of the Edwards Group outcrop across the aquifer, and each have subtly distinct clay mineralogies. Spatial variation in rainfall and differences in travel time could result in the appearance of these distinct sediment types at the spring at different times.

Finally, there are five different creek basins contributing flow to Barton Springs, each with discrete recharge points and different flowpaths and travel times. Thus, it cannot be expected that the mineralogic composition of the discharging sediment would be homogeneous.

Temporal changes in the PSDF may also reflect conditions both within and outside the aquifer. For both storms, d_{max} reaches a maximum at the same time that TSS peaks, a reflection of maximum flow velocity. The maximum particle size decreases from 8 to 12 hours after rainfall, possibly indicating that an initial flush of water from one source is later followed by an influx from another source. The late flush of clay minerals for storm 2, seen both in the mineralogy and as an increase in $N_{4\mu m,}$ indicates a newly accessed source of clay minerals.

Interestingly, the amount of sediment discharged in response to storm 2 was greater than that discharged in response to storm 1, even though only one-half as much rain fell. This may be a function of the intensity and location of rainfall, in which case the source of the sediment must be the surface. Alternatively, it may be the result of seasonal differences in sediment supply. The concept of sediment supply is used to describe and predict sediment transport by surface streams: as the wet season progresses, sediment concentrations for a given stream discharge decrease as sediment supplies are depleted. During the dry period that follows, supplies are "reset" by mass soil erosion processes, which may be caused by land-use practices such as construction and devegetation, or natural phenomena such as landslides (Van Sickle and Beschta, 1983). Storm 1 occurred

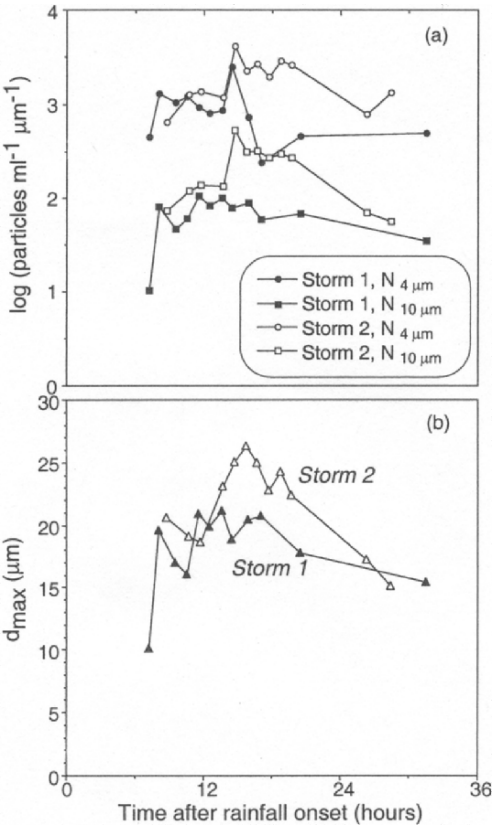

Figure 11. Changes in PSDF parameters $N_{4\mu m}$, $N_{10\mu m,}$ and d_{max} in response to storms 1 and 2.

at the end of a wet period and storm 2 after a long dry period. Based on the concept of sediment supply, storm 2 would be expected to transport more sediment than storm 1. This alternative also supports the hypothesis of an allochthonous source for the sediment: the processes that control sediment supply and depletion take place at the surface, not in the subsurface. Additionally, some sediment could be supplied to conduits during small rains, another form of "resetting" the supply, and then resuspended and flushed out during a large storm. Thus, in either case, the difference in the amount of sediment discharged indicates that the primary source of the discharging sediment is allochthonous, which could have important implications for decisions concerning land-use practices.

4. COLLECTION OF SUSPENDED SEDIMENTS DISCHARGING FROM SPRINGS FOR ANALYSIS

The presence of allochthonous sediment in discharge from Barton Springs raises the question: what role do these sediments play in the transport of hydrophobic contaminants (HCs) through the aquifer? The suspended sediments have a relatively high organic carbon content, and sorption of HCs onto solids is dominated by partitioning into organic carbon. The suspended sediments contain an important fraction of clay minerals, which, because of their large surface area, can also concentrate and transport HCs through direct sorption to the mineral surface. Clearly, these sediments have the potential to transport HCs through the aquifer to discharge at the spring, but are they actually doing so?

4.1. Large-Volume Filtration: Background

Occurrence and transport of HCs have important implications for health of biota as well as humans. Of the top 20 contaminants on the USEPA Hazardous Substances Priority List, 15 are hydrophobic (USEPA, 1999). These contaminants include trace elements, organochlorine compounds, and polycyclic aromatic hydrocarbons (PAHs). A major fraction of HCs are transported adhered to suspended sediment (Bradford and Horowitz, 1982; Garbarino et al., 1995; Rostad et al., 1995).

Using traditional methods of whole-water analysis, concentrations of these HCs are usually underestimated. Indeed, by these methods HCs may not even be detected, although they may occur on sediment at concentrations likely to have toxic effects on biota. The conventional approach for determining the concentration of HCs on suspended sediment is to analyze a whole-water sample and a filtered water sample and to assume that the difference between the two represents the fraction sorbed to suspended sediment. The major problem with this approach is that the amount of suspended sediment and associated contaminant in the whole-water sample may not be sufficient to produce a detection by whole-water analysis methods. This is particularly true if the suspended sediment concentration in the sample is small, as is generally the case for springs relative to surface water. For example, if a sample contains 50 mg/L of suspended sediment, and the sediment contains 300 μg/kg of polychlorinated biphenyls (PCBs) (a concentration likely to adversely affect biota health (Environment Canada, 1998)), the concentration of PCBs in the whole-water sample will be 0.015 μg/L. This concentration is well below most laboratory method detection limits—for example, the USGS National

Water Quality Laboratory (NWQL) method detection limit is 0.1 μg/L—yet the solid phase itself is highly contaminated.

Because of the tendency of HCs to associate with particles, suspended sediment is likely to be the vehicle for the vast majority of the transport of HCs. Once the sediment settles out of flow and settles to the floor of the receiving water body, it can represent a threat to the ecological community. Benzo[a]pyrene, for example, was not detected in any of 100 storm-event samples in residential sites in the Dallas-Fort Worth area and was detected in less than 5% of samples from commercial and industrial sites (Raines et al., 1997). Yet concentrations of benzo[a]pyrene have increased 20-fold in the Dallas-Fort Worth area, coincident with urban development, based on an age-dated sediment core from White Rock Lake in Dallas (Van Metre et al., 2000).

A more effective approach to determining the concentration of HCs on suspended sediments is to separate the sediment from the water column and analyze it directly. Although there are several approaches to this, as described by Horowitz (1995), the least expensive and most efficient method for use on low-TSS karst spring water is large-volume filtration (LVF). This involves *in situ* filtration of the spring water using an apparatus that allows both a sufficient amount of material to be collected for analysis and the material in a form that lends itself to analysis.

4.2. Large-Volume Filtration: Methods

A major motivation for the LVF method is the mass of sediment required to achieve reasonable analytical method detection limits. Target constituents include major and trace elements, organochlorine pesticides, PCBs, and PAHs. The amount of sediment required for the analysis of major and trace elements by the USGS NWQL, for example, is 300 to 500 mg dry weight (R. Sanzalone, USGS, oral commun.). The amount of sediment required for the analysis of the organic compounds is 3 to 5 g dry weight (E. Furlong, USGS, oral commun.). The more material that is supplied, the less the interference and the lower the detection limits (E. Furlong, USGS, oral commun.).

To obtain sufficient sample for major and trace element analysis, water is pumped through a polytetrafluoroethylene (PTFE) filter held in an acrylic filter holder. A 145-mm diameter, 0.5-μm pore-size PTFE filter is sprayed lightly with methanol to allow water to pass through, and water is pumped through until the filter clogs. (Although the particulate phase is often operationally defined to be >0.3 μm, it is very difficult to pass water through a PTFE filter of pore size <0.5 μm.) The filter is placed in a sealable plastic bag with a few milliliters of distilled water and massaged until all the sediment has been removed from the filter and is suspended in the small volume of water. More than 98% of the initial suspended sediment can be recovered in this fashion. The water containing the sediment is then poured into a small plastic dish, frozen, and freeze-dried for analysis. A single filter may allow 100 to 500 mg of sediment to be recovered, depending on the organic matter and algal content of the water.

To obtain sufficient sample for analysis of organochlorine compounds and PAHs, water is pumped through a glass-fiber filter held in a stainless-steel plate filter holder. The filters are pre-cleaned by baking and wrapped in aluminum foil pending use. Initially, water can be pumped through the 298-mm diameter, 0.7-μm pore-size glass-fiber filter (the minimum pore size available) at a rate of 1 L or more per minute; as the filter begins to clog, the flow rate slows. Once the filter has clogged, air is pumped

Table 1. Details of sampling during three storm events.

Event date	Rainfall (mm)	Sample timing (hrs after rainfall onset)	TSS range (mg/L)	Volume filtered (L)
5/27/99	50	11–22	2–16	1,189
5/01/00	69	12–20	2–9	1,043
5/02/00	36	12–19	5–9	500
6/09/00	112	12–14	28–35	90
6/10/00	20	6–10	36–42	72

through the filter to remove as much water as possible—drying the filter in this way improves laboratory minimum reporting levels by decreasing interference during the analysis. A graduated container is used to collect outflow from the filter, and the volume of water pumped to clog the filter is recorded. Experience indicates that about 0.5–2 g of sediment is trapped on each filter, so that 2 to 3 clogged filters are required to obtain enough material for analysis. The filters are placed (together) in a baked glass jar and chilled for shipment to the laboratory. Results are reported as mass of organic contaminant per liter of water filtered. The concentration is converted to mass of organic contaminant per mass of sediment based on the volume filtered and the suspended sediment concentration of the original sample; samples for TSS concentrations are collected before and after sample processing.

For the results presented here, elemental concentrations were determined on concentrated-acid digests using inductivity coupled plasma-atomic emission spectrometry (ICP–AES); concentrations of cadmium, chromium, lead, and zinc were determined on concentrated-acid digests using graphite furnace atomic adsorption (GFAA); and concentrations of mercury were determined by cold-vapor atomic adsorption (CVAA) (Fishman and Friedman, 1989). Organochlorine compounds and PAHs were measured in organic-solvent extracts using a dual capillary-column gas chromatograph with dual electron capture detector (Foreman et al., 1995; Furlong et al., 1996). The filters and the sediment they contain are extracted together. The method uses a soxhlet extraction with dichloromethane and methanol followed by gel permeation and adsorption chromatographic fractionation.

To date, three storm events have been sampled (Table 1). A sample for each event was collected *in situ* at Barton Springs. In addition, a flow-weighted composite sample for each event was collected from each of two sites from Barton Creek (Figure 6). The first site is located just upstream of the springs ("Barton Above"), where the watershed has been extensively developed with residential and commercial land-use. Water from this portion of the creek is not thought to recharge Barton Springs; however, Hauwert et al. (in press) determined a travel time of about 10 hours from a point of infiltration about 2 km upstream of this site to the springs. The second site is Barton Creek at Highway 71 ("Barton @ 71"), a reference site in the contributing zone, where there is relatively little development. Water from the contributing zone flows onto the western portion of the recharge zone—infiltration in this area discharges from Cold Springs, a small spring west of Barton Springs (Hauwert et al., 1998). Under high flow conditions, however, as recharge features in the western portion of the recharge zone become saturated, flow from the contributing zone may continue downstream to infiltrate through features in the

eastern portion of the recharge zone, which ultimately discharges from Barton Springs (N. Hauwert, unpublished data).

Concentrations of selected contaminants at the sites are shown in Table 2. Also shown are Environment Canada (1998) Sediment Quality Guidelines (SQGs); although these guidelines have no regulatory power, they are useful as a yardstick for gauging the degree of contamination of the sediment. The Threshold Effects Level (TEL) is the concentration below which biota is not expected to be adversely affected; the Probable Effects Level (PEL) is the level above which biota is expected to be adversely affected (Environment Canada, 1998; MacDonald et al., 2000). The effect of concentrations between the TEL and PEL on aquatic biota is uncertain. Canada has adopted the TELs as Interim Sediment Quality Guidelines.

At Barton Springs, contamination from trace elements was more serious than that from organic contaminants. None of the organochlorine compounds exceeded the method detection limits, and concentrations of PAHs were in all cases below the TEL. Arsenic concentrations, however, were consistently greater than those in either of the surface samples and exceeded the PEL in every sample. Chromium concentrations were also greater in the spring samples than in either of the surface water samples and exceeded the TEL in every sample. Zinc was almost 6 times the PEL in one sample, but in subsequent samples was below the TEL. At the level of development at the time of sampling, at Barton @ 71 (the reference site), none of the organochlorine compounds exceeded the detection limits, and the concentrations of PAHs, while greater than those at the springs, were still below the TEL in two of the three samples. The exceedance in one instance of the TEL for total PAH and benz[a]anthracene may be because the sample site is directly downstream of a major highway crossing. Arsenic, chromium, lead, and zinc all exceeded the TELs in one or more samples but not the PELs. It may be that with continued urbanization in the area around the Barton @ 71 site, the site will no longer be appropriate for use as a reference site. In contrast to Barton Springs, suspended sediment from Barton Above, the urban site, was more highly contaminated by organic contaminants than trace elements. Chlordane exceeded the PEL in two of three samples. DDT and its metabolite DDE exceeded the PEL in one and two samples, respectively. PAHs occurred at concentrations exceeding the PELs in two of the three samples; benzo[a]pyrene, which is on the USEPA (1999) Top 20 Hazardous Substances Priority List, exceeded the PEL in one sample by a factor of 3. In contrast, the trace elements exceeded the TEL, but exceeded the PEL in only one case (zinc).

4.3. Large-Volume Filtration: Results and Discussion

Large volume filtration proved to be an efficient way to obtain enough sediment from Barton Springs for analysis. The data indicate that urbanization may be having an effect on water quality at the springs, particularly in the case of trace elements. Arsenic, in particular, occurs on sediments at concentrations having probable deleterious effects on aquatic biota. Because concentrations of arsenic and chromium in the springs exceeded those at Barton Above, they probably have a source other than Barton Creek. The elevated concentrations of organic contaminants seen in the adjacent Barton Creek do not yet seem to be affecting the springs, as organochlorines were not detected in the spring samples. Contaminated sediments from Barton Above, however, may still have a deleterious effect on aquatic life in the pool (including the Barton Springs salamander)—when a rain event of sufficient magnitude occurs, as happens every few

Table 2. Concentrations of trace elements and hydrophobic organic compounds found on suspended sediments at Barton Springs and Barton Creek, in mg/kg. Sediment quality guidelines (PEL and TEL) are from Environment Canada (1998), except those for T-PAH, which are from MacDonald et al. (2000).

Date	Site	As	Cr	Pb	Zn	Chlor-dane	DDT	DDE	DDD	T-PAH	Benzo [a]-pyrene	Benz[a]-anthra-cene
5/27/99	Barton Springs	20.0	68.6	25.2	1,820	< 8.9	< 0.89	<0.89	<0.89	109	5.0	3.3
	Barton Above	12.0	64.0	55.8	214	E 17.0	13	7.6	4.6	51,400	2,300	1,500
	Barton @ 71	11.2	66.6	39.2	141	< 120	< 12	< 12	< 12	5,230	E 230	E 150
5/01/00	Barton Springs	22.3	80.7	31.7	113	< 13	< 21	< 1.3	< 1.3	389	25	30.6
	Barton Above	15.9	69.0	76.8	326	E 39	< 14	E 7.1	< 6.8	22,900	1200	679
	Barton @ 71	6.78	32.6	28.9	271	< 63	< 120	< 6.3	< 6.3	819	37	29.3
5/02/00	Barton Springs	19.3	67.5	24.6	120	< 16	< 96	< 1.6	< 1.6	481	24	12.9
6/09/00	Barton Springs	NA	NA	NA	NA	< 24	< 2.4	< 2.4	< 2.4	201	15	6.7
	Barton Above	11.7	61.5	35.8	301	< 11	< 50	< 1.1	<1.1	5,330	350	237
	Barton @ 71	8.16	37.2	15.7	57.6	< 5.5	< 0.55	<0.55	<0.55	95.6	1.5	2.5
6/10/00	Barton Springs	17.8	82.1	21.3	87.8	< 19	< 19	< 1.9	< 1.9	232	24	7.8
TEL		5.9	37.3	35.0	123	4.50	1.19	1.42	3.54	1,610	31.9	31.7
PEL		17.0	90.0	91.3	315	8.87	4.77	6.75	8.51	22,800	782	385

years, the creek overtops the dam and flows directly into Barton Springs Pool. Additional samples from this site and from additional recharging creeks will be very useful in determining the effects of changing land use on the water quality of this karst system.

5. CONCLUSION

The three investigations presented in this chapter taken together demonstrate not only that sediment is mobile in karst, but also that much of it probably originates at the surface, and it can and does act as a vector for contaminant transport, including transport of bacteria.

At the well field adjacent to Terrieu Creek in southern France, a large proportion of fecal coliform bacteria was associated with suspended sediment, at times up to 90%. Bacterial concentrations associated with sediment in surface water and in the subsurface were very similar, indicating a close connection between the two. The association of bacteria with sediment has important implications for public health. The bacteria may be protected from predation, may be able to use the substrate as a food source, and are less susceptible to standard methods of disinfection.

Although sediment concentrations may be low, large spring discharge can result in a substantial mass of sediment being transported. In Austin, Texas, as much as a metric ton of sediment was shown to discharge from Barton Springs in response to rainfalls of 45 to 90 mm. The timing of the arrival of peak sediment concentrations, combined with the mineralogy and relatively large organic carbon content, indicate that much of this sediment originates at the surface. Supporting this hypothesis is the fact that a rain event at the end of the wet season resulted in less sediment discharge than a rain event at the end of the dry season, despite the fact that more rain fell.

Large volume filtration is one approach for obtaining sufficient sediment from a karst spring for direct analysis of hydrophobic contaminants. By filtering up to 1,000 L in situ, enough sediment was obtained for hydrophobic organics analysis, and metals analysis was performed on sediment obtained from filtration of an additional 200 L. Analysis of suspended sediment from the adjacent surface stream demonstrated that surface sediments coming from urbanized areas may be highly contaminated with organochlorine compounds and PAHs. The spring sediments, however, showed the greatest contamination from trace elements, in particular arsenic, chromium, and zinc. Sampling of additional events using LVF should result in a valuable data set revealing the current extent of the effect of urbanization on this large spring system.

6. ACKNOWLEDGMENTS

The authors are grateful to William White, Marcus Gary, and Brian Katz for their thorough and insightful reviews of the manuscript. Any use of trade, product, or firm names is for descriptive purposes only and does not imply endorsement by the U.S. Government.

7. REFERENCES

Atteia, O., and Kozel, R., 1997, Particle size distributions in waters from a karstic aquifer: From particles to colloids, *J. Hydrol.*, **201**:102–119.

Bales, R. C., Li, S., Maguire, K. M., Yahya, M. T., Gerba, C. P., and Harvey, R. W., 1995, Virus and bacteria transport in a sandy aquifer, Cape Cod, MA., *Ground Water*, **33**:653–661.

Botton, R., 1984, Etude de certaines modalités du fonctionnement de l'aquifère karstique (zone d'infiltration et zone saturée) sur deux champs de forages nord-Montpellierains, PhD thesis, Université des Sciences et Techniques du Languedoc, Montpellier, France, 380 p.

Bradford, W. L., and Horowitz, A. J., 1982, The role of sediments in the chemistry of aquatic systems, *in* Proceedings of the Sediment Chemistry Workshop, February 8–12, 1982, U.S. Geological Survey Circular 969, 75 p.

Bretz, J. H., 1942, Vadose and phreatic features of limestone caves, *J. Geology*, **L**:675–811.

City of Austin, 2000, Update on Barton Springs water quality analysis: Water Quality Report Series COA–ERM–2000, 20 p.

Drogue, C., 1974, Structure de certains aquifères karstiques d'après les résultats de travaux de forages, *C.R. Acad. Sci. Paris*, **278**:2621–2624.

Environment Canada, 1998 (September 28, 1998); http://www.ec.gc.ca/ceqg-rcqg/sediment.htm.

Fishman, M. J., and Friedman, L. C., 1989, Methods for determination of inorganic substances in water and fluvial sediments: U.S. Geological Survey Techniques of Water-Resources Investigations (Book 5 Chapter A1), 545 p.

Fontes, D. E., Mills, A. L., Hornberger, G. M., and Herman, J. S., 1991, Physical and chemical factors influencing transport of microorganisms through porous media, *Applied and Environmental Microbiology*, **57**:2473–2481.

Ford, D. C., and Williams, P. W., 1989, *Karst Geomorphology and Hydrology*, Unwin Hyman Ltd., London.

Foreman, W. T., Connor, B. F., Furlong, E. T., Vaught, D. G., and Merten, L. M., 1995, *Methods of Analysis by the U.S. Geological Survey National Water Quality Laboratory—Determination of Organochlorine Pesticides and Polychlorinated Biphenyls in Bottom Sediment by Dual Capillary-Column Gas Chromatography with Electron-Capture Detection*, U.S. Geological Survey Open-File Report 95–140, 78 p.

Furlong, E. T., Vaught, D. G., Merton, L. M., Foreman, W. T., Gates, P. M., and Koleis, J. C., 1996, *Methods of Analysis by the U.S. Geological Survey National Water Quality Laboratory—Determination of Semivolatile Organic Compounds in Bottom Sediment by Solvent Extraction, Gel Permeation Chromatographic Fractionation, and Capillary-Column Chromatography/Mass Spectrometry*, U.S. Geological Survey Open-File Report 95–719, 67 p.

Gale, S. J., 1984, The hydraulics of conduit flow in carbonate aquifers, *J. Hydrol.*, **70**:309–327.

Garbarino, J. R., Hayes, H. C., Roth, D. A., Antweiler, R. C., Brinton, T. I., and Taylor, H. E., 1995, Heavy metals in the Mississippi River, in: *Contaminants in the Mississippi River, 1987–1992*, R. H. Meade, ed., U.S. Geological Survey Circular 1133, p. 53–72.

Harvey, R. W., Smith, R. L., and George, L., 1984, Effect of organic contamination upon microbial distribution and heterotrophic uptake in a Cape Cod, Mass., Aquifer, *Appl. Environ. Microbiol.*, **48**:1197–1202.

Hauwert, N.M, Johns, D. A., and Aley, T. J., 1998, *Preliminary Report on Groundwater Tracing Studies Within the Barton Creek and Williamson Creek Watersheds, Barton Springs/Edwards Aquifer*, prepared by the Barton Springs/Edwards Aquifer Conservation District and the City of Austin Watershed Protection Department, May 1998.

Hauwert, N. M, Johns, D. A., Aley, T. J., and Sansom, J. W., in press, Groundwater Tracing Study of the Barton Springs Segment of the Edwards Aquifer, Southern Travis and Northern Hays Counties, Texas, Barton Springs/Edwards Aquifer Conservation District and the City of Austin Watershed Protection Department.

Hauwert, N. and Vickers, S., 1994, Barton Springs/Edwards Aquifer Hydrogeology and Groundwater Quality, submitted by the Barton Springs/Edwards Aquifer Conservation District to the Texas Water Development Board.

Horowitz, A. J., 1995, The use of suspended sediment and associated trace elements in water quality studies, IAHS Special Publication No. 4, 58 p.

Jones, S. A., Van Metre, P. C., Moring, J. B., Braun, C. L., Wilson, J. T., and Mahler, B. J., 1997, Chemical Data for Bottom Sediment, Lake Water, Bottom-Sediment Pore Water, and Fish in Mountain Creek Lake, Dallas, Texas, 1994–96, U.S. Geological Survey Open-File Report 97–245, 50 p.

Lynch, F. L., 1997, Frio shale mineralogy and the stoichiometry of the smectite-to-illite reaction: the most important reaction in clastic sedimentary diagenesis, Clays and Clay Min., **45**:618–631.

MacDonald, D. D., Ingersoll, C. G., and Berger, T. A., 2000, Development and evaluation of consensus-based quality guidelines for freshwater ecosystems, *Arch. Env. Cont. Toxicol.* **39**:20–31.

Mahler, B. J., and Lynch, F. L., 1999, Muddy waters: temporal variation in sediment discharging from a karst spring, J. Hydrol, **214**:165–178.

Mahler, B. J., and Van Metre, P. C., 2000, Austin (December 2000); http://tx.usgs/gov/reports/dist/dist-2000-01.

Mahler, B. J., Lynch, L., and Bennett, P. C., 1999, Mobile sediment in an urbanizing karst aquifer: implications for contaminant transport, *Env. Geology*, **39**:25–38.

Malard, F., Reygrobellet, J. L., and Soulié, M., 1994, Transport and retention of fecal bacteria at sewage-polluted fractured rock sites, *J. Environ. Qual.*, **23**:1352–1363.

McCaulou, D. R., Bales, R. D., and Arnold, R. G., 1995, Effect of temperature-controlled motility on transport of bacteria and microspheres through saturated sediment, *Water Resources Res.* **31**:271–280.

Raines, T. H., Baldys III, S., Lizarraga, J. L., 1997, *Characterization of Storm Water Runoff from the Naval Air Station and Naval Weapons Industrial Reserve Plant, Dallas, Texas, 1994–1996*, U.S. Geological Survey Open-File Report 97–402, 80 p.

Rittman, B. E., 1993, The significance of biofilms in porous media, *Water Resources Res.*, 7:2195–2202.

Rostad, C. E., Bishop, L. M., Ellis, G. S., Leiker, T. J., Monsterleet, S. G., and Pereira, W. E., 1995, Polychlorinated biphenyls and other synthetic organic contaminants associated with sediment and fish in the Mississippi River, in: *Contaminants in the Mississippi River, 1987–1992,* R.H. Meade, ed., U.S. Geological Survey Circular 1133, pp. 103–114.

Ryan, M., and Meiman, J., 1996, An examination of short-term variations in water quality at a karst spring in Kentucky, *Ground Water*, **34**:23–30.

Schoenen, D., 1998, International perspective: health risk and water treatment, in: *AWWA: Source Water Protection Symposium: A Focus on Waterborne Pathogens*, Oct. 28–31, 1998, San Francisco.

Slade, R. M., Jr., Dorsey, M., and Stewart, S., 1986, *Hydrology and Water Quality of the Edwards Aquifer associated with Barton Springs in the Austin Area, Texas,* U.S. Geological Survey Water-Resources Investigations 86–4036.

U.S. Environmental Protection Agency, 1999; http://www.atsdr.cdc.gov/cxcx3.html

U.S. Environmental Protection Agency, 2000; http://www.epa.gov/owow/tmdl/sediment/source.html

U.S. Fish and Wildlife Service, 1997, Final rule to list the Barton Springs Salamander as endangered, *Federal Reg.*, **62**:23377–23392.

Van Metre, P. C., Callender, E., 1997, Water-Quality Trends in White Rock Creek Basin from 1912–1994 Identified Using Sediment Cores from White Rock Lake Reservoir, Dallas, Texas, *J. Paleolimnol.* **17**:239–249.

Van Metre, P. C., Mahler, B. J., and Furlong, E. T., 2000, Urban sprawl leaves its PAH signature, *Environ. Sci. Technol.* **34**:4064–4070.

Van Sickle, J., and Beschta, R. L., 1983, Supply-based models of suspended sediment transport in streams, *Water Resources Res.* **19**:768–778.

White, W. B., 1977, Characterization of karst soils by near infrared spectroscopy, *National Speleological Soc. Bull.* **39**:27–31.

White, W. B., 1988, *Geomorphology and Hydrology of Karst Terrains*, Oxford University Press, New York, 464 p.

White, E. L., and White, W. B., 1968, Dynamics of sediment transport in limestone caves, *National Speleological Soc. Bull.* **30**:115–129.

Williams, P., 1983, The role of the subcutaneous zone in karst hydrology, *J. Hydrol.*, **61**:45–67.

PALAEOMAGNETIC ANALYSIS OF SEDIMENTS IN THE BUCHAN CAVES, SOUTHEASTERN AUSTRALIA, PROVIDES A PRE-LATE PLEISTOCENE DATE FOR LANDSCAPE AND CLIMATE EVOLUTION

R. J. Musgrave and J. A. Webb*

1. INTRODUCTION

Studies of Quaternary geomorphological development in south-eastern Australia and throughout the world have often relied on surface features such as river terracing (e.g. Bishop and Brown, 1992). Difficulties in directly dating terraces have encouraged workers to look at limestone cave systems; these preserve a record of landscape evolution, including the development of passage levels, growth of speleothems, and accumulation of cave sediments, which can often be correlated with river terracing (e.g., White and White, 1974; Williams, 1982; Ford et al., 1983; Palmer, 1989; Webb et al., 1992). Dating the age of development of cave features can be challenging, however. Uranium series dating, commonly applied to speleothems, has an effective upper bound of 350 ka, and has proved useful in Europe and North America, where most cave development occurred during the late Pleistocene (Ford and Williams, 1989; Atkinson et al., 1978; Gascoyne et al., 1981; Gascoyne, 1984). However, there is an accumulating body of evidence that much cave development in Australia occurred during the Tertiary (Webb et al., 1991) or even earlier (Osborne and Branagan, 1988; Osborne, 1990), well beyond the limits of uranium series dating. For these caves, other techniques must be used, such as palaeomagnetic analysis of cave sediments; this has been applied to date cave development over the last 2 Ma (e.g., Schmidt, 1982; Schmidt et al., 1984; Noel and Thistlewood, 1989).

Limestone cave levels within the Dukes system in the Buchan district of East Gippsland in Victoria, southeastern Australia (Fig. 1) can be correlated with a series of three river terraces in the valley of the Buchan River (Webb et al., 1992). Both caves and terraces are thought to have developed in the Pleistocene, because uranium series dating of speleothems in this system gives ages of more than 350,000 years, and perhaps greater

* Department of Earth Sciences, La Trobe University, Bundoora, VIC 3086, Australia. E-mail: R.Musgrave@latrobe.edu.

than one million years (Webb et al., 1992). Given that this age range straddles, the Matuyama-Brunhes magnetic reversal, it was hoped that a palaeomagnetic study of the cave sediments from the Dukes system could clarify the age of development of these caves.

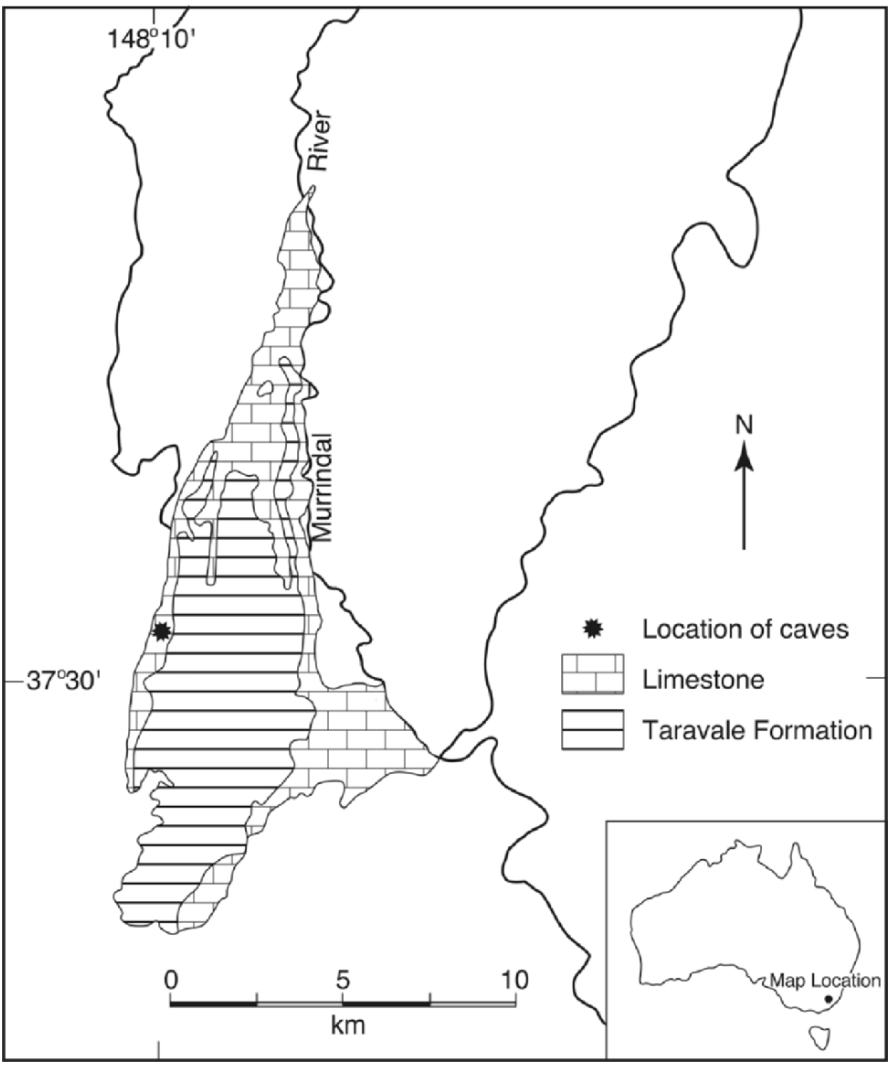

Figure 1. Generalised geology of the Buchan Synclinorium, showing the location of the Dukes Cave system.

2. GEOLOGICAL AND GEOMORPHOLOGICAL SETTING

The Buchan area, some 350 km east of Melbourne in eastern Victoria, comprises a large synclinorium of Early Devonian limestones and mudstones (Buchan Group) dis-

conformably overlying rhyolitic volcanics (Fig. 1). The Buchan Group has been divided into three units, two limestone formations (Buchan Caves Limestone and Murrindal Limestone) separated by the mudstones of the Taravale Formation (VandenBerg and O'Shea, 1981). In the northern part of the synclinorium the Taravale Formation lenses out and the two limestone units merge together.

Caves are present through much of the limestone. The topographically highest caves have formed in the Murrindal Limestone in the centre of the synclinorium. These caves vary from simple shafts to complex joint-controlled mazes of narrow passages, but all display predominantly vertical development. The Murrindal Limestone caves are believed to have formed beneath an Eocene river system, and were probably drained by incision of the rivers in the Late Eocene - Early Oligocene (Webb et al., 1991).

The topographically lower caves in the Buchan area are predominantly horizontal systems, usually developed sub-parallel to the strike of bedding, and are present only within the Buchan Caves Limestone. The main passages in these caves are less than 30 m above the nearest surface stream or river bed, and many contain active streams in their lowest levels. Thus these caves are of more recent origin than the Murrindal Limestone caves.

The longest of the topographically lower caves, the Dukes system, contains over 5 km of passage (Fig. 2), sections of which have been developed as the tourist caves at Buchan, because of their extensive and very attractive speleothem deposits (Fairy Cave: B5-B64, and Royal Cave: B6-B65). The cave system has formed entirely within the Buchan Caves Limestone, and consists of epiphreatic and vadose passages developed through pre-existing phreatically enlarged joints (terminology used follows Jennings, 1985). The epiphreatic cave passages run more or less parallel to the strike of the limestone, which is approximately north-south in this area. They are characterised by very well developed flat roofs, which are present throughout the cave system, trimmed cleanly across the bedding planes; the latter dip at 30-40°. This indicates that the roofs represent groundwater levels and are not structurally controlled. The flat roofs are absent only where the cave passages have been disrupted by rockfall. These epiphreatic levels correspond to "state 4" of the four-state model of phreatic and watertable cave development proposed by Ford and Williams (1989).

Within the Dukes cave system two extensive sub-horizontal cave passages are present, and in the lower passage there are two separate roof levels (Fig. 3). Thus three epiphreatic cave levels can be identified, termed here levels A to C from lowest to highest, and these can be correlated with three river terraces developed along the Buchan River (Webb et al., 1992), and with three knickpoints in the nearby Murrindal River (Fabel et al., 1996). Each level represents a stillstand in the denudational history of the area. In an effort to date these stillstands, a number of speleothem samples from the epiphreatic caves were dated by the U/Th method (Webb et al., 1991; Webb et al., 1992). A flowstone sample from Spring Creek Cave, just south of the Dukes system, gave an age of greater than 350,000 years. The $^{234}U/^{238}U$ ratio of this sample suggests that the age may be in excess of one million years. The flowstone was collected about 20 m above creek level, corresponding to the uppermost epiphreatic level in the Dukes cave system. This level must therefore have formed at least 350,000, and perhaps over one million, years ago.

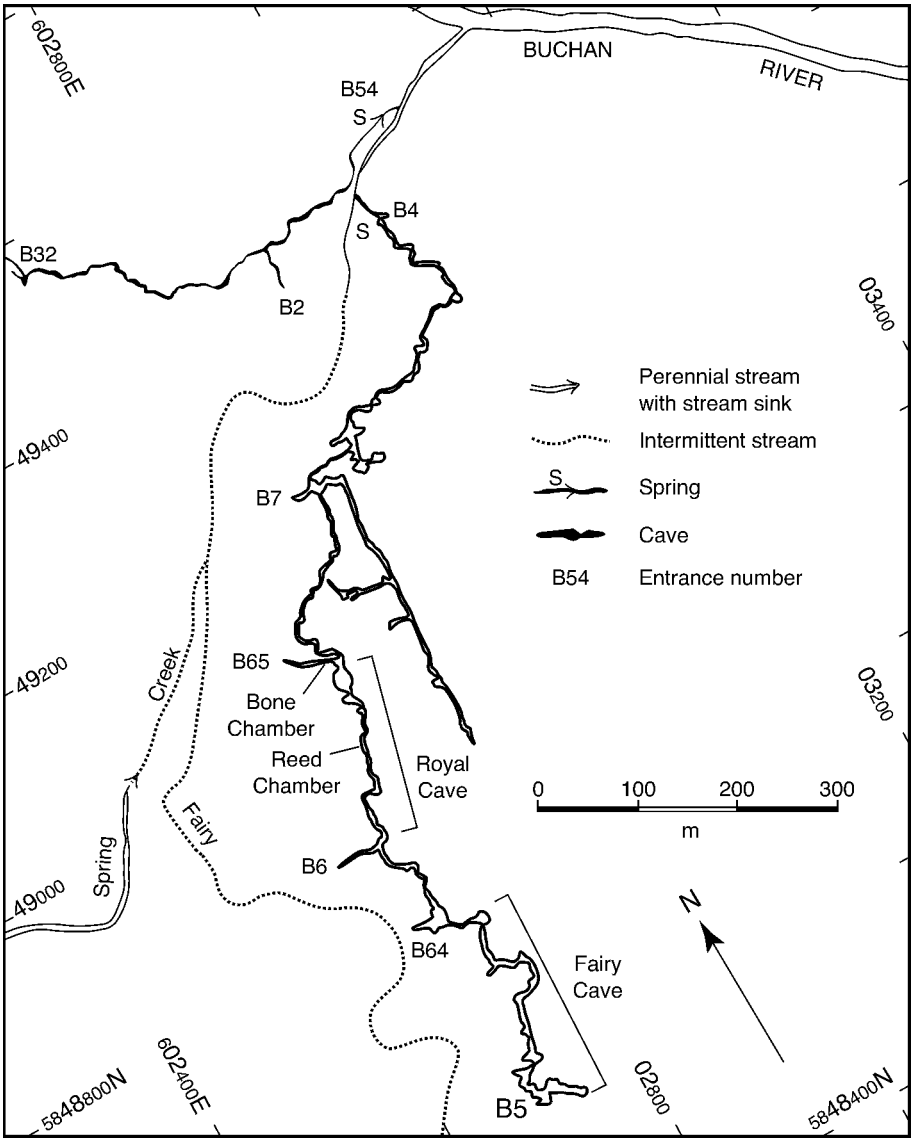

Figure 2. Plan view of the Dukes Cave system, showing the Royal Cave section (B6-B65) and the location of the two sampling sites, Reed Chamber and Bone Chamber, see Fig. 1 for overall location. Grids represent the Australian Map Grid, 1966, Zone 55, and are based on the Mount Tara 1:25 000 topographic sheet (8522-4-1).

Both the lowermost and uppermost epiphreatic passages in the Dukes system (Level A and Level C) contain extensive sediment deposits. These sediments were sampled for paleomagnetic analysis.

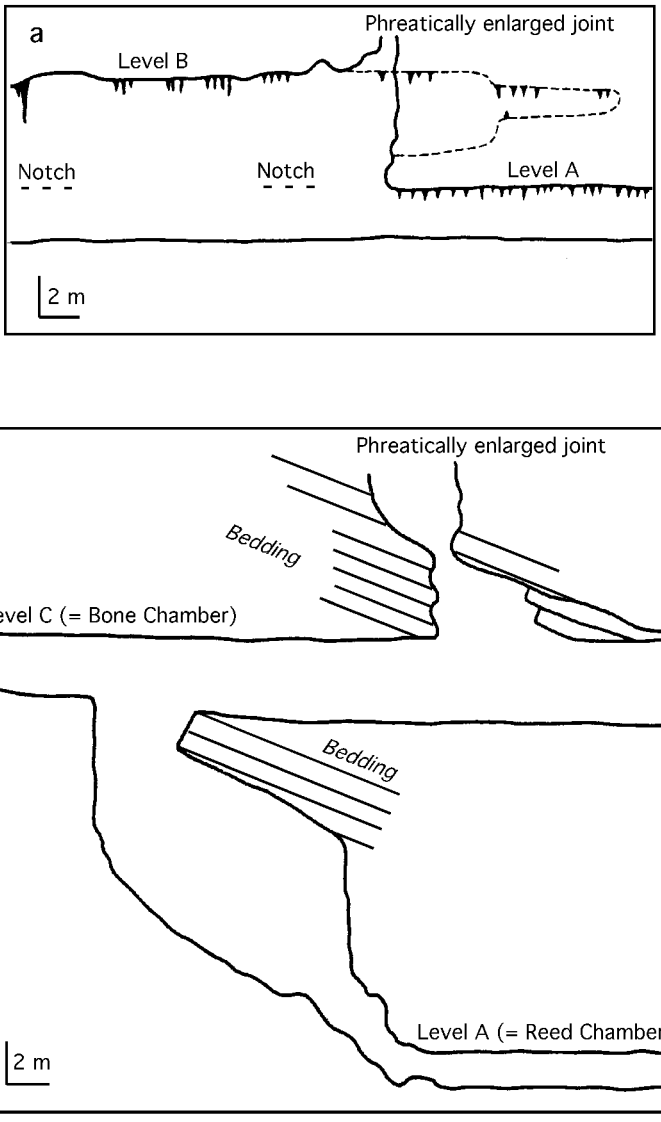

Figure 3. Detailed cross-sections at two sites in the Dukes cave system, illustrating the three flat-roofed epiphreatic levels and their relationship to the bedding and pre-existing phreatic passages (after Webb et al., 1992).

3. SAMPLING LOCALITIES

Two sites within the Royal Cave part of the Dukes cave system were selected for palaeomagnetic sampling; one within Level A ("Reed Chamber"), and one within Level C ("Bone Chamber"). The locations of both sites are indicated on Figure 2.

3.1. Level A (Reed Chamber)

Much of the Fairy and Royal Cave portions of the Dukes system consists of a flat-roofed epiphreatic passage at Level A (Fig. 4); the roof is a few meters above the level of the bed of Fairy Creek outside the cave. At one stage in its history this passage was almost completely filled with bedded fluvial sediments. Subsequently, the stream flowing through the cave has removed most of the sediment fill, although remnants are present in many places. Flowstone has covered much of this remaining sediment, but banks of unconsolidated material are exposed in the walls of the cave at several sites.

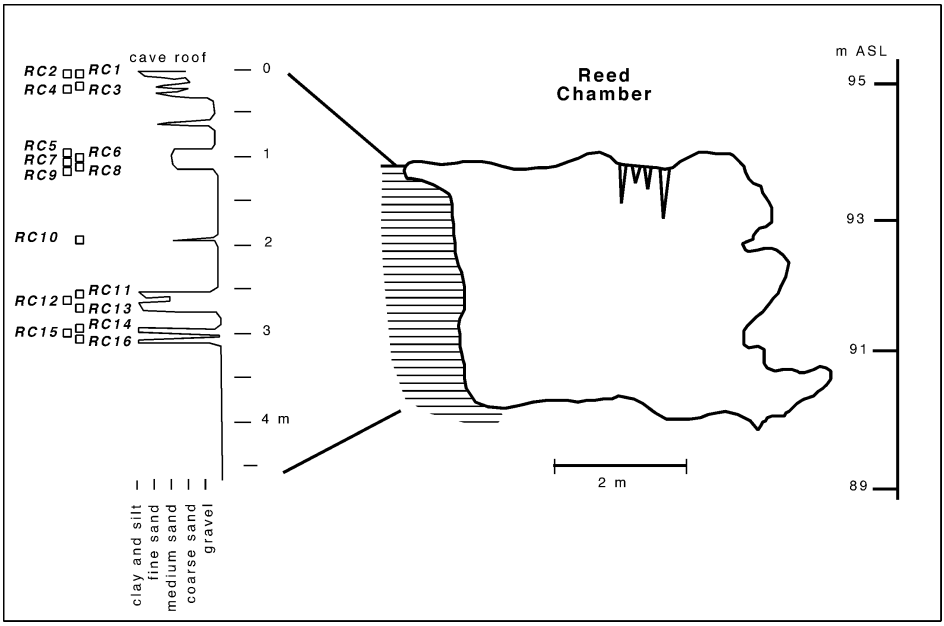

Figure 4. Cave cross-section within Reed Chamber (Level A), showing the location of cave sediment (hatched), grain size stratigraphy of the cave sediments, and the position of samples. Column at right indicates topographic height, surveyed to within 0.1% accuracy against local benchmarks (see Webb et al., 1992).

At Reed Chamber the sediment fills the passage almost to the roof (Fig. 4). The sediments are thin to medium-bedded and brownish black (10YR 2/3) to yellowish brown (10YR 5/6) in colour (occasionally bright brown - 7.5YR 5/6). Sands and gravels predominate (Fig. 4); the gravels are composed of well rounded pebbles and cobbles. Within the sand layers are numerous interbedded thin clay lenses. Grain size analysis of the sandy layers reveals peaks in grain size at round 3-4 mm and around 0.7-0.5 mm, with a tail of finer material into the silt range (Grotaers, 1995). Palaeomagnetic sampling at Reed Chamber (RC) concentrated on the finer sands and clays as the better palaeomagnetic targets (Fig. 4). Four principal fine-grained intervals were sampled,

spanning 3 m of stratigraphy, with from three to five samples in each. A single sample (RC10) was taken in an isolated thin sand layer. There is no evidence of bioturbation within the sediments, as bedding is undisturbed.

3.2. Level C (Bone Chamber)

The northern part of Royal Cave, near the B65 entrance (Fig. 2), consists of a high level passage, much of it with a flat roof (Level C; Fig. 3). In places, such as Bone Chamber, this flat roof is cut across a pre-existing phreatically enlarged joint (Fig. 5). This passage represents the uppermost epiphreatic level in the Dukes cave system, and is 16-18 m above Level A.

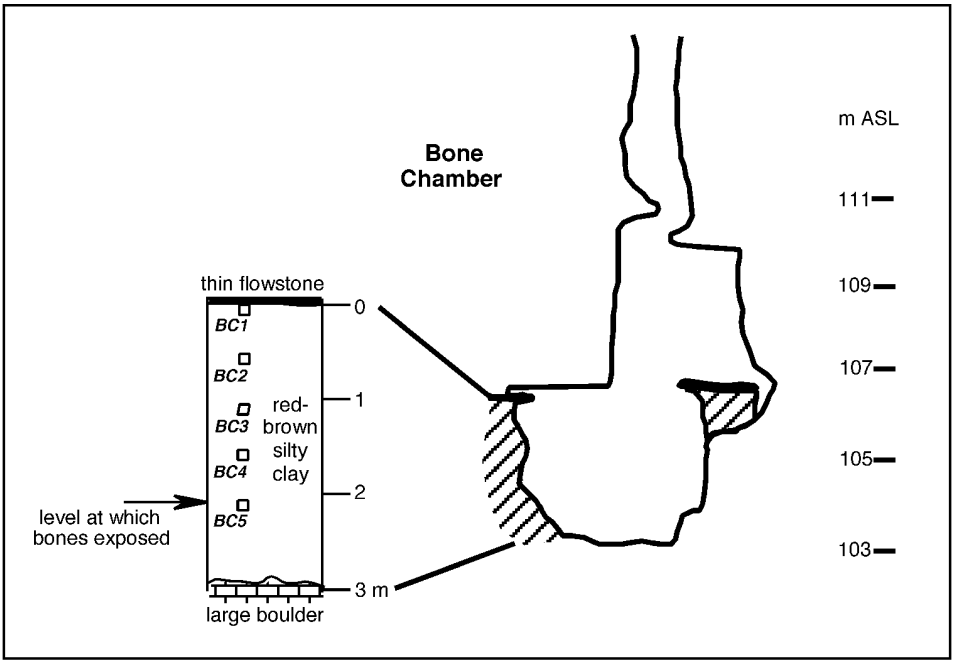

Figure 5. Cave cross-section within Bone Chamber (Level C), showing the location of cave sediment (hatched) and flowstone cap (black), and the position of samples within the cave sediment. Column at right indicates topographic height, as for Fig. 4.

Reddish brown (5YR 3/6 to 5/8) sediments are present almost throughout Level C, mostly in the epiphreatic passage (Fig. 5) but also within the enlarged joint that extends upwards beyond the flat roof. The sediments are highly uniform, and consist of abundant angular silt-sized quartz in a reddish clay matrix. Laser particle size analyses of sediment from Bone Chamber (Fig. 6) show that the grain size distribution is polymodal; the coarsest grain size (medium-coarse silt) comprises only a small proportion of the

sediment, about half of which is clay-sized (< 4 μm). There are no obvious bedding structures, but this is not due to bioturbation, as there is no evidence of burrowing of any kind. The upper surface of the sediments is covered by flowstone in several places.

Within the reddish brown sediments of Bone Chamber (also known as Skeleton Chamber), the bones of extinct marsupials, including *Sthenurus* sp., have been collected (Fig. 5; A. Tickner, pers. comm.). *Sthenurus* was a large kangaroo with a time range of Pliocene to Pleistocene (Rich and Thompson, 1982).

Five samples were taken in Bone Chamber (BC) at an approximately 50 cm vertical spacing from a section below a prominent flowstone layer (Fig. 5).

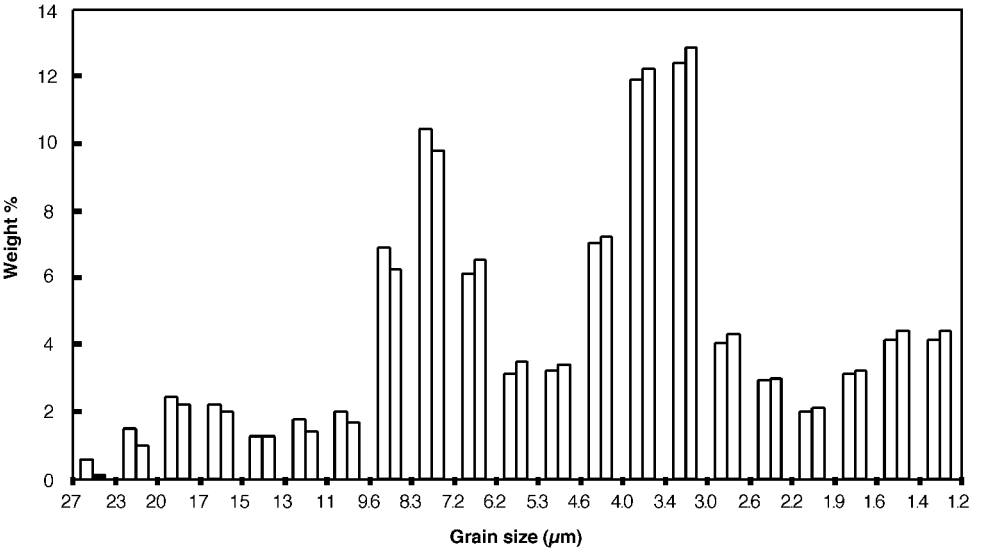

Figure 6. Laser grain size analyses of two separate sediment samples from Bone Chamber.

4. SAMPLING AND MEASUREMENT TECHNIQUES

To obtain samples, oriented plastic cubes were pushed gently into a flat vertical face cut into the unconsolidated cave sediments. Samples were demagnetised through a very closely spaced series of alternating field (AF) demagnetisation steps conducted with a coaxial AF-demagnetiser – cryogenic magnetometer system on board the Ocean Drilling Program ship *JOIDES Resolution*. Remanence was measured with the 3-axial 2G magnetometer in this system prior to demagnetisation (natural remanent magnetisation, or NRM), and after each successive demagnetisation step; the magnetometer had an effective sensitivity for the 6 cm^3 samples of 2×10^{-3} mA/m. Demagnetisation was carried out at 2 mT steps to 30 mT, which at the time was the operating limit of this instrument. Remanence was almost completely lost in most samples demagnetised at 30 mT (mean destructive fields were typically less than 10 mT); this was confirmed by continued demagnetisation and measurement of selected samples above 30 mT, using a Molspin spinner magnetometer (sensitivity 0.1 mA/m) and Molspin AF-demagnetiser at

the La Trobe PALM ("Palaeo/Archaeo/Litho- Magnetism") laboratory. Demagnetisation behaviour was analysed with the aid of Zijderveld and stereographic plots.

Hysteresis and isothermal remanence demagnetisation behaviour were analysed for a representative set of specimens on a Molspin Nuvo vibrating sample magnetometer, allowing the determination of saturation magnetisation (M_s), saturation remanence (M_{rs}), coercivity (H_c) and coercivity of remanence (H_{cr}). Bulk mass-normalised susceptibility (χ) was measured with a Bartington MS-2 system at both the 0.465 and 4.65 kHz settings. Frequency dependence of susceptibility (χ_{FD}) was calculated as the ratio $(\chi_{0.465kHz} - \chi_{4.65kHz})/\chi_{0.465kHz}$, expressed as a percentage.

Hysteresis analysis allows determination of magnetic grain size and discrimination between ferrimagnet- (e.g., magnetite) and antiferromagnet- (e.g., haematite) dominated magnetic assemblages. However, maghemite, a prominent component of many terrestrial sediments (e.g., Maher and Thompson, 1999), is also a ferrimagnet, and not readily distinguished from magnetite on the basis of hysteresis behaviour alone. Maghemite (γ-Fe_2O_3) inverts to haematite (α-Fe_2O_3) when heated above 300°C (Thompson and Oldfield, 1986). To test for the presence of maghemite, a subset of samples were heated in a series of 50°C steps to 600°C; the samples were cooled to room temperature after each heating step, and their susceptibility (on the low-frequency setting) was measured after each cooling. The samples became very fragile on heating, resulting in irregular sample shapes and the consequent introduction of some scatter in the susceptibility measurements.

5. RESULTS

5.1. Demagnetisation Behaviour

5.1.1. Bone Chamber

Most of the samples from Bone Chamber (Fig. 7) show simple demagnetisation paths dominated by one component with a direction broadly similar to the present-day field at Buchan (declination = 13°, inclination = -68°, based on the International Geomagnetic Reference Field for epoch 1995.0), after removal of soft post-sampling components by 4 mT demagnetisation. Remanence has very low coercivity, with mean destructive fields of <10 mT, and remanence remaining after 30 mT demagnetisation is less than 5% of natural remanent magnetisation (NRM). NRM varies between 172 mAm^{-1} (sample BC4) and 330 mAm^{-1} (sample BC2).

Every sample from Bone Chamber shows some evidence of the presence of additional magnetisation components, not revealed until after demagnetisation at fields of 12 mT or higher. In samples BC1, BC2, BC3 and BC5, these components are indicated by small deviations in the demagnetisation path; at least two additional components of magnetisation are present, of which the less stable (revealed over the demagnetisation interval from 16 to 24 mT) has a direction distinctly different from the present field; this component is not clearly isolated, however, and its direction (and so polarity) cannot be determined.

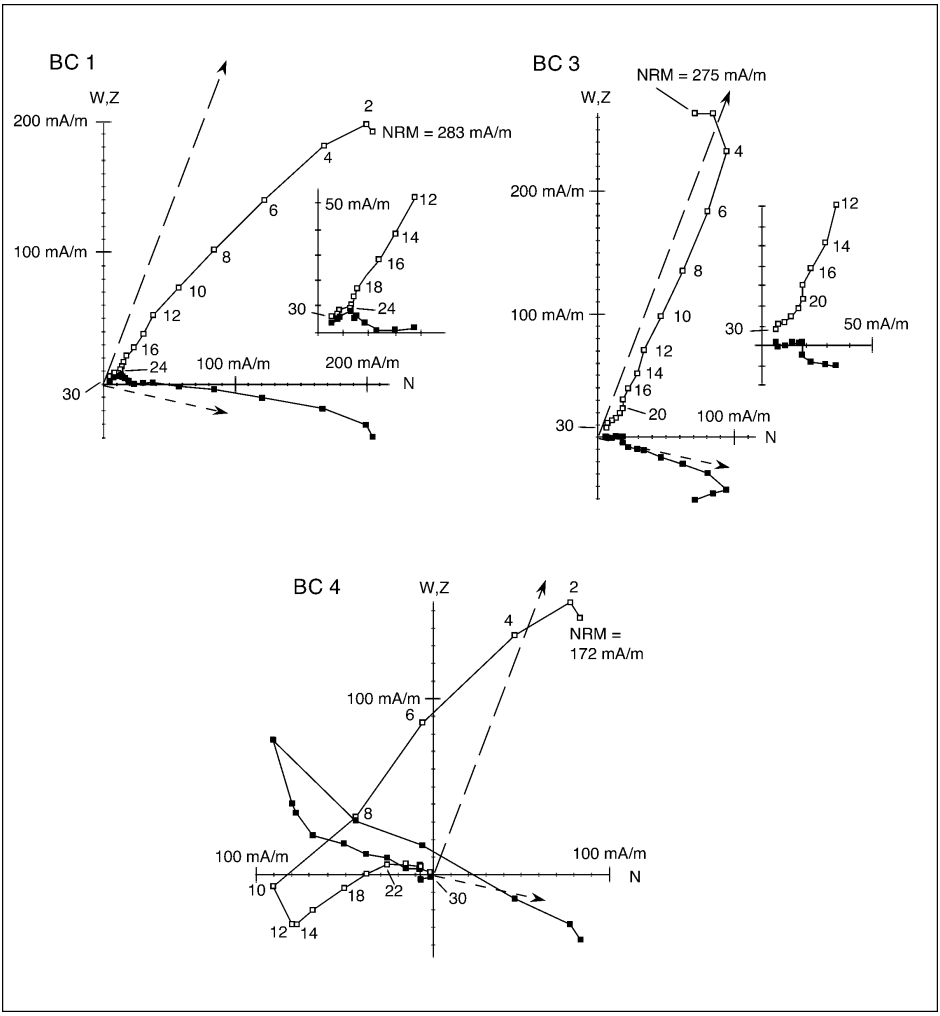

Figure 7. Zijderveld (orthogonal) plots for representative samples from Bone Chamber. Solid squares show projection of remanence after stepwise demagnetisation onto the horizontal plane (north to the right); open squares show equivalent projection onto north-south vertical plane (+Z = up). NRM = natural remanent magnetisation, prior to demagnetisation. AF demagnetisation at 2 mT intervals; selected steps are indicated. Dashed, arrowed lines show projection of a magnetisation parallel to the present-day field, representing a VRM with short relaxation time; short dashes = horizontal plane, long dashes = vertical plane. Insets for BCI and BC3 show enlargements of higher demagnetisation stages.

Demagnetisation of sample BC4 reveals these additional components more clearly. From 14 to 20 mT a reversed polarity component is removed. Above 22 mT the demagnetisation spectra of this reversed component and another component of unknown direction overlap, resulting in a curved demagnetisation interval. It is possible that the reversed polarity component is present in all the Bone Cave samples, but is propor-

tionally smaller and has a less clearly isolated stability spectrum in samples other than BC4.

5.1.2. Reed Chamber

Samples from Reed Chamber show more variation in NRM, from 22.8 mAm^{-1} (sample RC12) to 135 mAm^{-1} (sample RC4), and a wider range of demagnetisation behaviours than do those of Bone Chamber (Fig. 8). Some, such as RC11 and RC3, display simple, single component demagnetisation after cleaning of post-sampling components by 4-6 mT demagnetisation. Remanence in these samples is close to the direction of the present-day field, and there is no clear signal of additional components above the noise level.

Several samples from Reed Chamber display evidence for the presence of a reversed polarity component, but in none is it as clear as that seen in sample BC4. Sample RC2 has a complex demagnetisation above 10 mT, with an intermediate direction about 60° away from a reversed dipole direction. Samples RC4 and RC5 both display curved demagnetisation paths above 8 mT; the curvature indicates the presence of at least two components with overlapping stability spectra. In both RC4 and RC5 the trend approaching total demagnetisation remains along an intermediate direction, although in RC4 this trend is closer to a reversed field direction, while in RC5 it is closer to a normal field. Sample RC12, the most weakly magnetised of all the samples in this study, has an intermediate remanence, which becomes very weak and complex at demagnetisations above 14 mT.

Mean destructive fields (MDFs) for the Reed Chamber samples which display complex demagnetisation behaviour are generally higher (often above 12 mT) than MDFs for Bone Chamber samples or Reed Chamber samples with simple demagnetisation paths (usually < 10 mT).

5.2. Rock Magnetic Analysis

Rock magnetic parameters for representative samples from both sampling sites are listed in Table 1. Susceptibility is fairly uniform in the Bone Cave samples, ranging from 570 to 1030 $\times 10^{-8}$ m^3kg^{-1}, but is more variable in the Reed Chamber samples, ranging from 8 $\times 10^{-8}$ m^3kg^{-1} (RC12) to 1560 $\times 10^{-8}$ m^3kg^{-1} (RC11). Despite the red colour of many of the samples, which suggests the presence of haematite (an antiferro-magnet), the high susceptibility of most samples, and their low MDFs, suggest that ferrimagnetic minerals (magnetite and/or maghemite) dominate the magnetism. Note that the much higher susceptibility and saturation remanence of ferrimagnets compared to antiferromagnets will allow ferrimagnets to dominate magnetic properties, even where they constitute a much smaller proportion by weight than does haematite.

Susceptibility measured after the stepwise heating/cooling sequence showed little change in any of the samples (Fig. 9), indicating that maghemite does not constitute a significant component of the magnetic mineralogy. By elimination, magnetite dominates both the ferrimagnetic mineralogy and the magnetism of the samples overall.

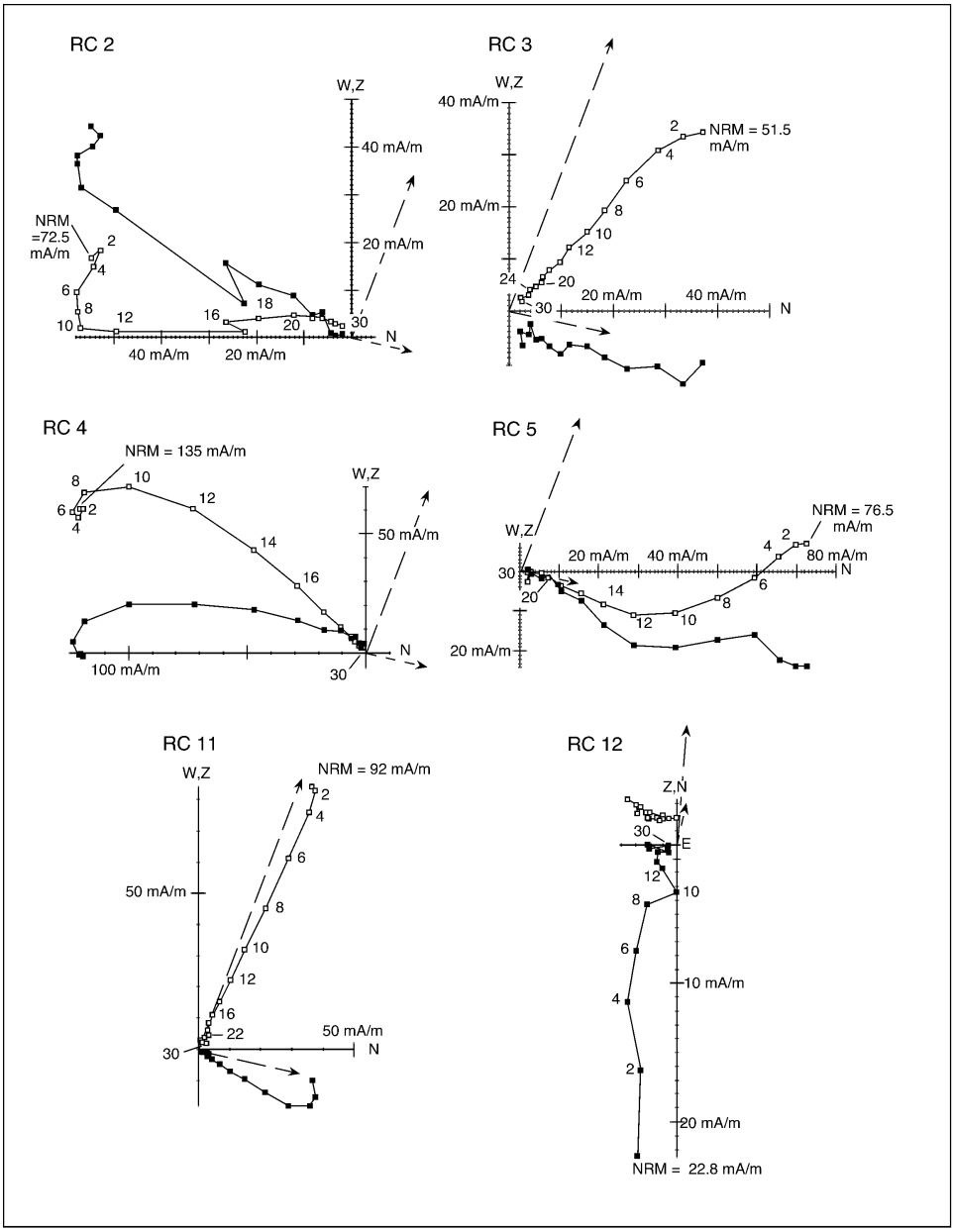

Figure 8. Zijderveld plots of representative samples from Red Chamber, Symbols as for Figure 7. For clarity, sample RC 12 is presented in the alternative orthogonal projection, with the vertical plane aligned east-west, and with north to the top on the horizontal projection.

Table 1. Rock magnetic parameters for representative samples from the Buchan cave sediments.

Sample	M_{rs} (mAm^2/kg)	M_s (mAm^2/kg)	H_{cr} (mT)	H_c (mT)	χ (10^{-8} m^3/kg)	χ_{FD} (%)
Bone Chamber						
BC1	16.7	149	12.0	3.0	575	10.94
BC3	31.1	232	13.0	4.0	571	11.41
BC4	56.2	377	13.5	5.5	1030	9.39
BC5	21.3	157	13.0	4.0	954	6.22
Reed Chamber						
RC2	6.80	33.4	25.0	6.5	129	8.64
RC3	6.09	36.5	17.5	6.5	93	8.11
RC4	16.3	86.8	19.0	2.4	287	5.99
RC5	13.7	63.9	25.0	9.0	112	6.11
RC11	46.9	462	12.5	3.0	1560	9.53
RC12	0.28	4.17	62.0	4.5	7.8	1.47

Coercivity and saturation magnetisation parameters are influenced by domain state (and hence by grain size of the magnetic fraction). Domain state in materials where the remanence is dominated by magnetite can be determined by position on a Day plot (Day et al., 1977); on such a plot, stability of remanence increases towards the upper left corner. Samples BC4, RC2, RC3, and RC5, all of which show evidence in their demagnetisation behaviour for the presence of a reversed-polarity component, plot closest to the stable part of the Day plot (Fig. 10). Samples BC1, BC3, BC5, and RC11, which do not show a clearly isolated reversed component, plot in less stable positions. Samples RC4 and RC12, which have complex demagnetisation, plot as outliers, well to the less stable side of the plot.

Admixtures of magnetite and haematite can be better categorised by a plot of saturation magnetisation normalised for susceptibility against coercivity of remanence (Bradshaw and Thompson, 1985). Stability of remanence generally increases to the upper right in this plot. Reed Chamber samples are generally more stable than those from Bone Chamber (Fig. 11), and there is a similar relationship between stability indicated by position on the Bradshaw and Thompson plot and evidence for a reversed polarity component of remanence as is seen for the Day plot. In this case, however, only the weakly magnetised sample RC12 is an obvious outlier; surprisingly, RC12 falls towards the more stable parts of this plot, in contrast with its position on the Day plot.

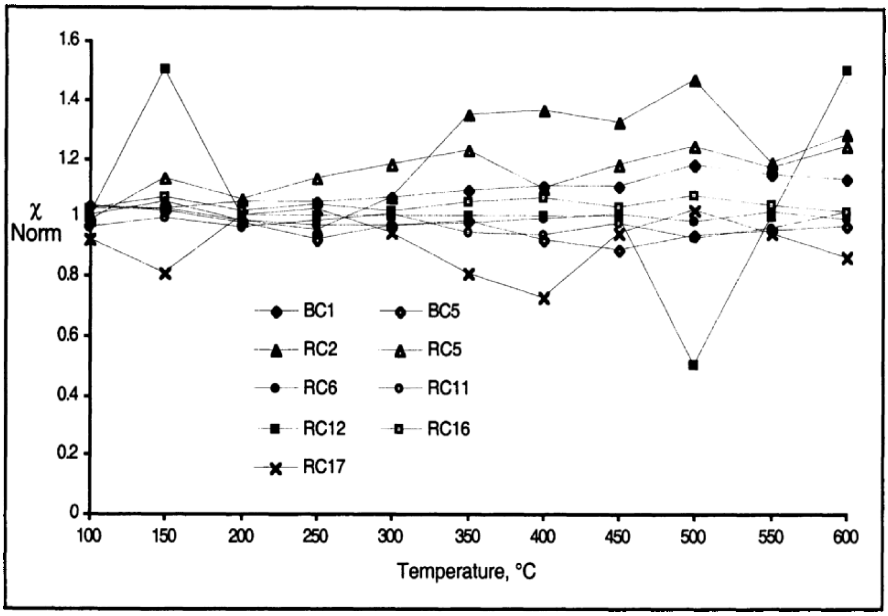

Figure 9. Plot showing variations in susceptibility measured after a series of heating and cooling steps for Bone Chamber and Reed Chamber sediments. Susceptibility is normalised relative to the initial susceptibility measured before heating.

Fields defining domain states for magnetite assemblages have been theoretically defined for the Day plot, and similar fields for both magnetite and haematite have been empirically determined for the Bradshaw and Thompson plot. The two plots appear to disagree over the Buchan samples: the bulk of the samples fall in the pseudo-single domain (PSD) field on the Day plot (representing grains around 0.1-1 μm in diameter), but in the multidomain (MD) field (grains larger than PSD size) on the Bradshaw and Thompson plot. Neither plot was designed to identify superparamagnetic (SP) grains, however. SP magnetite grains have dimensions smaller than about 0.03-0.05 μm (Butler and Banerjee, 1975), and contrast markedly in magnetic properties with single-domain (SD) grains, which are slightly larger. SP grains are too small to support a stable magnetic domain, and are characterised by high susceptibility but very short relaxation times, of the order of seconds: relaxation times increase dramatically over the transition from SP to SD grains (up to billions of years). In both the Day and the Bradshaw and Thompson plots SP grains are regarded as having essentially zero saturation remanence and coercivity, so that their admixture with other domain sizes shifts the position on both plots downward.

Frequency dependency of susceptibility (χ_{FD}) sharply increases with an increase in the proportion of ultrafine (0.01–0.03 μm) grains of magnetite, around the border between the superparamagnetic (SP) and single domain (SD) fields (Özdemir and Banerjee, 1982; Maher, 1988). Assemblages of larger grains, including SD, PSD and MD grains, display little frequency dependence of susceptibility. Most of the Buchan samples experience a substantial decrease in susceptibility at the higher measuring frequency: χ_{FD} exceeds 5% in all samples except RC12, indicating the presence of substantial

proportions of SP threshold grains (Dearing, 1994), and in two of the Bone Chamber samples (BC1 and BC3) χ_{FD} exceeds 10%, suggesting that SP-threshold grains dominate the remanence. Sample RC12, which has a bulk susceptibility one to two orders of magnitude less than all other samples, also has a much lower χ_{FD} (<2%), in the range where SP grains contribute little to the total remanence.

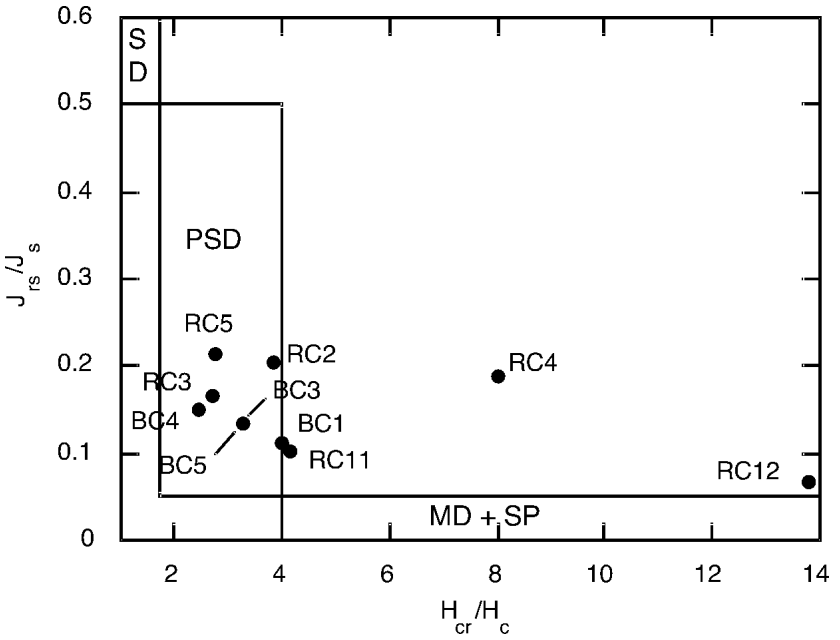

Figure 10. Day plot showing representative samples from the Buchan cave sediments. Theoretical fields for single-domain (SD), pseudo-single-somain (PSD), and multidomain and/or superparamagnetic (MD + SP) assemblages of magnetite are indicated.

Grains which contribute the strongest χ_{FD} are in a size range just below the lower limit of true single-domain behaviour (Dearing et al., 1985, 1996). As such, they exhibit behaviour transitional between true SP and SD grains: they can maintain a remanence for an appreciable period, and have a low but non-zero coercivity. This potentially makes them carriers of viscous remanence (VRM), more commonly thought of as being associated with PSD or MD grains. The presence of significant proportions of these ultrafine, "viscous SP" grains probably explains the anomalous position of the Buchan samples on the Day and Bradshaw and Thompson plots, and the disagreement between the two plots.

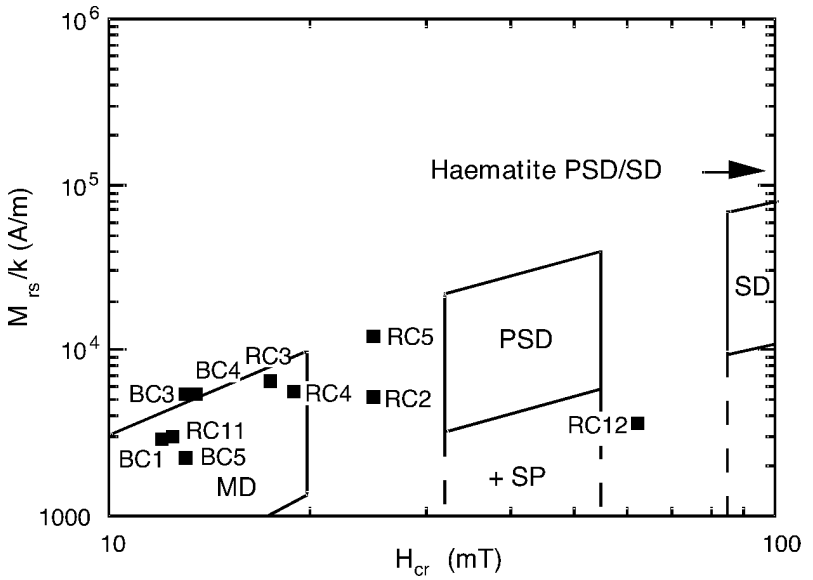

Figure 11. Bradshaw and Thompson (1985) plot showing representative samples from the Buchan cave sediments. Empirical fields for multidomain (MD), pseudo-single-domain (PSD) and single-domain (SD) assemblages of magnetite are indicated, as is the effect of adding superparamagnetic grains to these assemblages ("+SP"). Fields for pure haematite assemblages lie well to the right, beyond H_{cr} = 100 mT.

6. DISCUSSION

6.1.Palaeomagnetism

Given the rock-magnetic evidence that unstable, SP magnetite grains make up a substantial proportion of the magnetic carriers in the Buchan cave sediments, it is not surprising that a simple pattern of magnetic polarity has not emerged. The relatively simple, normal polarity component which dominates the magnetisation of most of the Bone Chamber samples is probably a viscous remanence (VRM) with a relatively short relaxation time, acquired over the last few tens to hundreds of years, and carried by ultrafine grains of around 0.01-0.03 μm diameter, just below the SP/SD threshold. In the case of sample BC4, the presence of the reversed polarity component can be explained by the slightly greater grain size of this magnetite component, towards the SD limit, resulting in an increase in remanence coercivity and the preservation of a "stable" remanence component. At least one other component, of slightly higher stability, also seems to be present in this sample; similar, relatively stable components are probably present in much smaller proportions in the other Bone Chamber samples, presumably being carried in each case by the coarser fraction of the SP magnetite grains.

Some of the Reed Chamber samples preserve only a VRM directed near the present field; the grain size of magnetite in these samples is presumably finer. Complex demagnetisation in other Reed Chamber samples implies the presence of two or more com-

ponents, with similar stability spectra; in at least some cases one of these appears to be reversed.

The presence of a reversed polarity component can be demonstrated in one Bone Chamber sample, and there is evidence for reversed polarity components in several of the samples from Reed Chamber. At some stage between deposition of the Buchan cave sediments and the present, they have been exposed to a reversed field. Although brief intervals of intermediate and reversed polarity are known from the Brunhes Chron (e.g., the Blake and Emperor events), these total only about 5% of its 780,000 year extent (Jacobs, 1984; Cande and Kent, 1995). Consequently, it is most likely that the cave sediments have been in place since at least 780 ka. Understanding how the age of acquisition of the reversed polarity component relates to the age of cave sedimentation depends on an appreciation of the magnetisation process involved.

6.2. Sedimentation and Diagenesis of the Magnetic Mineralogy of the Buchan Cave Sediments

6.2.1. Bone Chamber

Sediments in Bone Chamber, representing the uppermost level of cave sedimentation at Buchan (Level C), are much finer grained and redder in colour than sediments from the lower, Reed Chamber level (Level A). Unlike the Reed Chamber sediments, bedding features suggestive of fluvial deposition are entirely lacking from Bone Chamber. In addition, sediments in Bone Chamber are not confined to the epiphreatic part of the passage, but occur also in the narrow vertical joint which extends upwards, probably almost to the ground surface above the cave. It appears most likely that these sediments were washed down into the cave by rainwater percolating down the open joints.

Similar sediments, often called "red earths", are widespread in other caves in the Buchan area, and deposits several meters thick are also present within caves throughout southeastern Australia (Osborne, 1991). These sediments frequently contain the bones of extinct marsupials; the time ranges of the species recorded suggest that the age of the "red earths" is most likely Pleistocene (Osborne, 1983). The presence of thick deposits of reddish silt and clay, all probably Pleistocene in age, across such an extensive area suggests that a common mechanism is responsible. It is likely that the "red earths" represent wind-blown material washed into the caves, as they have an appropriate grain size (dominated by silt and clay), and the reddish colour suggests a derivation from the deserts of central Australia. The volume of material (particularly silt-sized quartz) is too great for the "red earths" to represent surface soil material derived by weathering of the limestone bedrock, as suggested by Frank (1975). The Buchan Caves Limestone contains less than 6% by weight of clay and quartz (Sweeting, 1960; Jenkin and Baxter, 1969), and the soil developed on the limestone, which is less than 30 cm (and often < 10 cm) thick, is dark reddish brown or dark brown (2.5YR 3/4 to 7.5YR 3/4) rather than reddish brown in colour.

The Bone Chamber sediments have mass susceptibilities of 500-1000 $\times$ 10^{-8} m^3kg^{-1}, greater than those for pristine aeolian sediments such as the Chinese loesses, which typically have mass susceptibilities of the order of 10-100 $\times$ 10^{-8} m^3kg^{-1} (e.g., Heller and Liu, 1984; Chen et al., 1999). Palaeosols developed within loess sequences, however,

have significantly enhanced susceptibilities (Heller and Evans, 1995), and are also characterised by a greatly increased content of ultrafine magnetite grains in the SP/SD threshold size (Maher and Thompson, 1992). Production of such ultrafine magnetite is now widely recognised as a feature of soil formation (e.g., Thompson and Oldfield, 1986; Dearing et al., 1996), and probably reflects the extracellular reduction of ferric iron by bacteria.

Maher and Thompson (1995) sought to quantify the pedogenic enhancement of susceptibility by a survey of loesses and other Northern Hemisphere soils, in which other sources of susceptibility enhancement could be discounted. Their maximum susceptibility values were around 500×10^{-8} m^3kg^{-1}, at the lower range of the Bone Chamber sediments. Indeed, the Bone Chamber sediments are in the upper part of the range of susceptibilities reported for all topsoils (Dearing, 1999). This may reflect the high availability of iron in the original aeolian red silts and clays, or differences in conditions influencing bacterial activity between surface soils and cave sediments.

It is unlikely that the enhanced susceptibility of the Bone Chamber samples could reflect a source as a burnt soil. Although such burnt soils have been shown to have susceptibilities ranging as high as 9000×10^{-8} m^3kg^{-1} (Dearing, 1999), they frequently contain maghemite (see Thompson and Oldfield, 1986, for a discussion), and would be expected to show other indications of burning, such as fragments of charcoal or baked clays. These were not observed in either the Bone Chamber or Reed Chamber samples.

The ultrafine magnetite in the Bone Chamber sediments is either a pre-existing part of aeolian sediments accumulating on the surface and subsequently washed into the cave, or it formed subsequent to aeolian deposition, either in a soil produced on such aeolian sediments, or within the cave sediments after these were washed down and redeposited inside the cave. High concentrations of ultrafine magnetite in dusts collected from Barbados (Prospero et al., 1981) have been interpreted as indicating soils that had been enriched in magnetite prior to transport. The polymodal grain size distribution of the Bone Chamber sediment, which contrasts with the usual unimodal distribution of loess, may reflect accumulation as a soil prior to transport into the cave. However, the demagnetisation behaviour of the Bone Chamber sediments accords best with *in situ* magnetite formation in the cave. Besides a viscous remanence (VRM), the Bone Chamber sample BC4 shows evidence of two other components, one reversed and the other indeterminate, with strongly overlapping stability spectra. The two components were blocked in by ultrafine, SP/SD threshold magnetite grains; these may have been produced during prolonged or episodic bacterial activity, spanning a period over which the direction or polarity of the earth's field changed. In-situ bacterial authigenesis of ultrafine magnetite, perhaps enhancing earlier pedogenesis, is our preferred interpretation of the cause of enhanced susceptibility in the Bone Chamber sediments. If this is so, then the reversed polarity component isolated in sample BC4 was acquired at some time after deposition of the Bone Chamber sediments.

6.2.2. Reed Chamber

The gravels, sands and clays in Reed Chamber in the lowermost epiphreatic level undoubtedly represent fluvial sediments deposited by the stream flowing through the cave at the time, as the sands occasionally show ripple cross-lamination.

Compositionally, the cave sediments match the stream sediments in the bed of Fairy Creek, particularly the pebbles and cobbles, which are predominantly rhyolitic volcanics.

Despite the difference in origin between the Bone Chamber and Reed Chamber sediments, the contrast between their rock-magnetic properties is not great. This may merely reflect a sampling bias towards the finer-grained parts of the Reed Chamber sequence, which may have originated on the surface from a similar source to that which washed in to fill Bone Chamber. Susceptibility is mostly lower in the Reed Chamber samples than in those from Bone Chamber, which may indicate a lower availability of iron in the original sediment, in accord with the less intense red colour of the Reed Chamber sediments. With the exception of sample RC12, the Reed Chamber samples contain substantial proportions of ultrafine magnetite grains, and the presence of at least two non-VRM components in several of the Reed Chamber samples argues for growth of at least some of this magnetite fraction after deposition in the cave.

Sample RC12 is a yellowish brown, laminated clay, similar to other Reed Chamber samples, but has strongly contrasting magnetic properties. In most of the samples from both Bone and Reed chambers, authigenic magnetite dominates the magnetic properties over any detrital haematite, because magnetite is so much more magnetic than haematite. The low susceptibility, remanence intensity, and χ_{FD} of sample RC12 indicate that relatively little authigenic magnetite is present. Detrital haematite plays a more significant role in the rock magnetism of this sample, which as a consequence plots as an outlier closer to the haematite field on the Bradshaw and Thompson plot. The difference between this sample and its neighbours may reflect a different provenance, providing a different detrital magnetic mineralogy; however, this is inconsistent with the similarity in appearance between RC12 and other Reed Chamber samples. Pedogenic magnetite production is highly dependent on organic content, water saturation, and pH (Taylor et al., 1987), and some variation in these may be the controlling factor.

6.3. Timing of Cave Development

At least some of the samples from both the lowermost (Level A – Reed Chamber) and uppermost (Level C – Bone Chamber) epiphreatic passages in the Dukes system show evidence for having been exposed to a reversed polarity field, implying deposition of the sediments at both levels before 780 ka. The relative timing of the deposition of the sediments and the formation of the cave passages is not certain. The sands and gravels of Level A may have infilled the passage while it was actively forming. In this case the sediments could have forced the continuing solutional enlargement of the passage upwards to the water table, so the passage would be of paragenetic origin (Ford and Williams, 1989). However, similar fluvial sediments are lacking from the other two epiphreatic levels within the Dukes cave system.

Alternatively, the fluvial sediments of Level A may have accumulated when a roof collapse blocked water flow through the cave. It is notable that the bulk of the sediments occur upstream of a major area of collapse in the cave.

Thus the development of the lowest epiphreatic cave level may have been contemporaneous with or pre-date the sediment deposition. This indicates that even the lowest cave level (and the river terrace with which it is correlated) formed in the mid-Pleistocene, or earlier. The sea level and climatic fluctuations of the late Pleistocene, responsible for the bulk of Northern Hemisphere karst geomorphology, have left little discernible trace in the Buchan area (Webb et al., 1992).

The uppermost epiphreatic level, Level C, must be considerably older than Level A. The palaeomagnetic evidence corroborates the U-series speleothem dates which suggest that Level C formed more than one million years ago.

6.4. Palaeoclimatic Implications

Substantial transport of wind-blown dust has occurred during the arid phases that have periodically characterised the climate of southern Australia in the Quaternary (Bowler, 1976, 1982; Colhoun, 1991). The palaeomagnetic minimum age for the "red earths" in the cave at Buchan suggests that these wind-blown sediments record a period of aridity older than 780 ka. Although the most intense periods of aridity in southern Australia occurred during the last 700 000 years (Bowler, 1982), seasonal aridity became established at about 6 Ma, and progressive desiccation was well advanced by 2.5 Ma (Bowler, 1976). In central Australia the onset of arid-zone aeolian facies may have been at around 1.1 Ma (Chen and Barton, 1991). Thus the "red earths" at Buchan appear to record the early imprint of these climatic changes on southern Australia, probably in the early Pleistocene.

7. CONCLUSIONS

Palaeomagnetism provides the only direct method of dating the Buchan cave sediments. Recognition of magnetic polarity was made more difficult by post-depositional authigenesis in the sediments, which involves generation of ultrafine magnetite, on the superparamagnetic – single-domain threshold, presumably through bacterial processes similar to those recognised in pedogenesis. Nevertheless, a reversed polarity component can be recognised in the demagnetisation of some samples, and can be inferred in others, suggesting that the sediments were deposited some time prior to the last major change in polarity at 780 ka.

Reversed polarity components appear to be present in samples from both the uppermost (Bone Chamber – Level C) and lowermost (Reed Chamber – level A) epiphreatic levels in the cave system. Thus level A, only a few meters above present stream level, must have formed before 780 ka. The caves have an antiquity not indicated by their present appearance or position in the landscape. This is in marked contrast to the Northern Hemisphere, where the effects of the Pleistocene glaciations have meant that the majority of the caves there probably developed in the late Pleistocene and Holocene.

The red clays and silts in the upper level of the cave probably represent wind-blown material washed into the cave from the ground surface. They presumably represent the effects of one of the major periods of aridity that affected the landscape of southeastern Australia in the early Pleistocene, prior to 780 ka.

The present study indicates clearly the principle of "karst immunity" (Jennings 1985), whereby caves often contain information that is lacking or less clearly expressed in non-limestone terrains. This conforms the utility of the study of caves and their contents to studies of landscape evolution and palaeoclimatology.

8. ACKNOWLEDGEMENTS

This project was initiated by an ARC grant to study the origin of the Buchan karst. Some measurements were made using facilities of the Ocean Drilling Program's ship, the *JOIDES Resolution*, during transit time at the start of Leg 164; we thank the ODP technical crew, and especially Margaret Hastedt, for their assistance. The Department of Conservation and Environment, and particularly the former Ranger in Charge at Buchan, Graham Parkes, are thanked for allowing access to the caves and the collection of samples. Derek Fabel supplied the cave maps and cross sections, and carried out the laser particle size analyses. Anna Klein assisted with redrafting of the figures. Discussions with Brian Finlayson and Armstrong Osborne helped to formulate some of the ideas in this paper, and the final version benefited greatly from reviews by W. Harbert and an anonymous reviewer.

9. REFERENCES

Atkinson, T. C., Harmon, R. S., Smart, P. L. and Waltham, A. C., 1978, Palaeoclimatic and geomorphic implications of $^{230}Th/^{234}U$ dates on speleothems from Britain, *Nature* **272**:24–28.

Bishop, P., and Brown, R., 1992, Denudational isostatic rebound of intraplate highlands: the Lachlan River valley, Australia, *Earth Surf. Proc. Landforms* **17**:345–360.

Bowler, J. M., 1976, Aridity in Australia: age, origins and expression in aeolian landforms and sediments, *Earth Sci. Rev.* **12**:279–310.

Bowler, J. M., 1982, Aridity in the late Tertiary and Quaternary of Australia, in: *Evolution of the Flora and Fauna of Arid Australia*, W. R. Barker and P. J. M. Greenslade, eds., Peacock Publications, Adelaide, pp. 35–45.

Bradshaw, R. H. W., and Thompson, R., 1985, The use of magnetic measurements to investigate the mineralogy of some Icelandic lake sediments and to study catchment processes, *Boreas* **14**:203–215.

Butler, R. F., and Banerjee, S. K., 1975, Theoretical single-domain size range in magnetite and titanomagnetite, *J. Geophys. Res.* **80**:4049–4058.

Cande, S. C., and Kent, D. V., 1995, Revised calibration of the geomagnetic polarity timescale for the Late Cretaceous and Cenozoic, *J. Geophys. Res.* **100**:6093–6095.

Chen, J., An, Z., and Head, J., 1999, Variation of Rb/Sr ratios in the loess-paleosol sequences of central China during the last 130,000 years and their implications for monsoon paleoclimatology, *Quat. Res.* **51**:215–219.

Chen, X. Y., and Barton, C. E., 1991, Onset of aridity and dune-building in central Australia: sedimentological and magnetostratigraphic evidence from Lake Amadeus, *Palaeogeogr., Palaeoclimatol., Palaeoecol.* **84**:55–73.

Colhoun, E. A., 1991, Climate during the last glacial maximum in Australia and New Guinea: evidence inferred from biogeographical and geomorphological data, *Australian and New Zealand Geomorphology Group Special Publication* **2**:1–71.

Day, R., Fuller, M., and Schmidt, V. A., 1977, Hysteresis properties of titanomagnetites: grain size and compositional dependence, *Phys. Earth Planet. Int.* **13**:260–277.

Dearing, J. A., 1994, *Environmental Magnetic Susceptibility*, Chi Publishing, Kenilworth, U.K.

Dearing, J. A., 1999, Magnetic susceptibility, in: *Environmental Magnetism: a Practical Guide*, J. Walden, F. Oldfield, and J. P. Smith, eds., Technical Guide No. 6, Quaternary Research Association, London, pp. 35–62.

Dearing, J. A., Hay, K. L., Baban, S. M. J., Huddleston, A. S., Wellington, E. M. H., and Loveland, P. J., 1996, Magnetic susceptibility of soil: an evaluation of conflicting theories using a national data set, *Geophys. J. Int.* **127**:728–734.

Dearing, J. A., Maher, B. A., and Oldfield, F., 1985, Geomorphological linkages between soils and sediments: the role of magnetic measurements, in: *Geomorphology and Soils*, K. S. Richards, R. Arnett, and S. Ellis, eds., George Allen and Unwin, London, pp. 245–266.

Fabel, D., Henricksen, D., Finlayson, B. L., and Webb, J. A., 1996, Nickpoint recession in karst terrains: an example from the Buchan Karst, southeastern Australia, *Earth Surf. Proc. Landforms* **21**:453–466.

Ford, T. D., Gascoyne, M., and Beck, J. S., 1983, Speleothem dates and Pleistocene chronology in the Peak district, Derbyshire, *Trans. Brit. Cave Res. Assoc.* **10**:103–115.

Ford, D. C., and Williams, P. W., 1989, *Karst Geomorphology and Hydrology*, Unwin Hyman, London.

Frank, R. M., 1975, Late Quaternary climatic change: evidence from cave sediments in central eastern New South Wales, *Australian Geograph. Studies* **13**:154–168.

Gascoyne, M., 1984, Twenty years of uranium-series dating of cave calcites, *Studies in Speleology* **5**:15–30.

Gascoyne, M., Ford, D. C., and Schwartz, H. P., 1981, Late Pleistocene chronology and paleoclimate of Vancouver Island determined from cave deposits, *Can. J. Earth Sci.* **18**:1643–1652.

Grotaers, L. D., 1995, The Buchan Caves Gravels: implications for past depositional environment, B.A. (Honours) thesis, Deakin University, Geelong, Australia (unpublished).

Heller, F., and Evans, M. E., 1995, Loess magnetism, *Rev. Geophys.* **33**:211–240.

Heller, F., and Liu, T. S., 1984, Magnetism of Chinese loess deposits, *Geophys. J. Roy. Astron. Soc.* **77**:125–141.

Jacobs, J. A., 1984, *Reversals of the Earth's Magnetic Field*, Adam Hilger Ltd, Bristol.

Jenkin, J. J., and Baxter, G. W., 1969, *Limestones and Dolomites of the Buchan-Murrindal Area*, BHP Exploration Report No. 744 (unpublished).

Jennings, J. N., 1985, *Karst Geomorphology*, Blackwell, Oxford.

Maher, B. A., 1988, Magnetic properties of some synthetic sub-micron magnetites, *Geophys. J.*, **94**:83–96.

Maher, B. A., and Thompson, R., 1992, Paleoclimatic significance of the mineral magnetic record of the Chinese loess and paleosols, *Quat. Res.* **37**:155–170.

Maher, B. A., and Thompson, R., 1995, Paleorainfall reconstructions from pedogenic magnetic susceptibility variations in the Chinese loess and paleosols, *Quat. Res.* **44**:383–391.

Maher, B. A., and Thompson, R., 1999, Palaeomonsoons I: the magnetic record of palaeoclimate in the terrestrial loess and palaeosol sequences, in: *Quaternary Climates, Environments and Magnetism*, B. A. Maher and R. Thompson, eds., Cambridge University Press, Cambridge, U.K., pp. 81–125.

Noel, M, 1986, The palaeomagnetism and magnetic fabric of cave sediments from Pwll y Gwynt, South Wales, *Phys. Earth Planet. Int.* **44**:62–71.

Noel, M., and Thistlewood, L., 1989, Developments in cave sediment palaeomagnetism, in: *Geomagnetism and Palaeomagnetism,* F. J. Lowes, et al., eds., Kluwer Academic Publishers, New York., pp. 91–106.

Osborne, R. A. L., 1983, Cainozoic stratigraphy at Wellington Caves, New South Wales, *Proc. Linn. Soc. New South Wales* **107**:131–147.

Osborne, R. A. L., 1990, Palaeokarst deposits at Jenolan Caves, New South Wales, *J. Proc. Roy. Soc. New South Wales* **123**:59–73.

Osborne, R. A. L., 1991, Red earth and bones: the history of cave sediment studies in New South Wales, Australia, *Earth Sci. Hist.* **10**:13–28.

Osborne, R. A. L., and Branagan, D. F., 1988, Karst landscapes of New South Wales, Australia, *Earth Sci. Rev.* **25**:467–480.

Özdemir, Ö., and Banerjee, S. K., 1982, A preliminary magnetic study of soil samples from west-central Minnesota, *Earth Planet. Sci. Lett.* **59**:393–403.

Palmer, A., 1989, Geomorphic history of the Mammoth Cave System, in: *Karst Hydrology – Concepts From the Mammoth Cave Area*, W. B. White and E. L. White, eds., Van Nostrand Reinhold, New York, pp. 317–337.

Prospero, J. M., Glaccum, R. A., and Nees, R. T., 1981, Atmospheric transport of soil dust from Africa to South America, *Nature* **289**:570–577.

Rich, P. V., and Thompson, E. M., 1982, *The fossil vertebrate record of Australasia*, Monash University, Clayton, Australia.

Schmidt, V. A., 1982, Magnetostratigraphy of sediments in Mammoth Cave, Kentucky, *Science* **217**:827–829.

Schmidt, V. A., Jennings, J. N.. and Haosheng, B., 1984, Dating of cave sediments at Wee Jasper, New South Wales, by magnetostratigraphy, *Aust. J. Earth Sci.* **31**:361–370.

Sweeting, M. M., 1960, The caves of the Buchan area, Victoria, Australia, *Zeitschrift Geomorph., Supplementband* **2**:81–91.

Taylor, R. M., Maher, B. A., and Self, P. G., 1987. Magnetite in soils: I. The synthesis of single-domain and superparamagnetic magnetite, *Clay Mins.* **22**:411–422.

Thompson, R., and Oldfield, F., 1986, *Environmental Magnetism*, Allen and Unwin, London.

VandenBerg, A. H. M., and O'Shea, P. J., 1981, *Explanatory Notes on the Bairnsdale 1:250,000 Geological Map*, Geological Survey of Victoria Report No. 65, pp. 1–61.

Webb, J. A., Fabel, D., Finlayson, B. L., Ellaway, M., Li Shu, and Spiertz, H.-P., 1992, Denudation chronology from cave and river terrace levels: the case of the Buchan Karst, southeastern Australia, *Geol. Mag.* **129**:307–317.

Webb, J. A., Finlayson, B. L., Fabel, D., and Ellaway, M., 1991, The geomorphology of the Buchan karst - implications for the landscape history of the Southeastern Highlands of Australia, *Geol. Soc. Aust. Spec. Pub.* **18**:210–234.

White, W. B., and White, E., 1974, Base-level control of underground drainage in the Potomac River Basin, in: *Proceedings of the 4th Conference on Karst Geology and Hydrology*, H. W. Rauch and E.Werner, eds., West Virginia Geological Survey, Charleston, pp. 41–53.

Williams, P. W., 1982, Speleothem dates, Quaternary terraces and uplift rates in New Zealand, *Nature* **298**:257–260.

PALEOMAGNETIC ANALYSIS OF A LONG-TERM SEDIMENT TRAP, KOOKEN CAVE, HUNTINGDON COUNTY, PENNSYLVANIA, USA

Ira D. Sasowsky, Rebecca A. Clotts, Bryan Crowell,
Selena M. Walko, Edward J. LaRock, and William Harbert*

1. ABSTRACT

Kooken Cave is an extensive, deep fissure system developed in Ordovician age limestones of the Valley and Ridge physiographic province, Pennsylvania, USA. The cave floods to significant depth each year, due to influent surface waters. The cave drains slowly, and 45 ft (15 m) of clastic sediments fill portions of the cave. The discharge area for groundwater flowing through the cave is unconfirmed, but appears to be the Little Juniata River, which is steeply incised into the limestone upland containing the cave. The lowest deposits in the cave contain clay, sand, and cobbles, which probably limit draining of the cave. The remainder of the sediments are exclusively fine-grained. Twenty-four paleomagnetic samples were collected and analyzed. They all show normal polarity, indicating deposition within the present chron (< 780 ka). Sample pairs show good correlation, indicating that the sediments maintain a good record of paleosecular variation. Declinations are generally eastward of the present-day field, and most inclinations show shallowing. Sediment accumulation rates extrapolated from recent individual floods suggest that the entire sedimentary package could have been deposited within 1,440 years. Expected river incision rates and other geomorphic constraints lead to an age of <320 ka for the cave. It is likely that Kooken Cave has been accumulating allochthonous sediments for 1,000-10,000 years.

---

* Ira D. Sasowsky, Rebecca A. Clotts, Dept. of Geology, University of Akron, Akron, Ohio 44325-4101. Bryan Crowell, Environmental Pollution Control Program, 209 Materials Research Lab, The Pennsylvania State University, University Park, PA 16802. Selena M. Walko, Dept. of Earth Resources, Colorado State University, Fort Collins, CO 80523. Edward J. LaRock, 4148 East 19th Ave, Denver, CO 80222. William Harbert, University of Pittsburgh, Dept. of Geology & Planetary Science, 321 Engineering Hall, Pittsburgh PA 15260 USA.

2. INTRODUCTION

Geomorphologists, climatologists, and hydrogeologists frequently try to decipher historical changes in earth systems by interpreting depositional records. In erosional (i.e. most continental) settings this is difficult because the deposits may be discontinuous and short-lived. However, clastic cave sediments have the potential to hold extensive paleoclimatic and paleohydrologic records under certain conditions. A cave can provide a protected environment, at least on timescales from 0 to 5 Ma. To provide the most useful records, the deposits should be continuous and contain material that is capable of being dated.

Kooken Cave is a laterally extensive karst void developed in steeply dipping limestones of the Valley and Ridge physiographic province of central Pennsylvania (Fig. 1). The cave is peculiar for the region, because it floods on at least an annual basis and takes a long time to drain. Therefore, we recognized the potential for the cave to be a long-term sediment trap, and undertook an investigation to evaluate the record that was contained therein.

3. DESCRIPTION OF THE STUDY SITE

The study site is located in Huntingdon County, Pennsylvania (Fig. 1). The area is within the westernmost part of the Valley and Ridge physiographic province, about 4 mi (6 km) east of the Allegheny Front, the boundary with the Appalachian Plateaus province. The entire Valley and Ridge province is characterized by extensive anticlines and synclines, and the structure of this particular area is complicated by the proximity to the Allegheny Front. The study area lies near the nose of Brush Mountain (shown as higher topography in lower left of Fig. 1), which is a southwest plunging syncline. The north-northeast trending Yellow Springs Fault, with numerous splays, is present just to the east of the mountain. The lack of good outcrops leaves the possibility open that other faults may be present. The cave is developed beneath a gently rolling, agricultural upland surface that is at about 1000 ft (300 m) amsl. The rocks are undifferentiated Ordovician limestones of the Coburn through Loysburg Formations (Berg and Dodge, 1981; Shultz, 1999). East of the fault the rocks are mainly dolomites. Further to the northeast the upland has been steeply incised by the Little Juniata River to an elevation of 750 ft (230 m) amsl (Fig. 1). This stream, which serves as local base level for surface and ground waters, is a tributary of the Juniata River, which subsequently joins the Susquehanna River on its journey to the North Atlantic Ocean.

Kooken Cave is primarily a fissure system developed along a steeply inclined (and possibly faulted) bedding plane. In the cave, at the vicinity of the samples, bedrock strikes 068° and dips 64° southeast. In plan view (Fig. 2) the cave follows a gently arcuate pattern. In cross-section (Figure 3) a series of interconnected overlying and underlying passages are seen. The cave has been known since the summer of 1930, when it was dug open (Devitt, 1953). It presented a serious challenge to explorers due to the vertical entrance shaft (requiring ropes), and numerous, large, mud-sided pits (or funnels). The eastern entrance of the cave is at a surface elevation of 988 feet (301 m) amsl, based upon a GPS survey. Most of the cave has a surveyed level of about 860 feet (260 m) amsl, though the high ceilings of the fissures and the depth of the pits make this figure only a generality. The lowest portion of the cave, 809 feet (247 m) amsl, is at the base of a pool in the easternmost portion of the cave.

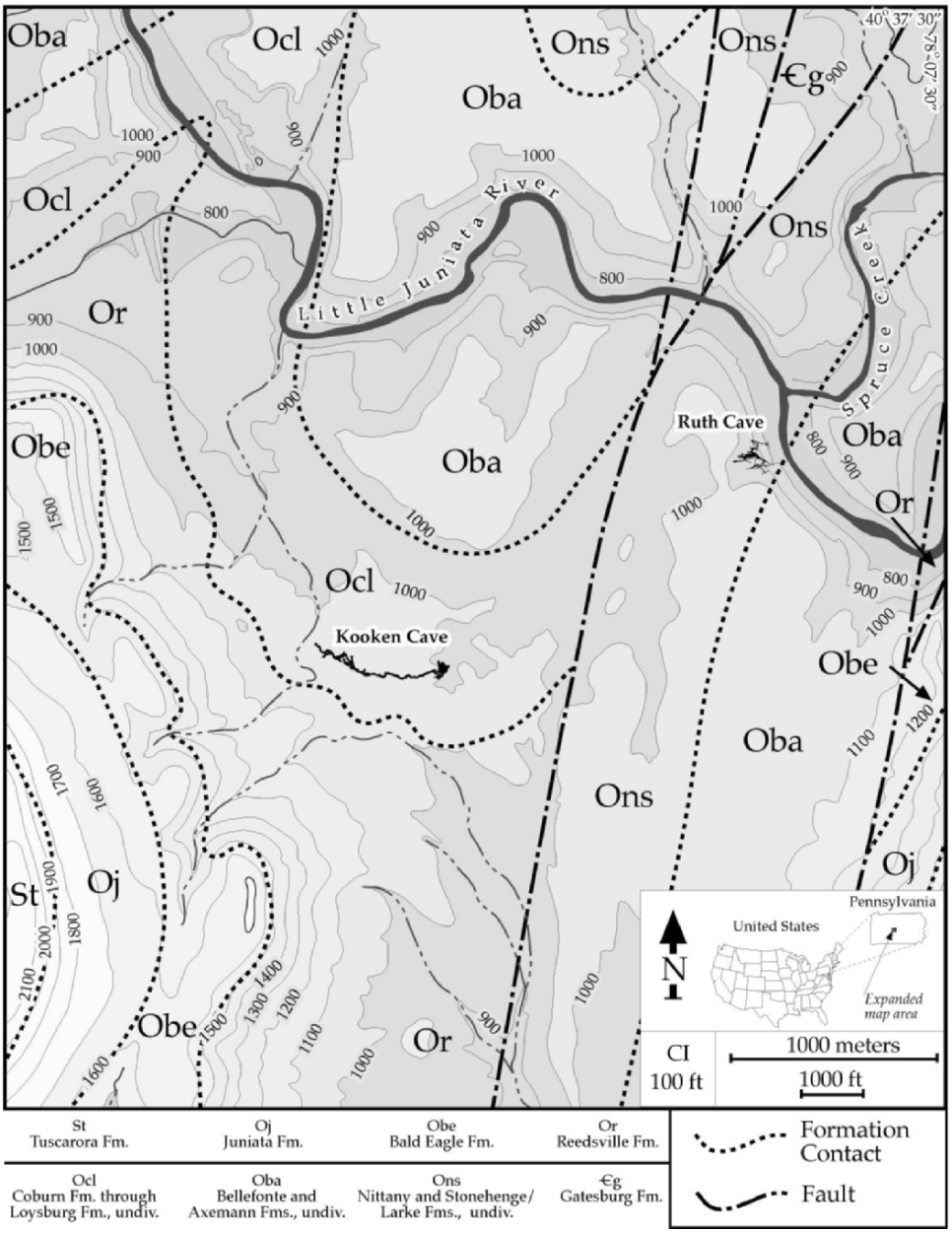

Figure 1. Map of the vicinity of Kooken Cave. Topography (100 foot contours) and hydrography from U.S.G.S. Spruce Creek 7.5′ quadrangle. Geology from Berg and Dodge (1981). Kooken Cave map modified from original map by Pittsburgh and Nittany Grottos (National Speleological Society). Ruth Cave map modified from original map by Jim Kennedy and Kevin Lear (Kennedy, 1990).

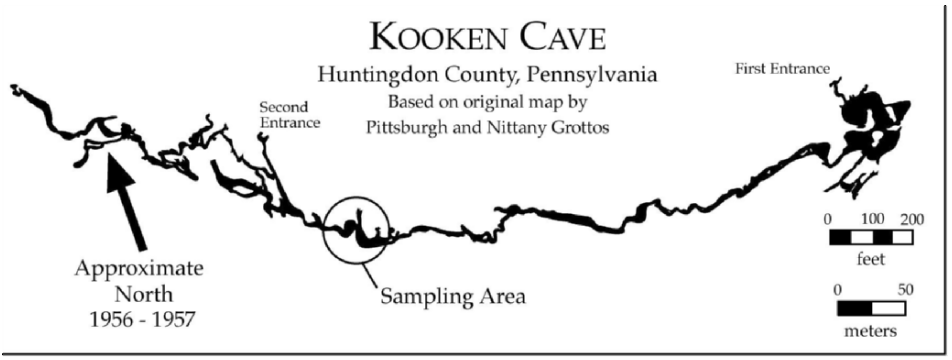

Figure 2. Map of Kooken Cave. Modified from original map by Pittsburgh and Nittany Grottos (National Speleological Society).

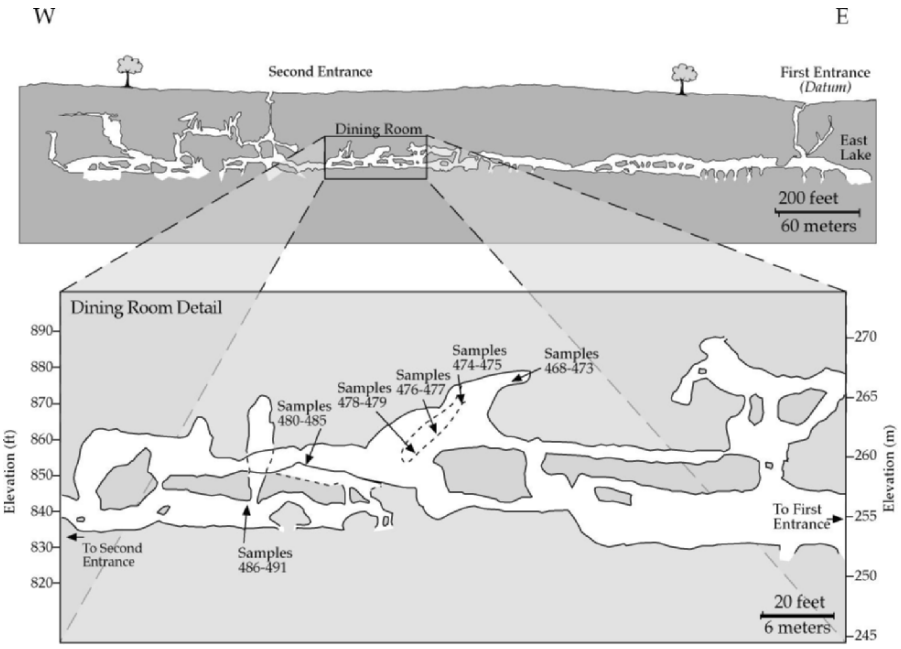

Figure 3. Cross section of Kooken Cave and overlying land surface. No vertical exaggeration. Lower portions of cave, with white tone and no black line, are unmapped, because they are underwater. The cave extends to unknown depth. General position of sample locations is indicated by number. Dashed lines show cave passages that are behind others. Modified from a map by Bryan Crowell.

Water flows in an overall eastward direction within the cave. The specific source of the water has not been identified, but is likely to be the unnamed surface stream shown on Figure 1 near the western end of the cave. Almost all drainage on the limestone upland is lost from intermittent streams to the groundwater system, which is typical in

this area of central Pennsylvania. There is very little evidence of channelized flow on the surface. This stream is also the likely source of clastic sediments found in the cave. Water flows through the lowermost portions of the cave toward the eastern end, where a pool (East Lake), with base elevation 809 feet (247 m) amsl is found. This pool has at least 6 ft (2 m) of water at all times. On December 9, 2000, SCUBA divers Dave Grimm and Bill Williams explored the East Lake to 26 ft (8 m) below water level, or an elevation of about 789 ft (240 m; author B.Crowell was present). They found that the cave narrows to a tight fissure, which was impenetrable using the equipment they had. It has been noted (W.B. White, personal communication) that dye placed in the eastern pool remained in the ponded water for some time. It was originally hypothesized that the water then moved slowly southward to the fault-controlled Tippery Spring, beyond the Southern boundary of Figure 1. However, recent leveling surveys (McCarthy, 2001) have shown that this spring is higher in elevation than the pool in the cave. Topographic position, along with geologic contacts, indicates that the water probably drains to the north or east from the cave, to springs on the Little Juniata River. The position of Ruth Cave (Kennedy, 1990), a dry cave in the valley wall above the Little Juniata River, along with the surface topography, suggests that the former could be an abandoned downstream outlet of the water from Kooken Cave (Fig. 1). However, the elevation of Ruth Cave is 977 ft (299 m) at its West end and 793 ft (242 m) at the East, which is relatively high in comparison to the present day Kooken Cave. Because of this, and the Yellow Springs Fault separating the two caves, we feel it is unlikely that the two caves were hydraulically connected.

The flooding and draining behavior of Kooken Cave provides insight in to the hydraulic function of the flow system, particularly the inaccessible portions. The cave has been known to flood since its discovery. Devitt (1953) indicated that water level rises of 30 ft (9 m) were common, particularly in the winter. Recent observations (1996-2001) have shown a maximum rise of 42 ft (13 m). Floods vary in magnitude and duration depending upon precipitation amount, precipitation intensity, and antecedent water conditions. During drought conditions, flooding is greatly minimized in both magnitude and duration. If soil moisture is relatively low, and a brief intense rain occurs, the flooding will recede in 3-7 days. If the soil has been saturated, and a large rain or snowmelt event occurs, several weeks may pass before the cave drains. This indicates a constriction in the downstream portions of the flow system.

4. METHODS

Methods employed to evaluate Kooken Cave as a long-term sediment trap included mapping, field observation, stratigraphic description, and paleomagnetic analysis of cave sediments. Field work has been ongoing in the cave, mainly for the purposes of exploration and mapping. This includes 55 visits by one of the authors (B. Crowell), resulting in excellent familiarity with the geologic and hydrologic features of the cave. The cave was mapped using compass and tape, from which maps and profiles were constructed. Paleomagnetic sampling was conducted during a one-day visit. The cave was examined westward from the eastern entrance, in a reconnaissance to find the most complete section of cave sediments. An area informally known as the Dining Room has the most complete section, and sampling was conducted in this vicinity (Figs. 2, 3, 4). Beginning with the top of the section, paired paleomagnetic samples were taken to provide broad coverage of the entire column. Samples were collected in specially designed, demagnetized plastic boxes (8 mL volume). The moist nature of the sediment

allowed for the boxes to be pressed in to the cleaned face of the outcrop. The number of the sample was written on the box while in position, and the strike, dip, and tilt of the sample were measured with a Brunton compass (Sasowsky et al., 1995) with declination set to zero. The samples were then excavated with a plastic spatula, capped, cleaned, and packaged for transport. The position of the sample with respect to a known (surveyed) elevation in the cave was measured with a fiberglass tape, and a description of the stratigraphy was made at that time. A total of 12 sample pairs (24 samples) were collected for paleomagnetic analysis (sample identification numbers IDS468 through IDS491).

Samples were analyzed intact in their plastic cubes, at the University of Pittsburgh Paleomagnetic Laboratory. First, the sample orientations were corrected for declination using the GeoMAG computer program and IGRF95 magnetic model (National Oceanic and Atmospheric Administration - National Geophysical Data Center, 2000). A declination of −10.2° and an inclination of 69° were found for the date and location of interest. Following this, a large-bore, 3-axis 2-G superconducting rock magnetometer (SRM) was used to measure sample magnetic orientation and strength. To further enhance sample signal, the device was zeroed before each sample. Stepwise alternating field (AF) demagnetization was used to progressively demagnetize the samples. Analytical instruments were housed in a magnetically shielded room that reduced the earth's present field (PDF) strength to below 2.5×10^{-4} millitesla (mT).

Samples were demagnetized in 5 to 7 steps ranging between 0 (NRM) to 110 mT. Orthogonal vector plots (Zijderveld, 1967) were constructed for each sample. Through inspection of the plots, points were chosen for principal component analysis to extract the characteristic remnant magnetic vector of interest (Kirschvink, 1980). Lower-coercivity demagnetization directions were visually removed from high-coercivity directions. Mean directions for sample pairs, as well as all 24 samples, were determined using Fisher (1953) statistics. Magnetic susceptibility of all samples was measured (2 orientations, 3 repeats) in a Sapphire Instruments Model SI-2 instrument.

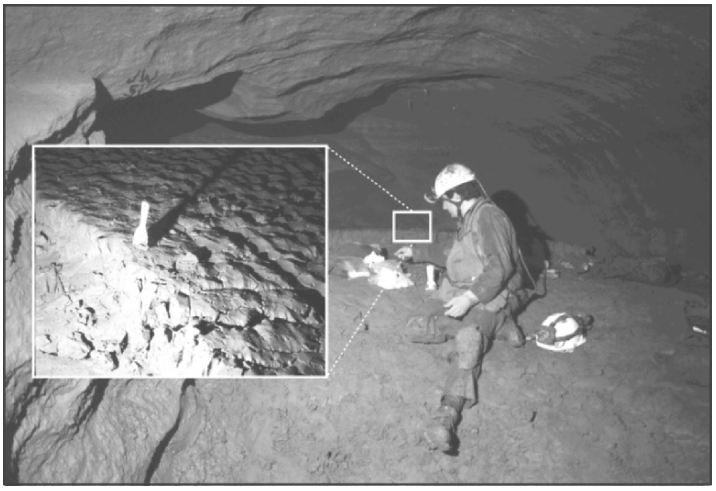

Figure 4. Photograph composite view of the uppermost sedimentary deposit investigated in Kooken Cave. The top surface is at an elevation of 875 feet amsl (267 m), and is moist and mud-cracked.

5. RESULTS & DISCUSSION

5.1. Sediments and Hydrology

The results of the sediment analysis are shown in Figure 5. The paleomagnetic results are all similar to those pictured in Figure 6 and all samples exhibit normal polarity (Figure 7). The exact source and fate of water and sediments in the cave has not been satisfactorily determined through dye-tracing, though this has been previously attempted (W. B. White, personal communication). The proximity of the western part of the cave to known influent surface streams (Fig. 1) suggests that one or more of these streams is the input source to the cave. Clastic sediments found within the cave are non-carbonate detrital materials derived from the flank of Brush Mountain. The cave floods rapidly following precipitation events, which is concordant with the model of input from a nearby sinking-stream.

What is peculiar about this flow system is the relatively lengthy recession of the flood, which must result from restriction in the downstream flow direction. We are handicapped by the inaccessibility of these parts of the flow route, but some basic features can be determined. Calculation along a hypothetical flow path to the Little Juniata River near Ruth Cave gives the following results for low-stage conditions. The elevation of East Lake water is 803 ft amsl (245 m). The straight-line distance from East Lake to Little Juniata River is 7000 ft (2130 m). The elevation of the Little Juniata River is 750 ft amsl (228 m). Using the difference in elevation (53 ft; 16 m) and the distance between points, a hypothetical horizontal hydraulic gradient of 0.0076 is obtained. This represents the driving force to drain the cave. Under extreme flood conditions, when the water in the cave has 42 ft (13 m) of additional head, this gradient would be 0.014; a 84% increase. Despite the differences in magnitude, both of these gradients are more than adequate to drive significant groundwater flow. In a non-karstified aquifer, flow rates on the order of feet per day might be expected. In an open karst conduit, much greater rates (up to 100's of feet per hour) would result. However, the open conduit rates are not found in this aquifer, as shown by the long time needed to drain the cave.

The sediments themselves give some indication of what causes the slow drainage of the cave after a flood. It is useful to envision an early time in the history of the cave, when it had been dissolved from the limestone, and was as yet unfilled with sediments. At some time after this, breaching of the cave by the surface stream allowed copious water and sediments to enter. These initial sediments are preserved in the cave, in the lowest positions. The left column in Figure 5 shows the stratigraphy of the examined sediment deposits. The lower 6 feet consists of sand and cobbles, along with moist, finely laminated clay. We believe that this coarse sediment is the initial flood-borne material emplaced soon after the cave was breached. These coarse sediments moved through the cave, until they reached a constriction in the bedrock channel where they were trapped. They would be difficult to move once deposited, due to decreased gradients away from the stream swallow point. Once the initial "plugging" of the outlet had occurred, subsequent deposits would likely be finer, due to the decreased competence of slower moving water. Figure 5 shows that the deposits above the coarse layer are moist, finely laminated, medium-brown clay.

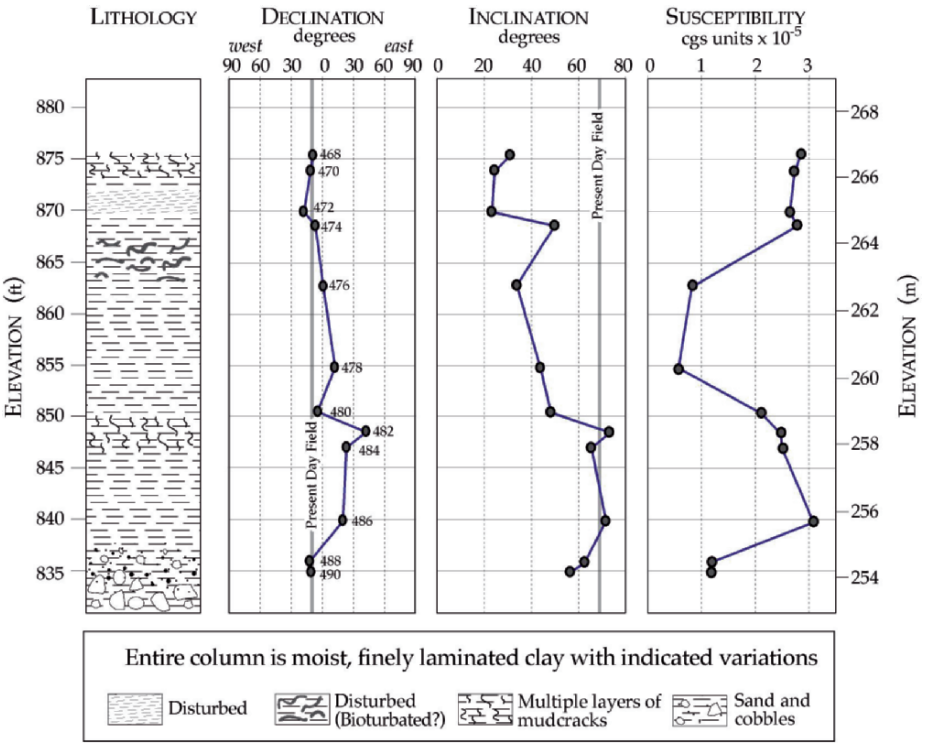

Figure 5. Summary diagram showing elevation, sediment lithology, and overall magnetic results from Kooken Cave. Each dot represents a sample pair (averaged), starting with samples IDS468/489 at top, and ending with IDS 490/491 at the bottom. Vertical gray lines show present-day field values for declination and inclination.

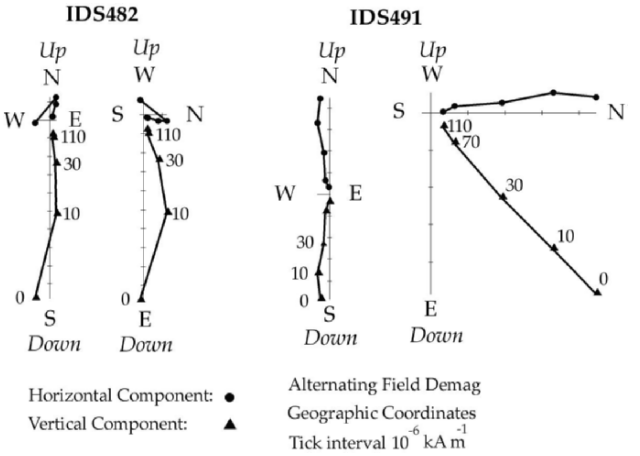

Figure 6. Vector endpoint (Zijderveld) diagrams for typical paleomagnetic samples from Kooken Cave. Both samples shown have normal polarity. Sample IDS482 shows a weak viscous magnetization that was removed by application of a 10 mT alternating field demagnetization.

5.2. Magnetism of sediments

Kooken Cave was chosen for study because of its potential to contain datable paleohydrologic records in its fine clastic sediments. In particular, the presence of magnetically reversed sediments would constrain the age of the cave. All of the samples had well-preserved depositional remnant magnetization (DRM). Typical vector endpoint diagrams are shown in Figure 6. A few of the samples had a weak viscous remnant magnetization (VRM) that was random, and easily removed by application of a 10 mT alternating field demagnetization. Magnetic behavior was straightforward, with decay of the magnetic vector directly toward the origin.

All magnetic samples exhibit normal polarity. This is an active area of sedimentary deposition, which strongly suggests that the deposit originated in the present magnetic chron, and has an age of less than 780 ka (Cande and Kent, 1995). A plot of field directions (Fig. 7) shows that the samples clustered around the present-day field (PDF), but with considerable scatter. Figure 5 shows the detailed magnetic behavior of the sediments in stratigraphic context. Most of the magnetic declinations are east of the expected value. Based on agreement between sample pairs, this appears to represent a true record of paleosecular variation (magnetic pole drift), rather than sampling error. Inclinations, for the most part, were less than predicted by the PDF. In our experience with cave sediments, this "shallowing" is normal, and results from depositional and post-depositional compaction of detrital grains. However, we usually find that the inclinations in the uppermost part of the column are closest to the PDF. The opposite is true in Kooken, for unknown reasons.

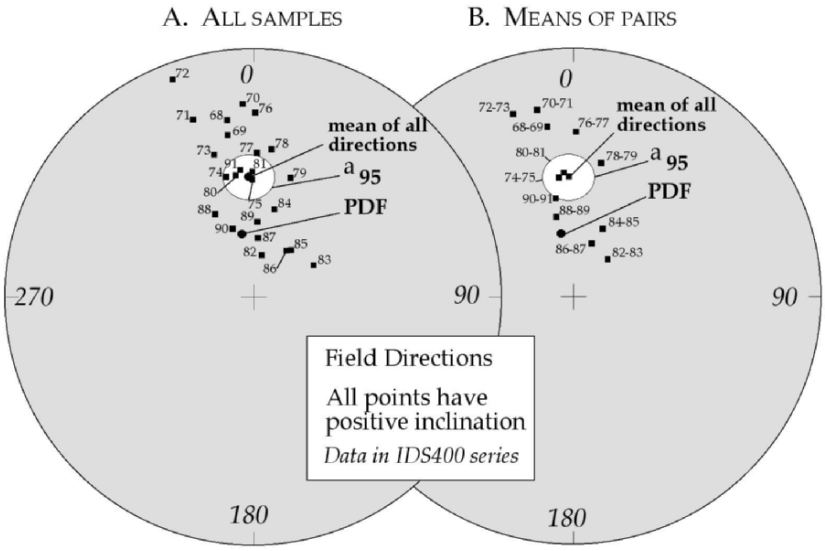

Figure 7. Lambert equal-area stereoplots of all magnetic sample directions (A) and means of sample pair directions (B). Present Day Field (PDF) is shown as a black dot. Mean of all directions and alpha-95 confidence interval (white ellipse) also shown. Sample numbers are all in IDS400 series (i.e. "72" means "IDS472").

Magnetic susceptibility (MS) is often used as a proxy for changes in sediment source or degree of weathering (e.g. Banerjee, 1995; Maher and Thompson, 1999). Measured MS values from the Kooken Cave deposit (Fig. 5) vary between 5.7×10^{-6} and 3.1×10^{-5} (dimensionless cgs units). These values are typical of those that we have seen from studies of other caves in the Appalachian Highlands. There seems is an apparent bimodal distribution of MS values, with some clustering near 1×10^{-5}, and others nearer to 3×10^{-5} (Fig. 5). This variation probably does represent a change in sediment characteristics, but with the limited sampling, it is not possible to attribute the change to any specific variable or event.

The absence of a reversal, and uncertainties about depositional continuity for paleosecular variation, make it difficult to assign an age (duration of sediment collection) to Kooken Cave on a paleomagnetic basis. Therefore, we used two other approaches to constrain the age; present sediment accumulation rates in the cave, and elevation of the cave relative to local base-level.

We can employ a rough calculation based upon sediment accumulation rates. Observations in the cave show that after each flood, approximately 1/16 to 1/4 inch (2 to 6 mm) of sediments accumulate. Assuming an average 1/8-inch (3 mm) accumulation, with 3 floods per year, an accumulation of 3/8-inch (9.5 mm) or 0.03125 feet (0.0095 m) per year could be expected. The overall thickness of sediments measured in the cave is about 45 feet (14 m), which at the stated accumulation rate could have accrued in 1,440 years. This number is based on the above assumptions, as well as continuous deposition and no erosion, all of which may be unmet.

The elevation of the cave in relation to local base-level may also serve to constrain the age of the cave. The morphology of the cave makes it reasonable to believe that it formed at or above local base-level. The lowest portions of the cave are presently at about 53 ft. (16 m) above the Little Juniata River. As an end-member calculation, let us assume that the cave formed at base-level and had a negligible gradient toward the surface stream. Furthermore, let us assume an incision rate of 0.05 m/ka (Sasowsky et al., 1995). Under such conditions the river could have cut this distance below the cave in 320 ka, yielding a similar age for the cave. Because we do not know the actual gradient that was present when the cave formed, this number should be considered a maximum possible value.

6. CONCLUSIONS

Kooken Cave has functioned as a long-duration trap for sediments washed in from a nearby sinking stream. The ultimate outlet for waters and sediments from the cave is unknown, but is likely to be springs on the Little Juniata River. Flooding in the cave occurs at least annually. This flooding results from partial blockage of flow in the karst system, probably by a mixture of fine and coarse sediments. Magnetic analysis of 45 ft (14 m) of the sediments reveals that they all have normal polarity, suggesting that they have been deposited in the present chron (<780 ka). However, paleosecular variation in the sediments reveals a record that could extend back hundreds or thousands of years. Rough calculation using estimated sediment accumulation rates shows that all sediments in the cave could have been deposited in 1,440 years. It is highly possible that wood harvesting and agricultural development of overlying land within the last 200 years has accelerated sediment accumulation in the cave. Expected river incision rates and other geomorphic constraints lead to an age of <320 ka for the cave. Based on all of these factors, it is likely that Kooken Cave has existed for at least 100 ka and has been

accumulating sediments for 1,000 to 10,000 years. An extremely detailed stratigraphic and paleomagnetic study might allow correlation with known secular variation records, and evaluation of agricultural impacts.

7. ACKNOWLEDGMENTS

We greatly appreciate receiving access to the cave through the owner, Luke Martin, and the Huntingdon County Cave Hunters (National Speleological Society). Please note that Kooken Cave is gated, and access is by written prior permission only. Photographs were taken by Peter Sasowsky. Mick O'Mahony helped with the field work. Karen Traugh helped with analysis of the paleomagnetic samples. Support for the University of Pittsburgh Paleomagnetic Laboratory was provided by the National Science Foundation. The efforts of Mark Jancin and an anonymous reviewer were very helpful in improving the paper.

8. REFERENCES

Banerjee, S.K., 1995, Chasing the paleomonsoon over China: Its magnetic proxy record: GSA Today, v. 5, p. 93-97.

Berg, T.M., and Dodge, C.M., 1981, Map 61 - Atlas of preliminary geologic quadrangle maps of Pennsylvania: Harrisburg, Pennsylvania Topographic and Geologic Survey (also available at http://www.dcnr.state.pa.us/topogeo/map61/61intro.htm).

Cande, S.C., and Kent, D.V., 1995, Revised calibration of the geomagnetic polarity timescale for the Late Cretaceous and Cenozoic: Journal of Geophysical Research, v. 100, p. 6093-6095.

Devitt, W.H., III, 1953, Kooken - Pennsylvania's toughest cave: National Speleological Society Bulletin, v. 15, p. 31-33.

Fisher, R.A., 1953, Dispersion on a sphere: Royal Society of London, Proceedings, Series A, v. 217, p. 295-305.

Kennedy, J.W., 1990, The Ruth Cave project report: Nittany Grotto News (Natlonal Speleogical Society), v. 38, p. 2-19.

Kirşchvink, J.L., 1980, The least-squares line and plane and the analysis of paleomagnetic data: Royal Astronomical Society Geophysical Journal, v. 62, p. 699-718.

Maher, B.A., and Thompson, R., 1999, Quaternary climates, environments, and magnetism: Cambridge, Cambridge University Press, p. 390.

McCarthy, S.C., 2001, Using dye tracers to delineate flow patterns through two karst basins:Kooken Cave, Huntingdon County and Tytoona Cave, Blair County, PA [B.S. thesis], The Pennsylvania State University, 71 p..

National Oceanic and Atmospheric Administration - National Geophysical Data Center, 2000, Geomagnetic Field Synthesis Program (GeoMAG): http://www.ngdc.noaa.gov/seg/potfld/faqgeom.html.

Sasowsky, I.D., White, W.B., and Schmidt, V.A., 1995, Determination of stream incision rate in the Appalachian plateaus by using cave-sediment magnetostratigraphy: Geology, v. 23, p. 415-418.

Shultz, C.H., 1999, The geology of Pennsylvania: Harrisburg - Pittsburgh, Pennsylvania Geological Survey - Pittsburgh Geological Society, 888 p.

Zijderveld, J.D.A., 1967, A.C. demagnetization of rocks: Analysis of results, *in* Collinson, D.W., Creer, K.M., and Runcorn, S.K., eds., Methods in paleomagnetism: Amsterdam, Elsevier, p. 254-286.

PROVENANCE OF SUSPENDED SEDIMENT DISCHARGED FROM A KARST AQUIFER DETERMINED BY CLAY MINERALOGY

F. Leo Lynch, Barbara J. Mahler, and Nico N. Hauwert*

1. INTRODUCTION

Barton Springs is the fourth largest spring in Texas (Brune, 1981). It is the major discharge point for a segment of the Cretaceous Edwards Limestone karst aquifer. Water from Barton Springs is a significant component of the water resource of Austin, the 21st largest city in the United States. Barton Springs is also a heavily used recreational spot, and it is the sole home of the Barton Springs Salamander (*Eurycea sosorum*), an endangered species that is extremely vulnerable to changes in water quality (Mahler and Lynch, 1999).

Although in general water quality at Barton Springs is good, there have been occurrences of contamination across the aquifer. Petroleum hydrocarbons, arsenic, lead, pesticides, and other compounds have been identified from aquifer wells (Hauwert and Vickers, 1994). Many of these compounds sorb onto solid surfaces in much higher concentrations than their concentration in water.

After high rainfall (~1") events in the watershed, the water discharged from Barton Springs is noticeably turbid. The purpose of this project was to investigate the mineralogy of the suspended sediment discharged from Barton Springs in order to learn about its provenance and its potential to serve as a vector for contaminant transport through the aquifer.

* F. Leo Lynch, Department of Geosciences, Mississippi State University, Mississippi State, Mississippi, 39762. Barbara J. Mahler, Department of Geological Sciences, The University of Texas at Austin, Austin, Texas, 78712 (Present address: U.S. Geological Survey, Austin, Texas, 78754). Nico N. Hauwert, Department of Geological Sciences, The University of Texas at Austin, Austin, Texas, 78712.

2. GEOLOGIC FRAMEWORK AND METHODS OF ANALYSIS

The Barton Springs segment of the Edwards aquifer (referred to here as the Barton Springs aquifer) extends across 391 km^2 southwest of Austin, Texas, and is composed of eastward-dipping limestones and dolomites of the Upper Cretaceous Edwards and Georgetown Limestones. The aquifer is bounded to the north by the Colorado River, to the west by the limit of the geologic units, to the south by a groundwater divide, and to the east by the "bad-water line, beyond which the water contains more than 1000 mg/l TDS (Slade et al., 1986). Karstification of Edwards lagoonal and rudist reef deposits began during periods of subareal exposure in the Cretaceous and continued in the Tertiary when formation of the NNE trending Balcones fault zone allowed further infiltration of meteoric waters (Rose, 1972; Maclay and Small, 1984; Slade, 1986). The Edwards Formation conformably overlies the lower Cretaceous Glen Rose Limestone, and is unconformably overlain by the Georgetown Limestone, which in turn is overlain by the relatively impermeable Del Rio Clay and the Buda Limestone.

The Barton Springs aquifer and its watershed are divided into three components (Fig. 1). The contributing zone is that portion of the watershed where the Glen Rose Limestone outcrops. The outcrop of the Edwards and Georgetown Limestones (hereafter referred to as simply the Edwards Limestone), and smaller amounts of Del Rio Clay and Buda Limestone, define the recharge zone. Eastward of the Balcones fault zone and the recharge zone, the Barton Springs aquifer system consists of the porous and permeable Edwards Limestone sandwiched between the relatively impermeable Del Rio Clay and Buda Limestone at the surface and the Glen Rose Limestone at depth. Surface water flows east across the contributing zone via one of six main creeks. As these creeks cross onto the recharge zone, surface water infiltrates through sinkholes and fractures in the streambed providing 85% of the total aquifer recharge (Slade et al., 1986). The direction of groundwater flow is NNE and follows the trend of the Balcones fault zone. Approximately 90% of aquifer flow discharges at Barton Springs in central Austin.

Suspended sediment from Barton Springs (20 samples) was collected during two flood events by in-line centrifugation of large volumes of water. Sediment and rock samples (n=120) were also collected from creeks, sinkholes, caves, soils, and outcrops in the contributing and recharge zones, and from caves , wells, and outcrops in the confined zone (Mahler and Lynch, 1999; Mahler et al., 1999). Whole rock and <2 μm fraction samples were analyzed by X-ray diffraction (XRD). The quantitative mineralogical composition of a representative subset of the samples was determined using the techniques described in Lynch (1997).

3. RESULTS

The suspended sediment discharged from Barton Springs consists of clay minerals (~35%), dolomite (~35%), calcite (~15%) and quartz (~15%) (Fig. 2A) (Mahler and Lynch, 1999). Sediments in karst aquifers can originate both at the surface (allochthonous) and within the aquifer (autochthonous). Figure 2B shows that the same mineral assemblage discharged from Barton Springs does exist autocthonously in the Edwards Limestone. However, with the exception of several marls, Figure 2B also shows that quartz and clay minerals do not occur in abundance in the Edwards. Figure

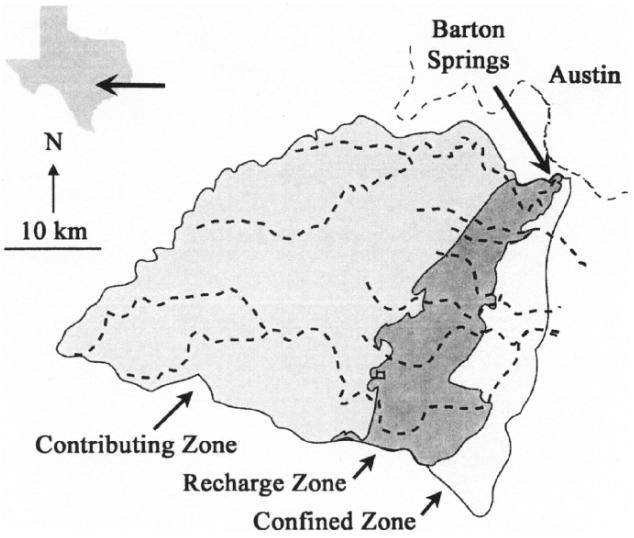

Figure 1. Location of the Barton Springs study area.

2C shows that calcite, quartz, and clay minerals also exist in the rocks and sediments found at the surface of the contributing and recharge zones.

The dolomite fraction of the suspended sediment is the only mineralogical component of the suspended sediment that is unambiguously autochthonous. Members of the Edwards Limestone that contain abundant dolomite are very rarely exposed at the surface in the recharge zone, and are almost totally absent in the soils and sediments of the contributing zone (Small et al., 1996). The "hollow box" texture of the dolomite observed in the discharged sediment (Fig. 3A) has been observed in petrographic study of Edwards rocks (Ellis, 1986). Clearly allochthonous components of the discharged sediment are woody organic matter (Fig. 3B), and pink, green, and blue filaments that are probably some type of man-made fiber (Fig. 3C).

Determination of an autochthonous or allochthonous source for the calcite, quartz, and clay mineral components of the discharged sediment is more problematic. The rocks of both the contributing and recharge zones, the Glen Rose and Edwards Limestones respectively, are grossly similar. Both are complex geological units composed of platform, lagoonal, shoreface, tidal flat, and shallow marine limestones and marls (Stricklin et al., 1970; Rose, 1972; Ellis, 1986; Woodruff, 1993; Woodruff et al., 1994; Havorka et al., 1996, and many others). The soils and sediments derived by the weathering of the rocks (calcite, clay minerals, and quartz), are also grossly similar. However, more detailed investigation of the clay mineral suites from the different samples does show significant differences.

3.1 Clay Mineralogy of Suspended Sediment

Figure 4 is the XRD pattern of the <2 μm fraction (oriented and glycol-solvated) of the suspended sediment discharged at Barton Springs. Though some quartz, calcite, and

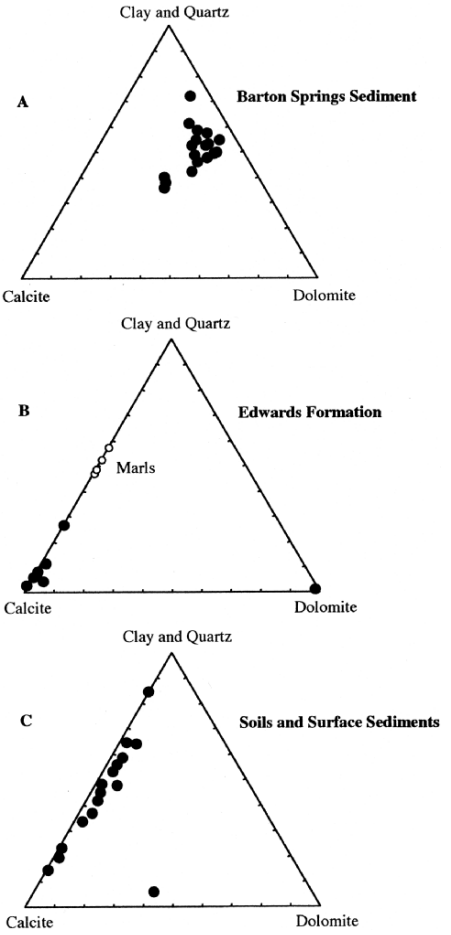

Figure 2. Relative mineralogy of (A) suspended sediment discharged at Barton Springs, (B) samples of the Edwards Formation, and (C) soil and stream sediment from the contributing and recharge zones.

dolomite does exist in the sample, it is composed predominately of clay minerals. The clay minerals present are kaolinite (38%), illite (24%), and mixed-layer illite/smectite (37%). The peak at 5.34 Å indicates that the illite/smectite (I/S) contains ~60% illite layers (60%I), and the 16.9 Å peak shows that the I/S is randomly interstratified (R0). For the purpose of this paper, randomly interstratified I/S with 55-65% I will be identified as Barton Springs I/S (BS I/S). For further explanation of clay mineralogy and mixed-layering, interested readers are referred to Moore and Reynolds (1997).

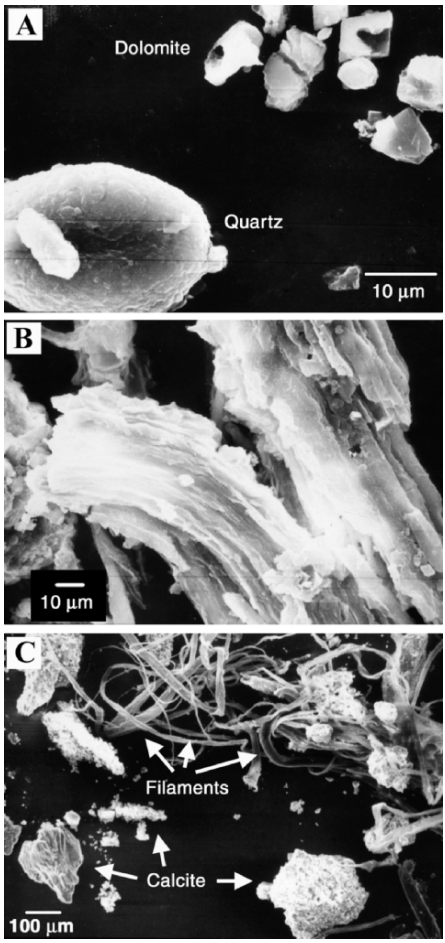

Figure 3. Scanning electron microscope images of suspended sediment discharged at Barton Springs.

3.2 Autochthonous Clays

Figure 5 shows XRD patterns of the <2 µm fraction (oriented and glycol-solvated) of samples of autochthonous clays in the Edwards Limestone, and the <2 µm fraction (oriented and glycol-solvated) of the suspended sediment discharged at Barton Springs. Marls in the Edwards Limestone are composed of kaolinite, illite, and I/S, however, the position of the I/S peak at 13.2 Å in the marl indicates ordered interstratification as opposed to the random interstratification in the BS I/S (16.9 Å peak). Furthermore, the peak at 5.2 Å shows that the I/S from the marl has a larger %I than the BS I/S (~80%I vs. ~60%I). This indicates that the marls in the Edwards Limestone are not the source of either the BS I/S or, by inference, the other clays and quartz in the sediment discharged from Barton Springs.

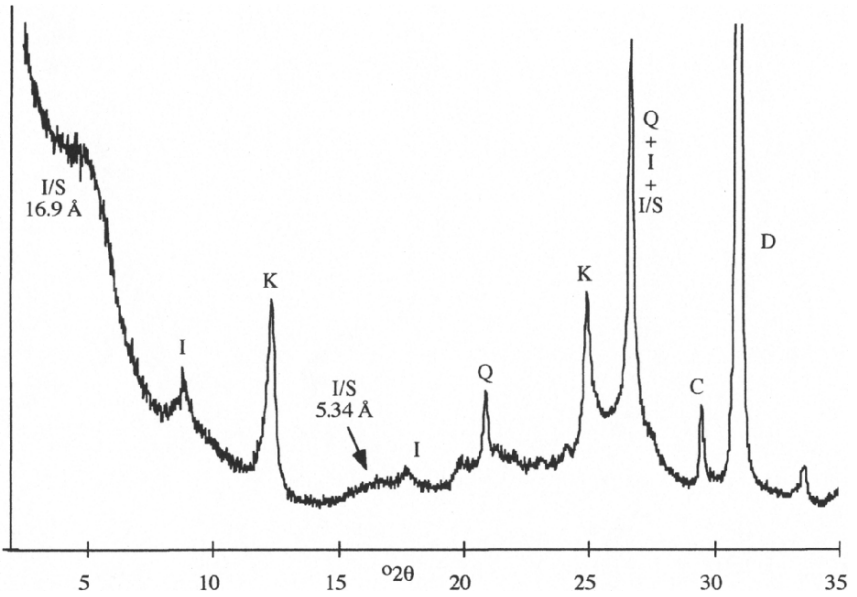

Figure 4. XRD pattern of the <2 μm fraction (oriented and glycol solvated) of suspended sediment discharged from Barton Springs. Minerals present are illite/smectite (I/S), illite (I), kaolinite (K), quartz (Q), calcite (C), and dolomite (D).

The Pleistocene *terra rossa* of central Texas is a soil that developed during times of tropical weathering between 0.7 and 2.0 m.y.b.p. Today it is found almost exclusively as an uncommon cave fill in the Edwards Limestone (Young, 1986). Analysis of the XRD pattern of the terra rossa indicates that it is composed of interstratified kaolinite/smectite and is clearly not the source for the BS I/S (Fig. 5).

Most caves in the Edwards Limestone do contain a clay suite very similar to the clays found in the suspended sediment discharged from Barton Springs. The I/S in the cave clays is identical to the BS I/S (Fig. 5). The presence of laminations in some cave clay deposits indicates that, like the *terra rossa*, the clastic material was washed into caves and was not derived from dissolution of the Edwards Limestone (Kastning, 1986; Ellis, 1986; Havorka et al., 1996). Similarity of clay suites in the caves and in the discharged sediment implies that the source area for the clays, and the processes leading to its deposition in caves or transport through the aquifer, have been the same for an extended period of time.

3.3 Allochthonous Clays: Recharge Zone Soils

Figure 6 shows XRD patterns of the <2 μm fraction (oriented and glycol-solvated) of samples of soils found in the recharge zone. The 17 Å, 8.4 Å and 5.64 Å peaks in the pattern of Edwards soil A show that smectite, not BS I/S, is present in that sample. Furthermore, Edwards soil A does not contain illite, which is present in the Barton Springs suspended sediment. Therefore, Edwards soil A is not the source of the clastic material discharged from Barton Springs. Neither is Edwards soil B, which is also found

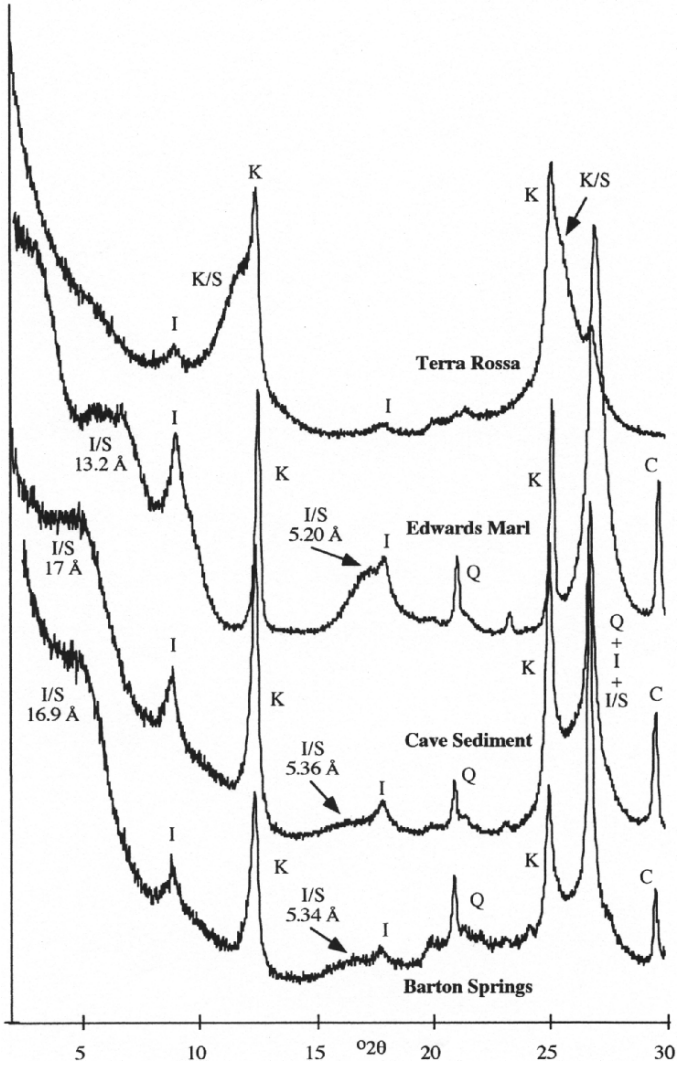

Figure 5. XRD patterns of the <2 μm fraction (oriented and glycol solvated) of Edwards Limestone autochthonous clay samples. K/S = kaolinite/smectite, other peak labels as in Figure 4.

on some members of the Edwards Limestone in the recharge zone, since it is dominated by interstratified kaolinite/smectite and does not contain BS I/S.

The I/S peak at 11.8 Å in the pattern of soil developed on the Del Rio Clay indicates ordered interstratification as opposed to the random interstratification in the BS I/S (16.9 Å peak). Soils developed on the Buda Limestone contain smectite and yield XRD patterns similar to Edwards soil A. Therefore, neither the Del Rio Clay nor the Buda Limestone is the source of the Barton Springs suspended sediment.

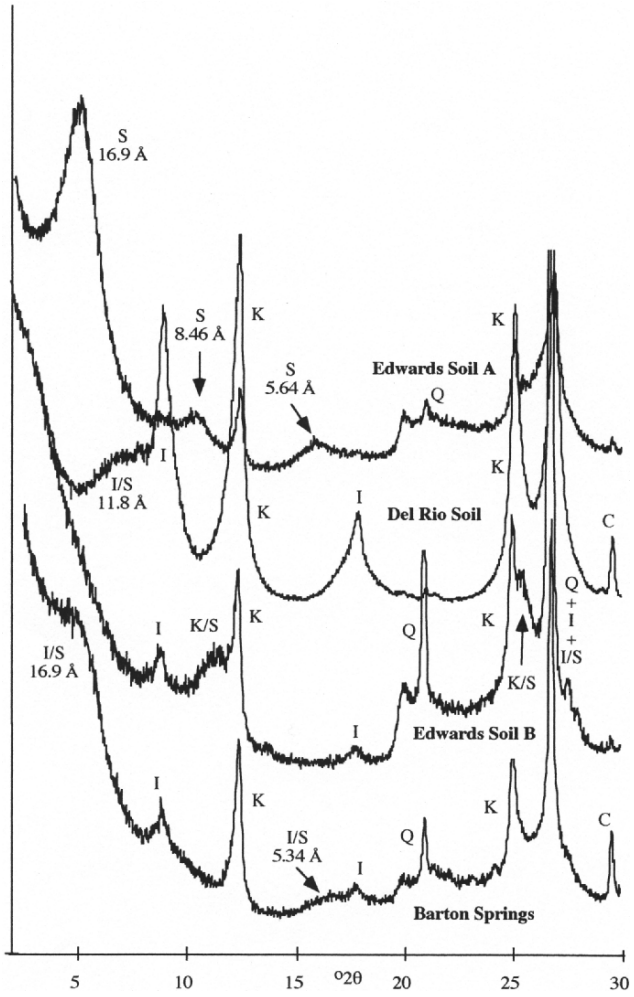

Figure 6. XRD patterns of the <2 μm fraction (oriented and glycol solvated) of soils from the recharge zone. S = smectite, other peak labels as in Figure 5.

3.4 Allochthonous Clays: Contributing Zone Soil and Stream Sediment

Soils developed on the Glen Rose Limestone in the contributing zone contain the identical clay mineral suite as is present in the suspended sediment discharged from Barton Springs (Fig. 7). The <2 μm fraction of samples of stream sediments from both the contributing and recharge zones also contain the same clay mineral suite. This data implies that at least the clastic component of the suspended material discharged from Barton Springs originated as soil in the contributing zone. Storm events mobilized the soil in the contributing zone and transported it to the recharge zone where it entered the

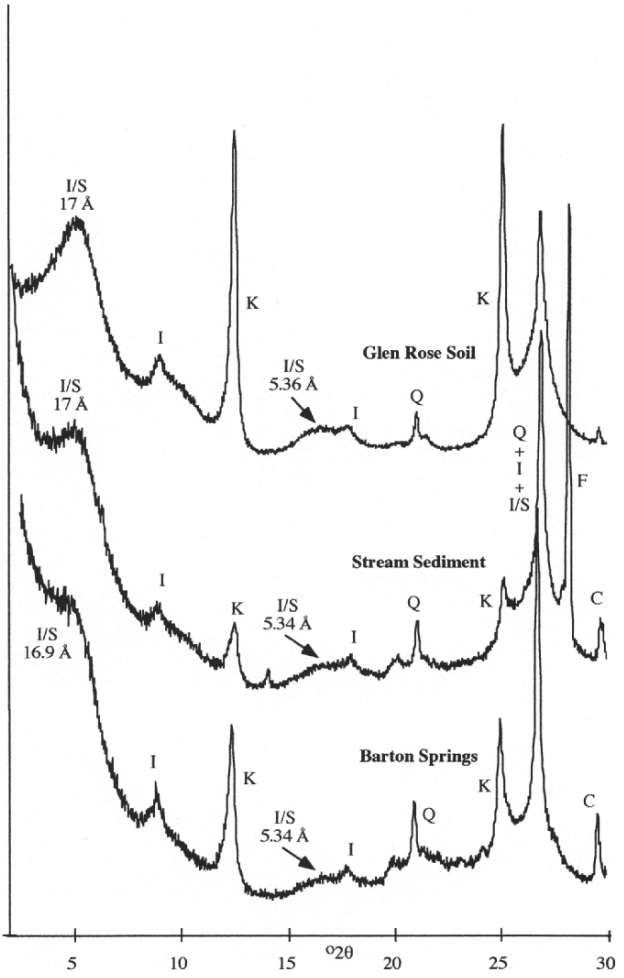

Figure 7. XRD patterns of the <2 μm fraction (oriented and glycol solvated) of soil and stream sediment from the contributing zone. F = feldspar, other peak labels as in Figure 4.

aquifer through losing streams. The sediment traveled through the aquifer and was discharged at Barton Springs.

Is this conclusion plausible? The contributing zone of the Barton Springs aquifer, which accounts for almost 75% of the aquifer watershed (Slade, 1986), is located in the Texas Hill Country. The stair-step morphology of the Texas Hill Country is due to alternating layers of hard limestone and soft marls (Wilding, 1993; Woodruff et al., 1994). Compared to the Edwards Limestone, the Glen Rose Formation is a marl-rich, therefore clay-rich, unit (R. L. Folk, pers. com.), so the source terrain for the discharged sediment does exist. Great potential for soil erosion also exists because the contributing zone contains abundant small, high gradient streams. Furthermore, the Austin area has

one of the highest probabilities of flood producing storms in the United States (Woodruff, 1993). Indeed, proof that this process is operating is apparent to anyone who lives near Barton Springs whenever it rains. Flowing creeks and Barton Springs are usually clear, however, after a heavy rain in the watershed, the creeks on the contributing and recharge zones are muddy and turbid water is discharged from Barton Springs.

4. CONCLUSIONS

The study shows the utility of clay studies to karst hydrology. These data show that suspended sediment discharged from a karst aquifer can be derived from erosion of soil tens of kilometers away from the recharge zone of the aquifer. The data also show that other clearly allochthonous material, such as wood and (probably man-made) fibers travel through the aquifer and are discharged at the springs.

In the specific case of Barton Springs, these results are troubling. Austin Texas is the 21st largest city in the United States, bracketed by Boston and Seattle. According to the U.S. census, the Austin metropolitan area, with a population of 1.1 million people, had the fifth highest growth rate in the nation in the 1990s, increasing by over 30%. Much of that growth is into the Texas Hill Country which is the contributing zone of the Barton Springs aquifer and the source area of the suspended sediment discharged from Barton Springs. Surface sediments with high organic and clay mineral content, such as those found in the contributing zone, can act as vectors of pollutant and bacterial transport (Hauwert and Vickers, 1994; Mahler et al., 1999). These results must be kept in mind while formulating plans for further growth and environmental protection.

5. ACKNOWLEDGMENTS

The authors are grateful to A. Foos and an unidentified reviewer for their helpful comments.

6. REFERENCES

Brune, J.H., 1981, *Springs of Texas*, Branch-Smith Inc., Fort Worth.

Ellis, P. M., 1986, Post-Miocene carbonate diagenesis of the lower Cretaceous Edwards Group in the Balcones fault zone area, South-Central Texas, in: *The Balcones Escarpment, Central Texas*, P. L. Abbott and C. M. Woodruff Jr., eds., Geological Society of America Annual Meeting, San Antonio, pp. 101-114.

Hauwert, N., and Vickers, S., 1994, *Barton Springs/Edwards Aquifer Hydrogeology and Groundwater Quality*, submitted by the Barton Springs Edwards Aquifer Conservation District to the Texas Water Development Board.

Havorka, S. D., Dutton, A. R., Ruppel, S. C., and Yeh, J. S., 1996, *Edwards aquifer ground-water resources: geologic controls on porosity development in platform carbonates, South Texas*, The University of Texas, Bureau of Economic Geology, Report of Investigations, **238**, Austin, 75 p.

Kastning, E. H., 1986, Cavern development in the New Braunfels are, Central Texas, in: *The Balcones Escarpment, Central Texas*, P. L. Abbott and C. M. Woodruff Jr., eds., Geological Society of America Annual Meeting, San Antonio, pp. 91-100.

Lynch, F. L., 1997, Frio shale mineralogy and the stoichiometry of the smectite-to-illlite reaction: the most important reaction in clastic sedimentary diagenesis, *Clays Clay Miner.* **45**: 618-631.

Maclay, R. W., and Small, T. A., 1984, *Carbonate geology and hydrology of the Edwards aquifer in the San Antonio area, Texas*, United States Geological Survey, Open-File Report 83-537.

Mahler, B. J., and Lynch, F. L., 1999, Muddy waters: temporal variation in sediment discharging from a karst spring, J. Hydrol, **214**:165–178.

Mahler, B. J., Lynch, L., and Bennett, P. C., 1999, Mobile sediment in an urbanizing karst aquifer: implications for contaminant transport, *Env. Geology*, **39**:25–38.

Moore, D. M., and Reynolds, R. C., Jr., 1997, *X-ray Diffraction and the Identification and Analysis of Clay Minerals, 2nd edition*, Oxford University Press, New York, 378 p.

Rose, P. R., 1972, *Edwards group, surface and subsurface, Central Texas*, The University of Texas, Bureau of Economic Geology, Report of Investigations, **74**, Austin.

Slade, R. J., Jr., 1986, Large rainstorms along the Balcones escarpment in Central Texas, in: *The Balcones Escarpment, Central Texas*, P. L. Abbott and C. M. Woodruff Jr., eds., Geological Society of America Annual Meeting, San Antonio, pp. 15-20.

Slade, R. M., Jr., Dorsey, M., and Stewart, S., 1986, *Hydrology and Water Quality of the Edwards Aquifer associated with Barton Springs in the Austin Area, Texas,* U.S. Geological Survey Water-Resources Investigations 86–4036.

Small, T. A., Hanson, J. A., and Hauwert, N. M., 1996, *Geologic framework and hydrogeologic characteristics of the Edwards aquifer outcrop (Barton Springs segment), NE Hays and SW Travis Co., Texas*, United States Geological Survey, WRI 96-4306.

Stricklin, F. L., Smith, C. I., and Lozo, F. E., 1970, Stratigraphy of the lower Cretaceous Trinity deposits of Central Texas, The University of Texas, Bureau of Economic Geology, Report of Investigations, **71**, Austin, 63 p.

Wilding, L. P., 1993, Soils of tributary sub-basins in the Barton Creek watershed – implication for a reappraisal of Hill Country soils, in: *Soils, landforms, hydrologic process, and land-use issue – Glen Rose Limestone terrains, Barton Creek watershed*, C. M. Woodruff Jr., W. M. Marsh, and L. P. Wilding, eds., Travis County, Texas, Society of Independent Professional Earth Scientists, Central Texas Chapter, Field report and guidebook, pp. 3-1- 3-12.

Woodruff, C. M., Jr., 1993, Geology and physiology of Glen Rose limestone terrains, Barton Creek watershed, Central Texas, in: *Soils, landforms, hydrologic process, and land-use issue – Glen Rose Limestone terrains, Barton Creek watershed*, C. M. Woodruff Jr., W. M. Marsh, and L. P. Wilding, eds., Travis County, Texas, Society of Independent Professional Earth Scientists, Central Texas Chapter, Field report and guidebook, pp. 2-1- 2-12.

Woodruff, C. M., Jr., Wilding, L. P., and Marsh, W. M., 1994, *Edwards aquifer–water quality and land development in the Austin area, Texas*, Gulf Coast Association of Geological Societies, 44th annual convention, Field trip guidebook, Austin, 66p.

Young, K., 1986, The Pleistocene *Terra Rossa* of Central Texas, in: *The Balcones Escarpment, Central Texas*, P. L. Abbott and C. M. Woodruff Jr., eds., Geological Society of America Annual Meeting, San Antonio, pp. 63-70.

READING VIRGINIA'S PALEOCLIMATE FROM THE GEOCHEMISTRY AND SEDIMENTOLOGY OF CLASTIC CAVE SEDIMENTS

Elizabeth P. Knapp, Dennis O. Terry, David J. Harbor, and Robert C. Thren*

1. ABSTRACT

Clastic sediments in Bathers Cave, Virginia, are divided into distinct packages that reflect changes in water velocity, sediment source, surficial weathering conditions, and the cave depositional setting that are a function of Quaternary climate change. These packages are found in the same stratigraphic order at various levels on ledges within passages of elliptical cross section in the upper part of the cave system. Sediment extractions performed on separate fractions from each layer indicate changes in oxide mineralogy and clay mineralogy through the sedimentary sequence. Additional samples from a nearby flood plain, a terrace soil, and a sinkhole pond also show mineralogical and geochemical changes. Goethite is abundant in the lower layers of the cave sequence, while the upper layers have mostly ferrihydrite and abundant kaolinite.

Paleomagnetic evidence and Maury River incision rates indicate an age of these deposits near the 6/5e isotope boundary (128 ka). This glacial-interglacial transition in Virginia represents a shift from colder and drier conditions to warmer and wetter conditions, providing the potential for change in water table position and cave flooding. The shift in iron and clay mineralogy suggests deposition beginning in a period of less intense weathering with possibly lower erosion rates and ending in a period of more intense weathering, erosion of nearby soils, and changes in sinkhole flushing or draining. The presence of significant ferrous iron and manganese minerals in the black silty layer suggests the collapse of a sinkhole that contained an anaerobic pond. Cyclic changes in

* Elizabeth P. Knapp, David J. Harbor, and Robert C. Thren, Department of Geology, Washington and Lee University, Lexington, Virginia, 24450. Dennis O. Terry, Department of Geology, Temple University, Philadelphia, Pennsylvania, 19122.

the laminated orange and yellow sediments at the base of the section reflect cyclic responses in cave hydrology and surficial processes as a function of paleoclimatic change during the Quaternary.

2. INTRODUCTION

Crossing the southern tip of the Shenandoah Valley, the Maury River is incised 60 m into a rolling upland. The Bathers Cave entrance is in the lower third of a steep cutbank of the Maury River (Fig. 1). Above the cave are several levels of river terraces strewn with river cobbles. The topographically highest terrace is inverted and extremely disrupted by sinkholes. Previous studies have established maximum incision rates for the upper James River of 150 m/Ma (Harbor, 1996; Erickson and Harbor, 1998). This fast rate of up to 6 times greater than surrounding Appalachian basins led to investigations of caves in the upper James River basin to find evidence verifying the incision rate (Harbor et al., 1999). The protected nature of the cave environment also provides the potential for the preservation of climatic signals in clastic sediments.

The cave slopes up from the Maury River and in cross section consists of upper and lower passages (Fig. 2A). The upper part of Bathers Cave is a tube-like, discontinuous room, containing up to 2.5 m of laminated silt and clay (Fig 2B). Both these deposits and the floor of the upper room have been incised by a narrow slot that connects to lower passages near the entrance of the cave. That upper tube-like passage is a paleophreatic passage that subsequently was filled with clastic sediments either from the back of the cave via a sinkhole or from the mouth via the Maury River (Fig. 3). These sediments are largely laminated silts and clay with varying amounts of authigenic iron, manganese, and organic matter (Fig. 4C-E). The lower passages at the rear of the cave contain cobbles derived from the superjacent sinkholes (Fig. 2A)

The distinctive stratigraphy of the study interval is repeated both vertically and laterally throughout the upper tube at the rear of the cave (Fig. 2B). The study interval consists of 10 - 40 cm thick sediment packages that include a yellow rubbly layer, a black silty layer, a red laminated layer, and an upper orange layer of laminated clays and silts (Fig 3). In the orange layer, (Harbor et al., 1999) discovered a short-lived paleomagnetic reversal correlated with the Blake event of 114-119 ka (Fang et al., 1997). This reversal yields an incision rate of the Maury River that is consistent with other rates in the valley. Below this reversal are a host of textural, mineralogical, and geochemical changes that may be related to climate changes in the basin at 128 ka. We sampled a single sediment block that best demonstrates the full variety of sedimentological and geochemical characteristics near the middle of the study interval (Fig. 4A).

3. METHODOLOGY

3.1. Sedimentology

Samples for oriented thin sections were collected by carving out a 40 cm x 20 cm x 20 cm rectangular block from the cave wall. Subsamples were air dried and impregnated with a low viscosity resin before sectioning. Subsequent analysis and photomicrographs were made with a Nikon Eclipse E600 polarizing microscope and auto-exposure camera

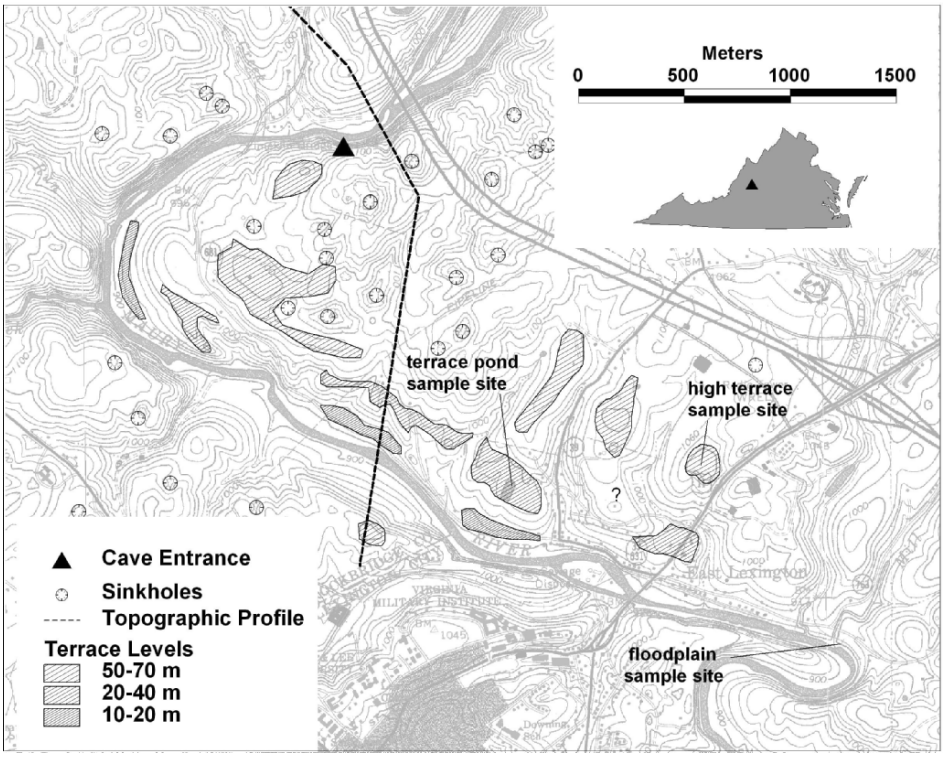

Figure 1. Topographic map of the study area showing the location of Bathers Cave in relation to major geomorphic features. Derived from a Lexington, Virginia, 1:24,000 USGS Quadrangle.

system. Clay mineralogy samples were prepared by disaggregating approximately 10 cm^3 of sediment in 500 ml of deionized water. Samples were stirred and allowed to set to check for flocculation. Flocculated samples were washed by removing the supernate and refilling with deionized water until clays remained suspended. Samples were then transferred to 1000 ml graduated cylinders and filled with deionized water to the 1000 ml level. Samples were stirred and allowed to settle for eight hours, after which the top 10 cm of sediment (2-4 micron clay) plus water were extracted. Oriented samples were created using the filter paper method described by (Moore et al., 1989).

Random powder mounts were made by mixing sediment with Duco cement on a glass slide. Clays were identified by comparing untreated, glycolated, and heated (550°C) samples. Samples were analyzed on a computerized Rigaku x-ray diffractometer using Cu k_ radiation at 35 kv and 15 ma with a scan rate of 1.2 deg/min and a step of 0.05. Diffractograms were interpreted using data from (Moore et al., 1989) and *Jade* mineral identification software. Samples for scanning electron microscopy were coated with gold and analyzed on a PGT-EDX system.

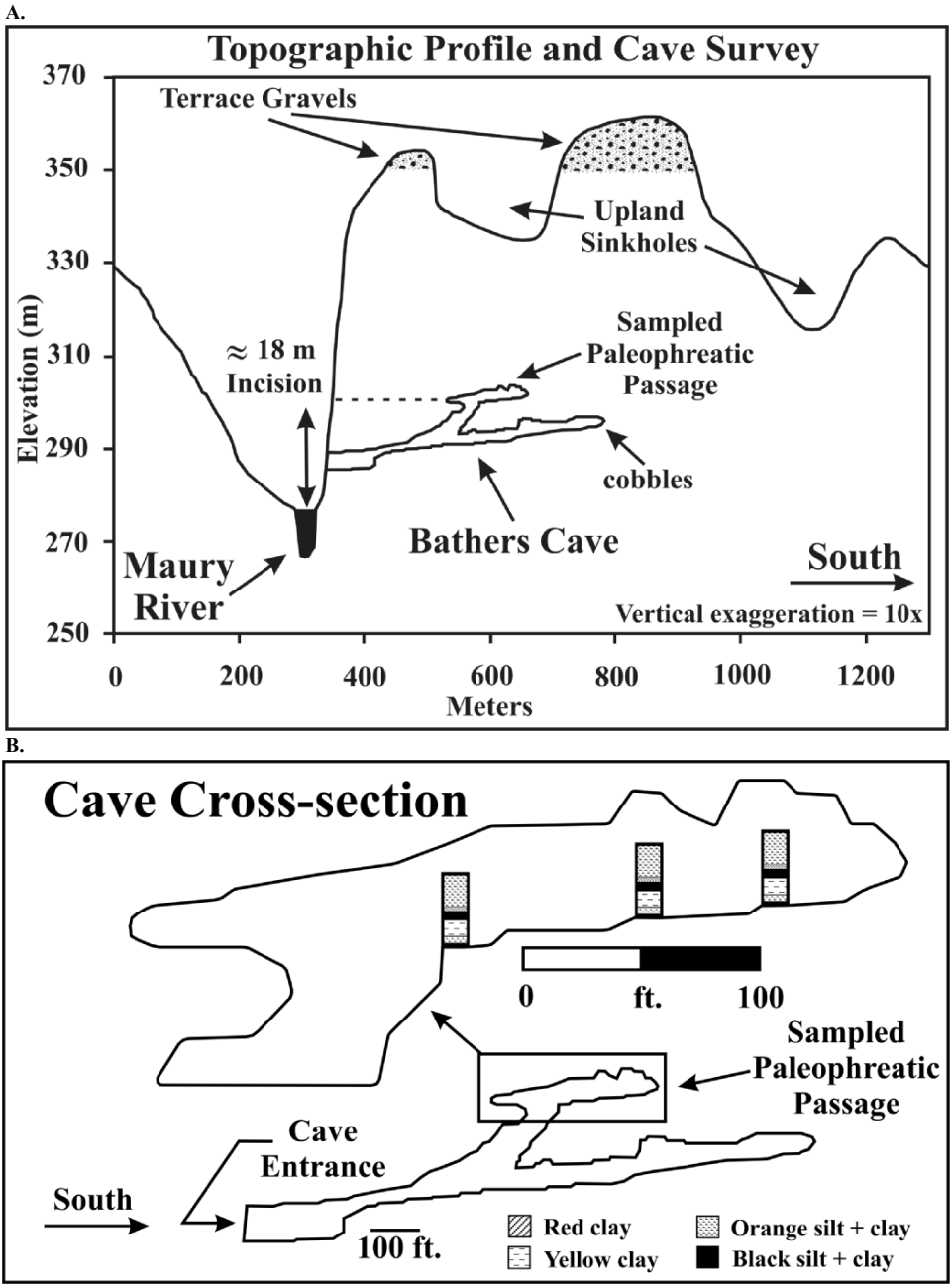

Figure 2. A. Cross section of Bathers Cave showing the location of the cave system and the study area relative to the Maury River and surrounding topographic features. **B.** Close up cross section of Bathers Cave showing the location of the study area and distribution of cave sediments within the passage. See Figure 3 for detailed measured section.

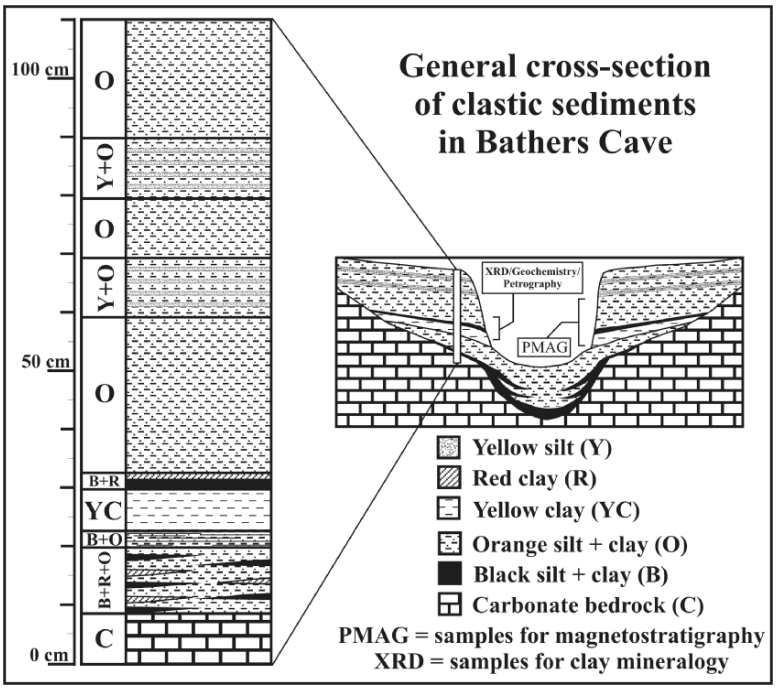

Figure 3. Measured section and cross section through the sample interval showing the relationship to the overall cave stratigraphy. XRD = x-ray diffraction, PMAG = paleomagnetic sample interval.

3.2. Geochemistry

Sediments were also subsampled from each of the four stratigraphic layers of the sequence. In order to examine the relationship of cave sediments to modern, nearby depositional settings, samples were also collected from a nearby sinkhole pond with hand operated coring device and from the high terrace and flood plain soils with a shovel (Fig. 1).

The geochemistry of cave samples from each of the stratigraphic layers and the nearby sediments was characterized using metal-oxide extractions on repeated 1-g sample splits for ferrous and ferric iron and manganese. The ammonium oxalate extraction removed poorly crystalline oxides (Phillips and Lovely, 1987). The dithionite citrate bicarbonate (DCB) method was used for extracting total metals (Mehra and Jackson, 1960). The 0.5 HCl extraction removed oxides, including crystalline Fe-oxides such as goethite, and was used for speciating reduced iron phases (Heron et al., 1994). Iron and manganese were determined by atomic absorption spectroscopy. Ferrous iron was determined by uv-vis spectroscopy using the ferrozine method (Gibbs, 1979). Organic carbon content of each of the layers was determined by loss on ignition. Samples from each layer were dried overnight at 100°C, weighed, heated to 450°C for two hours and then reweighed. The loss in weight is expressed in % C (Bierman et al., 1997).

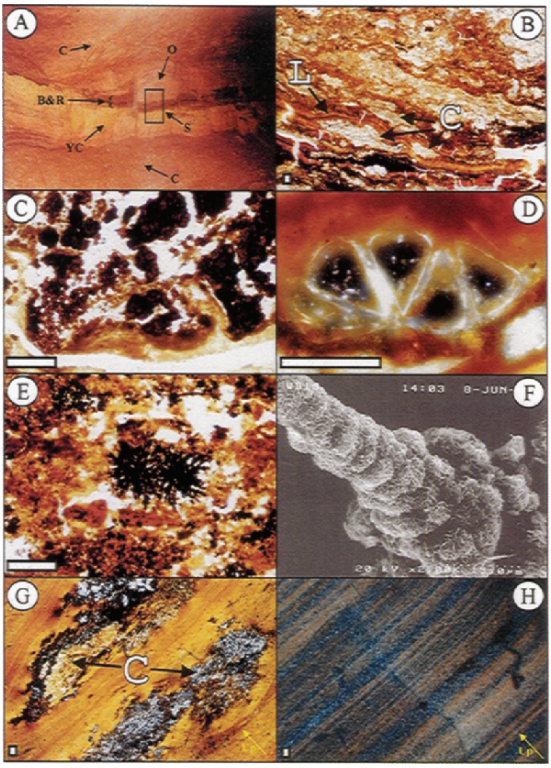

Figure 4. Photographs. **A**. The cave sediments and study interval from the section closest to the cave mouth. **B**. Photomicrograph of the lower yellow layer showing the disrupted, rubbly texture produced by alternating clay clasts (C) and laminae (L). **C**. Photomicrograph of authigenic iron oxides (ferrihydrite?) from the lower yellow layer. Note that individual blebs in the lower left coalesce and form larger masses in the upper right. **D**. Possible plant fragment from the lower yellow layer. Note that the far left chamber has collapsed. **E**. Photomicrograph of authigenic manganese dendrites in the black layer. **F**. Scanning electron microscope image of an authigenic manganese dendrite. **G**. Photomicrograph of the red layer showing the several clay clasts (C) within finely laminated clays. **H**. Photomicrograph of the upper orange layer showing the repetitious, laminated layers of silt and reddish-orange clay. Up is towards the top of the photograph unless indicated otherwise. Scale bar in all thin sections is 0.1 mm.

4. RESULTS

4.1. Sedimentology

4.1.1. Petrography

The cave sediments consist of distinct layers of yellow, black, red, and orange silt and clay that are punctuated by thin beds of yellow silt (Fig. 3). The main study interval is a 25 cm thick zone in the middle of this package that contains four distinct units, herein referred to as the bottom yellow, black, red, and top orange layers.

Macroscopically, the bottom yellow layer is a 8 cm thick rubbly zone of alternating silt and clay layers with occasional stringers of fine silt. On a microscopic scale, this layer is characterized by alternating zones of clay clasts that are covered by thin clay

laminae (Fig. 4B). Clay clasts are angular to subangular, equant to elongated masses that average 0.5 x 0.2 mm in size and consist of both yellow-orange masses with laminated internal fabrics and structureless silty gray clay masses. The laminated clasts have no consistent internal arrangement as a group, although elongated clasts are parallel to bedding. The outer edges of some clay clasts show realignment of fabric tangential to the clast. Laminae are dark red to orange in color and drape the clay clasts. Some laminae are truncated and overlain by clasts, whereas others are deformed by the clasts. A 0.75 to 1 cm layer of yellow clay near the top of this unit contains no clay clasts, but is strongly laminated at its top. The top of this clay layer is undulatory with truncated laminae and large clay clasts (predominantly the massive gray silty clay, up to 1 x 2 mm in size) resting on top and deforming the laminae. This layer of clay clasts is 5 mm thick and is capped by a sharp transition to the overlying silty black layer.

The black layer is a 3.5 cm thick, black to very dark gray clayey silt with weak lamination. The most notable feature of this layer is the abundance of euhedral, starburst shaped Mn oxide minerals that average 0.5 to 0.1 mm in diameter (Figs. 4E and 4F). The detrital component of this unit is dominated by quartz silt. The upper contact of this unit is slightly eroded and marked by clay clasts and a transition to red laminated clay.

The red layer is a 1 cm thick zone of red laminated clays and numerous clay clasts. In this interval are at least five sets of clay clasts overlain by clay laminae and capped by an iron-rich coating. The red clay laminae drape over individual clasts and are also deformed beneath clasts (Fig. 4G). Certain clast layers are predominantly composed of massive silty gray clay. Clasts are relatively large and elongated (up to 3 mm long x 1 mm wide) compared to other units. The upper contact with the upper orange layer is sharp and planar.

The top orange layer is 75-80 cm thick and composed of repetitive fining upwards sequences of silt and clay ranging from 0.1 to 1.5 mm in thickness (Fig. 4H). Siltier zones are marked by increased amounts of iron oxide staining and manganese mineralization in the upper parts of this unit. This zone is the thickest of the cave sediments and continues to the top of the cave passage. It is punctuated by several 1-3 cm layers of coarse silt in the upper part.

4.1.2. Clay Mineralogy

Illite, kaolinite, goethite, and quartz are present within the clay fraction of the cave sediments (Fig. 5). Original diffraction analysis by (Terry et al., 1999) suggested the presence of smectite, although this could not be replicated in repeat measurements. Illite is confirmed by the presence of the 001, 002, and 003 peaks at approximately 8.8°, 17.7°, and 26.3° 2_ respectively, and do not shift with e-glycol solvation or heating. Kaolinite is confirmed by the presence of peaks at 12.4° and 24.7° 2_ that do not shift with e-glycol solvation, but disappear with heating to 550° C. Goethite is suggested by the presence of a peak at 21.2° 2_ that disappears with heating at 550°C. According to (Moore et al., 1989), heating of goethite to 300°C will shift the 100% intensity peak to approximately 33.2° 2 _ (2.69d), although no such peak was found. Quartz is identified by its primary and secondary peaks at 26.64° and 20.8° 2 _, respectively, that do not shift with glycolation or heating.

Illite is present within all layers. Quartz is present in the clay fraction only in the top orange layer. Goethite is present within all but the top orange layer. Kaolinite is present within all layers, but is especially strong in the red layer. Based on visual comparison, and calculation of relative abundances of illite vs. kaolinite, the lower

yellow layer has the least amount of kaolinite. The identify of the authigenic manganese of the black layer is unknown as it was amorphous to x-rays.

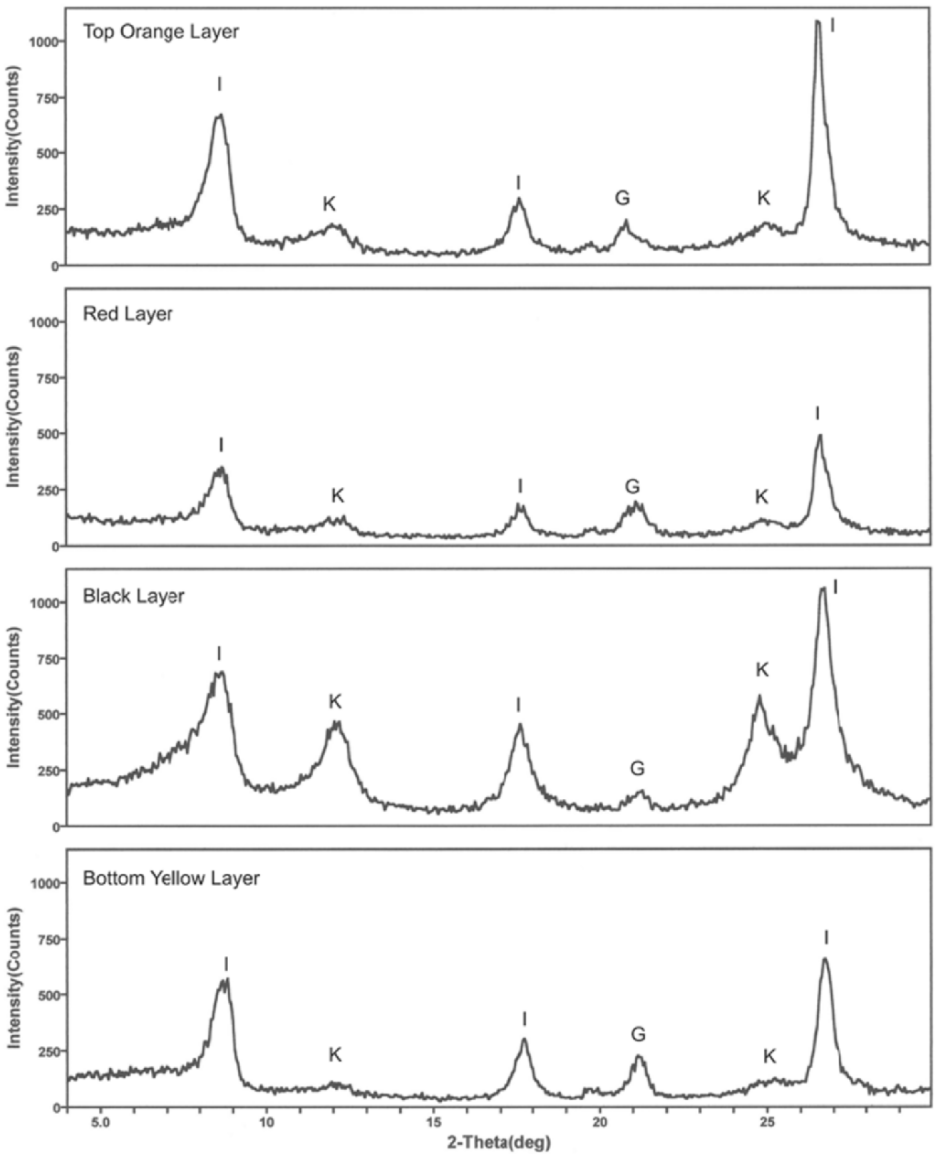

Figure 5. X-ray diffractogram of the four main layers. G = goethite, I = illite, K = kaolinite, and Q = quartz. Note that goethite is absent from the top orange layer, quartz appears in the top orange layer, and that kaolinite is greater in the red and orange layers than in the bottom yellow and black layers.

4.2. Geochemistry

Iron extraction values show that iron speciation varies significantly between layers in the cave (Fig. 6A). Values for amorphous, total, and ferrous iron range from 2.4 to 84 μmol/g. Extraction results indicate a significant amount of goethite in the lower layers of the sequence as determined by total minus ammonium-oxalate extractable iron (52 μmol/g in the bottom yellow layer) (Schwertmann and Taylor, 1977). The upper layers have total iron values represented almost entirely by ammonium-oxalate extractable iron (83 μmol/g in the red layer and 59 μmol/g in the top orange layer) suggestive of ferrihydrite (a necessary precursor to hematite formation). The ferrihydrite in the upper layers is indicative of formation by rapid oxidation of ferrous iron (Schwertmann, 1993). The black layer contains the only cave sediment with a significant amount (42 μmol/g) of extracted ferrous iron.

Results for the nearby high terrace, flood plain, and terrace pond show variability similar to the cave deposits (Fig. 6B). Values for amorphous, total, and ferrous iron range from 0.5 to 100 μmol/g. Compared with the flood plain, a significant amount of ferrous iron occurs in the pond sediments (43 μmol/g), and a high total iron (100 μmol/g) and amorphous iron (85 μmol/g) are extracted from the high terrace soil.

Extraction of amorphous and total manganese for the cave (Fig. 6C) and modern sediments (Fig. 6D) show great variability. The cave sediments range from 5 to 90 μmol/g, whereas the high terrace, flood plain, and terrace pond range from 0.01 to 42 μmol/g. Manganese minerals are concentrated in the black layer of the cave, with a total Mn of 90 μmol/g and an amorphous contribution of 68 μmol/g. Petrographic interpretation of the manganese in this layer indicates probable authigenic formation of dendrites. SEM / EDX analysis (shown in Fig. 4F) further supports the authigenic nature of the manganese deposits within the black layer sediments. Analysis of the modern sediments indicates that there is little manganese in the high terrace soil (0.1 μmol/g) and that the highest modern values found are in the sinkhole pond (31 - 42 μmol/g). The presence of manganese in the pond is consistent with formation in an anaerobic, organic-rich environment.

5. DISCUSSION

5.1. Interpretations

The distinct differences in mineralogy and sedimentology may indicate changes in climatic impacts on soil weathering, sinkhole pond change, and cave mouth flooding. However, because the modern samples also differ, the cave stratigraphy may also include potential changes in the sediment influx to the cave over time. In the following section we link the cave sedimentology and geochemistry to particular flow conditions and surface weathering conditions. Because of the near coincidence of the Blake paleomagnetic event with a glacial-interglacial climate shift, we end this discussion with a climatic interpretation.

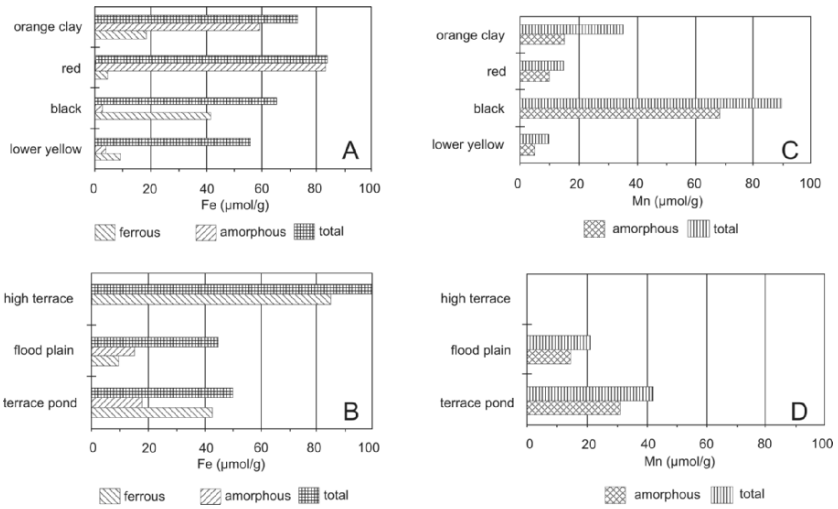

Figure 6. Geochemical analysis of Fe and Mn extractions from the four main cave sediment layers as compared to different surficial environments. **A**. Fe results for the cave sequence. **B**. Fe results for the surficial environments. **C**. Mn results for the cave sequence. **D**. Mn results for the surficial environments.

The extremely jumbled and rubbly nature of the bottom yellow layer is interpreted as the result of episodic high flow events through the karst system. Individual storm events were followed by quiet water conditions that allowed finer suspended particles to settle out and form the laminae followed by draining of the cave system. The previously deposited muds were later remobilized as rip-up clasts during initial phases of successive flooding events. The difference in orange laminated clay vs. massive gray silty clay clasts is likely a function of sediment source. The yellow-orange laminated clays were eroded from cave deposits. Gray clay clasts may represent the introduction of new material into the karst system, possibly from catastrophic collapse of overlying sinkholes or from the fluvial system via the cave mouth. Given that the fine sediments are eroded from soils and delivered to the cave from the sinkhole above or from the river, the presence of goethite represents lower amounts of organic matter in the soil and/or lower release rates of iron (Birkeland, 1984). Moreover, the lower amount of kaolinite in the yellow layer is consistent with less intense weathering and leaching in the sediment source area.

The black layer is a coarser sediment brought in by stronger flow conditions, possibly a catastrophic event such as sinkhole collapse. The contact with the underlying yellow layer is marked by numerous clay clasts, many of which are massive gray silty clay, reinforcing the idea that this layer was the result of a high flow event. The black coloration is due to post-deposition mineralization of manganese oxide. The delicate nature of the manganese dendrites precludes their transport into the cave system as a clastic sediment. The silty texture of this layer was conducive to manganese mineralization, as were other silty layers throughout the cave section. The formation of a significant amount extractable ferrous iron minerals in the black layer, in addition to manganese formation, is consistent with delivery from an anaerobic source. The

oxidation state of the metals plus the high organic matter content (3.38% organic carbon) likely reflects drainage from a sinkhole pond. The significant amount of ferrous iron and manganese in modern sinkhole pond sediments supports a sinkhole pond source for at least some of the cave sediments.

The thin, clay and iron-rich red layer caps a transition to a calmer water depositional environment. The red layer is predominantly composed of quiet water clay laminae, but at least five separate episodes of turbulent flow introduced clay rip-up clasts into the system. The red layer marks the last occurrence of remobilized clay clasts. These were in turn covered by laminae deposited during the quieter phase of flow. The high iron and kaolinite clay contents suggest an influx of weathered soil sediment. The iron enriched caps on fining upward laminae implies that an extraordinary amount of iron was allowed to settle or precipitate out in quiet water.

The top orange layer is the result of more flooded conditions. Storm events introduced sediments that became multiple fining upward silt-clay laminae. Water must have been present in the cave to promote differential sediment settling, while also preventing the creation of clay rip-up clasts. The laminae vary in thickness, and may represent an ancient record of storm/flooding events in this watershed during the Quaternary. Like the red layer, increased kaolinite and ferrihydrite indicate a more intensely weathered or more deeply eroded sediment source.

In summary, the sedimentological and geochemical changes through these four layers suggest a dramatic shift in cave hydrology, sediment delivery, and surface weathering. The dramatic change in iron species plus changes in clay signify a change in soil weathering during a shift from cool-dry to warm-wet climates or they reflect the degree of erosion and transport of soils and pond sediments from the surface. The presence and absence of rip-up clasts is consistent with an increase in the height of the water table and more persistent flooding.

5.2. Paleoclimatic Implications

Paleomagnetic evidence (Harbor et al., 1999) and Maury River incision rates indicate an age of these cave deposits near the 6/5e isotope boundary (128 ka). This period represents a shift from colder and drier glacial conditions to warmer and wetter interglacial conditions (Webb et al., 1998), which affects both weathering and local hydrology. Our interpretation of the synchronous sedimentological, geochemical, and mineralogical change in this section coordinates with a change from a time of less flooding, a lower water table, less soil leaching and erosion to a time of warmer, wetter, more weathered soils, increased flooding, and more erosion.

The change of this hydrologic system starts with the black layer. Just as rivers mobilize more sediment during transitions (Bull, 1991), the black layer formed as new kinds of sediments and dissolved ions were flushed into the cave. At the onset of interglacial conditions, the glacial anticyclone moved north (Webb et al., 1998), bringing increased moisture from the Gulf. With it came the potential for sinkhole flooding and collapse, increased weathering and erosion, larger, more frequent flooding, and a rising water table. We envision that the black and red layers were derived from a superjacent sinkhole, but might well have come from the watershed via riverbank flooding of the cave. Once the interglacial climate was established and the hydrologic system reached steady state, the rate of delivery of materials decreased, but they kept their warm and wet signature.

If in fact this sequence is the result of a change from glacial to interglacial

conditions, then there should be others above and below. Subsequent transitions were probably not recorded in the sediment layers because the river and cave system had incised. Thin bands of flowstone are present at the very top of the orange layer in some sections. In other parts of the cave, the study interval sits atop a number of thinner replicates of the study interval. This cave system serves as a repository for clastic sediments containing climate signals, but for only a finite time. As the passages open, they begin to receive surface sediments; but passage enlargement combined with river incision increasingly limits flooding of the cave.

6. REFERENCES

Bierman, P. R., Lini, A., Zehfuss, P., Church. A., Davis, P. T., Southon, J., and Baldwin, L., 1997, Postglacial ponds and alluvial fans: recorders of Holocene landscape history, *GSA Today* 7 no. 10:1-8.

Birkland, P. W., 1984, *Soils and Geomorphology*, Oxford University Press, New York, 372 p.

Bull, W. B., 1991, *Geomorphic Responses to Climate Change*, Oxford University Press, New York, 326 p.

Erickson, P. A. and Harbor, D. J., 1998, Bringing down Floyd: incision by the James River in the valley and ridge of Virginia, *Geol Soc Am Abstr Programs* 30 no. 7:142.

Fang, X., Li, J., Van der Voo, R., Niocaill, C., Dai, X., Kemp, R., Derbyshire, E., Cao, J., Wang, J., and Wang, G., 1997, A record of the Blake event during the last interglacial paleosol in the western Loess Plateau of China, *Earth Planetary Sci Lett* 146:73-82.

Gibbs, M. M., 1979, A simple method for the rapid determination of iron in natural waters, *Water Res* 13:295-297.

Harbor, D. J., Terry, D. O., Knapp, E. P., and Panuska, B. C., 1999, River incision and climate history revealed in cave stratigraphy, Maury River, Virginia, *Am Geophys Union Abstr Programs* 80 no. 17:S126.

Harbor, D. J., 1996, Nonuniform erosion patterns in the Appalachian mountains of Virginia, *Geol Soc Am Abstr Programs* 28 no. 7:116.

Heron, G., Crouzet, C., Bourg, A. C. M., and Christensen, T. H., 1994, Speciation of Fe(II) and Fe(III) in contaminated aquifer sediments using chemical extraction techniques, *Environ Sci Technol* 28:1698-1705.

Mehra, O. P. and Jackson, M. L., 1960, Iron oxide removal from soils and clays by a dithionite-citrate system buffered with sodium bicarbonate, *Clays Clay Miner* 5:317-327.

Moore, G., Crouzet, C., Bourg, A. C. M., and Christensen, T. H., 1989, *X-Ray Diffraction and the Identification and Analysis of Clay Mineral*, Oxford University Press, New York, 332 p.

Phillips, E. J. P. and Lovely, D. R., 1987, Determination of Fe(III) and Fe(II) in oxalate extracts of sediment, *Soil Sci Soc Am J* 51:938-941.

Schwertmann, U., 1993, Relations between iron oxides, soil color, and soil formation, *Soil Sci Soc Am, Spec Publ* no. 31:51-59.

Schwertmann, U. and Taylor, R. M., 1977, Iron oxides, in: *Minerals in Soil Environment*, Dinauer, R. C., Soil Science Society of America, Madison, Wisconsin, p.p. 145-181.

Terry, D. O., Jr., Knapp, E. P., Harbor, D. J., and Thren, R. C., 1999, Clastic sediments of Bathers Cave: a potential record of Quaternary climate change in west central Virginia, *Geol Soc Am Abstr Programs* 31 no. 7:A-233.

Webb, T., Anderson, K. H., Bartlein, P. J., and Webb, R. S., 1998, Later Quaternary climate change in eastern North America: a comparison of pollen-derived estimates with climate model results, *Quaternary Science Reviews* 17:587-606.

GLACIALLY-INFLUENCED SEDIMENT CYCLES IN THE LIME CREEK KARST, EAGLE COUNTY, COLORADO

Paul A. Burger*

ABSTRACT

Cave sediments in the Lime Creek area of Eagle County, Colorado were classified by composition and texture and were plotted on detailed maps of cave geomorphology. These maps were used to relate cave sediments to surface deposits and to assemble a depositional history of the caves.

Speleogenesis and karst development was strongly controlled by the advances and retreats of Pleistocene glaciers and advances of Holocene rock glaciers. Cave development probably began about 95-130 ka and continues to the present. During glacial periods, caves overrun by glacial ice were characterized by calcite deposition and roof breakdown. Periglacial caves were marked by active stream erosion and deposition, and calcite deposition in abandoned passages. Meltwater from glaciers increased stream energy and transported glacial materials completely filling some passages. During interglacial periods, speleogenesis in most of the caves was limited to roof collapse, calcite precipitation, and sediment deposition.

1. INTRODUCTION

Most cave sediment studies have focused on data obtained from sediment cores (i.e. Luiszer, 1987; Lauritzen, 1996) or sections of speleothems (Lauritzen, 1996). Paleomagnetic data and analyses of stable and unstable isotopes have been used to determine paleoclimate and long-term depositional history, but these techniques are expensive and not widely available. In some wilderness areas, coring, trenching, and speleothem removal may be prohibited, requiring alternative techniques.

The objectives of this study were to develop a method for cave sediment mapping, and to use that method to develop a sedimentary history for the caves of Lime Creek. Cave deposits were mapped using techniques generally applied to unconsolidated surface deposits. Correlation between surface glacial deposits and cave deposits allowed some

* Paul A. Burger, Carlsbad Caverns National Park, 3225 National Parks Highway, Carlsbad, NM 88220, paul_burger@nps.gov.

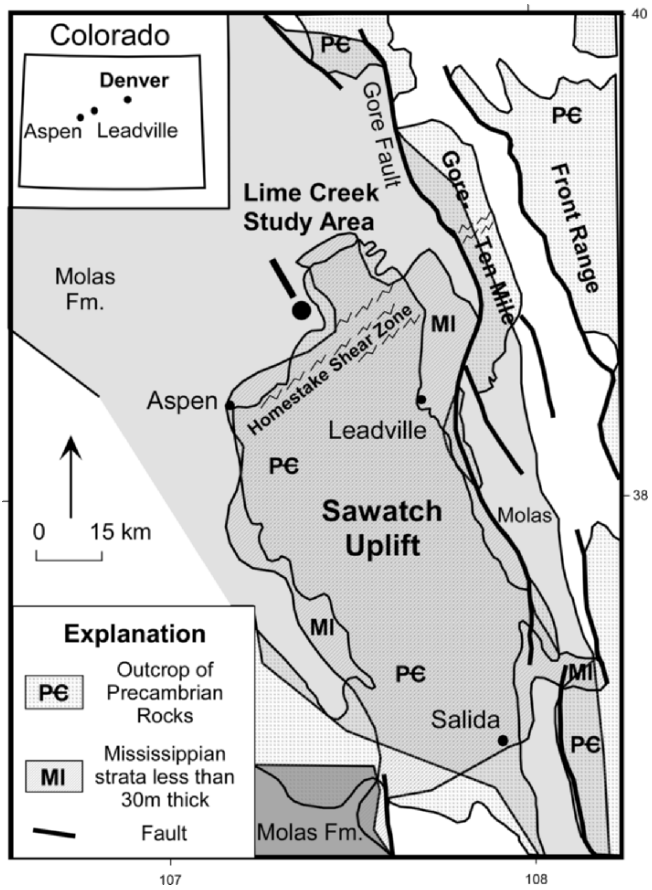

Figure 1. Location and tectonic features of the late-Mississippian, northern Sawatch Range showing distribution of Leadville Limestone (After DeVoto, 1990).

interpretation of how glacial processes affected cave development and sedimentation. Detailed classification and mapping of cave sediments were accomplished with very little cave disturbance.

2. GEOLOGIC SETTING

The Lime Creek drainage is an alpine karst system developed in Mississippian Leadville Limestone on the west slope of the Sawatch Range, approximately 20 kilometers (12 miles) northeast of Aspen, Colorado (Fig. 1). The mapped area is approximately 23 km^2 (9 mi^2), at elevations between 2,740 and 3,350 m (9,000 to 11,000 ft). The area is bounded by tributary valleys of the Fryingpan River on the north, south, and and west. The eastern extent of the study area is defined by uplifted and exposed Precambrian granite, gneiss, and schist (Fig. 2).

The Leadville Limestone is part of a carbonate shelf northwest of the Sawatch Uplift (Fig. 1). In Lime Creek, the Leadville is a massive to well-bedded, fossiliferous limestone

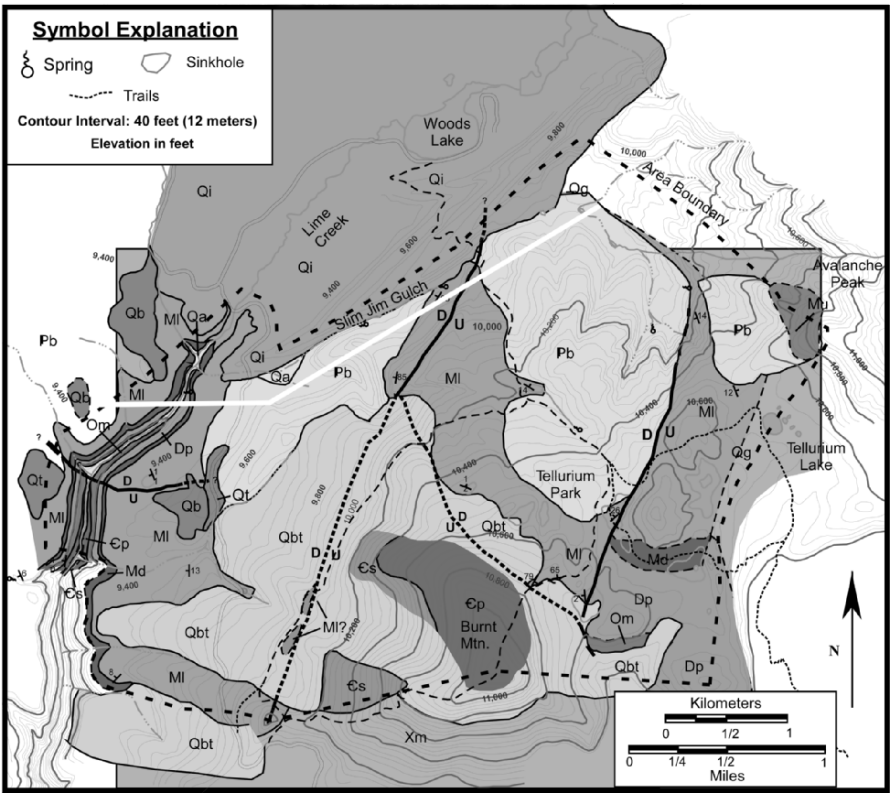

Figure 2. Geologic map of Lime Creek Study Area. Xm: Precambrian migmatite, Cs: Sawatch Quartzite, Cp: Peerless Shale, Om: Manitou Dolomite,Dp: Parting Quartzite, Md: Dyer Dolomite, Ml: Leadville Limestone, Mu: undifferentiated Mississippian, Pb: Belden Shale, Qi: Ivanhoe Till, Qb: Biglow Till, Qt: Thomasville Till, Qg: undifferentiated till, Qbt: Burnt Mtn. Talus, Qa: alluvium: White line indicates line of section shown in figure 4.

containing discontinuous layers of black chert. The Sawatch Uplift has existed as a topographic high from the late Cambrian to late Pennsylvanian, and influenced the thickness and facies of rock units deposited along its flank.

During late-Mississippian, the Leadville Limestone was subjected to subaerial erosion and karstification. During this large-scale karst event, sinkholes developed on the surface of uplifted structural blocks (Maslyn, 1977) and cave passages were developed in patterns largely controlled by bedding planes and northeast-trending fractures and faults. As base level dropped, sinkholes and caves were filled with carbonate collapse breccia, carbonate sand and silt, and black chert (Maslyn, 1977; DeVoto, 1990). During the Pennsylvanian, a transgression deposited the Belden formation on the Leadville karst surface and filled some open sinkholes and near-surface conduits with calcareous black shale (Maslyn, 1977; Hall, 1987; DeVoto, 1990).

In the southern part of the Sawatch Uplift, the Laramide Orogeny began about 72 Ma, forming a north-trending, asymmetrical anticline with reverse faults on the west side (Wallace, 1990). During the Laramide, igneous material was intruded into faults along the northeast-trending Colorado Mineral Belt (Tweto, 1980). Mineral-rich waters

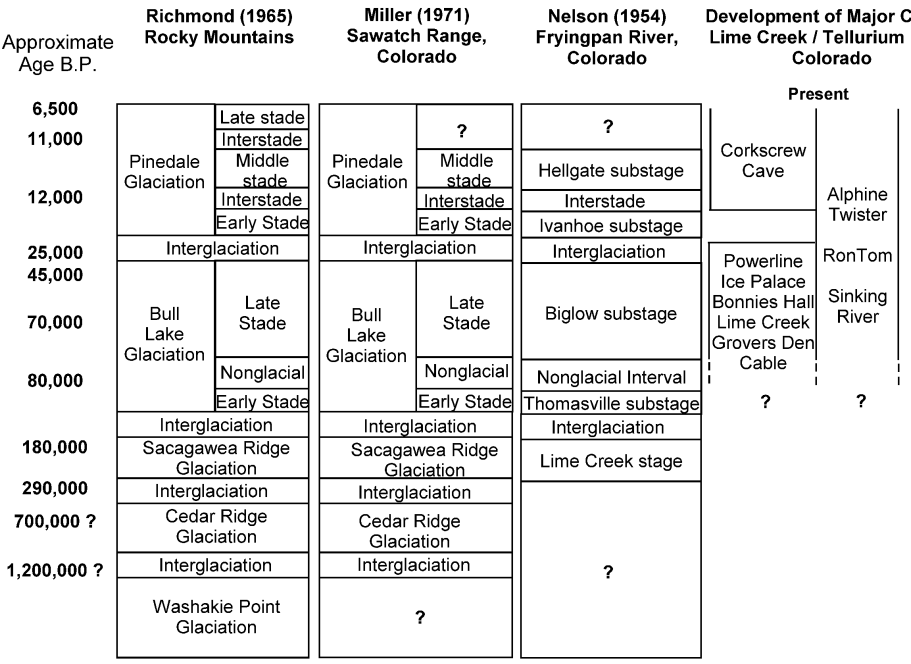

Figure 3. Correlation of glacial events and speleogenesis.

associated with these intrusions altered the rock near the faults and emplaced silver-lead-zinc and some gold into Mississippian paleokarst features.

By the late Eocene to mid Oligocene (about 37 Ma) uplift and erosion had ceased, and the topography was subdued (Epis et al., 1980; Wallace, 1990). During the mid-Oligocene, extension along the Rio Grande Rift cut the Sawatch Uplift into the Sawatch Range and the Mosquito Range (Wallace, 1990). This extension reactivated older faults, causing normal motion on some older reverse faults, and initiated downcutting of older deposits, including Paleozoic sedimentary rocks.

Alpine glaciation (Pre-Bull Lake, Pre-Wisconsin) began in Colorado about 450 ka (Wallace, 1990; Meierding and Birkeland, 1980; Miller, 1971; Nelson, 1954). By using the relative position and degree of preservation of glacial landforms, Nelson (1954) mapped five major glacial advances in the Lime Creek valley. Miller (1971) used a statistical approach to divide the glacial deposits of four drainages located north of the Lime Creek study area. Miller used the weathering characteristics of granite boulders and measurements of glacial landforms (height and length of till ridges, end moraines, etc.) to divide the deposits into five statistical groups. He then used the relationships between the deposits to assign relative ages. Miller's results generally agree with the stages of Nelson (1954) and Richmond's (1965) sequence for the Rocky Mountains as a whole (Fig. 3).

Large rock volumes and angular moraine morphology are characteristic of relatively young Ivanhoe deposits (17,250 years b.p.). Older glacial deposits are weathered and have more subdued topography. The Hellgate substage (11, 500 years b.p.) is characterized by small moraines with very little rock.

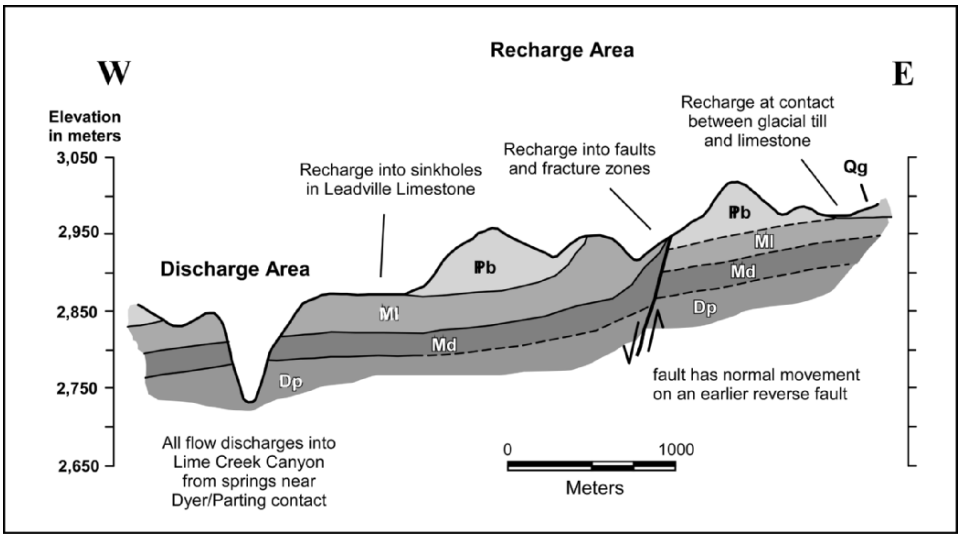

Figure 4. Section through Slim Jim Gulch showing recharge and discharge areas. Symbols as in Figure 2.

3. HYDROLOGIC SETTING

The study area can be divided into two general regions, an active karst recharge area and a flow and discharge area (Fig. 4). The two areas are separated by a north-northeast trending fault along the west side of Burnt Mountain (Fig. 2).

The recharge area consists of a relatively flat-lying Leadville Limestone bench between 2,960 and 3,200 m (9,700 to 10,500 ft) elevation. Some of the limestone is covered by Belden Shale and/or glacial deposits. The recharge area is a moderately well-developed karst bench with poor surface drainage, numerous large sinkholes, one major sinking stream, and two known caves over 150 m (500 ft) long.

The flow and discharge area is a Leadville Limestone bench, underlain by Paleozoic sedimentary rocks and partially covered with glacial materials and talus, with an elevation between 2,740 and 3,140 m (9,000 and 10,300 ft) elevation. Paleozoic rocks along the dividing fault are nearly vertical, while rocks in the Lime Creek valley dip less than twenty degrees. The discharge area has numerous sinkholes, sinking streams, caves, and a major karst spring, Clark Spring, which discharges into Lime Creek.

4. METHODS

The caves in Lime Creek were mapped with compass and tape and then drafted using a computer drawing program (Canvas 5, Deneba Software) at 2.4 m/cm (20 ft/inch). Longitudinal profiles of the caves were generated during this mapping and standard cave mapping symbols were used to indicate floor detail.

Cave sediments were differentiated based on color, grain size, and general composition. Sediments were mapped and digitally drawn onto the plan and profile cave maps. The classification and descriptions of mapped sediments are shown in Table 1. The distribution of sediments were mapped onto cave profiles Ato determine the vertical

Table 1. Sediment types found in the caves of Lime Creek

Sediment (map symbol)	Description
Red Sandy fill (Fs)	fill comprised of sand-sized chert, limestone, and other rocks derived from the Leadville
Red Clay fill (Fc)	fill comprised of red clay derived from weathering of the Leadville
Brown fill (Frs)	brown to tan, dry cave fill
Brown fill (Frc)	brown to tan, wet cave fill
Reworked fill (Fml)	reworked breakdown and cave sediment; mostly subangular to rounded limestone and chert, ranging from sand- to cobble-sized.
Till-derived fill (Ft)	sand to cobble-sized rounded to sub-rounded igneous and metamorphic rocks. Some are calcite-cemented and occur only in remnant pockets above current base level.
Gray Clay fill (Fg)	gray to black, organic-rich, clay deposit
Breakdown (Fm)	mostly angular blocks of limestone and chert fallen from the ceiling
Calcite-cemented fill (Fb)	calcite-cemented breakdown or calcite-coated floor; angular to subangular fragments of limestone and chert up to cobble-sized; calcite-coated bedrock or other cave fill.
Flowstone (Ff)	flowstone
Organic fill (Fo)	primarily rat midden, pine needles, and washed-in surface debris

relationships between different deposits. Sedimentation sequences were visible in some stream cuts and in trenches made by cavers during exploration, and were drawn onto the cave profiles.

5. SPELEOGENESIS

Cave development probably began once the sedimentary rocks overlying the Leadville had been removed after the Laramide Orogeny, 65 Ma. The three primary controls on cave development in the study area are structure, lithology, and glaciation. Paleokarst and mineralization are present in the study area but have had little effect on recent cave development (Burger, 1998). Faults and fractures act as capture zones for water and control the orientation of cave passages. Bedding in the Leadville controls the slope of the cave passages. Downcutting into the resistant Dyer Dolomite and Sawatch Quartzite is limited. Glaciation controlled water flow in the area, and in some cases, buried or eradicated earlier karst features.

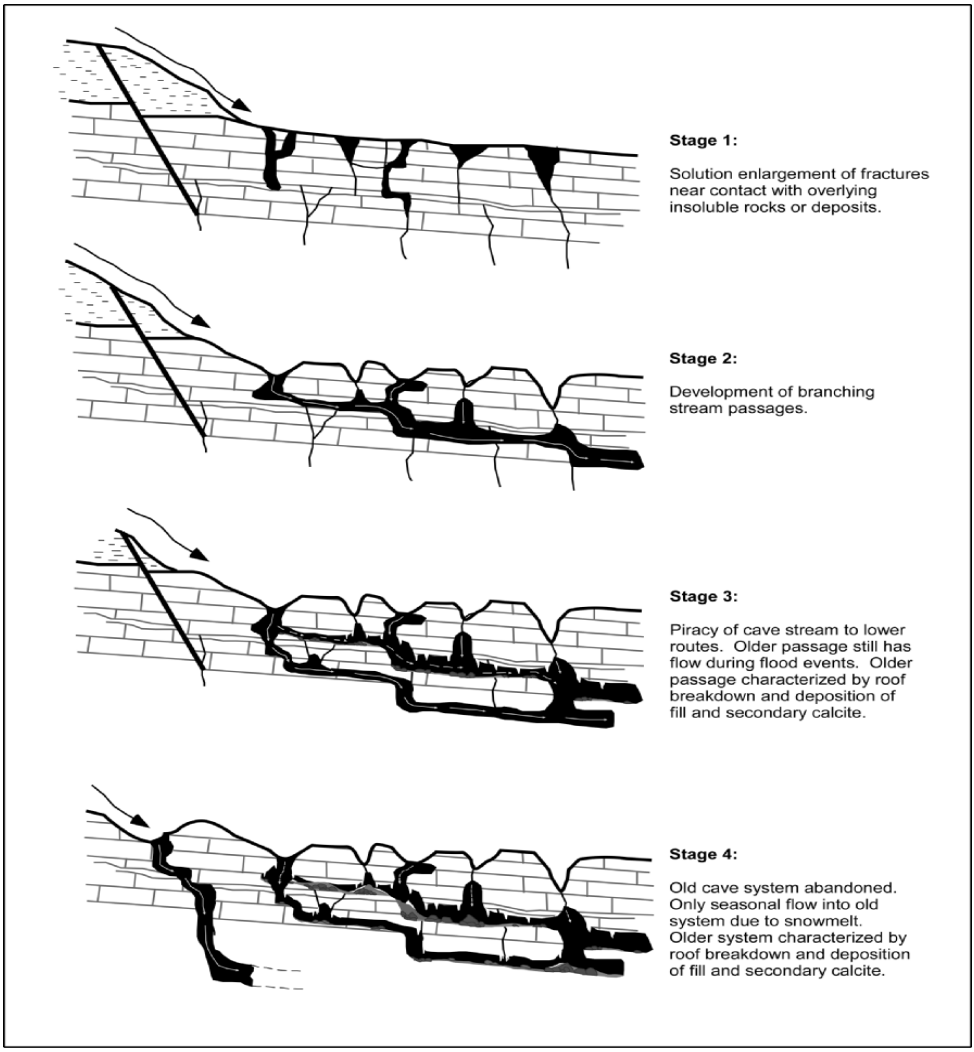

Figure 5. General stages of cave development.

The caves of Lime Creek have gone through four general stages of development (Fig. 5) based on the ability of the system to transport material over a long distance. The first stage is enlargement of fractures or faults to capture runoff. This occurs preferentially along the contact with less soluble, overlying material, especially poorly-sorted glacial deposits and the Belden Shale. Development in the vadose zone consists of enlarged fissures and solution domes and is characterized by limited transport of sediment.

During the second stage, flow from the enlarged fissures and domes coalesced and formed branchwork stream passages that could carry sediments over a greater distance. Aggressive downcutting was focused along vertical joints and bedding planes in the

limestone. Except in caves along the Lime Creek valley there is no evidence of significant development in the phreatic zone.

The third stage of passage development was piracy of stream flow into new channels. As water cut deeper into the limestone, new flow routes were developed and the older channels were abandoned. Some of the sediments in the abandoned channels became cemented with calcite or covered with breakdown and organic material. In the caves with active streams, these older channels presently take flow only during spring flood events.

The fourth general stage of development in the caves of Lime Creek was abandonment. Downcutting and piracy of cave streams to lower routes left some of the lower caves near Lime Creek Canyon without significant flow. Presently, these caves take water captured as snow and rain in sinkhole entrances and through open fractures.

It is important to note that these stages actually represent a continuum of cave development. It is likely that different parts of the same cave system were at different stages of development at the same time.

6. CAVE SEDIMENTS

Clay, sand, and gravel deposits were mapped to determine likely sources of cave fill and relative flow system energy (Table 1). The vertical relationships between sediments indicate the sequence of sedimentation in most of the caves of Lime Creek. Older deposits are buried by younger ones, or can be preserved in pockets and cemented by calcite above current base level. Older deposits may have been completely removed by later stream activity, so a complete sediment record may not be preserved.

The oldest preserved deposit is sand to cobble-sized sediment composed of subangular to rounded limestone and chert (Fml). These deposits are generally preserved in calcite-cemented pockets above current base level or in higher-level passages where they overlie the limestone bedrock.

Lime Creek Cave and Alphine Twister Cave contain sand to cobble-sized fill derived from igneous and metamorphic rock (Ft). In Alphine Twister, these deposits overlie a bedrock floor, and are 1 m (3 ft) below the cemented Fml deposit. In Lime Creek Cave, these sediments are cemented by calcite and are, in turn, overlain by reworked fill (Fml). This relationship is contrary to what is observed in Alphine Twister Cave where the Fml deposit appears to be older. This may indicate that there were two episodes of Fml deposition, separated by an episode of Ft deposition.

The brown fill deposits (Frs, Frc) are silt to clay-sized with almost no organic components. These deposits are generally found overlying the limestone bedrock in higher-level cave passages. The overall relationship between these deposits and the Fml and Ft deposits is unclear. In Lime Creek Cave, both the Ft and Fr deposits are overlain by Fml.

In several caves, gray, organic-rich clay deposits (Fg) overlie the Fml, Ft, and Fr deposits. These deposits often contain bits of charcoal and other organic material and are generally found in shallow, inactive cave stream basins and pit bottoms.

Some older sediment deposits have been covered by flowstone (Ff) or cemented by calcite (Fb). Organic deposits (Fo), such as pack rat nests and midden, overlie older deposits including some flowstone and calcite-cemented areas.

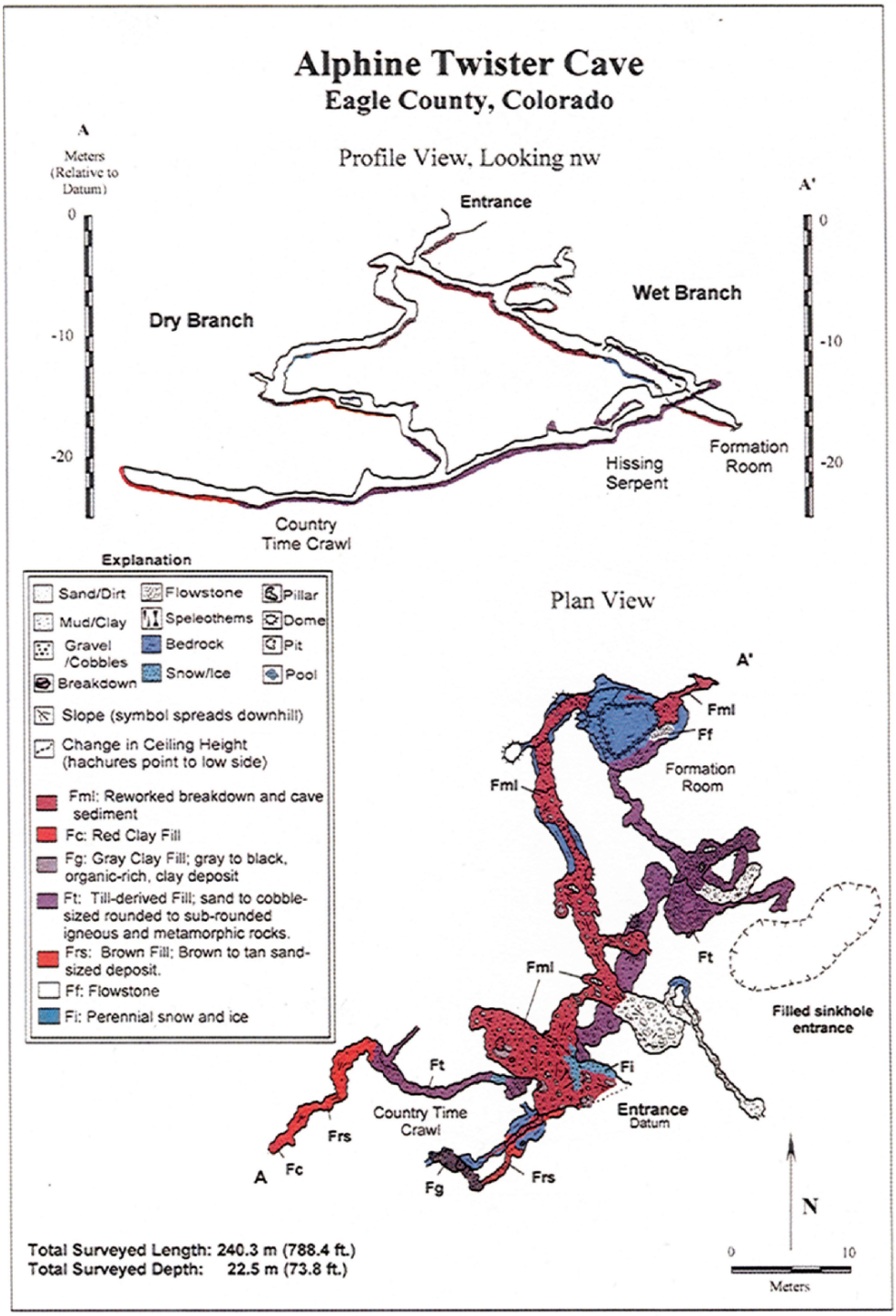

Figure 6. Alphine Twister Cave.

7. DEPOSITIONAL HISTORY

By mapping the distribution and types of cave sediments it is possible to determine the depositional history of the caves. The similarity between the cave sediments and surface deposits provide some clues as to the provenance of cave sediment. The relationship between the caves and surface features can provide an idea as to when and how the caves were formed.

Fine-grained deposits are indicative of either low energy or a long distance from the source rock. In some cases these deposits may represent fine-grained material winnowed from older, poorly-sorted deposits. Rounded, sand to cobble-sized deposits are indicative of relatively high energy stream deposition.

Flowstone and calcite cement were used as indicators of relatively low energy. In active stream passages, older calcite-cemented sediments are actively being incised. Presumably, the calcite could have been deposited in the stream paths only during full glacial conditions when streamflow would have been minimal (Ford, 1979). In Alphine Twister, calcite speleothems are currently being deposited in parts of the cave away from active streams.

During full glaciation, there was some limited flow along previous stream passages which cemented previous deposits. Away from the stream passage, calcite deposition was minimal. During early and late glacial conditions, the system became more active, probably re-dissolved calcite-cemented sediments and began to incise into the bedrock again. During this period, very few speleothems could grow near the stream because of the amount of stream action. During interglacial periods, active stream passages would continue to cut through previous sediments and the bedrock. In passages out of the influence of the active stream, both floor and ceiling calcite deposition could occur. In passages with active streams, only ceiling speleothems could grow.

This is best illustrated in Alphine Twister Cave (Fig. 6). A stream runs through half of the cave during the spring snowmelt. In this part of the cave, stalactites are actively forming, but flowstone and calcite-cemented sedimentary deposits are being eroded and reworked into the present stream bed. In the part of the cave that no longer takes an active stream, stalactites, stalagmites, and flowstone are being deposited over the old stream sediments and cave breakdown.

Organic deposits (Fo) such as pack rat nests were used as indicators of relatively stable, low-energy conditions. In a few cases, organic sediments were transported by water instead of animals and may indicate flooding events, or forest fire and erosion events above the caves.

Lime Creek Cave and Alphine Twister Cave contain high-energy fill derived from igneous and metamorphic rock (Ft). Both caves are located a long distance from outcrops of igneous and metamorphic bedrock and there are no major ephemeral or perennial streams currently entering the caves. There is no evidence that there were any surface streams in the past capable of bringing this material from uplifted Precambrian rocks from the east into the caves. The most likely mechanism which could have brought these materials onto the limestone was glacial ice. Fill containing igneous and metamorphic rock has been interpreted as an indicator of glacial deposits proximal to sinkhole cave entrances. Using the ages of nearby glacial deposits, it is possible to bracket the ages of the caves.

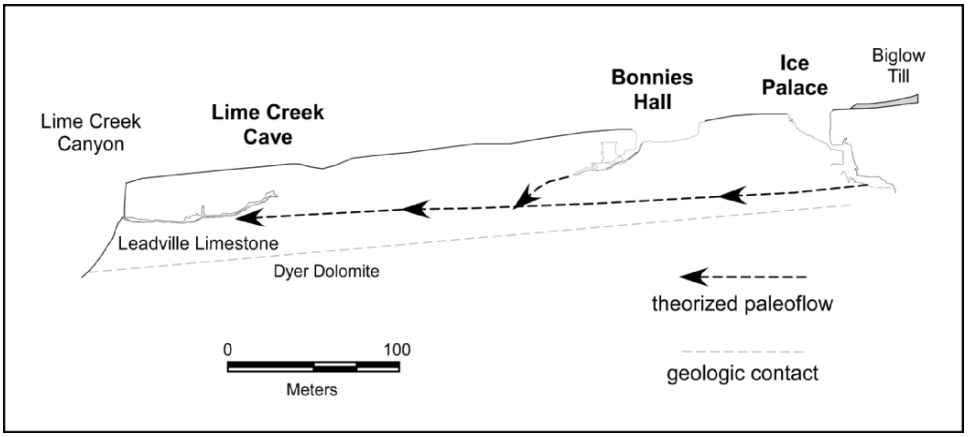

Figure 7. Relative positions of Lime Creek, Bonnies Hall, Ice Palace and glacial deposits shown in profile.

7.1 Lime Creek Cave, Ice Palace and Bonnies Hall

If the ages assigned by Nelson (1954) and Miller (1971) to the glacial deposits in the northern Sawatch are accurate, it is possible to assume ages for the caves near these deposits. Both the Thomasville glaciation (63,250 years b.p.) and the Biglow glaciation (46,000 years b.p.) extended beyond the entrances of Ice Palace and Bonnies Hall. Surface karst features tend to be removed by ice movement or buried by glacial debris (Ford, 1979). The entrances to all of these caves are sinkholes, so it seems unlikely that these entrances would have survived the glaciations.

Initial fracture and fault enlargement probably began during the Biglow glaciation, but the present entrances most likely formed during the retreat of the Biglow ice. At this time, the lower passages in Lime Creek Cave were probably forming at or near the water table.

After the end of the Biglow substage and before the Ivanhoe substage (17,250 years b.p.), Lime Creek Canyon formed. It is likely that Lime Creek Cave was one of several springs fed by Ice Palace and Bonnies Hall (Fig. 7). The glacial deposits observed in the front section of Lime Creek Cave (Fig. 8) were probably Biglow deposits washed into Bonnies Hall and Ice Palace, and transported through now-filled passages.

As water stopped flowing into Ice Palace and Bonnies Hall, Lime Creek Cave and the similar springs around it stopped flowing and began to fill with breakdown and secondary calcite deposits. Whether the water stopped flowing because all of the ice had melted, or because flow was pirated elsewhere is unknown.

7.2 Alphine Twister

Alphine Twister (Fig. 6) has gone through at least two stages of development. A cemented deposit located about one meter above the current base level in Alphine Twister Cave contains no igneous or metamorphic rocks. This suggests that there was a stage of cave development before the main influx of glacial material. A sinkhole east of the entrance to Alphine Twister is filled with glacial debris, suggesting there was a karst surface before the glacial debris was deposited.

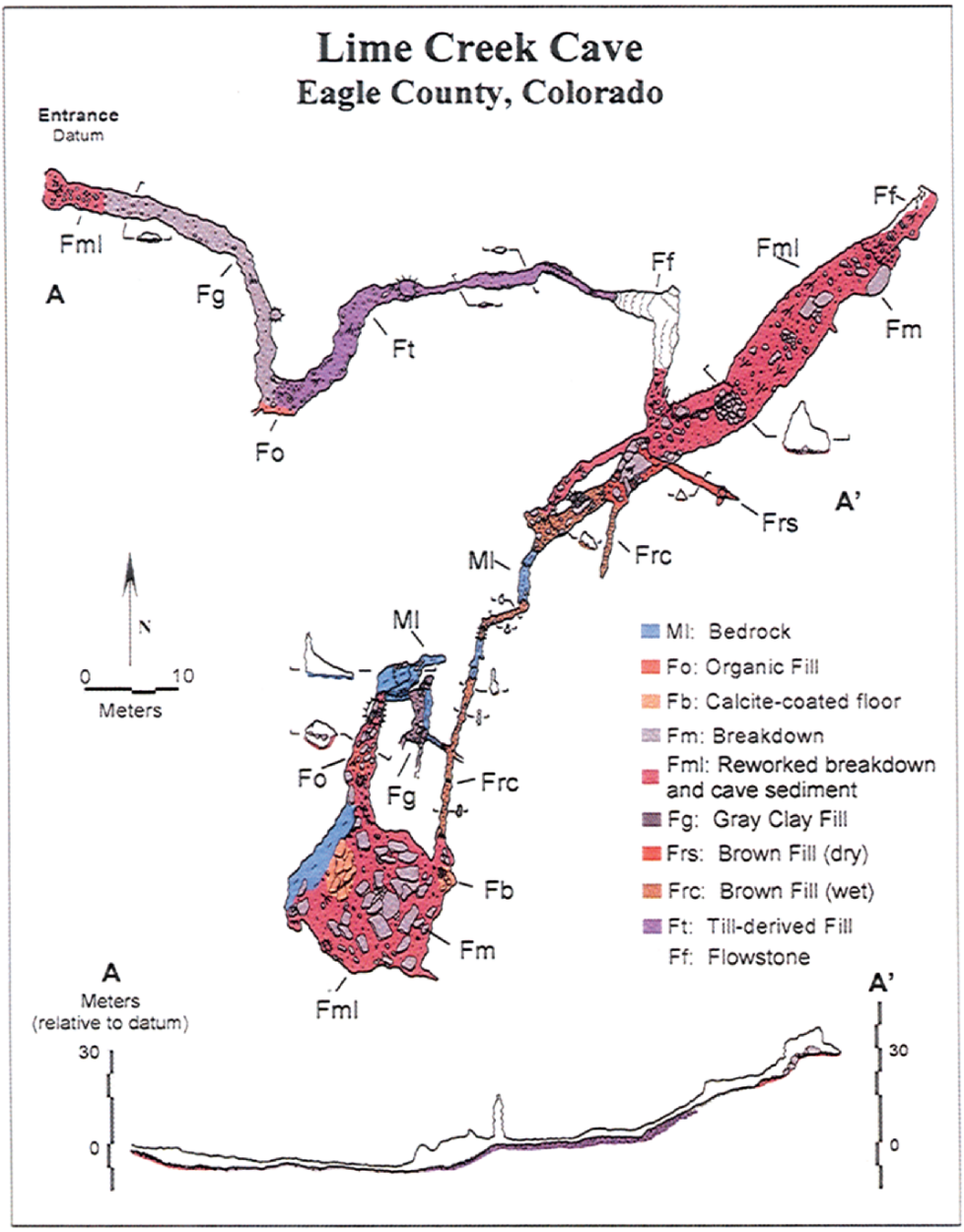

Figure 8. Lime Creek Cave.

It appears that a karst surface formed soon after the Belden Shale was removed. After the Leadville was exposed, a main, lower branch to the cave, and a high-water overpass into the Formation Room were formed. The cave stream carried limestone and chert gravel and cobbles derived from surface exposures of the Leadville Limestone and from material eroded from the cave walls.

Eventually, active flow ceased or slowed enough so that the older deposits were cemented. The cave stream again became active, incised the older deposits, and began to cut into the limestone. During this stage, glacially-derived materials washed into the cave and some passages were completely filled, including the entrance sinkhole.

Although some water entered through the buried entrance, most of the water in the cave stream flowed into the current entrance of the cave. The initial flow path was the now-abandoned Dry Branch of the cave. Most of the sediment in the Dry Branch is limestone and chert, indicating that most of the igneous and metamorphic glacial material near the entrance had been removed. As water cut deeper into the limestone near the entrance, flow was pirated downward, into the Wet Branch through the Formation Room. The Wet Branch reconnected to the older route near the beginning of the Country Time Crawl. Currently, the Dry Branch no longer takes water, even during high-flow events.

The moraines near the cave are well-preserved and contain a great deal of rock derived from the Precambrian granite, gneiss, and schist. Based on topographic characteristics, it is likely that the glacial materials along the eastern edge of Tellurium Park are Ivanhoe deposits.

It is likely that Alphine Twister probably began to form at the end of the Biglow stage (46,000 years b.p.), and that development continued until the Ivanhoe. The Ivanhoe advance partially filled the sinkhole east of the cave while cementation was going on inside the cave. During retreat of the Ivanhoe Ice, the old entrance and several passages were filled, and the current entrance formed. Subsequent flow into the cave was dominated by spring snowmelt, and calcite deposition was controlled by larger-scale climatic changes.

8. THE IMPACT OF GLACIATION ON CAVE SEDIMENTATION

The effects of glaciation on karst development depend on the proximity of glacial ice to the caves and karst surfaces (Mylroie, 1984, Ford, 1979, Glover, 1977). Ice advance and retreat can change the type of effects that are seen on the surface and in sediments preserved in the caves (Glover, 1977). In the Lime Creek area, the most important effects of glaciation area were glacial quarrying and sediment transport by ice and water.

Glacial ice may have been responsible for removing some of the rock that overlies the Leadville Limestone, exposing the limestone to karstification. As discussed previously, glacial ice also transported igneous and metamorphic material from exposed Precambrian bedrock westward, onto the limestone. Glacial effects on cave sedimentation and karst development vary throughout Lime Creek.

There is evidence that there were sinkholes along the flanks of Lime Creek prior to glaciation, but those sinkholes are now completely filled with glacial till. Currently-accessible caves in areas overridden by glacial ice probably did not form until after the ice retreated. The caves in these areas are characterized by an initial active stream phase

Table 2. Observed sedimentary history of Lime Creek caves.

Caves Overridden by Glacial Ice

Cave Name	Herbies Deli	Bonnies Hall	Powerline Cave	Ice Palace
Current Deposition	Secondaries, breakdown, organics	Organics, breakdown	Organics, secondaries, ice	Ice, breakdown
	Calcite deposition	Calcite?	Breakdown	Fault enlargement
	Breakdown-dirt fill	Active stream?	Calcite (dams?)	
	Active stream		Organics	
			Breakdown	
			Dirt fill	
Oldest event			Active stream	

Periglacial Caves

Cave Name	Alphine Twister Upper	Alphine Twister Lower	Corkscrew Lower	Corkscrew Upper
Current Deposition	Organic fill, breakdown	Active stream	Active stream	Breakdown, secondaries, organics
	Calcite cementation	Cementation, breakdown		Active stream
	Active stream	Active stream		
	Calcite cementation			
Oldest event	Active stream			

Possible Spring Caves in Lime Creek Canyon

Cave Name	Lime Creek Cave	Grovers Den	Cable Cave
Current Deposition	Secondaries, organics, breakdown	Organics, secondaries	Organics, secondaries, breakdown
	Breakdown	Breakdown	Active stream
	Calcite depostion	Active stream	
	Breakdown (organics)		
Oldest event	Glacial cobbles - active stream		

followed by deposition of low-energy deposits such as roof breakdown, calcite, and organic materials.

Periglacial caves in Lime Creek have the longest preserved sediment record. These caves have evidence of development before and after glaciation, and possibly multiple glacial episodes.

In general, the periglacial caves preserve two main stages. Initially there was a period of active stream dowcutting and sedimentation. Some of this material was derived from fallen rock in the cave passage, and some was derived from the surface, including chert, red clay, and in some cases, till. During high-energy stages of cave development, this material was reworked and transported deeper into the cave system. At the same time, the water was cutting deeper into the limestone.

The second stage is characterized by relatively low-energy deposits. During these quiescent periods, stream deposits were cemented together with calcite. Some of the deposition during these periods included organic material washed into the caves during periodic flood events, or brought in by pack rats as nesting material.

Alphine Twister Cave has evidence of a second major period of stream activity that downcut and reworked earlier deposits. Current deposition may be characteristic of the quiescent phase of sedimentation. A perennial stream flows in the lower part of the cave and transports silt and sand-sized materials. The upper part of the cave is characterized by calcite accumulation, breakdown, and organic fill brought in by animals.

Deposits in the caves of Lime Creek indicate at least two cycles of active downcutting of stream passages followed by relative quiescence. It seems likely that these cycles reflect accumulation and melting of ice during alpine glaciations of the Pleistocene and Holocene. Water flow during rejuvenated periods of downcutting destroyed most evidence of previous deposition and cementation, so it is impossible to tell how many of these events affected cave sedimentation. Table 2 summarizes the observed sedimentary history of the caves in the study area as well as the current stage of each.

9. CONCLUSIONS

The sedimentary maps were developed using standard cave mapping techniques and techniques generally used for mapping unconsolidated surface deposits. With virtually no disturbance to the deposits in the cave, it was possible to reconstruct the sedimentary record of the caves of Lime Creek. The cave sediment record made it possible to determine the speleogenesis of the caves and to evaluate the effects of glaciation on karst development.

Cave development probably began about 95-130 ka and continues to the present. Caves overrun by glacial ice are characterized by calcite deposition and roof breakdown. Periglacial caves had active stream erosion and deposition, and calcite was deposited in abandoned cave passages. Meltwater from glaciers increased stream energy causing some passages to be completely filled with glacial materials. During interglacial periods, speleogenesis in most of the caves consisted of roof collapse, calcite precipitation, and sediment deposition.

REFERENCES

Burger, P.A., 1998, *Alpine Karst Development and Speleogenesis in the Lime Creek Hydrologic System, Eagle County, Colorado* [Master's thesis], Colorado School of Mines, 59 p.

DeVoto, R.H., 1990, Paleozoic stratigraphy, tectonism, thermal history, and basin evolution of central Colorado, in: *Economic Geology Monograph Number 7: Carbonate-hosted sulfide deposits of the central Colorado mineral belt,* D.W. Beaty, G.P. Landis, and T.B. Thompson, eds., Harwood Academic Publishers, Chur, Switzerland, pp. 29-44.

Epis, R.C., Scott, G.R., Taylor, R.B., and Chapin, C.E., 1980, Summary of Cenozoic geomorphic, volcanic, and tectonic features of central Colorado and adjoing areas, in: *Colorado Geology*, H.C. Kent and K.W. Porter, eds., Rocky Mountain Association of Geologists, Denver, Colorado, p. 135-156.

Ford, D.C., 1976, Development of the principal types of solution caves in limestone, in: *Proceedings, 6th International Congress of Speleology* , pp. 83-84.

Ford, D.C. 1979, A review of the alpine karst in the southern Rocky Mountains of Canada, *National Speleological Society Bulletin*, **41:** 3, pp. 53-65.

Glover, R.R., 1977, A conceptual model of cave development in a glaciated region, in: *Proceedings, 7th International Congress of Speleology*, pp. 220-221.

Hall, J.F. Jr., 1987, *Paleokarst and other Dissolution Features of the Devonian Dyer and Mississippian Leadville Formations, Central Colorado* [Master's thesis], Colorado School of Mines, 136 p.

Lauritzen, Stein-Erik, ed., 1996, *Climate change: the Karst Record,* Charlestown, West Virginia, Karst Waters Institute, 196 p.

Luiszer, F.G., 1987, *Genesis of Cave of the Winds, Manitou Springs, Colorado* [PhD. thesis], Boulder, University of Colorado, 137 p.

Maslyn, R.M., 1977, *Late-Mississippian Paleokarst in the Aspen, Colorado Area* [Master's thesis], Colorado School of Mines, 123 p.

Meierding, T.C. and Birkeland , P.W., 1980, Quaternary glaciation of Colorado, in: *Colorado Geology*, H.C. Kent and K.W. Porter, eds., Rocky Mountain Association of Geologists, Denver, Colorado, pp. 165-174.

Miller, C.D., 1971, *Quaternary Glacial Events in the Northern Sawatch Range, Colorado* [PhD. thesis], Boulder, University of Colorado, 340 p.

Mylroie, J.E., 1984, Pleistocene climatic variation and cave development, *Norsk geogr. Tidsskr,* **38**, pp. 151-156.

Nelson, R.L., 1954, Glacial geology of the Fryingpan River drainage, Colorado, *Journal of Geology*, **62:**4, pp. 325-343.

Richmond, G.M., 1965, Glaciation of the Rocky Mountains, in: *The Quaternary of the United States*, Princeton University Press, Princeton, Massachusetts, pp. 217-230.

Tweto, Ogden, 1980, Summary of the Laramide Orogeny in Colorado, in: *Colorado Geology*, H.C. Kent and K.W. Porter, eds., Rocky Mountain Association of Geologists, Denver, Colorado, pp. 129-134.

Wallace, A.R., 1990, Regional Geologic and Tectonic Setting of the Central Colorado Mineral Belt, in: *Economic Geology Monograph Number 7: Carbonate-hosted sulfide deposits of the central Colorado mineral belt,* D.W. Beaty, G.P. Landis, and T.B. Thompson, eds., Harwood Academic Publishers, Chur, Switzerland, pp. 19-28.

CAVE SEDIMENTS AND DENUDED CAVERNS IN THE LAŠKI RAVNIK, CLASSICAL KARST OF SLOVENIA

France Šušteršič[1]

1. ABSTRACT

Recent studies of denuded caverns ("unroofed caves") in Slovenia have revealed that features previously supposed to be exceptional occur widely as typical parts of the karst surface. This paper sets out to demonstrate that detailed, systematic, field mapping of denuded cave features ("surface caving") not only increases the number of caves known in a given area, but also yields a better insight into the spatial organization of cave systems, by casting more light upon their history. This paper sets out to present the results of "surface caving" in an area east of the Planinsko polje, within the classical karst of Slovenia. Here, observation of the sediments within denuded caves provides a means of recognizing individual cave system sectors that display apparently different histories of sedimentation, outwash and re-sedimentation, as well as possibly different sediment source areas. Additionally, such observations provide information about the spatial relationships of karst channels within a flow corridor.

2. INTRODUCTION

Most textbook authors mention "denuded underground phenomena" explicitly among their standard inventory of surface karst features. As a rule these examples are presented as curiosities, and cover only a small part of the full suite of endokarstic phenomena. Such an approach is one of passive recording, and tends not to promote active research designed to extract wider conclusions. Recognition of "roofless caves" (Mihevc, 1996, 1998; Mihevc and Zupan Hajna, 1996; Mihevc et al., 1998) revealed that features previously supposed to be exceptional actually occur as a typical part of the karst

[1] France Šušteršič, University of Ljubljana, Department of Geology, Aškerčeva 12, SI-1000 Ljubljana, Slovenia, E-mail: france.sustersic@ntfgeo.uni-lj.si.

surface and the layer close beneath it (Šušteršič, 1999a). Though its discussion is limited deliberately to the cave sediments, this paper is intended to demonstrate that detailed, systematic, field mapping of denuded cave features increases the number of known caves in a given area. This approach also yields a better insight into the relationship between the geological setting and the spatial organization of cave systems, insofar as it casts more light upon their history. The paper sets out to demonstrate the power of the method, rather than to present new factual data.

Systematic study of denuded caves undoubtedly began during preparatory work for the construction of the motorway between Divača and Sezzzana (Classical Karst, southwest Slovenia). The whole area is an excellent example of contact karst, characterized by large active and dry horizontal, epiphreatic channels at several levels, draining an Eocene flysch territory towards the Adriatic. Even in "true" caves, it is evident that only a small part of the full system is actually accessible to humans. Most of the inactive part (assumed to be more than 80%) is choked by various sediments, predominantly flysch gravel and loam, deposited by sinking rivers. Though several impressive surface outcrops of large stalagmites were known previously, the first unroofed cave (about 200 m long) was recognized in 1994 (Mihevc, 1996). It was completely filled with still-recognizable cave sediments that were later cleared. Re - inspection of pre-existing infrared aerial photographs revealed that the course of this passage - and, by analogy, many others in the neighborhood - was clearly recognizable. Additional field indicators of buried caves were soon recognized, and this was followed by the discovery of several kilometers of "surface" extensions to the Škocjanske jame system (Mihevc et al., 1998).

A somewhat different approach to that used by A. Mihevc and his colleagues (Mihevc, 1996, 1998; Mihevc and Zupan Hajna, 1996; Mihevc et al., 1998) was adopted by the present author. It began as a detailed geomorphic mapping program on the karst surface in Laški Ravnik, intended as a framework for detailed study of solution dolines (Šušteršič, 1994). With recognition of the similarities and significance of unroofed cave channels, the recording of denuded underground phenomena became a systematic project on a complete cave system.

3. STUDY AREA AND GEOLOGICAL SETTING

Laški Ravnik (Fig. 1) forms part of a low-relief corridor about 18 km long and 1 to 3 km wide, lying about 3km northeast of Planinsko polje (south - central Slovenia). The area is generally flat and extremely rich in solution dolines (Šušteršič, 1994b). Some of the main streams of the underground Ljubljanica system are anticipated to flow beneath the area (Gospodarič and Habič, 1976), but no active stream cave has yet been found among a number of short cave fragments of evident phreatic origin.

Like the whole of the Classical Karst of Slovenia, the area investigated lies on the Adriatic sub-plate, a part of the African macroplate. The contact with the European continent lies about 80km to the north. During the last 2 Ma, changes in the motion of the Adriatic sub - plate have led to the establishment of several dextral strike - slip faults of Dinaric trend (i.e. southeast to northwest direction). As a reflection of its 12 km displacement and ongoing neotectonic activity, the Idria Fault is usually considered the

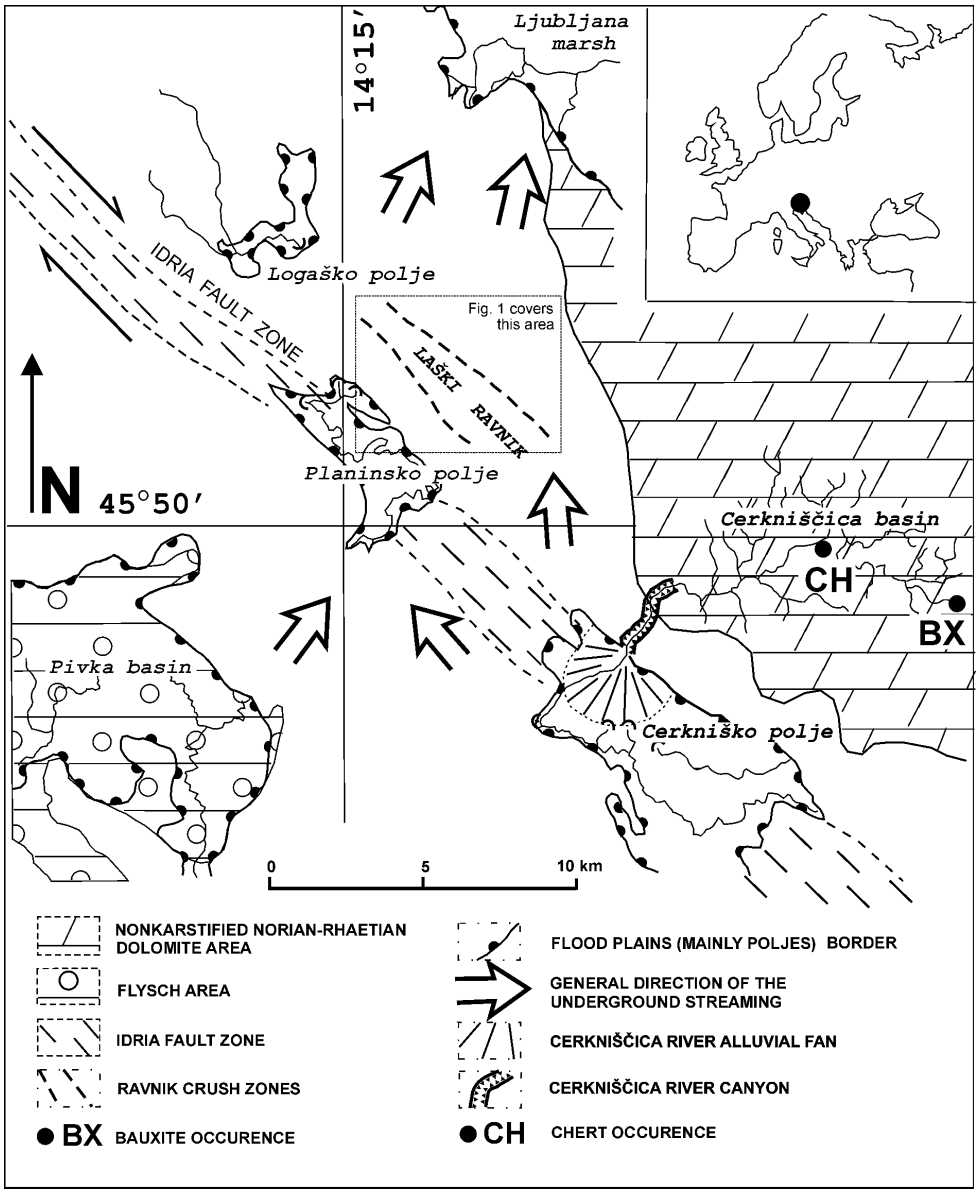

Figure 1. Location of the study area, showing important geological details.

most important. Statistical study of cave fragments in the general area revealed that the earliest cave systems were formed before the displacement along the Idria Fault (Šušteršič, 1996, 2000), i.e. 2 Ma ago. The conclusion reached was that most of the present underground streams make use of partly - adapted channels, inherited from a hydrogeological situation essentially different from the present one.

Structurally the area is a monocline, with beds dipping at 25° to 30° towards the

westsouthwest. The oldest beds, in the east, comprise Middle Triassic clastic rocks and dolomites. These are overlain by the c.6,850 m - thick Dinaric carbonate sequence, topped in turn by Eocene flysch deposits on the western side. The study area coincides with the contact between Jurassic and Cretaceous rocks. Early mapping identified a c.300 m - wide outcrop of coarse-grained secondary dolomite at the top of the Jurassic sequence, whereas more recent fieldwork has revealed that in fact, rather than a single dolomite package, there is an interfingering of wider or narrower dolomite/limestone stripes (Fig. 2).

The low-lying Ravnik corridor runs parallel to the Idria Fault, which lies about 2 km to the southwest, running in the Dinaric (NW to SE) direction. Additionally, two lineaments, until recently only partially recognised as major crush zones, run parallel to both sides of the Ravnik. As demonstrated in the following discussion, these tectonic lines act as delimiters between zones of somewhat different cave sedimentation, whereas minor fractures appear to be insignificant in this respect (see Šušteršič, 1998a).

A previous statistical study of the known cave distribution within the Ljubljanica sinking river basin (Šušteršič, 1996, Fig. 5) showed a slightly increased cave density in the general area of Laški Ravnik, but no obvious distinctive peak. At that stage it seemed reasonable to assume that the increased cave density could be interpreted as a reflection of the presumed main underground streams of Ljubljanica that pass beneath (Gospodarič and Habič, 1976). Subsequent study revealed a previously unknown cave system, with a morphology that simply could not be attributed to development by water from the present Ljubljanica river system.

Mapping at 1:5,000 or larger scale began in 1994, with the seemingly un-ambitious intention of providing a wider background for a detailed study of solution dolines (Šušteršič, 1994b). Not only solution and collapse dolines (Šušteršič, 1998a), but also geological structure and lithology, as well as karren fields and other small - scale superficial karst phenomena, including outcrops of what was previously described as *terra rossa*, were mapped on separate sheets. The area is entirely covered by dense coniferous forest, so all of the mapping was done in the field, and potential over-simplifications that are common in remote sensing interpretations were avoided.

In the Najdena jama-Vranja jama-Jama Kloka cave system (Šušteršič, 1994a) the bedding plane partings on the (Cretaceous) limestone-dolomite contacts acted as inception horizons - i.e. these planes were most prone to early karstification (Lowe and Gunn, 1997). Based on the experience gained in this study, special care was directed into investigation of the (Jurassic) limestone-dolomite contacts. Thus, the presence of several outcrops of denuded cave channels became apparent.

The area studied by Mihevc and his colleagues, included large, horizontal, epiphreatic caves. In contrast, all of the features currently accessible on the surface of Laški Ravnik were originally deep phreatic, oblique (reflecting the dip of the enclosing strata), and relatively small. All of the denuded channels in the area are filled with a variety of clastic sediments, and localized flowstone deposits also occur. Where visible and washed clean, the channel walls are seen to be modified to some extent by small-scale spalling.

The set of "derived" denuded underground karst phenomena that is now detectable at the surface is much larger than was previously believed. With recognition of this abundant information, it soon became clear that the organization of the cave system is far more structured, and much less chaotic, than was ever imagined previously, and the

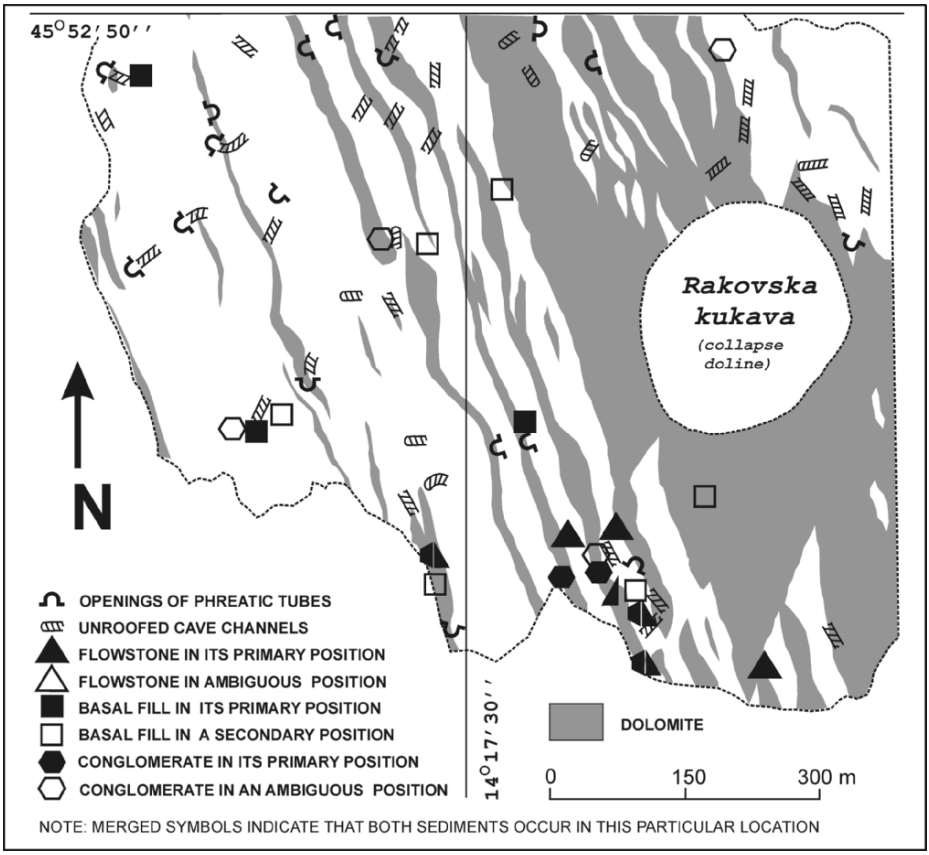

Figure 2. Morphological and sedimentological indicators of denuded caves in the southern part of the study area. Note: Combined symbols indicate that both sediment types occur at this particular location. The blank area indicates the position of a collapse doline.

relationship to the geological structure and lithology appear much clearer than before. Additionally, the application of "surface caving" has led to the identification of some previously unsuspected features, such as *phantom caves* and *aureole flowstone*.

4. CHANNELS AND SEDIMENTS

The known set of denuded underground karst phenomena includes morphological features and various cave sediments that are preserved, intact or reworked, at the karst surface.

4.1 Directly Detectable Channels

Except for some vertical vadose shafts, which appear to be very young, all of the cave channels identified to date are wholly phreatic in origin, and most of them are

sediment-filled (Fig. 2).

The most common sequence of denudational decay of an average, unroofed, inclined, cave, synthesised on the basis of observations at various sites, is presented in Fig.3. Because the process is continuous, the "stages" illustrated are intended merely to represent "milestones", rather than defining seemingly discrete phases of development.

After the corrosional front (cf. Gams, 1997) has touched the roof of the infilled cavern, the loosened blocks in the arch will settle down into the loam (Fig. 3, "stage" B). Now, "floating" blocks appear to disintegrate faster in the abundant soil that has developed from former cave sediments (Geršl et al., 1999), and for some time an unroofed cave looks like a green, grassy strip between the clints.

Commonly the loam is gradually washed away, so that a trench-like depression appears within the former cave (Fig. 3, "stages" C, D). Once the sediment has been removed completely, denudation continues from the bottom of the former cave and acts preferentially downwards. So, until chaotic weathering finally erases the "trench" completely (Fig. 3, "stage" E), the "negative volume" of the cave is imprinted into the formerly underlying parent rock. Considering the deepest depression of this kind still recognizable is about 2m deep (Šušteršič, 1998b, Fig. 4), and assuming an average denudation rate of 65 m Ma^{-1} (Gams, 1966) such trenches may survive for at least 30 ka. In cases where the outwash of loam is faster than previously described, an overhang will appear during "stage" A (Šušteršič, 1997, Fig. 2).

4.2 Fine - Grained Cave Sediments

The structures discussed above (Fig. 3, "stages" C to E) have partly been washed clear of sedimentary fill and are thus relatively easy to recognize as cave remnants. More commonly, deposits of cave infill remain virtually untouched as the cave walls disintegrate (*primary position* - Figs.3, A; 4), and the outcrop of a denuded cave looks similar to a lens of loam at the surface.

The most widespread fill material is reddish brown (2.5 YR 4/4, 5 YR 4/4) loam with a minor admixture of relatively large oolitic bauxite pebbles (derived from the Late Triassic - Carnian - beds) and coarse clasts of black chert. Pilot X-ray diffraction analysis revealed mostly muscovite/illite, plus mixed-layer clay minerals of illite/montmorillonite type, chlorite plus mixed-layer clay minerals of chlorite/montmorillonite type, calcium montmorillonite, and diaspore plus gibbsite, or just traces of bauxite minerals (Mišič, 2000). The mineral composition is not as uniform as might be expected, and further research, intended for application of factorial analysis, is in progress. A potential sediment source area in the present Cerkniščica River basin (Fig. 1) appears obvious at first glance, but similar outcrops of bauxite and chert do also appear at other sites that are not much more remote.

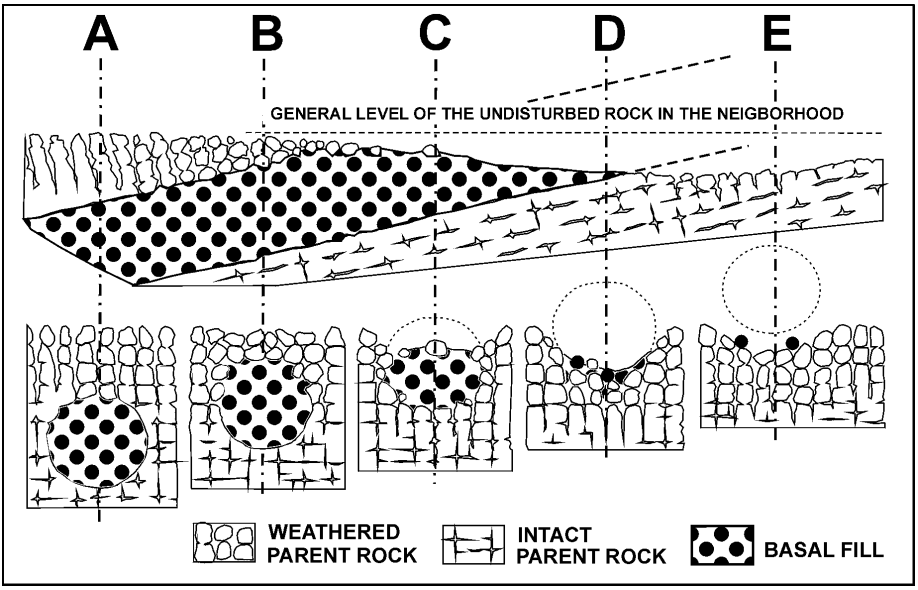

Figure 3. Stages in the gradual decay of an inclined, sediment-filled, phreatic channel, showing longitudinal section (above) and cross sections (below).

A: Original phreatic channel, not yet influenced by the zone of surface-weathering.

B: The sediment-filled channel is intersected by the surface-weathering zone. Breakdown of the channel ceiling takes place, and the fill supports large isolated blocks of parent rock.

C: The passage ceiling and the upper parts of its walls are removed as surface downcutting continues. Washing-out of sediment is somewhat faster than general surface lowering, and a small depression develops at the surface. Large insoluble clasts gradually concentrate in the floor of the depression.

D: Most of the cave walls have been removed, together with most of the former infill. Fragments of decayed flowstone and insoluble pebbles are preserved along the line of the former cave floor.

E: Both the cave and its parent rock have been totally denuded. A slight secondary depression persists within the new land surface for some time. Insoluble pebbles preserved in its former floor are the only evidence of the original cave's presence. Remnant concentrations of loamy infill are preserved only locally, within isolated pockets.

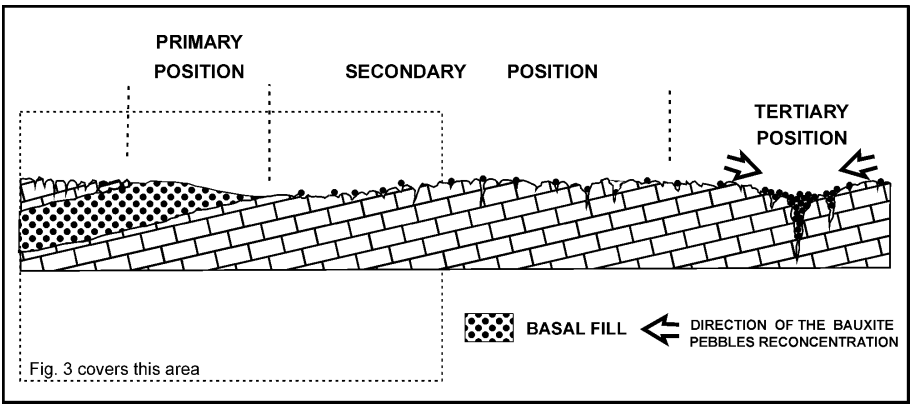

Figure 4. Possible positions of the cave infill.

Because no flowstone is found on the underlying cave walls, such sediments appear to have been deposited in the original cave systems when they were completely water-filled. As these deposits are nearly ubiquitous, and lie beneath most of the other preserved cave sediments, the sediment is referred to as *basal fill* (Šušteršič, 1998b).

At some locations all of the parent rock around, and some beneath, the previously filled cave has disintegrated, whereas the insoluble basal fill remained on the subsequent land surface *(secondary position,* Fig. 4*)*, where it would gradually be dispersed by continued terrain lowering. Locally it is still possible to distinguish the resultant pattern by observing concentrations of bauxite pebbles and chert on the modern land surface. In some cases they can be related to an adjacent outcrop of a denuded cavern, or at least to a recognizable inception horizon. Such features are referred to as *phantom caves*.

Ongoing terrain lowering would increase sediment dispersion and possibly re-concentrate any insoluble pebbles into newly formed pocket deposits (*tertiary position,* Fig. 4).

4.3 Laminated Sandstone

Partly cemented quartz sand was described formerly as an "exotic" sediment (Šušteršič, 1998b, p.128). Since then, other occurrences have been found, unfortunately mostly in obscure situations. However, it is now clear that the sediment in question is composed of fine quartz sand, cemented by calcite, which was later partly disintegrated again by ongoing surface chemical weathering. Some lamination is evident in unaffected "sandstone". Visual inspection reveals no significant differences from a number of similar occurrences distributed all over the Julian Alps and Dinaric Alps of Slovenia (Habič, 1992). As the "sandstone" generally lies lower, topographically, than the *basal fill*, and at one location lies just below its *secondary position*, it may be hypothesized that the *laminated sandstone* is older than the *basal fill*. Further research is in progress.

4.4 Coarse - Grained Cave Sediments

Outcrops of conglomerates that were deposited in now - denuded caves, are much less common. Clast size varies greatly, from coarse sands to large pebbles a few centimeters in diameter. The clasts are predominantly of Upper Triassic dolomite (which might originate from the same area as the oolitic bauxite discussed previously), with an admixture of Jurassic limestone clasts that are probably more local. Many of the dolomite pebbles were hollowed out during vadose diagenesis. Small quantities of bauxite and chert occur too, but it is not yet possible to say whether they were brought in as part of the stream load or simply admixed on the spot. Coarse rubble, originating from the channel roof or walls, is present locally.

Generally, the conglomerate displays typically alluvial features, such as graded bedding and laminated sedimentation. The matrix, which is loamy, ranges from barely present to comprising more than 70% of the rock. In the latter case, large pebbles are found "floating", supported by the matrix. At some locations flowstone occurs with the conglomerate. Unfortunately, no large clear section of a profile including conglomerate and flowstone has yet been found. Nevertheless, it appears that there were several alternating phases of conglomerate sedimentation and flowstone deposition. As flowstone is an indicator of subaerial sedimentation, its mere existence indicates that at

the time of conglomerate sedimentation the conditions in the cave system were no longer deep phreatic.

4.5 Flowstone in the Denuded Caves

Little can be said about the flowstone. It is evident that it is younger than the *basal fill*, as it lies above it, but it is also contemporaneous with the conglomerate. Relatively dry periods of flowstone deposition alternated with possibly catastrophic flood events, during which gravel-laden water rushed into dry caves. Determination of the age of the flowstone deposits in the denuded caverns is clearly beyond the reach of the U-Th series method. Following a single failed attempt, at Bergen University (Mihevc, 2000), no further direct attempts have been made to measure their date(s) of emplacement.

The completely recrystallized flowstone is of various types, ranging from nearly pure glassy calcite to heavily clay-stained formations. Most is in the form of wall-flowstone or half-stalactites. Flowstone cave bottom crusts and massive stalagmites are also found, whereas true stalactites appear to be absent. As mentioned above, with very few exceptions most of the flowstone is found associated with conglomerate. Flowstone crusts survive on the walls of nearly completely washed-out caverns, or in the form of highly corroded flowstone "clints". Much of the flowstone appears either within confirmed former caves or in situations where the presence of a former cave is at least strongly implied.

Some deposits occur in fractures and other narrow openings, which may be completely filled with the flowstone. Typically, such deposits did not grow concentrically from the walls inwards, as they might in true shafts or dome pits, but from one wall towards another, until the whole space was consumed. Without exception these occurrences are no more than 20m from a larger (at least 5m) cavern. This flowstone variety is described as *"aureole flowstone"*, and its origin is still a matter of discussion (Šušteršič, 1998b).

One possible explanation is that it was deposited at comparatively great depth beneath the surface, where the rock mass is relatively poorly ventilated. Saturated percolation water in small voids could generally not give up its surplus CO_2, except where close to larger, better ventilated, caverns. Consequently, the rocky mass around better - aired voids became impregnated with flowstone, whereas vadose water channels farther away remained free of flowstone.

5. THE LAŠKI RAVNIK CAVE SYSTEM

"Surface caving" should, in theory, provide details of a planar section through a cave system and thus give much more information about its 3-D pattern than any other speleological method, especially if the channels are inclined. On consideration of the visible morphological and sedimentological information, the exhumed cave segments detected in the Laški Ravnik are quite clearly of deep phreatic origin.

5.1 Organization of the Cave Maze

Though more than 100 surface occurrences of denuded caverns have been noted,

their dimensions have not yet been measured precisely enough to allow fair statistical analysis. Nevertheless, the disposable data imply strongly enough that such phreatic mazes are fractal, as concluded by Curl (1986). If the positions of these channels are considered relative to the lithology, it becomes clear that most of the phreatic tubes lie within or close to one or other of the upper or lower limestone/dolomite contacts. In this way, D.J.Lowe's Inception Horizon Hypothesis (Lowe and Gunn, 1997), arguing that primary tubes are formed along only a small number of somehow favoured bedding planes within the stratigraphic column, appears to be proven on a large scale. It indicates especially that bedding planes marking trans-bedding contrasts are among the most prone to early karstification.

Minor faults do not appear to affect the system to any great extent, except that major phreatic jumps are likely to be found in their close neighbourhood.

5.2 Distribution of the sediments

At least from the viewpoint of cave fill, the spatial distribution of cave sediments implies that the system must be split in two parts, separated by the NE Ravnik crush zone (Fig. 5). The best - studied area is on the western side. There, the *basal fill* must have been deposited within the channels when the system was still phreatic.

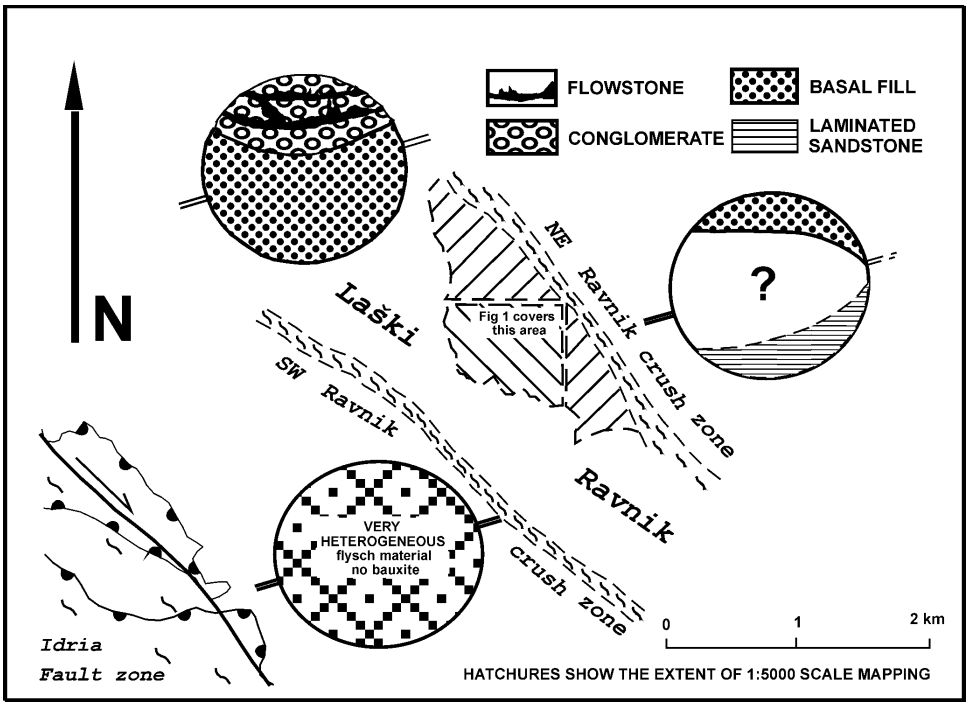

Figure 5. Cave sediment distribution within the study area. The ovals represent idealized cross-sections of infilled phreatic tubes.

The length of the time gap between the *basal fill* deposition and the last phase of partial outwash is unclear. At a time when conditions were to some extent similar to today's, with catchment area boundaries comparable to modern ones, flowstone development and conglomerate sedimentation apparently took place under vadose conditions. On one hand, the dolomite pebbles within the conglomerate do not differ from those in late Pleistocene gravel in the Cerkniščica river alluvial fan in the Cerkniško polje (Gospodarič and Habič, 1979). On the other, conglomerate-filled caves are exposed in the slopes of most of the larger collapse dolines, which suffered their essential transformation during the last glacial episode (Šušteršič, 1998a). Based on the nature and the number of pebbles in the conglomerate, one may conclude that the conglomerate (and flowstone) sedimentation took place during the Pleistocene, but not at its very end.

The situation on the other side of the same crush zone is rather different. The *basal fill* is preserved at higher elevations, whereas *laminated sandstone* appears at lower elevations. In areas where laminated sandstone has not been found, there are some larger caverns, which are accessible to humans. Close to the caverns are larger, unroofed, caves containing *basal fill* (Geršl et al., 1999). No conglomerate has yet been found in this area.

It is evident that only during emplacement of the *basal fill* was sedimentation comparable in cave systems on both sides of the crush zone. Because the other sediments differ completely across the crush zone, it can be concluded that the history of the cave systems on opposite sides might also be quite different.

Unroofed caves and, consequently, the sediments within them, have not yet been studied systematically westward of the southwest Ravnik crush zone. According to some pilot analyses, the loamy component of the fill is quite heterogeneous, and locally it may overlie flowstone. Bauxite pebbles appear to be completely absent, whereas an admixture of flysch-derived quartz sand is obvious.

6. CONCLUSIONS

Two conclusions may be drawn.

Firstly, observation of sediments within the denuded caves provides a way to recognize individual sectors within the cave system with possibly different histories of sedimentation, out-wash and re-sedimentation, as well as possibly different sediment source areas.

Secondly, a wide crush-zone may function not only as an obstacle to karst water movement (as suggested by many hydrogeologists), but may also act as a delimiter between tectonically-defined blocks, each of which may record a different history of sedimentation and, possibly, of speleogenesis.

7. ACKNOWLEDGEMENTS

Thank you to all those who's dedicated work has contributed to the recognition and interpretation of the many features of unroofed caves in the karst of Slovenia. Also, I

thank two anonymous reviewers, whose valuable comments on an early draft not only helped to make the text clearer, but also made me think! Finally, my thanks to David Lowe, for suggesting final small adjustments to my English translation.

8. REFERENCES

Curl, R.L., 1986, Fractal dimensions and geometries of caves, *Mathematical Geology*, 18: pp. 765-783.

Gams, I., 1966, Faktorji in dinamika korozije na karbonatnih kamninah dinarskega in alpskega krasa Slovenije [Factors and dynamics of corrosion of the carbonatic rocks in the Dinaric and Alpine karst of Slovenia; in Slovene, English summary], *Geografski vestnik*, **38**: pp. 11-68.

Gams, I., 1997, Climatic and lithological influence on cave depth development, *Acta carsologica*, **26**: pp. 321-336.

Geršl., M., Stepišnik, U., and Šušteršič, S., 1999, Brezstropa "jama pri bunkerju" (Laški Ravnik) [The "unroofed cave" near the bunker (Laški Ravnik); in Slovene, English summary], *Acta carsologica*, **28**: pp. 77-90.

Gospodarič, R., and Habič, P, 1976, *Underground water tracing*, Institute for the Karst Research SAZU, Postojna, pp. 1-309.

Gospodarič, R., and Habič, P., 1979: Kraški pojavi Cerkniškega polja [Karst phenomena of Cerkniško polje; in Slovene, English summary], *Acta carsologica*, **8:** pp. 7-162.

Habič, P., 1992, Les phénomenes paléokarstiques du karst alpin et dinarique en Slovénie. In: *Karst et évolutions climatiques: hommage q Jean Nicod,* Salomon, J.-N. and Maire, R., eds., Presses Universitaires de Bordeaux, Bordeaux, pp. 412-429.

Lowe, D. J., and Gunn, J., 1997, Carbonate speleogensis: an inception horizon hypothesis, *Acta carsologica*, **26**: pp. 457-488.

Mihevc, A., 1996, Jama Brezstropa jama pri Povirju [The cave Brezstropa jama near Povir; in Slovene, English abstract], *Naše jame*, **38**: pp. 65-75.

Mihevc, A., 1998, Brezstropa jama pri Povirju in denudirane jame v okolici Divače [Roofless cave near Povir and denuded caves in the vicinity of Divača; in Slovene, English abstract], *Geografski obzornik*, **45**: pp. 12-17.

Mihevc, A., 2000: Personal communication.

Mihevc, A., Slabe, T., and Šebela S., 1998, Denuded caves - an inherited element in the karst morphology: the case from Kras, *Acta carsologica*, **27**: pp. 165-174.

Mihevc, A., and Zupan Hajna, N., 1996, Clastic Sediments from Dolines and Caves Found During the Construction of the Motorway near Divača, on the Classical Karst, *Acta carsologica*, **25**: pp.169-191.

Mišič, M., 2000: personal communication.

Rus, J., 1925: Morfogenetske skice z notranjskih strani [Morphogenetic sketches from south-central Slovenia (in Slovene, with untitled French summary)], *Geografski vestnik*, **1**: pp. 29-32, 105-112.

Šebela, S., 1999, Morphological and geological characteristics of two denuded caves in SW Slovenia, *Acta carsologica*, **28**: pp. 175-185.

Šušteršič, F., 1994a, Jama Kloka in začetje [The Kloka cave and speleo-inception; in Slovene, English summary], *Naše jame*, **36**: pp. 9-30.

Šušteršič, F., 1994b, Classic dolines of classical site, *Acta carsologica*, **23**: pp. 123-154.

Šušteršič, F., 1996, Poljes and caves of Notranjska, *Acta carsologica*, **25**: pp. 251-289.

Šušteršič, F., 1998a, Rakovska kukava - collapse or tumour doline?, *Acta carsologica*, **27**: pp. 231 - 259.

Šušteršič, F., 1998b, Interaction between a cave system and the lowering karst surface; Case study: Laški Ravnik, *Acta carsologica*, **27**: pp. 115-138.

Šušteršič, F., 1999a, Vertical zonation of the speleogenetic space, *Acta carsologica*, **28**: pp. 187-201.

Šušteršič, F., 2000, Speleogenesis in the Ljubljanica River Drainage Basin, Slovenia, in: *Speleogenesis, Evolution of Karst Aquifers*, Klimchouk, A., B., Ford, D. C., Palmer, A., N., and Dreybrodt, W., eds., National Speleological Society, Huntsville, pp. 397 - 406.

PALEOCLIMATE RECORDS FROM SPELEOTHEMS IN LIMESTONE CAVES

William B. White*

1. ABSTRACT

Limestone caves provide a stable environment for the deposition of dense uniform masses of calcite in the form of stalactites, stalagmites, and flowstone (speleothems). Variations in trace element concentration, isotopic composition, and trace organic compounds incorporated into the calcite provide a highly detailed record that should correlate with temperature and rainfall variations at the land surface. Growth rates of calcite layers are highly variable and range from 5 to 200 μm/year as determined by direct measurement and geochemical models for the kinetics of calcite deposition. Uranium-thorium dating provides time scales for flowstone and stalagmite sequences. At the largest time scales, the mass of deposited calcite relates to glacial and interglacial periods at more northerly latitudes. At intermediate time scales, thousands of years, detailed records of carbon and oxygen isotopes and to a lesser extent Sr/Mg concentrations provide temperature information. Color banding resulting from variations in humic acid concentration and luminescence banding resulting from variations in fulvic acid concentration provide precipitation records with a resolution of one year or better. At the smallest time scales, tens to hundreds of years, historical records can be correlated with observed banding to obtain some insight into the additional influences of soil properties and flow paths in the vadose zone.

* William B. White, Department of Geosciences and Materials Research Laboratory, The Pennsylvania State University, University Park PA 16802.

2. INTRODUCTION

2.1. Background

Limestone caves provide a depositional environment for secondary carbonate minerals, mostly calcite, occasionally aragonite, precipitated from seepage waters entering the cave from the land surface above. The carbonate minerals are deposited in an environment specified by a certain water vapor partial pressure, usually the saturation pressure, a certain carbon dioxide partial pressure, and a certain temperature. The carbon dioxide partial pressure relates to vegetative cover and biological activity in overlying soils and exhibits an annual cycle related to the growing seasons. Typically, the carbon dioxide partial pressure is about ten times the atmospheric background although much higher CO_2 pressures have been recorded. In most caves, the temperature is nearly constant and equal to the mean annual temperature at the cave site. Most caves are sufficiently deep and sufficiently isolated from the surface for annual temperature cycles to be averaged out. They do respond, however, to longer-term temperature fluctuations so that climatic scale temperature changes will be reflected in the caves.

Limestone caves in moderate relief terrains often form in tiers - individual caves or passages within caves stacked in vertical sequences. The tiers represent sequential stages in cave development with the oldest passages on top and the youngest passages – sometimes completely water-filled – on the bottom (although there are some caveats; see Palmer (1987)). Tiered caves preserve the speleothem records over very long periods of time with little disruption or modification. Typically, the ages of caves range from late Pliocene to the present with some definitely older. Trace elements and trace organic compounds incorporated in the secondary carbonates provide a record of past environmental conditions on the land surface with which the caves are intimately connected.

Speleothem records have been probed extensively, especially during the past decade. Special symposia (e.g. Lauritzen, 1996) and special issues of journals dedicated to the topic have begun to appear (e.g. Lauritzen and Lundberg, 1999). Researchers at the University of Mons, Belgium have launched a journal, *Speleochronos*, devoted to speleothems and related cave records. Perrette (1999) gives an excellent recent review. It is the purpose of the present review to sort out the various kinds of information recorded in speleothems and to offer a somewhat subjective evaluation of these records as paleoclimate indicators.

2.2. Time Scales

Data derived from speleothems must mesh in a consistent way with paleoclimatic records collected by other techniques and also track with accepted time scales. The types of records that have been collected are quite diverse and there are differences in the labeling of the time scales. For reference, the sequence of time scales used in the context of most speleothem investigations is illustrated in figure 1.

The longest time scale spans the entire Pleistocene and part of the Pliocene. The time markers are the magnetic reversals that are shown with the chronology set forth by Cande and Kent (1995) and Berggren et al. (1995). The proposed number of glacial advances in the northern hemisphere ranges from 8 to 12 and possibly more (Easterbrook, 1999) so figure 1 subdivides the Pleistocene but omits the pre-Illinoian glacial periods. The oldest "hard" dates for caves are those for caves in the Guadalupe Mountains of New

Mexico (Polyak et al, 1998). These range from 3.9 to 11 Ma, taking development of this group of caves well back into the Miocene. A single date of 87-98 Ma on a spar crystal (Lundberg et al., 2000) suggests some precursor cave development as far back as the Laramide. Caves deposits could contribute to sorting out events of the Pliocene and early Pleistocene providing that methods such as paleomagnetism, cosmogenic isotope dating and U/Pb dating can establish the necessary time scales.

Most relevant to speleothem investigations is the middle to late Pleistocene – the past half-million years. This is the time scale of U/Th dating. Paleoclimatic signals are often matched to variations in oxygen isotope ratios derived from measurements on deep sea cores. This record has been subdivided into isotope stages that in turn correlate with sea level stands and with temperatures. The version of the isotope stage record shown in figure 1 is the SPECMAP compilation here reconstructed from Bradley (1999).

The Holocene spans the past 11,500 years. Much of the Holocene time scale is obtained from Greenland and Antarctic ice-core data, from stratigraphic pollen records, and other records of floral, faunal, and landscape changes. Records younger then 45,000 years are also within the range of radiocarbon dating. The recent Holocene is the historic period when some written records are available and finally the past century or so, the contemporary period, where directly measured climatic data are available for comparison.

In deciphering the records archived in speleothems, there is the challenge of ascertaining the meaning of the record itself – what (if any) climatic parameters correlate with the records. In addition to the determination of the absolute age of the individual records, there is also the question of the time resolution of the records. The various records that have been extracted from caves and their deposits fall into three broad categories with respect to time resolution.

Low resolution records (Thousands of years)
- Geomorphic interpretation of tiered caves
- Magnetic reversals recorded in clastic sediments

Intermediate resolution records (Tens to hundreds of years)
- U/Th and other age dating of speleothems
- Isotopic profiles through speleothems
- Cosmogenic isotope dating of clastic sediments

High-resolution records (One year or less)
- Luminescence banding
- Color (gray scale) banding
- Trace element profiles

Because this review is only concerned with speleothems, not all of these records will be discussed.

3. SPELEOTHEM DEPOSITIONAL MECHANISMS

3.1. Speleothems

Because speleothems are deposited from seeping, dripping, and flowing water in a variety of geochemical regimes, their macroscopic forms and internal structures are highly variable. Because speleothems are often of great beauty and fascinate cave scientists, cave explorers, and casual visitors alike, they have accumulated a lengthy list of names (Hill and Forti, 1997). For speleothems to be of value in deciphering paleoenvironments and

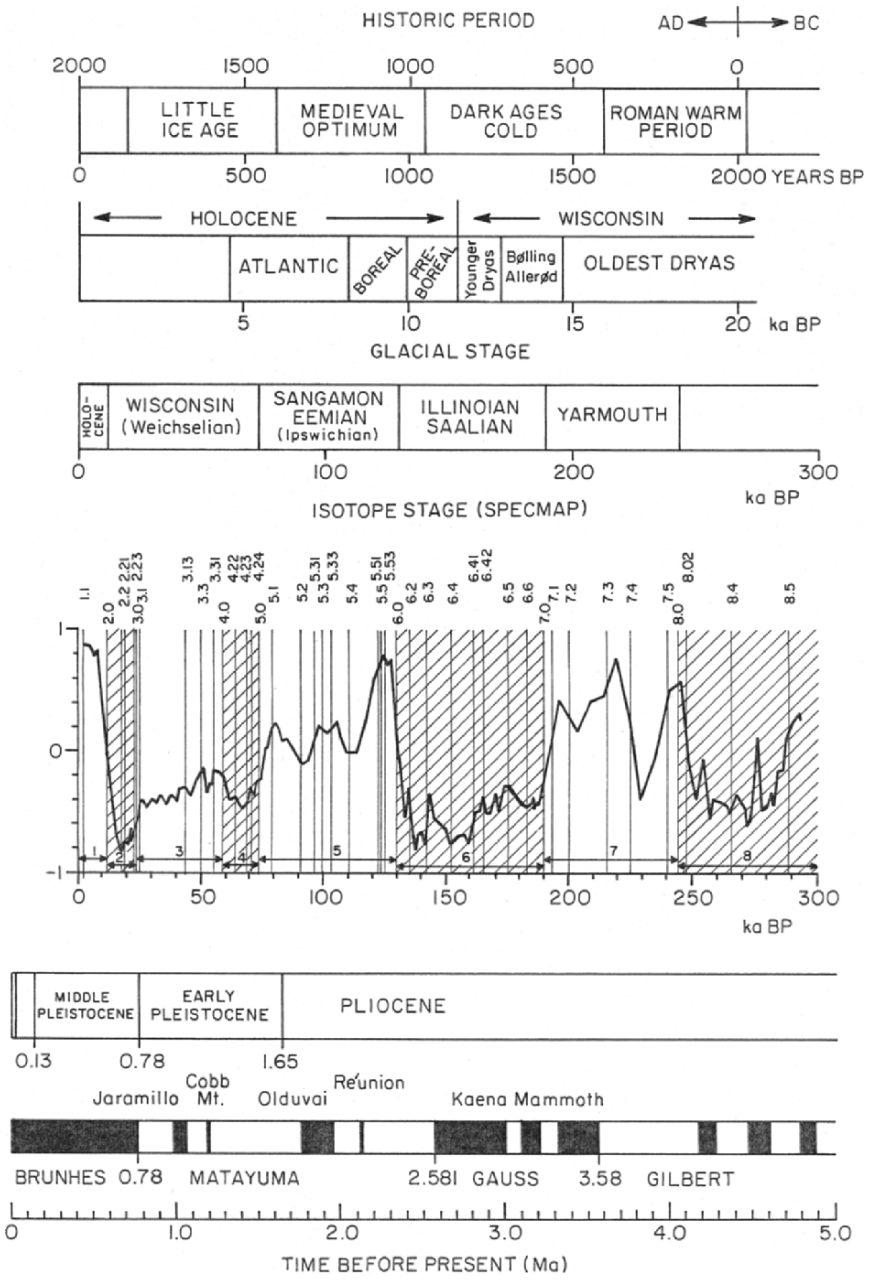

Figure 1. Time scales. Paleomagnetic scale constructed from Cande and Kent (1995) and Berggren et al. (1995). Oxygen isotope stages from SPECMAP and redrawn from Bradley (1999). Late Pleistocene consistent with Greenland ice core records (Alley et al., 1993). Historical period from Lauritzen and Lundberg (1999).

paleoclimates they must contain a definable time axis – a microstratigraphy of sequentially deposited layers. Speleothems in which deposition has taken place erratically or which have undergone dissolution and reprecipitation are generally less suitable for preserving climatic records because they may lack a traceable time line. The speleothems of most value for paleoclimatic studies are stalagmites and flowstone. Mostly these are composed of calcite so it is the deposition of calcite and its uptake of various isotopes, trace elements, and organic compounds that must be interpreted.

Flowstone forms on the walls and floors of caves. It is generally built up of parallel layers which form in sequence from bottom to top or from the wall outward. Because of variations in the flow of water down the walls or across the floor, the thickness of flowstone often varies greatly from one place to the next across the deposit. Stalactites, although also layered structures, are generally much less suitable. The water that feeds stalactites flows both through a central canal and as water films moving down the outside. Although cross sections of stalactites show concentric banding, the time sequence may be distorted and is difficult to define. Stalagmites generally contain the most traceable time lines and a higher resolution stratigraphy than do stalactites and flowstone. Stalagmites reflect all of the complexity of dripping water and as a result are found in a great variety of shapes (Fig. 2). Tall cylindrical stalagmites (often referred to as "candles" or "broomhandles") are generally the most useful. Cylindrical stalagmites occur with a range of diameters and with heights ranging from a few centimeters to many meters (Fig. 3). Their internal stratigraphy consists of a sequence of superimposed caps so that the core of the stalagmite provides a consistant time line. Stalagmites are usually sliced longitudinally and polished to produce a slab with the microstratigraphy displayed (Fig. 4). Observations, direct measurements, and sampling are usually taken along the central axis of the specimen.

3.2. Geochemistry of Cave Carbonate Deposition

The overall geochemical processes describing the deposition of calcite speleothems as set down long ago by Holland et al. (1964) remain valid. They are spelled out in much detail in such textbooks as White (1988) and Langmuir (1997). Only a qualitative description is given below. Figure 5 shows the essential features. Rainfall is usually quoted as having a carbon dioxide partial pressure of about $10^{-3.5}$ bars. More precisely, with the 1998 values for atmospheric CO_2 concentration of 367 parts/million, it is $10^{-3.44}$ (C.D. Keeling and T.P. Whorf, data from Mauna Loa Observatory taken from web site http://cdiac.esd.ornl.gov/ftp/maunaloa-co2). Rainfall percolates through the soil where it dissolves a great deal of additional CO_2 that has been released into the soil atmosphere by respiration of plant roots and by the microbially-mediated decay of organic materials. Soil atmospheres may reach CO_2 concentrations of 10%, much of which is lost by diffusion upward to the atmosphere. CO_2 -rich soil water also extracts various humic substances from the organic matter in the soil. The highly corrosive water then infiltrates downward through the more sterile B-horizon until it reaches the contact with the carbonate bedrock. $CaCO_3$ is dissolved until the water approaches equilibrium at the CO_2 partial pressure brought down from the soil. How close the water approaches equilibrium depends on residence time at the bedrock interface. Trace elements from the bedrock are also taken into solution.

Because the infiltrating water enters the bedrock close to saturation, it migrates downward along fractures carrying its load of dissolved carbonates and other substances with little further dissolution. When the infiltrating water emerges from the roof of an underlying cave passage, it is again out of equilibrium with the local environment. CO_2

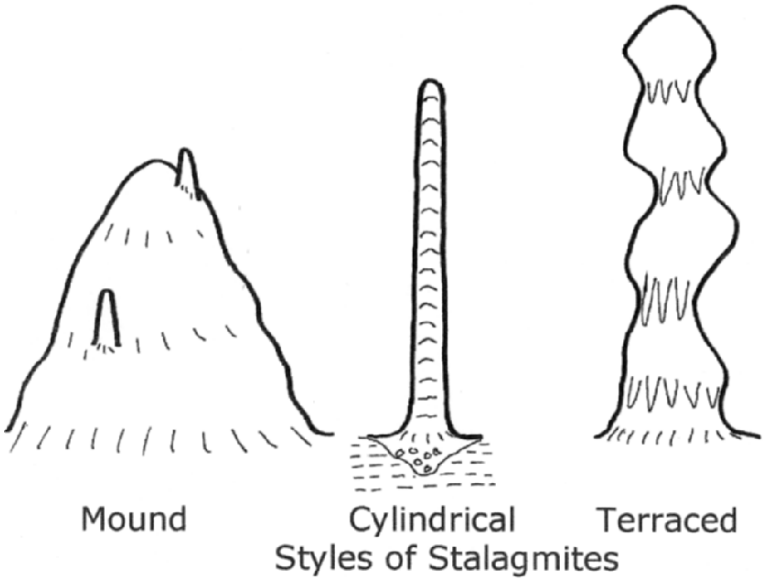

Figure 2. Sketch showing common style of stalagmites.

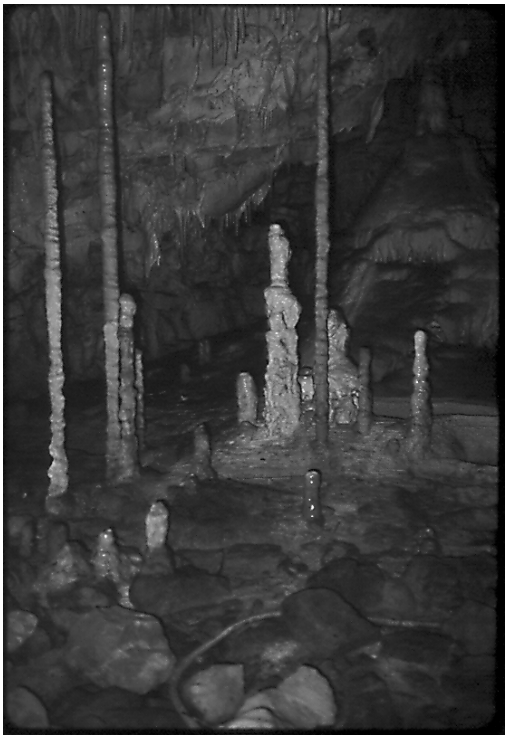

Figure 3. Cylindrical stalagmites in the Catherine Cave, Moravian Karst, Czech Republic.

Figure 4. Longitudinal slice through 25 cm high stalagmite showing alternating light and dark bands. White Arch Cave, Norway. Specimen loaned by S.-E. Lauritzen.

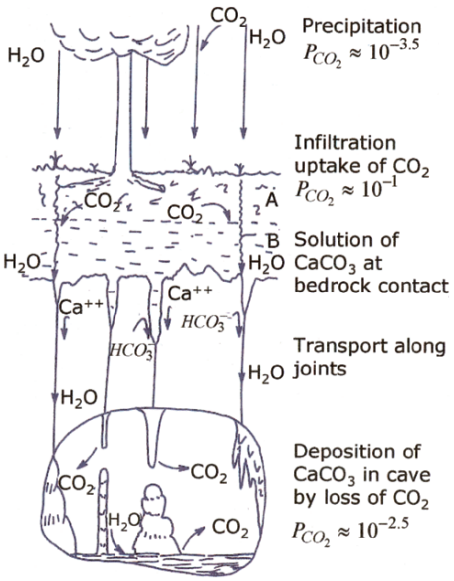

Figure 5. Conceptual model for the deposition of calcite speleothems.

partial pressures in caves are typically about ten time the atmospheric value, or approximately $10^{-2.5}$ bars. The seeping infiltration water dripping from the ceiling, splashing onto the floor, or flowing down the wall, degases CO_2 to the cave atmosphere, becomes supersaturated, and deposits calcite on the growing stalactites, stalagmites, or flowstone. In the deposition process, both organics and trace elements are partitioned into the growing crystals of calcite. The complexity of the generation, transport, and deposition of the calcite in speleothems must be taken into account in trying to interpret the patterns in isotopes, trace elements, and organic molecules found in the speleothem layers.

3.3. Crystal Growth and Textures

The growth of calcite crystals to form speleothems is a delicately balanced process depending on the degree of supersaturation of the water and its total concentration of dissolved carbonates. Waters dripping onto speleothems require supersaturations on the order of $SI_c = +0.5$ in order to overcome nucleation barriers (where Si_c is the saturation index defined in the textbooks cited above). However, the critical supersaturation for 2-dimensional nucleation and the continued growth of a single crystal is only slightly

lower than the supersaturation required for 3-dimensional nucleation of new crystals. Speleothems growing from waters just above the critical supersaturation will form with the internal structure of a single crystal. Such speleothems are easily recognized because they fracture along a single cleavage plane. Very high supersaturations cause the formation of multiple nuclei and result in a speleothem consisting of a large number of small, randomly oriented crystals.

Most speleothems grow in an intermediate range of supersaturations resulting in polycrystalline speleothems with large and partially oriented grains. The fast growth direction in calcite is along the c-crystallographic axis so that grains tend to be elongate in the c-axis direction. The shape, size, and orientation of crystal grains in a solid is known as a "fabric" or "texture" to petrologists (and as "microstructure" to materials scientists looking at the same patterns in ceramics) (Fig. 6).

Inspection of the broken surfaces of damaged speleothems shows that many consist of very coarse crystals – grain sizes on the order of centimeters – while the outermost layer of the speleothem is composed of extremely small crystals, suggesting a major change in depositional mechanism. Some of these dramatic changes in fabric may represent the creation of cave entrances with corresponding changes in CO_2 and water vapor pressures. No systematic investigations seem to have been made.

Studies of speleothem fabrics (Folk and Assereto, 1976; Kendall and Broughton, 1978) show that many flowstones in particular tend to grow as sets of columnar crystals oriented perpendicular to the growth surface (Fig. 6). Each of the columns grew from a separate nucleus. The columnar crystal morphology results from the fast growth of calcite along the c-axis. The size of the crystals and the degree of orientation has been used to deduce information on the paleoenvironment in which the flowstone deposited (Gradzinski et al., 1997). The fabric of recent speleothems deposited in the abandoned Godarville Tunnel in Belgium show much the same form as the fabrics of much older speleothems found in caves (Genty, 1992). Because the columnar structures originate from independent nuclei, the space between the columns can act as depositional sites for clay, sand, pollen, and other particulate material that may be carried into the speleothem by the seepage water.

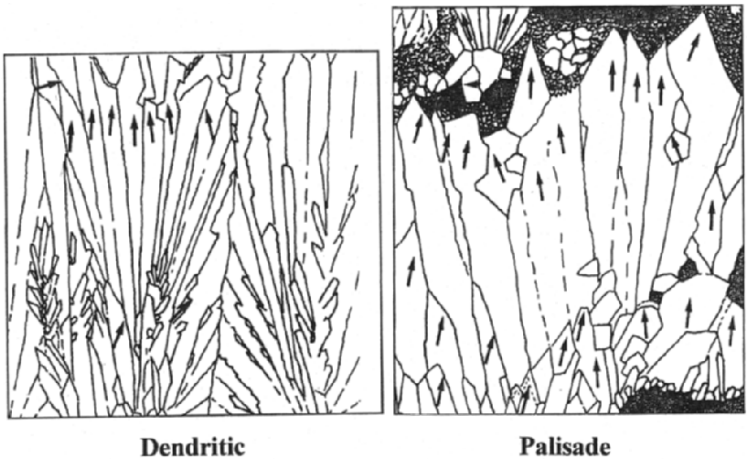

Figure 6. Two common speleothem fabrics. Adapted from Frisia (1994).

3.4. Speleothem Mineralogy

Bulk speleothems generally are composed entirely of calcite. However, aragonite does occur, sometimes interlayered with the calcite. Aragonite is metastable with respect to calcite at atmospheric pressure and is about 11% more soluble than calcite at any specified CO_2 partial pressure. For aragonite to precipitate, the supersaturation must exceed its equilibrium solubility. In order for aragonite to deposit in competition with calcite, either nucleation of aragonite must be enhanced or the nucleation of calcite must be inhibited. The occurrence of metastable aragonite in both freshwater and marine carbonates has been a nagging problem that has accumulated an immense literature (Carlson, 1983). Trace elements play a role. Sr^{2+} is thought to promote aragonite nucleation. Once aragonite nuclei are formed, they will continue to grow at the expense of calcite, which has a higher nucleation barrier. Mg^{2+} acts to inhibit calcite nucleation, thus allowing the solution to build up the necessary supersaturation for the precipitation of aragonite (Berner, 1975). Other trace elements and quite possibly trace organics also have an effect. Many of the details of calcite growth are being worked out with the use of the atomic force microscope (Teng et al., 2000; Davis et al., 2000).

In addition to the modifying influences of trace elements, only the rate of precipitation is important. High rates of precipitation can overdrive the system so that the necessary supersaturation is achieved for aragonite deposition. In completely sealed caves the water vapor partial pressure is at saturation and CO_2 partial pressures may rise to approach those of the seepage waters. As a result, carbonate deposition takes place slowly and coarse-grained calcite is the product. In dry caves or at deposition sites close to cave entrances, water vapor partial pressures are lower and CO_2 partial pressures are closer to the atmospheric background value. Deposition rates are higher and it appears that aragonite can be deposited in these environments (Bar-Matthews et al., 1991).

Denniston et al. (2000) have made use of the alternating deposition of calcite and aragonite to interpret changes in the Indian monsoon season. Aragonite layers in dated speleothems in the Siddha Baba Cave in central Nepal suggest that the period 2300 to 1500 B.P. represents a dry period with greatly decreased monsoon precipitation. After 1500 B.P. calcite layers appear suggesting an abrupt increase in precipitation rate.

4. DATING SPELEOTHEMS

The technological advance that moved speleothem studies into a prominent place in the study of paleoclimates was the development of reliable and accurate methods for assigning absolute dates to individual calcite layers (Thompson et al., 1975). Such methods as U/Th dating and ^{14}C dating are now well established. A brief review is given here only because all of the other speleothem data depend on these techniques to establish time scales.

4.1. U/Th Dating and Related Techniques

The extraction of dates from the uranium and thorium isotope ratios in speleothems depends on a quirk in the geochemistry of these two elements. Uranium is easily oxidized to the U^{6+} state where it usually appears as the UO_2^{2+} ion. The uranyl ion in addition to its intrinsic solubility also forms soluble carbonate complexes that further mobilize the element in karstic ground waters (Langmuir, 1978, 1997). Thorium is firmly locked into the insoluble Th^{4+} state and is immobile in ground water (Langmuir

and Herman, 1980). Thus speleothem-depositing infiltration waters may incorporate uranium into the speleothem, but not thorium. It can then be assumed that any thorium found in the speleothem has formed by the decay of uranium and thus is a measure of the time since the speleothem was deposited.

The dominant isotope, ^{238}U, has a half life of 4.510×10^9 years. It heads a long decay chain of daughter isotopes (Fig. 7) which contains only two moderately long-lived isotopes: ^{234}U with a half life of 2.48×10^5 years and ^{230}Th with a half life of 7.52×10^4 years. The relationships between these interlocking decay schemes have been worked out in detail for some time (Faure, 1986; Ivanovich and Harmon, 1992). The final equations are

$$\frac{U^{234}}{U^{238}} = 1 + \left[\left(\frac{U^{234}}{U^{238}}\right)_0 - 1\right] e^{-\lambda_4 t} \quad (1)$$

$$\frac{Th^{230}}{U^{234}} = \frac{\left(1-e^{-\lambda_0 t}\right)}{\left(U^{234}/U^{238}\right)} + \frac{\lambda_0}{\lambda_0 - \lambda_4}\left[\left(\frac{U^{234}}{U^{238}}\right)_0 - 1\right]\left(e^{-\lambda_4 t} - e^{-\lambda_0 t}\right) \quad (2)$$

where λ_0 and λ_4 are the decay constants for ^{230}Th and ^{234}U respectively. Thus there are two equations in two unknowns, time, t, and the initial $^{234}U/^{238}U$ ratio. By measuring the isotopic ratios defined by equations (1) and (2), the age of the specimen can be calculated. In the past, the isotopic ratios were measured by α-counting spectroscopy (Harmon et al., 1975). More recent work has made use of heavy ion mass spectrometry to improve both sensitivity and accuracy (Edwards et al., 1987; Li et al., 1989).

The mathematics places some intrinsic limits on U/Th age dating. Figure 8 shows the relation between the isotope ratios for various ages. For ages less then about 200,000 years, the age scales with the Th/U ratio. At ages greater than 200,000 years, the age contours begin to coalesce as the system approaches isotopic equilibrium. It is for this reason that the age limit for α-counting techniques is 350,000 years. The higher precision of mass spectrometric measurements allows dates to be extended to perhaps 600,000 years.

Successful dating of speleothems by U/Th methods depends on satisfying three criteria: (1) The specimen must contain enough uranium to measure. The required concentration varies with technique with mass spectrometry offering major advantages over decay counting. Many dates have been obtained with uranium concentrations of hundreds of ppb. (2) The specimen must contain negligible or calculatable initial ^{230}Th. The presence of the isotope ^{232}Th is a criterion for contamination because it will be present in any thorium-bearing minerals that may occur in the insoluble detritus, but is not part of the uranium decay chain. (3) The specimen must not have undergone dissolution and recrystallization that would scramble the U/Th isotopic composition. See the article by Dorale et al. in this volume for a more detailed discussion of the method and its limitations. The principles of U/Th dating are well established although only a few laboratories make a specialty of the technique.

An alternative dating technique that also makes use of the uranium incorporated in speleothems is to treat the speleothem as a dosimeter. The α-particles emitted during uranium decay create defects in the calcite structure. The longer the speleothem has been exposed to the radiation, the greater the number of defects. These defects contain trapped

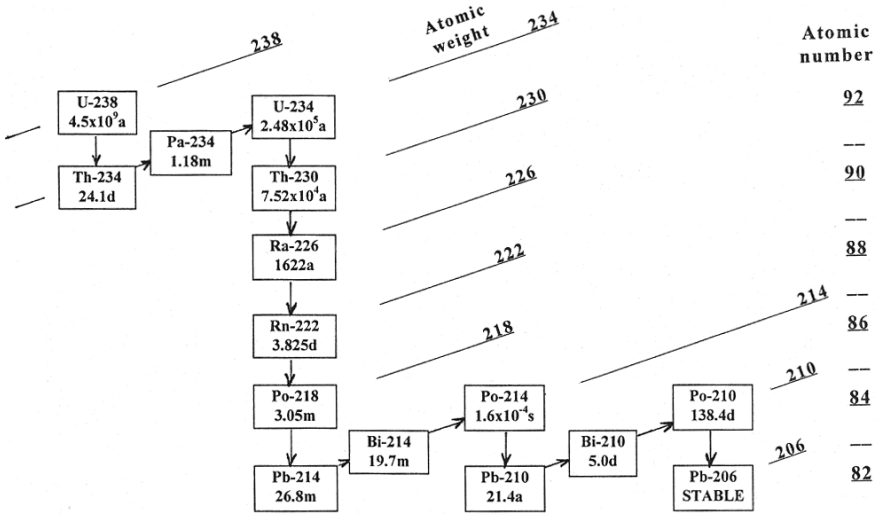

Figure 7. Decay chain for ^{238}U. Alpha decays are shown by vertical down arrows; beta decays by diagonally up arrows. Half lives of isotopes are given in the boxes as years (a), days (d), minutes (m), or seconds (s) as appropriate.

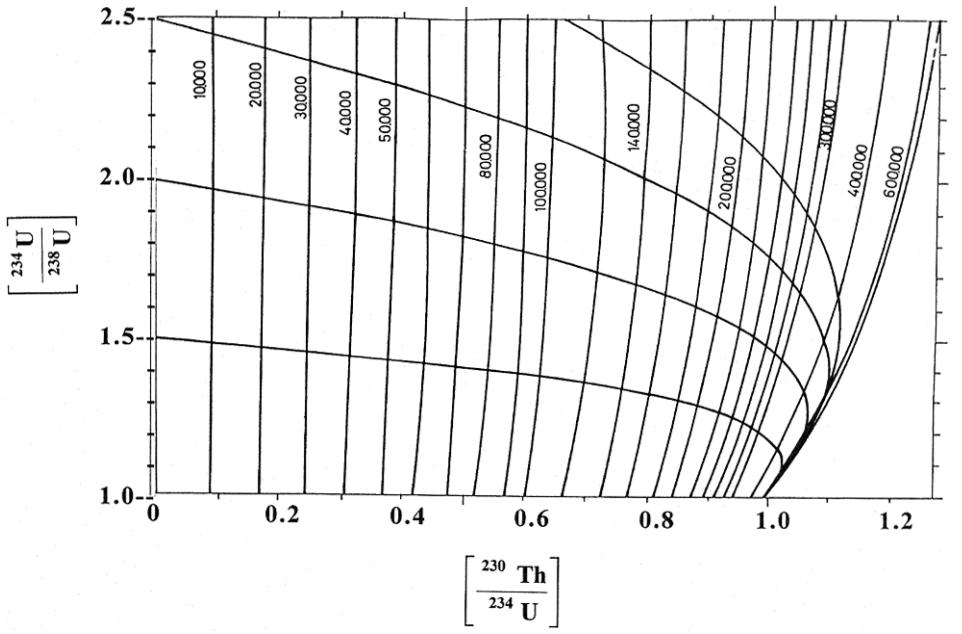

Figure 8. Isochrons for various $^{234}U/^{238}U$ and $^{230}Th/^{234}U$ ratios. Contours are in years. This identical diagram appears in Harmon et al. (1975) and in Quinif (1989). Neither is credited to any other sources.

electrons, the concentration of which can be measured by electron spin resonance (ESR) spectroscopy (also known as electron paramagnetic resonance (EPR) spectroscopy). Alternatively, the concentration of defects can be determined by measuring thermoluminescence. Heating the speleothem allows the electrons to escape from the traps and release their stored energy as a flash of light that can be measured. Comparisons between ESR dates and U/Th dates are sparse but agreement between the methods has not been particularly good (Hercman and Lauritzen, 1996). No systematic evaluation of thermoluminescence dating seems to have been applied to speleothems.

4.2. Uranium/Lead Dating

It is possible, in principle, to use the isotope ratios $^{238}U/^{206}Pb$ or $^{235}U/^{207}Pb$ to calculate speleothem ages on the million-year scale. Such measurements could provide dates for the oldest speleothems that anyone is likely to find. With these isotopes, it is the half-lives of ^{238}U and ^{235}U that determine the time scale. The difficulty is that lead is also mobile in the karst environment. It is difficult to separate lead that resulted from uranium decay in the speleothem from other lead that may have precipitated directly from the drip-water. Richards et al. (1996) determined the age of a stalactite from Winnats Head Cave in the UK as 250 ± 12 ka compared with 255 ± 30 ka determined by U/Th methods. Lundberg et al. (2000) found 87-98 Ma for a calcite spar crystal from a Guadalupe Mountain cave. The U/Pb technique has promise but requires a great deal of development.

4.3. Carbon-14 Dating

Dating by the natural decay of ^{14}C is a well-established technique for carbon-bearing materials with ages less than perhaps 50,000 years. In principle it should work for young speleothems. The problem that arises is isotope exchange. The CO_2 extracted from the soil by infiltrating ground water is derived from the atmosphere and from active biological processes in the soil so it should be composed mainly of young carbon. However, the reaction of this water with limestone at the base of the soil and below is

$$CaCO_3 + CO_2 + H_2O \Leftrightarrow 2\,HCO_3^- + Ca^{2+}$$

The carbon derived from the limestone is old carbon with no residual ^{14}C. In the deposition of speleothems, the above reaction is reversed. In the absence of any isotope exchange, the carbon that is deposited in speleothems should be 50% old carbon and 50% young carbon. In reality, there is extensive isotope exchange during the complex process of dissolution, transport, and redeposition. It appears that speleothems contain about 85% young carbon (Hennig, et al., 1983), a proportion that has been confirmed by other measurements (Genty and Massault, 1997). The uptake of radiocarbon in calcitic speleothems has recorded the pulse of ^{14}C produced by nuclear weapons testing in the late 1950's and early 1960's (Genty et al., 1998).

Dating of young speleothems in Red Spider Cave, Georgia, with the assumption of 85% young carbon, gave good results (Brook and Nickmann, 1996). Holmgren et al. (1994) made a detailed comparison, on a stalagmite from Botswana, of the dates obtained by U/Th alpha-counting methods and dates on the same location in the stalagmite obtained by ^{14}C methods. The results suggest that speleothems can give usable ^{14}C dates back to about 20,000 years. Older dates show a great deal of scatter. The <20,000 year ^{14}C dates were consistently about 10% lower than the corresponding U/Th dates. The

issue of the accuracy of ^{14}C-dating of speleothems was addressed by mass-spectrometry (Richards et al., 1999). If it can be surmised that the dead carbon effect has remained constant back through time, speleothems, with the advantages of high-resolution and long-term continuity, may represent the best of materials to accurately calibrate the ^{14}C timescale.

4.4. Lead-210 Dating

Many karst waters contain significant quantities of ^{222}Rn. Radon decays rapidly through intermediate short-lived isotopes (Fig. 7) to ^{210}Pb, which has a half-life of 21.4 years. The ^{210}Pb is deposited in growing stalactites from the ^{222}Rn in the drip water. By measuring ^{210}Pb along the axis of a soda straw stalactite (Baskaran and Iliffe, 1993) it was possible to date the stalactite and thus its growth rate over a time range up to about 100 years. This is a potentially useful method for relating other records in young speleothems to contemporary climatic records.

4.5. Dating by Magnetic Measurements

Some speleothems, at least, contain enough magnetic minerals to allow the determination of the natural remanent magnetism. Determination of magnetic orientations along the growth direction of a speleothem, combined with U/Th dating to assign absolute ages, allows the compilation of a curve of secular variation for the region in which the cave is located. Measurements on speleothems from western Canada and Mexico gave results in good agreement with the accepted secular variation curves for those sites (Latham et al., 1979, 1982, 1986, 1987). In principle, one could extract dates from magnetic measurements by matching secular variation curves determined from speleothems with the known secular variation curves for the region. It is a rather difficult approach and does not seem to have been followed up beyond the work cited above. It is also possible that magnetic reversals could be observed in speleothems that would give a fixed time reference. Since the first reversal at 780 ka is beyond the range of U/Th dating, such reversals would provide useful isochrones for old speleothems.

5. GROWTH RATES FOR SPELEOTHEMS

5.1. Growth Rates Over Long Time Scales

It was proposed early on that cylindrical stalagmites should grow at near-constant rates. Drops falling onto the stalagmite flow outward over the top of the stalagmite depositing calcite until the water film comes approximately into equilibrium with the cave atmosphere. The diameter of the stalagmite then depends on both the drip rate and on the degree of supersaturation. Franke (1965) used a mass balance argument to show that the diameter of a cylindrical stalagmite was given by

$$d = 2\sqrt{\frac{q(C - C_s)}{\pi \, dz/dt}} \tag{3}$$

where d is the stalagmite diameter, q is the drip rate, C is the concentration of the inflowing water, C_s is the saturation concentration at the CO_2 pressure of the cave atmosphere, and dz/dt is the growth rate of the stalagmite along its axis.

Curl (1973) published more detailed and quantitative calculations on the rate of stalagmite growth and showed that there are actually two growth regimes. There is a rapid flow regime in which the equilibrium diameter varies with the square root of the flow rate as in Franke's theory and there is a slow flow regime which is independent of the flow rate. The slow flow regime leads to a minimum diameter for stalagmites given by

$$d_{\min} = 2\sqrt{\frac{\nu}{\pi\delta}} \tag{4}$$

where ν is the volume of the water drop and δ is the thickness of the moisture film left on the surface of the stalagmite by the falling drop. The minimum diameter was calculated to be about 3 cm, which is generally consistent with observations.

A more direct way to determine the average growth rate over long time periods is to measure U/Th ages along the axis of the stalagmite. Not only does a plot of age against the height above the base give a growth rate but, if the dates along the axis of the stalagmite are taken at sufficiently close intervals, the measurements reveal variations and hiatuses in the growth. Further, such data show the beginning and end of growth. The top of the stalagmite may be old with growth having ceased perhaps thousands of years before present.

A number of such measurements have been made and some results are plotted in figure 9. The available data span many geographical locations and climatic regimes. The growth rates based on the linear slopes in figure 9 are summarized in Table 1. With an average growth rate of 40 μm/year, a 1-meter stalagmite would be expected to provide a record of 25,000 years.

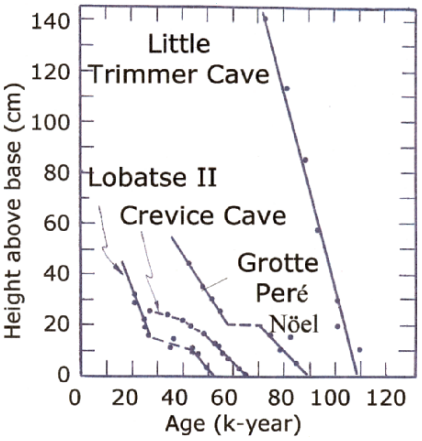

Figure 9. Growth of cylindrical stalagmites based on U/Th dating. Lobatse II Cave, Botswana, (Holmgren et al, 1994); Crevice Cave, Missouri, (Dorale et al., 1998); Grotte Pere Noel, Belgium, (Quinif, 1991); Little Trimmer Cave, Tasmania, (Goede et al., 1986).

Several complications are apparent in the data of figure 9. Although some stalagmites have grown uniformly, so that there is a linear relation between height and age, two of the four sets of measurements show a distinct hiatus where growth stopped for periods of 10,000 to 20,000 years and then resumed again. One stalagmite, that from Crevice Cave, Missouri, apparently underwent a decrease in growth rate from a slow initial rate to an even slower rate late in its history. All of these specimens are fossil stalagmites, that is, growth began, continued for a period of time on the order of a few tens of thousands of years, and then stopped.

Table 1. Growth rates of stalagmites determined by U/Th dating along the stalagmite axis.

Location	Growth Rate (mm/year	Age Range (years)*	Reference
Little Trimmer Cave, Tasmania	0.039	73,000 – 110,000	Goede et al (1986)
Crevice Cave, Missouri	0.0095	49,000 – 65,000	Dorale et al. (1998)
Grotto Pere Noel, Belgium	0.016	42,000 – 55,000	Quinif (1991)
Lobatse II Cave, Botswana	0.027	20,000 – 27,000	Holmgren et al. (1994)
White Arch Cave, Norway	0.113	6500 - 8200	Lauritzen (Pers. Comm.)

*Age range for linear portion of data from which growth rate was extracted. Hiatuses not included.

5.2. Direct Measurements of Growth Rates

Growth rates can be determined in young speleothems by direct observation. If the time of growth initiation can be established, for example by speleothems growing in abandoned mines or in caves where new growth has occurred over some known excavation, growth rate can be determined from flowstone thickness or stalagmite height combined with the time interval since initiation. Baker and Smart (1995) used this approach for flowstone buildup in Kents Cavern and for the Dolebury Levy mine in the United Kingdom (Table 2). For these sites, the theoretical growth rate was also modeled from the water chemistry using the early growth rate calculations of Buhmann and Dreybrodt (1985a,b; 1987). Calculated growth rates were a factor of 2–4 times faster than measured ones.

Direct measurements of growth rates can also be obtained by counting laminations much in the manner of counting tree rings. This approach assumes that the laminations are annual and, of course, that the speleothem is still growing. Measurements by Baker et al. (1998) in the Browns Folly Mine in the United Kingdom show good agreement between growth rates estimated from counting laminations and growth rates determined by total speleothem growth over a known time period. A summary of growth rate data (Table 2) shows that growth rates vary considerable from a few tens to a few hundreds of micrometers/year. Growth rates scale roughly with the hardness of the drip water but there are a number of controlling factors involved. As a result, it is difficult to correlate growth rate directly with environmental parameters.

5.3. Theoretical Growth Rates

Determination of the rate of flowstone growth or stalagmite growth from geochemical models is complicated. Growth rates depend on dissolved carbonate concentration in the drip water, on the ratio of the CO_2 pressure of the drip water to the CO_2 pressure of the

Table 2. Some Representative Growth Rate Data for Flowstone and Stalagmites

Sample Site	Growth Rate (mm/year)	Rate from Laminae (mm/year)	Model Rate (mm/year)	Reference
Kents Cavern	0.201		0.09	Baker & Smart (1995)
Kents Cavern	0.019		0.09	Baker & Smart (1995)
Kents Cavern	0.018		0.06	Baker & Smart (1995)
Kents Cavern	0.039		0.10	Baker & Smart (1995)
Kents Caverns	0.041		0.10	Baker & Smart (1995)
Dolebury Levy	0.019		0.07	Baker & Smart (1995)
Dolebury Levy	0.018		0.07	Baker & Smart (1995)
Dolebury Levy	0.019		0.07	Baker & Smart (1995)
Browns Folly	0.023	0.10		Baker (1998)
Browns Folly	0.064	0.23		Baker (1998)
Browns Folly	0.078	0.08		Baker (1998)
Browns Folly	0.083	0.09		Baker (1998)
Browns Folly	0.157	0.13		Baker (1998)
Grotte de Villars	0.55			Baker (1998)
Godarville Tunnel	0.89			Baker (1998)

cave atmosphere, on the thickness of the moisture film from which the CO_2 is degassing, and on the rate at which drip water is supplied. Dreybrodt and his associates have constructed the most comprehensive models which have been evolving for several decades (Dreybrodt, 1980, 1981; Buhmann and Dreybrodt, 1985; Dreybrodt and Buhmann, 1987; Dreybrodt (1988); Dreybrodt et al. (1998).

According to the Dreybrodt model, the rate of deposition from a thick moisture film where ion motion is determined by diffusion is given by the deceptively simple equation

$$R = \alpha (C - C_s) \tag{5}$$

where R is the deposition rate in mmole $cm^{-2}sec^{-1}$, α is a the kinetic rate constant with units of cm sec^{-1} which is dependent on temperature, and C_s is the saturation concentration which is dependent on CO_2 partial pressure and on temperature. For thin moisture films of thickness δ, the drip rate becomes important. For the range $0.04 > \delta > 0.02$ cm the rates do not depend on δ. The molecular accumulation rate between two drops falling onto a thin film in a time interval t_d is given by

$$R_{acc} = (C - C_s)\frac{\delta}{t_d}(1 - e^{\frac{t_d}{\tau}}) \tag{6}$$

where $\tau = \delta/\alpha$ is the time constant for the exponential decay in growth rate. According to Baker et al. (1998), if $t_d < 0.2\ \delta/\alpha$, the accumulation rate can be estimated from equation (5) to within 10%. Some predictions of the Dreybrodt model are given in figure 10 and Table 2.

6. BULK DEPOSITION OF SPELEOTHEMS

A huge number of U/Th dates have been obtained in many contexts (Ivanovich and Harmon, 1992) including many dates on speleothems. Data on 664 speleothem dates

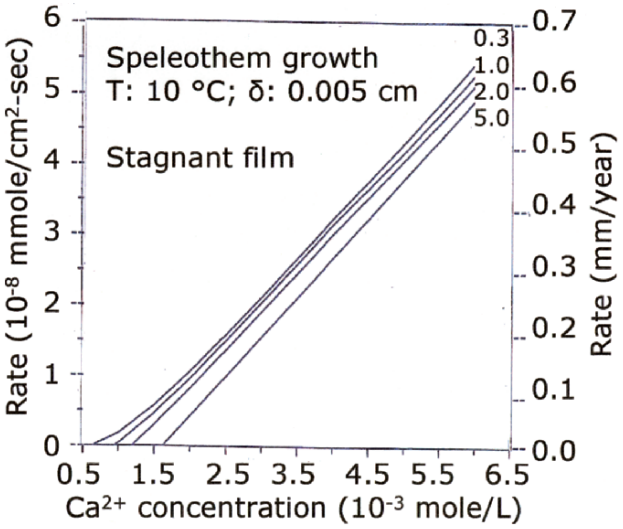

Figure 10. Theoretical growth rates of calcite from thin water films. Contours are CO_2 partial pressures in units of 10^{-3} atm. Adapted from Baker et al. (1998).

obtained through the early 1980's are summarized by Hennig et al. (1983). The first results from U/Th dating of speleothems revealed ages from essentially modern to what was at that time the limit of the age dating technique (350,000 years) and some speleothems that were too old to be dated.

One of the immediate applications of speleothem dates was that they provided minimum ages for the cave passages from which they were collected. The dates could be used to lock in the time scale for landscape evolution, rates of denudation, and establish time scales for tiered caves (Atkinson et al., 1978; Gascoyne et al., 1983). Results through 1990 are summarized by Atkinson and Rowe (1992). A recent application is to the Demanova Valley in Slovakia, which contains one of the classic examples of a tiered cave system. U/Th dating of level IV speleothems combined with magnetic reversals measured in the clastic sediments allowed level IV to be placed in the range of 780 – 685 ka, older than previously proposed, thus shifting the entire time scale for the cave system (Hercman et al., 1997).

6.1. Direct Climatic Correlations

Because speleothem growth depends on a supply of drip water, breaks in speleothem growth could be interpreted as an interruption of the water supply. That in turn could be the result of increased aridity at the land surface or of frozen ground and glacial advance. These breaks can occur within individual speleothems as illustrated by the hiatuses that appear in the growth curves shown in figure 9 or they can be recognized by the absence of speleothems in certain age ranges. Either case requires evaluation of a sufficiently large number of speleothems to be confident that the signal is of regional significance and not the result of a quirk in local hydrology.

The absence of speleothem deposition in the Nullarbor caves in southern Australia more recently than 400 ka was explained in terms of increasing aridity in the middle and

late Pleistocene (Goede et al., 1990). Other speleothem data from Australia correlated relative aridity with interglacials (Ayliffe et al., 1998).

Brook et al. (1990) found pollen grains incorporated in the pore spaces within the speleothem fabric. Since the age of the encapsulating calcite could be determined by U/Th methods, the age of the pollen could also be determined far beyond the usual limitation of carbon-14 dating. From pollen speciation in speleothems, Brook et al. concluded that the Chihuahuan Desert of southwestern United States and the Kalahari Desert of northwestern Botswana were wetter during northern hemisphere glacial and interstadial times. In contrast, wetter conditions in the Somali-Chalbi Desert corresponded with interglacials and to a lesser extent with interstadials.

Similar observations in Red Spider Cave, northwest Georgia, provided a good pollen record over the past 40,000 years, thus allowing interpretation of the local climate through the last glaciation in an area well south of the glacier margins (Brook and Nickmann, 1996).

6.2. Pleistocene Deposition of Speleothems at Northern Latitudes

Many of the early speleothem dates were measured on specimens taken from caves in northern latitudes, notably Canada (Harmon et al., 1977; Gascoyne et al., 1981), Britain (Gascoyne et al., 1983; Gascoyne, 1984; Atkinson et al., 1986) and Norway (Lauritzen and Gascoyne, 1980). It was quickly apparent that the speleothem ages were clustered. There were many Holocene specimens as might have been expected, but there were also many specimens with ages in the range of 100,000 years whereas there were other time periods when there seems to have been little speleothem growth. Lauritzen (1991) used the Norway data to construct a series of "speleothem chronozones" which he matched with reasonable success against the isotope stage record. Hennig et al (1983) attempted to transform simple bar graphs of date distributions into a continuous function. There has been some discussion concerning the choice of weighting function used to take account of the greater experimental uncertainties in the older dates (Gordon and Smart, 1984). Gordon et al. (1989) used the large collection of dates from Britain to construct a speleothem deposition distribution function. Figure 11 shows Lauritzen's (1993) compilation of his distribution function from Norway, the distribution function from Britain, and a bar-graph distribution of dates from more southern regions of Europe and North America (drawn from Hennig et al., 1983).

The deposition of speleothems in northern latitudes has been punctuated by advances and retreats of the Pleistocene glaciations. The most obvious feature in the Norwegian data is the peak at 125 ka, which correlates with isotope stage 5e, a major warm period that allowed extensive speleothem growth even at the latitude of Norway. The same peak appears in the data from Britain but the peak is more spread out, spanning essentially all of the interglacial marked by isotope stage 5. Other peaks and dips are possibly related to retreats and advances during the Wisconsinan glaciation. The distribution function is truncated at the Holocene and does not show the very extensive speleothem deposition of the past 11 ka. Data from more southern latitudes are more spread out with less contrast between stadials and interstadials although the isotope stage 5 maximum is apparent. Curiously, speleothem dates from the Helderberg Plateau of New York fail to show any speleothem activity at isotope stage 5e (Lauritzen and Mylroie, 2000).

The mechanisms for the shut-down of speleothem growth in glacial and periglacial climates include blockage of seepage water by perennially frozen ground, by ice cover and by dramatic decreases in biogenic CO_2 because of sparse vegetation and cold temperatures. Dreybrodt (1982) has presented an argument for modest speleothem

growth in the absence of biogenic CO_2 sources. If infiltration water is in equilibrium of atmospheric CO_2 at a temperature close to the freezing point of water, this water will be warmed somewhat as it passes down to the cave. The small temperature rise will be sufficient to supersaturate the water and cause calcite to be deposited. Dreybrodt estimates a maximum growth rate of 10 μm per year.

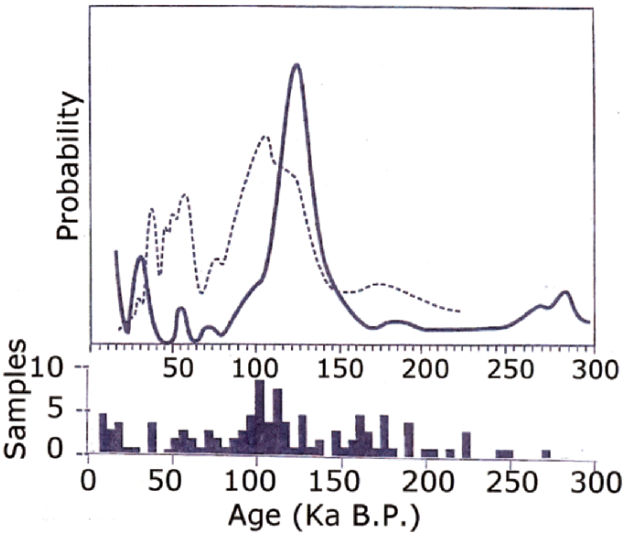

Figure 11. Distribution of speleothem growth over time for the middle and late Pleistocene. Solid curve represents 100 speleothem dates from Nordland, Norway. Dashed curve represents 260 dates from Britain drawn from Gordon et al. (1989). The bar graph is the distribution of 116 dates from southern regions of Europe and North America drawn from Henning et al. (1983). Compilation from Lauritzen (1993).

6.3. Speleothem Deposition in Relation to Sea Level Changes

In low relief coastal karst, such as the Yucatan and the Bahamian Platform, caves that have developed during the sea level minima associated with glacial maxima are flooded by the sea level rise during interglacial periods. Speleothems develop in many of these caves during glacial episodes when sea levels are low. Dates from these speleothems thus indicate the chronology of sea level lowering (Gascoyne and Harmon, 1992). Speleothems collected from relatively shallow (0 < 15 m) depths in underwater caves in Bermuda (Harmon et al., 1978-a) and the Bahamas (Li et al., 1989; Lundberg and Ford, 1994) show a succession of speleothem ages indicating sea level lows and missing speleothem deposition that indicates sea level highs. In general these agree with the isotope stage record and with the speleothem record at northern latitudes. Lundberg and Ford specify sea level highs at 100, 125, 215, and 233 ka BP.

There are deeper caves that contain stalactites and stalagmites that could only have formed when the cave was air-filled. Using mass spectrometric U/Th dating, Richards et al. (1994) measured sea level low stands down to 50 meters below present sea level. The last extensive thrust of the Wisconsinan ice sheet at about 20 ka is clearly shown. Speleothems recovered from a cave on Andros Island, Bahamas at −45 meters was dated at 139 – 160 ka, showing that sea level must have been at least this low at that time

(Gascoyne et al., 1979). These data are indicators of the sea level minima associated with the glaciation of isotope stage 6.

The reverse interpretation can be applied to presently air-filled coastal caves that contain speleothems with the rough textured overgrowths characteristic of deposition under water. Such dated deposits observed on Mallorca were correlated with sea level highs on the Mediterranean coast (Vesica et al, 2000).

7. ISOTOPE AND TRACE ELEMENT STUDIES OF SPELEOTHEMS

Given that flowstone and stalagmites may provide relatively continuously time lines that can be accurately calibrated by U/Th dating, it is possible to extract paleoclimatic signals beyond the bulk deposition of the calcite itself. This has been accomplished by tracking various isotope and trace element profiles. Samples can be drilled at sufficiently close intervals along a sawed slab of stalagmite or flowstone to provide profiles with a time resolution of a few tens to a few hundred years.

7.1. Fluid Inclusion and Drip Water Studies

Most speleothem crystals are translucent rather than transparent. This is because of the presence of myriad tiny bubbles trapped in the growing calcite. The bubbles provide a sample of the water from which a particular bit of calcite grew. Measurements can also be made on the drip water from actively growing speleothems. The calibration is important because of the complicated pathway taken by the infiltration water from its origin as rainfall, through soil water, to water dissolving limestone at the bedrock interface, to drip water and finally to incorporation in the speleothem. If speleothem isotope ratios are to provide useful climatic information, it must be shown that the isotope record incorporated in the speleothem accurately reflects the isotope composition of the original rainfall.

From drip water and from the water in fluid inclusions, oxygen isotope ratios and deuterium/hydrogen (D/H) ratios can be determined. These are usually expressed as a shift in parts per thousand from the isotope ratios in a standard. For oxygen

$$\delta^{18}O = \left[\left({}^{18}O/{}^{16}O\right)_{sample} / \left({}^{18}O/{}^{16}O\right)_{standard} - 1\right] x\,1000 \qquad (7)$$

The usual reference for water is "standard mean ocean water" (SMOW). However, oxygen (and carbon) isotope ratios in speleothems are often reported using the PDB (Peedee belemnite) standard (Faure, 1986). Currently, one should report relative to the VPDB standard.

Measurements of δD and $\delta^{18}O$ from both drip waters and fluid inclusions (Schwarcz et al, 1976; Yonge et al., 1985) showed that isotope ratios of these waters fell on the meteoric water line (equation 8).

$$\delta D_w = 8\delta\,{}^{18}O_w + 10 \qquad (8)$$

The D/H ratios of the fluid inclusions should not have shifted because of isotope exchange with the encapsulating calcite since calcite does not contain these isotopes. Thus, equation (8) can be used to estimate the oxygen isotope ratios in fluid inclusions.

Given evidence for isotopic equilibrium (Hendy, 1971; Gascoyne, 1992), the isotopic composition of speleothem calcite will then be determined by the fractionation that takes place during crystallization.

If the system is at isotopic equilibrium, the fractionation constant for calcite precipitating from dripwater is given by

$$\alpha_{cw} = \frac{1+10^{-3}\,\delta\,^{18}O_c}{1+10^{-3}\,\delta\,^{18}O_w} \tag{9}$$

The fractionation constant is temperature dependent. Thus if one can determine $\delta^{18}O_c$ and $\delta^{18}O_w$ independently, the temperature can be calculated from it. The experimental relationship determined by Friedman and O'Neill (1977) is

$$1000\,\ell n\,\alpha_{cw} = 2.78\,x10^6\,T^{-2} - 2.89 \tag{10}$$

This equation was used by Gascoyne et al. (1980) in their temperature determinations.

Early work on oxygen and hydrogen isotope ratios from caves in North America (Harmon et al., 1978b), including West Virginia (Thompson et al., 1976) and Kentucky (Harmon et al., 1978c), allowed the construction of a sequence of warm and cold periods back to 200 ka. These were more or less in agreement with the glacial sequences as known at the time and illustrated the potential of oxygen using isotope ratios as a paleothermometer.

7.2. Oxygen Isotope Profiles

To determine $\delta^{18}O_w$ using equation (8) requires measuring D/H ratios which in turn means capturing the water in speleothem fluid inclusions. Analysis of fluid inclusions is technically difficult and requires larger samples than would be necessary if one needed only to determine $\delta^{18}O_c$ from the calcite. Accordingly, many investigators have chosen to generate higher resolution records by analyzing only $\delta^{18}O_c$ from many closely spaced samples. Because $\delta^{18}O_w$ is not known, a temperature equation must be derived and calibrated, for example the equation used by Dorale et al. (1992).

Lauritzen (1995) and Lauritzen and Lundberg (1999) have proposed a "speleothem delta function". Using the expression for the calcite-water fractionation constant (equation 9) combined with the known exponential dependence of the fractionation constant, α_{cw}, on temperature and adding some correction terms the following was obtained.

$$\delta\,^{18}O_c = \left\{\exp\left[\frac{a}{(T_1+273.15)} - b\right]\left[F(T_2,t,g)+10^3\right]\right\} - 10^3 \tag{11}$$

T_1 is the cave temperature in degrees Celsius, a and b are empirically derived constants and $F(T_2, t, g)$ is a "dripwater function" that depends on the mean annual precipitation temperature, time, t, and geographical location, g. Cave temperatures are usually very close to the mean annual air temperature at the surface so $T_1 = T_2$ to a good approximation. The dripwater function is really a measure of the missing $\delta^{18}O_w$ which can be taken as the average isotope concentration in the precipitation at the land surface,

$\delta^{18}O_p$. Lauritzen and Lundberg (1999) modified existing equations to arrive at an empirical expression for the dripwater function

$$F(T_2, t, g) \approx \delta^{18} O_p = cT + d + \Delta_{SMOW} \tag{12}$$

By calibrating the dripwater function with isotope ratios from speleothems deposited at known temperatures, numerical values for the empirical coefficients can be obtained. Under present and similar conditions, $\Delta_{SMOW} = 0$, but must be adjusted for changes in ocean water during periods when glacial ice has modified ocean water. Note that $\delta^{18}O_w$ is measured with respect to the SMOW standard while $\delta^{18}O_c$ is often measured with respect to the PDB standard. With the use of equations (11) and (12), oxygen isotope ratios determined from speleothem calcite can be converted into actual temperatures. It is important to realize, however, that the calculated temperatures are accurate only to the extent that the empirical coefficients are accurate and that the coefficients have remained constant through time. In reality, this is difficult to know.

The Holocene temperature record extracted from a speleothem in Soylegrotta in northern Norway by Lauritzen and Lundberg (1999) is in reasonable agreement with the temperature record deduced from the Greenland ice core GISP2 (Fig. 12). Note that the short exceptionally cold period at 8200 years that is a dominant features in the ice core record (Alley et al., 1997) does not appear in the speleothem record, a mismatch that would merit further investigation. The great value of these oxygen isotope records and calculations is that, if properly calibrated, they can attach an actual temperature scale to periods that can otherwise be described only as "colder" and "warmer" (e.g. a half million year old flowstone from Lapphullet Cave in northern Norway, Lauritzen et al., 1990). A key assumption in these calculations is that the relation between $\delta^{18}O_p$ (precipitation) and temperature has remained constant over time. Work by Cuffey et al. (1994) on the Greenland ice cores cast doubt on this assumption.

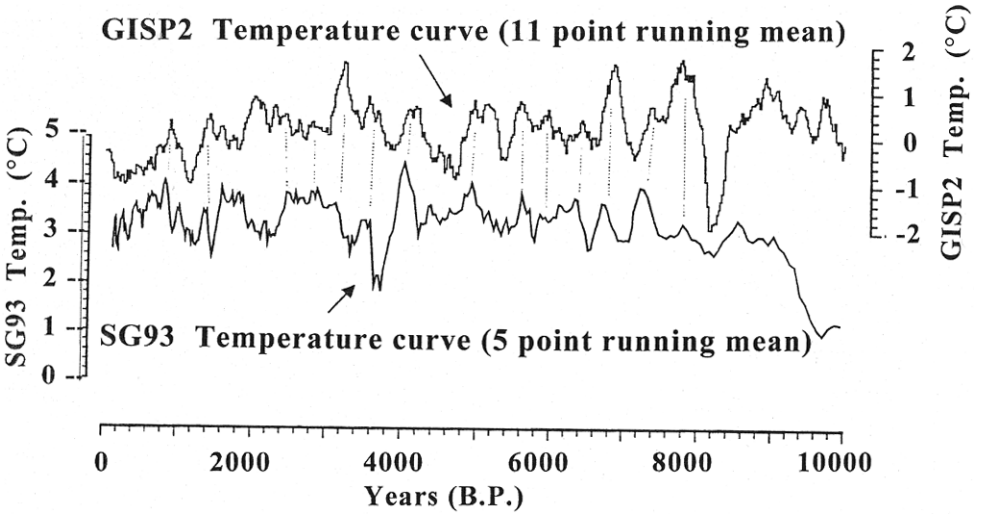

Figure 12. Comparison of a temperature curve calculated from oxygen isotope ratios in a speleothem (SG93) from Norway with the temperature curve from the Greenland ice core, GISP2. From Lauritzen and Lundberg (1999).

One of the longest speleothem isotope records was obtained from a uniform, underwater, slow-growing flowstone from Devils Hole, Nevada (Winograd et al., 1988; Winograd et al., 1992; Ludwig et al., 1992; Coplen et al., 1994; Szabo et al., 1994). The Devils Hole flowstone has one of the slowest recorded growth rates, about 0.5 μm/year compared with the 20 – 100 μm rates given in Tables 1 and 2. As a result, a 36 cm core collected 30 m below the water table spans 500,000 years. For unknown reasons, flowstone deposition apparently ceased at 60 ka BP. The oxygen and carbon isotope record is reproduced in figure 13. The cyclical warm and cold periods of the middle and late Pleistocene are clearly displayed. The main problem in detailed intepretation of these records is the unknown travel time of ground water from its recharge area to its discharge in the Ash Meadows Springs near Devils Hole. The travel time is long, as much as 10,000 years or perhaps longer. There has recently been demonstrated a close correlation of the Devils Hole isotope record with Mg/Ca and oxygen isotope records from equatorial Pacific foraminfera (Lea et al., 2000).

At middle and southern European latitudes, farther from the immediate impact of glacier advances and retreats, well-dated isotope records from speleothems from widely spaced caves allow comparison of regional climate shifts. McDermott et al. (1999) found, for example that early Holocene warm conditions prevailed on the Atlantic seaboard (southern Ireland) while relatively cool conditions occurred in the Mediterranean region of southern France. At 3500 years these conditions were shown to reverse. In the eastern Mediterranean, oxygen and carbon isotope ratios have been used to determine wet and dry periods (Frumkin et al., 1994; Frumkin et al., 1999a, b; Bar-Matthews et al., 1996). The wetter climate of the Holocene is recorded in the speleothems.

A useful application of speleothem records is that they can permit a comparison between climatic events in the northern and southern hemispheres. Early investigations in Tasmania (Goede, et al., 1986; Goede etal., 1990) provided data in the time range of 100 to 55 ka. Surprisingly, they found a positive relation between $\delta^{18}O$ and temperature, the reverse of what is usually observed. The relation was thought to be due to ocean influences. One of the oldest southern hemisphere records came from Victoria Fossil Cave in South Australia (Desmarchelier et al., 2000). A stalagmite gave a continuous record from 185 to 157 ka. Oxygen isotope ratios revealed cold temperatures at the beginning of growth but there was a warm interstadial between 178 and 162 ka with temperature similar to present day values. Finally came a period of rapid cooling until the end of the record at 157 ka. Speleothem records from the late Pleistocene provide evidence for a Younger Dryas cool period in the southern hemisphere (Goede et al., 1996; Hellstrom et al., 1998). Hellstrom et al. also suggested that the Younger Dryas in New Zealand began slightly before the Younger Dryas recorded in the Greenland ice cores. Measurements of oxygen and carbon isotope ratios on contemporary straw stalactites show fluctuations over a 100 year period comparable to the fluctuations over the entire Holocene showing that local climatic effects are recorded on very short time scales (Williams et al., 1999).

A young speleothem from Cold Air Cave in the Makapansgat Valley in South Africa (Holmgren et al., 1999; Tyson et al., 2000) provides a clear record of the historic period. The medieval warming (950 to 1300 AD) and the "little ice age" from 1300 to 1800 AD are shown to be distinctive features in South Africa as well as in Europe.

7.3. Carbon Isotope Profiles

Measurement of $\delta^{13}C$ from speleothems provides a useful record of vegetative cover at the time the speleothem was deposited. Nearly all trees, shrubs, and cool-season grasses

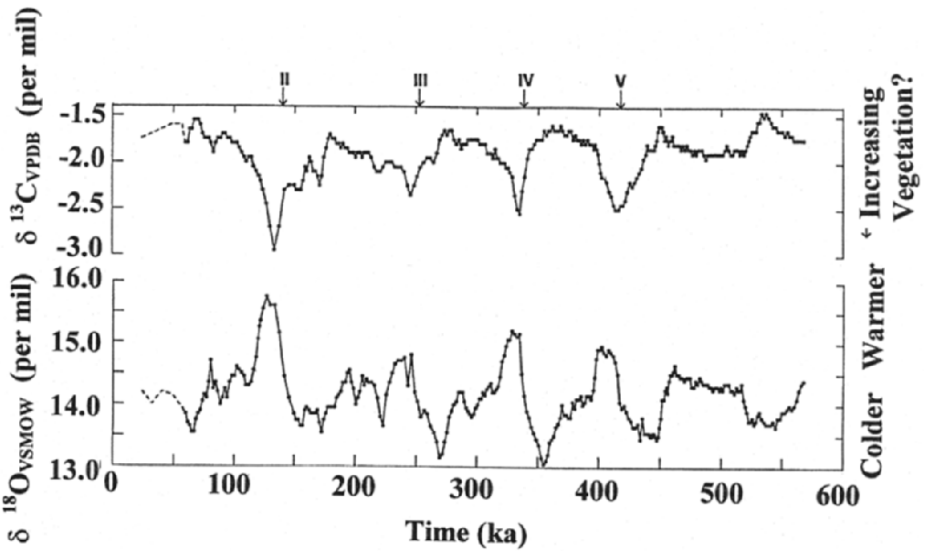

Figure 13. Oxygen and Carbon isotope ratios from underwater flowstone in Devils Hole, Nevada. From Coplan et al. (1994).

preferentially take up the lighter ^{12}C isotope. This is referred to as C_3 vegetation and is isotopically more negative than C_4 plants, mainly grasses that utilize a less discriminatory photosynthetic pathway. $\delta^{13}C$ ranges from −32 o/oo to −22 o/oo for C_3 vegetation and from −18 o/oo to −9 o/oo for C_4 vegetation (Tieszen and Boutton, 1989). The values are with respect to the VPDB standard. The mix of C_4 and C_3 vegetation varies with climate (Teeri and Stowe, 1976) and this is reflected in the carbon isotope ratios found in the speleothems (Dorale et al., 1992). Evaporation, degassing, or short residence times of water in the soil may shift isotopic compositions in the deposited speleothem as noted by Baker et al. (1997) from Stump Cross Caverns in the UK.

Some of the greatest success in tracking vegetation changes has taken place in the American mid-west. Both oxygen and carbon isotope ratios from a Cold Water Cave, Iowa, speleothem allowed the tracking of Holocene climate changes which suggested a rapid warming at 5900 years BP, and then cooling at 3600 years BP (Dorale et al., 1992). Dorale et al. (1998) were able to track changes from forest to savanna to prairie and back to forest from $\delta^{13}C$ data taken from speleothems from Crevice Cave, Missouri, over the period from 75 to 25 ka. The speleotherm $\delta^{13}C$ data show the changes in vegetation that accompanied the temperatures deduced from the oxygen isotope data and these speleothem data agreed well with the record from a nearby alluvial deposit that contained pollen and plant macrofossils (Baker et al., 1998). Collectively, the data showed prairie replacing mesic deciduous forest at 5900 years BP and the return of oak savanna around 3600 years BP. The $\delta^{13}C$ measurements on the alluvial organic matter showed variations that agreed well with the speleothem data. Data from the Ozark Highlands has been interpreted in a similar fashion to help understand vegetation changes farther south in the mid-west (Denniston et al., 1999a; Denniston et al., 2000). These records also revealed the short intense cold period at 8200 years BP found in the Greenland ice cores (Alley et al., 1997) and recently measured in mid-Europe ostracod data (von Grafenstein et al., 1999). Well-dated speleothems collected from a group of

caves can show the migration of climatic boundaries (or at least the associated vegetative changes) across the area as a function of time (Denniston et al., 1999b).

7.4. Strontium Isotopes

Strontium isotope ratios in speleothems have only recently been considered in the literature. The $^{87}Sr/^{86}Sr$ ratios in speleothems are a possible indicator of moisture conditions in the overlying soils (Banner et al., 1996; Ayalon et al., 1999). The shift in isotope ratio is due to differentiation in the soil and depends on residence time. According to Banner et al. (1996) during periods of diminished recharge, the drip waters will carry a soil zone signature (lower $^{87}Sr/^{86}Sr$ ratio). During periods of high recharge, the infiltrating water will seek mainly open pathways with shorter residence time and thus produce a higher $^{87}Sr/^{86}Sr$ ratio. In contrast, from measurements in the Soreq Cave in Israel, Ayalon et al. (1999) found a sharp drop in the $^{87}Sr/^{86}Sr$ ratio at 17 ka when there was a abrupt shift from a cool dry climate to a warmer a wetter climate. These opposite interpretations reflect the emerging status of strontium isotope work in speleothems.

7.5 Trace Element Studies

The $CaCO_3$ minerals that make up speleothems can accept small quantities of other ions in solid solution in the mineral structure. Sr^{2+} and Mg^{2+} are the most important, although Ba^{2+}, and transition group ions such as Fe^{2+}, Ni^{2+}, and Cu^{2+} are occasionally found. Sr^{2+} is a large ion radius = 132 pm) compared to Ca^{2+} (radius = 112 pm) while Mg^{2+} is a smaller ion (radius = 86 pm). As such, Sr^{2+} would be expected to have a higher solubility in aragonite with its large 9-coordinated cation site while Mg^{2+} should be more soluble in calcite with its smaller 6-coordinated cation site. Indeed, there is a very systematic relationship between Sr^{2+} and Mg^{2+} contents in calcite and aragonite samples as shown in figure 14 (White, 1994).

The incorporation of trace element into calcite or aragonite can be thought of as a simple exchage reaction

$$CaCO_3 + Tr^{2+} \Leftrightarrow TrCO_3 + Ca^{2+}$$

The equilibrium constant for this reation is called a distribution coefficient, k_D, defined as

$$k_D = \frac{[Ca^{2+}]^{liquid}[TrCO_3]^{crystal}}{[Tr^{2+}]^{liquid}[CaCO_3]^{crystal}} \tag{13}$$

The quantities in brackets represent activies of ions in solution and of components in the solid phase. Application of the defining equation directly would require knowing activity coefficients for the ions in solution and also the Henry's law coefficient for the trace carbonate in solid solution. A practical approach is to rewrite equation (13) in terms of an effective or empirical distribution coefficient

$$k'_D = \frac{m_{Ca}}{m_{Tr}} N_f(TrCO_3) \tag{14}$$

where the m's are the molal concentrations of ions in solution and N_f is the mole fraction of the trace carbonate in solid calcite or aragonite.

The distribution coefficient of Mg^{2+} in calcite is strongly temperature dependent. One such relation is (Katz, 1973).

$$k'_{Mg} = 0.0351 + 0.000894T \tag{15}$$

The temperature dependence of k'_{Mg} has led to proposals to use the magnesium concentration as a paleothermometer. Gascoyne (1983) found a substantial difference in k'_{Mg} between calcites and seepage waters from Jamaica and from Vancouver Island, which correlated, with the mean temperature differences. Unfortunately, the magnesium paleothermometer requires that the Mg^{2+} concentration in the drip water remain constant and as later work has shown, this is seldom the case.

The thermodynamic distribution coefficient requires that equilibrium be maintained between the crystallizing solid and the parent liquid. However, diffusion rates in the solid are so slow that there is negligible interchange between trace elements in the crystal and trace elements in solution except at the surface. The measured empirical distribution coefficients describe an instantaneous or surface partitioning. This requires that a careful distinction be made between a static system, such as a closed pocket or pond from which crystals are growing and a flow-through system in which the growing crystals are continuously bathed in fresh solution.

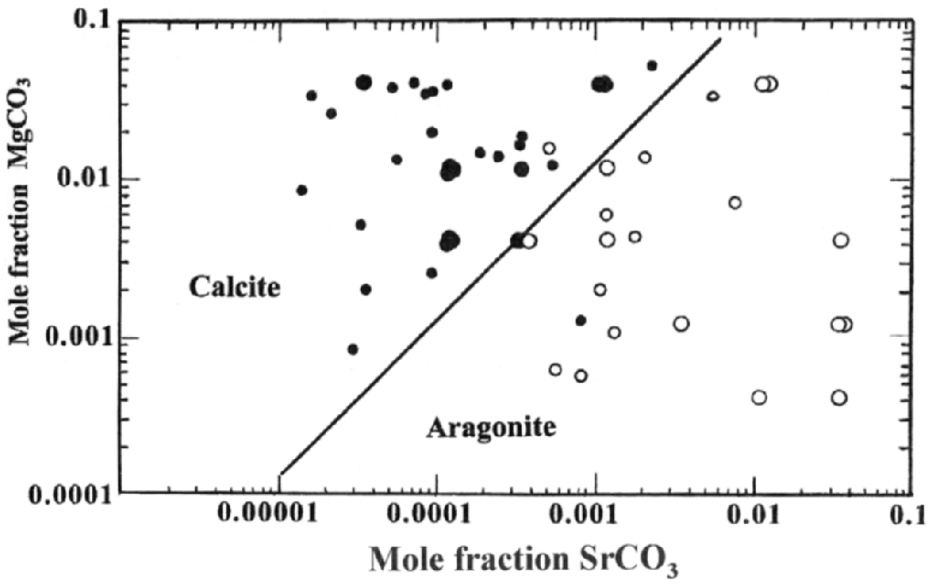

Figure 14. Sr^{2+} and Mg^{2+} distributions in calcite and aragonite. Solid circles indicate calcite; open circles indicate aragonite. Data from White (1994) with additional data from Harm and White (unpublished).

In a static system, the trace elements are either gradually enriched or gradually depleted in the liquid depending on whether the distribution coefficients are less than or greater than unity. The concentrations of trace elements in the growing crystal are zoned. The relations between the initial and final concentrations are described by the Doerner-Hoskins equation (Kinsman and Holland, 1969)

$$\log \frac{\left(m_{Tr}^{l}\right)_i}{\left(m_{Tr}^{l}\right)_f} = k_{Tr} \log \frac{\left(m_{Ca}^{l}\right)_i}{\left(m_{Ca}^{l}\right)_f} \tag{16}$$

where m_{Tr} and m_{Ca} are the molal concentrations of trace element and Ca^{2+} in the initial liquid (i) and final liquid (f). A version of the static system that appears in the cavern environment is the flowstone cascade. Water emerges from a crevice and flows distances of perhaps tens of meters as a uniform thin film, depositing calcite over the surface of the cascade. There should be a concentration gradient in various trace elements between the top of the cascade and the bottom, related to the changing water chemistry from top to bottom as described by the Doerner-Hoskins equation.

The flow-through system need provide only a single sampling point for liquid which is regarded as being in a steady state relation with the crystallizing solid. Another version of the Doerner-Hoskins equation provides a relationship between the concentrations of the trace elements in the flowing liquid and the crystalline solid which has just been deposited from it.

$$\log\left[1+\frac{\left(M_{Tr}^{c}\right)}{\left(M_{Tr}^{l}\right)}\right] = k_{Tr} \log\left[1+\frac{\left(M_{Ca}^{c}\right)}{\left(M_{Ca}^{l}\right)}\right] \tag{17}$$

where M is the number of moles of trace element and calcium in crystal (c) or liquid (l). There have been few tests of these equations in caves, although Holland et al. (1964) found that strontium concentrations in stalactites and flowstone in Luray Caverns could be calculated from the Sr/Ca ratio in the water using the laboratory determined distribution coefficient.

The trace element content of drip water does not remain constant and thus factors other than temperature variations must be responsible for the varying Sr^{2+} and Mg^{2+} concentrations in speleothems (Roberts et al., 1999). Among the factors listed by Fairchild et al. (2000) are residence time of the infiltration water in the epikarst, prior calcite precipitation along the flow path, and selective leaching of Mg and Sr with respect to Ca. Calcite dissolves more rapidly than dolomite. If limestone and dolomite are intermixed along the flow path, longer water residence times will allow more dolomite to be dissolved than when residence times are shorter. There is also the possibility of alternate flow paths with the distribution of infiltration water along these paths changing with recharge rate. Goede (1994) and Goede et al. (1998) found a bimodal distribution of strontium in a 70 ka Tasmanian speleothem that was interpreted by $^{87}Sr/^{86}Sr$ isotope ratios to be due to a contribution of wind-blown dust during interstadial times. In general, it seems that trace elements in speleothems would be a fruitful field for investigation but the results would require careful interpretation in terms of the local geological setting.

Perrette et al. (2000) measured Mn^{2+} concentration by ESR spectroscopy and found that the Mn^{2+} varied with other precipitation indicators such as color banding. ESR spectroscopy is an intrinsically low-resolution measurement. Cathodoluminescence imaging should reveal Mn^{2+} banding. Cathodoluminescence imaging is a common technique in sedimentary petrography but does not seem to have been applied to speleothems.

Modern analytical techniques such as secondary ion mass spectrometry (SIMS) and the electron microprobe allow chemical analysis with a spatial resolution of a few micrometers. In the few investigations that have been made, Sr^{2+} and Mg^{2+} are found to exhibit banding on the scale expected from the annual growth rate (Fig. 15). The data from Uamh an Tartair Cave in northern Scotland show Mg and Sr to vary in antiphase to each other. Data from Butler Cave, west central Virginia show Mg and Sr to vary in phase. Further, in the Butler Cave sample, the seasonal low concentrations are sharp downward spikes compared with the much broader high concentrations. The presence of a systematic annual pattern in Sr and Mg has been demonstrated for two examples. The interpretation of these results remains to be worked out.

8. COLOR AND LUMINESCENCE OF SPELEOTHEMS

8.1. Speleothem Color

A striking feature of calcite speleothems is their color. Although calcite itself is colorless, stalactites, stalagmites, and flowstone usually exhibit an array of colors from pale tans and oranges to reds and deep browns. White speleothems are quite rare. Conventional wisdom was that the pigmentation came from small amounts of iron oxides and hydroxides carried into the growing speleothem by the same seepage water that grew the speleothem. Indeed, the matter seemed so obvious that it was largely accepted without question. Lack of correlation between the depth of color and the iron content of the speleothems persuaded Gascoyne (1977) to suggest that the colors were due to organic substances derived from the overlying soils rather than from iron compounds, an hypothesis that was confirmed by spectroscopic measurements (White, 1981). Chemical extraction of humic material from cave calcites left no doubt that it was present in speleothems (Lauritzen et al., 1986). Pigmentation by hematite, goethite and ferrihydrite does occur in some speleothems and can be recognized by a characteristic absorption band in the near infrared (850 nm for hematite; 950 nm for goethite and ferrihydrite). The near-infrared spectra of most speleothems lack the characteristic signature of iron compounds and instead exhibit the smooth absorption edge expected of humic substances.

The location of the humic substances in speleothems has not been satisfactorily determined. If the speleothem has a columnar fabric, organic material can deposit in the pore spaces between the columnar crystals. However, speleothems with large close-packed crystals or which are composed of single crystals are also colored and the color bands are observed to be continuous across crystal boundaries. Fulvic and humic acids are large molecules that would not fit into the calcite structure, but it is possible that calcite could grow around these molecules with no break in crystal growth. Thus it is possible that the organic molecules are incorporated in the calcite on a molecular scale. It is also possible that the organic material is incorporated as second-phase inclusions at a submicroscopic scale. The two possibilities are not mutually exclusive.

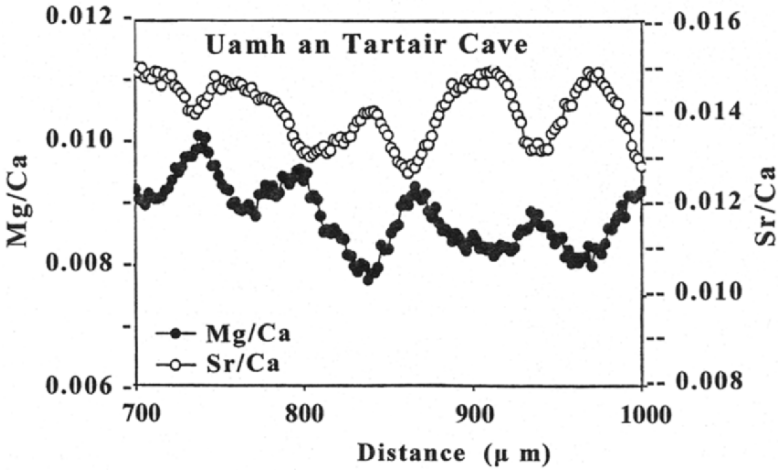

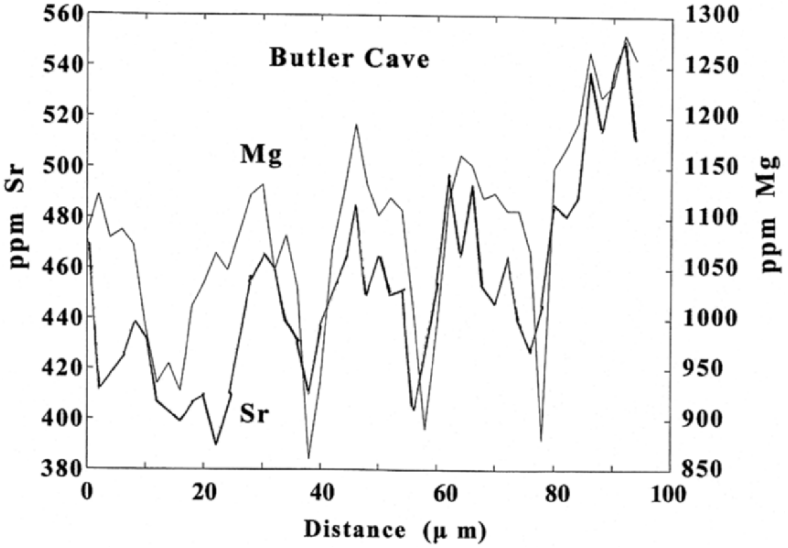

Figure 15. Strontium and magnesium banding in speleothems. (15A): Uamh an Tartair Cave, Scotland showing antiphase relation in strontium and magnesium (Roberts et al., 1998). (15B): Butler Cave, Virginia showing in-phase relation (Crowell and White, unpublished data).

A visible-scale color banding is immediately obvious in polished sections of speleothems stalactites, stalagmites, and flowstone (see Fig. 4). The colors of the bands of calcite vary from pure white to deep browns with all colors in between. In general the banding is coarse with band widths from a fraction of a millimeter to many millimeters. The transport of humic substances that make up the color bands has clearly varied over the growth history of most speleothems.

Most quantitative measurements of the color banding have used optical arrangements that limit the spatial resolution to a few hundred micrometers. Reflected light intensities are converted into electrical signals by a photomultiplier for recording and display. Some have used digital cameras. Two-dimensional imaging is possible. Holmgren et al. (1999) used false color imaging to display the growth layer structure in a stalagmite. Improvements are possible. Certainly, higher spatial resolution can be achieved since the diffraction limit for visible light is on the order of one micrometer.

"Brown" is a difficult color to characterize. The reflectance spectrum of a tan, beige or brown object is a continuous function of high reflectance in the red end of the spectrum gradually falling through yellow and green with little or no reflectance in the blue. The function is non-linear and its precise shape describes the depth and hue of "brown". In attempting to describe the bulk color of speleothems, it was found useful to construct two color variables, one the logarithmic ratio of reflected blue light to red light and the other the logarithmic ratio of reflected green light to red light (White, 1981). Using these two variables, all humic-substance pigmented speleothems plotted on a single straight line. The variability of the B/R and G/R ratios along a sequence of color banding has not been examined.

8.2. Speleothem Luminescence

It has long been known that most calcitic speleothems are phosphorescent. Photographers noted that speleothems would glow a pale greenish to bluish white for several seconds after excitation by a flash bulb or strobe lamp (O'Brien, 1956). It was suspected that the phosphorescence, like the color, was due to humic substances incorporated in the calcite crystals of the speleothems (White, 1986). The luminescence spectra were consistent with humic substances with the main contribution coming from the fulvic acid fraction (White and Brennan, 1989). Further characterization of the organic component of speleothems and the drip water shows that the luminescent component is extracted from overlying soils and carried into the cave with drip water (Ramseyer et al., 1997; Toth, 1998; McGarry and Baker, 2000).

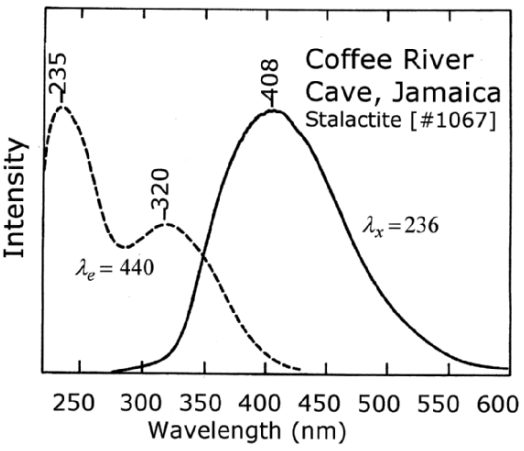

Figure 16. Luminescence spectrum of stalactite from Coffee River Cave, Jamaica. Brennan and White, unpublished data.

The emission spectra of speleothems tend to contain only a single broad band peaking in the range of 400 – 500 nm (Fig. 16). The wavelength of the band maximum, however, varies between speleothem samples. The excitation spectra are more complicated, often containing several bands. The humic substances are a mix of molecular structures and the mix varies from sample to sample. It appears that the fulvic acid component has the strongest luminescence signal. The characteristic fulvic acid peak occurs in the range of 400 – 450 nm. However, some specimens also exhibit luminescence from the humic acid component, which peaks at longer wavelengths.

To obtain more information on the chemistry of humic substances, a set of speleothems was dissolved in hydrochloric acid (Smailer and White, unpublished data). Gel chromatography was used to separate the molecular weight fractions of the solutions and luminescence spectra were measured on each fraction as it came off the column. The resulting plot, for an orange stalactite with an oily yellow luminescence, shows two dominant fractions, one in the humic acid range of 100,000 daltons and the other in the fulvic acid range of 1000 – 2000 daltons (Fig. 17). What is measured in any luminescence investigation is a composite of whatever mix of organic molecules that happen to be present in the specimen.

An important discovery by Yavor Shopov in the mid-1980's was that the luminescence also exhibits a banding, in this case, on a scale of tens of micrometers. These bands take the form of alternating bright and less bright luminescence intensity. The thickness of the luminescence bands is comparable to annual growth rates. It is reasonably well established that the smallest scale luminescence bands represent a seasonal record (Baker et al., 1993; Shopov et al., 1994). Superimposed on the annual records are longer time scale fluctuations that must represent longer scale variations in depositional conditions (Fig. 18).

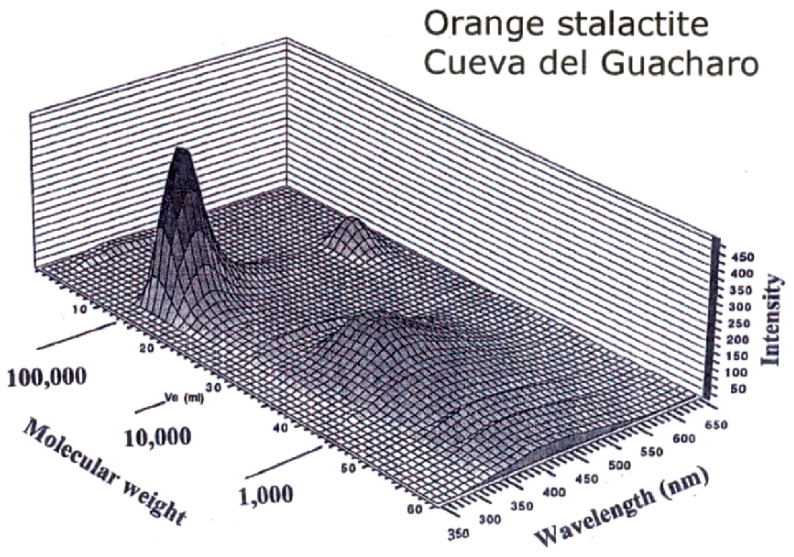

Figure 17. Distribution of luminescence according to molecular weight. Smailer and White, unpublished data.

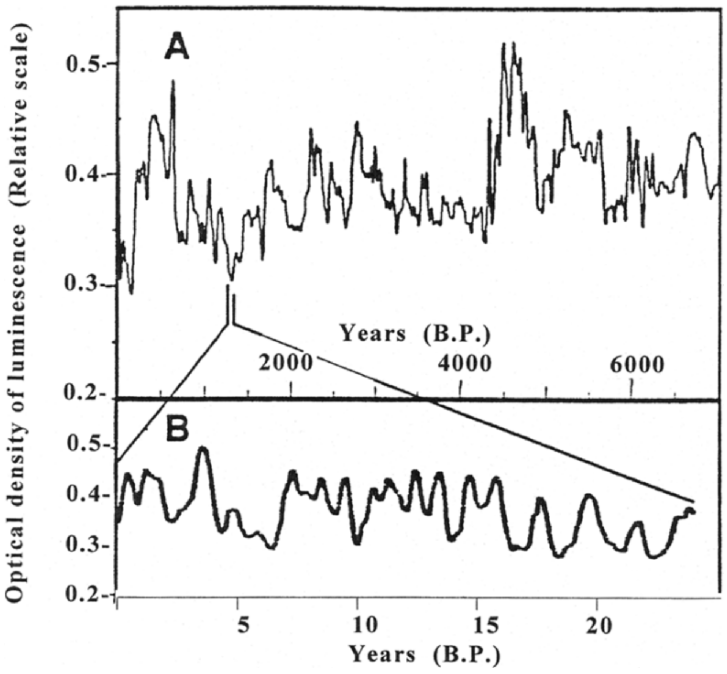

Figure 18. An early measurement of luminescence banding using the optical density of photographic film. Coldwater Cave, Iowa. Upper curve shows variation in the luminescent intensity on the scale of thousands of years. Insert curve shows details of resolution at an annual scale. From Shopov et al. (1994).

The original measurement of luminescence banding was photographic. A polished slab of speleothem was illuminated with ultraviolet light and a high resolution photograph taken. Densitometer measurements on the photographic film produced a pattern of bright and dark bands along the growth axis. More recent measurements have utilized a laser source – a Cd-Ne laser emitting at 325 nm in the case of Baker's extensive research – or a UV microscope with photographic recording. The microfocus Raman spectrometer, available in many university laboratories, has proved an effective tool for measuring luminescence banding (White, 1997). In this instrument, a laser – typically an argon ion laser – is focused on the specimen through a microscope objective. The luminescence radiation is also collected by the microscope objective and passed through a beam-splitter into a high-resolution monochromator. This permits constructing banding profiles at different wavelengths and thus traces the distribution of different mixes of organic species in the speleothem. With a precision mechanical translation stage, which may be computer controlled, spatial resolution of a few micrometers is possible.

Comparison of gray-scale banding with luminescence banding for caves in France and Belgium (Genty et al., 1997) showed that in these examples both measures gave very similar patterns. However, Perrette et al. (2000) comment that there is no consistent correlation between reflectance and luminescence banding.

8.3. Speleothem Microstratigraphy as a Paleoclimate Record

Considering stalagmites and flowstone simply as stratigraphic sequences in the same fashion as other sedimentary sequences, the textures of the individual layers themselves become paleoclimatic indicators. Annual laminations appear because of seasonal variations in flow rate of drip water (Genty and Quinif 1996). Increased layer thickness is usually a measure of higher growth rate that correlates with the infiltration rate, which in turn is a measure of excess precipitation over evapotranspiration. Brook et al. (1999) found stalagmites in the Anjohibe Cave, Madagascar that exhibited alternating layers, one inclusion-poor calcite (or aragonite) with high Sr^{2+} content, the other inclusion-rich with low Sr^{2+}, each about 40 μm thick. These were interpreted as representing dry season and wet season respectively. The thickness of the layers correlated with rainfall and temperature data over the time period 1951–1992. A longer, 415-year stalagmite thickness agrees with the historical records of El Niño events. Holmgren et al. (1999) found excellent agreement between laminae thickness and the rainfall index northeastern South Africa (Fig. 19).

The discovery of luminescence banding aroused a great deal of interest because it was immediately apparent that here was a record with a time resolution of one year or less that clearly seemed to be carrying a paleoclimatic signal. Many banding sequences have been measured, many from Britain, France, Belgium, and some from Germany (Richter et al., 1997; Niggemann et al., 2000). Much of the work cited in earlier sections was devoted to demonstrating the existence of luminescence banding and to attaching significance to the banding patterns. Some unique events appeared such as an anomaly in the banding pattern in a stalagmite from Uamh an Tartair Cave, Scotland, which Baker et al. (1995) assigned to the Hekla 3 volcanic eruption which occurred about 1159 BC.

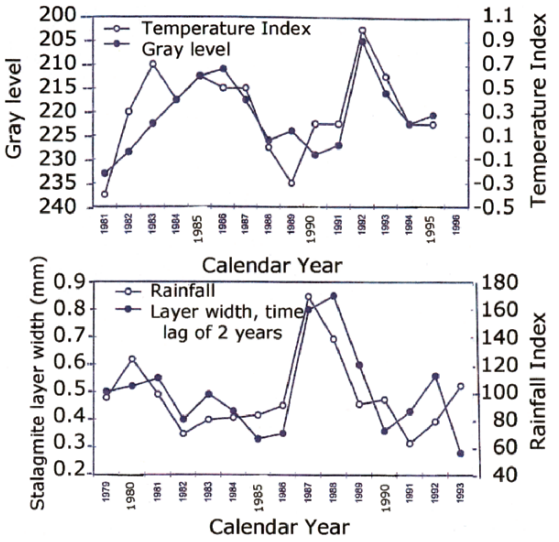

Figure 19. Correlation of gray scale banding with temperature index and laminae thickness with rainfall index for contemporary stalagmite growth in Cold Air Cave, Makapansgat Valley, South Africa. From Holmgren et al. (1999).

It has been tempting to treat the banding pattern as a time series with a dominant high frequency component, the annual cycle, and then look for lower frequency components by Fourier transform or other spectral analysis. Qin et al (1999) performed spectral analysis over 1000 years of record in a stalagmite from Shihua Cavern near Beijing, China and claimed to have found cycles in the laminae thickness of 2, 3.3, 5-6, 10-12, 14-18, 133 and 194 years. Little work has been done on the intrinsic error in the various laminae measurements or in their reproducibility. Until this is done, it is difficult to assign significance to such a sequence of climatic cycles in a single record.

It appears that the luminescence and color banding records relate to excess precipitation, the infiltration component that remains from the total precipitation after soil moisture and evapotranspiration have been deducted (Baker et al., 1999a, b). Band width, contrast between light and dark bands, spectral characteristics of the bands, and comparisons between luminescence and color banding are all parameters that can be measured at one-year resolution along the time line of the speleothem. The potential is excellent. However, this record has the same problem as the trace element record. The mix of humic and fulvic acids that appear in speleothems depends on the primary mixture of humic substances in the soil which in turn is related to vegetative cover, depth and characteristics of soils, and the rate of weathering of the organic debris. Although related to excess precipitation, the banding also depends on the residence time of the water in the soil and on the various pathways that the water follows from the surface down to the cave. Cave drip water during the dry season is fed mainly by water stored in the epikarst and by long travel time pathways through small fissures and primary pore spaces. Baker et al., 1999b determined dry-season lags of 10 to 20 days. Cave drip water in the wet season may arrive by much more direct pathways. The dark bands are thought to represent winter high flows that extract more humic acid whereas the light bands, also the bright luminescence bands are formed in the autumn after leaf-fall which provides a surge of fulvic acid. The origin of luminescence banding is clearly more complicated because speleothem banding also occurs in caves beneath prairies and in tropical caves where there are no seasonal changes in vegetation.

9. CONCLUSIONS

One can think of a cylindrical stalagmite as a core, already prepared, with no drilling needed. With a time scale provided by U/Th dating, the stalagmite provides a microstratigraphic record with a resolution of one year or less spanning a time interval of many thousands of years. Cores drilled from flowstone sheets provide similar records. Investigations began with the establishment of the U/Th dating technique and early isotope measurements in the 1970's and have appeared with increasing frequency and increasing number of investigators right up to the present moment. Useful records include the following:

- The sequence of variations in speleothem fabric along with identified breaks in the depositional record can be related to changes in flow rate and chemistry of the infiltrating drip water and thus indirectly to climatic changes on the land surface.
- Profiles of oxygen isotope ratios taken along the growth axis record surface temperatures in reasonable agreement with other temperature proxies. Important progress has been made on converting isotope ratios to accurate numerical temperatures, although complications still exist.

- Profiles of carbon isotope ratios relate well to surface vegetation with some care needed to take into account carbon isotope redistribution along the flow path.
- There are variations in the concentrations of trace elements, particularly Sr and Mg, both at coarse scales along the speleothem and at the scale of annual growth layers. Interpretation is at an early stage with a combination of climate and local geologic factors to be taken into account.
- Color and luminescence banding provide a very high-resolution record that seems to relate to excess precipitation. Instrumentation techniques allow very high spatial resolution. Improved interpretation of the relation between color (gray scale) banding and luminescence banding is needed. This will require improved understanding of the mechanisms of extraction of humic and fulvic acids from overlying soils and their incorporation into speleothems. It is still not clear whether luminescence and color banding will provide a quantitative record of excess precipitation.

The great value of speleothem records is that they are continental records with high time resolution and the possibility of accurate dating. Enough data have been collected to show that the speleothem records very often agree well with other indicators of paleoclimate. A likely application for speleothem records will be to fill in much detail on the timing of climate shifts across continental masses where local climate can vary substantially over relatively short distances.

10. ACKNOWLEDGEMENTS

Our work on luminescence banding in speleothems, from which this review derives, is supported by the National Science Foundation. This review draws on the research of many investigators from many countries. I am grateful to these colleagues for sharing information and reprints. For experimental work at Penn State acknowledgement is due to graduate students Edward Brennan, Steven Smailer, and Bryan Crowell. I am grateful to Richard Alley for a colleague review and to reviewers Arthur and Margaret Palmer and Jeffrey Dorale for many useful suggestions.

11. REFERENCES

Alley, R.B., Meese, D.A., Shuman, C.A., Gow, A.J., Taylor, K.C., Grootes, P.M., White, J.W.C., Ram, M., Waddington, E.D., Mayewski, and Zielinski, G.A., 1993, Abrupt increase in Greenland snow accumulation at the end of the Younger Dryas event, *Nature* **362**:527-529.

Alley, R.B., Mayewski, P.A., Sowers, T., Stuiver, M., Taylor, K.C. and Clark, P.U., 1997, Holocene climatic stability: A prominent, widespread event 8200 yr ago, *Geology* **25**:483-486.

Atkinson, T.C., Smart, P.L. Harmon, R.S., and Waltham, A.C., 1978, Palaeoclimatic and geomorphic implications of $^{230}Th/^{234}U$ dates on speleothems from Britain, *Nature* **272**:24-28.

Atkinson, T.C., Lawson,T.J., Smart, P.L., Harmon, R.S., and Hess, J.W., 1986, New data on speleothem deposition and palaeoclimate in Britain over the last forty thousand years, *J. Quat. Res.* **1**:67-72.

Atkinson, T.C. and Rowe, P.J., 1992, Application of dating to denudation chronology and landscape evolution, in: *Uranium-Series Disequilibrium*, (2nd ed.) M. Ivanovich and R.S. Harmon, eds., Clarendon Press, Oxford, pp.670-703.

Ayalon, A., Bar-Matthews, M. and Kaufman, A., 1999, Petrography, strontium, barium and uranium concentrations and strontium and uranium isotope ratios in speleothems as palaeoclimatic proxies: Soreq Cave, Israel, *Holocene* **9**:715-722.

Ayliffe, L.K., Marianelli, P.C., Moriarty, K.C., Wells, R.T., McCulloch, M.T., Mortimer, G.E. and Hellstrom, J.C., 1998, 500 ka precipitation record from southeastern Australia: Evidence for interglacial relative aridity, *Geology* **26**:147-150.

Baker, A., Smart, P.L., Edwards, R.L., and Richards, D.A., 1993, Annual growth banding in a cave stalagmite, *Nature* **364**:518-520.

Baker, A. and Smart, P.L., 1995, Recent flowstone growth rates: Field measurements in comparison to theoretical predictions, *Chem. Geol.* **122**:121-128.

Baker, A., Smart, P.L., Barnes, W.L, Edwards, R.L. and Farrant, A., 1995, The Hekla 3 volcanic eruption recorded in a Scottish speleothem, *Holocene* **5**:336-342.

Baker, A., Ito, E., Smart, P.L., and McEwan, R.F., 1997, Elevated and variable values of ^{13}C in speleothems in a British cave system, *Chem. Geol.*, **136**:263-270.

Baker, A., Genty, D., Dreybrodt, W., Barnes, W.L., Mockler, N.J. and Grapes, J., 1998, Testing theoretically predicted stalagmite growth rate with Recent annually laminated samples: Implications for past stalagmite deposition, *Geochim. Cosmochim. Acta* **62**:393-404.

Baker, A., Proctor, C.J., and Barnes, W.L., 1999a, Variations in stalagmite luminescence laminae structure at Poole's Cavern, England, AD 1910-1996: calibration of a palaeoprecipitation proxy, *Holocene* **9**:683-688.

Baker, A., Caseldine, C.J., Gilmour, M.A., Charman, C., Proctor, C.J., Hawkesworth, C.J. and Phillips, N., 1999b, Stalagmite luminescence and peat humification records of palaeomoisture for the last 2500 years, *Earth Planet. Sci. Lett.* **165**:157-162.

Baker, A., Mockler, and Barnes, W.L., 1999c, Fluorescence intensity variations of speleothem-forming groundwaters: Implications for paleoclimate reconstruction *Water Resources Res.* **35**:407-413.

Baker, R.G., Gonzalez, L.A., Raymo, M., Bettis, E.A. III, Reagan, M.K., and Dorale, J.A., 1998, Comparison of multiple proxy records of Holocene environments in the Midwestern United States, *Geology* **26**:1131-1134.

Banner, J.L., Musgrove, M.L., Asmerom, Y., Edwards, R.L. and Hoff, J.A., 1996, High-resolution temporal record of Holocene ground-water chemistry: Tracing links between climate and hydrology, *Geology* **24**:1049-1053.

Bar-Matthews, M., Matthews, A., and Ayalon, A., 1991, Environmental controls of speleothem mineralogy in a karstic dolomitic terrain (Soreq Cave, Israel), *J. Geol.* **99**:189-207.

Bar-Matthews, M., Ayalon, A., Matthews, A., Sass, E. and Halicz, L., 1996, Carbon and oxygen isotope study of the active water-carbonate system in a karstic Mediterranean cave: Implications for paleoclimate research in semiarid regions, *Geochim. Cosmochim. Acta* **60**:337-347.

Baskaran, M. and Iliffe, T.M., 1993, Age determination of recent cave deposits using excess ^{210}Pb- a new technique, *Geophys. Res. Lett.* **20**:603-606.

Berggren, W.A., Kent, D.V. Swisher, III, C.C. and Aubry, M.-P., 1995, A revised Cenozoic geochronology and chronostratigraphy in *Geochronology, Time Scales and Global Stratigraphic Correlation*, W.A. Berggren, D.V. Kent, M.-P. Aubry, and J. Hardenbol, eds., Soc. Sedimentary Geol. Spec. Pub. 54, pp. 129-212.

Berner, R.A., 1975, The role of magnesium in the crystal growth of calcite and aragonite from sea water, *Geochim. Cosmochim. Acta* **39**:489-504.

Bradley, R.S., 1999, *Paleoclimatology*, 2nd Ed., Academic Press, San Diego

Brook, G.A., Burney, D.A., and Cowart, J.B., 1990, Desert paleoenvironmental data from cave speleothems with examples from the Chihuahuan, Somali-Chalbi, and Kalahari deserts, Palaeogeography, Palaeoclimatology, Palaeoecology **76**:311-329.

Brook, G.A. and Nickmann, R.J., 1996, Evidence of late Quaternary environments in northwestern Georgia from sediments preserved in Red Spider Cave, *Phys. Geograph.* **17**:465-484.

Brook, G.A., Rafter, M.A., Railsback, L.B., Sheen, S.-W. and Lundberg, J., 1999, A high-resolution proxy record of rainfall and ENSO since AD 1550 from layering in stalagmites from Anjohibe Cave, Madagascar, *Holocene* **9**:695-705.

Buhmann, D. and Dreybrodt, W., 1985a, The kinetics of calcite dissolution and precipitation in geologically relevant situations of karst areas. 1. Open system, *Chem. Geol.* **43**:189-211.

Buhmann, D. and Dreybrodt, W., 1985b, The kinetics of calcite dissolution and precipitation in geologically relevant situations of karst areas. 2. Closed system, *Chem. Geol.* **53**:109-124.

Buhmann, D. and Dreybrodt, W., 1987, Calcite dissolution kinetics in the system H_2O-CO_2–$CaCO_3$ with the participation of foreign ions, *Chem. Geol.* **64**:89-102.

Cande,S.C. and Kent, D.V., 1995, Revised calibration of the geomagnetic polarity timescale for the Late Cretaceous and Cenozoic, *J. Geophys. Res.* **100**:6093-6095.

Carlson, W.D., 1983, The polymorphs of $CaCO_3$ and the aragonite – calcite transformation. Chap. 6 in *Carbonates: Mineralogy and Chemistry*, R.J. Reeder, ed., *Reviews in Mineralogy*, **11**:191-225.

Coplen, T.B., Winograd, I.J., Landwehr, J.M. and Riggs, A.C., 1994, 500,000-year stable carbon isotopic record from Devils Hole, Nevada, *Science* **263**:361-365.

Cuffey, K.M., Alley, R.B., Grootes, P.M., Bolzan, J.M. and Anandakrishnan, S., 1994, Calibration of $\delta^{18}O$ isotopic paleothermomenter for central Greenland, using borehole temperatures, *J. Glaciology* **40**:341-

Curl, R.L., 1973, Minimum diameter stalagmites, *Natl. Speleol. Soc. Bull.* **35**:1-9.

Davis, K.J., Dove, P.M., and De Yoreo, J.J., 2000, The role of Mg^{2+} as an impurity in calcite growth, Science **290**:1134-1137.

Denniston, R.F., Gonzalez, L.A., Semken, Jr., H.A., Asmerom,Y., Baker, R.G. Recelli-Snyder, H., Reagan, M.K. and Bettis III, E.A., 1999a, Integrating stalagmite, vertebrate, and pollen sequences to investigate Holocene vegetation and climate change in the southern Midwestern United States, *Quat. Res.* **52**:381-387.

Denniston, R.F., Gonzalez, L.A., Baker, R.G., Asmerom, Y., Reagan, M.K., Edwards, R.L., and Alexander, E.C., 1999b, Speleothem evidence for Holocene fluctuations of the prairie-forest ecotone, north-central USA, *Holocene* **9**:671-676.

Denniston, R.F., Gonzalez, L.A., Asmerom, Y., Sharma, R.H. and Reagan, M.K., 2000a, Speleothem evidence for changes in Indian summer monsoon precipitation over the last ~2300 years, *Quat. Res.* **53**:196-202.

Denniston, R.F., Gonzalez, L.A., Asmerom, Y., Reagan, M.K. and Recelli-Snyder, H., 2000b, Speleothem carbon isotopic records of Holocene environments in the Ozark Highlands, USA, *Quat. Internatl.* **67**:21-27.

Desmarchelier, J.M., Goede, A., Ayliffe, L.K., McCulloch, M.T., and Moriarty, K., 2000, Stable isotope record and its palaeoenvironmental interpretation for a late Middle Pleistocene speleothem from Victoria Fossil Cave, Naracoorte, South Australia, *Quat. Sci. Rev.* **19**:763-774.

Dorale, J.A., Gonzalez, L.A., Reagan, M.K., Pickett, D.A., Murrell, M.T. and Baker, R.G., 1992, A high-resolution record of Holocene climate change in speleothem calcite from Cold Water Cave, northeast Iowa, *Science* **258**:1626-1630.

Dorale, J.A., Edwards, R.L., Ito, E. and Gonzalez, L.A., 1998, Climate and vegetation history of the midcontinent from 75 to 25 ka: A speleothem record from Crevice Cave, Missouri, USA, *Science* **282**:1871-1874.

Dreybrodt, W., 1980, Deposition of calcite from thin films of natural calcareous solutions and the growth of speleothems, *Chem. Geol.* **29**:89-105.

Dreybrodt, W., 1981, The kinetics of calcite precipitation from thin films of calcareous solutions and the growth of speleothems: Revisited, *Chem. Geol.* **32**:237-245.

Dreybrodt, W., 1982, A possible mechanism for growth of calcite speleothems without participation of biogenic carbon dioxide, *Earth Planet. Sci. Lett.* **58**:293-299..

Dreybrodt, W. and Buhmann, D., 1987, A mass transfer model for dissolution and precipitation of calcite from solutions in turbulent motion, *Chem. Geol.* **90**:107-122.

Dreybrodt, W., 1988, *Processes in Karst Systems,* Springer Verlag, Berlin, 288 pp.

Dreybrodt, W., Eisenlohr, B., Madry, B. and Ringer, S., 1997, Precipitation kinetics of calcite in the system $CaCO_3 - H_2O - CO_2$: The conversion to CO_2 by the slow process $H^+ + HCO_3^- \Leftrightarrow CO_2 + H_2O$ and the inhibition of surface controlled reactions as rate limiting steps, *Geochim. Cosmochim. Acta* **61**:3897-3904.

Easterbrook, D.J., 1999, *Surface Processes and Landforms,* 2nd Edition, Prentice Hall, Upper Saddle River, NJ, 546 pp.

Edwards, R.L., Chen, J.H. and Wasserburg, G.J., 1987, ^{238}U- ^{234}U- ^{230}Th- ^{232}Th systematics and precise measurement of time over the past 500,000 y, *Earth Planet. Sci. Lett.* **81**:175-192.

Fairchild, I.J., Borsato, A., Tooth, A.F., Frisia, S., Hawkesworth, C.J., Huang, Y., McDermott, F. and Spiro, B., 2000, Controls on trace element (Sr – Mg) compositions of carbonate cave waters: implications for speleothem climatic records, *Chem. Geol.* **166**:255-269.

Faure, G., 1986, *Principles of Isotope Geology,* John Wiley, New York, 589 pp.

Folk, R.L. and Assereto, R., 1976, Comparative fabrics of length-slow and length-fast calcite and calcitized aragonite in a Holocene speleothem, Carlsbad Caverns, New Mexico, *J. Sed. Petrol.* **46**:486-496.

Franke, H.W., 1965, The theory behind stalagmite shapes, *Studies Speleol.* **1**:89-95.

Friedman, I. and O'Neill, J.R., 1977, Compilation of stable isotope fractionation factors of geochemical interest. *U.S. Geol. Survey Prof. Pap.* **440-KK**, 3.

Frumkin, A., Schwarcz, H.P. and Ford, D.C., 1994, Evidence for isotopic equilibrium in stalagmites from caves in a dry region: Jerusalem, Israel, *Israel J. Earth Sci.* **43**:221-230.

Frumkin, A., Ford, D.C., and Schwarcz, H.P., 1999a, Continental oxygen isotopic record of the last 170,000 years in Jerusalem, *Quat. Res.* **51**:317-327.

Frumkin, A., Carmi, I., Gopher, A., Ford, D.C., Schwarcz, H.P. and Tsuk, T., 1999b, A Holocene millennial-scale climatic cycle from a speleothem in Nahal Qanah Cave, Israel, *Holocene* **9**:677-682.

Gascoyne, M., 1977, Trace element geochemistry of speleothems, *Proc. 7th Internatl. Congress Speleol.,* p.205-208.

Gascoyne, M., Benjamin, G.J., Schwarcz, H.P. and Ford, D.C., 1979, Sea-level lowering during the Illinoian Glaciation: Evidence from a Bahama "blue hole", *Science* **205**:806-808.

Gascoyne, M., Ford, D.C. and Schwarcz, H.P., 1981, Late Pleistocene chronology and paleoclimate of Vancouver Island determined from cave deposits, *Canad. J. Earth Sci.* **18**:1643-1652.

Gascoyne, M., 1983, Trace-element partition coefficients in the calcite-water system and their paleoclimatic significance in cave studies, *J. Hydrol.* **61**:213-222.

Gascoyne, M., Ford, D.C. and Schwarcz, H.P., 1983, Rates of cave and landform development in the Yorkshire Dales from speleothem age data, *Earth Surface Processes Landforms* **6**:557-568.

Gascoyne, M., Schwarcz, H.P. and Ford, D.C., 1983, Uranium-series ages of speleothem from Northwest England: Correlation with Quaternary climate, *Phil. Trans. Royal Soc. London* **B301**:143-164.

Gascoyne, M., 1984, Twenty years of uranium-series dating of cave calcites: A review of results, problems and new directions, *Studies Speleol.* **5**:15-30.

Gascoyne, M., 1992, Palaeoclimate determination from cave deposits, *Quat. Sci. Rev.* **11**:609-632.

Gascoyne, M. and Harmon, R.S., 1992, Palaeoclimatology and palaeosea levels. Chapt. 16 in *Uranium Series Disequilibrium*, M. Ivanovich and R.S. Harmon, eds, Clarendon Press, Oxford, 553-582.

Genty, D., 1992, Les spéléothèms du tunnel de Godarville (Belgique) – un exemple exceptionnel de concrétionnement moderne – intérêt pour l'étude de la cinétique de la précipitation de la calcite et de sa relation avec les variations d'environement, *Speleochronos* **4**:3-29.

Genty, D. and Quinif, Y., 1996, Annually laminated sequences in the internal structure of some Belgian stalagmites - importance for paleoclimatology, *J. Sed. Res.* **66**:275-288.

Genty, D., Baker, A. and Barnes, W., 1997, Comparaison entre les lamines luminescentes et les lamines visibles annuelles de stalagmites, *Compt. Rend. Acad. Sci. Paris, Earth Planet. Sci.* **325**:193-200.

Genty, D. and Massault, M., 1997, Bomb ^{14}C recorded in laminated speleothems: Calculation of dead carbon proportion, *Radiocarbon*, **39**:33-48.

Genty, D., Vokal, B. Obelic, B. and Massault, M., 1998, Bomb ^{14}C time history recorded in two modern stalagmites -- importance for soil organic matter dynamics and bomb ^{14}C distribution over continents, *Earth Planet. Sci. Lett.* **160**:795-809.

Goede, A., Green, D.C. and Harmon, R.S., 1986, Late Pleistocene palaeotemperature record from a Tasmanian speleothem, *Austral. J. Earth Sci.* **33**:333-342.

Goede, A, Harmon, R.S., Atkinson, T.C. and Rowe, P.J., 1990, Pleistocene climatic change in Southern Australia and its effect on speleothem deposition in some Nullabor caves, *J. Quat. Sci.* **5**:29-38.

Goede, A., Veeh, H.H. and Ayliffe, L.K., 1990, Late Quaternary palaeotemperature records for two Tasmanian speleothems, *Austral. J. Earth Sci.* **37**:267-278.

Goede, A., 1994, Continuous early last glacial palaeoenvironmental record from a Tasmanian speleothem based on stable isotope and minor element variations, *Quat. Sci. Rev.* **13**:283-291

Goede, A., McDermott, F., Hawkesworth, C., Webb, J. and Finlayson, B., 1996, Evidence of Younger Dryas and Neoglacial cooling in a Late Quaternary palaeotemperature record from a speleothem in eastern Victoria, Australia, *J. Quat. Sci.* **11**:1-7

Goede, A., McCulloch, M., McDermott, F. and Hawkesworth, C., 1998, Aeolian contribution to strontium and strontium isotope variations in a Tasmanian speleothem, *Chem. Geol.* **149**:37-50.

Gordon, D. and Smart, P.L., 1984, Comments on "Speleothems, travertines and paleoclimates" by G.J. Henning, R. Grun, and K. Brunnacker, *Quat. Res.* **22**:144-147.

Gordon, D., Smart, P.L., Ford, D.C., Andrews, J.N., Atkinson, T.C., Rowe, P.J., and Christopher, N.S.J., 1989, Dating the late Pleistocene interglacial and interstadial periods in the United Kingdom from speleothem growth frequency, *Quat. Res.* **31**:14-26,

Gradzinski, M., Rospondek, M. and Szulc, J., 1997 Paleoenvironmental controls and microfacies variability of the flowstone cover from the Zvoniva Cave in the Slovakian Karst, *Slovak Geol. Mag.* **3** 299-313.

Harmon, R.S., Thompson, P., Schwarcz, H.P. and Ford, D.C., 1975, Uranium-series dating of speleothems, *Natl. Speleol. Soc. Bull.* **37**:21-33.

Harmon, R.S., Ford, D.C. and Schwarcz, H.P., 1977, Interglacial chronology of the Rocky and Mackenzie Mountains based upon ^{230}Th-^{234}U dating of calcite speleothems, *Canad. J. Earth Sci.* **14**:2543-2552

Harmon, R.S., Schwarcz, H.P. and Ford, D.C., 1978a, Late Pleistocene sea level history of Bermuda, *Quat. Res.* **9**:205-218

Harmon, R.S., Thompson, P., Schwarcz, H.P. and Ford, D.C., 1978b, Late Pleistocene paleoclimates of North America as inferred from stable isotope studies of speleothems, *Quat. Res.* **9**:54-70.

Harmon, R.S., Schwarcz, H.P. and Ford, D.C., 1978c, Stable isotope geochemistry of speleothems and cave waters from the Flint Ridge-Mammoth Cave System, Kentucky: Implications for terrestrial climate change during the period 230,000 to 100,000 years B.P., *J. Geol.* **86**:373-384.

Hellstrom, J., McCulloch, M. and Stone, J., 1998, A detailed 31,000-year record of climate and vegetation change, from the isotope geochemistry of two New Zealand speleothems, *Quat. Res.* **50**:167-178.

Hendy, C.H., 1971, The isotopic geochemistry of speleothems-I. The calculation of the effects of different modes of formation on the isotopic composition of speleothems and their applicability as palaeoclimatic indicators, *Geochim. Cosmochim. Acta* **35**:801-824.

Hennig, G.J., Grun, R. and Brunnacker, K., 1983, Speleothems, travertines, and paleoclimates, *Quat. Res.* **20**:1-29.

Hercman, H. and Lauritzen, S.-E., 1996, Comparison of speleothem dating by the TL, ESR, ^{14}C and $^{230}Th/^{234}U$ methods, in *Climate Change: The Karst Record,* S.-E. Lauritzen, ed., Karst Waters Institute Special Publication No. 2:47-50.

Hercman, H., Bella, P., Glazek, J., Gradzinski, M, Lauritzen, S.-E. and Lovlie, R., 1997, Uranium-series dating of speleothems from Demanova Ice Cave: A step to age estimation of the Demanova Cave System (the Nizke Tatry Mts., Slovakia), *Ann. Soc. Geol. Poloniae* **67**:439-450.

Hill, C. and Forti, P., 1997, *Cave Minerals of the World.* (2nd edition), National Speleological Society, Huntsville, AL, 463 pp.

Holland, H.D., Kirsipu, T.V., Huebner, J.S., and Oxburgh, U.M., 1964, On some aspects of the chemical evolution of cave waters, *J. Geol.* **72**:36-67.

Holmgren, K., Lauritzen, S.-E. and Possnert, G., 1994, $^{230}Th/^{234}U$ and ^{14}C dating of a late Pleistocene stalagmite in Labatse II Cave, Botswana, *Quat. Geochron.* **13**:111-119.

Holmgren, K., Karlen, W., Lauritzen, S.-E., Lee-Thorp, J.A., Partridge, T.C., Piketh, S., Repinski, P., Stevenson, C. Svanered, O., and Tyson, P.D., 1999, A 3000-year high-resolution stalagmite-based record of palaeoclimate for northeastern South Africa, *Holocene* **9**:295-309.

Ivanovich, M. and Harmon, R.S., 1992, *Uranium-Series Disequilibrium,* Clarendon Press, Oxford.

Katz, A., 1973, The interaction of magnesium with calcite during crystal growth at 25 – 90 °C and one atmosphere, *Geochim. Cosmochim. Acta* **37**:1563-1586.

Kendall, A.C. and Broughton, P.L., 1978, Origin of fabrics in speleothems composed of columnar calcite crystals, *J. Sed. Petrol.* **48**:519-538.

Kinsman, D.J.J. and Holland, H.D., 1969, The co-precipitation of cations with $CaCO_3$. IV. The co-precipitation of Sr^{2+} with aragonite between 16° and 96° C, *Geochim. Cosmochim.* Acta **33**:1-17.

Langmuir, D., 1978, Uranium solution-mineral equilibria at low temperatures with applications to sedimentary ore deposits, *Geochim. Cosmochim.* Acta **42**:547-569.

Langmuir, D. and Herman, J.S., 1980, The mobility of thorium in natural waters at low temperatures, *Geochim. Cosmochim. Acta* **44**:1753-1766.

Langmuir, D., 1997, *Aqueous Environmental Geochemistry,* Prentice Hall, Upper Saddle River, NJ, 600 p.

Latham, A.G, Schwarcz, H.P. and Ford, D.C., 1979, Palaeomagnetism of stalagmite deposits, *Nature* **280**:383-85.

Latham, A.G., Schwarcz, H.P., Ford, D.C. and Pearce, G.W., 1982, The paleomagnetism and U-Th dating of three Canadian speleothems: evidence for the westward drift, 5.4 – 2.1 ka BP, *Canad. J. Earth Sci.* **19**:1985-1995.

Latham, A.G., Schwarcz, H.P. and Ford, D.C., 1986, The paleomagnetism and U-Th dating of Mexican stalagmite, DAS2, *Earth Planet. Sci. Lett.* **79**:195-207.

Latham, A.G., Schwarcz, H.P. and Ford, D.C., 1987, Secular variation of the Earth's magnetic field from 18.5 to 15.0 ka BP, as recorded in a Vancouver Island stalagmite, *Canad. J. Earth Sci.* **24**:1235-1241.

Lauritzen, S.-E. and Gascoyne, M., 1980, The first radiometric dating of Norwegian stalagmites - evidence of pre-Weichselian karst caves, *Norsk geografische Tidsskrift* **34**:77-82.

Lauritzen, S.-E., Ford, D.C. and Schwarcz, H.P., 1986, Humic substances in speleothem matrix - paleoclimatic significance *Proc. 9th Internatl. Congress Speleol.* **2**: 77-79.

Lauritzen, S.-E., Lovlie, R., Moe, D and Ostbye, E., 1990, Paleoclimate deduced from a multidisciplinary study of a half-million-year-old stalagmite from Rana, northern Norway, *Quat. Res.* **34**:306-316.

Lauritzen, S.-E., 1991, Uranium series dating of speleothems: A glacial chronology for Nordland, Norway, for the last 600 ka, *Striae* **34**:127-133.

Lauritzen, S.-E., 1993, Natural environment change in karst: The Quaternary record, *Catena Suppl.* **25**:21-40.

Lauritzen, S.-E., 1995, High-resolution paleotemperature proxy record for the last interglaciation based on Norwegian speleothems, *Quat. Res.* **43**:133-146.

Lauritzen, S.-E., 1996, *Climate Change: The Karst Record,* Karst Waters Inst. Spec. Pub. No. 2, 196 pp.

Lauritzen, S.-E. and Lundberg, J., 1999, Speleothems and climate: a special issue of The Holocene, *Holocene* **9**:643-647.

Lauritzen, S.-E. and Lundberg, J., 1999, Calibration of the speleothem delta function: an absolute temperature record for the Holocene in northern Norway, *Holocene* **9**:659-669.

Lauritzen, S.-E. and Mylroie, J.E., 2000, Results of a speleothem U/Th dating reconnaissance from the Helderberg Plateau, New York, *J. Cave Karst Stud.* **62**:20-26.

Lea, D.W., Pak, D.K. and Spera, H.J., 2000, Climate impact of late Quaternary equatorial Pacific sea surface temperature variations, *Science* **289**:1719-1724.

Li, W.-X., Lundberg, J., Dickin, A.P., Ford, D.C., Schwarcz, H.P., McNutt, R. & Williams, D., 1989, High-precision mass-spectrometric uranium-series dating of cave deposits and implications for palaeoclimate studies, *Nature* **339**:534-536.

Ludwig, K.R., Simmons, K.R., Szabo, B.J., Winograd, I.J., Landwehr, J.M., Riggs, A.C. and Hoffman, R.J., 1992, Mass-spectrometric ^{230}Th- ^{234}U- ^{238}U dating of the Devils Hole calcite vein, *Science*, **258**:284-287

Lundberg, J. and Ford, D.C., 1994, Late Pleistocene sea level change in the Bahamas from mass spectrometric U-series dating of submerged speleothem, *Quat. Sci. Rev.* **13**:1-14.

Lundberg, J., Ford, D.C., and Hill, C.A., 2000, A preliminary U-Pb date on cave spar, Big Canyon, Guadalupe Mountains, New Mexico, USA, *J. Cave Karst Stud.* **62**:144-146.

McDermott, F., Frisia, S. Huang, Y., Longinelli, A., Spiro, B., Heaton, T.H.E., Hawkesworth, C.J., Borsato, A., Keppens, E., Fairchild, I.J., van der Borg, K., Verheyden, S. and Selmo, E., 1999, Holocene climate variability in Europe: Evidence from δ^{18}O, textural and extension-rate variations in three speleothems, *Quat. Sci. Rev.* **18**:1021-1038.

McGarry, S.F. and Baker, A., 2000, Organic acid fluorescence: applications to speleothem palaeoenvironmental reconstruction, *Quat. Sci. Rev.* **19**:1087-1101.

Niggemann, S., Frank, N., Mangini, A., Richter, D.K. and Wurth, G., 2000, Holozane Stalagmiten des Sauerlandes (Deutschland) als Klimaarchive, *Mitt. Verbandes deutsch. Hohlen Karstforscher e.V. Munchen*, **46**:84-90.

O'Brien, B.J., 1956, "After glow" of cave calcite, *Natl. Speleol. Soc. Bull.* **18**:50-51.

Palmer, A.N., 1987, Cave levels and their interpretation, *Natl. Speleol. Soc. Bull.* **49**:50-66.

Perrette, Y., 1999, Les stalagmites: archives environnementales et climatiques à haute resolution, *Karstologia* **34**:23-44.

Perrette, Y., Delannoy, J.-J., Bolvin, H., Cordonnier, M., Destombes, J.-L., Zhilinskaya, E.A. and Aboukais, A., 2000, Comparative study of a stalagmite sample by stratigraphy, laser induced fluorescence spectroscopy, EPR spectrometry and reflectance imaging, *Chem. Geol.* **162**:221-243.

Polyak, V.J., McIntosh, W.G., Guven, N., and Provencio, P., 1998, Age and origin of Carlsbad Cavern and related caves from ^{40}Ar/^{39}Ar of alunite, *Science* **279**:1919-1922.

Qin, X., Tan, M., Liu, T., Wang, X., Li T., and Lu, J., 1999, Spectral analysis of a 1000-year stalagmite lamina-thickness record from Shihua Cavern, Beijing, China, and its climatic significance, *Holocene* **9**:689-694.

Quinif, Y., 1989, La datation uranium-thorium, *Speleochronos* **1**:3-22.

Quinif, Y., 1991, La courbe de croissance interpolée, *Speleochronos* **3**:11-16.

Ramseyer, K., Miano, T.M., D'Orazio, V., Wildberger, A., Wagner, T. and Geister, J., 1997, Nature and origin of organic matter in carbonates from speleothems, marine cement and coral skeletons, *Org. Geochem.* **26**:361-378.

Richards, D.A, Smart, P.L., and Edwards, R.L., 1994, Maximum sea levels for the last glacial period from U-series ages of submerged speleothems, *Nature* **367**:357-360.

Richards, D.A., Bottrell, S.H., Cliff, R.A. and Ströhle, K.-D., 1996, U-Pb dating of Quaternary age speleothems, in *Climate Change: The Karst Record*, S.-E. Lauritzen, ed., Karst Waters Institute Special Publication No. 2, 136-137.

Richards, D.S., Beck, J.W., Donahue, J.W., Smart, P.L. and Edwards, R.L., 1999, Th-230 and C-14 dating of speleothems from the Bahamas: Implications for the calibration of the radiocarbon timescale, in *Ninth Annual V.M. Goldschmidt Conference*, LPI Contribution No. 971, Lunar and Planetary Institute, Houston, p. 245.

Richter, D.L., Niggemann, S., Oelze, R. and Wurth, G., 1997, Geochemische Rhythmik an quartaren Spelaothemen und ihre Bedeutung fur den mitteleuropaischen Raum-Ziele und erste Ergebnisse, *Mitt. Verband. deutsch. Hohlen-und Karstforscher e.v. Munchen*, **43**:118-121

Roberts, M.S., Smart, P.L. and Baker, A., 1998, Annual trace element variations in a Holocene speleothem, *Earth Planet. Sci. Lett.* **154**:237-246.

Roberts, M.S., Smart, P.L., Hawkesworth, C.J., Perkins, W.T. and Pearce, N.J.G., 1999, Trace element variations in coeval Holocene speleothems from GB Cave, southwest England, *Holocene* **9**:707-713.

Schwarcz, H.P., Harmon, R.S., Thompson, P. and Ford, D.C., 1976, Stable isotope studies of fluid inclusions in speleothems and their paleoclimatic significance, *Geochim. Cosmochim. Acta* **40**:657-665.

Shopov, Y.Y., Ford, D.C. and Schwarcz, H.P., 1994, Luminescent microbanding in speleothems: High-resolution chronology and paleoclimate, *Geology* **22**:407-410.

Szabo, B.J., Kolesar, P.T., Riggs, A.C., Winograd, I.J. and Ludwig, K.R., 1994, Paleoclimatic inferences from a 120,000-yr calcite record of water-table fluctuation in Browns Room of Devils Hole, Nevada, *Quat. Res.* **41**:59-69.

Teeri, J.A. and Stowe, L.G., 1976, Climatic patterns and the distribution of C4 grasses in North America, Oecologia **23**:1-12.

Teng, H.H, Dove, P.M., and De Yoreo, J.J., 2000, Kinetics of calcite growth: Surface processes and relationships to macroscopic rate laws, *Geochim. Cosmochim. Acta* **64**:2255-2266.

Thompson, P., Ford, D.C. and Schwarcz, H.P., 1975, U^{234}/U^{238} ratios in limestone cave seepage waters and speleothem from West Virginia, *Geochim. Cosmochim. Acta* **39**:661-669.

Thompson, P., Schwarcz, H.P., and Ford, D.C., 1976, Stable isotope geochemistry, geothermometry and geochronology of speleothems from West Virginia, *Geol. Soc. Amer. Bull.* **87**:1730-1738.

Tieszen, L.L. and Boutton, T., 1989, Applications of stable isotopic ratios in terrestrial ecosystems, in *Stable Isotopes in Ecological Research*, P.W. Rundel, J.R. Ehlerlinger, and K.A. Nagy, eds., Springer-Verlag, New York, pp. 167-195.

Toth, V.A., 1998, Spatial and temporal variations in the dissolved organic carbon concentrations in the vadose karst waters of Marengo Cave, Indiana, *J. Cave Karst Stud.* **60**:167-171.

Tyson, P.D., Karlen, W., Holmgren, K. and Heiss, G.A., 2000, The Little Ice Age and medieval warming in South Africa, *South African J. Sci.* **96**:121-126.

Vesica, P.L., Tuccimei, P., Turi, B., Fornos,J.J., Gines,A. and Gines, J., 2000, Late Pleistocene paleoclimates and sea-level change in the Mediterranean as inferred from stable isotope and U-series studies of overgrowths on speleothems, Mallorca, Spain, *Quat. Sci. Rev.* **19**:865-879.

Von Grafenstein, U., Erienkeuser, H., Brauer, A., Jouzel, J. and Johnsen, S.J., 1999, A mid-European decadal isotope-climate record from 15,500 to 5000 years B.P., *Science* **284**:1654-1657.

White, W.B., 1981, Reflectance spectra and color in speleothems, *Natl. Speleol. Soc. Bull.* **43**:20-26.

White, W.B., 1986, Luminescence in cave calcite deposits: A current appraisal, *Natl. Speleol. Soc. Bull.* **48**:40

White, W.B., 1988, *Geomorphology and Hydrology of Karst Terrains,* Oxford University Press, New York, 464 pp.

White, W.B., 1994, The anthodites from Skyline Caverns, Virginia: The type locality, *Natl. Speleol. Soc. Bull.* **57**:23-26.

White, W.B., 1997, Precise measurement of luminescence banding profiles in speleothems for paleoclimatic interpretation, *Proc. 12th Internatl. Congress Speleol.* **1**:89-92.

White, W.B. and Brennan,E.S., 1989, Luminescence of speleothems due to fulvic acid and other activators, *Proc. 10th Internatl. Congress Speleol.* pp. 212-214.

Williams, P.W., Marshall, A. Ford, D.C. and Jenkinson, A.V., 1999, Palaeoclimatic interpretation of stable isotope data from Holocene speleothems of the Waitomo district, North Island, New Zealand, *Holocene* **9**:649-657.

Winograd, I.J., Szabo, B.J., Coplen, T.B. and Riggs, A.C., 1988, A 250,000-year climatic record from Great Basin vein calcite: Implications for Milankovitch theory, *Science* **242**:1275-1280.

Winograd, I.J., Coplen, T.B., Landwehr, J.M., Riggs, A.C., Ludwig, K.R., Szabo, B.J., Kolesar P.T., and Revesz, K.M., 1992, Continuous 500,000-year climate record from vein calcite in Devils Hole, Nevada, *Science* **258**:255-260.

Yonge, C.J., Ford, D.C., Gray, J. and Schwarcz, H.P., 1985, Stable isotope studies of cave seepage water, *Chem. Geol.* **58**:97-105.

URANIUM-SERIES DATING OF SPELEOTHEMS: CURRENT TECHNIQUES, LIMITS, & APPLICATIONS

Jeffrey A. Dorale, R. Lawrence Edwards, E. Calvin Alexander, Jr., Chuan-Chou Shen, David A. Richards, and Hai Cheng*

1. ABSTRACT

Carbonate speleothems that contain ppb-ppm levels of uranium can be dated by the ^{238}U-^{234}U-^{230}Th and ^{235}U-^{231}Pa disequilibrium techniques. Accurate ages are possible if the initial concentrations of ^{230}Th and ^{231}Pa are well constrained and if the system has remained closed to post-depositional exchange of uranium, thorium, and protactinium. An estimate of the plausible range of initial $^{230}Th/^{232}Th$ values combined with the measured $^{232}Th/^{238}U$ ratio reveal, to first order, whether initial ^{230}Th is significant. If significant, initial ^{230}Th can be constrained by monitoring ^{232}Th and employing isochron techniques to closely estimate the value of the contaminant $^{230}Th/^{232}Th$ ratio. The sensitivity of the age error to uncertainties in the initial $^{230}Th/^{232}Th$ ratio decreases with increasing U concentration, increasing age, and decreasing detrital contamination. For many speleothems, particularly those composed of nearly pure calcite, initial ^{230}Th may be trivial. Because Pa is more soluble than Th, ^{232}Th is a poor analog for ^{231}Pa. Therefore, initial ^{231}Pa tends to be more significant than initial ^{230}Th for young samples, although this problem becomes less significant or even insignificant with increasing age. Closed-system behavior can be judged by petrographic considerations, stratigraphic ordering of ages, and ^{230}Th-^{231}Pa concordance. Thermal ionization mass spectrometry (TIMS) and inductively coupled plasma mass spectrometry (ICP-MS) offer significant improvements in counting efficiency and sample throughput compared to traditional decay-counting techniques. For ~ 100 mg samples containing ~ 1.0 ppm ^{238}U, best-scenario ^{230}Th age errors, based on the analytical errors (2σ) of current TIMS and ICP-MS techniques, are approximately: 500 ± 6 yrs, 10,000 ± 40 yrs, 50,000 ± 180 yrs, 120,000 ± 500 yrs, and 500,000 ± 15,000 yrs. Materials as young as tens of years and older than 600,000 years are potentially dateable by the ^{238}U-^{234}U-^{230}Th method.

* Jeffrey A. Dorale, Department of Geological Sciences, University of Missouri, Columbia, MO, 65211, USA. R. Lawrence Edwards, E. Calvin Alexander, Jr., Chuan-Chou Shen, and Hai Cheng, Department of Geology and Geophysics, University of Minnesota, Minneapolis, MN, 55455, USA. David A. Richards, School of Geographical Sciences, University of Bristol, Bristol BS8 1SS, UK.

2. INTRODUCTION

The principles of uranium-series dating, which include ^{238}U-^{234}U-^{230}Th and ^{235}U-^{231}Pa disequilibrium dating, have been known since the early part of the last century (Bateman, 1910), shortly after the discovery of radioactivity (Becquerel, 1896; Curie, 1898) and actually before the discovery of isotopes (Thomson, 1914). However, uranium-series dating was not done prior to the 1950's because of problems with measuring concentrations of rare uranium-series isotopes. The first U-Th measurements were made on corals (Barnes et al., 1956), using decay-counting techniques that would become the standard for the next three decades. Although early applications of U-Th-Pa dating included measurements on marine sediment cores (Rosholt et al., 1961) and cave calcites (Rosholt and Antal, 1962; Cherdyntsev et al., 1965), much of the focus was on fossil corals, whose age provided estimates on the timing of past sea levels (e.g. Broecker et al., 1968; Ku, 1968). The routine application of ^{230}Th dating to speleothems gained prominence in the early 1970's (Ford et al., 1972; Thompson et al., 1974; Harmon et al., 1975), which provided access to a new source of paleoenvironmental information. Dating capabilities advanced in the late 1980's with the development of thermal ionization mass spectrometric (TIMS) techniques for measuring ^{234}U (Chen et al., 1986) and ^{230}Th (Edwards et al., 1987). These techniques improved the precision with which ^{230}Th ages could be determined, decreased sample size requirements, and extended the range of ^{230}Th dating to both younger and older times. The first mass-spectrometric U-Th measurements on speleothems were made by Li et al. (1989). Since the late 1980's, there have been additional improvements in uranium and thorium isotopic measurements, including measurements made by inductively coupled plasma mass spectrometry (ICP-MS) using instruments with sector magnets (Luo et al., 1997). Another recent advance was the development of TIMS techniques for measuring ^{231}Pa (Pickett et al., 1994) and the application of these methods to the dating of carbonates (Edwards et al., 1997). The utility of ^{231}Pa dating lies in its combination with ^{230}Th dating as a test for age concordance and closed-system behavior (Cheng et al., 1998). By applying these techniques to appropriate materials (e.g. inorganic carbonates, coralline aragonite), one can obtain precise, and potentially accurate ages over the past half million years. These methods promise to place the chronology of a wide range of late Quaternary events on a precise, calendarial time scale.

The extensive number of published ^{230}Th dates on speleothems has made it clear that well chosen speleothem sub-samples are nearly ideal candidates for ^{230}Th dating (Schwarcz, 1986; Gascoyne, 1992a). In this regard, three fundamental issues are (1) the precision with which ^{230}Th ages can be determined, (2) the level of initial ^{230}Th in samples and methods of correcting for initial ^{230}Th, and (3) the degree to which diagenesis may affect the accuracy of the ages and methods for detecting diagenesis. The purpose of this paper is to review these three issues in light of current techniques and analytical capabilities. In addition to reviewing current capabilities, we present some of the first high-precision TIMS ^{231}Pa data on speleothems and some of the first ICP-MS ^{230}Th data on speleothems. We elaborate on the issue of initial ^{230}Th using a series of examples and simple isochron techniques. All errors quoted in this paper are given as two standard deviations of the mean (2σ), including errors on half-life values, which may differ from the original reference. All age determinations reported in this paper are given in years before present.

3. BACKGROUND

The activity, or the number of disintegrations per unit time (dN/dT), of any radioactive nuclide is equal to $N\lambda$, where N is the number of atoms, λ is the decay constant for that nuclide, and T is time. The half-life of the nuclide is equal to $(\ln 2)/\lambda$. ^{234}U and ^{230}Th are the longest-lived intermediate daughters in a decay series that starts with ^{238}U and ends with stable ^{206}Pb. That series with only the nuclides pertinent to this discussion and their respective half-lives is:

$$^{238}U \underset{4.468 \times 10^9\ y}{\Rightarrow} {}^{234}U \underset{2.453 \times 10^5\ y}{\Rightarrow} {}^{230}Th \underset{7.569 \times 10^4\ y}{\Rightarrow} {}^{206}Pb$$

The half-life of ^{238}U is four orders of magnitude greater than any of the intermediate daughters. Therefore, any closed system, regardless of the initial state, will approach a state of "secular equilibrium" such that the activities of all the intermediate daughters are the same and are equal to the ^{238}U activity (Bateman, 1910). External processes that fractionate nuclides within the decay chain disrupt the state of secular equilibrium. The subsequent growth or decay of the intermediate nuclides back towards equilibrium with ^{238}U can be used to date the fractionation event (see Ivanovich et al., 1992).

Uranium-thorium dating of speleothems is possible because of the extreme fractionation of Th from U in ground water. Uranium is easily oxidized to the U^{6+} state and is soluble as the UO_2^{2+} (uranyl) ion, and as various uranyl carbonate complexes, but Th is locked into the Th^{4+} state and has an extremely low solubility (Langmuir, 1978; Gascoyne, 1992b). Surface waters, therefore, have very low $^{230}Th/^{238}U$ ratios. This condition is examined more fully in a subsequent section, but for the moment we can assume that a growing speleothem includes U into its crystal lattice but incorporates negligible ^{230}Th. If the crystal lattice remains a closed system with respect to the loss or gain of U and Th, the equations for radioactive production and decay of ^{238}U, ^{234}U, and ^{230}Th govern the geochemical evolution of the system as follows:

$$\left[\frac{^{230}Th}{^{238}U}\right] = 1 - e^{-\lambda_{230}T} + \left(\frac{\delta^{234}U_{(m)}}{1000}\right)\left(\frac{\lambda_{230}}{\lambda_{230} - \lambda_{234}}\right)\left(1 - e^{(\lambda_{234} - \lambda_{230})T}\right) \quad (1)$$

(modified from Kaufman and Broecker, 1965), and

$$\delta^{234}U_{(i)} = \delta^{234}U_{(m)}e^{\lambda_{234}T} \quad (2)$$

(modified from Edwards et al., 1987),

where the λ's denote the decay constants, $[^{230}Th/^{238}U]$ denotes the $^{230}Th/^{238}U$ activity ratio, $\delta^{234}U_{(m)} = ([^{234}U/^{238}U] - 1)*1000$, and T is the age. Equation (1) shows that the age can be calculated if $[^{230}Th/^{238}U]$ and $\delta^{234}U_{(m)}$ can be measured and the decay constants are known. Equation (2) relates the measured $\delta^{234}U$ value ($\delta^{234}U_{(m)}$) to the initial state ($\delta^{234}U_{(i)}$) when the system was isolated with $^{230}Th = 0$. Figure 1 shows $[^{230}Th/^{238}U]$ plotted as a function of T and contoured in units of $\delta^{234}U_{(i)}$. This shows that as T becomes

large, [^{230}Th/^{238}U] approaches unity, and that at some point between 400,000 and 800,000 years an age limit to the technique is reached. The exact limit depends on several factors, including $\delta^{234}U_{(i)}$ and the precision of the isotopic measurements.

Reported uncertainties in T are introduced primarily by uncertainties in the measured values for [^{230}Th/^{238}U] and $\delta^{234}U_{(m)}$, but also depend on T itself, because the slope d[^{230}Th/^{238}U]/dT, generally decreases with increasing T, approaching a slope of zero near secular equilibrium (Fig. 1). The smallest fractional age errors are obtained for materials several thousands to several tens of thousands of years old. Samples of this age are old enough to have enough ^{230}Th atoms for a high-precision analysis, yet are young enough to fall on the initial high-slope part of the [^{230}Th/^{238}U] evolution curve (Fig. 1). For example, [^{230}Th/^{238}U] and $\delta^{234}U_{(m)}$ measured to the 2.0-3.0 ‰ level yield the approximate age errors: ± 40 yrs at 10,000 yrs, ± 200 yrs at 50,000 yrs, ± 1,200 yrs at 200,000 yrs, and ± 15,000 yrs at 500,000 yrs.

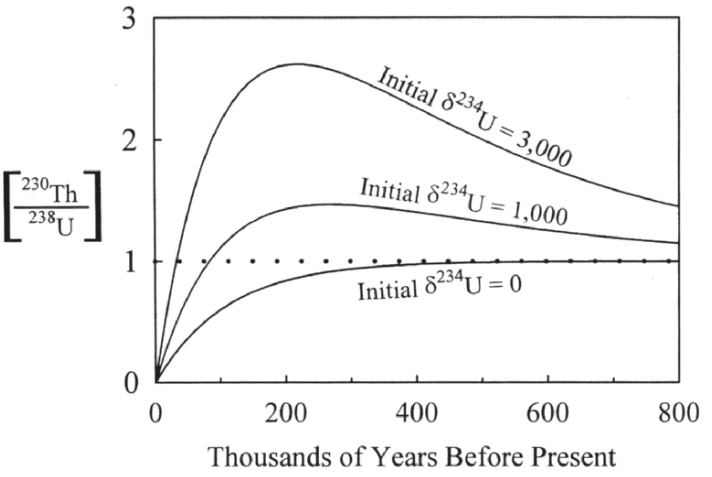

Figure 1. This shows the change in the ^{230}Th/^{238}U activity ratio ([^{230}Th/^{238}U]) with time for different initial δ^{234} values ($\delta^{234}U_{(i)}$) and is calculated assuming a closed system and initial ^{230}Th = 0 (Eqs. (1) and (2)). For those cases where [^{230}Th/^{238}U] > 1, a unique combination of [^{230}Th/^{238}U] and $\delta^{234}U_{(m)}$ defines the age T. Initial δ^{234}U values of 0 to 3,000 are common for many of the speleothems discussed in the paper.

The analytical errors in [^{230}Th/^{238}U] and $\delta^{234}U_{(m)}$ generally follow counting statistics, such that the fractional error is inversely proportional to the square root of the number of counts per analysis. At the 2σ level:

$$2\sigma = \frac{2}{\sqrt{\text{total counts}}} \tag{3}$$

Thus, precision at the 2 % level requires at least 10^4 counts, whereas precision at the 2 ‰ level requires at least 10^6 counts. Because of their relatively long half-lives, decay

counting is on the order of 10^4 times less efficient for measuring the abundances of ^{234}U and ^{230}Th than is mass spectrometry for the same sample size (Chen et al, 1992).

In practice, measured isotope ratios are reported as mean and standard error. For analyses with stable ion-beam intensities, the "within-run" statistical errors are typically similar to those predicted by counting statistics. Uncertainties in sample weight, spike weight, spike concentration, chemical blanks, and filament blanks are typically small compared to the analytical uncertainty, but are also included in the error propagation through Eq. (1).

Accurate values for half-lives are clearly required for accurate age calculations. Table 1 lists the nuclides discussed in this paper, their half-lives, decay constants, and sources. Of the three pertinent nuclides used in ^{230}Th dating, the fractional error in the half-life of ^{238}U, $4.4683 \pm 0.0048 \times 10^9$ y (Jaffey et al., 1971), is the smallest. For ^{234}U, De Bievre et al. (1971) determined a half-life of 244,600 ± 730 years and Lounsbury and Durham (1971) determined a value of 244,400 ± 1,200 years. A commonly used value in geochronology is the mean value: 244,500 years. More recently, Holden (1989) reviewed the available literature on ^{234}U and proposed a weighted average value of 245,500 ± 1,000 years. A commonly used value for ^{230}Th is 75,380 ± 590 years (Meadows et al., 1980). Most recently Cheng et al. (2000) re-determined the half-lives of ^{234}U and ^{230}Th to be 245,250 ± 490 years and 75,690 ± 230 years. These new values are within error of the previously used values but have smaller errors. We have therefore adopted the Cheng et al. (2000) half-lives and recommend universal use of these values.

It is important to note that uncertainties in decay constants are *not* typically propagated through Eq. (1). This is permissible when comparing ages determined by the same dating technique because any inaccuracy due to decay constants will affect the ages in the same sense. However, when comparing ages determined by different chronometers, it is important to consider errors in decay constants (Renne et al., 1998).

Table 1. Half-lives and decay constants and recommended values*

Nuclide	Half-life ($t_{½}$)[a]	Decay constant (λ)	Source
^{238}U	$4.4683 \pm 0.0048 \times 10^9$ y	1.55125×10^{-10} y^{-1}	Jaffey et al., 1971*
^{235}U	$7.0381 \pm 0.0096 \times 10^8$ y	9.8485×10^{-10} y^{-1}	Jaffey et al., 1971*
^{234}U	247,500 ± 3,200 y	2.8006×10^{-6} y^{-1}	Fleming et al., 1952
^{234}U	244,600 ± 730 y	2.8338×10^{-6} y^{-1}	De Bievre et al., 1971
^{234}U	244,400 ± 1,200 y	2.8361×10^{-6} y^{-1}	Lounsbury & Durham, 1971
^{234}U	245,500 ± 1,000 y	2.8234×10^{-6} y^{-1}	Holden, 1989
^{234}U	245,250 ± 490 y	2.8263×10^{-6} y^{-1}	Cheng et al., 2000 *
^{230}Th	75,200 ± 3,200 y	9.2174×10^{-6} y^{-1}	Attree et al., 1961
^{230}Th	75,381 ± 590 y	9.1953×10^{-6} y^{-1}	Meadows et al., 1980
^{230}Th	75,690 ± 230 y	9.1577×10^{-6} y^{-1}	Cheng et al., 2000 *
^{232}Th	1.401×10^{10} y	4.9475×10^{-11} y^{-1}	LeRoux & Glendenin, 1963 *
^{231}Pa	32,760 ± 220 y	2.1158×10^{-5} y^{-1}	Robert et al., 1969 *

* These are the values used in our calculations and the values we recommend.

[a] All errors are quoted at the 2σ level; this may differ from the original source.

^{231}Pa is the only long-lived intermediate daughter ($t_{½}$ = 32,760 years) in the decay series starting with ^{235}U and ending with stable ^{207}Pb. ^{235}U-^{231}Pa dating is analogous to ^{238}U-^{234}U-^{230}Th dating, but the system only involves two nuclides:

$$\left[\frac{^{231}\text{Pa}}{^{235}\text{U}}\right] = 1 - e^{-\lambda_{231}T} \tag{4}$$

For a closed-system material at secular equilibrium, the ^{230}Th/^{231}Pa atomic ratio is equal to $(\lambda_{238}*\lambda_{231}*137.88)/(\lambda_{235}*\lambda_{230})$ = 50.9, where 137.88 is the present-day value for the natural ^{238}U/^{235}U atomic ratio (Steiger and Jäger, 1977). Because ^{231}Pa is 50 times less abundant than ^{230}Th, ^{231}Pa dating is inherently less precise than ^{230}Th dating, and because the half-life of ^{231}Pa is roughly half that of ^{230}Th, the upper limit to ^{231}Pa dating is approximately 250,000 years given current capabilities (Edwards et al., 1997).

The discussion thus far has not been restricted to speleothems. Any material that (1) forms with appreciable U, (2) forms with negligible Th and Pa, and (3) remains a closed system, is potentially datable by U-Th-Pa techniques. Despite such simple criteria, few natural materials meet all three conditions. Corals commonly satisfy criteria (1) and (2) exceedingly well but become increasingly likely to violate criterion (3) with increasing age, because coralline aragonite is thermodynamically metastable and is typically highly porous. Materials such as bone, teeth, and mollusk shells also violate criterion (3) because they exclude U while the organism is alive, but then take up U after death (Kaufman et al., 1971; Szabo, 1979). Dense calcite speleothems, on the other hand, are excellent candidates for true closed-system behavior and accurate age dating.

4. SAMPLING CONSIDERATIONS

For ^{230}Th dating by mass spectrometry, the factors that determine a given level of precision include (1) U concentration, (2) $\delta^{234}U_{(i)}$, (3) sample age, (4) chemical yield (generally > 90%), and (5) ionization/transmission efficiency. For ^{235}U-^{231}Pa dating, $\delta^{234}U_{(i)}$ is not a factor, and for decay counting, the decay rates of the pertinent nuclides are important. The ionization/transmission efficiency refers to the number of atoms actually detected versus the number of atoms introduced to the system, a variable number dependent on technique but typically in the range of 10^{-3} to 10^{-5} (Chen et al., 1992).

Suppose we seek to measure ^{234}U with a precision of 2 ‰ (2σ). Counting statistics predicts a requirement of at least 10^6 counts, and assuming a typical ionization efficiency of 10^{-4}, such precision would require 10^{10} atoms of ^{234}U. Assuming that the sample contains 1 ppm ^{238}U, the chemical yield is 100 %, and that for simplicity ^{234}U and ^{238}U are in secular equilibrium, i.e. $\delta^{234}U = 0$ and the ^{234}U/^{238}U atomic ratio = $\lambda_{238}/\lambda_{234}$. Given these constraints the sample size required for a 2 ‰ ^{234}U analysis is:

$$\text{sample size (g)} = \frac{(10^{10}\,\text{atoms}\ ^{234}\text{U})\left(238.051\,\frac{\text{g}\ ^{238}\text{U}}{\text{mole}\ ^{238}\text{U}}\right)}{\left(10^{-6}\,\frac{\text{g}\ ^{238}\text{U}}{\text{g calcite}}\right)\left(\frac{\lambda_{238}}{\lambda_{234}}\right)\left(6.022 \times 10^{23}\,\frac{\text{atoms}}{\text{mole}}\right)} = 0.72\ \text{g calcite} \tag{5}$$

In speleothem and other inorganic calcite work, both sample size and precision are related to the error in age (Ludwig et al., 1992). Deposition rates of speleothems are often low, so that large sub-samples will integrate large time intervals and introduce error in age if uranium concentrations and growth rates are not constant in that interval. On the other hand, large sub-samples contain more ^{230}Th atoms and therefore result in higher precision measurements. Thus, there is a tradeoff between spatial resolution in sub-sampling (for which small sub-samples are ideal) and precision in ^{230}Th age (for which large samples are ideal). The optimal strategy is to balance sampling resolution and analytical precision to obtain the most scientifically useful result.

Improvements in the ionization/transmission efficiency directly result in improved counting statistics and/or smaller sample sizes. Such improvements generally benefit all of the sub-disciplines that utilize isotopic measurements, but hold especially important practical implications for dating slow-growth speleothems.

5. EXPERIMENTAL METHODS

5.1. Sampling

Sub-samples for dating are typically obtained by either sawing or milling. Milling is generally less destructive to the formation. For high-resolution work, milling from polished surfaces using a hand-held or computerized dental drill offers excellent control. Particularly when the layering is not horizontally uniform, milling allows the tracing of specific layers in a manner that is not possible by sawing. We typically use carbide dental burrs that range in size from 0.5 to 1.2 mm in diameter. Sub-samples smaller than ~ 300 mg can be milled in approximately 20 to 40 minutes. In preparation for sampling, the polished speleothem surface is cleaned with deionized water, and the dental burr is turned in 0.1*N* HCl and then methanol. The milled powders are gently scraped from the surface of the speleothem onto weighing paper and are then transferred to a pre-weighed polyethylene vial and weighed. For those cases where solid sub-samples are preferable to powders, slow-speed saws and wire saws provide reasonably precise control.

5.2. Chemical Separation of Uranium and Thorium

The basic chemical procedure is similar to that described for coral work by Edwards et al., (1987), although the smaller sub-gram sample sizes of the speleothem analyses described here generally involve reduced reagent volumes compared to that described in the reference. Sub-samples are transferred from the polyethylene vials to pre-weighed 30 ml Teflon vials and are re-weighed. The samples are covered with ~ 5 ml of deionized water and are then dissolved by incrementally adding small amounts of 7*N* HNO_3. For clean, powdered samples it is unusual to observe any acid-insoluble residue. For samples with detrital impurities, acid-insoluble residue may remain after nitric acid dissolution. Although in earlier studies the residue was commonly discarded, recent studies have demonstrated that significant and unpredictable exchange of U and Th between the residues and the leachates can take place and render the results inaccurate (Bischoff and Fitzpatrick, 1991; Luo and Ku, 1991). For this reason, the most effective procedure is to completely dissolve the residue with concentrated HF-HCl-$HClO_4$. Isochron techniques,

to be discussed in a subsequent section, can be used to estimate the U and Th contribution of the detrital phase for those samples with significant contamination.

Once dissolved, the samples are spiked with a mixed ^{229}Th-^{233}U-^{236}U tracer of known concentration and isotopic composition. Organics are destroyed by the addition of 3-6 drops of concentrated $HClO_4$, and the sample is dried on a hot plate. While still hot, the residue is re-dissolved in ~ 1*N* HCl, and ~ 0.3 mg of Fe in chloride solution is added. The U and Th are co-precipitated with Fe by dropwise addition of concentrated NH_4OH. The mixture is centrifuged and the supernate discarded. The residue is then rinsed 2-3 times, dissolved in 14*N* HNO_3, dried and re-dissolved twice in 14*N* HNO_3, then dried and dissolved in ~ 0.5 ml 7*N* HNO_3. The solution is loaded on an anion exchange column (SPECTRUM Spectra Gel Ion Exchange 1 X 8, chloride form, particle size = 75-150 μm, mesh size = 100-200) with a volume of 0.5 ml. Iron is eluted using 1.5 column volumes of 7*N* HNO_3, thorium is eluted using 2 column volumes of 8*N* HCl, and uranium is eluted using 4 column volumes of water. The U and Th fractions are dried and generally contain only trace amounts of Fe (just visible). Rarely, significant amounts of Fe may require an additional clean-up column, but unless this is the case, the samples are ready either for loading onto rhenium filaments for TIMS analysis or dissolution in a weak nitric acid solution for ICP-MS analysis.

5.3. Instrumental Procedure

Measurements were made at the Minnesota Isotope Lab by TIMS on a Finnigan-MAT 262 instrument, equipped with ion-counting capabilities and a retarding potential quadrapole. Uranium is run using the double-filament technique with an evaporation-filament current of 0.3 to 1.5 amps and an ionization-filament current of 4.0 to 5.3 amps (corresponding to ionization-filament temperatures of 1600-1850 °C). Runs typically last 1-2 hours. Because of dead time and intensity bias constraints on the multipliers, ion currents are not allowed to exceed 200,000 counts per second (cps) for ^{235}U. Ionization efficiencies are typically in the range of 10^{-4} to 5 x 10^{-4}. Thorium is loaded with colloidal graphite on a single rhenium filament and run at temperatures of 1500-1900 °C for 1-2 hours. Throughout the course of a Th analysis, both temperature and ion beams increase as the graphite burns away. Typical loads of 10^{11} atoms of ^{229}Th yield ion currents that range from ~ 500-2,000 cps at the beginning of a run to ~ 10,000-40,000 cps near the end of a run, resulting in overall ionization efficiencies that range from 10^{-4} to 10^{-3}.

Measurements made at the Minnesota Isotope Lab by ICP-MS were done on a Finnigan-MAT *ELEMENT*, equipped with a double-focusing sector field/energy filter of reversed Nier-Johnson geometry, and a single electron multiplier. Shen et al. (2001) provide details on the instrumental modifications and procedures. Uranium samples are diluted with 0.1*N* HNO_3 to a volume of 1.0 ml and run for ~ 20 minutes at a flow rate of ~ 50 μl/min using a microconcentric desolvation nebulizer (Cetac MCN 6000). As the nebulized and dried sample is introduced into a plasma, ionization efficiencies are extremely high. However, in this sort of instrument significant losses occur during transmission of the plasma to the high vacuum in the main part of the mass spectrometer. A combined ionization/transmission efficiency of ~ 3 x 10^{-3} has been attained for uranium. Thorium samples are diluted with 0.1*N* HNO_3 + ~ 0.01*N* HF to a volume of 0.5 ml and run for ~ 10 minutes at a flow rate of ~ 50 μl/min. A combined ionization/transmission efficiency of ~ 2 x 10^{-3} has been attained for thorium. The

implications of the shorter run times and the improved ionization/transmission efficiency of ICP-MS method are significant and are discussed in a subsequent section.

6. INITIAL ^{230}Th AND ^{231}Pa

The derivations of the ^{238}U-^{234}U-^{230}Th and ^{235}U-^{231}Pa age equations assume zero initial contents of the daughter isotopes ^{230}Th and ^{231}Pa. This assumption is generally reasonable, because Th^{4+} and Pa^{5+} (rarely Pa^{4+}) have low solubilities in surface waters. For example, the surface sea water ^{230}Th/^{238}U atomic ratio is ~ 3 x 10^{-10} and the ^{231}Pa/^{235}U ratio is ~ 3 x 10^{-9} (Chen et al., 1986 for U; Moran et al., 1995 for ^{230}Th; Edmonds et al., 1998 for ^{231}Pa). By dating recent corals with low ^{232}Th concentrations, and whose age was known independently by band-counting, Edwards (1988) demonstrated that the maximum amount of initial ^{230}Th that could have been incorporated during growth was equivalent to the amount of ^{230}Th produced by radioactive decay in 3-6 years. A 6-year offset is comparable to the 2σ analytical errors for a 500-year-old coral (1 g sample, 3 ppm ^{238}U). The age error is ~ ± 3 years for a 20-year-old coral and ~ ± 20 years at 4,000 years. Thus, for clean corals older than 20-500 years, initial ^{230}Th may be negligible.

Although Th^{4+} and Pa^{5+} have low solubilities, they strongly adsorb to surfaces and may be readily introduced into a growing carbonate matrix with detrital materials such as clays. The initial ^{230}Th associated with such a detrital component is the main problem with dating "dirty" speleothems and other carbonates. Also, the behavior of Th^{4+} and Pa^{5+} in karst ground waters is less studied than in ocean surface waters. It is possible that ^{230}Th and ^{231}Pa could be carried in solution in colloidal phases (Short et al., 1988; Dearlove et al., 1991), attached to organic molecules (Langmuir and Herman, 1980; Gaffney et al., 1992), or in carbonate complexes (Dervin and Faucherre, 1973a,b; Joao et al., 1987). Thus, multiple sources may potentially contribute variable amounts of initial ^{230}Th and ^{231}Pa to a developing speleothem. Whitehead et al. (1999) suggested that for some young New Zealand speleothems, initial ^{230}Th and ^{231}Pa may account for age offsets from the true age that are larger than 2,000 years, clearly a significant issue.

The first step in evaluating initial ^{230}Th is to measure the ^{230}Th/^{232}Th ratio. ^{232}Th is an abundant radioactive, non-radiogenic isotope with a half-life of 1.401 x 10^{10} years and is measured during a typical thorium analysis. Because ^{230}Th and ^{232}Th are chemically equivalent, ^{232}Th is a potential monitor of the initial ^{230}Th content of a growing speleothem if the ^{230}Th/^{232}Th ratio of the contamination can be determined.

The ^{230}Th/^{232}Th ratio of the contamination can be estimated using an isochron technique (Ludwig, 1993; Kaufman, 1993; Ludwig and Titterington, 1994). The technique depends on the ability to obtain sub-samples of the same age (i.e. carefully milling within the boundaries of a given stratigraphic layer) that differ in ^{232}Th/^{238}U values, which generally correlate with detrital content. Many stalagmites lend themselves to such sampling because they are commonly cleanest near the center of a given layer and are dirtier near the edges, presumably because the falling drip flushes particulates away from the point of impact.

The importance of the total sample dissolution technique mentioned earlier becomes apparent because the detrital phase contains Th and U that is both lattice-bound and adsorbed but in unknown proportions. Bischoff and Fitzpatrick (1991) demonstrated that it is not possible to quantitatively separate these two components by selective leaching.

Also, ^{230}Th released from the carbonate phase during acid dissolution may unpredictably adsorb to detrital particles if they are present. For these reasons, both Bischoff and Fitzpatrick (1991) and Luo and Ku (1991) independently concluded that isochron techniques that employ total sample dissolution give the most reliable results.

The isochrons that we depict in this paper are simple two-dimensional isochrons. A rigorous treatment of isochron techniques requires the use of three-dimensional isochrons (e.g. Ludwig and Titterington, 1994). However, for our particular examples, variation in the ^{234}U/^{238}U ratio among sub-samples used to construct each isochron is negligible. Therefore, two-dimensional isochrons are advantageous in their simplicity in illustrating the concepts discussed here. Such a two-dimensional, three-point isochron using total sample dissolution for a stalagmite from Spring Valley Caverns, Minnesota is shown in Fig. 2 (data in Table 2). The regression y-intercept value of 4.4 ppm (the atomic ^{230}Th/^{232}Th ratio * 10^6) is the present-day ^{230}Th/^{232}Th ratio of the contamination. The excellent fit of a straight line to the three points in Fig. 2 is consistent with initial ^{230}Th being dominated by a single component that has a constant ^{230}Th/^{232}Th value.

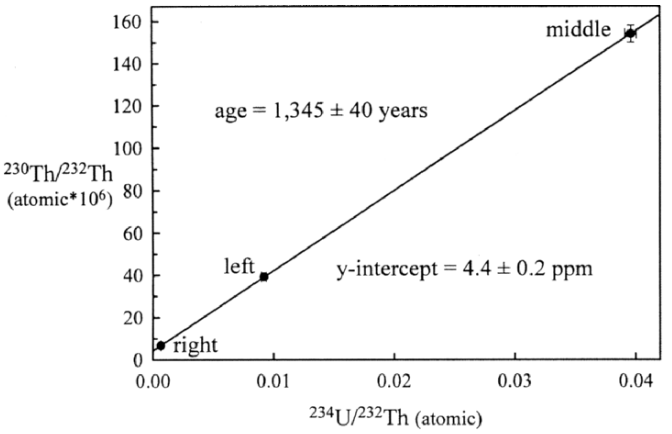

Figure 2. A two-dimensional isochron diagram for stalagmite SVC-98-3.B from Spring Valley Caverns, Minnesota (the third dimension, not shown here, would be ^{234}U/^{238}U). The three sub-samples, labeled left, middle, and right, are horizontally spaced 1-1.5 cm from one another within the same stratigraphic layer and are from locations with visually obvious differences in detrital content. Sub-sample widths are about 1.0 mm. The regression y-intercept value of 4.4 ± 0.2 ppm represents the present-day ^{230}Th/^{232}Th ratio of the contamination. The true ^{230}Th/^{232}Th initial value, that is the value at the actual time of calcite deposition when $T = 0$, can be approximated by multiplying the present-day value by $e^{-\lambda 230 T}$.

Table 2. Isochron data for Spring Valley Caverns stalagmite SVC-98-3.B

Isochron Sub-sample	Sample Weight (mg)	^{238}U conc. (ppm)	^{232}Th conc. (ppb)	Uncorrected Age	Corrected Age[a]
Middle	40.5	2.55	5.4	1,383 ± 34	1,344 ± 34
Left	42.8	2.54	22.8	1,519 ± 46	1,349 ± 44
Right	37.7	2.25	291.6	3,797 ± 55	1,348 ± 51

[a]Ages corrected using an initial ^{230}Th/ ^{232}Th atomic ratio of 4.4 ppm.

The contamination in this particular example is almost certainly clay particles, as such particles were clearly visible in the two dirtier sub-samples. The $^{230}Th/^{232}Th$ ratio of 4.4 ppm is almost the exact value predicted by the chondritic $^{232}Th/^{238}U$ atomic ratio of 3.8, which at secular equilibrium gives a $^{230}Th/^{232}Th$ atomic ratio equal to $\lambda_{238}/\lambda_{230}$ *3.8 = 4.44×10^{-6}. Such a perfect match is doubtless fortuitous, but it is still reassuring validation of a value commonly used for correcting initial ^{230}Th. A 4.4 ppm correction results in corrected ages that are impressively concordant (Table 2).

A second isochron example from Crevice Cave, Missouri (Dorale et al., 1998) illustrates a slightly more complex scenario (Fig. 3). The regression y-intercept value of 6.1 ± 0.2 ppm is certainly a reasonable value within the range of common detrital $^{232}Th/^{238}U$ values. As Table 3 shows, however, applying a 6.1 ppm correction to each of the three sub-samples results in ages that are slightly discordant at face value. Such a data set is consistent with the hypothesis that there is more than one source of initial ^{230}Th and that these multiple sources have different $^{230}Th/^{232}Th$ ratios. The simplest scenario is a two-component system in which the high ^{232}Th component has a low $^{230}Th/^{232}Th$ ratio and the low ^{232}Th component has a high $^{230}Th/^{232}Th$ ratio. Indeed, Table 3 illustrates that the two dirtier sub-samples (left and right) give an initial $^{230}Th/^{232}Th$ value of 2.4 ppm, while the two cleaner sub-samples (middle and left) give a value of 11.0 ppm.

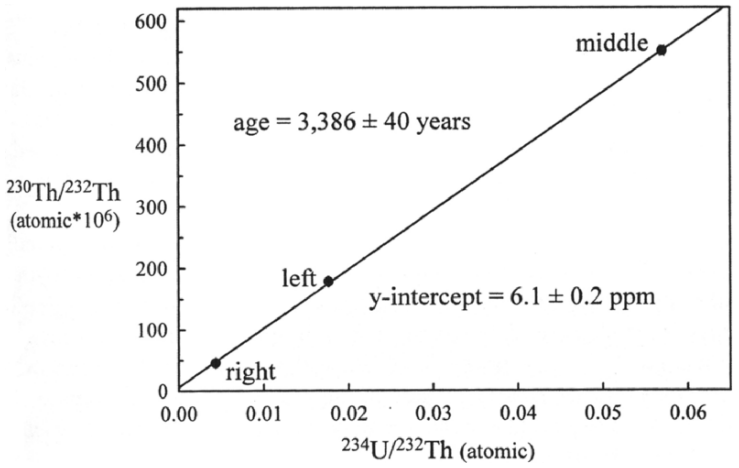

Figure 3. A two-dimensional isochron diagram for stalagmite CC-99-12-A from Crevice Cave, Missouri. The three sub-samples, labeled left, middle, and right, are horizontally spaced 1-1.5 cm from one another within the same stratigraphic layer and are from locations with visually obvious differences in detrital content. Sub-sample widths are about 2.0 mm. The regression y-intercept value of 6.1 ± 0.2 ppm represents the average, present-day $^{230}Th/^{232}Th$ atomic ratio of the contamination. Although the scaling of this figure makes it difficult to see, the three points are not exactly co-linear. A two-point line using the two dirtier sub-samples (left and right) gives a regression y-intercept value of 2.4 ppm, and a similar exercise for the two cleaner sub-samples (middle and left) gives a value of 11.0 ppm. Such a data set is consistent with the hypothesis that there is more than one source of initial ^{230}Th and that these multiple sources have different $^{230}Th/^{232}Th$ ratios. The simplest scenario (one that fits the data in this example) is a two-component system in which the high ^{232}Th component has a low $^{230}Th/^{232}Th$ value and the low ^{232}Th component has a high $^{230}Th/^{232}Th$ value.

Table 3. Isochron U-Th-Pa data for Crevice Cave stalagmite CC-99-12-A-102.5

	Left	Middle	Right
^{238}U (ppb)	1,198	1,205	1,162
^{232}Th (ppb)	12	3.7	47
Uncorrected ^{230}Th age	3,604 ± 22	3,453 ± 20	3,752 ± 25
Corrected 6.1 ± 3.05 ppm	3,482 ± 64	3,415 ± 28	3,257 ± 248
Corrected 2.4 ± 1.2 ppm[a]	*3,556 ± 32*	3,438 ± 22	*3,557 ± 100*
Corrected 11.0 ± 5.5 ppm[a]	*3,385 ± 111*	*3,385 ± 40*	2,857 ± 450
Uncorrected ^{231}Pa age	4,815 ± 210	4,875 ± 193	3,853 ± 170
Corrected ^{231}Pa age[b]	4,689 ± 219	4,836 ± 194	3,338 ± 307
Calculated initial $^{231}Pa/^{232}Th$[c]	1,020 ± 30 ppb	3,425 ± 95 ppb	81 ± 7 ppb

[a] Italicized ages highlight concordant sub-samples for a particular $^{230}Th/^{232}Th$ corrective value.
[b] Corrected for initial ^{231}Pa using an atomic $^{231}Pa/^{232}Th$ value of 88.8 ± 44.4 ppb. This is the secular equilibrium value for the chondritic $^{232}Th/^{238}U$ atomic ratio of 3.8.
[c] Calculated using the ^{230}Th age of 3,385 ± 40 years.

Speleothems from other regions help provide perspective for the midwestern examples given here. Richards et al. (1999) analyzed a stalagmite from the Bahamas and calculated an initial $^{230}Th/^{232}Th$ ratio of 89 ppm, significantly higher than the Minnesota and Missouri examples. The carbonate platforms that comprise the Bahamas are expected to have significantly lower silicate-related ^{232}Th. The high initial $^{230}Th/^{232}Th$ values of these speleothems most likely reflect the production of ^{230}Th by uranium decay in a ground water setting that is deficient in ^{232}Th, or indicate that the primary limestone itself has high $^{230}Th/^{232}Th$ ratios. The transport mechanism for this excess ^{230}Th is possibly by colloids, organic complexes, or carbonate complexes as mentioned earlier. Other workers have referred to a high ^{230}Th component such as this as "hydrogenous" (e.g. Lin et al., 1996).

^{231}Pa dating adds another dimension to the issue of initial daughter/parent ratios. Whitehead et al. (1999) described discordant ^{231}Pa and ^{230}Th ages for several young New Zealand speleothems (measured by α-counting) and reinforced earlier suggestions that Pa^{5+} and Th^{4+} may have slightly different behaviors in ground water. Gascoyne (1985), for example, measured ^{227}Th as a proxy for ^{231}Pa and suggested the possibility of ^{231}Pa excess in speleothems. We also observe small but significant ^{231}Pa –^{230}Th discordance for our Holocene Crevice Cave stalagmite, as the uncorrected ^{231}Pa ages are older than the ^{230}Th ages, suggesting ^{231}Pa excess (Table 3).

For the two sub-samples with lower ^{232}Th concentrations, ^{231}Pa-^{230}Th discordance remains after initial ^{231}Pa is corrected assuming secular equilibrium and a $^{232}Th/^{238}U$ value of 3.8 ($^{231}Pa/^{232}Th = \lambda_{235}/(\lambda_{231}*3.8*137.88) = 8.9 \times 10^{-8}$ (89 ppb)). This indicates that ^{232}Th is a poor analog for ^{231}Pa in these samples. Using the ^{230}Th age of 3,385 ± 40 years as the true age, we calculate initial $^{231}Pa/^{232}Th$ ratios of 3,425 ± 95 ppb, 1,020 ± 30 ppb, and 81 ± 7 for the middle (low ^{232}Th), left (moderate ^{232}Th), and right (high ^{232}Th) sub-samples, respectively. This suggests that a hydrogenous ^{231}Pa component is significant for those samples with low ^{232}Th concentrations, and that ^{231}Pa is considerably more soluble than ^{230}Th in karst ground waters. This observation is consistent with the significantly longer residence time of ^{231}Pa (~ 200 years) versus ^{230}Th (~ 20 years) in the oceans (Broecker and Peng, 1982; Yu et al., 1996).

To what extent do initial ^{230}Th and ^{231}Pa affect the validity of disequilibrium ages? In some cases initial ^{230}Th and ^{231}Pa can cause an offset from the true age that is significantly larger than the analytical error. However, these tend to be unusual cases for samples that are young, have low U concentrations, have a high hydrogenous component, have high detrital content, or have a combination of the four factors. The sensitivity of the age error to uncertainties in the initial concentrations of ^{230}Th and ^{231}Pa decreases with the sample age because (1) *in situ* radiogenic production of ^{230}Th and ^{231}Pa and (2) the unsupported decay of the initial ^{230}Th and ^{231}Pa, gradually shift the radiogenic/initial ratio toward higher values. Our data suggest that initial ^{231}Pa is more problematic in young speleothems than initial ^{230}Th, because ^{230}Th is less soluble than ^{231}Pa, and because we can correct for initial ^{230}Th using estimates of the initial $^{230}Th/^{232}Th$ ratio.

The Spring Valley Caverns stalagmite provides an excellent example of initial ^{230}Th sensitivity. Using an isochron technique (Fig. 2; Table 2), we calculated an initial $^{230}Th/^{232}Th$ value of 4.4 ppm for this particular stalagmite. We can test the sensitivity of the three sub-samples to uncertainties on this initial $^{230}Th/^{232}Th$ value as shown in Table 4. The exercise clearly shows that the most sensitive sample is the right sub-sample, which has the highest ^{232}Th concentration. For the cleanest sub-sample (middle), initial $^{230}Th/^{232}Th$ uncertainties of 100% (e.g. 4.4 ± 4.4 ppm), after propagation through Eq. (1), are relatively small and are comparable to the analytical error (34 yrs vs. 52 yrs).

Table 4. Sensitivity to initial ^{230}Th corrections for stalagmite SVC\98-3.B

Sample ID	^{232}Th (ppb)	$[^{230}Th/^{232}Th]$ activity	Uncorrected Age	Corrected 4.4 ppm	Corrected 4.4 ± 2.2 ppm	Corrected 4.4 ± 4.4 ppm
Middle	5	29	1,383 ± 34	1,344 ± 34	1,344 ± 39	1,344 ± 52
Left	23	7	1,519 ± 46	1,349 ± 44	1,349 ± 95	1,349 ± 175
Right	291	1	3,797 ± 55	1,348 ± 51	1,348 ± 1,220	1,348 ± 2,450

By alpha-counting techniques, the general rule of thumb was that samples with $^{230}Th/^{232}Th$ activity ratios > ~ 20 did not have significant initial ^{230}Th corrections relative to analytical error (Schwarcz, 1986). However, because mass spectrometric techniques have increased the precision of the isotopic measurements, the $[^{230}Th/^{232}Th] > 20$ guideline no longer accurately reflects the relationship between initial ^{230}Th corrections and the magnitude of the analytical errors. Table 5 lists a number of examples in order of increasing $[^{230}Th/^{232}Th]$ to help illustrate the spectrum of this relationship. Sample 97-8-K-4.5, for example, has a $[^{230}Th/^{232}Th] = 48$, yet the initial ^{230}Th correction (± 45 years) is still larger than the analytical error (± 17 years). Sample 99-12-3-3.0, because of its young age (it was collected while active and the sub-sample is from very near the top surface) and relatively high ^{232}Th concentration, demonstrates extreme initial ^{230}Th sensitivity. Using a 4.4 ppm corrective value results in a negative age (-13 ± 9 years), so clearly the 4.4 ppm value can not be correct. A 4.2 ppm corrective value, however, results in an age of 18 ± 9 years. This particular example is clearly a good candidate for the type of careful isochron work described above, as the sample age is extremely sensitive to the initial $^{230}Th/^{232}Th$ ratio. On the opposite end of the spectrum, sample CC-99-3-Y-485.5 is corrected using an initial $^{230}Th/^{232}Th$ value of 4.4 ± 2.2 ppm, but the difference between the corrected and uncorrected ages is less than one year, far smaller

than the analytical error of ± 375 years. Most speleothem samples fall somewhere between these two extremes, although, generally speaking, speleothems with sufficiently high $^{238}U/^{232}Th$ ratios commonly have initial ^{230}Th corrections that range from moderate (i.e. comparable to the analytical error) to trivial (e.g. the last four entries in Table 5). As mentioned earlier, exceptions to this general statement typically involve samples that are very young and/or those that have an unusually high hydrogenous ^{230}Th component.

Table 5. Corrected vs. uncorrected ages for some Crevice Cave stalagmite sub-samples

Sample ID	^{238}U (ppb)	^{232}Th (ppb)	$[^{230}Th/^{232}Th]$ activity	Uncorrected Age	Corrected Age[a]
99-3-B-3.8[b]	840	83	1	682 ± 8	-13 ± 9
99-3-B-3.8[c]	840	83	1	682 ± 8	18 ± 9
94-DBL-S-199.0	444	132	18	66,651 ± 493	64,521 ± 1,167
99-12-J-3.0	405	28	26	18,259 ± 153	17,741 ± 300
97-8-K-4.5	822	4.4	48	2,662 ± 17	2,617 ± 28
99-12-B-19.0	1,652	0.6	77	332 ± 6	329 ± 6
99-3-B-251.9	1,454	1.6	290	2,364 ± 10	2,358 ± 10
99-3-B-203.0	973	0.2	1,000	1,514 ± 8	1,513 ± 8
99-3-W-382.5	1,208	2.2	3,480	99,479 ± 389	99,466 ± 389
99-3-E-119.5	445	0.3	23,800	244,072 ± 1,759	244,070 ± 1,759
99-3-Y-485.5	2,102	0.02	560,000	83,172 ± 375	83,172 ± 375

[a] All ages except the first two entries are corrected using a $^{230}Th/^{232}Th$ atomic ratio of 4.4 ± 2.2 ppm.
[b] Corrected using a $^{230}Th/^{232}Th$ atomic ratio of 4.4 ppm.
[c] Corrected using a $^{230}Th/^{232}Th$ atomic ratio of 4.2 ppm.

Isochron data in Fig. 3 was used to suggest that initial ^{230}Th in some cases likely has more than one component. A two-component system was inferred in which the high ^{232}Th component has a low $^{230}Th/^{232}Th$ ratio (e.g. clays) and the low ^{232}Th component has a high $^{230}Th/^{232}Th$ ratio (e.g. hydrogenous forms). How is this knowledge best accommodated in the initial ^{230}Th correction procedure? For many speleothems, such as the Spring Valley Caverns example, isochron-derived $^{230}Th/^{232}Th$ initial values that are low and are close to the chondritic secular equilibrium value of 4.4 ppm suggest that the high $^{230}Th/^{232}Th$ hydrogenous component, although it likely exists, is of secondary importance. For many samples such as these, using a single appropriate value with generous errors of 50-100 % (i.e. 4.4 ± 2.2 or 4.4 ± 4.4 ppm) is a reasonable way of correcting for initial ^{230}Th. For the Crevice Cave isochron example, the range of 2.4-11.0 ppm implied a moderate two-component contribution of initial ^{230}Th. This situation can be addressed either by (1) applying different initial $^{230}Th/^{232}Th$ corrective values to the dirtier and cleaner sub-samples within the guidelines provided by the isochron data, and then remaining conservative with respect to the errors, or (2) using a single $^{230}Th/^{232}Th$ value with errors that encompass the range of initial values. For those exceptional cases where hydrogenous ^{230}Th is more significant, such as the Bahamas example, multiple isochrons may be required for any given speleothem.

On the basis of the arguments presented above, we disagree with some of the conclusions of Whitehead et al. (1999), who dated several speleothems presumed to be

close to zero-age but gave ages from 2,000-3,000 years. They concluded that because of initial ^{230}Th, *all* speleothem ages less than 2,000-3,000 years are possibly inaccurate and should be viewed with suspicion. Based on the same data, they also concluded that a speleothem sample dated by Li et al. (1989) at 40,000 ± 700 years could have systematic errors (related to initial ^{230}Th) that would increase the age error to ± 2,000 years. The authors imply that the initial ^{230}Th and ^{231}Pa conditions specific to their cave settings in New Zealand have general application to other cave systems worldwide. We have shown that initial ^{230}Th corrections for many of the speleothems we have studied are orders of magnitude smaller than the inferred New Zealand values, and therefore stress that each cave system and perhaps each speleothem demands individual evaluation.

7. TIMS VERSUS ICP-MS

Table 6 lists three stalagmite sub-samples dated by both TIMS and ICP-MS. Both methods give the same ages within error. These sub-samples contained between 0.8 and 1.0 ppm ^{238}U, and ~ 80 % of the U and Th fractions was loaded for the TIMS analysis and ~ 20 % was reserved for analysis by ICP-MS. Comparable precision for the two methods attests to the higher ionization efficiency of the ICP-MS method. Shorter analysis times also allow higher throughput on the ICP-MS. TIMS analyses are more labor intensive (e.g. filament loading) and more prone to accident (e.g. filament burn-out, premature graphite loss). By comparison, source stability of the ICP-MS is generally inferior to TIMS. For ultra-high precision work (~ 1 ‰) on sufficiently large samples, the source stability of TIMS is a distinct advantage. For analyses in the 2-3 ‰ range, however, ICP-MS offers some distinct advantages over TIMS and has particular appeal to speleothem work, which typically benefits from analyzing very small sub-samples.

Table 6. Comparison between TIMS and ICP-MS methods

Sample ID	Sample Size (g)	Method	Measured δ^{234}U	[^{230}Th/^{238}U] activity	Corrected Age[a]
DBL-L-27.5	0.3004	TIMS	3,031.9 ± 3.4	1.2234 ± 0.0039	37,710 ± 140
		ICP-MS	3,037.7 ± 5.8	1.2303 ± 0.0046	37,890 ± 170
DBL-L-75.2	0.2997	TIMS	2,509.0 ± 4.6	1.2375 ± 0.0044	45,000 ± 200
		ICP-MS	2,506.0 ± 5.5	1.2424 ± 0.0050	45,260 ± 230
VA2-1-BR	0.1831	TIMS	427.0 ± 1.8	1.2787 ± 0.0086	198,170 ± 3,420
		ICP-MS	427.4 ± 2.8	1.2768 ± 0.0053	197,300 ± 2,310

[a] Ages corrected for initial ^{230}Th using a ^{230}Th/^{232}Th value of 4.4 ± 2.2 ppm. All corrections are < 25 years.

Prospects for further improvements in sensitivity and precision of mass spectrometric measurements of these nuclides require improvements in either ionization efficiency or transmission efficiency or both. For TIMS methods, the possibility exists for increasing ionization efficiencies using different loading techniques. In addition, small but significant increases in transmission efficiency could plausibly be obtained with improved TIMS instruments, perhaps including the Finnigan *TRITON*. For ICP-MS

methods, it is likely that small but significant improvements will continue to be made through modifications in "front end" design. Recent improvements include the use of micro-concentric nebulizers, desolvation nebulizers, guard electrodes, and refinements in cone geometry (see refs in Shen et al., 2001). The use of larger geometry ICP-MS instruments may also lead to significant improvements in transmission. Finally, the use of multiple electron multipliers or channeltrons (on a multi-collector ICP-MS, MC-ICP-MS), obviates the problems associated with the ICP source instability and also maximizes the amount of time that the isotope of interest can be counted. While requiring careful work to cross-calibrate multipliers, this will lead to an improvement of on the order of a factor of two in numbers of ions counted. Taken together, all of these potential improvements bode well for yet additional improvements in the precision and sensitivity with which we will be able measure rare uranium-series nuclides in coming years.

8. ACCURACY OF AGES

The issues of initial ^{230}Th and ^{231}Pa are ones of accuracy, that is, how close the age determination is to the true age of the sample. A second concern, one that increases with the sample age, is the closed-system behavior of the U-Th-Pa decay chains. In general, older samples are more at risk because of the longer opportunity for diagenetic changes to have taken place. Speleothems with significant porosity are poorer candidates for closed-system behavior than are speleothems with dense fabrics. Fluid inclusions are a ubiquitous source of micron-scale fabric porosity but are generally isolated and thus do not translate to permeability with diagenetic implications.

Combined ^{230}Th-^{231}Pa dating is a powerful test of open-system behavior because diagenesis will often result in discordant ages (Cheng et al., 1998). Table 7 shows U-Th-Pa data for a Crevice Cave stalagmite that suggests closed-system behavior for at least the last 90,000 years. The larger errors of the ^{231}Pa ages reflect both the lower ^{231}Pa concentrations (compared to ^{230}Th) and the larger fractional errors related to large T for the ^{235}U-^{231}Pa clock (limit ~ 250 ka). Initial ^{230}Th is insignificant for these sub-samples because of their relatively old age and low ^{232}Th content. The age concordance also indicates that any offset from the true age due to initial ^{231}Pa is insignificant relative to the analytical error for these particular (old) sub-samples.

Table 7. Comparison between ^{230}Th and ^{231}Pa ages for Crevice Cave stalagmite CC-J

ID	[^{230}Th/^{238}U] activity	[^{230}Th/^{232}Th] activity	[^{231}Pa/^{235}U] activity	^{230}Th Age corrected[a] uncorrected	^{231}Pa Age corrected[a] uncorrected
222.0	1.4176 ± 0.0042	9,990	0.8101 ± 0.0058	78,860 ± 330[a]	78,520 ± 1,470[a]
				78,870 ± 330	78,530 ± 1,470
315.5	1.8191 ± 0.0065	3,020	0.8507 ± 0.0053	89,740 ± 530[a]	89,900 ± 1,720[a]
				89,770 ± 530	89,920 ± 1,720

[a] Ages are corrected for initial ^{230}Th using an atomic ^{230}Th/^{232}Th value of 4.4 ± 4.4 ppm and for initial ^{231}Pa using an atomic ^{231}Pa/^{232}Th value of 88.8 ± 88.8 ppb. These are the secular equilibrium values for the chondritic ^{232}Th/^{238}U atomic ratio of 3.8.

Another indication of closed-system behavior is the stratigraphic ordering of ages and the absence of any age reversals. Although simple, this straightforward criterion becomes an impressive argument for those speleothems with a large number of densely spaced ages such as is shown for stalagmite CC-94-9-DBL-L in Table 8. Stalagmite CC-94-9-DBL-L is composed of dense, yellowish, translucent calcite with ubiquitous fluid inclusions in the 3-10 micron range. The stalagmite stopped growing ~ 23,000 years ago and was found in the cave lying in a stream. A 0.5-1.0 mm rind indicates leaching of the outer surface but the interior is pristine and optically unaltered. The U-Th systematics also suggest it has remained a completely closed system. The stalagmite contains a high-resolution record of past changes in climate and vegetation in the form of stable carbon and oxygen isotopic variations (Dorale et al., 1998). The importance of a precise and accurate ^{230}Th chronology for records such as this cannot be overstated. Dense calcite that remains completely closed to the diagenetic loss and/or gain of both parent and daughter isotopes is a key reason why speleothems can be dated with great accuracy.

Table 8. U-Th data for stalagmite CC-94-9-DBL-L from Crevice Cave, Missouri[a]

ID[b]	Sample Size (mg)	^{238}U (ppb)	Measured δ^{234}U	[^{230}Th/^{238}U] activity	[^{230}Th/^{232}Th] activity	Corrected Age[c]
1.5	180	556	3,555.4 ± 8.6	0.9410 ± 0.0067	690	24,530 ± 190
4.0	284	561	3,452.7 ± 3.2	1.0033 ± 0.0037	320	26,990 ± 110
7.9	203	803	3,365.6 ± 6.6	1.0969 ± 0.0050	1,430	30,450 ± 160*
11.0	293	928	3,321.5 ± 3.4	1.1183 ± 0.0034	7,800	31,470 ± 110
18.5	185	843	3,182.9 ± 5.1	1.1571 ± 0.0041	5,580	33,930 ± 140
27.5	300	812	3,032.4 ± 2.5	1.2264 ± 0.0033	1,050	37,810 ± 120**
30.8	230	957	2,973.3 ± 2.8	1.2315 ± 0.0035	1,800	38,650 ± 130
41.8	220	1,026	2,813.6 ± 3.0	1.2282 ± 0.0032	12,100	40,420 ± 130
50.0	279	1,000	2,774.1 ± 10.7	1.2540 ± 0.0116	20,900	41,920 ± 470*
67.2	212	915	2,567.8 ± 5.2	1.2172 ± 0.0041	22,600	43,270 ± 190
75.2	300	796	2,508.3 ± 2.8	1.2400 ± 0.0036	7,500	45,120 ± 160**
80.2	242	753	2,477.1 ± 3.4	1.2529 ± 0.0035	9,700	46,170 ± 160
95.1	197	571	2,303.0 ± 3.3	1.2372 ± 0.0059	6,360	48,400 ± 280
116.0	318	605	2,357.8 ± 5.8	1.3316 ± 0.0055	6,170	51,810 ± 280*
133.6	220	643	2,303.3 ± 4.5	1.3455 ± 0.0046	3,470	53,540 ± 250
143.1	293	631	2,352.0 ± 4.0	1.3881 ± 0.0045	9,630	54,620 ± 230*
150.2	225	646	2,337.6 ± 2.6	1.3880 ± 0.0039	7,110	54,900 ± 200
160.9	309	760	2,411.0 ± 3.7	1.4349 ± 0.0045	1,820	55,650 ± 230*
173.8	238	641	2,336.4 ± 2.6	1.4189 ± 0.0048	320	56,430 ± 240
191.0	246	649	2,336.6 ± 3.4	1.4540 ± 0.0044	420	58,160 ± 230
202.0	366	566	2,249.4 ± 4.0	1.4458 ± 0.0051	290	59,730 ± 280*
225.5	238	521	2,191.4 ± 8.1	1.4741 ± 0.0102	91	62,630 ± 580
238.0	435	433	2,274.2 ± 4.6	1.5541 ± 0.0100	44	64,780 ± 540*
247.8	296	489	2,444.2 ± 13.0	1.6485 ± 0.0291	15	65,370 ± 1,500

[a] All measurements made by TIMS except those denoted * which where made by ICP-MS and those denoted ** which were made by both TIMS and ICP-MS.

[b] ID denotes distance in mm from the top surface of stalagmite to the midpoint of the sub-sample boring.

[c] Ages are corrected for initial ^{230}Th using a ^{230}Th/^{232}Th atomic ratio of 4.4 ± 2.2 ppm.

9. CONCLUSIONS

The range over which useful age data on speleothems can be obtained by uranium-series disequilibrium techniques extends from tens of years to ~ 600,000 years. Compared to decay-counting, TIMS and ICP-MS techniques have significantly extended the datable time range, greatly reduced age errors, reduced sample-size requirements to a level more compatible with the slow growth rates common to many speleothems, and reduced the time and effort invested per analysis. These improvements now allow for high-resolution dating that is typically more precise than that obtained by ^{14}C. For the past half million years, U-Th dated speleothem records represent an excellent source of Quaternary paleoenvironmental information.

Accurate dating is possible if the initial concentrations of ^{230}Th and ^{231}Pa are well constrained and the system remains closed to post-depositional loss and/or gain of U, Th, and Pa. Initial ^{230}Th can be constrained by monitoring ^{232}Th and employing isochron techniques. The small sample size requirements of mass spectrometry allow effective application of precise isochron sub-sampling on slow-growth speleothems. The sensitivity of the age error to uncertainties in initial ^{230}Th decreases with increasing U concentration, increasing age, and decreasing detrital contamination. For many speleothems the uncertainties regarding initial ^{230}Th are smaller than those associated with the analytical precision of the measurements and are trivial. Because Pa is more soluble than Th, ^{232}Th is a poor analog for ^{231}Pa. Therefore, initial ^{231}Pa is more problematic than initial ^{230}Th for young samples, although this problem becomes less significant or even insignificant with increasing age. Closed-system behavior can be judged by petrographic considerations, stratigraphic ordering of ages, and ^{230}Th-^{231}Pa concordance. Dense, calcite speleothems seem capable of maintaining closed-system U-series behavior over the timescales of effective U-Th-Pa dating.

10. ACKNOWLEDGEMENTS

Cave and sample-related thanks go to John Ackerman, Paul Hauck, Richard Young, Bev Shade, Bob Osburn, Paul Cutler, Julie Morris, Jess Adkins, and Bill Zanner. Laboratory help from John Hoff is gratefully acknowledged. The work was supported by National Science Foundation grants to Larry Edwards. During the years of the analyses, Jeff Dorale was supported by a NSF-sponsored Research Training Grant (to Margaret Davis) and a Graduate Research Training Grant (to Mark Person), and a University of Minnesota Doctoral Dissertation Fellowship.

11. REFERENCES

Attree, R. W., Cabell, M. J., Cushing, R. L., and Pieron, J. J., 1962, A calorimetric determination of the half life of Th-230 and consequent revision of its neutron capture cross-section, *Can. J. Phys.* **40**:194.

Barnes, J. W., Lang, E. J., and Potratz, H. A., 1956, The ratio of ionium to uranium in coral limestone, *Science* **124**:175.

Bateman, H., 1910, The solution of a system of differential equations occurring in the theory of radioactive transformations, *Proc. Cambridge Phil. Soc.* **15**:423.

Becquerel, H., 1896, Sur les radiations invisibles emises par phosphorescence, *Compt. Rend.* **122**:420.

Bischoff, J. L., and Fitzpatrick, J. A., 1991, U-series dating of impure carbonates: an isochron technique using total-sample dissolution, *Geochim. Cosmohcim. Acta* **55**:543.

Broecker, W. S., Thurber, D. L., Goddard, J., Ku, T.-L., Matthews, R. K., and Mesolella, K. J., 1968, Milankovitch hypothesis supported by precise dating of coral reef and deep-sea sediments, *Science* **159**:297.

Broecker, W. S., and Peng, T.-H., 1982, *Tracers in the Sea*, Lamont-Doherty Geological Observatory, Columbia University, Palisades, New York, pp. 690.

Chen, J. H., Edwards, R. L., and Wasserburg, G. J., 1986, ^{238}U, ^{234}U and ^{232}Th in seawater, *Earth Planet. Sci. Lett.* **80**:241.

Chen, J. H., Edwards, R. L., and Wasserburg, G. J., 1992, Mass spectrometry and application to uranium-series disequilibrium, in: *Uranium-Series Disequilibrium: Applications to Earth, Marine, and Environmental Sciences*, 2nd edition, M. Ivanovich and R. S. Harmon, eds., Clarendon Press, Oxford, pp. 174-206.

Cheng, H., Edwards, R. L., Murrell, M. T., and Benjamin, T. M., 1998, Uranium-thorium-protactinium dating systematics, *Geochim. Cosmohcim. Acta* **62**:3437.

Cheng, H., Edwards, R. L., Hoff, J., Gallup, C. D., Richards, D. A., and Asmeron, Y., 2000, The half-lives of uranium-234 and thorium-230, *Chem. Geol.* **169**:17.

Cherdyntsev, V. V., Kazachevskiy, I. V., and Kuz'mina, Ye. A., 1965, Age of Pleistocene carbonate determined from the isotopes of thorium and uranium, *Geochem. Int.* **2**:749.

Curie, M. S., 1898, Rayons emis par les composes de l'uranium et du thorium, *Compt. Rend.* **126**:1101.

Dearlove, J. P. L., Longworth, G., Ivanovich, M., Kim, J. I., Delakowitz, B., and Zeh, P., 1991, A study of groundwater-colloids and their geochemical interactions with natural radionuclides in the Gorleben aquifer systems, *Radiochim. Acta* **52/53**:83.

De Bievre, P., Lauer, K. F., Le Duigon, Y., Moret, H., Muschenborn, G., Spaepen, J., Spernol, A., Vaninbroukx, R., and Verdingh, V., 1971, The half-life of 234-U, in: *Proc. Intl. Conf. Chem. Nucl. Data, Measurement and Applications, Canterbury*, M. L. Hurrell, ed., Inst. Civil Engineers, London, pp. 221-225.

Dervin, J., and Faucherre, J., 1973a, Study of carbonate complexes of thorium and cerium, II. Constitution of the complexes in solution, *Bull. Soc. Chim. Fr.*, 2926.

Dervin, J., and Faucherre, J., 1973b, Study of carbonate complexes of thorium and cerium, III. Solubility and nature of the complex ions in solution, *Bull. Soc. Chim. Fr.*, 2930.

Dorale, J. A., Edwards, R. L., Ito, E., and González, L. A., 1998, Climate and vegetation history of the midcontinent from 75 to 25 ka: a speleothem record from Crevice Cave, Missouri, USA, *Science* **282**:1871.

Edmonds, H. N., Moran, S. B., Hoff, J. A., Smith, J. N., and Edwards, R. L., 1998, Protactinium-231 and thorium-230 abundances and high scavenging rates in the Western Arctic Ocean, *Science* **280**:405.

Edwards, R. L., 1988, High precision thorium-230 ages of corals and the timing of sea level fluctuations in the late Quaternary, *Ph.D thesis*, California Institute of Technology.

Edwards, R. L., Chen J. H., and Wasserburg G. J., 1987, ^{238}U-^{234}U-^{230}Th-^{232}Th systematics and the precise measurement of time over the past 500,000 y, *Earth Planet. Sci. Lett.* **81**:175.

Edwards, R. L., Cheng, H., Murrell, M. T., and Goldstein, S. J., 1997, Protactinium-231 dating of carbonates by thermal ionization mass spectrometry: implications for Quaternary climate change, *Science* **276**:782.

Fleming, E. H., Jr., Ghiorso, A., and Cunningham, B. B., 1952, The specific alphaactivities and half-lives of ^{234}U, ^{235}U, and ^{236}U, *Phys. Rev. C* **38**:642.

Ford, D. C., Thompson, P. L., and Schwarcz, H. P., 1972, Dating cave calcite by the uranium disequilibrium method; some preliminary results from Crowsnest Pass, Alberta, *International Geography 1972--La Geographie Internationale, Technical Program Abstracts - International Geographical Congress* **22**:21.

Gaffney, J. S., Marley, N. S., and Orlandini, K. A., 1992, Evidence for thorium isotopic disequilibria due to organic complexation in natural waters, *Environ. Sci. Technol.* **26**:1248.

Gascoyne, M., 1985, Application of the $^{227}Th/^{230}Th$ method to dating Pleistocene carbonates and comparisons with other dating methods, *Geochim. Cosmohcim. Acta* **49**:1165.

Gascoyne, M., 1992a, Palaeoclimate determination from cave calcite deposits, *Quat. Sci. Rev.* **11**:609.

Gascoyne, M., 1992b, Geochemistry of the actinides and their daughters, in: *Uranium-Series Disequilibrium: Applications to Earth, Marine, and Environmental Sciences*, 2nd edition, M. Ivanovich and R. S. Harmon, eds., Clarendon Press, Oxford, pp. 34-61.

Harmon, R. S., Thompson, P., Schwarcz, H. P., and Ford, D. C., 1975, Uranium-series dating of speleothems, *NSS Bull.* **37**:21.

Ivanovich, M., Latham, A. G., and Ku, T.-L., 1992, Uranium-series disequilibrium applications in geochronology, in: *Uranium-Series Disequilibrium: Applications to Earth, Marine, and Environmental Sciences*, 2nd edition, M. Ivanovich and R. S. Harmon, eds., Clarendon Press, Oxford, pp. 62-89.

Holden, N. E., 1989, Total and spontaneous fission half-lives for uranium, plutonium, americium, and curium nuclides, *Pure and Appl. Chem.* **61**:1483.

Jaffey, A. H., Flynn, K. F., Glendenin, L. E., Bentley, W. C., and Essling, A. M., 1971, Precision measurement of half-lives and specific activities of ^{235}U and ^{238}U, *Phys. Rev.* C **4**:1889.

Joao, A., Bigot, S., and Fromage, F., 1987, Study of the carbonate complexes of IVB elements: I. Determination of the stability constant of Th (IV) pentacarbonate, *Bull. Soc. Chim. Fr.*, 42.

Kaufman, A., and Broecker, W. S., 1965, Comparison of ^{230}Th and ^{14}C ages for carbonate materials from Lakes Lahontan and Bonneville, *J. Geophys. Res.* **70**:4039.

Kaufman, A., Broecker, W. S., Ku, T.-L., and Thurber, D. L., 1971, The status of U-series methods of mollusk dating, *Geochim. Cosmohcim. Acta* **35**:1155.

Kaufman, A., 1993, An evaluation of several methods for determining $^{230}Th/U$ ages in impure carbonates, *Geochim. Cosmohcim. Acta* **57**:2303.

Ku, T.-L., 1968, Protactinium-231 method of dating coral from Barbados Island, *J. Geophys. Res.* **73**:2271.

Langmuir, D., 1978, Uranium solution-mineral equilibria at low temperatures with applications to sedimentary ore deposits, *Geochim. Cosmohcim. Acta* **42**:547.

Langmuir, D., and Herman, J. S., 1980, The mobility of thorium in natural waters at low temperatures, *Geochim. Cosmohcim. Acta* **44**:1753.

Le Roux, L. J., and Glendenin, L. E., 1963, Half-life of ^{232}Th, in: *Proc. Natl. Meet. On Nuclear Energy*, Pretoria, South Africa, (April), pp. 83-94.

Li, W. X., Lundberg, J., Dickin, A. P., Ford, D. C., Schwarcz, H. P., McNutt, R., and Williams, D., 1989, High precision mass-spectrometric uranium-series dating of cave deposits and implications for paleoclimate studies, *Nature* **339**:534.

Lin, J. C., Broecker, W. S., Anderson, R. F., Hemming, S., Rubenstone, J. L., and Bonani, G., 1996, New Th-230/U and C-14 ages from Lake Lahontan carbonates, Nevada, USA, and a discusion of the origin of initial thorium, *Geochim. Cosmochim. Acta* **60**:2817.

Lounsbury, M., and Durham, R. W., 1971, The alpha half-life of ^{234}U, in: *Proc. Intl. Conf. Chem. Nucl. Data, Measurement and Applications, Canterbury*, M. L. Hurrell, ed., Inst. Civil Engineers, London, pp. 215-219.

Ludwig, K. R., Simmons, K. R., Szabo, B. J., Winograd, I. J., Landwehr, J. M., Riggs, A. C., Hoffman, R. J., 1992, Mass-spectrometric ^{230}Th-^{234}U-^{238}U dating of the Devils Hole calcite vein, *Science* **258**:284.

Ludwig, K. R., 1993, UISO—A program for calculation of ^{230}Th-^{234}U-^{238}U isochrons, *US Geological Survey Open-File Report 93-531* (disk available from author).

Ludwig, K. R., and Titterington, D. M., 1994, Calculation of $^{230}Th/U$ isochrons, ages, and errors, *Geochim. Cosmohcim. Acta* **58**:5031.

Luo, S., and Ku, T.-L., 1991, U-series isochron dating: a generalized method employing total sample dissolution, *Geochim. Cosmohcim. Acta* **55**:555.

Luo, X., Rehkämper, M., Lee, D., and Halliday, A. N., 1997, High precision $^{230}Th/^{232}Th$ and $^{234}U/^{238}U$ measurements using energy-filtered ICP magnetic sector multiple collector mass spectrometry, *Int. J. Mass Spectrom. and Ion Processes* **171**:105.

Meadows, J. W., Armani, R. J., Callis, E. L., and Essling, A. M., 1980, Half-life of ^{230}Th, *Phys. Rev.* C **22**:750.

Moran, S. B., Hoff, J. A., Buesseler, K. O., and Edwards, R. L., 1995, High precision ^{230}Th and ^{232}Th in the Norwegian Sea and Denmark Strait by thermal ionization mass spectrometry, *Geophys. Res. Lett.* **22**:2589.

Pickett, D. A., Murrell, M. T., and Williams, R. W., 1994, Determination of femtogram quantities of protactinium in geologic samples by thermal ionization mass spectrometry, *Anal. Chem.* **66**:1044.

Renne, P. R., Karner, D. B., and Ludwig, K. R., 1998, Enhanced: absolute ages aren't exactly, *Science* **282**:1840.

Richards, D. A., Beck, J. W., Donahue, D. J., Smart, P. L., and Edwards, R. L., 1999, Th-230 and C-14 dating of speleothems from the Bahamas: implications for the calibration of the radiocarbon timescale, in: *Ninth Annual V. M. Goldschmidt Conference*, LPI Contribution No. **971**, Houston, p. 245.

Robert, J., Miranda C. F., and Muxart, R., 1969, Mesure de la période du protactinium-231 par microcalorimétrie, *Radiochim. Acta* **11**:104.

Rosholt, J. N., Emiliani, C., Geiss, J., Koczy, F. F., and Wangersky, P. J., 1961, Absolute dating of deep-sea cores by the $^{231}Pa/^{230}Th$ method, *J. Geol.* **69**:162.

Rosholt, J. N., and Antal, P. S., 1962, Evaluation of the $^{231}Pa/U$-$^{230}Th/U$ method for dating Pleistocene carbonate rocks, *US Geological Survey Prof. Paper* **450-E**:108.

Shen, C.-C., Edwards, R. L., Cheng, H., Dorale, J. A., Thomas, R. B., Moran, S. B., Weinstein, S., and Edmonds, H. N., 2001, Uranium and thorium isotopic and concentration measurements by inductively coupled plasma mass spectrometry, *Chem. Geol.*, in review.

Short, S. A., Lowson, R. T., and Ellis, J., 1988, $^{234}U/^{238}U$ and $^{230}Th/^{234}U$ activity ratios in the colloidal phases of aquifers in lateritic weathered zones, *Geochim. Cosmohcim. Acta* **52**:2555.

Schwarcz, H. P., 1986, Geochronology and isotopic geochemistry of speleothems, in: *Handbook of Environmental Geochemistry: The Terrestrial Environment*, P. Fritz and J. C. Fontes, eds., Elsevier, Amsterdam, pp. 271-303.

Steiger, R. H., and Jäger, E., 1977, Subcommission on geochronology: convention on the use of decay constants in geo- and cosmochronology, *Earth Planet. Sci. Lett.* **36**:359.

Szabo, B. J., 1979, ^{230}Th, ^{231}Pa and open system dating of fossil corals and shells, *J. Geophys. Res.* **84**:4927.

Thomson, J. J., 1914, Rays of positive electricity, *Proc. Roy. Soc., Lond. A* **89**:1.

Thompson, P., Schwarcz, H. P., and Ford, D. C., 1974, Continental Pleistocene climatic variations from speleothem age and isotopic data, *Science* **184**:893.

Whitehead, N. E., Ditchburn, R. G., Williams, P. W., and McCabe, W. J., 1999, ^{231}Pa and ^{230}Th contamination at zero age: a possible limitation on U/Th series dating of speleothem material, *Chem. Geol.* **156**:359.

Yu, E.-F., Francois, R., and Bacon, M. P., 1996, Similar rates of modern and last-glacial ocean thermohaline circulation inferred from radiochemical data, *Nature* **379**:689.

PALEOCLIMATE INFORMATION FROM SPELEOTHEMS: THE PRESENT AS A GUIDE TO THE PAST

Russell S. Harmon, Henry P. Schwarcz, Mel Gascoyne, John W. Hess, and Derek C. Ford*

1. INTRODUCTION

Speleothems are the secondary mineral deposits formed in caves. The most common type of speleothems are the calcium carbonate ($CaCO_3$) stalactites, stalagmites, and flowstones which are a ubiquitous feature of caves worldwide. Variations in the $^{18}O/^{16}O$ and $^{13}C/^{12}C$ ratios in calcite speleothems can provide important information about terrestrial paleoclimate, if deposition occurred under equilibrium conditions because (i) they contain a well-defined internal stratigraphy, (ii) their absolute age of deposition can be determined accurately with high precision through mass spectrometric U-series disequilibrium geochronology (Edwards et al., 1987; Li et al., 1989), (iii) variations in their internal chemical and isotopic composition are determined by the environmental conditions at the time of deposition, (iv) they may trap surface-derived dust, pollen, and organic acids as the calcite layers are sequentially deposited and (v) they tend to behave as geochemically closed systems (see e.g. Schwarcz, 1986; Gascoyne, 1992).

The temperature dependence of equilibrium isotope exchange in the calcite-water system has been intensively studied since Urey (1947) first suggested that the paleotemperature of the ancient oceans could be estimated by the O-isotope distribution between seawater and the calcium carbonate precipitated from it. Urey et al. (1951) argued that O-isotope equilibrium between seawater and $CaCO_3$ was likely and support for this idea has come from the close agreement between the $CaCO_3$-H_2O isotopic fractionation observed in natural systems and those derived from both thermodynamic calculations and laboratory experiments (e.g. Epstein et al., 1951, 1953; Emiliani, 1955; O'Neil et al., 1969; O'Neil et al., 1975).

* Russell S. Harmon, Army Research Office/Army Research Laboratory, P.O. Box 12211, Research Triangle Park, NC 27709 USA. Henry P. Schwarcz, School of Geography and Geology, McMaster University, Hamilton, Ontario, L8S 4M1 Canada. Mel Gascoyne, Gascoyne Geoprojects Inc., P.O. Box 141, Pinawa, Manitoba, R0E 1L0 Canada. John W. Hess, Geological Society of America, P.O. Box 9140, Boulder, CO 80301USA. Derek C. Ford, School of Geography and Geology, McMaster University Hamilton, Ontario, L8S 4K1, Canada.

Some three decades ago, researchers in New Zealand (Hendy and Wilson, 1968) and Europe (Galimov et al., 1965; Labeyrie et al., 1967; Duplessy et al.,1970; Fantidis and Ehhalt, 1970) called attention to the fact that changes in terrestrial climate might be recorded in the O- and C-isotope compositions of speleothems. Subsequently Hendy (1971). geochemically modeled the isotope effects which accompany different modes of speleothem deposition. These earliest studies recognized that:

(i) records of past climate fluctuation can only be obtained from stable isotope ratio (i.e. speleothems that formed in isotopic equilibrium with parent seepage water and subsequently have remained closed to isotopic re-equilibration, and
(ii) paleotemperatures could not be directly inferred from speleothem $^{18}O/^{16}O$ ratio variations because the calcite O-isotope signal was a function of several different factors that could not be explicitly determined.

Subsequent research at McMaster University over the period 1970-1985 (Thompson et. al., 1974, 1976; Schwarcz et al., 1976; Harmon et al., 1977, 1978a,b, 1979a,b; Harmon and Schwarcz, 1981; Gascoyne et al., 1980, 1981; Gascoyne, 1983; Schwarcz and Yonge, 1983; Yonge et al., 1985; Gascoyne, 1992) examined different aspects of speleothem deposition across a spectrum of climates. These studies made several important observations:

(i) speleothem deposition frequently occurs under conditions of isotopic equilibrium, but not always,
(ii) cave seepage waters in temperate climates tend to be representative of meteoric precipitation on the surface above the cave,
(iii) the fluid inclusions present in speleothems are a relict sample of the parent seepage water from which the speleothem was deposited, and
(iv) the effect of temperature change on isotopic fractionation between water and calcite is not necessarily the primary cause of O-isotope variation in speleothems.

During the last decade, there has been a renewed interest in speleothem paleoclimatology which has produced some very exciting and, in some instances, contradictory interpretations (Lauritzen et al., 1990; Dorale et al., 1992; 1998; Lauritzen, 1995; Goede et al., 1996; Baker et al., 1997; Bar Matthews et al., 1996, 1997; Burns et al., 1998; Hellstrom et al., 1998; Holmgren et al., 1995; Frumkin et al., 1999; Lauritzen and Onac, 1999). However, not all of these recent studies have given the necessary attention either to demonstrating speleothem equilibrium deposition or to placing the paleoclimate interpretations within the context of the modern depositional setting. A major purpose of this contribution is to illustrate the importance of understanding the modern depositional environment when conducting paleoclimate studies on speleothems.

In this paper, we will examine the physiochemical processes that act in concert to determine the isotopic composition of speleothem calcite and, based upon a worldwide data compilation, argue that it is important to base any speleothem paleoclimatology study upon as thorough an understanding of the modern cave depositional environment as is possible. The focus of the discussion will be on oxygen isotopes, but we also will discuss carbon isotopes to a limited extent. Our observations and comments are based upon a comprehensive isotopic database compiled for precipitation, cave seepage water,

and both modern and fossil speleothems for 35 karst areas worldwide (Fig. 1) that has been assembled from the published literature and from our unpublished work.

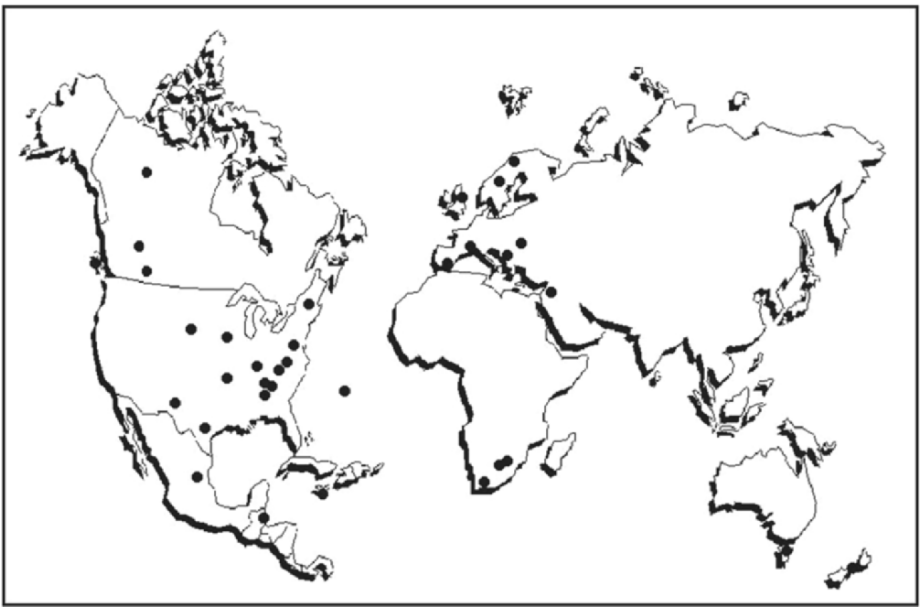

Figure 1. Cave sites worldwide for which rainfall, cave drip water, and modern and fossil speleothem stable isotope data were compiled for this study. Data from: Gross, 1964; Hendy and Wilson, 1968; Duplessy et al., 1971; Talma et al., 1974; Thompson et al., 1974, 1975; Harmon et al., 1977; 1978a,b; 1979b; Gascoyne et al., 1981; Gascoyne and Nelson, 1983; Schwarcz and Yonge, 1983; Goede and Hitchman, 1984; Yonge et al., 1985; Urbanc et al., 1987; Goede et al., 1986; Miller and Dicken, 1987; Goede et al., 1990; Ingraham et al., 1990; Lauritzen et al., 1990; Chapman et al., 1992; Dorale et al., 1992; Talma and Vogel, 1992; Holmgren et al., 1995; Lauritzen, 1995; Bar Matthews et al., 1996; Caballero et al., 1996; Goede et al., 1996; Baker et al., 1997; Bar Matthews et al., 1997; Hellstrom et al., 1998; Dorale et al., 1999; Frumkin et al., 1999; Lauritzen and Onac, 1999) and our unpublished data (Harmon, 1976; Gascoyne, 1979; Atkinson et al., 1983; and Hess et al., unpub).

2. OXYGEN ISOTOPES

Calcite speleothems are deposited in a cave when downward-percolating, carbonate-saturated groundwaters, with a partial pressure of CO_2 exceeding that of the cave atmosphere, enter a cave and become supersaturated with respect to calcium carbonate. If the degassing of CO_2 from solution is slow and isotopic equilibrium is maintained between aqueous carbon phases and deposited carbonate, then two climatically-dependent variables (a *fractionation effect* and a *water effect*) will determine the O-isotopic composition of the speleothem calcite deposited in a cave.

.

2.1. Equilibrium vs. Non-Equilibrium Deposition

Three common mechanisms for the precipitation of calcite speleothems in caves have been recognized: (i) precipitation due to the slow loss of CO_2 from solution, (ii) precipitation due to the rapid outgassing of CO_2 from solution, and (iii) evaporation. Only the first of these processes results in the deposition of speleothem of calcite that is in

Table 1. Comparison of measured cave temperatures (T_m) with the temperatures of deposition calculated for modern speleothems (T_c). Data from the sources cited in Figure 1.

Cave Site	Cave Temp. (°C)	Avg. $\delta^{18}O_{dw}$, (---------- ‰ SMOW ---------)	Avg. $\delta^{18}O_{ct}$	Calculated Temp. (°C)	T_m- T_c
Natural Bridge Cavern, TX, USA	21.8	-3.41	26.66	18.8	+ 3.0
Inner Space Cavern, TX, USA	20.7	-3.20	26.55	20.2	+0.5
Crystal Cave, Bermuda	20.1	-2.69	27.26	19.4	-0.4
Freshwater Cave, Bermuda	19.6	-1.31	28.33	20.9	-1.3
Grotto Bay Cave, Bermuda	19.4	-1.94	28.26	18.4	+1.0
Soreq Cave, Israel	19.2	-4.84	24.81	20.4	-1.2
Cango Cave, South Africa	17.5	-5.44	24.92	17.3	+0.2
Moon's Cave, Victoria, Australia	15.0	-5.68	25.01	15.8	-0.8
Mammoth-Flint Ridge, KY, USA	14.0	-5.87	25.77	11.9	-2.1
M-FR winter seepage		-5.97	"	11.4	+2.6
M-FR summer seepage		-5.77	"	12.3	+1.7
Tumbling Creek, MO, USA	14.0	-6.20	24.78	14.5	+0.5
Norman-Bone Cave, WV, USA	10.8	-9.70	22.67	8.4	+2.4
N-B winter seepage	"	-10.20	"	6.4	+4.4
N-B summer seepage	"	-9.15	"	10.7	+0.1
Wind Cave, SD, USA	13.8	-12.13	18.54	15.0	+1.2
Baker's Cave, KY, USA	13.8	-5.75	26.55	9.2	-4.6
Stab Cave, KY, USA	13.5	-5.79	25.46	13.5	0
Indian Echo Cave, PA	10.0	-7.50	24.06	12.0	+2.0
Predjama Cave, Slovenia	10.0	-6.42	24.02	16.8	-6.8
Little Trimmer Cave, Tasmania, Australia	9.5	-5.04	27.00	10.4	+0.9
LT winter seepage	"	-5.68	"	7.8	-1.7
Coldwater Cave, IA, USA	9.0	-7.71	24.12	10.8	-1.8
Divaca Cave, Slovenia	8.7	-5.06	25.65	15.8	-7.1
White Scar Cave, Yorkshire, UK	8.4	-6.78	25.53	9.1	-0.7
Frankencombe Cave, Tasmania, Australia	8.3	-5.17	26.74	10.3	-2.0
FC winter seepage	"	-5.70	"	8.7	-0.4
Mackova Cave, Slovenia	8.1	-6.77	23.89	15.8	-7.7
McFail's Cave, NY, USA	8.0	-7.20	23.13	17.2	+9.2
Cascade Cave, BC, Canada	6.9	-11.10	21.34	8.0	-1.1
Castleguard Cave, ALTA, Canada	1.9	-13.40	13.40	6.1	-4.2
Yorkshire Pot, ALTA, Canada	1.3	-19.26	18.24	3.0	-1.7

isotopic equilibrium with its parent seepage water (Labeyrie et al., 1967; Fornaca-Rinaldi et al., 1968; Fantidis and Ehhalt, 1970; Hendy, 1971). The very stable environments that prevail within the deep interiors of many caves, particularly those portions of a cave where the humidity is high and air circulation is restricted, are conducive to conditions that promote equilibrium deposition. Modern speleothems are frequently observed to form under equilibrium conditions. Of the 32 cave sites for which drip water – modern calcite data are available (Table 1), 21 measured isotopic fractionations yield isotopic temperatures which are within 2°C of the measured cave temperature. This observation suggests that speleothem deposition in these instances is presently occurring under conditions of isotopic equilibrium The 8 cases where the difference is >3°C, either the seepage water isotopic composition was based upon a very limited number of measurements and, therefore not representative of the mean annual cave seepage water isotopic composition (*e.g.* Natural Bridge Cavern and Baker's Cave – Harmon, 1975; McFail's Cave – Yonge et al., 1985; Predjama Cave, Divaca Cave, Mackova Cave – Urbanc et al., 1987) or present-day calcite precipitation in the cave is influenced by non-equilibrium effects (e.g. Castleguard Cave – Harmon et al., 1983). Rapid degassing of CO_2 during and evaporation produce a fractionation of both O- and C- isotopes, with ^{13}C being more enriched than ^{18}O in the speleothem calcite along individual growth layers in a predictable manner (Fornaca-Rinaldi et al., 1968; Hendy, 1971)

Few of the studies that have analyzed fossil speleothems as paleoclimate monitors have tested samples for equilibrium deposition because this is not always a straightforward task. The recognition and definition of individual growth layers, either in thin or thick section, can be difficult. This is particularly the case for speleothems that consist of a small number of large and optically transparent single crystals of nearly chemically pure and homogeneous $CaCO_3$ or for speleothems that are strongly colored due to high contents of organic matter. Growth layers in speleothems can pinch, swell, and merge in ways that makes stratigraphic correlation difficult. Deviations from a growth layer during sampling in the laboratory can generate a spurious $^{13}C/^{12}C$-$^{18}O/^{16}O$ covariation, particularly in instances where large changes in O-isotope compositions have been recorded by a speleothem in response to rapid climate fluctuations. Also, for flowstones, it can be difficult to reconstruct the direction of seepage flow. Where such tests have been made (e.g. Harmon, 1976; Thompson et al., 1976; Lauritzen, 1995; Goede et al., 1996; Frumkin et al., 1999), both equilibrium and non-equilibrium deposition has been observed (Fig. 2).

In the past, when samples of a few tenths of a milligram were required for a stable isotope analysis, the case could be made that single growth layers were difficult, if not impossible, to sample. Today, with the capability for ultra-precision sampling techniques and only micrograms of calcite required for an isotopic analysis, there is no analytical reason not to test for equilibrium deposition. However, rather than sampling along a growth layer (e.g. top of a stalagmite), the most secure approach is to trace O- and C-isotopic variation down a growth layer in the direction of water flow (i.e., which is the direction in which deposited calcite would be isotopically enriched as the result of either rapid degassing or evaporation).

The other strategy that has been followed by some researchers is to analyze modern speleothem material and present-day seepage waters from a cave site being studied to at least ascertain if equilibrium deposition is occurring under present-day conditions (e.g. Thompson et al., 1976; Harmon et al., 1987; Goede et al., 1986, 1990; Bar-Matthews et

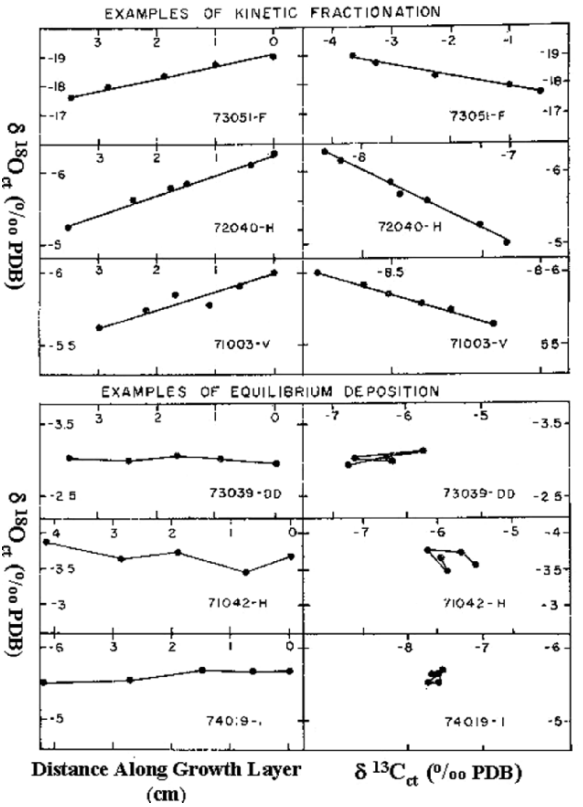

Figure 2. Co-variations of $\delta^{13}C_{ct}$ and $\delta^{18}O_{ct}$ (given relative to the PDB standard) for some fossil speleothems (73951 – Igloo Cave, Nahanni Region, NWT, Canada; 72040 – El Sotano de Soyate, SLP, Mexico; 71003 – El Sotano de la Tinaja, SLP, Mexico; 73039 – Crystal Cave, Bermuda; 71042 – El Sotano del Arroyo, SLP, Mexico; 74019 – Coldwater Cave, IA, USA) illustrating isotopic relationships that characterize deposition under equilibrium and non-equilibrium situations (from Harmon, 1975). Meaningful paleoclimate information can only be retrieved from speleothem calcite deposited under conditions of isotopic equilibrium.

al., 1996). If equilibrium deposition is documented, then the assumption is made that fossil speleothem material in the same cave was also deposited under equilibrium conditions.

As a consequence of the temperature dependence of the O-isotopic fractionation between water and calcite and the general isotopic equivalence of local meteoric precipitation and cave seepage water at a give cave locality (see below), the prevalence of equilibrium deposition should result in multiple speleothems within a single cave or local

area exhibiting concordant $\delta^{18}O_c$-time profiles. This would be the most convincing evidence for equilibrium deposition and has been demonstrated for some caves (see e.g. Harmon, 1975, Bar Matthews et al., 1997; Hellstrom et al., 1998; Dorale et al., 1999; Frumkin et al., 1999). It is highly unlikely (although not impossible) that two or more kinetically fractionated speleothems would exhibit a long-term synchronicity in their O-isotope variations. As we shall demonstrate below, however, it is also possible for two or more equilibrium speleothems to exhibit significantly different $\delta^{18}O_{ct}$ and $\delta^{13}C_{ct}$ records.

2.2. Oxygen Isotope Fractionation Effects

The temperature-dependent fractionation of oxygen isotopes between calcite (ct) and water (w), can be written in terms of the isotopic exchange reaction:

$$^1/3CaC^{16}O_3 + H_2{}^{18}O \leftrightarrow {}^1/3CaC^{18}O_3 + H_2{}^{18}O. \quad (1)$$

At equilibrium, the partition of isotopes in this system is described by a fractionation factor, $\alpha_{ct\text{-}w}$, defined to be:

$$\alpha_{ct\text{-}w} = (^{18}O/^{16}O)_{ct}/(^{18}O/^{16}O)_w, \quad (2)$$

which is more conveniently expressed as:

$$\alpha_{ct\text{-}w} = [\delta^{18}O_{ct} + 1000]/[[\delta^{18}O_w + 1000], \quad (3)$$

where,

$$\delta^{18}O_{ct} = 1000([(^{18}O/^{16}O)_{ct} - (^{18}O/^{16}O)_{std}]/[(^{18}O/^{16}O)_{std}]). \quad (4)$$

The units of $\delta^{18}O$ are per mil (‰) and $\delta^{18}O_{ct}$ values are commonly reported relative to either the Standard Mean Ocean Water (SMOW) or the Pee Dee belemnite (PDB) standards (Craig, 1957, 1961), where $\delta^{18}O_{SMOW} = 1.030864\delta^{18}O_{PDB} + 30.864$. A similar expression to Eq. (4) defines C-isotope variations, with $\delta^{13}C$ values always reported relative to the PDB standard. The $\delta^{18}O$ values for water cited in this paper are given relative to the SMOW standard; $\delta^{18}O$ values for calcite and all $\delta^{13}C$ values are given relative to the PDB standards for oxygen and carbon respectively.

The temperature dependence of the stable isotope fractionation between calcite and water was experimentally determined by O'Neil et. al., 1969, 1975), as:

$$10^3 \ln \alpha_{ct\text{-}w} = 2.78\,[10^6(T(^oK)^{-2})] - 2.89. \quad (5)$$

According to this relationship, $\alpha_{ct\text{-}w}$ decreases with increasing temperature. Over the temperature range that speleothem deposition has occurred in caves during the Quaternary, there is a decrease in the rate of decrease of $\alpha_{ct\text{-}w}$ with temperature from about -0.28 to -0.20‰ per °C as indicated in Table 2.

Table 2. Comparison of the rate of decrease of the calcite-water fractionation factor (α_{ct-w}) as a function of temperature over the range 5-25°C based upon O'Neil et al. (1969, 1975).

T (°C)	5	10	15	20	25
$[-d\alpha_{ct-w}/dT]/‰$ per °C	0.27	0.25	0.24	0.22	0.21

The inverse relationship between speleothem O-isotope composition and depositional temperature forms the basis for a paleothermometer (Epstein et al.,1951, 1953), given that $\delta^{18}O$ values can be routinely determined to a precision of better than 0.05‰ by modern isotope ratio mass spectrometry. However, the use of $\delta^{18}O$ values to determine paleotemperatures according to Eq. (5) depends critically on an inference of the $^{18}O/^{16}O$ ratio of the paleowater from which a speleothem was deposited.

2.3. Water Effects

The second variable determining the O-isotope composition of speleothem derives from the dependence of the O isotopic composition of cave seepage water (dw), $\delta^{18}O_{dw}$, on climate and the environment at the site of speleothem deposition. It is a complex function of at least four interrelated factors. These are:

(i) the $\delta^{18}O$ value of the surface seawater (sw) at source, $\delta^{18}O_{sw}$, of the meteoric precipitation (pptn), $\delta^{18}O_{pptn}$, that falls at the local cave site,
(ii) the temperature of seawater evaporation and subsequent vapor condensation over the cave site;
(iii) effects during moisture transport from source to cave site including variable storm tracks and differential amounts of ^{18}O "rainout" during moisture transport between ocean source and the site of precipitation; and
(iv) the history of moisture in the soil zone and seepage water in the epikarst zone (i.e., the part of the Earth's surface above the cave through which recharge occurs).

An expression for the effect of long-term change in climate on the oxygen isotopic composition of speleothem calcite deposited at a cave site in response to climate change can be formulated as follows:

$$\Delta\delta^{18}O_{ct} = [(d\,\alpha_{ct-w}/dT]\,\Delta T + [d(\delta^{18}O_{dw})/dT]\,\Delta T + \Delta(\delta^{18}O_{sw}). \quad (6)$$

The three terms in this expression describe the important factors that interact to determine the O-isotope signal recorded by a calcite speleothem. The first term, $d\alpha_{ct-w}/dT$, is the temperature dependence of the ^{18}O fractionation between cave seepage water and speleothem calcite from Eq. (5) above. The second term, $[(d\delta^{18}O_{dw})/dT)]\Delta T$, is the change in $^{18}O/^{16}O$ ratio of cave seepage waters as a function of temperature variation over the period of speleothem deposition (see discussion below). The third term, $\Delta(\delta^{18}O_{sw})$, is the long-term change in the O-isotope composition of surface sea water at the source

region for meteoric precipitation at the cave site, that occurred over the time interval corresponding to ΔT. For each 1‰ change in sea water isotopic composition, there will be an equal change in $\delta^{18}O$ of precipitation, if all other factors remain constant.

The first and third terms of Eq. (6) would cause speleothem to become enriched in ^{18}O as temperature decreases, as would occur during the transition from interglacial to glacial climate conditions. As indicated above, the calcite-water O-isotope fractionation ($\alpha_{ct\text{-}w}$) decreases with increasing temperature at a rate of -0.28 to -0.20‰ per °C (e.g. Table 2). The $\delta^{18}O$ value of seawater, $\delta^{18}O_{sw}$, the ultimate source of meteoric precipitation, increases in response to increasing amounts of low-^{18}O glacial ice present on the continents. The magnitude of the ^{18}O shift of the oceans during glacial/interglacial transitions can be estimated from changes in the $^{18}O/^{16}O$ ratio of oceanic benthic foraminifera. The maximum *ice-volume effect* is on the order of -1.2‰ (Shackleton and Opdyke, 1973; Fairbanks, 1989)

The second term reflects changes in the isotopic composition of cave seepage water over time and is influenced by both short-term and long-term factors. It is closely related to the average isotopic composition of meteoric precipitation above the cave and is similar in form to the temperature dependence of the O-isotopic composition of meteoric precipitation. Over the short term (over years to decades), the value of $d(\delta^{18}O_{pptn})/dT$ on a regional geographic scale has been shown to be ~ +0.7‰per °C for temperate maritime sites (Dansgaard, 1964); it is less for continental sites based upon studies of meteoric precipitation (Stuiver, 1968; Yurtsever and Gat, 1981; Fritz et al., 1987) and cave drip waters (Harmon et al., 1978; Yonge et al., 1985). This is clearly illustrated in Figure 3, where cave seepage water O-isotopic compositions are plotted as a function of cave temperature. Overall, the data define a non-linear array with a slope that decreases with increasing temperature. The middle section of the data set, which is derived from caves in temperate locations, defines a sub-linear array with a slope of ~ +0.5‰ per °C. However, when all data (including that for subtropical, arid/semi-arid, alpine, and arctic) sites are considered, the overall $\delta^{18}O_{dw}$-T trend, as noted by Yonge et al. (1985), closely approximates the arcuate form defined by Yurtsever and Gat (1981) for continental rainfall. In a paleoclimate context at a particular location, this parameter can be conceptualized as a shifting $d(\delta^{18}O_{pptn})/dT$ or $d(\delta^{18}O_{dw})/dT$ boundary that varies in time as the local climate changes from one dominant state to another (e.g. warm to cold or wet to dry). Its magnitude is determined by the cumulative effect of a set of variables that can not be explicitly quantified. These include: (i) the temperature of evaporation at the seawater source and subsequently of vapor condensation at the cave site, (ii) atmospheric effects during moisture transport (e.g. the air moisture content, storm tracks, the seasonality of precipitation, the amount of prior precipitation, and the degree of isotopic exchange of raindrops during precipitation), and (iii) seepage water effects (e.g. evaporation, storage, and mixing within the soil and epikarst zones). As a result, $d(\delta^{18}O_{dw})/dT$ at continental locations may have differed significantly in the past from the range of values of $d(\delta^{18}O_{pptn})/dT$ observed in modern times, but in general should lead to a decrease in $\delta^{18}O_{dw}$ with decreasing temperature and a corresponding decrease in speleothem $\delta^{18}O_{ct}$. By contrast, the situation for coastal locations is less complex. Here, the temperature dependence of $\delta^{18}O_{pptn}$ has a magnitude that tends to outweigh the effects of both $\alpha_{ct\text{-}w}$ and $\delta^{18}O_{sw}$, so that a decrease in temperature results in a decrease in speleothem $\delta^{18}O_{ct}$.

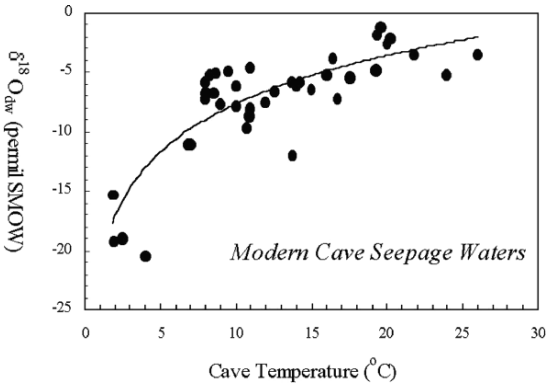

Figure 3. Plot of average cave drip water $\delta^{18}O$ values (relative to the SMOW standard) for modern cave seepage water as a function of cave temperature. The non-linear trend in the data closely resembles that recorded by Yurtsever and Gat (1981) for continental rainfall.

The complexities discussed above can make the interpretation of speleothem $\delta^{18}O_{ct}$ profiles problematic because of the difficulties in quantitatively determining the net response of Eq. 6 to climate change at any specific cave locality. The sum of the terms in Eq. 6 can vary quite widely depending on the relative magnitude of the positive- and negative- trending terms, and a given change in climate (effectively, ΔT) can lead to a change in isotopic composition of calcite, $\Delta\delta^{18}O_{ct,}$ which may be positive, negative or even zero. Unless the isotopic composition of cave seepage water at the time of speleothem formation can be estimated (e.g. through the analysis of fluid inclusions contained within the speleothem calcite as described Schwarcz et al., 1976 and Harmon et al., 1979b), the interpretation of measured $\delta^{18}O$ variations can be problematic because a decrease in speleothem $^{18}O/^{16}O$ ratio may be interpreted as indicative of either warming or cooling conditions, depending on the sign and magnitude of the *water effect* over time. An early literature example from France (Fig. 4) demonstrates the dilemma. When unconstrained by information about either the isotopic composition of the cave seepage water from which calcite precipitation occurred or modern speleothem calcite, a measured increase in the $^{18}O/^{16}O$ ratio of speleothem calcite could be interpreted as indicative of either warming conditions, as advocated by Duplessy et al. (1971) in their initial interpretation of the Aven d'Organc O-isotope profile, or indicative of cooling conditions as Emiliani (1971) subsequently reinterpreted the Aven d'Orgnac results.

Another way in which the sense of speleothem $\delta^{18}O$ change can be estimated is by reference to modern speleothem calcite that is actively forming in the same cave at the present time, once equilibrium deposition of the modern calcite has been established through analysis of $^{18}O/^{16}O$ ratios for modern speleothem calcite-water pairs (Table 1). By assuming that the $\delta^{18}O_{ct}$ value of the modern material is representative of the O-isotopic composition of speleothem calcite formed under interglacial conditions, both at present and in the past, then a record of $\delta^{18}O_{ct}$ variation for a fossil speleothem can be interpreted in terms of its climatic significance (e.g. Fig. 5). However, only a few recent speleothem paleoclimate studies have taken this approach to estimating the sense of $\delta^{18}O_{ct}$ variation for fossil speleothem calcite as a function of climate change.

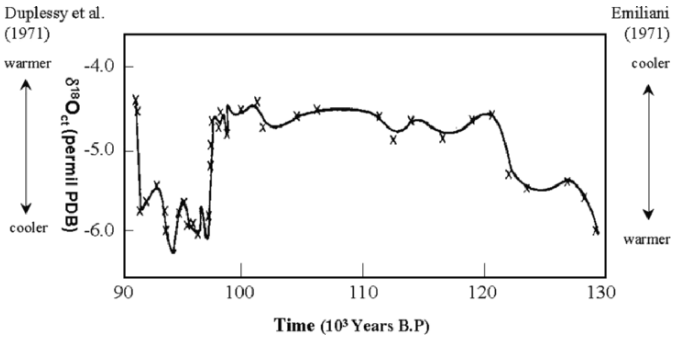

Figure 4. Axial $\delta^{18}O_{ct}$-time profile for a stalgamite from Aven d'Orgnac, France deposited from c. 130,000 to 90,000 years B. P. (after Duplessey et al., 1971)., O-isotope compositions are given relative to the PDB standard. Times of enrichments of speleothem calcite in ^{18}O have been interpreted as episodes of warm climate (Duplessy et al., 1971) and as episodes of cold climate (Emiliani, 1971). See text for discussion.

During the Holocene, the $\delta^{18}O$ value of seawater has remained constant and thus it can be assumed that present day value of $d[\delta^{18}O_{ppt}]/dT$ has been the principal control on $\delta^{18}O_{dw}$. The situation for Late Pleistocene time is more problematic. Dorale et al. (1992) have shown that $d(\delta^{18}O_{ct})/dT$ is positive for the mid-continent of North America during the Holocene. Earlier studies (Thompson et al., 1976; Harmon et al., 1978) indicated that a similar situation prevailed over the last two glacial-interglacial cycles in this region. However, Gascoyne et al. (1980, 1981), Goede et al. (1986, 1990), and Lauritzen (1995) have demonstrated that $d(\delta^{18}O_{ct})/dT$ is negative for certain high-latitude maritime situations. Data for fossil speleothems from 22 areas worldwide (Table 3) indicate that long-term trends for speleothem O-isotope variation can be either positive or negative as a function of changing climate. Hence, determination of $\delta^{18}O_{ct}$ of modern speleothem is recommended as a foundation for any speleothem paleoclimatology study. As well, speleothem fluid inclusion analysis (e.g. Schwarcz et al., 1976) should be conducted where feasible. To simply presume that the net *water effect* at a given site has been constant throughout the Late Pleistocene, as has been done in several recent studies, is a very tenuous assumption indeed.

2.4 Variability and Bias in Cave Drip Water Isotopic Composition

Continental precipitation exhibits distinct patterns of isotopic variation related to atmospheric circulation, geospatial position, and topography. Craig (1961) demonstrated that meteoric waters worldwide exhibit a well-defined relationship between D/H and $^{18}O/^{16}O$ ratios. It is well established that the stable isotopic composition of cave seepage waters in temperate and boreal karst areas conforms well to the meteoric water relationship (Schwarcz et al., 1976; Harmon and Schwarcz, 1981; Yonge et al., 1985) and that site-averaged $\delta^{18}O$ values for North American cave seepage waters exhibit the same geospatial distribution pattern as meteoric precipitation (Fig. 6). These two observations indicate that cave seepage waters in temperate to sub-arctic karst areas tend to be unfractionated samples of local meteoric precipitation.

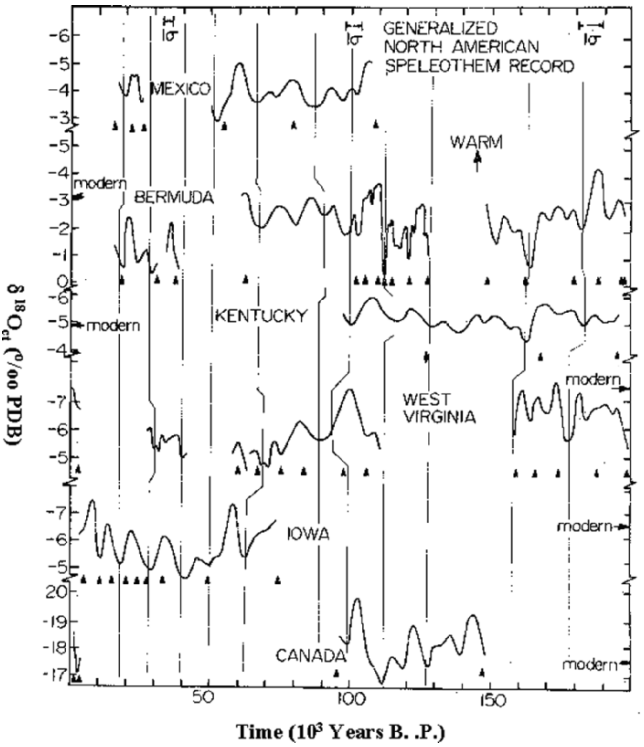

Figure 5. Records of $\delta^{18}O_{ct}$ variation (given relative to the PBD standard) for speleothems from six different karst regions between 22° and 62° north latitude in North America and Bermuda after Harmon et al. (1978a). Vertical lines indicate suggested correlation between isotopic maxima and minima that are interpreted to denote paleoclimatic events. Small upward pointing arrowheads indicate U-series age determinations. Horizontal arrows labeled *modern* indicate the $\delta^{18}O_{ct}$ value of calcite presently forming a particular speleothem locality.

However, the isotopic composition of seepage water at some localities is observed to be distinctly different from the annual average precipitation at the cave site, where cave drip waters may exhibit either a seasonal bias away from annual average rainfall, or large variations within individual cave systems or within local karst areas (Table 4)

In some cases, such as Bermuda and central Texas (Harmon, 1975), there is a distinct bias toward either winter or summer rainfall. In other instances, particularly in semi-arid areas of strongly seasonal precipitation like Israel (Bar-Matthews et al., 1996; Ayalon et al., 1998) and New Mexico (Chapman et al., 1992), the isotopic composition of recharge waters can be substantially modified by evaporation and mixing processes within the epikarst zone.

Table 3. Interpretation of the temperature dependence of changes in fossil speleothem O-isotopic composition. Data from the references cited in Figure 1.

Karst Area	Time Period (Ka)	$\Delta\delta^{18}O_{ct}/\Delta T$
Sierra de El Abra region, SLP, Mexico	20-110	negative
Central Kentucky, USA	120-200	negative
Northeastern Iowa, USA	1-81	negative
Southeastern West Virginia, USA	100-200	negative
Central Rocky Mountains, Canada	1-10 & 95-155	negative
Bermuda	40-200	negative
Southeastern France	90-130	negative
Yorkshire Dales, UK	190-300	negative
Israel	0-169	negative
New Zealand	0-35	negative
Transvaal area, South Africa	21-51	negative
Cape Town area, South Africa	0-5	negative
Southeastern Victoria, Australia	0-2 & 11-13	negative
Northern Oman	6-10 & 112-125	*near zero*
Cape Town area, South Africa	14-48	positive
Northwest Romania	55-130	positive
Tasmania, Australia	3-110	positive
Northern Norway	6-8, 82-145, & 580-710	positive
Southeastern Botswana	21-51	positive
Southeastern Missouri, USA	25-27	positive
Vancouver Island, BC, Canada	32-60	positive

A highly illustrative example of the complex isotopic variation that can be exhibited by cave seepage on a local scale is provided by the unique data set for the Ingleborough area of the Yorkshire Dales in England These data, for 11 drip sites along a 500m transect in White Scar Cave (Fig. 7) and 6 drip sites in four other nearby caves, were collected at approximately monthly intervals over a 13-month period from September 1980 through October 1981 (Atkinson et al., 1985; Hess et al., unpublished data). Several important points emerge from a comparison of the rainfall and cave seepage $\delta^{18}O$-time records for White Scar Cave (Fig. 8, Table 5). First, the combined mean $\delta^{18}O$ value for the seepage sites was -6.8‰, which is equivalent to the average $\delta^{18}O$ value of -6.6‰ measured for meteoric precipitation during the year. However, distinct isotopic signatures and different within and between site isotopic responses were observed for the same precipitation input. The annual $\delta^{18}O$ range for the individual drip sites in White Scar Cave varied from 1.3 to 2.9‰ and this range was 0.8 to 3.7‰ across all of caves sampled (Table 5). The difference between the highest and lowest $\delta^{18}O$ values observed for the monthly seepage water samples across the suite of White Scar drip sites was 1.8‰

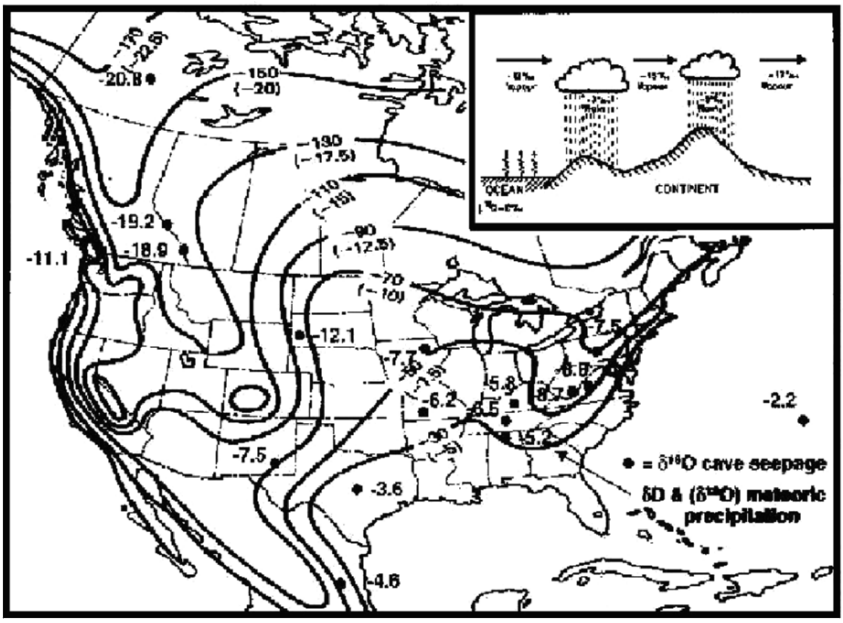

Figure 6. Map of North America showing (a) generalized contours of approximate δD and $\delta^{18}O$ values (given relative to the SMOW standard) of meteoric waters (after Taylor, 1974) and (b) site-averaged $\delta^{18}O_{dw}$ values for different karst areas. That the cave seepage waters exhibit the same geospatial distribution pattern as meteoric precipitation is an indication that cave seepage waters in temperate to sub-arctic karst areas tend to be unfractionated samples of local meteoric precipitation. The inset diagram is a schematic illustration of the multi-stage isotopic fractionation that occurs in the atmosphere during moisture transport from ocean source to a site of continental precipitation (after Siegenthaler, 1979).

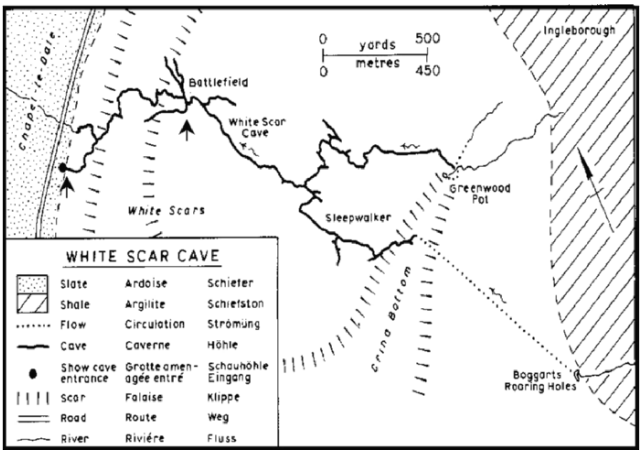

Figure 7. Map of White Scar Cave, Yorkshire Dales, UK (after Glover et al., 1977). The between the vertical arrows denote 500 m portion of the cave of the Entrance to the Battlefield sampled in our 1980-81 study (Hess et al., unpublished) of cave drip waters in the Yorkshire Dales karst area.

Table 4. O-isotope variations for surface precipitation and cave seepage waters in 11 karst areas worldwide (Δsw-pptn = the observed seepage water and precipitation difference). Data from the sources cited in Figure 1.

Karst Area	Average Annual Precipitation	Average Summer Precipitation	Average Winter Precipitation	Average Cave Seepage	Δsw-pptn
	[----------$\delta^{18}O$ (‰SMOW)---------- -----]				
Carlsbad Cave, NM, USA	-6.0	-4.0	-11.5		
<1100m asl				-7.9	-1.9
>1100m asl				-7.3	-1.3
Southeastern VA, USA	-6.9			-8.0	-1.1
Malaga, Spain	-4.6	-4.6		-5.2	-0.6
Southern MO, USA	-5.7			-6.2	-0.5
Yorkshire Dales, UK	-6.6	-6.2	-6.8	-6.7	-0.2
Tasmania, Australia	-4.9			-5.0	-0.1
Central KY, USA	-5.8	-5.0	-6.9	-5.8	0
Cape area, South Africa	-5.4			-5.4	0
Central TX, USA	-3.9	-2.2	-4.7	-3.6	+0.3
Israel	-6.4		---rainy season--	-5.4	+1.0
				-.5.7(f), -4.7(s)*	
Bermuda	-3.3	-2.6	-3.6	-2.2	+1.1

(s) = summer, (f) = fall

Table 5. O-isotope composition of (i) local meteoric precipitation, (ii) 11 drip sites in White Scar Cave, and (iii) 6 other drip sites four other local caves within the Yorkshire Dales of England, UK that were sampled monthly during the year from 9/80-10/81

Water Type/ Cave Drip Site	Range of Monthly $\delta^{18}O_{dw}$ Variation (‰)	Annual Average $^{18}O_{dw}$ (‰ SMOW)
Local Meteoric Precipitation		-6.6
White Scar Cave		
WSC-3	2.7	-7.1
WSC-4	3.3	-6.7
WSC-5	1.8	-7.1
WSC-8	2.3	-6.6
WSC-11	2.2	-6.9
WSC-13	2.9	-6.9
WSC-15	2.5	-6.6
WSC-16	3.3	-6.7
WSC-18	3.2	-7.4
WSC-19	3.2	-6.4
WSC-20	3.5	-6.8
Yordas Cave		
YC-1	2.9	-6.0
Jingling Cave		
JC-1	4.9	-6.1
Valley Cave		
VC-32	3.0	-6.9
VC-33	3.7	-6.9
VC-34	3.2	-6.5
Rowten Cave		
RC-1	3.5	-5.8

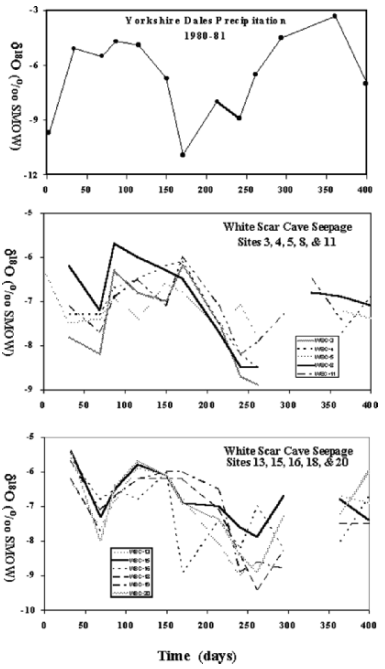

Figure 8. Comparison of temporal profiles of $\delta^{18}O$ variation for surface rainfall and cave seepage at different sites in White Scar Cave, Yorkshire Dales, UK over the period from 9/80 - 10/81 (Atkinson et al., 1983; Hess et al., unpublished data). See text for discussion.

compared to 3.1‰ across all four caves. Mean annual $\delta^{18}O$ values for the 11 White Scar Cave drip sites vary from −7.4 to −6.6‰, a range of almost 1‰ over only half a kilometer of cave passage. By comparison, mean annual drip site $\delta^{18}O$ values for the seven caves sampled vary from −7.4 to −5.8‰, a range of almost 2‰. Finally, some drip sites exhibit similar temporal $\delta^{18}O$ patterns, with major variations in isotopic composition in phase, but lagging behind the precipitation signal by some 50-60 days. By contrast, antithetic $\delta^{18}O$-time changes are observed for some other drip sites from one sampling time to the next. Together, this unusual set of data from the Yorkshire Dales indicates the isotopic composition of cave seepage drip waters is not necessarily a simple and direct response function of an input meteoric precipitation signal, but rather can be a complex derivative generated by a combination of physical effects such as different flow paths, residence times, and mixing histories of recharge water within the epikarst zone.

These observations also have important paleoclimatological as well as hydrological implications. Since cave temperatures throughout the Ingleborough cave system were closely similar (and equal to the average surface temperature), the speleothem calcite precipitated over the interval of the study from such drip waters sampled would exhibit the same difference in O-isotopic composition as the parent seepage waters. This would correspond to an apparent maximum difference of >6°C between contemporaneously deposited speleothem calcite.

The situation may be even more complicated when considering past climate regimes. The O-isotope data for the White Scar Cave system demonstrate that individual seepage

water drip sites, even those closely spaced over only 500m within a single cave, can have distinctly different isotopic signatures and response functions to a given hydrologic input signal. This characteristic is illustrative of the hydrological complexity that can exist within a geologically quite simple karst setting, such as that manifest in the horizontally-bedded limestones of the Yorkshire Dales. Based upon this case study, it is only reasonable to postulate that a large variety of different seepage water flow paths can exist within an epikarst zone as part of a complex seepage network that can be highly dynamic in character. More geologically complex folded and faulted karst settings have the potential to develop even more complicated and interconnected hydrological frameworks. Thus, it is to be expected that different epikarst flow paths may exhibit different rate responses to surface precipitation events and that distinct flow networks may be operating within any given epikarst zone, particularly during high or low recharge conditions.

Such a bias in the O-isotopic composition of drip waters ($\delta^{18}O_{dw}$) is likely to be present at many cave sites, particularly those located in semi-arid/arid and alpine and arctic regions, for the following reasons. First, there may be a large intra-annual variation in the O-isotopic composition of continental precipitation: typically at mid-latitude sites, $\delta^{18}O_{pptn}$ varies by about 10‰ or more, with the isotopically lightest (i.e. lowest $\delta^{18}O$ value) precipitation being snow that accumulates during the winter, and the heaviest being summer rainfall. Typically, melt water from winter snow contributes to recharge waters in the spring-summer of each year, but the distribution of this component of recharge may vary on a scale of tens to hundreds of meters on the land surface above the cave, depending on the timing of snow cover development, the amount of snow accumulated on different parts of the terrain, and the local topography. This would be especially true where an extensive cave system underlies irregular topography (e.g. a valley and ridge complex); caves beneath level plateau and plains would probably be less susceptible to such local variations in $\delta^{18}O$ of recharge.

Intra-site $\delta^{18}O_{dw}$ differences can arise for other reasons. For example, in regions where precipitation is temporally variable the timing of recharge may vary on a seasonal, annual, or decadal time scale. In other areas, rainfall may occur predominantly in one season of the year. In regions of semi-arid/arid climate subject to high rates of surface evaporation (in contrast to evapotranspiration), a differing extent of evaporative loss of the recharge water in thin soils prior to entry into the epikarst can generate recharge at different points above a cave that may be differentially enriched in ^{18}O. Ayalon et al. (1998) documented such variations in a study of the Soreq Cave in Israel. A difference in the isotopic composition of recharge water might also be expected within caves developed over a large depth interval. In such instances, the near-surface portions of the cave might receive a recharge derived almost entirely from local precipitation, compared to the deeper portions of the cave where seepage waters could be fed by a greater proportion of regional ground-water flow. Even more complex scenarios are possible. For example, Chapman et al. (1992) noted a 0.6‰ difference in $\delta^{18}O$ values for drip waters at Carlsbad Caverns, NM entering the cave above and below 1100 m elevation (Table 4), which was attributed to changes in amount of ^{18}O-enriched summer precipitation on a decadal time scale. Superimposed on this long-term isotopic signal was a complex cycle of intra-annual variability in seepage water isotopic composition that was attributed to seasonal changes in the cave climate. A combination of airflow-driven evaporation at the wallrock-cave chamber interface and vapor-dripwater isotopic exchange resulting from

air currents pumping ^{18}O-enriched vapor from the cave atmosphere into the wallrock generated isotopically distinct winter and summer cave drip water.

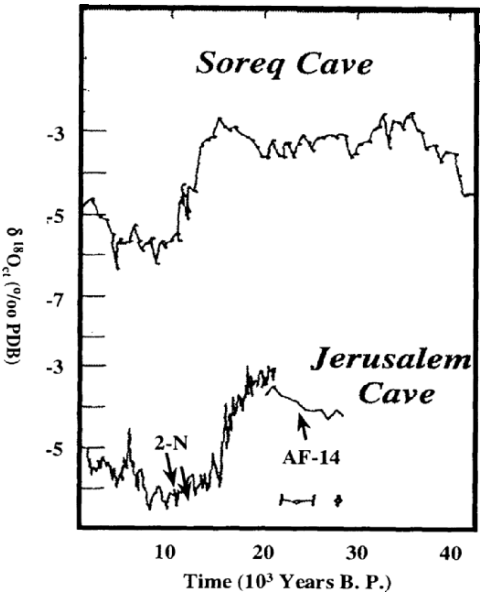

Figure 9. Concordant records of $\delta^{18}O_{ct}$ variation for speleothems from two caves in Israel (after Frumkin et al., 1999 and Bar Matthews et al., 1997).

Karst hydrologic systems are both highly complex and dynamic in character, both in the short and long term (Friedrich and Smart, 1982). For example, a partly different set of epikarst flow paths might be utilized during high- and low-recharge conditions. Similarly, the *quick flow* versus *base flow* components (Atkinson, 1977) of the seepage flow signal may vary as a function of intensity, duration, or timing of a precipitation input or may vary with a change in predominant climate regime. As a result of local nuances, there may be significant $\delta^{18}O_{dw}$ variations for seepage sites in a single cave, such as those illustrated in Tables 4 and 5. We would expect to see such differences reflected in $\delta^{18}O_{ct}$ of coeval speleothems from the same cave; this has been observed at some caves. Note that such differences in $\delta^{18}O_{dw}$ would be persistent at a given site even though $\delta^{18}O$ character of precipitation was changing seasonally or over the long term at a site. The important implication of this situation, from a paleoclimate perspective, is that the seepage water network within the epikarst zone feeding a particular cave drip site might

actually be of a variable hydrologic configuration under different climate regimes and be variable on a 10^2 to 10^3 year time scale. For example, a change in the transmission behavior of individual flow paths may result from sedimentation or calcite precipitation and cause variations in the relative proportions of high-flow/low-flow or winter/summer precipitation emerging at a particular drip site over a millennial time scale. Thus, it is entirely plausible that seepage waters of different isotopic composition may be generated during episodes of interglacial and glacial climate and yet not be a faithful reflection of average surface precipitation. As a result changes may be observed in the $^{18}O/^{16}O$ ratios of speleothem calcite which do not directly reflect changes in temperature at the cave site. As yet, there are no certain methods of elucidating such effects. The most robust approach would seem to be a documentation of the uniformity of coeval $\delta^{18}O$ profiles in two or more speleothems from the same or nearby caves. Some researchers have succeeded in finding two or more coeval speleothems at one site or two or more nearby sites (Fig. 9), which gave identical records of $\delta^{18}O_{ct}$ (Harmon et al., 1979; Gascoyne et al., 1981; Bar-Matthews et al., 1997; Dorale et al., 1998; Frumkin et al., 1999).

3. CARBON ISOTOPES

In theory, it should also be possible to use C-isotope variations in speleothems as a monitor of past climate change in a manner analogous to O-isotopes. The carbon isotopic signal in speleothem calcite arises from the $^{13}C/^{12}C$ ratio of dissolved inorganic carbon (DIC) in the drip water. This, in turn, is derived from processes occurring within the epikarst between biogenic and atmospheric CO_2, water, and the limestone of the bedrock (Hendy, 1971; Deines et al., 1974; Salomons and Mook, 1986):

$$CO_2 + H_2O + CaCO_3 \equiv 2HCO_3^- + Ca^{2+} \quad (7)$$

Surface vegetation and soil organic productivity determine the amount of biogenic CO_2 available for limestone dissolution (Quade et al., 1989; Cerling et al., 1991). In areas of low organic activity or sparse vegetation cover (*e.g.* in arid or alpine terrains with poorly developed soils), the proportion of CO_2 contributed by oxidation of biogenic matter in the soil will be small compared to the atmospheric contribution. As the level of soil biogenic activity increases, the $\delta^{13}C$ value of CO_2, and its aqueous dissociation products HCO_3^- and CO_3^{2-}, decrease because of the depletion of ^{13}C in organic matter with $\delta^{13}C$ = -26 to -12‰ compared with atmospheric CO_2 with $\delta^{13}C$ = -7‰ (Deines et al., 1974). Also, it has long been recognized that soil CO_2 concentrations, which are a direct reflection of extent of surface vegetation cover and soil biomass organic activity, can vary significantly between different soil and vegetation types within the same climatic regime (Miotke, 1974). Therefore, changes in $\delta^{13}C_{ct}$ of speleothem calcite will generally reflect changes in the level of organic activity in the soil zone above the cave and will respond accordingly to long-term changes in climate. This is clearly illustrated in Table 6, where large ranges of $\delta^{13}C_{ct}$ value variation (>6‰) are observed for modern speleothems within single caves or cave area and for different karst areas underlain by similar types of vegetation. Recently, it also has been recognized that the isotopic composition of atmospheric CO_2 is slightly different during intervals of glacial climate. Marino et al. (1992) estimated an interglacial-glacial $\delta^{13}C$ difference of -0.7‰.

Table 6. C-isotope ranges observed for modern speleothems from caves in different geographic regions. Data from the references cited in Figure 1.

Cave Site	$\delta^{13}OC_{ct}$ Range (‰ PDB)
Soreq Cave, Israel	−12.8 to −5.1
Yorkshire Dales, UK (5 Caves)	−11.7 to −4.5
Bermuda (5 caves)	−11.0 to −2.3
Vancouver Island, BC, Canada (3 caves)	−11.0 to −6.2
Moon's Cave, Victoria, Australia	−9.6 to −7.0
Mammoth-Flint Ridge, KY, USA	−9.4 to −7.3
Coldwater Cave, IA, USA	−9.3 to −6.3
Pulaski County, KY, USA (2 caves)	−8.8 to −5.8
Lynd's Cave, Tasmania, Australia	−8.6 to −6.7
Norman-Bone Cave, WV, USA	−8.1 to −7.7
Central TX, USA (2 caves)	−8.1 to −0.5
Wind Cave, SD, USA	−4.4 to −4.1
Yorkshire Pot, ATLA, Canada	−4.1 to −3.1

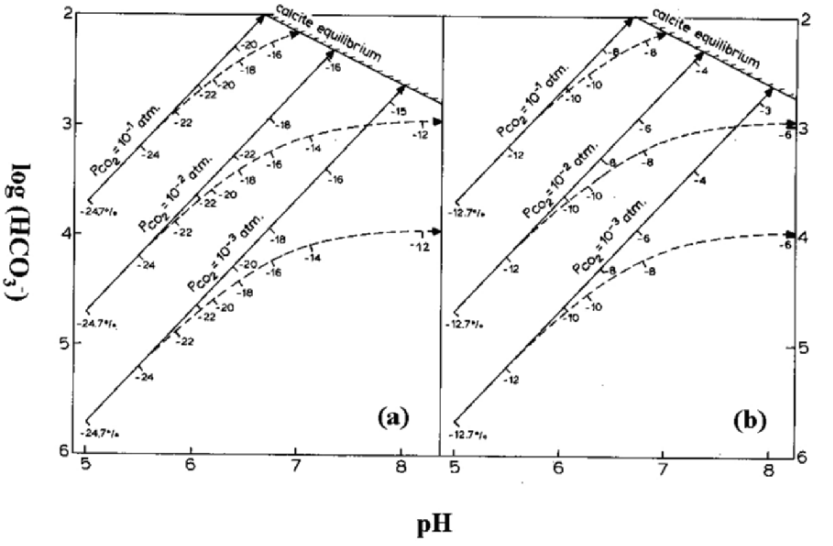

Figure 10. Comparison of the C-isotopic evolution at 25°C during dissolution of limestone (typically with $\delta^{13}C$ = −4 to +2‰; average. = 0‰, Deines et al., 1973) by soil waters initially equilibrated with CO_2 derived from a C_3-type vegetation source of $\delta^{13}C$ = −24‰ (a) and a C_4-type vegetation source of $\delta^{13}C$ = −12‰ (b) under *open* (solid line) and *closed* (dashed line) system conditions (after Salomons and Mook, 1986 and Deines et al., 1974). The lines and curves in each figure represent solution paths for different conditions of initial CO_2 partial pressure (PCO_2) conditions until equilibrium with calcite (i.e. saturation) is reached. The tick marks on the lines represent the C-isotope composition of the solution at that point of on evolutionary trajectory. Note that carbonate dissolution under *closed* system conditions leads to higher $\delta^{13}C$ values (‰ PDB) at saturation than *open* system dissolution, the lower the initial PCO_2 value, the greater the degree of ^{13}C enrichment at saturation.

In some regions of the world, where karst terrains are situated in locations that are transitional between regions of lower and higher rainfall, another factor may contribute to changes in $\delta^{13}C_{ct}$. The vegetation of hot, arid/subarid regions typically includes plants using the Hatch-Slack (C_4) photosynthetic process for which $\delta^{13}C$ value of the plant carbon is typically in the range of -14 to -12‰ (ranging to around -10‰ in the pre-industrial era before the burning of low-$\delta^{13}C$ fossil fuel). By contrast, vegetation of less arid regions is dominated by plants using the Calvin cycle (C_3) that have $\delta^{13}C$ values in the range of -27 to -24‰ (Hendy, 1971; Salomons and Mook, 1986; Cerling et al., 1991). As a result, long-term changes in the aridity immediately above a cave site in such regions may lead to changes in the proportion of C_3 to C_4 plants, and a corresponding shift in $\delta^{13}C$ value of HCO_3^- in cave drip waters (Fig. 10). Speleothem calcite deposited from seepage waters which had derived their dissolved carbon from a C_4-type vegetation should be some 7-9‰ enriched in ^{13}C by comparison to those formed from seepage waters that had equilibrated with soil CO_2 derived from C_3-type vegetation.

To some highly variable extent that is difficult to measure and quantify, a variety of processes within the epikarst zone and cave microclimate can also play a role in determining the C-isotopic composition of cave drip waters (Hendy, 1971; Baker et al., 1997; Bar-Matthews et al, 1998). The extent of evaporation of recharge water within the soil zone (Sonntag et al., 1983), the extent of isotopic equilibrium between water and CO_2 in the soil zone (Wigley et al., 1978), the degree of *closed* or *open* system chemical evolution during carbonate dissolution within the epikarst zone (Deines et al., 1974; Salomons and Mook, 1986), CO_2 loss during degassing of groundwater within the epikarst zone (Baker et al., 1997), and CO_2 loss from water upon entering a cave due to either evaporation (Fantidis and Ehhalt, 1970; Hendy, 1971) or high seepage water flow rate (Hendy, 1971) are all processes that can modify significantly the $\delta^{13}C_{ct}$ value that is recorded by a speleothem. Also, changes in the routing of recharge water from surface regions of greater or lesser soil activity through an epikarst flow network may result in long-term changes in $\delta^{13}C_{ct}$ in a similar manner to the effects discussed above for oxygen isotopes.

In terms of the paleoclimatic interpretation of $\delta^{13}C_{ct}$ records for speleothems, it is observed that generally cooler or drier climates will lead to higher $\delta^{13}C_{ct}$ values at sites where soil biogenic activity is the dominant control because temperature change has a relatively small effect on the fractionation between HCO_3^- and calcite (Deines et al, 1974). In areas where transitions between C_3 and C_4 plants are implicated, higher $\delta^{13}C_{ct}$ values would correspond to warmer and drier conditions. Therefore, there may be some ambiguity as to the interpretation of changes in speleothem C-isotopic composition. Added to this are the possibility of isotopic effects related to changes in the routing through the epikarst of recharge to a drip site, making the interpretation of $\delta^{13}C_{ct}$ variations in speleothems even more difficult and problematic to interpret than $\delta^{18}O_{ct}$ fluctuations.

Several examples illustrate this point. From Table 6, it is seen that high $\delta^{13}C_{ct}$ values (> -7‰) are observed for modern speleothems presently forming in caves in physiographic settings as diverse as the Yorkshire Dales of England, the Eastern Mediterranean region of Israel, and the Central Canadian Rocky Mountains where the overlying vegetation is entirely C_3 in character. Also, significant differences in C-isotopic composition are observed within individual caves (e.g. -11.7 to -8.7‰in Ingleborough

Cave, UK; Gascoyne, 1979 or -12.8 to -5.1‰ in Soreq Cave, Israel; Bar-Matthews et al., 1996) or karst areas (e.g. -11.0 to -2.3‰for five Bermudian caves or in Central Texas, -2.6‰for Natural Bridge Caverns *vs.* -5.1‰ for Inner Space Cave; Harmon, 1975) that cannot be attributed to differences in type of surface vegetation.

From Figure 9, it is also clear that large differences in C-isotopic composition of dissolved carbon can also be generated in seepage waters, depending on whether their transit through the epikarst zone occurs under *open* or *closed* system conditions (Hendy, 1971; Deines et al., 1974; Salomons and Mook, 1986). Under *open* system conditions, infiltrating seepage is able to maintain exchange and remain in isotopic equilibrium with the soil CO_2 reservoir during the time it is dissolving carbonate rock. By contrast, exchange is not maintained during the downward passage of seepage water through the epikarst zone under *closed* system conditions, so that carbon is consumed during carbonate dissolution. For example, it is seen from Figure 10 that, regardless of surface vegetation type, $\delta^{13}C$ values for dissolved carbon (and precipitated speleothem calcite) will be several permil enriched in ^{13}C if *closed* system, rather than *open* system, conditions prevail during groundwater recharge. It is even possible for seepage waters to attain positive $\delta^{13}C$ values at calcite saturation, if dissolution occurred under *closed* system conditions in a seepage water initially equilibrated at a low PCO_2 value (e.g. Castleguard Cave, Table 5; Harmon et al, 1983)

From a paleoclimate standpoint, it would be expected that *open* system conditions would be more likely to be realized during times of high precipitation and groundwater recharge, whereas *closed* system conditions would be more likely to occur during times of reduced precipitation and diminished or highly seasonal recharge. Thus, a positive shift in speleothem $\delta^{13}C_c$ values on the order of several permil could be a simple response to a change from wet to dry conditions which can occur in response to global climate fluctuation. Lacking other information, such a $\delta^{13}C_{ct}$ shift could be misinterpreted as reflecting a change from a C_3-type to C_4-type of surface vegetation.

From these data, it is clear that high $\delta^{13}C_c$ values in excess of about -7‰ are not necessarily diagnostic of a C_4-type of surface vegetation, but instead can be due to other causes. In the Yorkshire Dales, it is likely that the ^{13}C enrichments observed reflect a combination of short soil residence times and physical effects related to hydrologic processes within epikarst zone above the cave (Baker et al., 1997). By contrast, the ^{13}C enrichments at Castleguard Cave in the Canadian Rockies are the direct manifestation of the facts that the atmosphere is the predominant source of CO_2 for cave seepage waters and carbonate dissolution occurs under "closed" system conditions in this glacio-alpine environment (Harmon et al., 1983). That similarly high $\delta^{13}C_{ct}$ values are observed for fossil speleothem material from Castleguard Cave during the Holocene and last interglacial indicates that the atmosphere has been the primary source of dissolved CO_2 at this location during times of speleothem deposition in this alpine environment (Harmon et al., 1983). A striking example of a speleothem $\delta^{13}C_{ct}$ transition from low to high $^{13}C/^{12}C$ ratios that is not a result of a C_3 to C_4 vegetation change is given by Bar-Matthews et al. (1996). In Soreq Cave (Israel), the combination of high $\delta^{13}C$ and low $\delta^{18}O$ values are observed in portions of speleothems deposited over the period from 10 to 7 Ka that are characterized by thin laminae of various colors and high detritus contents. A convincing argument is presented by these authors that this combination of features is a result of paleoflood events, resulting from high surface rainfall rates, that largely removed the surface soil cover in the Eastern Mediterranean during Younger Dryas time.

Also, Frumkin et al. (2000) observed a rapid and large (c. 11 ‰) increase in $\delta^{13}C$ at the end of isotope stage 6 in a speleothem from Jerusalem. They attributed this increase to rapid deforestation of the Judean Hills at this climatic transition.

Recently, several studies (Dorale et al., 1992, 1998; Holmgren et al., 1995; Hellstrom et al., 1998) have interpreted trends of ^{13}C enrichment in fossil speleothems as diagnostic of a change in surface vegetation from plants that utilize a C_3-type photosynthetic pathway and favor moister growing conditions to those grasses that utilize a C_4-type pathway for photosynthesis and prefer hot and arid environmental conditions. For example, in their study of a Late Pleistocene stalagmite from Lobatse II Cave in Botswana, Holmgren et al. (1995) conclude that measured $\delta^{13}C_{ct}$ values of –6.5 to +1‰ are clear evidence that C_4-type plants were the predominant surface vegetation throughout the period of deposition of the stalagmite without considering other possible causes for the ^{13}C enrichment. It is more likely, however, that much of this change is due to changes in the level of biological activity in the soil zone rather than to changes in the proportion of C_4 grasses above the caves, since such vegetation is not generally abundant in the region today and would have been even less so in cooler periods of the Pleistocene.

4. SUMMARY AND CONCLUSIONS

Variations of $^{18}O/^{16}O$ and $^{13}C/^{12}C$ ratios in calcite speleothems can provide important information about terrestrial paleoclimate, if deposition occurred under equilibrium conditions. Fluctuations in $\delta^{18}O$ along the growth axis of a speleothem reflect a combination of two factors: the temperature dependent calcite-water ^{18}O fractionation and temporal change in the $^{18}O/^{16}O$ ratio cave seepage water, which is a complex and variable function of the integrated history of seepage water from its seawater source through its transit within the meteoric water cycle to a cave. It is only possible to estimate paleotemperatures in instances when these two effects can be differentiated and the isotopic composition of the parent cave seepage water constrained over the time interval of speleothem formation. However, the stable isotope variations observed in a fossil speleothem may not be totally determined by climate change because multiple processes can contribute to the $^{18}O/^{16}O$ and $^{13}C/^{12}C$ ratios recorded in speleothem calcite. Modern speleothem deposition occurs under equilibrium conditions in many deep-cave settings, with speleothems forming at temperatures from 1-23°C having $\delta^{18}O$ values of <12 to >28‰ (SMOW) and $\delta^{13}C$ values of <-10 to >+1.5‰ (PDB). Cave seepage isotopic composition closely reflects that of local rainfall, although the ^{18}O signature observed at an individual drip site can be biased away from average surface precipitation and variations in seepage water $\delta^{18}O$ of up to 5‰ are observed for different sites within individual caves.

Temporal records of speleothem stable isotope variation have the potential to yield very important and perhaps unique information about past terrestrial climate. However, significant problems may be associated with the interpretation of these long-term records of change in the $^{18}O/^{16}O$ and $^{13}C/^{12}C$ ratios of cave-deposited calcite. In particular, it might be expected that enrichment in the heavy isotopes of these elements (C, O) should correspond to different senses of climate change as one goes from one cave site to another. The isotopic variability of modern speleothems is considered to reflect a combination of seasonal effects on meteoric precipitation, the extent of evaporation in the

soil zone, and the variable manner in which recharge is transmitted through, and mixed within, the local epikarst zone during different flow conditions. The importance of these influences is likely to vary at any given site through time for both climatic and geologic reasons. Additionally, fluctuations in stalagmite C-isotopic composition will reflect the degree of soil zone organic productivity, the extent and type of surface vegetation, the amount of bedrock dissolution, the nature of water movement through the epikarst zone, cave drip rate, and CO_2 outgassing during deposition. For calcite speleothem O-isotope ratios, the most reliable test of the climatic significance of changing isotopic composition would seem to be comparison between ancient and modern speleothems because the O-isotopic composition of modern calcite is likely to be representative of warm climate conditions. Thus, the sense (positive, negative, or zero) of change in $\delta^{18}O_{ct}$ with climate will be indicated in this way, since pre-Holocene speleothems should reflect equivalent or cooler climatic conditions. From this standpoint, it may be supposed that speleothem isotopic variations could be used as relative indications of major climate change at those sites where large positive or negative shifts in $\delta^{18}O_{ct}$ values are observed. O-isotope records from fossil speleothems ought to be readily correlated with other paleoclimate indicators, specifically changes in speleothem C-isotope composition (Harmon et al., 1979; Dorale et al., 1998; Frumkin et al., 1999) and $\delta^{18}O_{ct}$ records for subaqueous calcite deposits (Coplen et al., 1994; Winograd et al., 1992) from other continental localities, terrestrial pollen (Heusser et al., 1980) or mollusc (Goodfriend, 1991) records, glacial stratigraphies (*e.g.* Mangarud et al., 1979; Heusser et al., 1980) or mollusc (Goodfriend, 1991) records, the chemical, and gas fluctuations of continental ice sheets (Bond et al., 1993; Dansgaard et al., 1993), and deep-sea foraminifera isotopic records (Shackleton et al., 1983). The use of speleothem $\delta^{18}O_{ct}$-time profiles as paleotemperature records remains a tantalizing possibility, but its full realization depends on better knowledge of the coeval changes in $\delta^{18}O$ of drip waters that formed these interesting deposits, possibly through further study of their fluid inclusions. Speleothem C-isotope records also hold promise for deciphering past climate change, but a better quantitative understanding of the processes that produce $^{13}C/^{12}C$ variations in speleothem calcite and an application of this knowledge in the interpretation of $\delta^{13}C_{ct}$-time profiles is required before this potential will be realized.

4.0 ACKNOWLEDGEMENTS

Support for the research reported in this paper was provided by the National Research Council (Canada), the Natural Sciences and Engineering Research Council (UK), and the Scottish Universities Research and Reactor Centre.

5.0 REFERENCES

Atkinson, T. C., 1977, Diffuse flow and conduit flow in limestone terrain in the Mendip Hills, Somerset (Great Britain), J. Hydrol. **35**:93-110.

Atkinson, T. C., Harmon, R. S., Smart, P., and Waltham, A. C., Paleoclimate and geomorphic implications of $^{230}Th/^{234}U$ dates on speleothems from Britain, Nature. **272**:24-28.

Atkinson, T. C., Hess, J. W., and Harmon, R. S., 1985, Stable Isotope Variations in recharge to a karst aquifer, Yorkshire Dales: preliminary work, Ann. Soc. Geol. Begique. **T108**:225.

Ayalon, A., Bar-Matthews, M., and Sass, E., 1998, Rainfall-recharge relationships within a karstic terrain in the eastern Mediterranean semi-arid region, Israel: $\delta^{18}O$ and δD characteristics, J. Hydrol. **207**:18-31.

Baker, A., Ito, E., Smart, P., and McEwan, R. F.,1997, Elevated and variable values of ^{13}C in speleothems in a British cave system, Chem. Geol. **36**: 263-270.

Bar-Matthews, M., Ayalon, A., Matthews, A., Sass, E., and Halicz, L., 1996, Carbon and oxygen isotope study of the active water-carbonate system in a karstic Mediterranean cave: implications for paleoclimate research in semiarid regions, Geochim. Cosmochim. Acta. **60**: 337-347.

Bar-Matthews, M., Ayalon, and Kaufman, A., 1997, Late Quaternary paleoclimate in the eastern Mediterranean region from stable isotope analysis of speleothems at Soreq Cave, Israel, Quat. Res. **47**:155-168.

Bond, J., Broecker, W. S., Johnsen, S., McManus, J., Labeyrie, L., Jouzel, J., and Bonani, R., 1993, Correlations between climate records from North Atlantic sediments and Greenland ice, Nature. **365**:143-147.

Burns, S. J., Matter, A., Frank., N, and Mangini, A., 1998, speleothem-based paleoclimate record from northern Oman, Geology. **26**:499-502.

Caballero, E., Jimenez de Cisneros, C., and Reyes, E., 1996, A stable isotope study of cave seepage waters. Appl. Geochem. **11**:583-587.

Cerling, T. E., Quade, J., Solomon, D. K., and Bowman, J. R., 1991, On the carbon isotopic composition of soil carbon dioxide, Geochim. Cosmochim. Acta. **55**:3403-3405.

Chapman, J. B., Ingraham, N. L., and Hess, J. W., 1992, Isotopic investigation of infiltration and unsaturated zone flow processes at Carlsbad Caverns, New Mexico, J. Hydrol. **133**:343-363.

Coplen, T. B., Winograd, I. J., Landwehr, J. M., and Riggs, A. C., 1994, 500,000-year stable carbon isotope record from Devils Hole, Nevada, Science. **263**:361-365.

Craig, H., 1957, Isotopic standards for carbon and oxygen and correction factors for mass-spectrometric analysis, Geochim. Cosmochim. Acta. **12**:133-149.

Craig, H., 1961, Isotopic variations in meteoric waters, Science.**133**:1702-1703.

Dansgaard, W., 1964, Stable isotopes in precipitation, Tellus. **16**:436-468.

Dansgaard, W., Johnsen, S.J., Claussen, H. B., Dahl-Jensen, D., Gundestrup, N. S., Hammer, C. U., Hvidberg, C. S., Steffensen, J. P., Sveinbjornsdottir, A. E., Jousel, J., and Bond, G., 1993, Evidence for general instability of past climate from a 250-kyr ice core record, Nature. **364**:218-220.

Deines, P., Langmuir, D., and Harmon, R. S., 1974: Stable carbon isotope ratios and the existence of a gas phase in the evolution of carbonate ground waters, Geochim. Cosmochim. Acta. **26**:1147-1154.

Dorale, J. A., Gonzalez, L. A., Reagan, M. K. Pickett, D. A., Murrell., M. T., and Baker, R. G., 1992, a high-resolution record of Holocene climate change in speleothem calcite from Cold Water Cave, northeast Iowa, Science. **258**:1626-1630.

Dorale, J. A., Edwards, R.L., Ito, E., and Gonzalez, L. A., 1998, Climate and vegetation history of the midcontinent from 75 to 25 ka: a speleothem record from Crevice Cave, Missouri, USA, Science. **282**:1871-1874.

Duplessy, J. C., Labeyrie, J., Lalou, C., Nguyen, H. V., 1970, continental climatic variations between 130,000 and 90,000 years B.P., Nature. **226**:631-633.

Duplessy, J. C., Labeyrie, J., Lalou, C., Nguyen, H. V., 1971, La mesure des variations climatiques continentales application a la periode comprise entre 130.000 et 90.000 ans B.P., Quat. Res. **1**:162-174.

Edwards, R. L., Chen, J. H., and Wasserburg, G. J., 1987, ^{238}U-^{234}U-^{230}Th systematics and the precise measurement of time over the past 500,000 years, Earth Planet. Sci. Lett. **81**:175-192.

Emiliani, C, 1955, Pleistocene paleotemperatures, J. Geol. **63**:538-378.

Emilani, C., 1971, The last interglacial paleotemperatures and chronology, Science. **171**:571-573.

Epstein, S., Buchsbaum, R., Lowenstam, H. A., and Urey, H. C., 1951: Carbonate-water isotopic temperature scale, Bull. Geol. Soc. Amer. **62**:417-426.

Epstein, S., Buchsbaum, R., Lowenstam, H. A., and Urey, H. C., 1953: Revised carbonate-water isotopic temperature scale, Bull. Geol. Soc. Amer. **64**:1315-1326.

Fantidis, J. and Ehhalt, D. H., 1970, Variations of the carbon and oxygen isotopic composition in stalagmites and stalactites: evidence of non-equilibrium isotopic fractionation, Earth Planet. Sci. Lett. **10**:136-144.

Fornaca-Rinaldi, G., Panichi, C., and Tongiorgi, E., 1968, Some causes of the variations of the isotopic composition of carbon and oxygen in cave concretions, Earth Planet. Sci. Lett. **4**: 321-324.

Friedrich, H. and Smart, P. L., 1982, the classification of autogenic percolation waters in karst aquifers: a study in G.B. Cave, Mendip Hills, England, Proc. Bristol Univ. Speleol. Soc. **16**:143-159.

Fritz, P., Drimmie, R. J., Frape, S. K., and O'Shea, K., 1987, The isotopic composition of precipitation and groundwater in Canada, in *International Symposium on the use of Isotope Techniques in Water Resources Development.* International Atomic Energy Agency, Vienna, IAEA-SM299, pp.39-550.

Frumkin, A., Ford, D. C., and Schwarcz, H. P., 1999, continental oxygen isotopic record of the last 170,000 years in Jerusalem, Quat. Res. **51**:317-327.

Galimov, E. M., Grinenko, V. A., and Gubkin, I. M., 1965, Effect of leaching under surface conditions on the isotopic composition of carbon in secondary calcite, Geochem. Int. **2**:79-82.

Gascoyne, M., 1979, Isotopic and geochronological studies of speleothems, Unpub. PhD Thesis, McMaster University, Hamilton (Ont.), Canada.

Gascoyne, M., 1980, Trace-element partition coefficients in the calcite-water system and their paleoclimate significance in cave studies, J. Hydrol. **61**:212-222.

Gascoyne, M, 1992, Paleoclimate determination from cave calcite deposits, Quat. Sci. Rev. **11**:609-632.

Gascoyne, M., Ford, D. C., and Schwarcz, H. P., 1981, Late Pleistocene chronology and paleoclimate of Vancouver Island determined from cave deposits, Can. J. Earth Sci.**18**:1643-1652.

Gascoyne, M. and Nelson, D. E., 1983, Growth mechanisms of recent speleothems from Castleguard Cave, Columbia Icefields, Alberta, Canada, inferred from a comparison of uranium-series and carbon-14 age data, Arctic Alpine Res. **15**:537-542.

Gascoyne, M., Schwarcz, H. P., and Ford, D. C., 1980, A paleotemperature record for the Mid-Wisconsin in Vancouver Island, Nature. **285**:74-76.

Glover, R. R., Pitty, A. F., and Waltham, A. C., 1977, Caves and karst of the Yorkshire Dales: Guidebook for the International Congress of Speleology, 37p.

Goede, A., Green, D. C., and Harmon, R. S., 1986, Late Pleistocene paleotemperature record from a Tasmanian speleothem, Austral. J. Earth Sci. **33**:333-342.

Goede, A. and Hitchman, M. A., 1983, Late Quaternary climatic change: evidence from a Tasmanian speleothem, in J. C. Vogel, ed., *Late Cainozoic Paleoclimates of the Southern Hemisphere,* Balkema Press, Rotterdam, pp. 221-232.

Goede, A., McDermott, F., Hawkesworth, C. J., Webb, J., and Finlayson, B., 1996, Evidence of Younger Dryas and Neoglacial cooling in a Late Quaternary paleotemperature record from a speleothem in eastern Victoria, Australia, J. Quat. Sci.**11**:1-7.

Goede, A., Veeh, H. H., and Ayliffe, L. K., 1990, Late Quaternary paleotemperature records for two Tasmanian speleothems, Austral. J. Earth Sci. **37**:267-278.

Goodfriend, G. A., 1991, Holocene trends in ^{18}O in land snail shells from the Negev Desert and their implications for changes in rainfall source areas, Quat. Res., **35**:417-426.

Harmon, R .S., 1975, Late Pleistocene paleoclimates in North America as inferred from isotopic variations in speleothems. Unpublished PhD Thesis, McMaster University, Hamilton (Ont.), Canada.

Harmon, R. S., Atkinson, T.C., and Atkinson, J.L., 1983, The mineralogy of Castleguard Cave, Columbia Icefields, Canada, Arctic Alpine Res. **15**:503-516.

Harmon, R .S., Ford, D.C., and Schwarcz, H.P., 1977, Interglacial chronology of the Rocky and MacKenzie Mountains based upon ^{230}Th-^{234}U dating of calcite speleothems, Can. J. Earth Sci. **14**:2543-2552.

Harmon, R. S. and Schwarcz, H. P., 1981, Changes in ^{2}H and ^{18}O enrichment of meteoric water and Pleistocene glaciation, Nature. **290**:125-128.

Harmon, R. S., Schwarcz, H. P., and Ford, D. C., 1978a, Late Pleistocene paleoclimates of North America as determined from stable isotope studies of speleothems, Quat. Res. **9**:54-70.

Harmon, R. S., Schwarcz, H. P., and Ford, D. C., 1978b, Stable isotope geochemistry of speleothems and cave waters from the Flint Ridge-Mammoth Cave System: implications for terrestrial climate change during the period 230,000 to 100,000 years B.P., Jour. Geol. **86**:373-384.

Harmon, R. S., Schwarcz, H. P., Ford, D. C., and Koch, D. L., 1979a, an isotopic paleotemperature record for Late Wisconsinan time in northeast Iowa, Geology. **7**:430-433.

Harmon, R.S., Schwarcz, H.P., and O'Neil, J.R., 1979b, D/h ratios in speleothem fluid inclusions: a guide to variations in the isotopic composition of meteoric precipitation?, Earth Planet. Sci. Lett. **42**:254-266.

Hellstrom, J., McCulloch, M., and Stone, J., 1998, A detailed 31,000-year record of climate and vegetation change from the isotope geochemistry of two New Zealand speleothems, Quat. Res. **50**:167-178.

Hendy, C. H., 1971, The isotopic geochemistry of speleothems – I. the calculation of the effects of different modes of formation on the isotopic composition of speleothems and their applicability as paleoclimate indicators, Geochim. Cosmochim. Acta. **35**:801-824.

Hendy, C. H. and Wilson, A. T., 1968, Paleoclimate data from speleothems, Nature. **219**:48-51.

Hess, J.W., Atkinson, T.C., and Harmon, R.S., Unpublished Data.

Heusser, C. J., Heusser, L. E., and Streeter, S. S., 1980, quaternary temperatures and precipitation for the north-west coast of North America, Nature. **286**:702-704.

Holmgren, K., Karlen, W., and Shaw, P. A., 1995, Paleoclimatic significance of the stable isotopic composition and petrology of a Late Pleistocene stalagmite from Botswana, Quat. Res. **43**:320-328.

Ingraham, N. L., Chapman, J. B., and Hess, J. W., 1990, Stable isotopes in cave pool systems: Carlsbad Caverns, New Mexico, U. S. A., Chem. Geol. **86**:65-74.

Labeyrie, J., Duplessy, J.C., Delibrais, G. and Letolle, R., 1967, Etude des tempereatures des climates anciens par la mesure de l'oxygen-18 du carbone-13 et du carbone-14 dans les concretions des caverenes, in

Symposium on Radioactive Dating and Methods of Low Level Counting, Proceedings of the International Atomic Energy Agency, Vienna, IAEA-SM87/5, pp.153-160.

Lauritzen, S.-E., 1995, high-resolution paleotemperature proxy record for the last interglaciation based on Norwegian speleothems, Quat. Res. **43**:133-146.

Lauritzen, S.-E., Lovlie, R., Moe, D., and Ostbye, E., 1990, Paleoclimate deduced from a multidisciplinary study of a half-million-year-old stalagmite from Rana, northern Norway, Quat. Res. **34**:306-316.

Lauritzen, S.-E. and Onac, B. P., 1999, Isotopic stratigraphy of a last interglacial stalagmite from northwestern Romania: correlation with the deep-sea record and northern-latitude speleothem, J. Cave Karst Studies. **6**:22-30.

Li, W.-X., Lundberg, J., Dickin, A. P., Ford, D. C., Schwarcz, H. P., McNutt, R., and Williams, D., 1989, High precision mass spectrometric uranium-series dating of cave deposits and implications for paleoclimate studies, Nature. **339**:534-536.

Mangarud, J., Sonstergaard., E., and Sejrup, H. P., 1979, Correlation of the Eemian and Weichselian with deep sea oxygen isotope stratigraphy, Quat. Int. **3/4**: 1-4.

Marino, B. D, McElroy, M. B., Salawitch, R. J., and Spauling, W. G., 1992, Glacial-to-interglacial variations in the carbon isotopic composition of atmospheric CO_2, Nature. **357**:461-466.

Millen, T. M. and Dickey, D. N., 1987, a stable isotopic investigation of waters and speleothems in Wind Cave, South Dakota: an application of speleothem isotope paleothermometry, Nat. Speleol. Soc. Bull. **49**:10-12.

Miotke, F.-D., 1974, Carbon dioxide and the soil atmosphere, Abhand. Karst Hohl. Ser. A, **9**:1-49.

O'Neil, J. R., Clayton, R. N., and Mayeda, T. K., 1969, oxygen isotope fractionation in divalent metal carbonates, J. Chem. Phys. **51**:5547-5558.

O'Neil, J. R., Adami, L. H., and Epstein, S., 1975, Revised value for the ^{18}O fractionation between CO_2 and H_2O at 25°C, J. Res. U.S. Geol. Surv. **3**:623-624.

Quade, J., Cerling, T. E., and Bowman, J. R., 1989, Systematic variations in the carbon and oxygen isotopic composition of pedogenic carbonate along elevation transects in the southern Great Basin, United States, Geol. Soc. Amer. Bull. **101**:464-475.

Salomons, W. and Mook, W. G., 1986, Isotope geochemistry of carbonates in the weathering zone, in *Handbook of Environmental Isotope Geochemistry,* P. Fritz and C. Fontes, eds., Elsevier, Amsterdam, **2**:239-270.

Schwarcz, H. P., 1986, Geochronology and isotope geochemistry of speleothems, in *Handbook of Environmental Isotope Geochemistry,* P. Fritz and C. Fontes, eds., Elsevier, Amsterdam, **2**:271-303.

Schwarcz, H. P., Harmon, R. S. Thompson, P., and Ford, D. C., 1976, Stable isotope studies of fluid inclusions in speleothems and their paleoclimate significance, Geochim. Cosmochim. Acta. **40**:657-665.

Schwarcz, H. P. and Yonge, C. J., 1983, Isotopic composition of paleowaters as inferred from speleothem and its fluid inclusions, in *Paleoclimates and Paleowaters: A Collection of Environmental Isotope Studies.* International Atomic Energy Agency, Vienna, IAEA-STI/PUB621, pp.115-133.

Shackleton, N. J., Imbrie, J., and Hall, M. A., 1983, Oxygen and carbon isotope record of East Pacific core V19-30: implications for the formation of deep water in the Late Pleistocene North Atlantic, Earth Planet. Sci. Lett. **65**:233-244.

Shackleton, N. J. and Opdyke, N. D., 1973, oxygen isotope and paleomagnetic stratigraphy of equatorial Pacific core V28-238: oxygen isotope temperatures and ice volumes on a 10^5 and 10^6 year time scale, Quat. Res., **3**:39-53.

Siegenthaler, U., 1979, Stable hydrogen and oxygen in the water cycle, in *Lectures in Isotope Geology*, E. Jager and J.C. Hunziker, eds., Springer, Berlin, pp. 264-273.

Sonntag, C, Munnich, K. O., and Jacob, H., 1983, Variations of deuterium and oxygen-18 in continental precipitation and groundwater, and their causes, in *Variations in the Global Water Budget,* A. Street-Perrot and A. Beran, eds., D. Reidel, Dordrecht, pp 107-124.

Stuiver, M., 1968, Oxygen-18 content of atmospheric precipitation during the last 11,000 years in the Great Lakes region, Science. **162**:994-997.

Talma, A. S. and Vogel., J. C., 1992, Late quaternary paleotemperatures derived from a speleothem from Cango Caves, Cape Province, South Africa: Quat. Res. **37**:203-213.

Talma, A. S., Vogel, J. C., and Partridge, T. C., 1974, isotopic contents of some Transvaal speleothems and their paleoclimate significance, South African J. Sci. **70**:135-140.

Taylor, H. P., 1974, The Application of Oxygen and Hydrogen Isotope Studies to Problems of Hydrothermal Alteration and Ore Deposition: Econ. Geol. **69**:843-883.

Thompson, P., Schwarcz, H. P., and Ford, D. C., 1974, Continental Pleistocene climatic variations from speleothem age and isotopic data, Science, **184**:894-896.

Thompson, P., Schwarcz, H. P., and Ford, D. C., 1976, Stable isotope geochemistry, geothermometry, and geochronology of speleothems from West Virginia, Geol. Soc. Amer. Bull. **87**: 730-1738.

Urbanc, J., Pezdic, J., Bronc, I.K., and Scdoc, D., 1987, Comparison of isotopic composition of different forms of calcite precipitated from fresh water, *Proceedings International Symposium on the Use of Isotope Techniques in Water Resources Development*, International Atomic Energy Agency, Vienna, IAEA-SM-131P, pp. 783-787.

Urey, H. C., 1947, The thermodynamic properties of isotopic substances, J. Chem. Soc. (London), 562-581.

Urey, H. C., Lowenstam, H. A., Epstein, S., and McKinney, C. R., 1951, measurement of paleotemperatures and temperatures of the Upper Cretaceous of England, Denmark, and the southeastern United States, Bull. Geol. Soc. Amer. **62**:399-416.

Wigley, T. M. L., Plummer, L. N., and Pearson, F. J., 1979, mass transfer and carbon isotope evolution in natural water systems, Geochim. Cosmochim. Acta, **42**:1117-1139.

Winograd, I. J., Coplen, T. B., Landwehr, J. M., Riggs, A. C., Ludwig, K. R., Szabo, B. J., Kolesar, P. T., and Revez, K. M., 1992, Continuous 500,000-year climate record from vein calcite in Devils Hole, Nevada, Science. **258**:255-260.

Yonge, C. J., Ford, D. C., Gray, J., and Schwarz, H. P., 1985, stable isotope studies of cave seepage water, Chem. Geol. **58**:97-105.

Yurtsever, M., and Gat, J. R., 1981, Stable isotope hydrology: deuterium and oxygen-18 in the water cycle: in *Atmospheric Waters*, International Atomic Energy Agency, Vienna, IAEA TRS-210, pp.103-142.

INFLUENCE OF DEPOSITIONAL ENVIRONMENT ON DEVILS HOLE CALCITE MORPHOLOGY AND PETROLOGY

Peter T. Kolesar and Alan C. Riggs*

1. ABSTRACT

Devils Hole, a steeply dipping (~80°) tectonically formed planar fissure >165 m deep (Riggs et al., 1994), has been accumulating calcite speleothems that contain at least two different paleoclimate records. Below water table deposits contain a 560,000 year paleoclimate isotopic record (Winograd et al., 1992), while above water table deposits record 120,000 years of changing water table elevation (Szabo et al., 1994). The different depositional environments in Devils Hole control the form of the speleothems.

Below the water table, mammillary calcite (vein calcite of Winograd et al., 1992) precipitates as a massive, uniformly thick coating of very coarsely crystalline calcite. Petrographically, the coating consists solely of densely intergrown, up-to-23-mm long, length-slow crystals. Mammillary calcite is the only calcite morph occurring from approximately 1 meter below water surface to as deep as exploration has gone, currently about 140 meters below water surface.

Rafts and folia form at/near the water table. Calcite rafts precipitate directly at the water surface, supported by surface tension. Folia, which resemble bracket fungi in shape, form on vertical to overhung surfaces and accumulate within the intertidal range of the water table.

Above-water-table deposits consist of popcorn and flowstone. Popcorn probably originates by capillary rise of water from the water table, with subsequent evaporation

* Peter T. Kolesar, Dept. of Geology, Utah State University, Logan, UT 84322-4505. Alan C. Riggs, U. S. Geological Survey, Box 25406, DFC, MS 413, Lakewood, CO 80225-0046.

producing the calcite precipitates. Flowstone deposits form as thin films of calcite-supersaturated water flow over exposed walls. They characteristically have 0.1 to 3 mm thick bands separated by discontinuities.

Because we have been able to integrate the gross morphologic and the petrographic characteristics of several common, and uncommon, speleothem types with their depositional environment, we now have the ability to interpret progressions of depositional environments from petrography alone. From the speleothem type, we can then select the best samples for whichever paleoclimate record we need. For example, mammillary calcite best preserves the paleotemperature record, whereas folia best preserve the paleohydrologic record. Thus we are no longer tied to having to interpret the gross morphology of the calcite deposit to recover the climate records we're after.

2. INTRODUCTION

Devils Hole is a tectonic fissure cave in southern Nevada that extends >165m below ground surface. All but the upper 16m of Devils Hole are below the water table of the Ash Meadows flow system, a regional-scale groundwater flow system whose 32-34 °C waters are slightly supersaturated with respect to calcite. Devils Hole hosts a variety of morpho-logically distinctive speleothem types, each of which seems to have formed in response to a particular set of environmental conditions. The correlation between precipitational envi-ronment and speleothem morphology was noted during visits to Devils Hole to collect samples for paleoclimatic studies. Several of the speleothem types were found to store excellent paleoenvironmental records, including a 120 kyr record of water table variation in Devils Hole (Szabo et al., 1994), and continuous 0.5 My oxygen- and inorganic-carbon-isotope records of groundwater in the southern Great Basin (Winograd et al., 1988; Coplen et al., 1990, 1994; Winograd et al., 1992). In addition, mammillary calcite (= the vein calcite of Winograd et al., 1988; 1992), one of the speleothem types found in Devils Hole, collected from a variety of locations in the southern Great Basin has yielded a 750 kyr-long record of water table decline in the southern Great Basin (Winograd and Szabo, 1988), as well as a 2My-long record of deuterium depletion in ground water that probably resulted from the uplift of the Sierras and the Transverse Ranges (Winograd et al., 1985). Despite the importance of the paleo-environmental records stored in some of the speleothem morphologies, there has been no description of their petrology, except for two abstracts (Kolesar, 1989; Kolesar and Riggs, 1999). The body of this paper describes the petrology of the different speleothem types deposited in Devils Hole, which should allow future investigators to identify each type, even in cases where the diagnostic gross form has been lost.

2.1 Geologic and Hydrologic Setting

Devils Hole is in the arid southern Great Basin, approximately 90 km west-northwest of Las Vegas, Nevada (Fig. 1). Average annual precipitation in Pahrump, NV, about 65 km

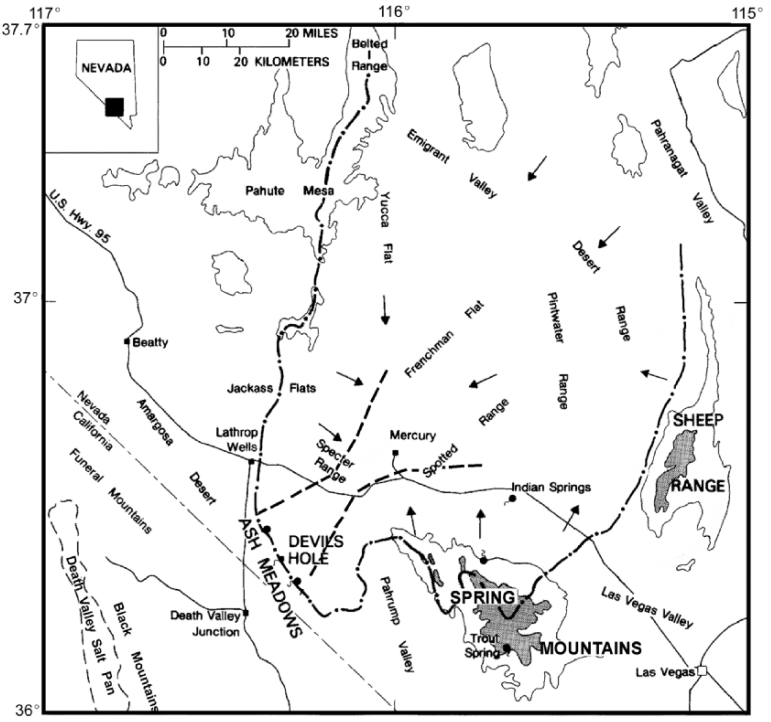

Figure 1. Location of Devils Hole and salient features in its vicinity. Dashed-dotted line marks approximate boundary of the Ash Meadows groundwater system. Dashed line marks approximate boundary of highly transmissive aquifer. They also coincide with approximate position of the Spotted Range-Mine Mountain structural zone. Arrows indicate the inferred direction of groundwater flow. Shaded areas are approximate recharge areas. Adapted from Winograd et al. (1992).

south of, and ~70 m higher than, Devils Hole is 12.09 cm (4.76 in) (www.wrcc.dri.edu, 2000a) and in Beatty, NV, about 65 km northwest of, and ~245 m higher than, Devils Hole, the average annual precipitation is 10.44 cm (4.11 in.) (www.wrcc.dri.edu, 2000b).

The northwest-striking Walker Lane structural corridor is the dominant structural trend in the vicinity of Devils Hole. However, most recent tectonic activity has taken place on conjugate northeast-striking structures of the Spotted Range-Mine Mountain structural zone, (Carr, 1984). Though just outside of the Spotted Range-Mine Mountain structural zone, Devils Hole lies within an area (Fig. 1) in which present stress conditions compress northwest-striking faults, tending to keep them tightly shut (Carr, 1974). Conversely, the less common northeast-striking structures currently are active, tending to open during fault movement. The Cambrian Bonanza King Formation at Devils Hole is one unit of the lower Paleozoic rocks that comprise the regional carbonate-rock-aquifer Ash Meadows ground-water system (Winograd and Pearson, 1976; Winograd and Thordarson, 1975). Because the regional stress field tends to open faults and fractures in the lower Paleozoic rocks, the main flow conduits forming the aquifer are so transmissive that Winograd and Thordarson (1975) found hydraulic gradients as low as 0.06 m/km.

Devils Hole is a steeply dipping (~80°) planar fissure with a surface opening (Fig. 2, 3) of approximately 8 meters by 24 meters in plan view (Carr, 1988). The fissure intersects the regional water table approximately 16 meters below the adjacent land surface (Carr, 1988). Total depth of Devils Hole is unknown, however, mixed-gas scuba exploration has shown that Devils Hole extends more than 145 m below the water table. The water table in Devils Hole has a mixed semi-diurnal solid earth(?) tide with a maximum tidal range of ~11 cm during maximum-amplitude spring tides, and ~3 cm during minimum-amplitude neap tides. These tidal variations are superimposed on other water-level changes due to barometric pressure, seismicity, and long-term water level changes that result from a variety of causes. Strong seismic disturbances can cause the water table to rise and fall rapidly, with consequent resuspension of any uncemented sediment on the footwall.

Surface water temperature is approximately 32°C throughout the year. Water temperature is 34.25°C at a depth of 51 meters (R.J. Hoffman, U.S. Geological Survey, 1990, personal communication). Water in Devils Hole is slightly supersaturated with respect to calcite (saturation index averages about 0.18) with calculated P_{CO2} values from 0.0123 to 0.0141 atm (Plummer et al., 2000). The water has been supersaturated with calcite for at least 500,000 years.

Browns Room (Fig. 3), an air-filled chamber, is accessible only by diving to a depth of about 25 meters in Devils Hole and ascending a different branch of the fissure back to the water table (Hoffman, 1988, p. 6; Riggs et al., 1994). Browns Room has a blocky shape that results from breakdown blocks falling from between splays of the fault (Riggs et al., 1994). The room extends approximately 9 meters above the present water table. An 8 m by 7 m pool of warm Ash Meadows groundwater occupies the southwest end of Browns Room. Millers

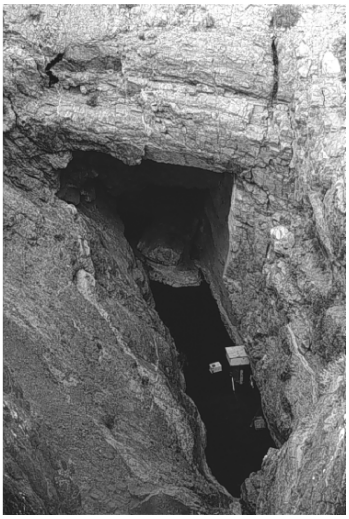

Figure 2. View northeast into Devils Hole. The left side of the opening is the footwall of the fault. The width of the opening at the water table is about 2 to 2.5 meters.

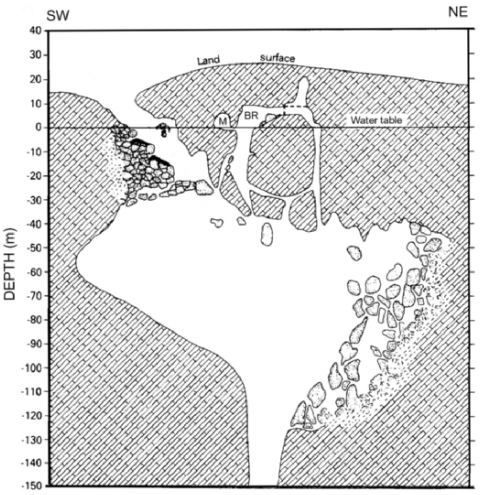

Figure 3. Map of Devils Hole. BR is Browns Room, and M is Millers Chamber. Mammillary calcite is the only speleothem morph below the water table. Rafts currently form on the surface on the main chamber and in Browns Room. Folia only form in Browns Room, and popcorn forms in both Millers Chamber and Browns Room.

Chamber is a second, much smaller air-filled room that is connected to Browns Room by a short, water-filled passage.

3. MORPHOLOGIC DESCRIPTION

Devils Hole contains five distinct morphologies of speleothems that are readily discriminated by the naked eye. Their form is mainly a consequence of the carbonate precipitation environment, that is, whether the carbonate precipitated above, at, or on the water table in humid air, or below the water table. As a result, once we learn to recognize the different speleothem morphologies, and relate them to their precipitation environments, we can quickly begin to reconstruct the progression of environmental conditions at a site from the arrangement of speleothem morphologies deposited there.

3.1 Mammillary Calcite

By far the most common of the precipitated morphologies, mammillary calcite forms a massive, uniformly thick coating of very coarsely crystalline calcite on most underwater surfaces. The outer surface of the coating has many gently dome-shaped protuberances (Fig. 4) that may result from convexities in the underlying bedrock surface on which the coating precipitated. In the Devils Hole system, mammillary calcite forms only below the water table (Kolesar and Riggs, 1999), and is the only coating present from approximately 1 meter below the water table to the present limit of exploration about 140 meters below the water surface. It is mammillary calcite that preserves the TIMS U-series dated (Ludwig et al., 1992) 560-kyr-long paleoclimate record of $\delta^{18}O$ (Winograd et al., 1988, 1992) and $\delta^{13}C$ (Coplen et al., 1990, 1994) changes.

In thin section, mammillary calcite resembles the palisade calcite of Folk and Assereto (1976), with very large (up to 23 mm long and 2 mm wide), columnar (Logan and Semeniuk, 1976) crystals oriented mostly normal to the surfaces it coats. Each columnar crystal is

Figure 4. Mammillary calcite coating the walls of Devils Hole about 23 m below water table. Note the gently rounded protuberances that characterize the coating. A core of mammillary calcite about 42 cm thick was recovered from approximately 30 meters below the water table. Photograph courtesy of Ray J. Hoffman.

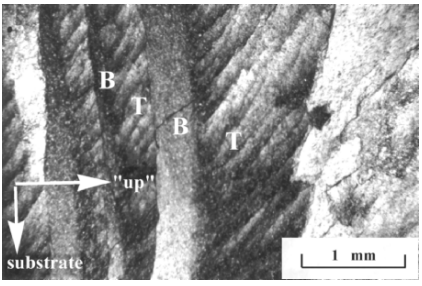

Figure 5. Photomicrograph of mammillary calcite in cross-polarized light. Note the closely packed "comb" structure of the crystals with the "teeth" (T) of the comb meeting the "back" (B) of the comb at an acute angle. White arrow indicates direction to the substrate.

composed of numerous elongate subcrystals, or crystallites. The crystallites commonly form patterns that resemble closely packed teeth on a comb (Fig. 5). Elongate crystallites have the c-axis generally oriented at greater than 60° to the direction of elongation and are length-slow, in marked contrast to the observation of Kendall and Broughton (1978) who found most of the speleothem calcite they examined to be length-fast ("normal"). Crystal growth of the compound crystals is approximately normal to the substrate. This suite of petrographic characters allows us to distinguish mammillary calcite from flowstone in complex samples.

Mammillary calcite on the hanging wall of Devils Hole is white, translucent, and unbanded. Footwall mammillary calcite, on the other hand, is strongly banded because silt and clay debris that settled on the up-facing surfaces were incorporated into the mammillary coating by continuing calcite precipitation. Well-developed bands on cross sections of up-facing mammillary calcite surfaces disappear abruptly wherever the depositional surface rolls over to vertical or overhanging.

Rapid accumulation of silt and clay on mammillary surfaces stops crystal growth. Large numbers of very small, equant to columnar crystals that grade quickly to a few large columnar crystals (Fig. 6) mark the reinitiation of crystal growth.

Growth rate of mammillary calcite ranges from about 0.3 to 1.3 mm/1,000 years (Ludwig et al., 1992; Plummer et al., 2000).

Mammillary calcite is very dense, with porosities much less than 1%. Pore spaces are of two different types. The first type consists of irregularly shaped pore spaces with fluid inclusions that are commonly oriented parallel with the crystallite boundaries. In "traditional" speleothems, spindle-shaped inclusions mark the sites where columnar crystals have coalesced (Kendall and Broughton, 1978). In mammillary calcite, the irregular inclusions probably mark

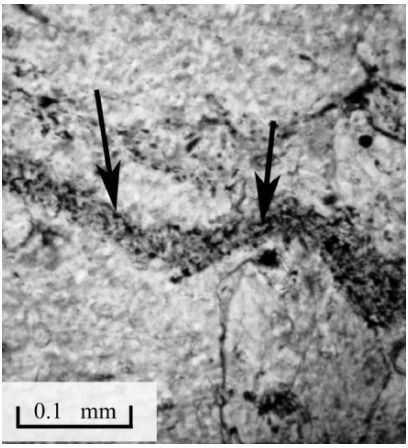

Figure 6. Photomicrograph (plane polarized light) of a zone of irregular pore spaces (arrows) that are elongated parallel with buried crystal terminations. Pore spaces probably resulted from small irregularities on the upper surfaces of the crystals created by accumulations of clay-sized debris.

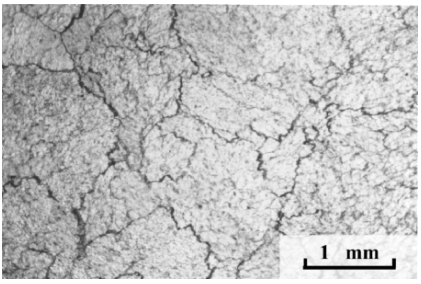

Figure 7. Photomicrograph of mammillary calcite perpendicular to the long crystal axis. Note the very irregular crystal outlines. Partial coalescence of these irregular crystals may be responsible for the irregular nature of fluid inclusions in mammillary travertine. Plane polarized light.

the sites of juncture of "micro-crystals" or crystallites that have coalesced to form large columnar crystals. Kendall and Broughton commented that most of the speleothems they studied were composed of length-fast calcite. In such crystals the c-axis is parallel with the long dimension of the crystal, and views of thin sections cut normal to the c-axis show the coalescence of triangular crystallites (Kendall and Broughton, 1978, Fig. 7). Although mammillary calcite crystals are also columnar, they are length-slow, and sections cut normal to the long axis of the crystals (approximately parallel with the c-axis) show very irregular crystal outlines (Fig. 7). This suggests that the irregularity of inclusion shape in mammillary calcite is a direct consequence of the crystal morphology.

The second pore and fluid inclusion type was formed when debris settling onto up-facing mammillary calcite surfaces trapped spaces in the plane of the crystal terminations (i.e., parallel to the growing surface) (Fig. 6).

3.2 Rafts, Folia, Popcorn, and Flowstone

Calcite precipitated at/on the water table or in the intertidal range forms as rafts and as folia.

3.2.1 Rafts

Calcite that precipitates directly at the water-air interface forms rafts of calcite crystals. The rafts float on the surface, supported by surface tension (Hill and Forti, 1997). When the water surface is disturbed by wind, seismicity, tidal fluctuations, flood inflow, or divers' air bubbles, the rafts sink and often become cemented to the bottom (Fig. 8) (Riggs et al., 1994). Rafts start out as roughly circular aggregations of crystals that, if undisturbed, coalesce into large (up to 10 cm across) aggregations that are variable in general outline. Because the water surface in Browns Room is protected from disturbance by wind or flood inflow, rafts in Browns Room consistently are much larger than those that form in the open part of Devils

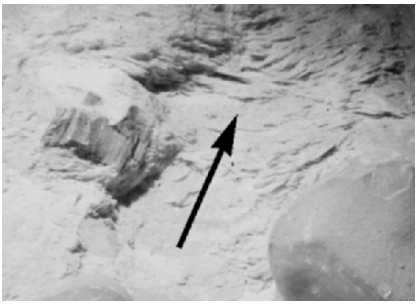

Figure 8. Accumulation of rafts (arrows) at a depth of about 28 meters below Browns Room in Devils Hole. Rafts have been cemented in place by continued precipitation of mammillary calcite. Thickness of bedrock block left of the arrow is about 15 cm.

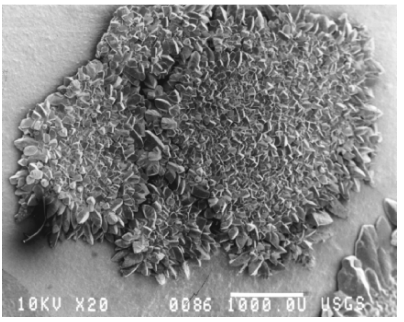

Figure 9. Scanning electron micrograph of the underside of a calcite raft that precipitated at the water-air interface in Browns Room. Perimeter has long crystals, whereas the central part of the raft is characterized by mostly equant crystals. Four small rafts coalesced to form this large one. Scale bar is 1 mm.

Hole, which commonly appear as a whitish dust haze on the water surface.

Because rafts grow on the water's surface, their upper surfaces are vastly different from their under surfaces. Crystal growth takes place only below water, so that upper surfaces are flat and nearly featureless, except for the holes where crystals forming the raft have incompletely coalesced, especially along the boundaries where two or more rafts have fused to form a larger one. Euhedral length-fast columnar crystals up to a mm or longer com-monly project out and down from the edges of the rafts, whereas the bottom surfaces nearer the center are studded with equant euhedral calcite crystals averaging about 5-10 um (Fig. 9). Rafts from Devils Hole are similar to the single-sided spar calcite rafts described by Jones (1989), but without the paper-thin soluble core.

While rafts make up an insignificant volume of the precipitated material in Devils Hole, their presence does have a an impact on underwater exploration of Devils Hole. Because rafts only form on a free water surface, and because they sink to the bottom whenever the surface tension of that free surface is disturbed, presence of rafts on the footwall in Devils Hole tells us that there is an air-filled chamber above.

3.2.2 Folia

Folia (Hill and Forti, 1997, p. 73-74) are a distinctive speleothem morphology that are strikingly beautiful when well developed (Fig. 10). Folia, which are abundant in Browns Room (Riggs et al., 1994; Kolesar and Riggs, 1999), appear to form only under a very specific combination of conditions which include: (i) a vertical-to-overhanging surface; (ii) an air-water interface, such as a pool surface; (iii) relatively frequent vertical oscillations of the air-water interface; (iv) pCO_2 gradient from the water to the air; (v) calcite saturation index of the water sufficiently large that when the pCO_2 of the water equilibrates with that of the air, the water becomes distinctly supersaturated with respect to calcite; (vi) high humidity; and (vii) no major biological activity. All of these conditions are fulfilled in Browns Room, where the diurnal tides cause water level to migrate up and down; the pCO_2 gradient from water to air is steep enough that outgassing drives the water well into calcite supersaturation; high humidity and minuscule biological activity are assured by poor communication with the outside world and perpetual darkness. In Browns Room, the intertidal zone is the 3-to-11-cm-high (depending primarily on the phase of the moon) band of wall centered at mean pool-surface level that is alternately submerged and exposed to the air. On a falling tide, the thin film of water left on the wall outgases CO_2, driving rapid precipitation of dissolved calcite. The next high tide exchanges the spent water film with fresh, and the cycle repeats, resulting in unusually rapid precipitation of calcite on the chamber walls at the level of the intertidal zone. The reason foliar morphology develops on vertical-to-overhanging surfaces is less clear, but probably has to do with the preferential precipitation of carbonate where the pCO_2 gradient from the water film to the atmosphere is steepest -- i.e. away from the pool surface (up) and away from the wall (out). The other player, gravity, tends to drag the water film down. Folia are an expression of the final compromise; they are wedge-shaped in vertical section and grow out and slightly down.

From the material presented above it's apparent that folia indicate the elevation of water table at the time they formed. As water table rises or falls, a trail of folia is left in its wake. The presence of well-developed folia on the ceiling of Browns Room, at least 9m above the present water table clearly demonstrates the long-term range of water table fluctuation, as

well as signaling the ubiquity of folia on all vertical-to-overhanging subaerial surfaces in Browns Room, though in many places the folia are covered in turn by flowstone and popcorn (described below). A final point is that a rising water table will deposit folia over the deposits on the previously subaerial walls – typically bare bedrock, flowstone, popcorn, or older folia left from a previous highstand. Similarly, a falling water table will deposit folia over the previously submerged surface – typically mammillary calcite in Devils Hole. So by identifying the material on which the folia precipitated, we can generally tell whether the water table was rising or falling when the folia formed.

Internally, folia generally consist of large numbers of relatively small (a few tenths of a mm to a few mm) equant to slightly elongate length-fast crystals (Fig. 11). Initial precipitates exhibit a dendritic habit, with most of the growth occurring on the upper surface of the folia. With continued calcite precipitation, the very open, dendritic habit fills in, with eventual formation of relatively long (up to 10 mm or so) columnar, length-fast calcite crystals.

Folia commonly exhibit internal banding. Most foliar bands, like the foot-wall-mammillary-calcite bands described earlier, are accumulations of silt- and clay-sized detritus that settled on top of the folia during growth. Too-rapid sediment accumulation on the actively growing rhombohedral crystal surfaces disrupts crystal growth. Large numbers of very small "seed" crystals on top of the sediment accumulations (Fig. 12) mark the resumption of calcite precipitation.

3.2.3 Popcorn

Popcorn (Hill and Forti, 1997; Riggs et al., 1994), a speleothem type common in many caves, is abundant in the perpetually humid Browns Room, and especially in Miller's Chamber

Figure 10. Well-developed folia in Browns Room. Because folia form within the semidiurnal tide range of the aquifer, this one meter exposure of folia has recorded a falling water table.

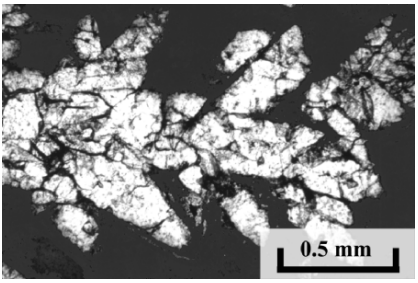

Figure 11. Photomicrograph (plane polarized light) of the crystal morphology characteristic of folia. Note the dendritic habit and the very porous nature of the precipitate. The dark material surrounding the crystals is opaque epoxy resin used to impregnate the sample before thin sectioning.

(Fig. 13), but does not occur on the dry walls of Devils Hole proper. Hill and Forti (1997) ascribe the precipitation of popcorn calcite to subaerial evaporation of calcite-rich water supplied by; capillary rise of water up a cavern wall, condensation of water vapor on cavern walls, splash from dripping water, or seepage of groundwater through cavern walls. Subsequent evaporation of the water causes the calcite to precipitate into globular-to-dendritic efflorescences. Alternatively, Dublyansky and Pashenko (1997) have suggested that popcorn results from deposition of aerosol-borne material. Because popcorn seems limited to the high humidity areas of Millers Chamber, where aerosol inputs are highly unlikely, and Browns Room, we believe that condensation of water vapor on cavern walls is most plausibly responsible for popcorn formation in Devils Hole.

Popcorn deposits are composed of radiating to subradiating (Logan and Semeniuk, 1976) accumulations of acicular crystals. The acicular crystals coalesce over time to form columnar crystals with aligned elongate fluid inclusions (Fig. 14) like those described by Kendall and Broughton (1978). The dense, coalesced calcite or aragonite crystals exhibit sweeping extinction.

3.2.4 Flowstone

The final Devils Hole speleothem type is flowstone (Hill and Forti, 1997, p. 70-72), which precipitated from films of calcite-supersaturated water flowing down the exposed walls of Browns Room. Flowstone deposits in Browns Room characteristically are banded in cross section, with bands from about 0.1 to 3 mm thick (Fig. 15, 17). Each band is a depositional unit, with major or minor discontinuities on either side. Outer surfaces of bands commonly are etched and corroded, and may have thin coatings of clay-sized material. The inner, older bases of the bands are composed of large numbers of micron- and decami-cron-sized equant calcite crystals. The equant crystals rapidly grade into fewer elongate, length-fast calcite

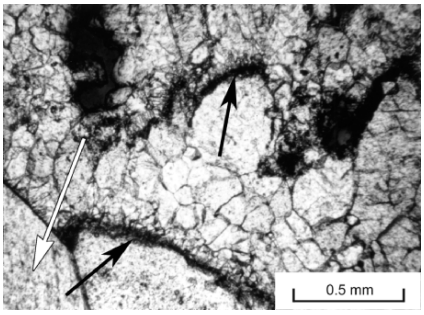

Figure 12. Foliar growth is commonly discontinuous. This photomicrograph (plane polarized light) displays two well-developed discontinuities (black arrows) caused by accumulations of silt and clay-sized debris, topped by numerous small seed crystals that mark resumption of deposition. The white arrow points toward the substrate. "Up" is toward the viewer.

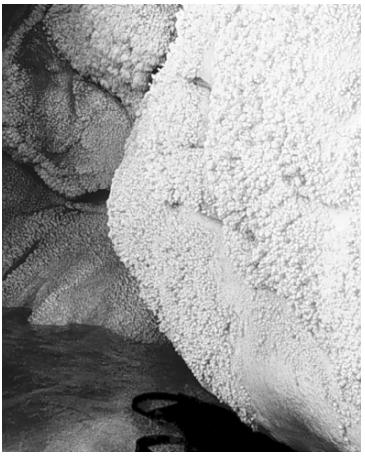

Figure 13. Popcorn covering surfaces in Millers Chamber, Devils Hole. Swim fins at bottom center, for scale.

crystals (Fig. 15). Devils Hole flowstone petrography is most similar to the petrography of stalactites described by Kendall and Broughton (1978).

Individual flowstone bands are petrographically variable over their extent. One part of a band may consist of elongate, length-fast calcite crystals, whereas other parts of the same band may be composed of accumulations of approximately equant, micron- and decamicron-sized calcite together with abundant clay-sized material. Changes along a band typically are gradational, and the differences between the different parts of a particular band is a consequence of their orientation. Up-facing surfaces accumulate much clay-sized debris and equant calcite crystals, whereas down-facing parts of the same band are composed of debris-free elongate calcite crystals.

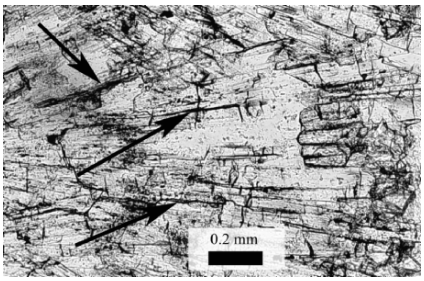

Figure 14. Photomicrograph (plane polarized light) of coalesced aragonite needles in Millers Chamber popcorn deposit. Arrows point to several of the elongate inclusions developed along the seams where adjacent needles coalesced.

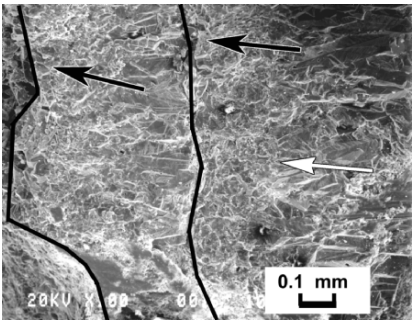

Figure 15. Scanning electron micrograph of flowstone from Devils Hole. The white arrow points toward the substrate. Flowstone characteristically has many irregular depositional discontinuities, and two discontinuities are shown here (solid lines). Note at the top (right) of each discontinuity the many small crystals (black arrows) that indicate recommencement of rapid precipitation. The small crystals rapidly grade into a few large, length-fast crystals.

4. DISCUSSION

4.1 Possible Cause of Length-slow Calcite in Mammillary Deposits.

Kendall and Broughton (1978) examined speleothems from what may be considered "normal" caves, that is, caves in karst areas. Their observation that most of the speleothems they studied were composed of columnar, length-fast calcite crystals is counter to our observation that Devils Hole mammillary deposits are composed of length-slow calcite crystals. One possible interpretation for the difference in crystal orientation may be related to the difference in rates of crystal growth. "Normal" speleothem growth rates are on the order of 50 to 80 mm/ka (Johnson et al., 2001; Daoxian, 2001), whereas the documented growth rate of mammillary calcite is only 1.3 mm/ka at its maximum. The c-axis may be the most favorably oriented axis for growth during rapid precipitation.

4.2 Rapid Interpretation of Depositional Site

Because new calcite in Devils Hole and Browns Room precipitates over material that is already present, a cross section from the underlying bedrock to the outer surface of a deposit is a stratigraphic section. The contact between the coating and the bedrock is oldest, and the outermost surface is youngest.

Figure 16 shows the broken edge of an approximately 20 cm-thick coating on the above-water-table wall in Browns Room. Examination of the section shows that three different units make up the deposit. Based only on the morphology, two of the units are folia, and the third unit is flowstone.

Figure 17 is a positive print of a thin section from a section of Brown's Room wall coating. The sample was taken approximately 6 meters above the present water table and from the general vicinity of the section shown in Fig. 16. Different crystallographic and morphologic zones are marked on the figure. Note several features:

The sample is morphologically and crystallographically complex. The far left side of the figure exhibits the characteristic mammillary calcite morphology. Directly to the right of the mammillary calcite is a typical band of folia. The right edge of the foliar band is a transition zone containing both mammillary calcite and folia. To the right of the transition zone is a band of mammillary calcite. The right edge of the mammillary calcite zone is etched and corroded, with broadly rhombic crystal terminations. Finally, directly to the right of the etched and corroded zone is the youngest deposit-flowstone.

This sample, collected about + 6 meters above the datum, current water table, is a graphic record of a changing water table in Devils Hole. The water table was originally higher than

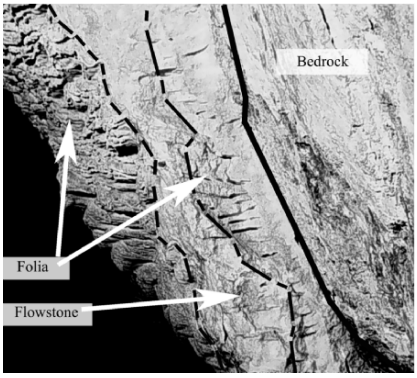

Figure 16. Cross section of a wall coating in Browns Room, Devils Hole. The coating is approximately 20 cm thick. The thick, solid line marks the contact between the calcite coating to the left, and the Cambrian Bonanza King Formation bedrock to the right. Folia and flowstone morphologies (arrows) are immediately distinguishable.

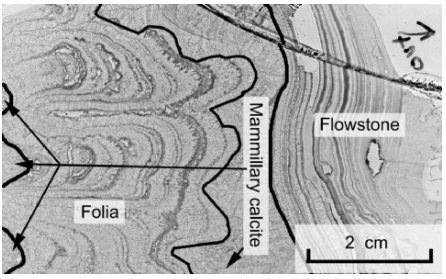

Figure 17. Positive print of a 2″×3″ thin section from Browns Room (DH-BR-2) that shows a very complex depositional history. The different calcite morphologies are labeled. The substrate is toward the left side of the figure. See text for interpretation.

+6 meters as indicated by the innermost mammillary calcite. It then fell to +6 meters, as shown by the folia, stayed there for probably less than 1,000 years (based on the up-to-8-cm/ka growth rate of folia), then rose above +6 meters - the outer mammillary calcite layer. After several thousand years (growth rate of mammillary calcite is approximately 0.3 - 1.3 mm/ka), the water table dropped below +6 meters as indicated by the youngest deposit, flowstone. Szabo et al. (1994) presented a 120 kyr chronology of water table rise and fall in the southern Great Basin, based on these same criteria.

4.3 Implications of flowstone

The presence of flowstone coatings on the walls of Browns Room raises an interesting possibility for an additional paleoclimate(?) record. The flowstone originates as thin films of carbonate-saturated water flow over the exposed walls, with the most probable source for that carbonate-saturated water being external to Browns Room, that is, from the land surface. Therefore, the flowstone is likely recording periods of local recharge directly into Browns Room.

5. CONCLUSIONS

Gross morphology of speleothems deposited in Devils Hole reflects their depositional environment. Mammillary calcite is deposited subaqueously. Because the water is only slightly supersaturated with respect to calcite (SI = 0.16 to 0.21), growth rate is slow, resulting in a very dense deposit composed of complex, elongate, length-slow crystals. Because mammillary calcite is so dense, and because it has precipitated below the water table continuously for more than a half million years, it has recorded and retained an outstanding paleoclimate record.

Folia are precipitated in the intertidal range on vertical-to-overhanging walls. Because CO_2 degassing at the water surface causes the water to become supersaturated with respect to calcite, precipitation of calcite occurs rapidly, forming many small crystals. These crystals tend to produce a dendritic habit. The deposits are quite porous, and have a readily recognizable gross morphology that resembles bracket fungi. Petrographic characteristics of folia are also distinct from flowstone and mammillary calcite. Because folia are precipitated in the intertidal range, they chronicle the behavior of the water table over time.

Flowstone precipitates from carbonate-saturated, externally derived water as it flows down the above-water-table walls of Browns Room. Its crystal structure is most similar to the speleothems described by Kendall and Broughton, (1978) and is petrographically distinct from folia, rafts, and mammillary calcite. By identifying flowstone deposits in Devils Hole, we have a second proxy record for the elevation of the water table

In the search for tools to help the paleoclimatologist or the speleologist interpret what (s)/he sees in a cave, we have been able to integrate the gross morphologic and the petrographic characteristics of several common, and uncommon, speleothem types with their depositional environment. As a result, we now have the ability to interpret progressions of paleoclimatic conditions from either the petrography of a deposit or the gross morphology of a deposit. We are no longer limited to having to interpret the gross morphology of the calcite deposit to recover the climate records we're after.

6. REFERENCES

Carr, W. J., 1974, Summary of tectonic and structural evidence for stress orientation at the Nevada Test Site, *U.S. Geol. Survey Open-File Report 74-176.*

Carr, W. J., 1984, Regional structural setting of Yucca Mountain, southwestern Nevada, and Late Cenozoic rates of tectonic activity in part of the southwestern Great Basin, Nevada and California, *U. S. Geol. Survey Open-File Report 84-854.*

Carr, W. J., 1988, Geology of the Devils Hole area, Nevada, *U.S. Geol. Survey Open-File Report 87-560*, 32 p.

Coplen, T. B., Winograd, I. J., Ludwig, K. R., Szabo, B. J., Landwehr, J. M., Kolesar, P.T., and Hoffman, R. J., 1990, Continuous 500,000-year climatic record from Great Basin vein calcite: 2. the $\delta^{13}C$ time series, *Geol. Soc. Amer. Abs.with Prog.*, **22**(7):A209.

Coplen, T. B., Winograd, I. J., Landwehr, J. M., and Riggs, A.C., 1994, 500.000-year stable carbon isotopic record from Devils Hole, Nevada, *Science*, **263**:361-365.

Daoxian, Yuan, 2001, IGCP in 1993: report to IGCP, (March 25, 2001) http://www.glnet.edu.cn/KDL/IGCP/IGCP299/1994/part1.htm

Dublyansky, Y. V., and Pashenko, S. E., 1997, Cave popcorn; an aerosol speleothem?, in: *Proceedings of the 12th international congress of Speleology; Symposium 7, Physical speleology; Symposium 8, Karst geomorphology*, P. Y. Jeannin, ed., Proceedings of the International Congress of Speleology 12, **1**:271-274.

Folk, R. L., and Assereto, R., 1976, Comparative fabrics of length-slow and length-fast calcite and calcitized aragonite in a Holocene speleothem, Carlsbad Caverns, New Mexico, *Jour. Sed. Pet.*, **46**:486-496.

Hill, C.A., and Forti, P., 1997, Cave Minerals of the World, 2nd ed., National Speleological Society, Huntsville, AL, 463 p.

Hoffman, R. J., 1988, Chronology of diving activities and underground surveys in Devils Hole and Devils Hole Cave, Nye County, Nevada, 1950-1986, *U.S. Geol. Survey Open-File Report 88-93*, 12 p.

Johnson, K. R., Ingram, B. L, Roark, E. B., and Lamble, G., 2001, Major and minor element variations in speleothems as a high resolution paleoclimatic record (March 25, 2001); http://alspubs.lbl.gov/AbstractManager/uploads/johnson.pdf

Jones, B., 1989, Calcite rafts, peloids, and micrite in cave deposits from Cayman Brac, British West Indies, *Can. Jour. Earth Sci.*, **26**:654-664.

Kendall, A. C., and Broughton, P. L., 1978, Origin of fabrics in speleothems composed of columnar calcite crystals, *Jour. Sed. Pet.*, **48**:519-538.

Kolesar, P. T., 1989, Calcite deposits in Devil's Hole, Nevada: A record of the fall and rise of the water table in the southern Great Basin, *Geol. Soc. Amer. Abs. with Prog.*, **21(5)**: 103.

Kolesar, P. T., and Riggs, A. C., 1999, Form and formation: speleothems in Devils Hole, a tectonic cave in southern Nevada, *Geol. Soc. Amer. Abs. with Prog.*, **31**(7):A-90.

Logan, B. W., and Semeniuk, V., 1976, Dynamic metamorphism; processes and products in Devonian carbonate rocks, Canning Basin, Western Australia, *Geol. Soc. Australia, Inc., Spec. Pub. No. 6*, 138 pp.

Ludwig, K. R., Simmons, K. R., Szabo, B. J., Winograd, I. J., Landwehr, J. M., Riggs, A. C., and Hoffman, R. J., 1992, Mass-spectrometric ^{230}Th - ^{234}U - ^{238}U dating of the Devils Hole calcite vein, *Science* **258**:284-287.

Plummer, L. N., Busenberg, E., and Riggs, A. C., 2000, In-situ growth of calcite at Devils Hole, Nevada: Comparison of field and laboratory rates to a 500,000 year record of near-equilibrium calcite growth, *Aquatic Geochem.*, **6**:257-274.

Riggs, A. C., Carr, W. J., Kolesar, P. T., and Hoffman, R. J., 1994, The tectonic speleogenesis of Devils Hole, Nevada, and implications for hydrogeology and the development of long, continuous paleoenvironmental records, *Quat. Res.*, **42**:241-254.

Szabo, B. J., Kolesar, P. T., Riggs, A. C., Winograd, I. J., and Ludwig, K. R., 1994, Paleoclimatic inferences from a 120,000-yr calcite record of water-table fluctuation in Browns Room of Devils Hole, Nevada, *Quat. Res.*, **41**:59-69.

Winograd, I. J., and Pearson, F. J., Jr., 1976, Major carbon-14 anomaly in a regional carbonate aquifer--Possible evidence for mega-scale channeling, south-central Great Basin, *Water Resources Res.* **12**:1125-1143.

Winograd, I. J., and Szabo, B. J., 1988, Water-table decline in the south-central Great Basin during the Quaternary period--implications for toxic waste disposal, in: *Geologic and Hydro-logic Investigations of a Potential Nuclear Waste Disposal Site at Yucca Mountain, U.S. Geol. Surv. Bulletin 1790*, pp. 147-152.

Winograd, I. J., and Thordarson, W., 1975, Hydrogeologic and hydrochemical framework, south-central Great Basin, Nevada-California, with special reference to the Nevada Test Site: *U.S. Geol. Surv. Prof. Paper 712-C*, 126 p.

Winograd, I. J., Szabo, B. J., Coplen, T. B., Riggs, A. C., and Kolesar, P. T., 1985, Two-million-year record of deuterium depletion in Great Basin ground waters: *Science* **227**:519-522.

Winograd, I. J., Szabo, B. J., Coplen, T. B., and Riggs, A. C., 1988, A 250,000-year climatic record from Great Basin vein calcite; implications for Milankovitch theory, *Science* **242**:1275-1280.

Winograd, I. J., Coplen, T. B., Landwehr, J. M., Riggs, A. C., Ludwig, K. R., Szabo, B. J., Kolesar, P. T., and Revesz, K. M., 1992, Continuous 500,000-year climatic record from vein calcite in Devils Hole, Nevada, *Science* **258**:255-260.

www.wrcc.dri.edu, 2000a, http://www.wrcc.dri.edu/cgi-bin/cliNORMtM.pl?nvpahr (January 02, 2000)

www.wrcc.dri.edu, 2000b, http://www.wrcc.dri.edu/cgi-bin/cliNORMtM.pl?nvbeat (January 02, 2000)

SPELEOTHEMS FROM THE HIGH-ALPINE SPANNAGEL CAVE, ZILLERTAL ALPS (AUSTRIA)

Christoph Spötl, Augusto Mangini, Stephen J. Burns, Norbert Frank, and Rudolf Pavuza*

1. ABSTRACT

Spannagel Cave is a fairly extensive cave system (currently nine kilometers of explored passages) which developed in Jurassic marbles sandwiched between gneiss in the western part of the Zillertal Alps, Tyrol. The cave system extends from 2195 m to 2521 m a.s.l. and is adjacent to the actively retreating Hintertux Glacier. Marginal moraines of the glacial advance during the "Little Ice Age" (about 1850) show that even fairly recently parts of the cave system were in a subglacial position. Despite its high altitude well above timber line, this cave hosts speleothems, some of which are actively forming today. Modern speleothem deposition includes stalactites, soda straws, stalagmites, moonmilk and flowstones, whereas the latter are the most abundant variety of ancient speleothems in this cave. Th-U TIMS dating demonstrates that speleothem deposition occurred repeatedly during the past few hundred thousand years at this site. Stable isotope data of modern and ancient speleothems yielded a large spread both in C (-11.1 to +10.8‰ VPDB) and O (-15.5 to -6.2‰ VPDB). The C isotope values are biased toward high and commonly positive values, reflecting a low proportion of soil-derived CO_2 in the karst system, largely buffered by the host rock. C isotope values as high as +10.8‰ indicate kinetically controlled fractionation. Speleothems of Holocene age show O isotopic compositions consistent with near-equilibrium fractionation from modern dripwaters. In contrast, fossil speleothems commonly show lower O isotope values and higher and more variable C isotope values, reflecting the impact of isotopically depleted glacier meltwaters and the sensitivity of the karst system to changes in the high-alpine vegetation cover.

* Christoph Spötl, Institut für Geologie und Paläontologie, Universität Innsbruck, Innrain 52, 6020 Innsbruck, Austria. Augusto Mangini, Norbert Frank, Institut für Umweltphysik, Forschungsstelle Radiometrie, Heidelberger Akademie der Wissenschaften, Im Neuenheimer Feld 229, 69120 Heidelberg, Germany. Stephen J. Burns, Department of Geosciences, Morrill Science Center, University of Massachusetts, Amherst, MA 01003, USA. Rudolf Pavuza, Naturhistorisches Museum Wien, Karst- und Höhlenkundliche Abteilung, Museumsplatz 1, 1070 Wien, Austria.

2. INTRODUCTION

The Eastern Alps of Austria comprise several long-known, classic karst regions, most notably the Northern Calcareous Alps, which contain many extensive cave systems. Caves are conspicuously less abundant in the Central-Alpine region, which constitutes — tectonically speaking — the backbone of the East Alpine segment of the Alpine orogen (e.g., Bauer and Zötl, 1972). A noteworthy exception is the caves close to the Hintertux Glacier in Tyrol. The main entrance to the system known as Spannagel Cave is located at 2521 m a.s.l. and the entire system is located above modern timber line (which is approximately 1900-2000 m in this region). With over nine kilometers of surveyed passages (as of beginning of year 2002) the cave is not only the largest in Tyrol (a small portion of the cave is developed as a tourist cave), it is also interesting in terms of its speleothems, some of which are active at present. As part of a larger paleoenvironmental research project, this cave system and its speleothems are currently being investigated in detail. In this article we give a first description of this exceptional cave and its deposits.

3. GEOLOGIC SETTING

Spannagel Cave is developed in Upper Jurassic marbles (Hochstegen Marble) within the western portion of the Zillertal Alps (Fig. 1). This area is the western segment of the "Tauern Window", a prominent tectonic feature of the Eastern Alps where medium- to high-grade metamorphic units of the former Penninic ocean are exposed due to tectonic uplift and large-scale lateral extension (Selverstone, 1988; Fügenschuh et al., 1997; Lammerer and Weger, 1998). Despite the strong tectonic overprint, the Hochstegen Marble is still in primary sedimentary contact with the underlying basement, a green-grayish phengite-rich gneiss which represents metamorphosed arkosic sediments of (?)Permo-Triassic age (Höck 1969, 1970). In the area northwest of the Spannagel Hut the Hochstegen Marble is exposed at the surface, and the cave is mostly between 20 and 30 m below the surface. Several additional cave entrances showing a high extent of destruction by frost splitting are present. With one exception none of these caves has a proven connection to the main cave system. Toward the west the Hochstegen Marble is tectonically overlain by a slab of granitic gneiss (Permian Zentralgneis — Fig. 1) which results in greater overburden (up to 190 m at the westernmost cave limit). In this area, the adjacent Hintertux Glacier is actively retreating. A prominent lateral moraine deposited during the mid-19th century "Little Ice Age" advance separates the largely unvegetated glacial foreland in the west (where Zentralgneis crops out) from the karstified carbonate terrane to the east. Inasmuch as the western branch of the cave system extends some 650 m beyond the moraine ridge, at least half of the cave was in a subglacial position during the "Little Ice Age" (Fig. 1).

The Hochstegen Marble is a medium to dark gray cherty marble showing rhythmic bedding and banding with individual layers typically a few centimeters thick. When crushed, a H_2S smell is commonly perceptible. The highly regular internal stratigraphy most likely reflects the primary sedimentary bedding of this basinal pelagic carbonate

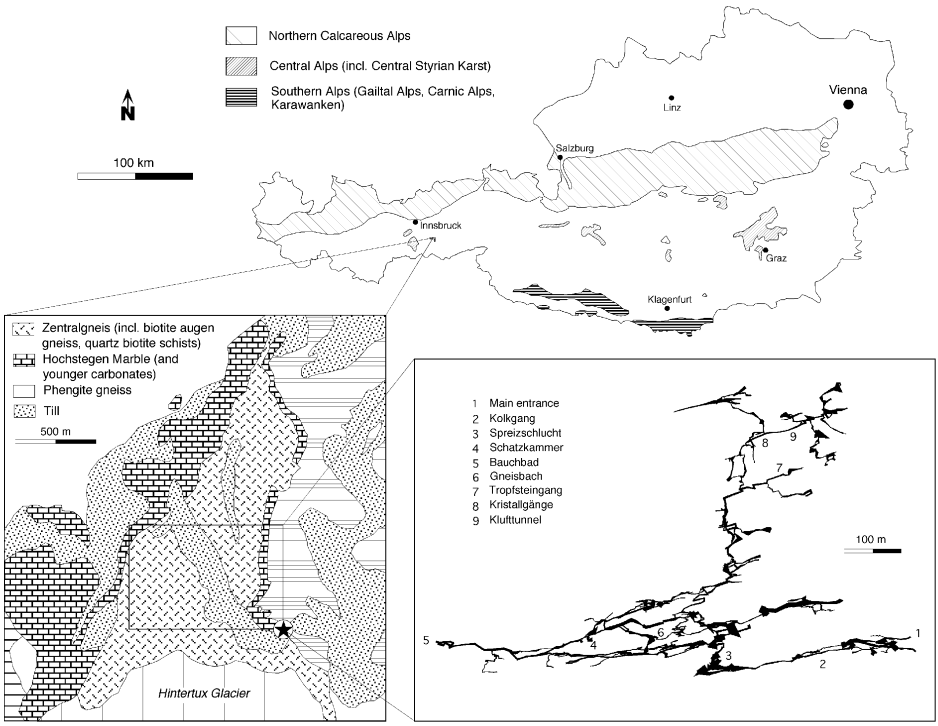

Figure 1. Map of Austria (top) showing major karst regions. Lower left diagram: geologic sketch map of the area surrounding Spannagel Cave (after Höck, 1969). The location of the Spannagel Hut is indicated by the encircled asterisk. Lower right diagram: plan view of Spannagel Cave and location of some of the localities mentioned in the text.

sediment (e.g., Kiessling, 1992). The vast majority of the marble is calcitic in composition. The lowermost portion immediately above the gneiss is rich in quartz and mica, suggesting a significant siliciclastic input into this basin during the early stages of carbonate deposition.

4. CAVE DEVELOPMENT

The initiation and development of the Spannagel Cave System are controlled primarily by stratigraphy and tectonics. Because the Hochstegen Marble constitutes a 20 m thick slab of carbonate sandwiched between gneiss its NW to NNW dip dictates the general orientation of the cave system (Fig. 1): it forms a layer of karstified marble extending from its southernmost (and highest) occurrence (Spannagel Hut, main entrance) toward the north and west. The lower boundary of the karst system follows the lithological boundary between Hochstegen Marble and underlying phengite gneiss in

which cave streams locally cut channels up to 4 m deep. The upper boundary is the ground surface in the eastern part and the structurally overlying Zentralgneis in the western part.

As has been shown previously (Jacoby and Krejci, 1992), most passages follow faults, especially those oriented parallel to the E-W strike of the "Tauern Window". Whereas the principal directions of the cave system are stratigraphically and tectonically defined, cave development was the result of two complementary processes: mechanical erosion and karst dissolution. The important role of erosion by turbulent waters is clearly indicated by the presence of potholes, i.e. funnel-shaped or cylindrical holes up to 3 m wide and up to 3.5 m deep, typically formed at the marble-gneiss interface. These potholes resemble giant's kettles ("glacial mills") and are commonly filled by coarse-grained siliciclastic sediment. A 4 m deep pothole excavated during development of the show cave (Fig. 2A) contained a few well-rounded granite cobbles about 40 cm in diameter embedded in a sandy matrix. The present cave lacks high-discharge streams capable of transporting such large components and forming potholes. Most conduits and passages of the Spannagel Cave, particularly those located near the main entrance, are either dry year around or show only seepage waters and insignificant water flow. The presence of these potholes and the abundance of allochthonous granitic cobbles in virtually all explored cave galleries (Figs. 2E & 2F) underscore the role high-energy waters played during cave development. The most likely source for turbulent water invading the cave in the past is glacial meltwater. Today, the cave is situated outside the reach of meltwaters from the nearby Hintertux Glacier (the western part extends beneath the foreland of the Hintertux Glacier, but no high-discharge flows are present inside the cave, which is probably due to the fairly thick overburden of Zentralgneis). It is highly conceivable, however, that such meltwaters entered the cave system during periods of glacial advances and in particular during Pleistocene glaciations and deglaciations.

In addition to mechanical erosion, the cave also hosts clear-cut evidence of chemical dissolution. This includes various forms of scallops and flute structures (Fig. 2B) on walls and ceilings. The most spectacular features, however, are sword-like inclusions of chert in the marble which form delicate projections out of cave walls up to half a meter long and commonly a few centimeters wide and less than a centimeter thick (Fig. 2C). These chert projections, which are tectonically stretched silica nodules, therefore allow minimum estimates of cave enlargement by chemical dissolution along cave walls.

5. CAVE CLIMATE

Spannagel Cave is a well-ventilated cave system with upward air flow during the cold season and reversed flow between June and October. The air temperature in distal portions of the cave shows no daily or seasonal variation and falls within a narrow range of +1.2 to +1.8°C (measured at eight sites using data loggers over a period of at least two years). These values are only slightly higher than the long-term mean annual air temperature (MAAT) for the altitude of the main entrance (approximately -1°C). The westernmost (and deepest) location has a slightly higher air temperature of +2.4°C, consistent with its lower elevation and thick gneiss overburden (Bauchbad — Fig. 1).

Consistent with the measured cave air temperatures, Spannagel Cave lakes perennial ice, expect for a neighboring cave (near the main entrance of Spannagel Cave) that contains a small accumulation of ice, the volume of which has steadily decreased during the past few years.

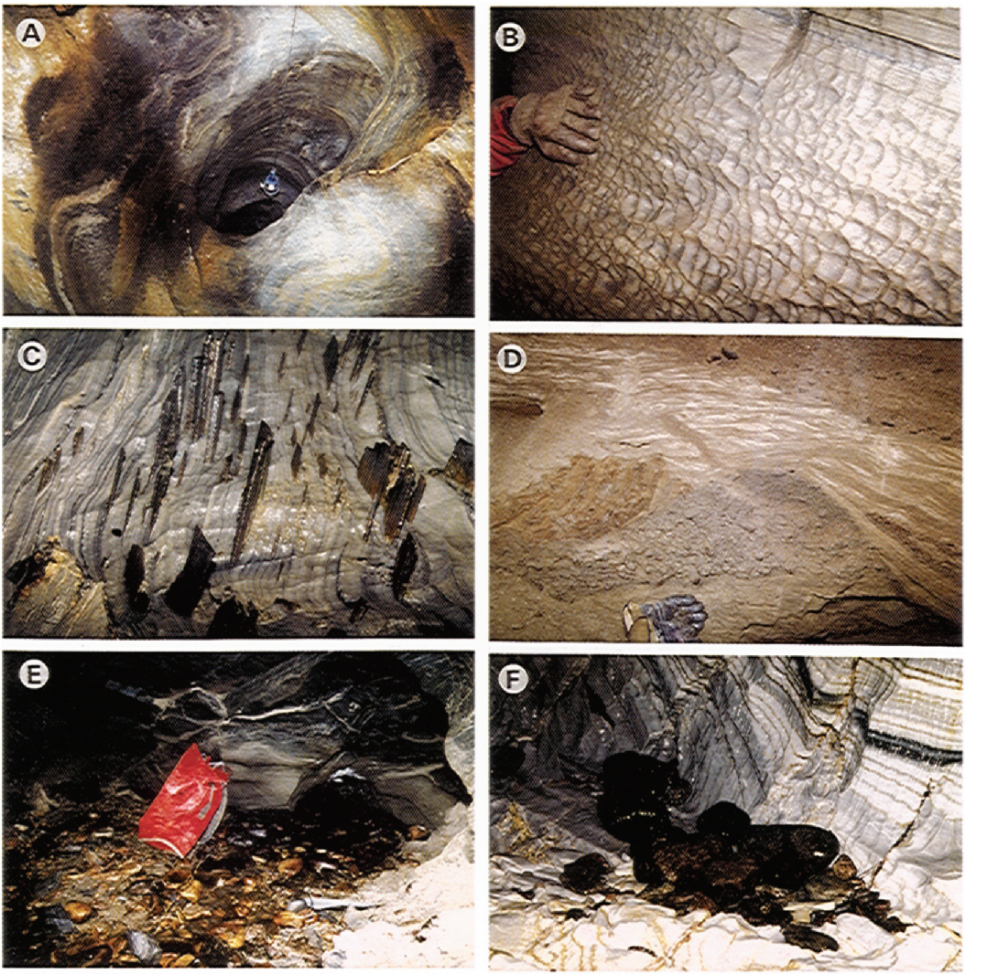

Figure 2. Erosional features and clastic cave deposits. (A) Excavated pothole, 4 m deep, cut into the underlying gneiss. Eingangslabyrinth (part of the show cave). Lamp (c. 15 cm diameter, on wire) for scale. (B) Scalloped wall surface of Hochstegen Marble. Flow was from right to left. (C) Sheet- and spear-like protrusions of tectonically strained chert nodules allowing minimum estimates of karst dissolution. The photo is rotated 90 degrees counterclockwise. Long axis of picture approximately 2 m. (D) Section of clastic sediments showing complex internal stratigraphy, including trough-crossbedding (right), ripple-crossbedding (upper half) and erosional relics of older sediments incorporated into younger ones (left-central). Gloves for scale. (E) Westernmost termination of Spannagel Cave (locality Bauchbad), where a small stream disappears (right-center). Note abundant well rounded allochthonous gneiss cobbles. 75-cm-long speleo bag for scale. (F) Pocket of well-rounded gneiss cobbles left behind by an ancient cave stream on banded Hochstegen Marble. Note coating of cobbles by iron minerals. Width of picture 1.5 m.

Relative humidity in the cave interior approaches the dew point (measured values are invariably higher than 96%) and actual condensation was verified at several sites by the presence of water droplets on data loggers within a period of two months.

Concentration of carbon dioxide in the cave air as determined by a calibrated infrared CO_2 meter is equal to, or only slightly higher than, the outside atmospheric value for this altitude (approximately 285 ppmv) and shows only minor variations in different parts of the cave. This is consistent with the sparse development of soil and vegetation above the cave, the long period of snow cover (8-10 months) and the good ventilation of the system.

6. CAVE DEPOSITS

Several types of clastic and chemical deposits are present in Spannagel Cave. The former include accumulations of cobbles, gravel, sand and silty-clayey material. The latter encompass calcitic speleothems and local gypsum precipitates. Fine-grained sediments are less abundant than coarse sand and gravel, reflecting the proximity of the source of these siliciclastics, i.e. nearby glaciers and their meltwaters. All of these clastics are allochthonous, with the exception of a rather small proportion derived locally from the incision of passages into the phengitic gneiss underlying the Hochstegen Marble.

The majority of the clastic sediment is unlithified. Cemented clastics were only observed locally as erosional relics typically at higher than present levels within individual passages. The thickness of the clastic cave sediments never exceeds a few meters. Where exposed, sections through these sediments show planar and trough crossbedding, graded bedding, as well as small current ripples in finer grained sands (Fig. 2D). As modern high-discharge streams transporting clastic sediment are absent, these unconsolidated sediments are most likely pre-Holocene in age. Indeed, small stalagmites resting on top of these clastic sediments yielded basal Th-U ages of 9-10 kyr.

A conspicuous feature of Spannagel Cave is the almost ubiquitous presence of well-rounded cobbles of granitic gneiss (Figs. 2E & 2F). The presence of this material testifies to the role high-energy waters played during cave development. The majority of these cobbles are characterized by a dark-brown coating, presumably iron oxides/hydroxides derived from mafic components (mostly biotite) inside the cobbles. Observations in the proglacial area, as well as in a temporary exposure of subglacial fluvial sediments beneath the modern Hintertux Glacier, revealed that such coated cobbles are absent there, suggesting that these iron minerals formed *in situ* in the cave environment (Fig. 2F). The lack or imperfect development of such a coating on the lower side of many cobbles implies that only those parts of the cobbles bathed in flowing water were exposed to water-rock interactions, giving rise to iron oxide/hydroxide precipitation.

Despite its high altitude well above modern timber line, Spannagel Cave is locally decorated by speleothems, including soda straws, stalactites, helictites, stalagmites, flowstones, moonmilk and spar (in order of decreasing abundance). The vast majority of

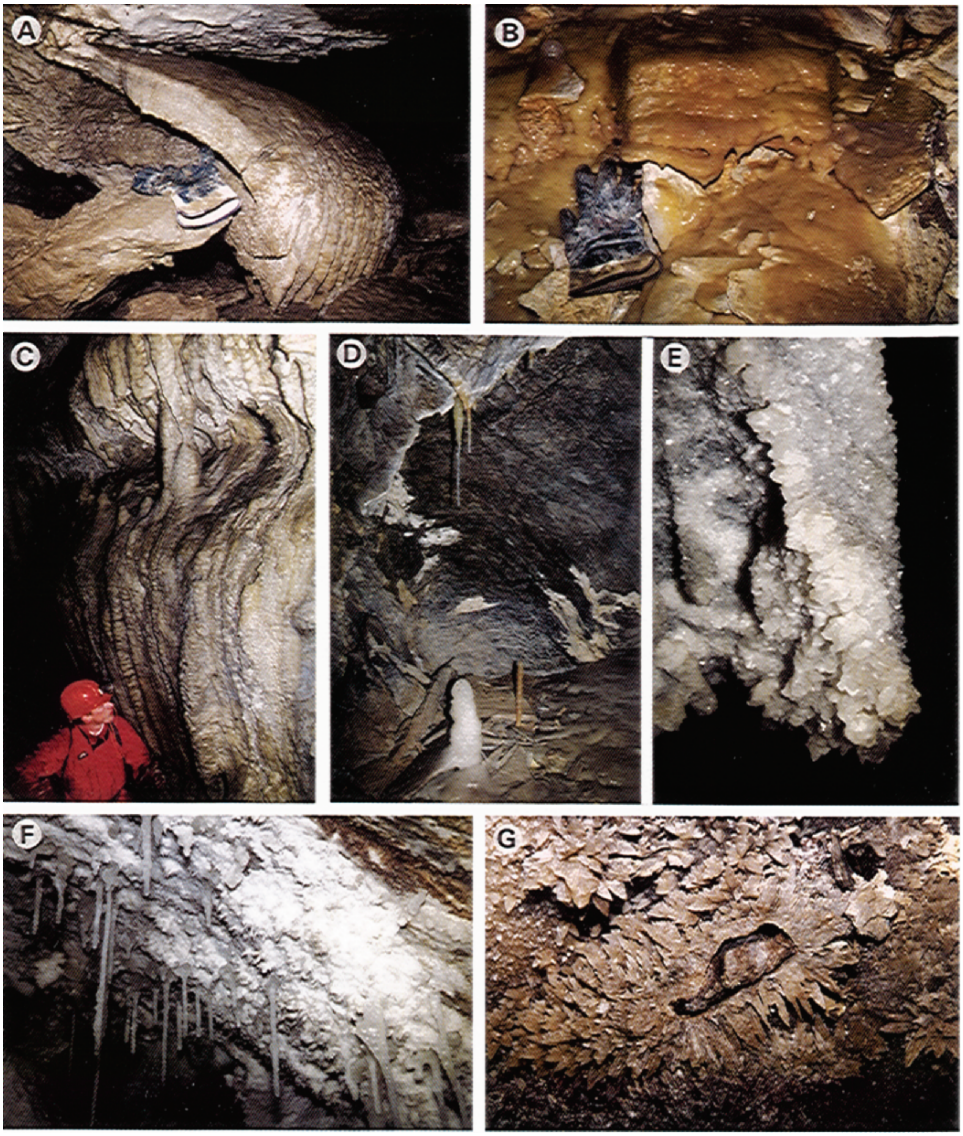

Figure 3. Chemical cave deposits. (A) Fossil flowstone partially exposed due to later erosion. Glove for scale. (B) Actively forming, light-brown flowstone, in the Tropfsteingang. Glove for scale. (C) Example of an area with fairly extensive, but currently inactive, speleothem deposition, in the Spreizschlucht. (D) Holocene stalagmites, stalactites, soda straws and flowstone, in the Trosfsteingang. Height of larger stalagmite approximately 25 cm. (E) Coarsely crystalline gypsum covering a cave wall, in the Kristallgange. Width of photograph 20 cm. (F) Stalactites and soda straws and abundant white, microcrystalling gypsum growing on ceiling in the Kristallgange. Width of photograph approximately 1 m. (G) Detailed view of partially eroded scalenohedral calcite crystals, which probably formed in a phreatic environment. Width of photograph 25 cm.

the deposits are white with occasional light-yellow or orange color, reflecting the low abundance of noncarbonate detritus. Flowstones locally reach up to about 30 cm in thickness, in particular those that are inactive at present (Fig. 3A, B). Stalagmites are up to about 30 cm in height and are cylindrical (Fig. 3C, D) or, more commonly, slightly conical in shape. Soda straws as long as 80 cm in length are present, although most are in the 5-10 cm range. Moonmilk is confined to the northern segment of the cave, where it forms a rather thin layer coating cave walls. Scalenohedral calcite crystals were found only in three localities (Fig. 3G). Active phreatic calcite deposition, however, has not been observed.

An interesting feature of Spannagel Cave is the presence of gypsum. It occurs both as encrustations on stalactites (e.g., Kristallgänge, Klufttunnel), as fragile encrustations on cave walls (e.g., Schatzkammer), and as clear, euhedral crystals up to 1 cm in diameter (Kristallgänge — Figs. 3E & 3F). The presence of these evaporites strongly suggests that relative humidity locally drops below the dew point allowing the necessary evaporation of cave seepage water. In one of these localities (Kristallgänge) we performed actual measurements of relative air humidity at 2-months intervals but failed to detect values significantly lower than the dew point (all measurements showed 96% relative humidity or higher). It remains to be clarified whether this small amount of potential evaporation is sufficient to explain the presence of fairly abundant gypsum at this site. Cave air flow plays a significant role in intensifying evaporation. This explanation may apply to this particular site (Kristallgänge) where air flow is clearly perceptible year around; it does not help to account, however, for the presence of gypsum encrustations in another locality (Schatzkammer), which is a fairly isolated chamber.

7. GEOCHEMICAL COMPOSITION OF SPELEOTHEMS

Carbonate speleothems at Spannagel Cave are invariably calcite. The Mg content as determined in a suite of flowstone and stalagmite samples ranges from 109 ppm to as high as 14072 ppm (mean 2520 ppm). Sr values (93 to 2416 ppm, mean 793 ppm) are weakly correlated with Mg values, whereas Fe is generally low (4-14 ppm). An interesting geochemical feature of Spannagel speleothems is their high U content, ranging from 3 to 218 ppm. The average U content is 37 ppm. Cave waters are likewise rich in U and range from 5 ppb for a small streamflow in the central cave system to 33 ppb measured in stalactite dripwaters (measured by ICP-MS). These values are up to 100 times higher than U concentrations in karst waters from typical limestone caves in other parts of the Eastern Alps (authors' unpublished data). U is most likely sourced from the overlying Zentralgneis which yielded significantly higher U concentrations (3.4-12.0 ppm) than the Hochstegen Marble (0.3-2.2 ppm; measured by ICP-MS).

Petrographically, Spannagel flowstone and stalagmites are composed of coarsely crystalline, columnar calcite indicating slow precipitation rates (e.g., Frisia et al., 2000). Lamination is rare in these samples, although faint laminae of possible annual origin were identified in thin section by epifluorescence microscopy. Postdepositional alteration is confined to macroscopic dissolution features, while there is little evidence of *in-situ* recrystallization in our samples.

A fairly extensive stable isotope data set for various types of speleothems has been developed for Spannagel Cave (Fig. 4). Both C and O isotope values show large variations: $d^{13}C$ values range from –11.1‰ to as high as +10.8‰ VPDB, reflecting locally significant in-cave fractionation processes. $d^{18}O$ values are also highly variable and range from -15.5‰ to -6.2‰ VPDB. Holocene and currently active speleothems, including soda straws and radiometrically dated stalagmites, define a field between -7‰ and +3‰ $d^{13}C$ and -10‰ and -6.4‰ $d^{18}O$. These values overlap only marginally with the isotopic composition of the host rock: $d^{13}C$ mostly +2 to +3‰ and $d^{18}O$ -10 to -3‰ (Fig. 4). In contrast, various inactive pre-Holocene speleothems (including many flowstones) depict a much larger variability, particularly in $d^{13}C$ (-6.5‰ to +11‰; — Fig. 4). Although there is overlap in the data, pre-Holocene speleothems generally have lower $d^{18}O$ values and more variable and locally highly positive $d^{13}C$ values than their modern counterparts (Fig. 4).

We also obtained S isotope analyses of five gypsum samples from Spannagel Cave. $d^{34}S$ values range from –7.3 to +1.2‰ VCDT, suggesting that the sulfate-S was derived from the oxidation of sulphide-S, most likely pyrite, which is common in the marble.

8. ISOTOPIC DATING OF SPELEOTHEMS

A large number of samples (over 80) from various locations inside the cave — both active and inactive speleothems — were analyzed using the ^{230}Th-^{234}U thermal ionization mass spectrometry (TIMS) method and only a brief summary will be given here (see also Spötl et al., 2002). U contents are invariably high (see above) and $^{234}U/^{238}U$ activity ratios are close to unity. The resulting ages range from 68 to > 350.000 yr (Fig. 5). As there is no evidence of open-system behavior subsequent to calcite deposition, the data demonstrate that speleothem deposition occurred repeatedly during the past few hundred thousand years at this site. The earlier suggestion that Spannagel Cave was formed largely by glacier meltwaters during the last glaciation (Jacoby, 1977) is thus a great underestimation of the age of the cave system.

In addition to Holocene and Eemian (Last Interglacial) speleothems we also found evidence for calcite deposition during marine isotope stages 3, 6, 7, 8 and 9 (Fig. 5). We also sampled flowstone covering the walls inside a large fossil pothole clearly postdating its formation (Kolkgang). This sample yielded an age > 350 kyr, strongly suggesting that these prominent erosion features are at least several hundreds of thousands of years old.

9. DISCUSSION

In the following section we will focus on the chemical deposits in Spannagel Cave because of their genetic and chronological significance to the cave history. The siliciclastics are likewise of importance (as outlined above), but the difficulty of dating these deposits limits their significance.

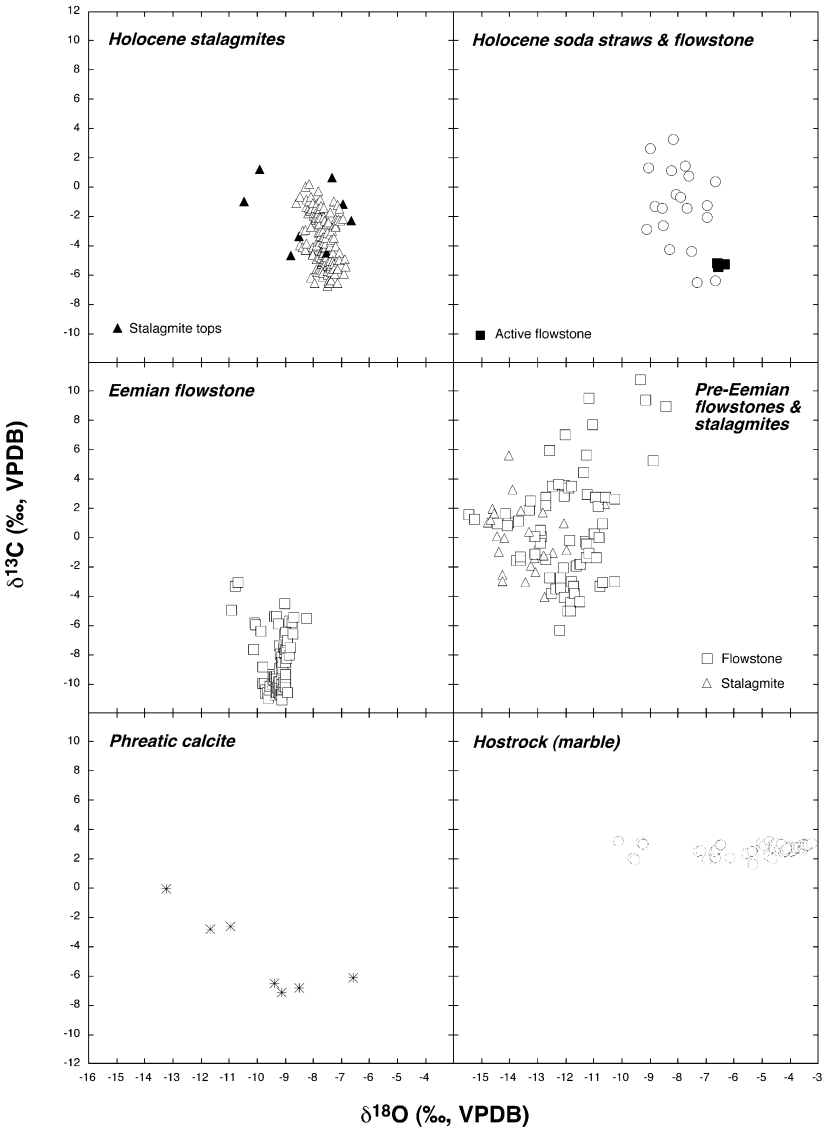

Figure 4. Stable isotopic composition of active and fossil calcite speleothems and the Hochstegen Marble, Spannagel Cave. The diagram contain single sample data and data from multiple subsamples.

High-altitude caves are not uncommon in the Eastern Alps, but the vast majority do not show active speleothem deposition. In addition, the origin of many of these alpinecave systems presently situated above timber line probably dates back well into the Tertiary (e.g., Frisch et al., 2000, 2001). Spannagel Cave is an exception inasmuch as it contains both active and fossil speleothems that can be reliably dated using U-series

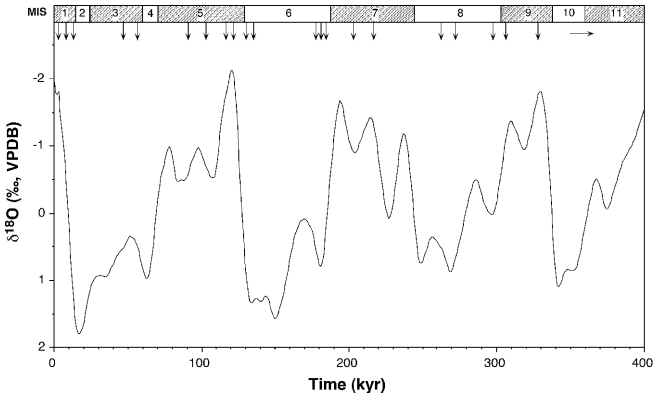

Figure 5. Th-U ages of calcite speleothems from Spannagel Cave (arrows) superimposed on the marine oxygen isotope curve (SPECMAP) to facilitate correlation with the marine isotope stages (MIS). Two Spannagel samples yielded dates > 350 kyr.

techniques. Naturally, speleothems of Spannagel Cave are less abundant and of smaller size than their counterparts in warmer, low-lying caves. The presence of these carbonates, however, is a clear testimony that conditions had to be — at least temporarily and locally — above freezing even during some of the glacial periods (cf. Fig. 5). As the present-day air temperature inside the cave is only slightly above freezing, this is a highly sensitive system.

Stable isotopes are particularly useful in helping to understand the conditions of speleothem deposition in Spannagel Cave. Under equilibrium conditions, calcite precipitating from modern dripwaters at this site ($d^{18}O$ = −14 to −10‰ VSMOW) at +1 to +2°C should have $d^{18}O$ values between −10.6‰ and −6.3‰ VPDB, which is the range of measured calcite compositions (cf. Fig. 4). As it is impossible to precipitate calcite at subzero temperatures, the only way to account for calcite of lower O isotopic composition (cf. Fig. 4) is to introduce ^{18}O-depleted seepage water. The O isotopic composition of rain and snow is a complex function of several parameters, including the moisture source, the O isotopic composition of the evaporating ocean surface waters, the path the air masses take and the in-cloud temperature of condensation. Keeping other variables constant, the latter process results in a near-linear relationship between MAAT (a proxy for cloud condensation temperature) and stable isotopic composition of precipitation (e.g., Rozanski et al., 1993). Lowering MAAT would thus provide a means to shift toward lower $d^{18}O$ precipitation values. Using the present-day mid-European averaged $d^{18}O$-MAAT gradient of 0.6‰/°C or 1.7°C/‰ as a guide (Rozanski et al., 1992; Grafenstein et al., 1996), calcite $d^{18}O$ values of as low as −15.5‰ suggest a temperature drop of up to several degrees C below present-day MAAT. Such a temperature decrease, however, would inevitably result in the development of permafrost and freezing conditions inside the cave, which are difficult to reconcile with the presence of speleothems. The most likely explanation for ^{18}O-depleted speleothems at this site therefore is flushing of the karst fissure network by meltwaters derived from decaying glaciers which stored cold and ^{18}O-depleted precipitation. A detailed study of a complex

flowstone sample from the northern part of the cave shows that such low $d^{18}O$ values occurred for instance during the penultimate deglaciation 135 kyr ago (Spötl et al., 2002).

The C sources in Spannagel Cave are threefold: C derived from dissolved host rock, soil-derived CO_2 and atmospheric CO_2. Pedogenic CO_2 should give rise to calcite $d^{13}C$ values of about -12‰ to -9‰, taking into account the fact that (i) vegetation at this site is (and most likely was) entirely C_3 (Körner, 1999), (ii) assuming isotopic equilibrium between aqueous C species and precipitating calcite, (iii) applying an isotopic enrichment factor between calcite and CO_2 of +11.7‰ (@2°C — Romanek et al., 1992) and (iv) considering that soil $CO_{2(g)}$ tends to be a few permil heavier in $d^{13}C$ than the soil organic matter (e.g., Yakir and Sternberg, 2000). Mixing of pedogenic CO_2 with bicarbonate-C derived from the host rock (+2 to +3‰) and/or atmospheric CO_2 (preindustrial $d^{13}C$ = -6‰) can explain most of the observed $d^{13}C$ values (Fig. 4). Under isotopic equilibrium, carbonates derived from a purely atmospheric CO_2 source can be as heavy as +6‰ (@2°C). Values higher than that indicate kinetic isotope fractionation during speleothem growth, most likely due to excessive CO_2 degassing as a result of very low drip rates possibly enhanced by evaporation (Hendy, 1971) and/or freezing. Such highly positive C isotopic values are not uncommon in other high-alpine caves where overlying soils are immature or missing (Geyh et al., 1982; authors' unpublished data). Holocene speleothems from Spannagel Cave show $d^{13}C$ values that are consistent with near-equilibrium precipitation provided that significant mixing with marble-derived C (and/or atmospheric C) took place. In addition, isotopic analyses of active soda straw tips demonstrate that these dripwaters have a significant host rock C component (Fig. 4). Some pre-Holocene speleothems are characterized by highly positive and variable $d^{13}C$ values (Fig. 4) that demand only a very small (or possibly absent) pedogenic CO_2 component in conjunction with excessive degassing (either within the karst aquifer and/or at the drip site).

Isotopic signatures not unlike those measured on Spannagel samples have previously been attributed to different mechanisms of high-altitude carbonate deposition. Magaritz (1973) studied secondary calcite (including speleothems) from Mount Hermon, Israel and from high-alpine sites in the Austrian and Swiss Alps and found anomalously low $d^{18}O$ values in combination with high (commonly positive) $d^{13}C$ values. He attributed these values to the influence of snow melt waters in areas devoid of soil. Dreybrodt (1982) elaborated this model further and suggested, on the basis of a simple kinetic model, that the principal control of carbonate precipitation in such high-alpine caves may be a slight temperature increase that subglacial or proglacial meltwaters experience upon their journey into the (warmer) cave. Although Dreybrodt's model is consistent with the highly positive C isotope values in high-alpine caves (e.g., Geyh et al., 1982), it is based on the fundamental assumption that the cave is warmer than the outside air temperature. This apparently contradicts theoretical and empirical observations that the interior cave air (and rock) temperature closely matches the MAAT above the cave, provided that the cave is well ventilated (e.g., Wigley and Brown, 1976; Ford and Williams, 1989). A possible solution was suggested by Dreybrodt (1982), i.e., "heating" of the cave due to an elevated geothermal gradient. An example is Castleguard Cave which extends beyond Columbia Icefield in Alberta and whose air temperature in distal parts of the cave is significantly warmer (up to +3.8°C) than the MAAT at the level of

the entrance (c. -4°C). This apparent internal warming has been attributed to a locally higher heat flow (Ford et al., 1976). In a subsequent study of Castleguard Cave, Atkinson (1983) concluded that such a warming of cave seepage waters by up to 4° is probably too small to account for the observed speleothem deposition, although he did not dismiss the possibility that this process may play a minor role. He instead favored carbonate precipitation as a result of oxidation of pyrite and subsequent release of CO_2 due to reaction of sulfuric acid with the host rock above the cave, possibly enhanced by evaporation.

We favor a similar model for Spannagel Cave which takes into account the highly variable C and O isotopic compositions, the age distribution of speleothems and the hydrochemistry of modern seepage waters (which will be detailed elsewhere). The latter shows elevated sulfate concentrations which in conjunction with gypsum precipitates and their low S isotope values point to the important role of sulfide oxidation and concomitant dissolution of marble. This process appears to have been the dominant mode during climate periods when no or very little vegetation and soil were present above the cave. The classic karst process prevailed only during fully interglacial periods and probably involved a time lag due to the slow buildup of soil at this altitude.

10. CONCLUSIONS

The very fact that calcite speleothems formed repeatedly during the Pleistocene and some are still actively forming today demonstrates the presence of liquid water in the karst fissure network. Interior cave air temperatures slightly above the outside MAAT imply a somewhat elevated geothermal gradient that may have provided extra heat preventing the system from converting into an ice cave. The actual processes that promoted marble dissolution and secondary redeposition as speleothems probably switched between two different modes, an interglacial mode when input of carbon dioxide from the soil dominated the system, resulting in low C and high O isotopic values. In contrast, during colder periods and probably also during the early phase of an interglacial, pedogenic input was negligible and speleothems show low O (reflecting glacier meltwaters) and high (rock-buffered) C isotopic compositions. The most likely mechanism causing host rock dissolution during these periods is oxidation of pyrite giving rise to acidic seepage waters which are capable of dissolving the marble. Slow drip rates and concomitant prolonged degassing locally resulted in a kinetic enrichment of C isotopes in speleothem calcite, particularly during cold periods.

11. ACKNOWLEDGMENTS

Research at Spannagel Cave is funded by the Austrian Science Fonds through grants P12458-GEO and START Y122-GEO to CS. The following individuals are thanked for their support during this ongoing project: Roman Erler, Renate Tobitsch, Rene Eichstätter and the team from the Spannagel Hut (in particular Sepp Klausner). Fred J. Longstaffe kindly provided S isotope data. Careful reviews Peter T. Kolesar, Arthur N. Palmer and Margaret V. Palmer are gratefully acknowledged.

12. REFERENCES

Atkinson, T.C., 1983, Growth mechanisms of speleothems in Castleguard Cave, Columbia Icefields, Alberta, Canada, *Arctic and Alpine Research* **15**: 523-536.

Bauer, F., and Zötl, J., 1972, Karst of Austria, in *Karst. Important Karst Regions of the Northern Hemisphere*, M. Herak and V.T. Stringfield, eds., Elsevier, Amsterdam, pp. 225-265.

Dreybrodt, W., 1982, A possible mechanism for growth of calcite speleothems without participation of biogenic carbon dioxide, *Earth Planetary Science Letters* **58**: 293-299.

Ford, D.C., Harmon, R.S., Schwarcz, H.P., Wigley, T.M.L., and Thompson, P., 1976, Geo-hydrologic and thermometric observations in the vicinity of the Columbia Icefield, Alberta and British Columbia, Canada, *Journal of Glaciology* **16**: 219-230.

Ford, D., and Williams, P., 1989, *Karst Geomorphology and Hydrology*, Chapman and Hall, London, 601 p.

Frisch, W., Székely, B., Kuhlemann, J., and Dunkl, I., 2000, Geomorphological evolution of the Eastern Alps in response to Miocene tectonics, *Zeitschrift für Geomorphologie* **44**: 103-138.

Frisch, W., Kuhlemann, J., Dunkl, I., and Székely, B., 2001, The Dachstein paleosurface and the Augenstein Formation in the Northern Calcareous Alps - a mosaic stone in the geomorphological evolution of the Eastern Alps. *Geologische Rundschau*, v. 90, p. 500-518.

Frisia, S., Borsato, A., Fairchild, I.J., and McDermott, F., 2000, Calcite fabrics, growth mechanisms, and environments of formation in speleothems from the Italian Alps and southwestern Ireland, *Journal of Sedimentary Research* **70**: 1183-1196.

Fügenschuh, B., Seward, D., and Mancktelow, N., 1997, Exhumation in a convergent orogen: the western Tauern window, *Terra Nova* **9**: 213-217.

Geyh, M.A., Franke, H.W., and Dreybrodt, W., 1982, Anomal große d13C-Werte von Hochgebirgssinter. Vergeblicher Versuch einer palaeoklimatischen Deutung, *Hölloch Nachrichten* **5**: 49-61.

Grafenstein, U. von, Erlenkeuser, H., Müller, J., Trimborn, P., and Alefs, J., 1996, A 200 year mid-European air temperature record preserved in lake sediments: an extension of the d18Op-air temperature relation into the past, *Geochimica et Cosmochimica Acta* **60**: 4025-4036.

Hendy, C.H., 1971, The isotopic geochemistry of speleothems — I. The calculation of the effects of different modes of formation on the isotopic composition of speleothems and their applicability as palaeoclimatic indicators, *Geochimica et Cosmochimica Acta* **35**: 801-824.

Höck, V., 1969, Zur Geologie des Gebietes zwischen Tuxer Joch und Olperer (Zillertal, Tirol), *Jahrbuch der Geologischen Bundesanstalt* **112**: 153-195.

Höck, V., 1970, Zur Kristallisationsgeschichte des penninischen Altkristallins beim Spannagelhaus (Tuxer Hauptkamm, Tirol), *Verhandlungen der Geologischen Bundesanstalt* **1970**: 316-323.

Jacoby, E., 1977, *Zur Geologie des Spannagelhöhlensystems und dessen näherer Umgebung*, Unpubl. Ph.D. thesis, Univ. of Innsbruck, 148 p.

Jacoby, E., and Krejci, G., 1992, Die Höhle beim Spannagelhaus, *Wissenschaftliche Beihefte zur Zeitschrift Die Höhle* **26**:1-148.

Kiessling, W., 1992, Palaeontological and facial features of the Upper Jurassic Hochstegen marble (Tauern window, Eastern Alps), *Terra Nova* **4**: 184-197.

Körner, C, 1999, Alpine Plant Life. 338 p., Berlin (Springer).

Lammerer, B., and Weger, M., 1998, Footwall uplift in an orogenic wedge: the Tauern Window in the Eastern Alps of Europe, *Tectonophysics* **285**: 213-230.

Magaritz, M., 1973, Precipitation of secondary calcite in glacier areas; carbon and oxygen isotopic composition from Mt. Hermon, Israel, and the European Alps, *Earth Planetary Sci. Letters* **17**: 385-390.

Romanek, C.S., Grossman, E.L., and Morse, J.W., 1992, Carbon isotopic fractionation in synthetic aragonite and calcite:Effects of temperature and precipitation rate, *Geochim. et Cosmochim. Acta* **56**: 419-430.

Rozanski, K., Araguás-Araguás, L., and Gonfiantini, R., 1992, Relation between long-term trends in oxygen-18 isotope composition of precipitation and climate, *Science* **258**: 981-985.

Rozanski, K., Araguás-Araguáz, L., and Gonfiantini, R., 1993, Isotopic patterns in modern global precipitation, in *Climate Change in Continental Isotopic Records*, P.K. Swart, K.C. Lohmann, J. McKenzie, and S. Savin, eds., *Geophysical Monograph Series* **78**: 1-36.

Selverstone, J., 1988, Evidence for east-west crustal extension in the Eastern Alps: implications for the unroofing history of the Tauern Window, *Tectonics* **7**: 87-105.

Spötl, C., Mangini, A., Frank, N., Eichstädter, R., and Burns, S.J., 2002, Start of the Last Interglacial at 135 ka: Evidence from a high-Alpine speleothem. *Geology* **30**: 815-818.

Wigley, T.M.L., and Brown, M.C., 1976, The physics of caves, in *The Science of Speleology*, T.D. Ford, and C.H.D. Cullingford, eds., Academic Press, London, pp. 329-358.

Yakir, D., and Sternberg, L. da S.L., 2000, The use of stable isotopes to study ecosystem gas exchange. *Oecologia*, v. 123, p. 297-311.

ISOTOPE STAGE 11, THE "SUPER-INTERGLACIAL", FROM A NORTH NORWEGIAN SPELEOTHEM

Stein-Erik Lauritzen and Joyce Lundberg*

1. ABSTRACT

A high resolution isotope profile (142 points in 75 mm) from LP-6, a corroded flowstone slab from Lapphullet cave at Mo i Rana, Norway, close to the Arctic Circle, is dated by nine TIMS U-series dates to isotope stages 13 and 11. The dates are in perfect stratigraphic order, putting the main growth periods of the speleothem at 502 ka, and 380-420 ka. Termination V occurred shortly before 421 ±10 ka, probably between 423 and 430 ka, an estimate that coincides with the orbitally tuned SPECMAP date. The duration of isotope stage 11 interglacial is at least 27 to 45.5 kyrs (depending on the growth model used) supporting the longer of the published estimates of ~30-40 kyrs (McManus *et al.*, 1999).

Calcite deposition began in isotope stage 13 with two growth periods separated by a drying horizon. A major dissolutional hiatus marks the isotope stage 12 glaciation. Renewed speleothem deposition at the end of the termination shows rapid growth, which coincides with the beginning of isotope stage 11 from Site 607 marine record. Speleothem growth continues throughout the interglacial peak and continues just beyond it, ending in a dissolutional hiatus. Isotopes and temperature are shown to have a negative relationship, in keeping with other speleothem records from northern Norway. The isotopic curve correlates very well with the Site 607 marine record from the North Atlantic. The isotopic values have a distinct relationship with the crystal form, the translucent palisade sections having less depleted values than the opaque laminated sections. Both are argued to be controlled by climatic variables. During the early part of isotope stage 11, from ~421 to ~412 ka, temperatures and biological activity were about the same as today. The speleothem shows a couple of detrital draping events (presumably floods), and one minor hiatus at the end of this cool, wet phase. During the isotope stage 11 peak, centered around 412 to 404 ka, temperatures and biological activity were noticeably higher than today in keeping with some other paleotemperature proxy estimates from this "super-interglacial". Pollen data from the interval 404-406 ka

*Stein-Erik Lauritzen, Geology Dept., Bergen University, Allégaten 41, N-5007 Bergen, Norway.
Joyce Lundberg (to whom all correspondence should be addressed), Dept. of Geography and Environmental Studies, Carleton University, Ottawa, K1S 5B6, Canada.

(Lauritzen *et al.*, 1990) confirm the presence of a Birch-Alder forest that was more dense than the modern vegetation. The speleothem contains fragments of charcoal, suggesting fire regimes in these forests.

2. INTRODUCTION

The value of speleothems as paleoclimate proxies has become apparent in the spate of recent publications on the subject (see, for example, the special issue of *The Holocene: Speleothems as high-resolution palaeoclimatic archives,* Lauritzen and Lundberg, 1999a). The paleoclimatic indicators include stable isotopes of oxygen and carbon, various types of laminations, crystallography, and growth rates. The advent of thermal ionization mass spectrometric (TIMS) dating has provided the basis for high resolution, accurately dated profiles.

Theoretically climates can be reconstructed for any period in the Quaternary back to the limit of U-Th TIMS dating, which is 600-700 ka. However, a focus on understanding modern, recent, and Holocene samples, where the environment is relatively well understood either from historical evidence or from other paleoclimatic proxies, is a necessary prelude to any longer-term climatic reconstructions. Speleothem work in Norway has been ongoing for several decades and the body of evidence now assembled on Holocene speleothems from northern Norway (Lauritzen and Lundberg, 1999b; Linge *et al.*, In prep, 2001a,b; Berstad, 1998) has given us confidence that the principles learned from Holocene samples can profitably be applied to older samples, at least to older interglacial samples where the climate systems are likely to have been similar to those of the Holocene. Here we have studied a much older sample from northern Norway which was originally shown by alpha U-U dating and paleomagnetic analysis to be in the region of half a million years old (Lauritzen *et al.*, 1990). Nine new TIMS dates place the sample into isotope stages 13 and 11; the date of Termination V and the duration of the stage 11 interglacial are estimated; a high resolution profile of oxygen and carbon isotopes provides a paleoclimate indicator together with the stratigraphy and crystal form. These new data are combined with the previously published information on pollen and charcoal content (Lauritzen *et al.*, 1990) to provide a paleoenvironmental reconstruction of the interglacial of isotope stage 11 in northern Norway.

Marine oxygen isotope stage (MIOS or MIS) 11 (~420-360 ka), referred to as the "Super Interglacial" (http://chht-ntsrv.er.usgs/gov.warmclimates/key_int.html, 2000), has recently become a focus of research because several proxy records suggest that MIS 11 is the longest and warmest interglacial of the past 500 kyr (Howard, 1997; Poore *et. al.*, 1999). With Milankovitch forcing similar to Holocene conditions, this period of past global warming may serve as a model for potential Holocene climate change in the absence of human intervention (Howard, 1999). Important questions about MIS 11 relate to its cause, its duration, and its temperature regime. For marine cores the dating of MIS 11 relies on spectral tuning or assumptions of sedimentation rates (Poore *et. al.*, 1999). In this north Norwegian stalagmite Termination V and MIS 11 are dated radiometrically and independently, thus circumventing the problem of circular arguments about timing of climate events and Milankovitch controls on climate.

The sample, LP6, comes from a cave in Rana County, Northern Norway, called Laphullet (Lauritzen *et al.*, 1990). Laphullet lies at the side of Rauvassdalen about 12 km south of the present terminus of the Svartisen glacier (Figure 1). The cave is in such a

position that it is strongly affected by glacial advance and retreat. In the present situation, with the ice limit far up-valley, the cave is air-filled and calcite deposition occurs freely. Expansion of the glacier would fill the valley and cause flooding of the cave preventing calcite deposition and probably causing some dissolutional damage to calcite already deposited; this would be apparent as an obvious non-depositional or erosional hiatus.

Laphullet is one part of what is probably a much more extensive system comprising more than 4.5 km of total passage with a depth of >350 m. The cave was originally formed in phreatic conditions; subsequent vadose conditions have caused little modification to the large tubular phreatic passages. Quaternary glacial advances and retreats forced the cave system into alternating phreatic and vadose conditions, which variations are mainly apparent in dissolution of the cave deposits rather than in passage form. The cave is formed in a narrow, steeply dipping band of marble forming a stripe karst. The sample grew in the main passage about 76 m below the modern topographic surface.

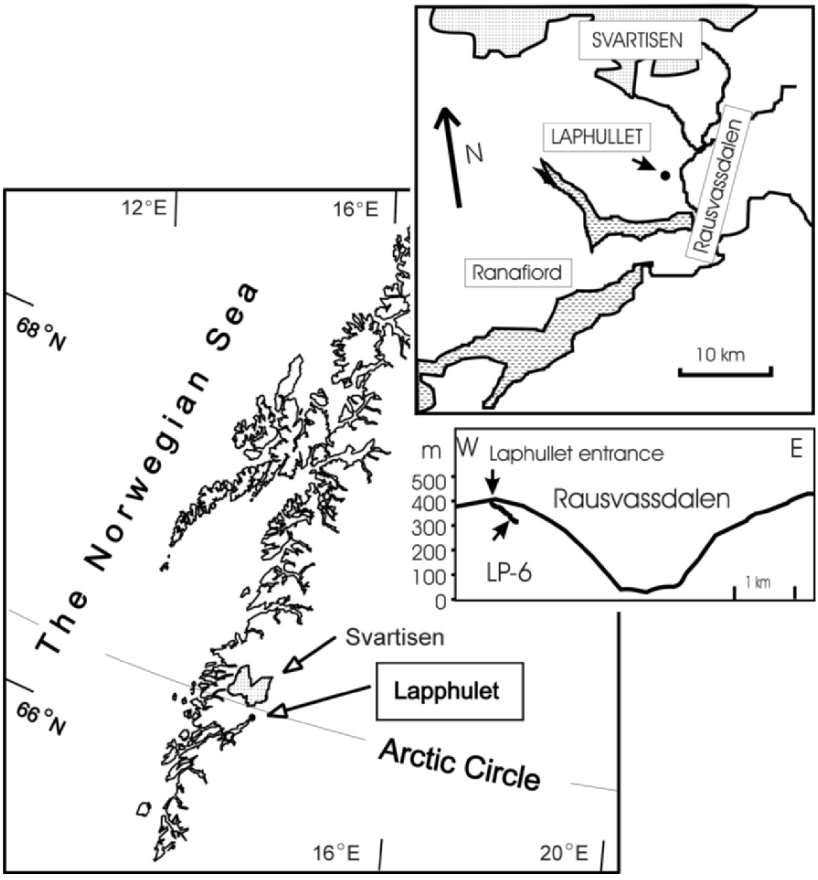

Figure 1. Location map of the cave, Laphullet, close to the Norwegian Sea, just south of the Arctic Circle, in a valley leading north to the small ice cap, Svartisen, with insets showing locality of the cave and valley cross section.

The cave is situated about 10 km from the head of Ranafiord, at an elevation of 400 m above sea level. The proximity to the coast and the position on the westward side of the mountain chain ensures a relatively simple climate-cave system, even in the past, because the source of air masses is likely to have remained the Norwegian Sea. The modern climatic setting is controlled by the North Atlantic Oscillation (NAO), the balance between the subtropical high-pressure center near the Azores and the subpolar low-pressure center south and east of Greenland (Lamb and Peppler, 1987; Cook *et al.*, 1998). The NAO index for winter varies between two extremes of very high subtropical pressure combined with very low subpolar pressures, a positive NAO index, and the opposite, a negative NAO index. A positive index results in more and stronger winter storms crossing the Atlantic Ocean on a more northerly track; Norway is dominated by zonal circulation with on-shore, westerly, frontal systems bringing more rain than usual and higher mean temperatures. A negative index results in fewer and weaker winter storms crossing on a more west-east pathway; enhanced meridional circulation brings cold air to northern Europe with more off-shore air flow, drier conditions and lower mean temperatures. The wintertime NAO exhibits significant interannual and interdecadal variability (Hurrell 1995).

3. MATERIALS AND METHODS

The sample (Figure 2), part of a 7.5 cm thick flowstone deposited on the bedrock wall of the main passage, was cut into slices and polished. The upper surface is dissolved into cusped forms. The flowstone stratigraphy (Figure 3) is complex, with various types of hiatuses and marked changes in color and texture. It is made up bands of dense, opaque, pale buff-colored, strongly laminated calcite with short crystals, alternating with less dense, translucent, buff to dark orange-colored, elongate pallisade crystals with few or weak laminations. Further details of the stratigraphy are considered along with the isotopic record in the discussion section. The division into zones shown in Figure 3 is based on color, crystal morphology, and discontinuities.

Nine subsamples for TIMS U-series dating of ~0.3 g were taken (Figure 3) and ignited in quartz crucibles at 800 °C for 4 - 6 h in order to destroy organics and expel CO_2. The resulting CaO was dissolved in H_2O/ HNO_3, a Fe carrier and spike added (JL369, DIL-E; ^{229}Th : ^{233}U : ^{236}U ~ 0.2 : 0.5 : 1.0). The radionuclides were scavenged on $Fe(OH)_3$, cleaned by anion exchange chromatography in 7.5 M HNO_3, and separated with 6 M HCl and 1 M HBr. The U and Th fractions were loaded in 0.1 M H_3PO_4. Both U and Th were loaded onto single Rhenium (5x zone-refined) filaments. All of the Th fraction, and an amount of U corresponding to ~ 100 ng ^{238}U was loaded. U was run as oxide from a silica gel bed, and Th was run as metal from a graphite bed. Mass abundances were measured on a Finnigan 262 RPQ instrument in dynamic (ion counting) mode. Samples for stable isotopes were taken at ~0.5 mm intervals up the cross section, of ~0.2 mg extracted with a 0.5 mm drill, giving 144 positions (Figure 3). Stable isotopes of carbon and oxygen were measured by CO_2 expulsion with H_3PO_4 and analyzed on a Finnigan 251 instrument at the Geological Mass Spectrometry lab in Bergen. Standard samples have an analytical reproducibility of ±0.06 and ±0.07‰ for $\delta^{13}C$ and $\delta^{18}O$ respectively. Results are reported as ‰ versus PDB.

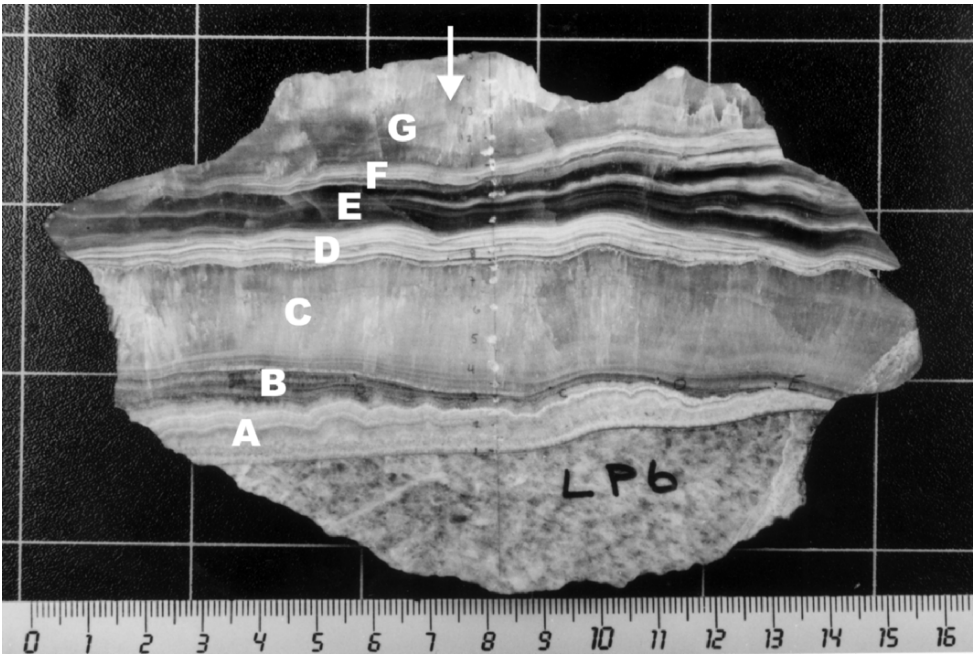

Figure 2. LP6, a slice from the 7.5 cm thick flowstone deposited onto the marble bedrock, is made up of alternating bands, one major hiatus close to the base of deposition. Its top surface is eroded. (The holes visible here are from a former low-resolution isotopic profile). Scale is in centimeters. The section shown in Figure 3 is not from this slice but its approximate position is shown by the white arrow. The zones as defined in Figure 3 are shown in white letters.

4. RESULTS

4.1 The dates and the age model

Table 1 shows the U-series data. These dates are close to the limit of the TIMS technique at this level of U, where a small variation in the measured isotopic ratios could significantly shift the calculated date. However, they are in perfect stratigraphic order (Figure 4). We would normally suggest caution in accepting the date as reliable if it were a single finite date so close to the limit, but the juxtaposition of the nine dates here lends credence to their values.

Table 1. TIMS uranium series data for LP6. 2Φ errors are shown in parentheses.

Sample	Position (mm from base)	Date (ka ± 2σ)	230/234 Activity Ratio	234/238 Activity Ratio	Initial 234/238 ratio	230/232 Act. Ratio	U ppm	Th ppm
183	4.0-6.0	502(+31−24)	1.0113(23)	1.0564(16)	1.2342(19)	108	0.497	0.3473
189	12.0-14.0	419.0(+10.0−9.2)	1.0012(19)	1.0650(09)	1.2132(10)	66	1.230	1.9569
175	27.0-28.0	416.8(+11.0−10.0)	1.0006(20)	1.0650(12)	1.2118(14)	58	0.778	0.2152
179	34.5-36.0	406.0(+11.2−10.1)	1.0001(23)	1.0715(13)	1.2259(15)	20	0.644	0.2247
174	41.5-43.5	405.6(+8.7−8.0)	0.9987(17)	1.0671(13)	1.2120(14)	43	0.715	0.4572
177	51.0-52.5	401.6(+9.6−8.8)	0.9961(19)	1.0624(14)	1.1948(15)	1040	0.533	0.2753
173	55.0-56.5	401.4(+10.5−9.6)	0.9960(21)	1.0620(14)	1.1935(16)	1357	0.534	0.1148
176	64.5-65.8	396.7(+7.8−7.3)	0.9950(17)	1.0630(10)	1.1939(12)	2861	0.614	0.1181
172	72.5-73.8	383.8(+7.0−6.2)	0.9933(18)	1.0696(10)	1.2064(11)	806	0.888	0.3819

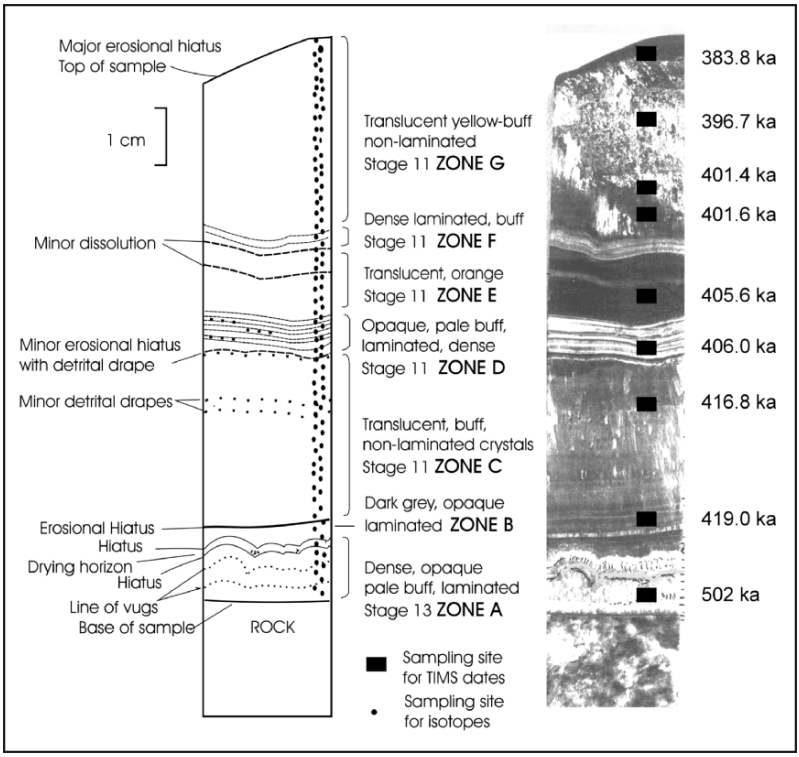

Figure 3. Diagram and scan of slab from LP6 showing stratigraphy and sampling positions for TIMS dating (solid black rectangles) and for stable isotopes (black dots). The sample is divided into zones A to G, based on crystal morphology and color.

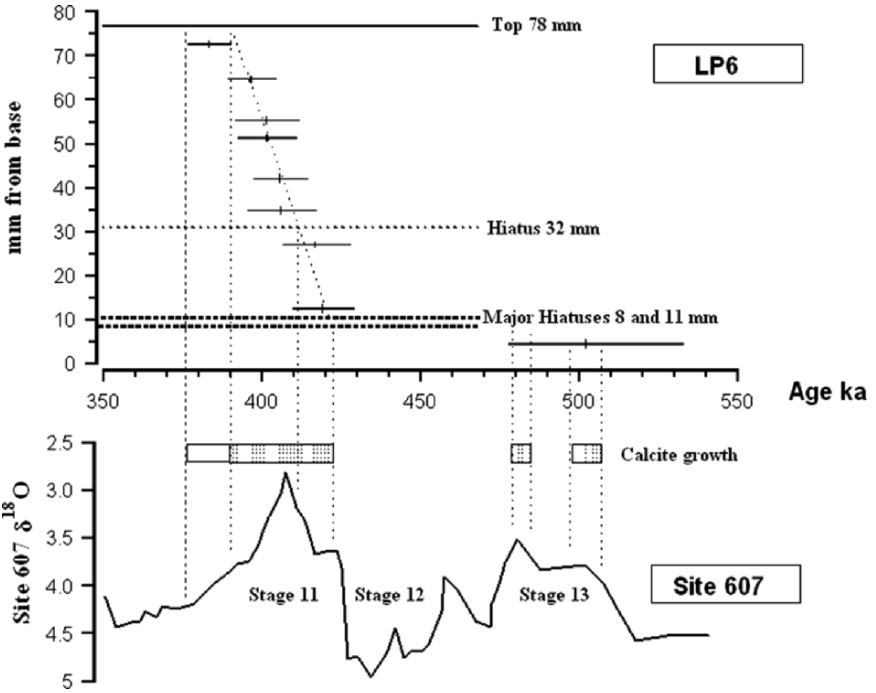

Figure 4. Dates on LP6 and growth model, in relation to marine isotope curve from Site 607. The periods of calcite growth are shown by the shaded boxes. If the topmost date is used then the period of calcite growth extends into the unshaded box.

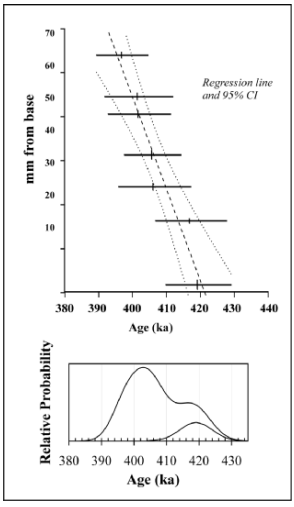

Figure 5. A: The seven MIS 11 dates from LP6 plotted with regression line (r^2 = 0.93) and 95% confidence intervals. B: The probability density function for the first date above Termination V, curve a, and for all seven dates, curve b.

The model by which ages were assigned to the hiatuses and to the isotopic values was constructed in the following way.

(i) With only one date for MIS 13 we simply assume that growth began at the start of the interglacial as indicated by the SPECMAP scale, at 508 ka, and that the major hiatuses represent glacial stage 12.

(ii) The next seven dates fall within MIS 11. The dates to either side of the minor hiatus at 32 mm have overlapping 2σ ranges (as do all the other consecutive dates). This suggests that the hiatus represents a minor erosional episode of no statistically significant duration. However, we offer two interpretations, the first being the better supported.

In the first model the seven dates for MIS 11 (Zones C to G) are treated as a single population with simple linear growth and no gap for the hiatus. Figure 5 shows the regression line and 95% confidence interval ($r^2 = 0.93$) together with the cumulative probability curve. The growth rate is 2.25 x 10^{-3} mm/a^{-1}. This results in an estimate for the beginning of calcite growth at 11 mm of 421±10 ka (ignoring the error of the regression).

If instead the seven dates are separated into two populations, divided by the hiatus at 32 mm, then the upper five dates represent a growth rate for Zones D to G of 3.3 x 10^{-3} mm/a^{-1}; the hiatus is 8 kyrs in duration; and the growth rate for Zone C is 6.6 x 10^{-3} mm/a^{-1}. In this case the estimate for the timing of the start of calcite growth at 11 mm, depending solely on two dates, is 419.3 ±10 ka. The quality of the dates do not justify this division into two since in this age range and $^{234}U/^{238}U$ activity ratio a very small modification in the measured isotopic ratios yields a very large difference in age.

(iii) No break in deposition is apparent between the seven dates of MIS 11 and the topmost date, and the crystal form suggests no change in conditions or in growth rate for the top of Zone G. However, we treated the topmost date separately because it falls out of MIS 11 on the SPECMAP scale and out of the regression line of the seven MIS 11 dates. If the last date is ignored and the simple linear model propagated, then the top of the sample falls at 392 ±10 ka. If growth for the topmost centimeter is modeled with a curve to fit the actual date, then the top of the deposit falls at 375.5 ±10 ka, but the growth rate is again constrained by only two dates.

4.2 U and Th systematics

Changes in U and Th systematics (Figure 6) give information about the stability of the soil-rock- percolation pathway system over time. It is quite common in speleothem to find that U concentration and initial $^{234}U/^{238}U$ activity ratios gradually decrease with time as the host rock becomes depleted of U and the more soluble ^{234}U is removed. This sample shows very little change with time of initial $^{234}U/^{238}U$ values, indicating a stable drip system. This may relate to the depth of the cave, 76 m being a long percolation pathway insensitive to variations in the weathering horizon. The values for U and Th concentration vary only a little, mainly in the sample immediately above the major hiatus. $^{230}Th/^{232}Th$ activity ratios are shown on a logarithmic scale because most of the values are so high; only two values indicate detrital content, at ~35 - 42 mm, but at this great age any small proportion of non-radiogenic ^{230}Th is irrelevant.

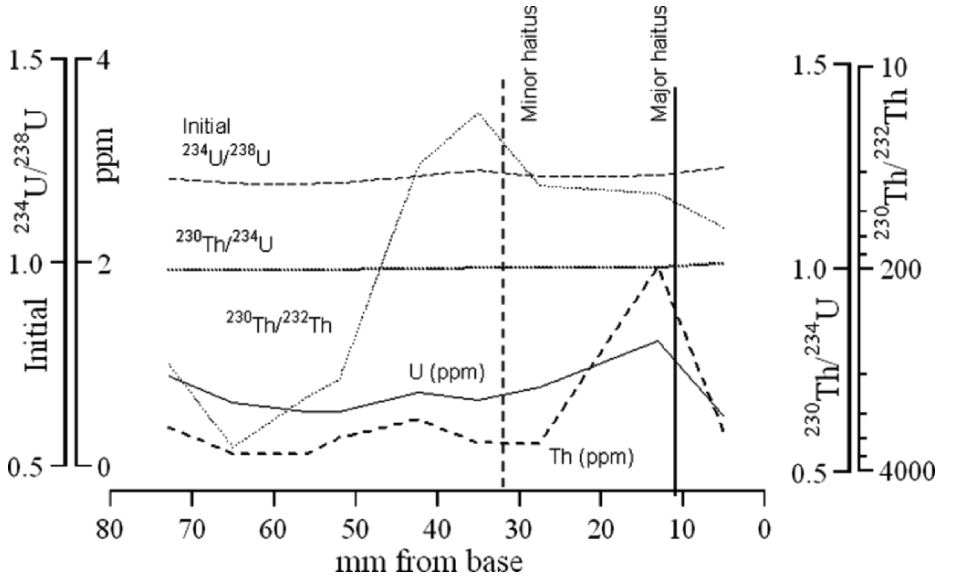

Figure 6. U and Th systematics for LP6 indicating a generally very stable system. 230Th/232Th is shown on a logarithmic scale, with lower values indicating higher detrital content at the top. The major hiatus of the Stage 12 glacial and the minor hiatus.

4.3 The isotopes

Figure 7 shows the $\delta^{18}O$ and $\delta^{13}C$ curves for LP6 in relation to position from base and stratigraphy as described in Figure 3. The range of $\delta^{18}O$ for modern calcite, of −6.9 to −6.3‰ come from active stalactite tips in the area (Lauritzen *et al*., 1990). The scales are placed such that the more depleted values lie at the top, representing the higher temperatures. This is done for three reasons: (i) because the more enriched values correlate with the early, cooler part of the interglacial as shown in the marine record; (ii) because the more depleted values are associated with the richer color which is usually related to a higher organic content from rich soils and high biogenic activity of warm times; and (iii) because this is in accordance with the commonly observed negative relationship of isotopes and temperature for north Norwegian caves (Lauritzen and Lundberg, 1999b; Linge *et al*. In prep, 2001a, b). Note that it is not consistent with Lauritzen *et al*. (1990) who argued for a positive relationship on theoretical grounds in the absence of detailed isotopic data and dates, and on the evidence of a positive relationship from Vancouver Island (Gascoyne *et al*., 1981). Figure 8 shows the stage 11 part of the isotopic curve in relation to age, using the linear growth model, and to the marine isotope curve from the North Atlantic ocean drilling site 607, the nearest core for which we can find data (Raymo *et al*., 1990).

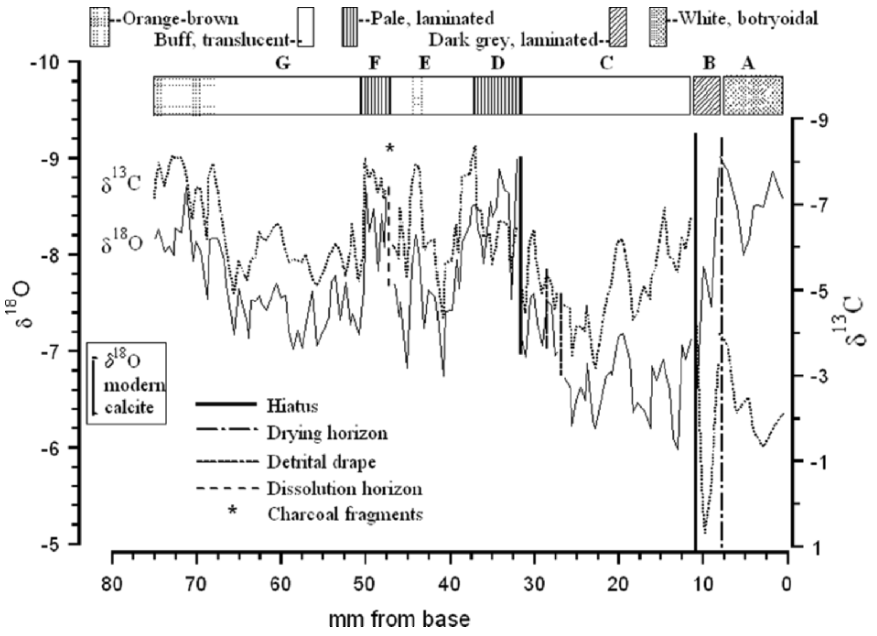

Figure 7. $\delta^{18}O$ and $\delta^{13}C$ curves for LP6 in relation to position from base and stratigraphic zones. The range of $\delta^{18}O$ for modern calcite, of −6.9 to −6.3‰ come from active stalactite tips in the area.

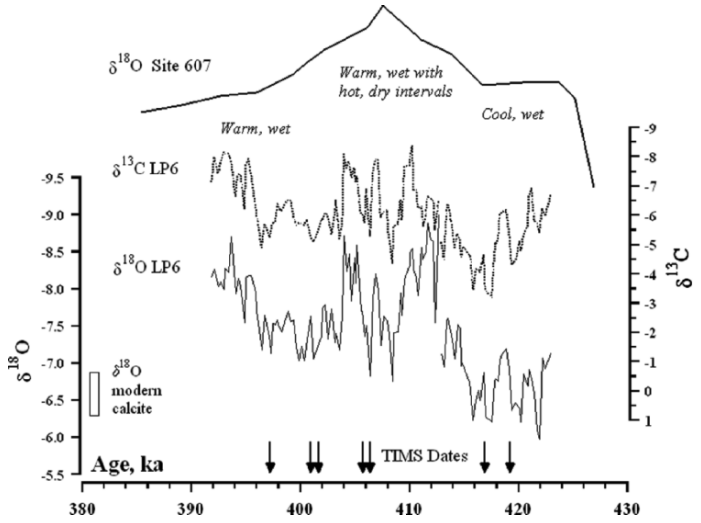

Figure 8. $\delta^{18}O$ and $\delta^{13}C$ curves in relation to age and to the marine isotope curve from Site 607. The isotope data points are assigned an age according to the linear age model described in the text. Values for modern calcite are included.

5. DISCUSSION

5.1 Termination V and the duration of isotope stage 11

Two of the most important questions not yet resolved in the literature are the dates of the beginning and the end of MIS 11; i.e., the timing of Termination V and the duration of the interglacial. The advantage of the present study is that it offers radiometrically-dated age estimates that are not tied to tuning techniques or any assumptions about orbital control of climate. The disadvantage is that neither the beginning nor the end is directly represented in these data.

Termination V is not directly represented because conditions suitable for calcite growth do not necessarily prevail immediately after the retreat of ice. Nevertheless, it is likely that calcite deposition resumed rapidly because the position of the cave high up on the valley side allows it to drain immediately after ice retreat from the uplands. Termination V must have occurred just before the earliest calcite growth at 421±10 ka (or 419.3 ±10 ka using the alternative model). The probability density function for this date is shown as curve *a* in Figure 5B and for all seven dates as curve *b*. Although the errors quoted here do not take into account the inter-relationship of the dates, the addition of other dates increases the probability that the age of the first calcite layer lies towards the centre or upper end of the 421±10 ka estimate (the mathematical expression of this probability is the subject of ongoing research). Termination V must lie to the right of this date, the probability rising from 421 ka and reaching its peak at 430 ka.

This estimate is generally in keeping with other published estimates, and adds to the small body of published radiometric dates. $^{40}Ar/^{39}Ar$ dates on volcanic ash layers in Rome placed Termination V within the broad interval 416-448 ka (Karner and Renne, 1998; Karner, 1999). The subaqueous calcite crust of Devils Hole, Nevada (Winograd et al. 1992; Coplen et al. 1994) grew throughout this time: Coplen et al. (1994) and Winograd et al. (1997) show the "approximate timing" of Termination V at 417 ka, but this timing is acknowledged to have large uncertainties. It is constrained by only two dates, one from the middle of MIS 11 at 402 ±10 ka and the other from the middle of MIS 12 at 438 ±15. In addition, the ages are minimum ages and need to be increased by groundwater travel times that may be several thousands of years (Coplen et al. 1994).

Other published estimates are not radiometric. Dating of the Vostok ice core based on ice-flow and accumulation models places the end of isotope stage 12 at 426 ka (Petit *et al.*, 1997). The SPECMAP record places Termination V at 423 ±5 ka (Imbrie *et al.*, 1984). Shackleton et al. (1990) date Termination V at 416 ka (ODP Site 677). These last two estimates rely on variations on astronomical tuning techniques.

Because of the inherent errors, all of these estimates overlap. The principal value of the LP6 estimate is that it limits the lower time range of possible ages. If we assume that calcite growth began within a few thousand years of ice retreat, then termination V in northern Norway occurred at ~424 ka, very close to the SPECMAP estimate. This supports the conclusion from the 1999 workshop on Marine Isotope Stage 11 (Poore *et al.*, 1999) that the SPECMAP time scale appears to represent the best model for dating MIS11.

The duration of the interglacial cannot be estimated directly from these data because the onset of MIS 10 glacial conditions is not directly represented in the LP6 calcite. Our transect was taken from the thickest part of the sample but the erosional hiatus at the top

may not represent the termination of deposition at the start of the isotope stage 10 glacial. Thus only the minimum duration of MIS 11 can be estimated. The date on end of calcite growth before MIS 10 glacial is 392 ±10 ka (or 375.5 ±10 ka, depending on the growth model used). The duration of MIS 11 was thus at least 27 kyr (419 to 392 ka) or up to 45.5 kyr (421 to 375.5ka). The longer estimate is based on the topmost measured date but the more conservative estimate is probably the more reasonable in view of the crystal form, isotopic results and colour as discussed below. SPECMAP suggests 20-30 kyrs (Imbrie *et al.*, 1984). Site 980 shows 30-40 kyrs (McManus *et al.*, 1999). The estimate from the Rome tephra site (Karner, 1999) is 15 kyr for the minimum duration and 41 kyr for the maximum duration; Winograd *et al.* (1997) suggested 20 kyr; Sarnthein and Tiedemann (1990) suggested 29 kyr. Even at the lower estimate of a minimum of 27 kyrs, the LP6 estimate supports the concept of a long stage 11 interglacial.

5.2 The isotopic record and sample stratigraphy

The minimally varying U and Th systematics over this record suggest stable drip routes; changes in percolation pathways can thus be ruled out as cause for the shifts in isotopic values.

From Figure 7 it can be seen that each obvious shift in the isotopic values is associated with a shift in the crystal form and in colour. This is not surprising since all are controlled by changing drip water properties and climate. Working from the base up, the first visible event is a double non-depositional hiatus 8 mm from the base made up of two minor hiatuses to either side of a white, opaque drying horizon. This is associated with a spike of depletion in both isotopes representing post-depositional alteration rather than evaporative dryness. The botryoidal crystal habit of Zone A is unique to this zone. The one date places it in isotope stage 13. The very few isotopic values do not allow strong conclusions to be made about paleoclimate: $\delta^{18}O$ values are more depleted than modern values suggesting a warm climate; $\delta^{13}C$ values are significantly higher than $\delta^{18}O$ perhaps indicating dry conditions. Although no date has been tried on the opaque, dark grey, laminated zone above this it has also been assigned to isotope stage 13 because it ends in a major hiatus. The placing of the dark grey zone, B, towards the end of interglacial is based on a rise in $\delta^{18}O$ values and on the requirement for a substantial time period for alteration of the white layer.

The second visible event is an erosional hiatus at 11 mm; although no detrital draping is apparent it is likely that this hiatus represents a major, long-term flooding event. The rest of the sample above the hiatus is dated to isotope stage 11; it is therefore assumed that the hiatus represents the isotope stage 12 glacial and Termination V. The hiatus has simply removed material; it has not caused any visible alteration in the calcite or in the isotopes.

The band of buff-colored, translucent pallisade calcite from 11 mm to 32 mm, Zone C, is relatively event-free, with only a few minor dissolution horizons or detrital drapes (not visible with the naked eye) representing short-term local flood events but not long-term glacial advance flooding. The isotopes show parallel oscillations and are somewhat more enriched than the upper zones of the sample. The oxygen isotopic values lie close to those of modern calcite in the cave, suggesting a moderately cool, wet climate similar to that of today. The oscillations in the carbon isotopic values follow the simple pattern of

greater depletion with greater biogenic activity during warmer times where humidity is not limiting. The absence of yellow or brown color suggests low organic content in the calcite and thus perhaps a relatively poor soil. The beginning of this zone lines up very well with the beginning of the isotope stage 11 interglacial from Site 607, the closest ocean site for which we have data. Pollen data (Sample #4, 25-28 mm, from Lauritzen *et al.*, 1990) show some carbonized elements interpreted as charcoal and some unidentified organic fragments, but otherwise no pollen or spores (as is quite normal for poorly ventilated caves).

The hiatus at 32 mm is minor, suggesting again a short-lived local event; the detrital drape is only barely apparent, very little erosion of underlying calcite has taken place, and there is only a small gap in the dates below and above the hiatus. The hiatus marks a change in form from translucent buff-coloured, pallisade crystals to dense, laminated, light coloured, opaque crystals.

The band of laminated calcite from 32 to 38 mm, Zone D, is not easy to interpret. It is associated with a shift to more depleted isotopic values. The depleted $\delta^{18}O$ values suggest high temperatures and the depleted $\delta^{13}C$ values suggest high biogenic activity. The position of the $\delta^{13}C$ values slightly below the $\delta^{18}O$ values suggests a slightly reduced drip rate from a possibly warm and slightly drier time. In addition, the laminae suggest drying out every summer. However, a high temperature with high biogenic activity would normally be accompanied by a high organic content in the speleothem calcite and this is not borne out by the pale color. The presence of occasional detrital traces indicates the occurrence of local flooding events. Pollen data (Sample #3, 33-37 mm) show extremely low counts (19 grains in total) but were interpreted by Lauritzen *et al.* (1990) as indicating open vegetation with birch, similar to the modern vegetation. The pollen are probably associated with the detrital traces visible in small lenses between some of the laminae, and thus carried in on a flood event. It is unlikely that the pollen was blown in on air currents because the cave would then have had higher ventilation and the isotopes would show enrichment from evaporation.

The sharp change in color and crystal form at 38 mm is accompanied by the shift to somewhat higher isotopic values. From 38 mm to 47 mm, Zone E, the translucent calcite is a rich dark orange color suggesting an organic-rich overlying soil. The generally depleted isotopic values and the rich color, along with the narrow spike of depletion in the middle coinciding with a narrow zone of deeper brown color, are interpreted here in the standard fashion as representing warm temperatures and high biogenic activity. The dates place this zone right at the peak of the interglacial. However, the pollen data (Sample #2) show only some unidentified organic fragments along with carbonized elements.

At 47 mm a minor dissolutional horizon with fragments of charcoal marks the beginning of another band of laminated pale-colored calcite, from 47 to 50 mm, Zone F, with depleted isotopes. The depleted $\delta^{18}O$ values suggest high temperatures and the even more depleted $\delta^{13}C$ values suggest high biogenic activity, with no diminution of the drip rate (a reduction of the drip rate would give more enriched $\delta^{13}C$ values). So the isotopes indicate warm, wet conditions but again the absence of color is not consistent with this picture of a rich flora. The pollen content of this zone was significant (Sample #1, 46-50 mm, Lauritzen *et al.*, 1990), indicating a diverse mixed forest dominated by birch and alder, along with a large proportion of carbonized elements. Presumably the visible charcoal fragments (10-50 μM) were carried into the cave with the minor flood event but

it is impossible to know if the pollen and carbonized dust were carried in on air currents. These carbonized elements suggest a fire regime in the forests, which would presumably mean some dry periods, consistent with the presence of visible laminations, which usually require a short but distinct break in deposition to give the sharp edge.

The rest of the sample, Zone G, is event-free translucent pallisade crystals with isotopic values similar to those of Zone E, slightly above modern values. The shift towards depletion for the top 10 mm coincides with an increase in the orange color, again paralleling the shift in Zone E.

Figure 8 shows LP6 isotopes from stage 11 plotted beside Site 607 isotopes, together with a summary of the interpreted climatic conditions. The isotopes are here plotted using the linear growth model for the upper part rather than the curved model based on the topmost measured date. This gives the more conservative timescale for the duration of the interglacial. Since the top of this flowstone shows depleted isotope values and richly colored palisade crystals, the final layers of growth from the cooling down phase of early isotope stage 10 are probably lost to erosion.

5.3 Paleoclimate of Isotope Stage 11

The paleoclimate indicated in LP6 for isotope stage 11 shows in the early part of the interglacial a cool, wet stage similar to the modern climate (Zone C); this gives way to alternating hot phases (Zones D and F) and warm, relatively wet phases (Zones E and G). The two warmest times occurred at ~412 and 405 ka. Most of the interglacial was warmer than today with a dense forest subject to occasional fires. This warmth seems to be in keeping with many other estimates of a warmer-than-today interglacial (Howard, 1997; Poore and Dowsett, 2001) although the evidence remains equivocal (Poore *et al.*, 1999). Several marine records indicate a cooler ocean temperature (Oppo *et al,* 1998), while many terrestrial records show that MIS 11 was either warmer than, or as warm as, MIS 5e or the Holocene (Rousseau, 1999), and in many cases wetter. Although the records are few, there seems to be some indication that the warmth was expressed more strongly in the northern latitudes, related to the extreme northern position of the Polar Front at this time and to the higher sea surface temperatures (Ruddiman *et al.*, 1989; Aksu *et al.*, 1992). Korejwo and Brigham-Grette (1999) find evidence in coastal Alaska for "an extremely warm interglacial"; biogenic silica production in Lake Baikal was among the highest of the last 800 kyrs during MIS 11 (Williams *et al,* 1997); while the record from France did not show increased warmth but only increased wetness (Rousseau, 1999).

The division into an early cool phase and a middle warm phase fits well with $\delta^{18}O$ variations from Site 607 (Raymo *et al.*, 1990) and Site 980 (Oppo *et al.*, 1998); the shift up to the warmer stage in both these orbitally-tuned marine records occurs at ~412 ka. In general the isotopic curve from LP6 closely parallels the relevant section from the Cariaco Basin curve shown in Poore and Dowsett (2001).

Millenial-scale but low-amplitude oscillations are shown on virtually all the MIS 11 records of sufficient resolution (eg, Oppo *et al.*, 1998); McManus *et al.* (1999) note that MIS 11 has the longest period of relative climatic stability in the last 500 kyrs where sea surface temperature variations were limited to 1-2°C. The resolution of the LP6 isotopic record and the dating basis for the growth model do not allow strong conclusions to be

made about the periodicity of oscillations. It can only be stated that the record shows that oscillations occurred in both the cool early stage and the warm middle to late stages, and that the oscillations appear to be on the order of 1.5 - 2 kyrs long.

6. CONCLUSION

The nine TIMS dates from this old flowstone from Laphullet, close to the Arctic Circle in north Norway, reveal it to have grown mainly during isotope stage 11. The dates are in perfect stratigraphic order in spite of their ages being close to the limit of the technique.

Termination V can be placed at approximately 423 ±10 ka, before ~421 ka and probably after 430 ka. The duration of isotope stage 11 is either 27 kyrs or 45.5 kyrs depending on the growth model used for the upper 15 mm of the sample.

The paleoclimatic interpretation for stage 11 interglacial shows that it began with a cool, wet phase similar to today; the majority of the interglacial was warmer than today, with a dense mixed forest, and some local flood events, and some forest fire events.

7. ACKNOWLEGEMENTS

Financial support was provided by a Norwegian Research Council grant to both authors. Dick Poole is thanked for his thoughtful and constructive review.

8. REFERENCES

Berstad, I. ,1998, *Uranseriedatering og stabilisotopanalyse av speleothemer fra Søylegrotta, Mo i Rana.* Cand. scient. thesis in Norwegian (unpublished), University of Bergen, 122 pp.

Cook, E.R., D'Arrigo, R.D. and Briffa, K.R. , 1998, A reconstruction of the North Atlantic Oscillation using tree ring chronologies from North America and Europe. *The Holocene*. v. 8, p. 9-19.

Coplen, T.B., Winograd, I.J., Landwehr, J.M., and Riggs, A.C., 1994, 500,000-year stable carbon isotopic record from Devil's Hole, Nevada. *Science*, 263: 361-365.

Howard, W.R., 1997, A warm future in the past. *Nature,* v. 388, p. 418-419.

Howard, W.R., 1999, The Marine Record of the MIS 11Oscillation. *In* Poore, R. Z., Burckle, L., Droxler, A., McNulty, W.E., Marine Oxygen Isotope Stage 11 and associated Terrestial Records: Workshop Report. *USGS Open File Report* 99-312. p. 31-34.

Hurrell, J. W., 1995, Decadal trends in the North Atlantic Oscillation regional temperatures and precipitation. *Science*, 269, 676-679.

Gascoyne, M., Ford, D.C., and Schwarcz, H.P., 1981, Late Pleistocene chronology and paleoclimate of Vancouver Island determined from cave deposits. *Canadian Journal of Earth Sciences* 18: 1643-1652.

Imbrie, J., Hays, J.D., Martinson, D.G., McIntyre, A., Mix., A.C., Morley, J.J., Pisias, N.G., Prell, W.L. and Shackleton, N.J., 1984, The orbital theory of Pleistocene climate: support for a revised chronology of the marine oxygen isotope record. In: Berger, A.L. et al (eds.) *Milankovitch and Climate.* Part 1. pp. 269-305. Riedel, Dordrecht.

Karner, D. B., and Renne, P. R., 1998, 40Ar/39Ar geochronology of Roman Volcanic Province tephra in the Tiber River valley: Age calibration of Middle Pleistocene sea-level changes. *Geological Society of America Bulletin*, 110, p. 740-747.

Karner, D.B. , 1999, $^{40}Ar/^{39}Ar$ dating of Glacial Termination V and duration of the Stage 11 highstand. *In* Poore, R. Z., Burckle, L., Droxler, A., McNulty, W.E., Marine Oxygen Isotope Stage 11 and associated Terrestial Records: Workshop Report. *USGS Open File Report* 99-312. p.35-40.

Korejwo, D.A. and Brigham-Grette, J., 1999, A paleoceanographic interpretation for a Middle Pleistocene interglacial based on micropaleontoloy and ostracode Mg/Ca shell chemistry, Arctic Coastal Plain, Alaska. *In* Poore, R. Z., Burckle, L., Droxler, A., McNulty, W.E., Marine Oxygen Isotope Stage 11 and associated Terrestial Records: Workshop Report. USGS *Open File Report* 99-312. p.41-43.

Lamb, P.J. and Peppler, R.A., 1987, North Atlantic Oscillation: concept and application. *Bull. Amer. Meteor. Soc.*, 68, 1218-1225.

Lauritzen, S-E. and Lundberg, J., 1999a, (Eds,) Holocene Special Issue: Speleothems as high-resolution palaeoclimatic archives". *The Holocene*, 9 (6), 643-726.

Lauritzen, S.-E. and Lundberg, J., 1999b, Calibration of the speleothem delta function: an absolute temperature record for the Holocene in northern Norway. *The Holocene,* v. 9, 659-670.

Lauritzen, S.-E., Løvlie, R., Moe, D. and Østbye, E., 1990, Paleoclimate deduced from a multidisciplinary study of a half-million-year-old stalagmite from Rana, Northern Norway. *Quaternary Research,* 34, 306-316.

Linge, H., Lundberg, J. and Lauritzen, S.-E., In prep., Isotope stratigraphy of Holocene speleothems: an example from Fauske, northern Norway.

Linge, H., Lauritzen, S.E., Lundberg, J. and Berstad, I.M., 2001a, Stable isotope stratigraphy of Holocene speleothems: examples from a cave system in Rana, northern Norway. *Palaeogeography, Palaeoclimatology, Palaeoecology*, v. 167, p. 209-224.

Linge, H., Lauritzen, S.-E. and Lundberg, J., 2001b, Stable isotope stratigraphy of a late last interglacial speleothem from Rana, northern Norway. *Quaternary Research,* v. 56. p. 155-164.

Linge, H., 1999, *Isotopic studies of some northern Norwegian speleothems and calcareous algae from Svalbard.* Unpublished Ph.D thesis, Geologic Institute, University of Bergen, Norway.

McManus, J.F., Oppo, D.W., and Cullen, J.L., 1999, A 0.5-Million-Year Record of Millenial-Scale Climate Variability in the North Atlantic. *Science*, 283, 971-975.

Oppo, D. W., McManus, J. F., and Cullen, J. L., 1998, Abrupt climate events 500,000 to 340,000 years ago: Evidence from subpolar North Atlantic sediments. *Science*, 279, p. 1335-1338.

Petit, J.R. and twelve others, 1997, Four climate cycles in Vostok ice core. *Nature*, 387, 359.

Poore, R.Z. and Dowsett, H.J., 2001, Pleistocene reduction of polar ice caps: evidence from Cariaco Basin marine sediments. *Geology*, v. 29, p. 71-74.

Poore, R. Z., Burckle, L., Droxler, A., McNulty, W.E., 1999, Marine Oxygen Isotope Stage 11 and associated Terrestial Records: Workshop Report. *USGS Open File Report* 99-312, 79p.

Raymo, M. E., Rudimann, W. F., Shackleton, N. J., and Oppo, D. W.,1990, Evolution of Atlantic-Pacific $\delta^{13}C$ gradients over the last 2.5 M.Y. *Earth Planetary Science Letters*, v. 97, p. 353-368.

Rousseau, D.-D., The Continental record of Stage 11. *In* Poore, R. Z., Burckle, L., Droxler, A., McNulty, W.E., 1999, Marine Oxygen Isotope Stage 11 and associated Terrestial Records: Workshop Report. *USGS Open File Report* 99-312. p.59-72.

Ruddiman, W.F., Raymo, M.E., Martinson, D.G., Clement, B.M. and Backman, J., 1989, Pleistocene evolution of northern hemisphere climate. *Paleoceanography*, 4, 353-412 .

Sarnthein, M. and Tiedemann, R., 1990, Younger Dryas-style cooling events at Glacial Terminations I-VI at ODP Site 658: associated benthic $\delta^{13}C$ anomalies constrain meltwater hypothesis. *Paleoceanography* 5, 1041-1055.

Shackleton, N.J., Nicholas, J., Berger, A. and Peltier, W.A., 1990, An alternative astronomical calibration of the lower Pleistocene timescale based on ODP Site 677, *Transactions of the Royal Society of Edinburgh – Earth Sciences*, 81, 251-261.

Williams, D.F., Peck, J., Karabanov, E.B., Prolopenko, A.A., Kravinsky, V., King, J. and Kuzmin, M.I. , 1997, Lake Baikal record of continental climate response to orbital insolation during the past 5 million years. *Science*, 278, 1114-1117.

Winograd, I.J., Coplen, T.B., Landwehr, J.M., Riggs, A.C., Ludwig, K.R., Szabo, B.J., Kolesar, P.T., and Revesz, K.M., 1992, Continuous 500,000-year climate record from vein calcite in Devils Hole, Navada. *Science*, 258: 255-260.

Winograd, I.J., Landwehr, J.M., Luwig, K.R., Coplen, T.B., and Riggs, A.C., 1997, Duration and structure of the past four interglaciations. *Quaternary Research*, 48: 141-154.

ESTABLISHING A SPELEOTHEM CHRONOLOGY FOR SOUTHWESTERN OREGON

Climatic controls and growth modeling

Steven C. Turgeon, and Joyce Lundberg*

1. ABSTRACT

Cave calcites from Oregon Caves National Monument (OCNM), a dissolutional Cave system located in the Klamath Mountains of southwest Oregon, are shown to refelect golobal paleoclimates. Given the high cost of obtaining numerous U-series dates and that many records lie beyond the range of the U-Th dating method (~500 ka), we have explored a technique for modelling the growth of speleothems both between dates and beyond 500 ka using theoretical and empirical growth data applied to OCNM speleothems. Fourtheen U-series TIMS dates indicate mean growth rates between 1.54×10^{-3} to 3.15×10^{-2} mm.a^{-1} mostly during early interglacials. Speleothem isotopes from dated intervals show direct relationships with temperature, and correlate well with high-frequency Holocene events (~200 years) in the GISP2 ice core, as well as to glacial to interglacial terminations. Contrary to theroretical predictions showing that temperature should predominantly control calcite growth, result from our samples indicate that growth rates are linear for given growth periods on time scales of $\sim 10^3$ to 10^4 years. The calculated growth rates, however, are broadly within the 2 to 5 x overpredication factors reported for theoretical growth rates. We suggest that in this area, both temperature and water film thickness control growth rates. Outcrop-scale discontinuities, representing prolonged hiatuses, are presumed to be caused by groundwater freezing during extended perigacial conditions. These hiatuses range from 14 to 102 kyrs are and get longer over the course of the Quaternary. An accompanying increase in growth rates suggests an opening of the cave system and shallowing of the rock overburden, which shifts the dissolutional system from closed to open. A simple "start-stop" growth model is presented, based on

* Steven C. Turgeon, Centre géoscientifique d'Ottawa-Carleton, Department of Earth Science Careleton University Ottawa, Ontario, Canada, KIS 5B6. Present address: Department of Earth and Atmospheric Sciences, University of Alberta, Edmonton, Alberta, Canada, T6G 2E3, e-mail: turgeonsc@ualberta.ca. Joyce Lundberg, Department of Geography and Environmental Studies, Carleton University, Ottawa, Ontario, Canada, KIS 5B6, e-mail: joyce_lundberg@carleton.ca.

minimum and maximum $\delta^{18}O$ isotopic values of marine records before or during terminations and shortly after the onset of climatic deterioration. Although this model shows a very good correspondence between growth periods of cave calcites and termination of glaciations, correlation with precipitation initiation and cessation lines show mixed results, possibly owing to uncertainties related to global records which might not be indicative of actual local conditions encountered at OCNM.

2. INTRODUCTION

Recently, much attention has been focused on cave calcites (speleothems) as archives of climatic and paleoenvironmental changes in terrestrial environments (Dorale et al., 1992; Matthews et al., 1996; Baker et al., 1998; Dorale et al., 1998; Dreybrodt, 1999; Lauritzen and Lundberg, 1999a). Factors contributing to make speleothems valuable paleoenvironmental indicators include: (i) their high preservation potential, shielded from Earth-surface erosional processes; (ii) their crystalline structure, frequently composed of coarsely crystalline inorganic calcite ($CaCO_3$) that records geochemical signatures of global and regional events transferred through atmospheric processes; and (iii) the resistance of speleothems to post-depositional recrystallisation and diagenesis.

Speleothems can be dated to a high accuracy and precision using uranium series disequilibrium methods (Edwards et al., 1986; Blackwell and Schwarcz, 1995). Thermal ionisation mass spectrometric (TIMS) U-Th is the preferred dating method because of its high precision (typically <1% 2σ errors), its potential age range (0-500 ka), its generally small sample size requirements (depending on U-content, but usually <1 g), and its suitability for use in terrestrial carbonates (owing to the solubility of uranium and its subsequent transport and incorporation into secondary carbonate minerals). Most high-resolution paleoclimatic reconstructions from speleothems rely on high-frequency dating along the growth axis of a speleothem. This, however, is time consuming and expensive. For large samples, it is often feasible to do only a few dates on a given speleothem, leaving the intervals between these chronological anchors devoid of absolute chronological control.

An alternative approach to modelling growth is hereby sought. Studies have shown that growth rates can be assessed using theoretical considerations of the chemical equilibria and kinetics of calcites in relation to climate (Buhmann and Dreybrodt, 1985a,b; Dreybrodt, 1999). In order to provide chronological controls for intervals between dates, this paper explores how these theoretical aspects might apply to modelling long-term growth for speleothems from a site on the west coast of North America. This is done by using $\delta^{18}O$ isotopic signatures from dated sections of speleothems, and comparing them to well-established high-resolution paleoclimatic records, since the oxygen isotopes contained within the $CaCO_3$ crystals of speleothems have been shown to vary with climate (Gascoyne, 1992; Bradley, 1999). These concepts can then be applied to paleoclimatic records from older speleothems, lying beyond the range of U-Th dating.

The following section provides an overview of the theoretical aspects of growth modelling, with emphasis on climatic influences. In the second part of this paper, we provide a brief description of the samples and assess their potential to contain

climatically-derived stable isotopic signatures. The third part of this paper focuses on modelling the deposition of our samples.

3. CAVE CALCITE DEPOSITION

The chemical reactions involved in inorganic calcite precipitation are fairly well known with respect to karst environments (Hendy, 1971; Buhmann and Dreybrodt, 1985a,b). As well, the contribution of individual factors involved in the growth of speleothem, such as CO_2 degassing, Ca^{2+} concentration ($[Ca^{2+}]$), and flow conditions over the surface of the speleothem, have been modelled (Dreybrodt, 1996; Dreybrodt, 1999). It has been shown that rates of calcite precipitation in thin sheets of water are mainly dependent on Ca^{2+} concentration and the type of flow (laminar vs. turbulent) over the surface of the speleothem (Dreybrodt, 1996), although most speleothems are only covered with thin films of water (typically <0.01 cm on average; Baker and Smart, 1995). Given the smooth surfaces encountered on most speleothems, flow of thin films of water should be either laminar or quasi-laminar (Boggs, 1987), leaving $[Ca^{2+}]$ as the major growth rate control. This section provides a brief overview of the processes involved in the dissolution of carbonate bedrock and precipitation of calcite within a spelean environment.

Three stages are involved in speleothem deposition (Holland et al., 1964; Hendy, 1971; Ford and Williams, 1989):

1) *Carbonation of meteoric water* occurs in soils overlying caves. During percolation through soil, meteoric waters, already in equilibrium with atmospheric CO_2, acquire pedogenic CO_2 as the partial pressure of soil carbon dioxide is much higher ($pCO_{2\,(soil)}$ is up to 5×10^{2} or about $10^{-1.3}$ at 25°C; Figure 1a) than atmospheric CO_2 ($pCO_{2\,(atm)} = 3\times10^{-4}$ or $10^{-3.5}$) owing to the oxidation of organic matter and biological respiration (Miotke, 1974; Rightmire, 1978). Carbonic acid, resulting from the mixing of meteoric water and soil CO_2, forms following $H_2O + CO_2 = H_2CO_3$. This weak acid solution is then channeled or percolated through the soil towards the water table and eventually reaches the carbonate bedrock.

The biogenic soil CO_2 ($pCO_{2\,(biogenic)}$) can be estimated using (Drake and Ford, 1981):

$$\log [pCO_{2\,(biogenic)}] = -2 + 0.04T_{air/gw} \quad \text{(Eq. 1)}$$

where $T_{air/gw}$ is the annual average air temperature or groundwater temperature (in °C). The actual $pCO_{2\,(soil)}$ is lower than this biogenic CO_2 because of inhibition processes caused by elevated CO_2 concentrations (or depleted oxygen concentrations). It can be estimated using Eq.2 (Drake, 1980):

$$pCO_{2\,(soil)} = [(0.21-pCO_{2\,(soil)})/0.21]\times pCO_{2\,(biogenic)} \quad \text{(Eq. 2)}$$

It has also been shown that $pCO_{2\,(soil)}$ values are reached only during summer growth seasons in temperate mid-latitudes climes (Rightmire, 1978): during winter, soil CO_2 equilibrates with atmospheric CO_2. Figure 1a illustrates the long-term influence of temperature on biogenic pCO_2 levels (upper curve) as well as the actual soil CO_2 ($pCO_{2\,(soil)}$), reaching approximately 5×10^{-2} atmosphere at 25°C.

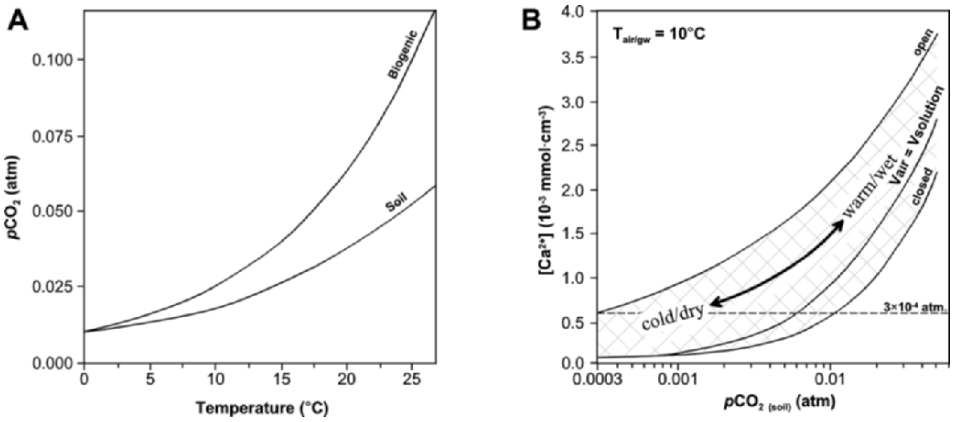

Figure 1. CO_2 partial pressure control on carbonate dissolution: A) effect of temperature on biogenic soil pCO_2 and total soil pCO_2; soil pCO_2 is lower than biogenic pCO_2 due to inhibition effects of high CO_2 or low oxygen levels (Drake, 1983); and, B) equilibrium concentrations of Ca^{2+} with respect to calcite for open, closed, and restricted air volume systems ($V_{air} = V_{solution}$). Equilibrium pCO_2 values below atmospheric equilibrium is where dissolution occurs, while the cross-hatched area indicates where precipitation occurs (figures modified from Dreybrodt, 1999).

2) *Dissolution of carbonate bedrock* by the groundwater solution follows $CaCO_3 + H_2CO_3 = Ca^{2+} + 2HCO_3$. Given that levels of soil CO_2 in humid environments are generally greater during the summer months, as well as during longer-term warm periods such as interglacials, higher bedrock $CaCO_3$ dissolution rates occur in response to increasing temperature and vegetation/microorganism levels (Rightmire, 1978; Lohmann, 1988).

Two dissolution system end-members can occur: the first is when the soil is free of carbonates and the meteoric waters reach equilibrium with $pCO_{2\,(soil)}$. This solution then percolates to bedrock and dissolves carbonates away from the CO_2 source under "closed" (also referred to as "sequential" by Drake, 1983) conditions (Garrels and Christ, 1965; Hendy, 1971). These conditions are illustrated in Figure 1b ("closed" curve). The dashed line represents $[Ca^{2+}]$ in equilibrium with atmospheric conditions (3×10^{-4} atm) (in most cave systems, cave air CO_2 is close to atmospheric CO_2). Below the dashed line, the solutions are undersaturated with respect to calcite and calcite dissolution occurs until equilibrium is reached. The second end-member is the "open" ("coincident" of Drake, 1983) system (Garrels and Christ, 1965; Hendy, 1971), where an "infinite" CO_2 source is in contact with carbonates ("open" curve of Figure 1b). This allows for the dissolution of calcite while maintaining high $pCO_{2\,(soil)}$ levels of the groundwater. Carbonate regoliths, shallow soils, or soils in contact with bedrock are examples of such settings (Drake, 1983). Conditions between these end-members are probably more common and can occur due to restricted soil air volumes interacting with percolating meteoric water. The $V_{air} = V_{solution}$ curve on Figure 1b illustrates the Ca^{2+} concentration with respect to $pCO_{2\,(soil)}$ for a mixed system comprised of equal air and solution volumes. In general, the pCO_2 of soils with little or no organic matter, such as those found in cold or dry environments, will lie

towards the left of the graph shown in Figure 1b. Soils with abundant organics (from warm and wet environments) display higher pCO_2 levels and require higher concentrations of Ca^{2+} to reach saturation (Figure 1b).

3) *Carbonate precipitation* follows. When the carbonate-bearing solution is transported into an air-filled cavity, $CaCO_3$ will precipitate if the solution becomes supersaturated (with respect to $CaCO_3$), either through loss of CO_2 to the cave atmosphere, evaporation, the common-ion effect and/or pressure-temperature changes (Hill and Forti, 1997). Loss of CO_2 by diffusion is the most common mechanism for saturation of $CaCO_3$-bearing drip waters for areas of high humidity removed from strong airflow (Dublyansky, 1995; Hill and Forti, 1997). Deposition from evaporation is limited to situations with high airflow, while the last two mechanisms rarely operate in standard meteoric water carbonate settings.

As shown above, if the initial dissolutional parameters are known (mean annual temperature, type of dissolution system), then the $[Ca^{2+}]$ of the cave dripwaters can be estimated: Drake and Wigley (1975) demonstrated an empirical correlation between regional temperatures and spring water pCO_2, and thus CO_2. The next section summarises the controls on precipitation and translates them into growth rates.

3.1. Parameters Involved in Speleothem Growth

Speleothem precipitation rates from thin water films open to the cave atmosphere are controlled by three processes (Baker and Smart, 1995; Baker et al., 1998): 1) chemical reactions at the calcite-solution interface as described by the rate equations of Plummer et al. (1978) through which precipitation rates can be calculated when the concentrations of reactants are known; 2) mass transport of reactants through the solution towards or away from the speleothem surface; and 3) the rate-limiting reaction $H^+ + HCO_3^- = H_2O + CO_2$, through which CO_2 is released into the cave atmosphere. Buhmann and Dreybrodt (1985a,b) have solved the transport equations taking into consideration these three mechanisms in order to obtain precipitation rates. For speleothems, Eq.3 can approximate these processes within 10%:

$$\text{Precipitation rate } (\text{mmol}\cdot\text{cm}^{-2}\cdot\text{s}^{-1}) = \alpha([Ca^{2+}]-[Ca^{2+}]_{equilibrium}) \quad \text{(Eq. 3)}$$

where α is a $pCO_{2\ (cave\ air)}$-, dripwater temperature- ($T_{dripwater}$) and flow characteristic-dependent (mainly film thickness) kinetic rate constant, in $cm\cdot s^{-1}$; $[Ca^{2+}]$ and $[Ca^{2+}]_{equilibrium}$ are respectively the actual and equilibrium concentrations of Ca^{2+} ions with respect to calcite, in $mmol\cdot cm^{-3}$, in the water film. $[Ca^{2+}]$ is controlled by the dissolution of the carbonate substrate, determined by the $pCO_{2\ (soil)}$, prior to the solution entering the cave. $[Ca^{2+}]_{equilibrium}$ is the equilibrium concentration of Ca^{2+} under atmospheric CO_2 conditions (for 3×10^{-4} atm). Equation 3 can be used in situations where solution flow over the speleothem is high: it has been calculated that high flow rates ($>>1\ cm^3\cdot s^{-1}$) should generate sizeable features of at least 2-3 m in diameter (Dreybrodt, 1999), such as the flowstones that are described below. Otherwise, drip rate must be taken into account (Dreybrodt and Franke, 1987; Dreybrodt, 1988). Both the value for α and for $[Ca^{2+}]_{equilibrium}$ can be obtained using Buhmann and Dreybrodt (1985a; Table 1). For example, under laminar or stagnant flow conditions, values of $6.35\times10^{-6}\ cm\cdot s^{-1}$ and

6.3×10^{-4} mmol·cm^{-3} were obtained for α and $[Ca^{2+}]_{equilibrium}$ respectively (for $T_{dripwater}$ = 10°C, water film thickness (d) = 0.01 cm and $pCO_{2\ (cave\ air)}$ = 3×10^{-4} atm). Within this range, $[Ca^{2+}]_{equilibrium}$ as a function a temperature can be summarized by (Dreybrodt, 1988):

$$[Ca^{2+}]_{equilibrium} = (-0.01T_{dripwater} + 0.72)/1000 \text{ mmol·cm}^{-3} \quad \text{(Eq. 4)}$$

where $T_{dripwater}$ is the dripwater temperature in °C. The use of Eqs. 3 and 4 to determine growth rates provides estimates for $[Ca^{2+}] > 1.5\times10^{-3}$ mmol·cm^{-3}, although inhibition processes might be present close to equilibrium, which may reduce the rates significantly (Dreybrodt et al., 1997).

Table 1. Growth rate changes in response to increases in growth parameters[a]

Parameter	Mean[b]	Modelled increase	Δ growth rate (mm·yr^{-1})
$[Ca^{2+}]$	2×10^{-3} mmol·cm^{-3} $\pm3\times10^{-4}$	$+1\times10^{-3}$ mmol·cm^{-3}	+0.037
d	0.08 mm ±0.06	+0.04 mm	+0.025
$T_{dripwater}$	10°C	+5°C	+0.018
$pCO_{2\ (cave\ air)}$	3×10^{-4} atm	$+1.5\times10^{-4}$ atm	+0.007

[a] After Baker and Smart (1995).
[b] Errors quoted as 1σ.

Figure 2 illustrates the response of various parameters to temperature. Figure 2a shows the effects of increasing $[Ca^{2+}]$ on growth rate for various thicknesses (d) of the supersaturated water film, illustrating a slight increase with thickness, although the rate becomes independent of thickness between 0.02 cm and 0.04 cm (Dreybrodt, 1996). One study reports a mean speleothem water film thickness of 7.5×10^{-3} cm, albeit with a $\pm5.5\times10^{-3}$ cm 1σ error (Baker and Smart, 1995). Figure 2b shows significant increases in precipitation rates for increasing temperature for a given film thickness and $pCO_{2\ (cave\ air)}$. Figure 2c illustrates the effect of $pCO_{2\ (cave\ air)}$, occasioning a slight reduction in growth rates with increased $pCO_{2\ (cave\ air)}$. This effect, however, is small. The average atmospheric pCO_2 is 3×10^{-4} atm, which is often taken as the average value for cave air pCO_2, although caves occasionally exhibit much higher values (Ek and Gewelt, 1985). The overall effect of these parameters on the actual value of α is illustrated in Figure 2d, showing a marked non-linear increase with temperature. Dreybrodt and Buhmann (1987) have shown that the presence of foreign ions does not affect precipitation rates.

Growth rates can be obtained by converting mmol·cm^{-2}·s^{-1} to mm·yr^{-1} by multiplying by 1.1677×10^{7} cm^3·s·mmol^{-1}·yr^{-1}, assuming a molecular weight of 100.09 g·mol^{-1} for $CaCO_3$, a density (ρ) for compact calcite of ≈2.7 g·cm^{-3} and time conversion factor of 3.156×10^{7} s per year (Dreybrodt, 1980). However, spelean calcites with up to 10% porosity have been reported (Genty et al., 1997). Some of this porosity arises from incomplete coalescence of crystallites forming common columnar crystals (Kendall and Broughton, 1978). As well, some types of speleothems with extensive micro-gour

development can have high porosities owing to the development of dog-tooth calcite crystals in standing water (Hill and Forti, 1997). Contrary to the speleothems discussed in this study (see Turgeon and Lundberg, in press), these gour speleothems require high-angle slopes (Hill and Forti, 1997) and are not commonly used in high-resolution paleoclimatic studies. Growth rates can be corrected by determining porosity in samples and adding this volume to the rates obtained from Eqs. 3 and 4 above. Given that porosities are generally small (<10%; Baker et al., 1998), this factor is not significant considering other uncertainties involved in the growth model.

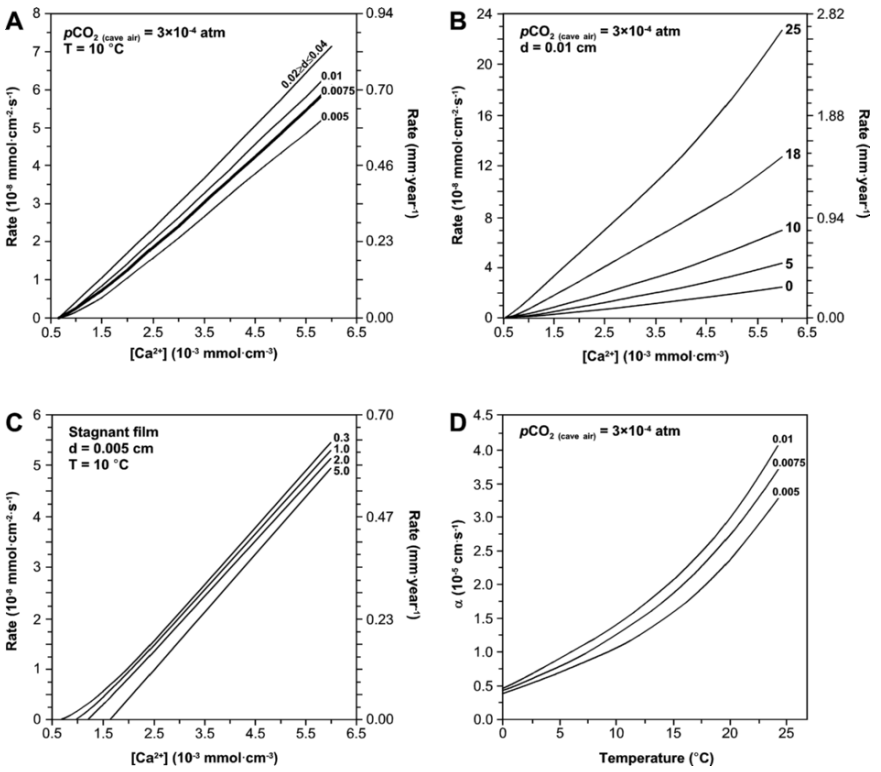

Figure 2. Effects of different parameters on cave calcite growth rate: A) precipitation rates for various film thicknesses (d in cm; the thicker line represents average film thickness of 7.5 cm^{-3}; Baker and Smart, 1995) as a function of $[Ca^{2+}]$ in the water film (T = 10°C, cave $pCO_2 = 3\times10^{-4}$ atm); B) precipitation rates (with d = 0.01 cm and cave $pCO_2 = 3\times10^{-4}$ atm) for various temperatures (in °C);C) precipitation rates for various cave pCO_2 levels (in 10^{-3} atm) (d = 0.005 cm, T = 10°C); D) values of the kinetic constant α as a function of temperature for different film thicknesses (d in cm)(cave $pCO_2 = 3\times10^{-4}$ atm). All figures after Baker et al. (1998).

Baker and Smart (1995) presented data calculated for a 50% increase in growth parameters modelled from the means of actual samples (Table 1). According to this table, changes in $[Ca^{2+}]$ account for 43% of the variability while 29% is explained by water film thickness, and temperature and CO_2 partial pressure account for 21% and 8% respectively. This is in agreement with Dreybrodt (1988). These data suggest that growth

rates are sensitive to temperature variations, with higher growth rates occurring in response to higher temperatures (assuming a constant film thickness d). Overall, this theoretical model has been shown to overestimate the actual growth rate by approximately 2 to 5 times for laminar flow conditions (Baker and Smart, 1995), owing to uncertainties associated with the rate equations of Plummer et al. (1978). These uncertainties could relate to differences in surface roughness between experimental and natural calcites, in addition to seasonal cessation and variations of water supply and soil pCO_2 that have yet to be accounted for and incorporated into this model. Although these parameters are known and can be measured with a satisfying degree of accuracy for present-day speleothem deposition (Baker and Smart, 1995; Baker et al., 1999), the individual effects of these parameters are difficult or impossible to isolate in older cave deposits. However, these theoretical considerations point out that temperature influences most of these parameters and mechanisms, including $pCO_{2\,(soil)}$ (film thickness is often assumed to be constant over stalagmites and flowstones owing to their slopes, hence recharge rates are thought to have little or no effect on film thickness). This points to the possibility of modelling speleothem growth rates as a function of temperature using well-established paleotemperature proxies (such as $\delta^{18}O$ and other signatures from marine-, ice-, and other long-term records). Paleotemperature records from speleothems include $\delta^{18}O$, although the effect of temperature on the proxy needs to be established for each site (Lauritzen and Lundberg, 1999b). The speleothem record can be anchored with whatever U-series dates are available. The growth rate function used to assign ages to the isotopic values can then be optimised so that the peaks and troughs of the speleothem curve conform to those of the well-established paleotemperature proxy. This can be tested first in the well-dated sections of the speleothem and then applied to other sections. Below we present the results of this exercise applied to speleothem samples from Oregon Caves National Monument.

4. STUDY AREA

Oregon Caves National Monument (OCNM) is located on steep, northwest facing slopes of the Klamath Mountains physiographic province in southwestern Oregon, approximately 65 km inland from the Pacific Ocean (Figure 3), from which the cave site's rainfall is derived (transported through westerly winds). The OCNM site is located south of the maximum limit of Pleistocene ice sheets (Figure 3), allowing us to rule out advancing continental ice sheets as a non-depositional control on speleothem formation at OCNM. The Monument is located at an altitude of approximately 1400 m ASL, covers 1.9 km^2, and is nested amidst old-growth Douglas- and white firs, providing abundant organic matter to the soils overlying the cave.

OCNM consists of a main dissolutional cave developed in a Triassic marble lens, bounded by pyrite-rich argillites. Cave development is controlled by a NE joint system and high-angle (60° to 85°), N-S trending normal faults within the marble lens, formed in response to tectonic activity during the Miocene (Wells and Heller 1988). These faults and joints allow the deep penetration of water into the subsurface and regulate passage alignment of the cave. The cave contains several subhorizontal levels representing former water table levels controlled by river down-cutting. The most laterally extensive level,

located at approximately 28 m above the main entrance, contains thick, well-developed flowstones from which most of our samples come. Few speleothems are located at higher levels, formed mainly by vadose drawdown shafts.

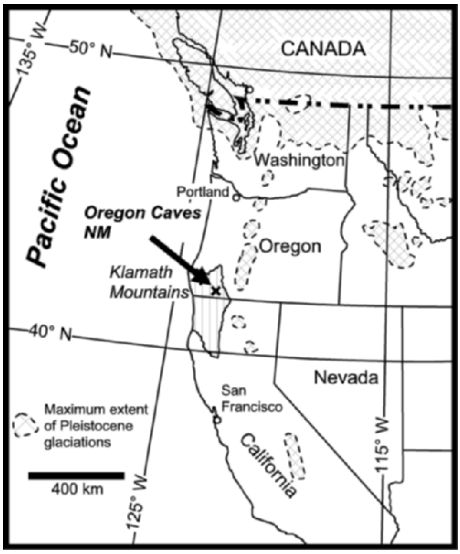

Figure 3. Location map of Oregon Caves National Monument. The cross-hatched areas indicate maximum extent of Pleistocene glaciers and continental ice sheets.

5. SAMPLE DESCRIPTION AND METHODOLOGY

Two flowstones, one approximately 13 cm thick from the *Exit Tunnel Cave* (ETC) and a 73 cm thick sequence from *Neptune's Grotto* (NG) (Figure 4), as well as a 5 cm high stalagmite from the *White Formation Passage* (WFP-2L), were analysed for this study. The NG and WFP-2L samples were taken from areas deep within the cave, away from the present-day main airflow in order to minimise evaporative effects and temperature variations stemming from airflow generated by the two known natural entrances. The ETC flowstone was collected in a cave discovered during the excavation of a tunnel in the 1930's allowing access to the cave at higher elevations. Since the ETC flowstone was collected from a cave with no known natural entrances, conditions of minimal evaporative and temperature variations are thought to have dominated the cave climate at this site.

In order to establish the depositional history of the speleothems, outcrop-scale features such as discontinuities were mapped. Four discontinuity surfaces were found within the NG flowstone (Figure 4). The discontinuities are laterally continuous over the entire outcrop of the specimen sampled. Debris such as broken soda straws and stalactites lie horizontally on these surfaces (Figure 4). Although columnar calcite crystals with rhombohedral terminations protrude from these sub-horizontal surfaces, they are

generally smooth, and are covered with a thin layer of allogenic brownish detritus of mineral origin.

X-ray diffraction analyses were undertaken on powdered samples of the speleothems, analysed with a Philips PW1730 apparatus at Carleton University, and used in conjunction with thin-section petrography to confirm the mineralogy of the crystals. Speleothem samples were cut normal to the growth axis. These surfaces were then ground and polished. The speleothems were sampled for stable isotopic analysis along the growth axis of the samples using a 0.6 mm drill bit. Oxygen stable isotope ratio measurements were done every 1 mm for the WFP-2L stalagmite and the lower section of the NG flowstone, while all the other samples were analysed every 2 mm. Standard extraction techniques, using H_3PO_4 digestion, were used to purify and isolate CO_2, which was analysed for oxygen stable isotopes using a Micromass Sira12 mass spectrometer located in the Earth Sciences Department of the University of Ottawa. The analytical errors on $\delta^{18}O$ values are ±0.1% and all results are reported as V-PDB.

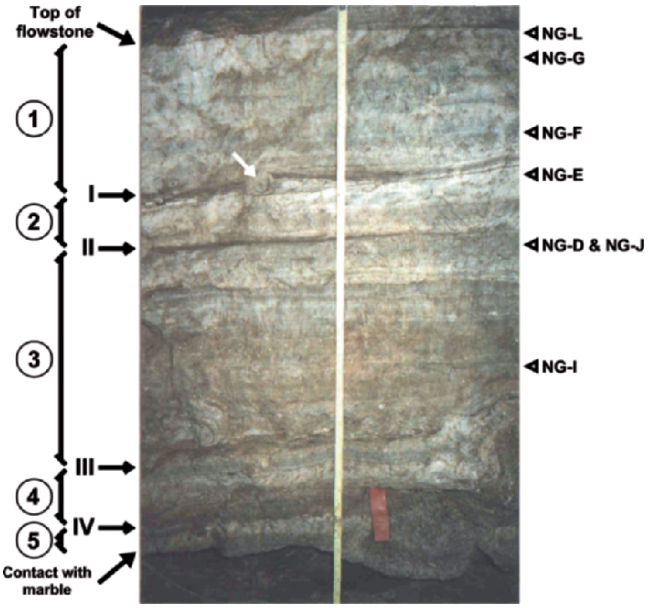

Figure 4. Cross-section of Neptune's Grotto flowstone (≈73 cm thick), unconformably overlying Triassic marble. Black arrows indicate outcrop-scale disconformities (numbered I to IV). Numbered sections on the left correspond to text descriptions. The white arrow shows a broken stalactite resting on a disconformity surface. The open triangles to the right of the graph indicate stratigraphic locations of U-series samples.

Chronological control is provided by 14 high-precision thermal ionisation mass spectrometry (TIMS) U-series dates performed at University of Bergen (Norway) on a Finnigan-MAT 262 RPQ solid source mass spectrometer following the analytical procedure described by Lundberg (1999). Owing to low uranium content, ranging from 0.086 to 0.233 ppm (Table 2), samples sizes varied from 1 to 2 g, representing vertical

Table 2. U-series dates for OCNM speleothems[a]

Sample	U (ppm)	Th (ppm)	Distance from base (mm)	$^{230}Th/^{234}U$ Age[b] (ka)	$^{230}Th/^{234}U$[c]	$(^{234}U/^{238}U)_{initial}$[d]	$^{234}U/^{238}U$[c]	$^{230}Th/^{232}Th$[c]	$^{234}U/^{232}Th$[c]
WFP-2-B	0.187	0.06	47-49	2.26 ±0.02	0.02058 ±0.00014	1.07468 ±0.00255	1.07420 ±0.00255	18.32 ±0.2	890 ±11
WFP-2-A	0.233	0.02	1-5	3.88 ±0.02	0.03508 ±0.00015	1.07091 ±0.00198	1.07013 ±0.00198	134.10 ±1.2	3822 ±38
ETC-B	0.168	0.66	127-129	11.98 ±0.13	0.10450 ±0.00103	1.12956 ±0.00163	1.12523 ±0.00163	7.99 ±0.1	76 ±1
ETC-E	0.169	0.77	109-112	14.29 ±0.05	0.12342 ±0.00037	1.11867 ±0.00220	1.11396 ±0.00219	7.94 ±0.0	64.3 ±0.4
ETC-D	0.183	0.53	74-77	116.69 ±0.45	0.67317 ±0.00135	1.15919 ±0.00128	1.11385 ±0.00123	69.25 ±0.5	103 ±1
ETC-A	0.197	0.42	36-38	117.50 ±0.39	0.66967 ±0.00114	1.13974 ±0.00149	1.10015 ±0.00144	91.66 ±0.7	137 ±1
ETC-C	0.189	0.16	1-7	119.25 ±0.75	0.67487 ±0.00212	1.13307 ±0.00315	1.09490 ±0.00305	224.42 ±2.3	332 ±4
NG-L	0.102	0.06	704-706	$122.92^{+1.01}_{-1.00}$	0.68187 ±0.00288	1.06698 ±0.00174	1.04727 ±0.00170	345.5 ±2.6	507 ±4
NG-G	0.167	0.05	681-684	$122.84^{+0.54}_{-0.53}$	0.68193 ±0.00150	1.07120 ±0.00123	1.05026 ±0.00121	384.10 ±5.0	563 ±7
NG-F	0.136	0.13	574-576	131.22 ±0.74	0.70513 ±0.00193	1.05588 ±0.00126	1.03852 ±0.00124	123.00 ±0.8	174 ±1
NG-E	0.085	0.09	508-511	$234.9^{+2.9}_{-2.8}$	0.89313 ±0.00289	1.07200 ±0.00122	1.03699 ±0.00118	142.70 ±1.6	160 ±2
NG-D	0.161	0.38	435-437	$315.3^{+6.9}_{-6.5}$	0.95525 ±0.00251	1.08543 ±0.00381	1.03495 ±0.00364	70.07 ±0.6	73 ±1
NG-J	0.169	0.39	435-437	$326.6^{+8.8}_{-8.0}$	0.96462 ±0.00296	1.11996 ±0.00425	1.04752 ±0.00398	115.60 ±0.6	120 ±1
NG-I	0.086	1.05	219-221	$359.3^{+9.8}_{-9.0}$	0.97931 ±0.00313	1.13926 ±0.00112	1.05029 ±0.00104	22.21 ±0.2	22.7 ±0.2

[a] All errors are quoted as 2σ.

[b] Calculated using Kaufman and Broecker's (1965) equation and half-lives of ^{230}Th and ^{234}U of 75 383 and 244 500 years respectively.

[c] Activity ratio.

[d] Initial $^{234}U/^{238}U$ activity ratio calculated for $^{230}Th/^{234}U$ age.

intervals between 2 and 7 mm. Samples were cleaned ultrasonically, ignited to remove organics, and a ^{229}Th-^{223}U-^{236}U spike was added. U and Th were separated in anion exchange columns, loaded onto single rhenium filaments with silica gel (U fraction) or graphite (Th fraction) and the isotopic ratios measured in peak switching, ion counting mode. Typical 2σ analytical precisions on isotopic ratios are 0.08% and 0.15% for U and Th respectively.

6. RESULTS AND DISCUSSION

6 .1. OCNM Cave Calcites as Paleoenvironmental Indicators

The first step towards utilising speleothem stable isotopes as paleoenvironmental indicators is to establish the primary nature of the calcite crystals comprising the bulk of the speleothems. One such verification involves searching for evidence of recrystallisation within the crystals, given evidence that suggests that some cave calcites are recrystallised from aragonite (Folk and Assereto 1976). Folk and Assereto (1976) proposed petrologic criteria to determine the presence of former aragonitic precursors within speleothems, namely: (i) preservation of the original aragonite crystals; (2) needle-like inclusions from possible surviving aragonite needle ghosts contained within a randomly-oriented recrystallised polycrystalline anhedral calcite mosaic; (3) presence of a randomly-oriented polycrystalline anhedral calcite crystal mosaic; (4) quadratic or feathery crystal termination possibly indicative of a former aragonitic crystal; (5) presence of extensive dissolution possibly occurring in less stable aragonitic layers. No evidence of recrystallisation was observed in the samples according to these criteria, including randomly-oriented equant calcite crystals. In addition, X-ray diffraction data confirm that no aragonite is present in the samples, indicating that the crystals are primary features and possibly reflect original environmental conditions.

The second step is to establish whether the calcites were deposited in isotopic equilibrium with the waters from which they are derived. During slow degassing, the isotopic fractionation between the aqueous and solid phases is controlled indirectly by cave temperature under equilibrium conditions. However, under an evaporative cave regime or rapid crystallisation, the isotopic fractionation is modulated by kinetic effects which inhibit isotopic equilibrium between the calcite and the dripwaters (Hendy, 1971).

A test for isotopic equilibrium deposition of speleothem calcite has been devised by Hendy (1971) based upon variations in C and O isotope ratio variations along coeval growth layers. Theoretically, $\delta^{13}C$ values of calcite should become progressively higher with distance from the source of dripwater as $^{12}CO_2$ is lost by degassing preferentially to $^{13}CO_2$. The $\delta^{18}O$ signal should remain constant owing to the relatively large amount of water available. Under evaporative conditions, both $^{12}CO_2$ and $H_2{}^{16}O$ molecules are preferentially fractionated as water travels down the speleothem, thereby producing synchronous enrichments of both ^{13}C and ^{18}O in the calcite deposited from solution.

Several drawbacks, however, are associated with the use of the Hendy test. The first concerns the physical sampling of single growth layers, typically only a few tens of microns thick, with drills burs ranging from approximately 0.3 mm up to 1 mm in diameter. This would not only induce an averaging of the isotopic values over the width

of the sample, but also create problems sampling the same group of coeval bands at several locations within a single speleothem. Secondly, although this test is theoretically sound for stalagmites with smooth surfaces (on which water flow direction is clearly downward), it could prove more difficult to establish the flow direction on flowstones, which typically have subhorizontal surfaces. However, as many dissolutional caves unaffected by air flow have high relative humidity levels (>90%), evaporation is thought to be of minor importance (Hill and Forti, 1997).

In the absence of any alternative, and in spite of the drawbacks enumerated above, Hendy tests were performed on the WFP-2L stalagmite and near the base of the NG flowstone (Figure 5). Figure 5a illustrates the results for sampling the WFP-2L stalagmite along coeval subsamples. Figure 5b illustrates the results for the lower parts of the NG flowstone. Sampling of the ETC flowstone for the Hendy test was not performed due to the lack of clear banding. For both the WFP-2L and the NG speleothem samples (Figure 5a and b, left panels), the results show the absence of parallel enrichment of $\delta^{13}C$ and $\delta^{18}O$ along "coeval" growth layers. Furthermore, Figure 5a and b (right panels) show that there is no synchronous enrichment of the carbon and the oxygen isotopes. This evidence, in conjunction with the physical setting of the samples (in areas with high humidity and away from natural entrance or areas of high air flow), indicates that the stable isotopes potentially contain paleoclimatic information.

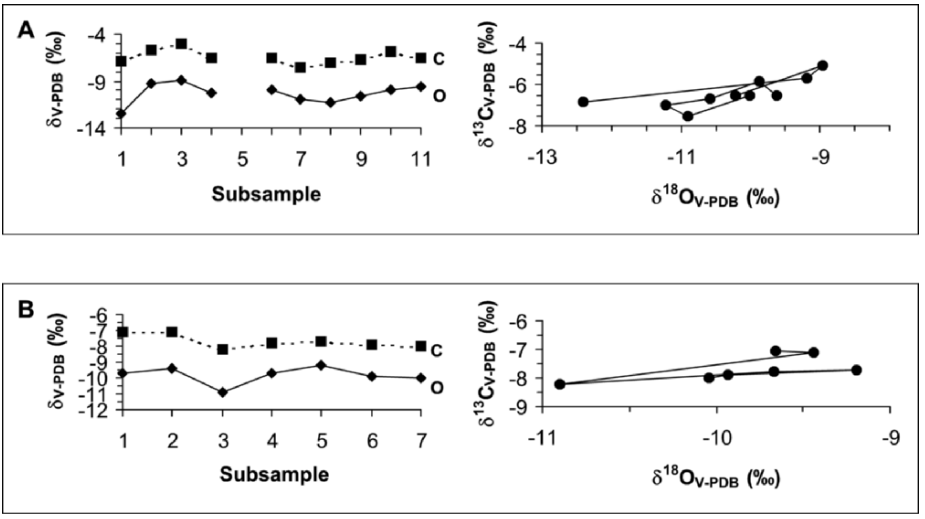

Figure 5. Hendy tests results for two speleothem samples: A) WFP-2L and, B) NG. For the left panel of sample WFP-2L, subsample 6 represents the apex (top) of the growth layer on the growth axis, with either side of the subsample representing sampling down the side of the stalagmite (subsample 5 was lost during laboratory analyses). The left panels show the absence of parallel enrichment of $\delta^{13}C$ and $\delta^{18}O$ with distance along coeval samples; the right panels show the absence of a progressive positive relationship between $\delta^{13}C$ and $\delta^{18}O$ in sequential samples.

The next step is to confirm the presence of paleoclimatic signals in our samples, and to determine the relationship of isotopic trends with climate. Several effects operating within the cave-surface-atmosphere-ocean system control oxygen isotope variations in speleothems. The *cave temperature effect* represents the thermodynamic fractionation of oxygen isotopes between water and calcite during equilibrium precipitation. The *ocean temperature effect* reflects the temperature-dependent fractionation of oxygen isotopes between liquid and vapour phases over ocean surfaces, the source of the atmospheric moisture. The *rainwater composition effect* describes the effect of atmospheric processes on oxygen isotope compositions of vapour and relates to the behaviour of air masses en route towards the site of rainfall in the vicinity of the cave: it is mainly a function of rainout before it reaches the site and relates to storm-tracks and temperature over the precipitation site (Dansgaard, 1964). The *ice-volume effect* represents changes in isotopic composition of ocean waters between glacial and interglacial periods, with seawater becoming enriched in heavy isotopes as ice volume increases (Shackleton and Opdyke, 1973).

The relative importance of these effects described above depends on the scale of the climatic changes. For example, during glacial-interglacial cycles, the ice-volume effect may be important, while cave temperature or rainout factors can be dominant during periods of less severe environmental changes such as within an interglacial. The overall relationship between climate and oxygen stable isotope ratios must be independently established for each study site and can be summarised using the speleothem delta function (SDF) as described by Lauritzen and Lundberg (1999b). Generally, the meteoric-dependent isotopic shifts will be greater than the cave temperature effect (Lauritzen and Lundberg, 1999b) so that the oxygen isotopes in the cave calcites will become more enriched as the temperature increases (positive relationship), although inverse correlations have also been established, mostly for cave sites influenced by maritime-derived moisture sources.

6.2. Speleothem Geochronology and Isotopic Signatures

Fourteen U-series dates were used as the basis for developing a speleothem growth chronology (Table 2). These ages ranged from 2.26 ka to 359 ka, while relative 2σ errors were from 0.32 to 2.62% of the actual age, with the greater errors occurring in older samples. All samples are in chronological order, except for two (NG-G and NG-L) that have overlapping 2σ errors. Two dates (NG-D and NG-J), taken from the same interval of overlapping samples within the Neptune's Grotto Section 1, gave overlapping 2σ errors. As well, two samples (ETC-B and ETC-E) presented low (<10) $^{230}Th/^{232}Th$ ratios (Table 2), which could be indicators of detrital contamination of the samples (Blackwell and Schwarcz, 1995). However, both samples had no visible detrital contamination and their absolute Th concentrations are below 1 ppm (0.66 and 0.77 respectively). These factors, in addition to the high $^{234}U/^{232}Th$ activity ratios encountered in these samples (76 and 64), contributed to our decision not to correct for an assumed initial $^{230}Th/^{232}Th$ activity ratio in these samples.

To facilitate preliminary comparisons, we have aligned the dated intervals of our speleothem isotopic records, plotted as distance from the base of the deposit, to the chronology of established global paleoclimatic records (from ice and marine cores) and

have assumed linear growth rates between these dated intervals. We utilised the highest resolution paleoclimatic isotopic record for given intervals, although our oldest samples could only be compared to the two longest records available (SPECMAP; Imbrie et al., 1984 and Devils Hole; Winograd et al., 1992).

Our youngest sample is the WFP-2L stalagmite, with a basal date of 3.88 ±0.17 ka (WFP-2-A) and a topmost date of 2.26 ±0.02 ka (WFP-2-B). These dates indicate a mean growth rate of 3.15×10^{-2} mm.a^{-1} during a short growth interval of approximately 1600 years. This growth rate agrees well with interglacial stalagmite growth rates from Norway (2.0×10^{-2} mm.a^{-1}; Linge, 1999), Ireland (2.8 to 3.4×10^{-2} mm.a^{-1}; Vesely, 2000), as well as growth rates calculated for the ETC flowstone (2.79×10^{-2} mm.a^{-1}). Figure 6 illustrates the oxygen isotope record of this sample in relation to the high-resolution ice cores from Greenland (GISP2; Grootes et al., 1993; Meese et al., 1994; Stuiver et al., 1995) and Antarctica (Vostok; Chappellaz and Jouzel, 1992). For both ice cores, an isotopic enrichment indicates an increase in global temperature (Grootes et al., 1993). The WFP-2L record seems to indicate a slight positive relationship of isotopic signal and temperatures as the 3rd-order polynomial best-fit lines indicate overall parallel trends. The WFP-2L record reveals a series of isotopic depletion events occurring about every 200

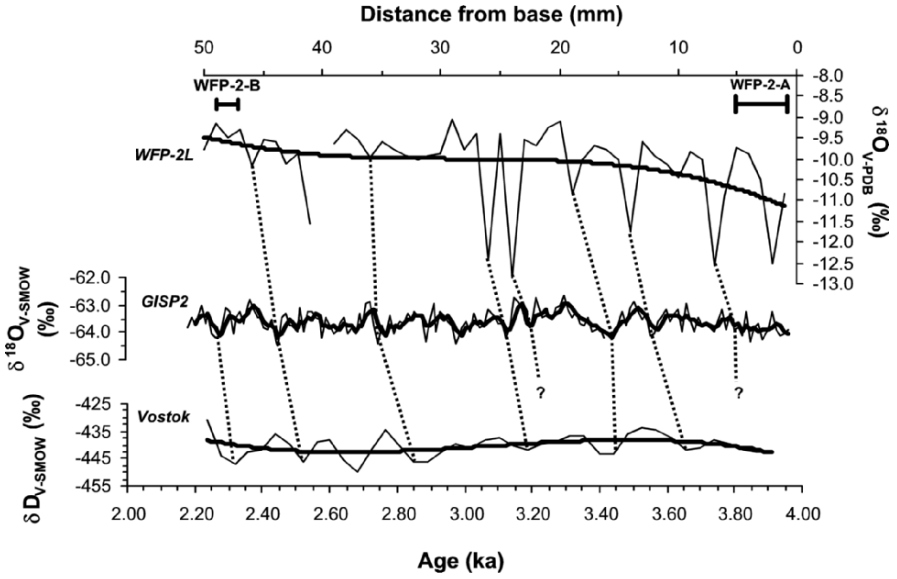

Figure 6. WFP-2L $\delta^{18}O$ values compared to the GIPS2 and Vostok ice-core records for similar time periods. 3rd-order polynomial best-fit lines are shown for the WFP-2L and Vostok isotope records. A 3-point running mean (thick line) is shown for the GISP2 record. This reduces the GISP2 record to a resolution similar to the WFP-2L's resolution (WFP-2L has 51 points while the GISP2 record has ≈ 160 points). $\delta^{18}O$ values are not available for the Vostok record. The speleothem isotopes are plotted relative to distance from base. Bars on the dates represent vertical sampling range and they have been lined up with the compared chronologies. One possible peak-correlation scenario is shown (dotted lines). The GISP2 data are from Grootes et al. (1993), Meese et al. (1994) and Stuiver et al. (1995). The Vostok data is from Chappellaz and Jouzel (1992).

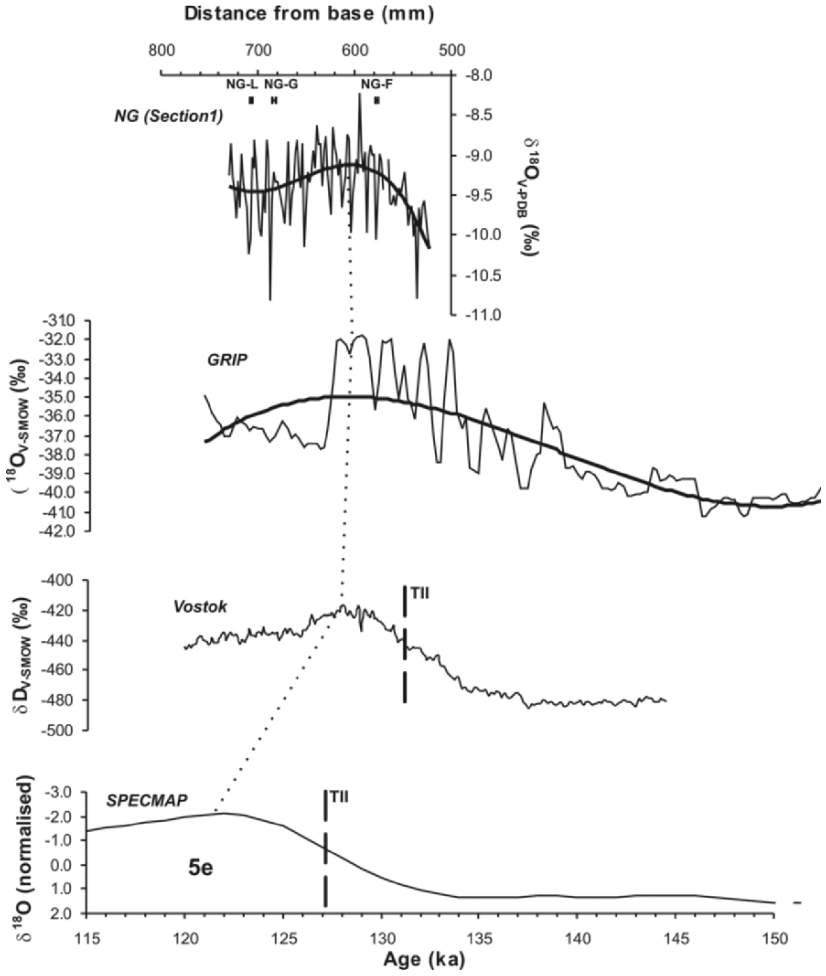

Figure 7. NG $\delta^{18}O$ values compared to the GRIP ($\delta^{18}O$; Johnsen et al., 1993) and Vostok ice cores (δD; Chappellaz and Jouzel, 1982), and the SPECMAP (Imbrie et al., 1984) marine record's $\delta^{18}O$ signature for the Termination II/5e period. A 3rd-order polynomial best-fit line is shown for the NG record. The speleothem isotopes are plotted relative to distance from base. The dated intervals for NG-L and NG-F have been lined up with the compared chronologies. Bars on the dates represent vertical sampling range. TII bars represent the SPECMAP curve.

years. These appear to correlate with events of similar periodicity in the GISP2 record (Grootes et al., 1993; Meese et al., 1994; Stuiver et al., 1995). The resolution of the Vostok ice core is too low to reveal these short-term shifts.

The chronology of deposition for the NG flowstone was established using seven U-series dates (Table 2). Figure 4 shows the distribution of outcrop-scale discontinuities within the NG flowstone. The top-most growth interval (Section 1; Figure 4) is defined by

three dates. A mean growth rate of 1.57×10^{-2} mm·a^{-1} was obtained based on the two dates, NG-F and NG-L (given the 2σ overlap of NG-L and NG-G, we chose the U-Th sample that was the farthest away from the basal NG-F U-Th sample along the growth axis). The stable isotopic record for this growth interval is plotted in Figure 7. It is compared to the Illinoian to Sangamon glacial-interglacial transition in the GRIP and Vostok ice core records, as well as the SPECMAP marine record. A 3rd-order best-fit polynomial trendline has been added to the NG and GRIP records in order to better illustrate similarities. The large-scale variations in data between all three records are strikingly similar in terms of major events within each data set.

Chronologic difference of the timing of peaks and troughs of the statistical trendlines are apparent, with the GRIP record showing its peak at approximately 130 ka, approximately 500 years earlier than on the NG record, and approximately 1 kyr earlier than the Vostok record. These offsets are well within the 2σ ranges and the timing is in good agreement with coral reef data from the Bahamas indicating the high sea-level stand during marine oxygen isotope substage 5e occurred between 132 and 129 ka (Chen et al., 1991). The similar shapes of the paleoclimatic curves suggests that the onset of the climatic amelioration in all three records was about of roughly equal intensity. The trough at ≈122 ka on the GRIP and NG records, resulting from a climatic degradation followed by a temperature increase, appears to be absent from the Vostok ice core record. Given the striking correspondence with both ice core records, we conclude that growth of the speleothem occurred during interglacial conditions (early marine isotope stage 5) (Table 2) during an interval of approximately 13,400 years. Comparing these records to the marine isotopic record of SPECMAP highlights the differences between the marine record and the ice and terrestrial records. A notable difference is the timing of the Termination II (terminations are defined as the middle of the transition between glacials to interglacial periods) within the records, which are offset by as much as 5000 years (Imbrie et al., 1984; Martinson et al., 1987). This difference is the subject of much on-going controversy, as much of the recently TIMS dated coral reef evidence supporting the earlier date for Termination II is in agreement with the ice core records (Chen et al., 1991; Gallup et al., 1994). In spite of timing differences between events, OCNM speleothem isotopes mirror the ice core and the inverted ocean core records for the last interglacial, establishing the positive relationship of speleothem oxygen isotopes and temperature. The rest of the NG record is less well dated or lies beyond the range of U-series dating.

The second interval of the NG flowstone (Section 2) is anchored by a single U-series date (≈235 ka). The NG isotope record for this interval has been compared to the GRIP ice core and SPECMAP marine records (Figure 8). All three records are similar and the NG and GRIP records show three peaks that can be tentatively correlated. However, the GRIP record terminates at 250 ka, leaving a short section of the NG (approximately 4 kyrs) record without any direct comparison to a record of similar resolution (Figure 8). Based on the tentative correlation of the NG and the GRIP records, a mean growth rate of ~2.9×10^{-3} mm·a^{-1} over a 22.4 kyr period from 253.8 to 231.4 ka have been estimated, indicating relatively slow speleothem growth during the marine oxygen isotope stage (MOIS) 7.

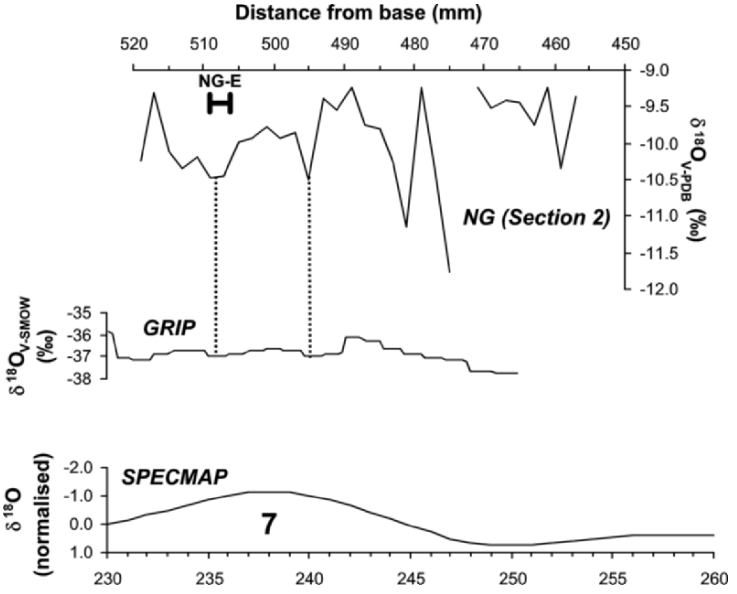

Figure 8. Tentative correlation of NG $\delta^{18}O$ values relative to the GRIP ice core (dotted lines)(Johnsen et al., 1993) and SPECMAP (Imbrie et al., 1984) stacked marine $\delta^{18}O$ records for parts of MIS 7. The speleothem isotopes are plotted relative to distance from base. The dated interval has been lined up with the compared chronology. Bars on the date represents the vertical sampling range. The marine isotope stage number is indicated on the SPECMAP curve.

The lowermost of the dated NG intervals (Section 3) is chronologically validated using the mean date provided by the overlapping samples (NG-D and NG-J) indicating MOIS 9 deposition, along with a third date (NG-I) from a lower interval (MOIS 10)(Figure 9). These dates provide a mean growth rate of 5.6×10^{-3} mm·a^{-1} between these two outcrop-scale discontinuities. Based on the mean growth rate, this interval represents approximately 51 kyrs of growth, possibly from marine isotope stages 9 through 11. Matching trends can be found between the NG speleothem and SPECMAP marine records for this section (Figure 9).

Three dates (ETC-C, ETC-A and ETC-D) from the Exit Tunnel Cave flowstone range in age from 116 to 119 ka (isotope substage 5e) and indicate a high growth rate (2.79×10^{-2} mm·a^{-1}) in the lower section of the flowstone, while two dates (ETC-E and ETC-B) in the upper reaches of the flowstone are clearly late Wisconsinan (MOIS 2) in age and indicate a growth rate of 7.6×10^{-3} mm·a^{-1}. The interval between ETC-D and ETC-E, broadly corresponding to the colder conditions of stages 4 through 2 (and including late 5), therefore represents either severely reduced growth ($\approx3.0\times10^{-4}$ mm·a^{-1}) or a hiatus in deposition of approximately 102 kyrs. No outcrop-scale discontinuity has been observed and no microscopic evidence of precipitation stoppage has been clearly identified, suggesting that growth was continuous throughout the Wisconsin glacial

period, although complete growth cessation could have occurred. The ETC isotopes for this section provide few clues to this puzzle as the $\delta^{18}O$ values have remained more or less constant between the two dates (ETC-D and ETC-E) constraining stages 4 through 2. The mean growth rates for the section spanning glacial intervals should therefore be considered as minimum growth rates.

7. GROWTH MODELLING

A simple theoretical model to determine growth rates for our interglacial samples can be obtained by using data in Figures 1 and 2. For example, using an approximate present-day mean annual temperature for OCNM of 7.5°C, a $pCO_{2\ (soil)}$ of 0.015 atm is obtained (Figure 1a). This translates into theoretical $[Ca^{2+}]$ values ranging from 0.75 to 2.3 $mmol \cdot cm^{-3}$ for closed and open systems respectively (Figure 1b) (preliminary testing of actual cave water at OCNM in 1992 reports mean values of approximately 0.68 $mmol \cdot cm^{-3}$, with a $2\sigma = \pm 0.52$ for n = 27; OCNM internal document). Thus the $([Ca^{2+}]–[Ca^{2+}]_{equilibrium})$ term, assuming an approximate $[Ca^{2+}]$ equilibrium value of 0.63 $mmol \cdot cm^{-3}$ (Dreybrodt, 1996, although he reports an apparent equilibrium value of 0.72 $mmol \cdot cm^{-1}$),

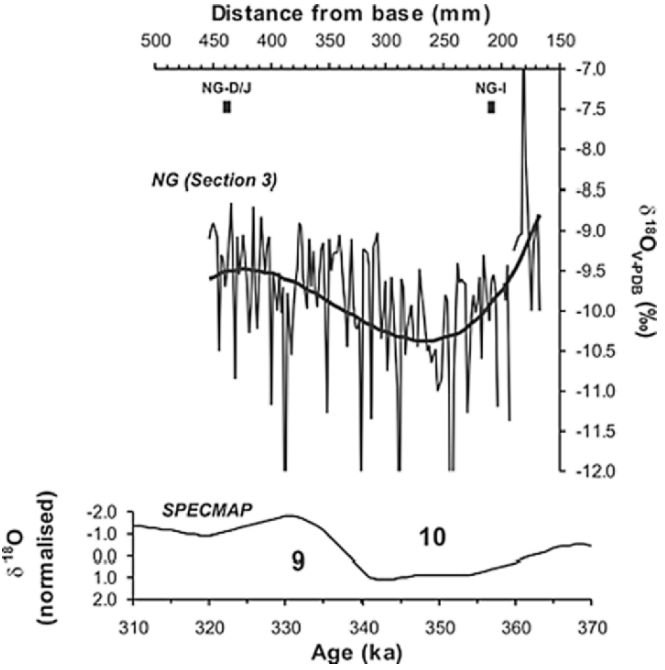

Figure 9. NG $\delta^{18}O$ values relative to the SPECMAP (Imbrie et al., 1984) stacked marine $\delta^{18}O$ record for parts of MIS 11 through 9. A 3rd-order polynomial best-fit line is shown for the NG isotopes. The speleothem isotopes are plotted relative to distance from base. The dated interval has been lined up with the compared chronology. Bars on the date represents the vertical sampling range. The marine isotope stage numbers are indicated on the SPECMAP curve.

becomes 0.15 to 1.7 mmol·cm^{-3}. Using a α value of 1.0 (from Figure 2d, for d = 7.5×10^{-3} cm and $pCO_{2\ (cave\ air)}$ = 3×10^{-4} atm), we obtain values ranging from 1.5×10^{-9} to 1.7×10^{-8} mmol·cm^{-2}·s^{-1}, translating into growth rates of 1.8×10^{-2} to 0.20 mm a year. The upper limit of 0.2 mm·a^{-1} should be considered an absolute maximum as no karst system is perfectly "open" (Drake, 1983). Furthermore, the air volume (≈pores) of soils is restricted with respect to water volume, further reducing the theoretical [Ca^{2+}] equilibrium at different $pCO_{2\ (soil)}$ (Drake, 1983). The upper values are in excess of the values reported for our samples ranging between 2.86×10^{-3} to 3.15×10^{-2} mm·a^{-1}, although our growth rates generally fall within the 5× overestimation factor of the theoretical growth model (Baker and Smart, 1995). These rates, however, are better represented by restricted air volume approximations (V_{air} = $V_{solution}$). In addition, as mentioned earlier, this simple model does not take into account the seasonality (winter stoppage) of calcite precipitation. As an example, for approximately 8 months of the year temperatures at OCNM, located at an altitude of approximately 1400 m asl, the monthly minimum temperature is below 0°C (OCNM internal document). This seasonality potentially allows for freezing of the ground above the cave, thereby substantially slowing down or stopping calcite precipitation. Also, long-term climatic variations, which could allow mean annual air temperatures above the cave to hover just above the freezing point, would further reduce the theoretical growth rate to approximately 7.6×10^{-3} mm·a^{-1} for an open system; hence, even at near-freezing temperatures, speleothem growth can be significant. Overall, our dated sections generally confirm the validity of this model, although the modelled growth rates obtained show a rather wide range (1.8×10^{-2} up to 0.2 mm·a^{-1}) for end-member dissolution systems. However, these climatic controls on growth rates might be negligible over significant time periods, as put forth in the next section.

7.1. Evidence for Linear Growth Rates

The model suggests that growth should relate strongly to temperature. This glacial-interglacial climate change probably explains the obvious reduction in the growth of ETC during MOIS 4-2. However, within the interglacials, it is apparent from the good fit of the speleothem $\delta^{18}O$ chronologies presented above with the other proxies that growth rates are linear rather that temperature controlled. Although variations in calcium concentrations over time are not available for the OCNM site, Baker et al. (1996) found [Ca^{2+}] to be generally constant for a given cave site. The models discussed above indicate that most of the growth rate changes (≈42.5%) can be attributed to long-term variations in Ca^{2+} concentration (Baker and Smart, 1995; Baker et al., 1996), although other parameters such as thickness of the water film (d) and atmosphere CO_2 also contribute to varying degrees. The assumption that our samples show linear growth between U-series dates is valid over the time scales for which we have chronological controls.

This apparent incompatibility between the theoretical and the empirical data could be reconciled by considering the water film thickness (d), which controls ≈29% of the growth variability. In climate systems that show alternating warm-dry and cool-wet periods, speleothem growth might be controlled alternately by the temperature and the water film thickness. Temperate maritime climates, controlled by depressions related to westerly winds and the polar front, do in fact show these extremes of climate (warm-wet or cool-dry conditions are relatively rare). In another climate system, temperature and

water film thickness controls may combine rather than alternate; this is probably true of a well-dated Bahamian speleothem which grew during Termination II with a logarithmic growth increase during the termination (Lundberg, 1997). The glacial to interglacial climate transition here was probably cool-dry to warm-wet.

Other empirical studies have also shown varying degrees of growth linearity for speleothems samples from similar climatic settings to OCNM's, most commonly after a slower growth period during the initial phases (of a few cm) of speleothem development (Hellstrom et al., 1998; Lauritzen and Lundberg, 1999b; Linge, 1999). The slower growth during early speleothem development could be associated with initial length-slow calcites representing the initial encrusting of an unconformity (Folk and Assereto, 1976; Dickson, 1978).

Our conclusions from this comparison of the theoretical and empirical is that growth cannot necessarily be simply modelled as a function of temperature, that water film thickness may act as either an alternate or as a complementary control along with temperature, and that the climate system(s) must be known in detail in order to model both controls.

7.2. Extending the Chronology OCNM Speleothems

The lower section of the NG flowstone could not be dated by TIMS U-Th dating owing to a generally low U content of the flowstone (Table 2). In addition, $^{234}U/^{238}U$ dating could not be performed owing to a non-constant initial $^{234}U/^{238}U$ content in our samples (Table 2). Using the linear growth rate assumption in conjunction with the positive relationship between climate and the oxygen isotope ratios of OCNM speleothems during interglacials, we therefore present peak-matching correlations of the lower sections of the NG flowstone isotopic record (lacking or beyond U-series chronological control) with other records of global paleoclimates such as the SPECMAP curve (Imbrie et al., 1984) and Devils Hole (Winograd et al., 1992). Figure 10 illustrates the correlation for NG Section 4. A 3rd-order polynomial best-fit trendline has been added to the NG curve on Figure 10. The best correlation between the paleoclimatic records occurs between 393 ka and 443 ka. In this interval, trends within all three records correlate well. This chronology indicates a mean growth rate for this NG interval of 3.24×10^{-3} mm·a^{-1}, which is roughly comparable to a rate of 2.05×10^{-3} mm·a^{-1} for a well-dated northern Norwegian flowstone from MOIS 11 (Lundberg and Lauritzen, in press) and suggest that our modelling attempt for this section of flowstone is not unreasonable.
Figure 11 shows the lowermost NG interval (Section 5), constrained by an outcrop-scale discontinuity at the top and resting directly on the marble bedrock (Figure 4). The 3rd-order best-fit polynomial trendline matches the shape of the SPECMAP record well. This indicates a growth period for this interval from c. 519 to c. 462 ka, placing the age of this section of flowstone at the beginning of MOIS 13. The mean growth rate for this interval is 1.54×10^{-3} mm·a^{-1}. The estimated age for the lower part of this interval indicates that initiation of speleothem deposition in this area of the cave probably started around 519 ka. Given that the NG flowstone is located on the most extensive level within the cave, this could be a good age estimate for the beginning of widespread speleothem deposition in the cave.

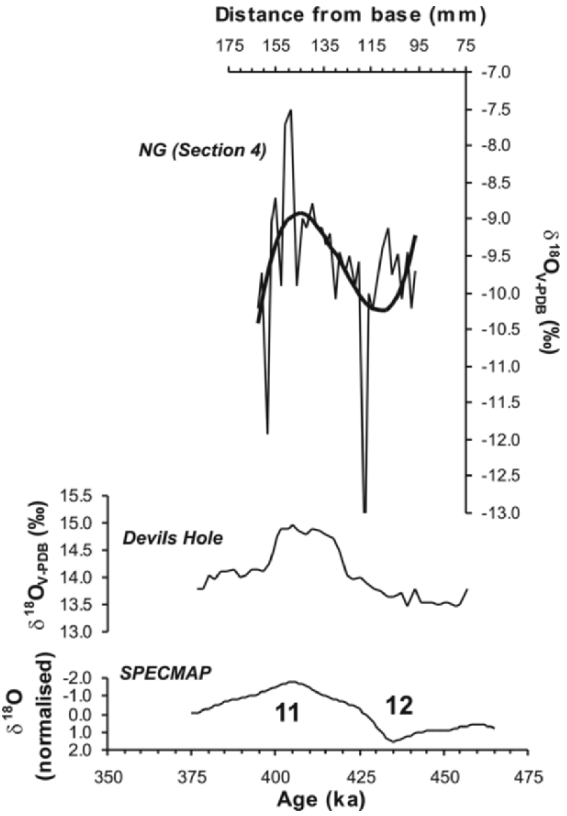

Figure 10. NG $\delta^{18}O$ values relative to the Devils Hole (Winograd et al., 1992) and SPECMAP stacked marine (Imbrie et al., 1984) $\delta^{18}O$ records for parts of MIS 12 through 11. A 3rd-order polynomial best-fit line is shown for the NG isotopes. The speleothem isotopes are plotted relative to distance from base. The marine isotope stage numbers are indicated on the SPECMAP curve.

7.3. Climatic Implications of Outcrop-scale Discontinuities

Figure 12a summarises all our data and the paleoclimatic proxies used for comparisons; the growth hiatuses within the OCNM speleothem are illustrated as cross-hatched areas. Through the use of the proposed chronology for the growth intervals of the NG flowstone, and U-series dates when available, we have estimated the time intervals represented by the outcrop-scale disconformities to be approximately 14 kyrs (IV), 22 kyrs (III), 63 kyrs (II), and 96 kyrs (I) (Figure 4) respectively. These hiatuses broadly correspond to the interglacial conditions of MOIS 12, 10, 8, and 6.

The ETC flowstone also corroborates this pattern: although no apparent precipitation cessation occurred (Turgeon and Lundberg, in press), a severe reduction of growth rates between two U-series dates (ETC-D and ETC-E) indicates the influence of climate on speleothem growth. This growth rate reduction observed in the ETC flowstone lasted approximately 102 kyrs during late MOIS 5 through MOIS 2.

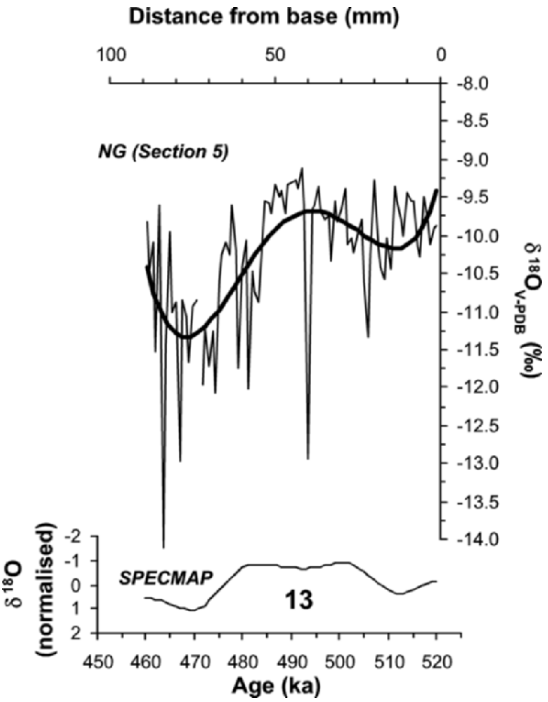

Figure 11. NG $\delta^{18}O$ values relative to the SPECMAP (Imbrie et al., 1984) stacked marine $\delta^{18}O$ record for parts of MIS 13. A 3rd-order polynomial best-fit line is shown for the NG isotopes. The speleothem isotopes are plotted relative to distance from base. The marine isotope stage number is indiciated on the SPECMAP curve.

These isotopic records and hiatuses indicate narrow growth intervals during early to mid-interglacial conditions. Although several growth frequency studies show that speleothem deposition occurs mainly during interglacial intervals in high-latitude environments (Gordon et al., 1989; Gascoyne et al., 1983; Gascoyne, 1992; Baker et al., 1993; Lauritzen, 1995), calcite precipitation in these studies was interrupted by continental ice sheet glaciation in most cases. No evidence of continental glaciation has been reported in the immediate vicinity of the study area, although cirque-like structures suggesting alpine-style glaciation have been observed at higher altitudes elsewhere in the Klamath Mountains (John Roth, U.S. Park Service, personal communication, 1994). This suggests that these growth hiatuses may be associated with periglacial conditions extending well below the alpine glacier limit. The increasing durations of these hiatuses indicates that precipitation could reflect an interplay between climate and additional effects related to cave development.

Glaciation thresholds in the northwestern United States suggest that climatic gradients during the last glacial maxima were similar to those of today, and that the change in summer temperature was about 5.5 ±1.5 °C (Porter, 1977; Porter et al., 1983). These glaciation thresholds allowed for changes in mountain snowline altitude (currently at about 3200 m ASL), which was depressed by approximately 1100 m during the last

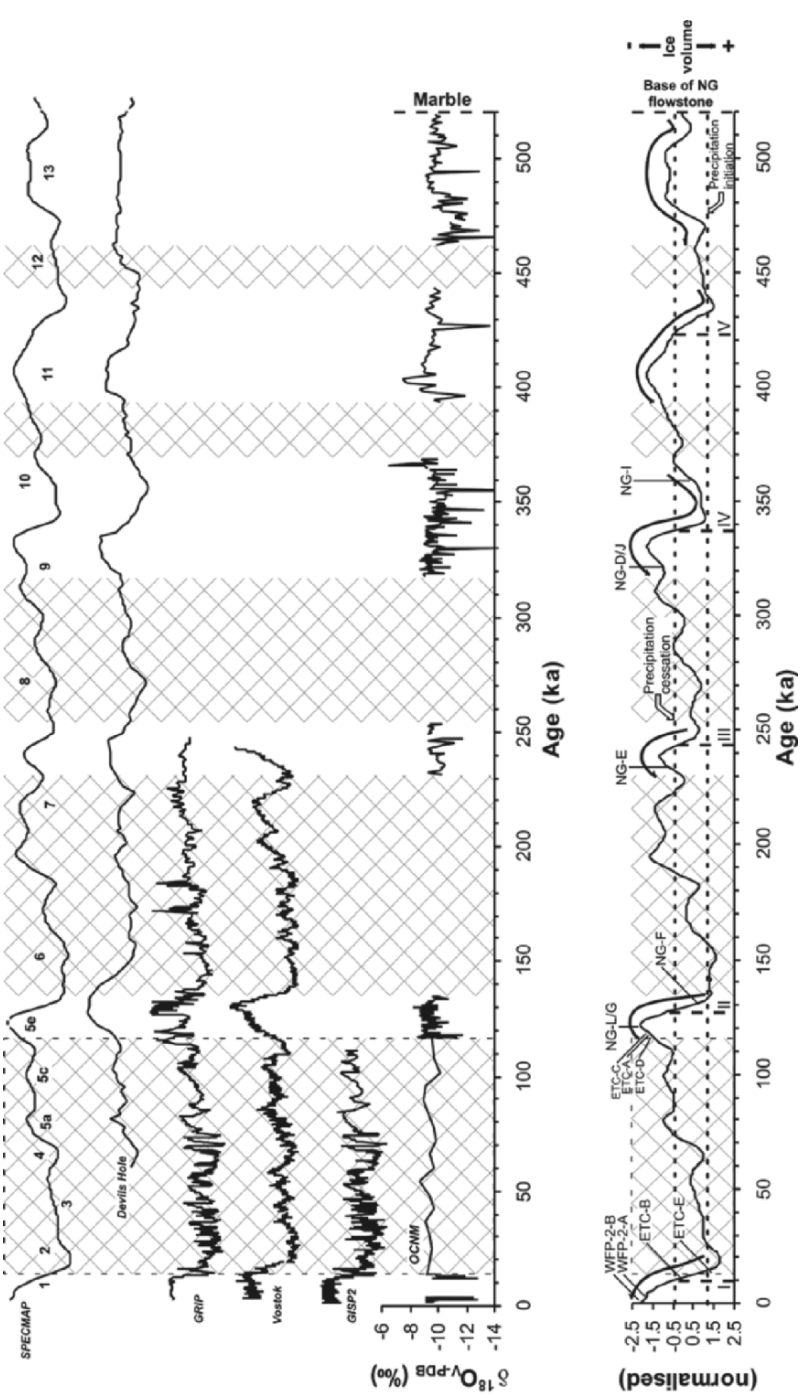

Figure 12. A) Composite OCNM ^{18}O record compared to the SPECMAP (Imbrie et al., 1984) stacked marine record (with marine isotope stage numbers), Devils Hole (Winograd et al., 1992) ^{18}O record, GRIP (Johnsen et al., 1993) ^{18}O ice core record, Vostok (Chappellaz and Jouzel, 1992) δD ice core record and GISP2 (Grootes et al., 1993; Meese et al., 1994; Stuiver et al., 1995) ^{18}O ice core record; B) southwestern Oregon speleothem growth model. Black arrows indicate speleothem growth intervals. The upper and lower dotted lines represent approximate upper and lower thresholds for speleothem precipitation according to the location of U-series dates on the marine curve. U-series dates are plotted against the oxygen isotope data from Imbrie et al. (1984). Dashed vertical lines represent location of Terminations. Cross-hatched areas represent inferred (outlined) and recorded precipitation cessation intervals (hiatuses).

glacial maximum at 42°N, to approximately 700 m above the cave site (Porter, 1977). In addition, Heusser and Heusser (1990) report that sub-alpine vegetation was established at elevations between 1300 and 1800 m lower than present-day conditions (owing to an inferred 5-7 °C temperature depression, in line with Porter's data), further suggesting that permafrost conditions could have occurred well below the 2100 m snowline during glacial conditions in the study area.

Colman and Pierce (1992) concluded that early Wisconsinan alpine glaciers of the western United States were more extensive than their late Wisconsinan counterparts in some areas, thereby contrasting with marine oxygen-isotope records which suggest that world-wide ice volumes were smaller during MOIS 4 than those in MOIS 2 (Emiliani and Shackleton, 1974; Martinson et al., 1987). This indicates that alpine areas could have responded more rapidly than continental ice sheets to climatic events associated with late MOIS 5 and MOIS 4 growth reduction. This sensitivity to climate change may also have been heightened owing to the location of the cave, which was probably very close to the lower permafrost limit during glacial periods, suggesting that speleothems are, at least partly, records of local paleoclimate.

Another feature of the growth hiatuses is their apparent increase in duration with time, associated with higher growth rates after MOIS 7. This could reflect an increasing intensity of glacial periods over time accompanied by warmer interglacials, although the influence of temperature on growth rates in OCNM speleothems, as shown in this study, is equivocal. This pattern might be linked to the predominance of the eccentricity parameter over the precession and tilt orbital parameters during the later parts of the Pleistocene (Berger and Loutre, 1991). Alternatively, these features could reflect the transition between closed to a more open dissolutional system in response to either a thinning of the overburden through erosional processes above the cave or a greater opening of the cave. Given that the cave is located in a marble lens of limited extent (and hence thickness), erosion above the cave would expose the cave to progressively shallower pedogenic processes until the marble lens is directly in contact with the soil overlying the cave. This would not only make the cave system more sensitive to environmental changes, it would also create a more open system of carbonate dissolution and precipitation. In addition, a greater number of natural entrances would develop in a shallower and enlarging cave system, creating additional ventilation of the cave, and thereby potentially lowering the pCO_2 of the cave air. Under these conditions, hiatuses would become progressively longer during glacial stages, while higher growth rates would be expected during interglacials.

8. THE START-STOP MODEL OF CAVE CALCITE PRECIPITATION

The model presented in the first section indicates that growth rates of speleothem calcite should be directly related to temperature. Nevertheless, our results show that growth rates during interglacials can be obtained by linear interpolation between dated sections, indicating little or no net influence of temperature on OCNM speleothem growth rates, but rather a probable interplay between the effects of temperature and film thickness. The precipitation is however influenced by climate on a broader scale. Results for terminations I and II clearly indicate that precipitation is initiated at the very end of a

glacial period, while precipitation cessation occurs very early in the climatic deterioration from interglacial to glacial. Therefore, if we assume that all growth intervals follow the same pattern, it is possible to approximate isotopic limitations on these precipitation/hiatus cycles as well as propagate the model back using established proxies of paleoclimate.

Figure 12b plots the 14 U-series dates obtained on our samples against the SPECMAP marine oxygen isotope curve (Imbrie et al., 1984). These dates cluster into four groups, indicating mean dates around 340 ka, 215 ka (one date only), 120 ka and 13 ka, suggesting that the samples were deposited mainly during interglacials. Using this distribution, we have broadly constrained the lowermost growth interval of our samples by using the lowermost (on the marine isotope curve) point for which we have any chronological control (ETC-E) at 14.3 ka (indicated as "precipitation initiation" line on Figure 12b). The upper growth limit ("precipitation cessation" line) can be similarly constrained (Figure 12b). In this case, it seems that growth stops shortly after major climatic cooling episodes. Note that owing to the low number of dates from our samples, these lines might not constrain growth perfectly. A major complicating factor is the question of the suitability of marine curves to reflect adequately the paleoclimatic régime of OCNM. The results of this simple model are mixed: while the growth intervals correspond well with growth during terminations (Figure 12b), the precipitation initiation and cessation lines are adequate only about half the time: this is probably due to generalised paleoclimatic curve (SPECMAP) used, that might not mimic the precise paleotemperature conditions at the OCNM site.

9. CONCLUSIONS

Cave calcites from Oregon Caves National Monument have been shown to be suitable as an indicator of global paleoclimates. Isotopes from dated interglacial intervals have been shown to record a direct relationship with temperature, controlled mainly by the temperature of the source ocean waters. Correlations with high-frequency Holocene events (~200 years) in the GISP2 ice core have been demonstrated, confirming the global nature of the signal.

In this paper we explored techniques for modelling growth for those parts of the record that were not well dated or were beyond the range of dating. According to theoretical modelling of calcite precipitation, growth rates of speleothems should respond mainly to temperature. The growth rates calculated for our speleothem, ranging from a lower value of 1.54×10^{-3} up to 3.15×10^{-2} mm·a^{-1}, are broadly within the growth rates predicted by the model (taking into account the 2 to 5× overprediction of the model). However, results from dated interglacial sections of our samples from OCNM indicate that precipitation rates are essentially linear on long-term scales (~10^3 to 10^4 years). We conclude that for this region, growth modelling simply as a function of temperature does not adequately describe growth, a conclusion that apparently contradicts the theoretical findings. This empirically-defined linear growth can be reconciled with the theoretical findings if both temperature and water film thickness are included. The relative balance of the two controls will depend on the climate system, where a warm-dry episode might produce the same growth rate as a cool-wet one. Thus film thickness must also be taken

into account when attempting to model growth rates and the climate system should be known.

Comparisons with well-established paleoclimatic records show that the speleothems growth started early in the terminations and ended shortly after the onset of climatic deterioration associated with glacial stadials or interstadials. Precipitation cessation, in most cases, is expressed as an outcrop-scale discontinuity within the Neptune's Grotto flowstone. These discontinuities probably reflect growth cessation through groundwater freezing brought about by periglacial conditions owing to the lowering of the alpine glacial limit. Based on established growth rates for various sections, along with associated dates and correlations of their oxygen isotope variations with global paleoclimatic records, these outcrop-scale discontinuities represent depositional hiatuses ranging from 14 to 102 kyrs. These hiatuses, which get longer with time, are accompanied by an increase in growth rates (also over time). These conditions are probably indicative of an opening of the cave system through cave enlargement and shallowing of the overburden through surficial erosional processes. This would allow not only for greater ventilation of the cave system, but could also shift the dissolutional system from closed (CO_2 source and carbonates separated) towards a more open system (where CO_2 and carbonates are coincident).

A simple growth model, based on minimum isotopic values of SPECMAP before or during terminations and after the beginning of climatic deterioration is presented. This "start-stop" model shows a very good correlation between growth periods and terminations. The precipitation initiation and cessation lines, however, show mixed results, possibly owing to uncertainties related to global records, which might not be indicative, on sub-orbital time-scales, of precise conditions encountered at OCNM.

Although not an aim of the research, it is of interest that the OCNM U-series dates and oxygen isotope data for the period ~135 to 121 ka support the estimates of the timing of Termination II from ice-cores and corals of ~134 to 132 ka rather than the later SPECMAP estimate.

10. ACKNOWLEDGMENTS

Samples were collected under a U.S. National Park Service sample collection permit. John Roth and Steve Knutson (OCNM/U.S. Park Service) provided both of the flowstone samples of this study. Their knowledge of the caves proved invaluable and their assistance is gratefully acknowledged. ST benefited from graduate scholarships from the *FCAR* (*Fonds pour la formation de chercheurs et l'aide à la recherche*) of Québec and NSERC (Natural Sciences and Engineering Research Council of Canada). This study was funded through an NSERC research grant to JL.

11. REFERENCES

Baker, A., Genty, D., Dreybrodt, W., Barnes, W.L., Mockler, N.J., and Grapes, J., 1998, Testing theoretically predicted stalagmite growth rate with recent annually laminated samples: Implications for past stalagmite deposition, Geochimica et Cosmochimica Acta, **62**: 393-404.

Baker, A., and Smart, P.L., 1995, Recent flowstone growth rate: Field measurements in comparison to theoretical predictions, Chemical Geology, **122**: 121-128.

Baker, A., Genty, D., and Barnes, W.L., 1996, Recent Stalagmite Growth Rates: Cave Measurements, Theoretical Predictions and the Environmental Record, in: *Climate Change: The Karst Record.* Karst Waters Institute Special Publication, no 2, pp. 7-9.

Baker, A., Smart, P.L., and Ford, D.C., 1993, Northwest European palaeoclimate as indicated by growth frequency variations of secondary calcite deposits, Palaeogeography, Palaeoclimatology, Palaeoecology, **100**: 291-301.

Baker, A., Proctor, C.J., Barnes, and Barnes, W.L., 1999, Variations in stalagmite luminescence laminae structure at Poole's Cavern, England, ad 1910-1996: calibration of a palaeoprecipitation proxy, The Holocene, **9**: 683-688.

Bar-Matthews, M., Ayalon, A., Matthews, A., Sass, E., and Halicz, L., 1996, Carbon and oxygen isotope study of the active water-carbonate system in a karstic mediterranean cave: implications for paleoclimate research in semiarid regions, Geochimica et Cosmochimica Acta, **60**: 337-349.

Berger, A., and Loutre, M.F., 1991, Insolation values for the climate of the last 10 million years, Quaternary Science Research, **10**: 297-317.

Blackwell, B., and Schwarcz, H.P., 1995, The Uranium Series Disequilibrium Dating Methods, in: *Dating methods for Quaternary deposits*, Rutter, N.W., and Catto, N.R., eds., Geological Association of Canada GEOtext 2, pp. 167-208.

Boggs, Jr., S., 1987, Principles of Sedimentology and Stratigraphy, Merrill, Columbus, 784 p.

Bradley, R.S., 1999, Paleoclimatology: Reconstructing Climates of the Quaternary (2^{nd} edition), Academic Press, San Diego, 610 p.

Buhmann, D., and Dreybrodt, W., 1985a, The kinetics of calcite dissolution and precipitation in geologically relevant situations of karst areas – 1. Open System, Chemical Geology, **48**: 189-211.

Buhmann, D., and Dreybrodt, W., 1985b, The kinetics of calcite dissolution and precipitation in geologically relevant situations of karst areas – 2. Closed System, Chemical Geology, **53**: 109-124.

Chappellaz, J., and Jouzel, J., 1992, Vostok Ice Core Data Set: IGBP PAGES/World Data Center-A for Paleoclimatology, Data Contribution Series 92-018.

Chen, J.H., Curran, H.A., White, B., and Wasserburg, G.J., 1991, Precise chronology of the last interglacial period: ^{234}U-^{230}Th data from fossil coral reefs in the Bahamas, Geological Society of America Bulletin, **103**: 82-97.

Colman, S.M., and Pierce, K.L., 1992, Varied records of early Wisconsinan alpine glaciation in the western United States derived from weathering-rind thickness, in: *The Last Interglacial-Glacial Transition in North America*, Clark, P.U. and Lea, P.D., eds., Geological Society of America Special Paper no 270, pp. 269-278.

Dansgaard, W., 1964, Stable isotopes in precipitation, Tellus, **16**: 436-468.

Dickson, J.A.D., 1978, Length-slow and length-fast calcite: A tale of two elongations, Geology, **6**: 560-561.

Dorale, J.A., Gonzalez, L.A., Reagan, M.K., Pickett, D.A., Murrel, M.T., and Backer, R.G., 1992, A high resolution record of Holocene climate change in speleothem calcite from Cold Water Cave, northeast Iowa, Science, **258**: 1626-1630.

Dorale, J.A., Edwards, R.L., Gonzalez, L., and Ito, E. 1998, Climate and vegetation history of the midcontinent from 75 to 25 ka: a speleothem record from Crevice Cave, Missouri, USA, Science, **282**: 1871-1874.

Drake, J.J., 1980, The effect of soil activity on the chemistry of carbonate groundwaters, Water Resources Research, **16**: 381-386.

Drake, J.J., 1983, The effects of geomorphology and seasonality on the chemistry of carbonate groundwater, Journal of Hydrology, **61**: 223-236.

Drake, J.J., and Ford, D.C., 1981, Karst solution: a global model for groundwater solute concentrations, Proceedings of the Japanese Geomorphological Union, **2**: 223-230.

Drake, J.J., and Wigley, T.M.L., 1975. The effect of climate on the chemistry of carbonate groundwater, Water Resources Research, **11**: 958-962.

Dreybrodt, W., 1980, Deposition of calcite from thin films of water of natural calcareous solutions and the growth of speleothems, Chemical Geology, **29**: 80-105.

Dreybrodt, W., 1988, Processes in Karst Systems – Physics, Chemistry and Geology: Springer Series in Physical Environments 5, Springer, Berlin, 288 p.

Dreybrodt, W., 1996, Chemical Kinetics, Speleothem Growth and Climate, in: *Climate Change: The Karst Record*, Karst Waters Institute Special Publication, no 2, pp. 33-34.

Dreybrodt, W., 1999, Chemical kinetics, speleothem growth and climate, Boreas, **28**: 347-356.

Dreybrodt, W., and Buhmann, D., 1987, A mass transfer model for dissolution and precipitation of calcite from solutions in turbulent motion, Chemical Geology, **90**: 107-122.

Dreybrodt, W., and Franke, H.W., 1987, Wachstumsgeschwindikeit und Durchmesser von Kerzenstalagmites, Die Höhle, **38**: 1-6.

Dreybrodt, W., Eisenlohr, L., Madry, B., and Ringer, S., 1997, Precipitation kinetics of calcite in the system: the conversion to CO_2 by the slow process $H^+ + HCO_3^- \rightarrow CO_2 + H_2O$ as a rate limiting step, Geochimica et Cosmochimica Acta, **60**: 3897-3904.

Dublyansky, Y.V., 1995, Speleogenetic history of the Hungarian hydrothermal karst, Environmental Geology, **25**: 24-36.

Edwards, R. L., Chen, J. H., and Wasserburg, G. J., 1986, ^{238}U-^{234}U-^{230}Th-^{232}Th systematics and the precise measurement of time over the past 500,000 years, Earth and Planetary Science Letters, **81**: 175-192.

Emiliani, C., and Shackleton, N.J., 1974, The Brunhes epoch: Isotopic paleotemperatures and geochronology, Science, **183**: 511-514.

Ek, C., and Gewelt, M., 1985, Carbon dioxide in cave atmospheres. New results in Belgium and comparison with other countries, Earth Surface Processes and Landforms, **10**: 173-187.

Folk, R.L., and Assereto, R., 1976, Comparative fabrics of length-slow and length-fast calcite and calcitized aragonite in a Holocene speleothem, Carlsbad Caverns, New Mexico, Journal of Sedimentary Petrology, **46**: 486-496.

Ford, D.C., and Williams, P.W., 1989, Karst Geomorphology and Hydrology, Unwin Hyman, London, 601 p.

Gallup, C.D., Edwards, R.L., and Johnson, R.G., 1994, The Timing of High Sea Levels Over the Past 200,000 Years, Science, **263**: 796-800.

Garrels, R.M., and Christ, C.L., 1965, Solutions, Minerals and Equilibria (2nd edition), Harper and Row, New York, 450 p.

Gascoyne, M., 1992, Palaeoclimate determination from cave calcite deposits, Quaternary Science Reviews, **11**: 609-632.

Gascoyne, M., Schwarcz, H.P., and Ford, D.C., 1983, Uranium-series ages of speleothem from northwest England: correlation with Quaternary climate, Philosophical Transactions of the Royal Society of London, **B301**: 143-164.

Genty, D., Baker, A., and Barnes, W.L., 1997, Comparaison entre les laminés luminescents et les laminés visibles annuels de stalagmites: Comptes Rendus de l'Académie des Sciences, Série II, Fascicule A - Sciences de la Terre et des Planètes, **325** : 193-200.

Gordon, D., Smart, P., Ford, D.C., Andrews, J.N., Atkinson, T., Rowe, P.J., and Christopher, N.S., 1989, Dating of late Pleistocene interglacial and interstadial periods in the United Kingdom from speleothem growth frequency, Quaternary Research, **31**: 14-26.

Grootes, P.M., Stuiver, M., White, J.W.C., Johnsen, S., and Jouzel, J.,1993, Comparison of oxygen isotope records from the GISP2 and GRIP Greenland ice cores, Nature, **366**: 552-554.

Hellstrom, J., McCulloch, M., and Stone, J., 1998, A detailed 31,000-year record of climate and vegetation change, from the isotope geochemistry of two New Zealand speleothems, Quaternary Research, **50**: 167-178.

Hendy, C.H., 1971, The isotopic geochemistry of speleothems I. The calculation of the effects of different modes of formation on the isotopic composition of speleothems and their applicability as paleoclimatic indicators, Geochimica et Cosmochimica Acta, **35**: 801-824.

Heusser, C.J., and Heusser. L.E., 1990, Long continental pollen sequence from Washington State (U.S.A.): correlation of upper levels with marine pollen-oxygen isotope stratigraphy through substage 5e, Palaeogeography, Palaeoclimatology, Palaeoecology, **79**: 63-71.

Hill, C., and Forti, P., 1997, Cave Minerals of the World (2nd Edition), National Speleological Society, Huntsville, 463 p.

Holland, H.D., Kirsipu, T.W., Huebner, J.S., and Oxburgh, U.M., 1964, On some aspects of the chemical evolution of cave waters, Journal of Geology, **72**: 36-67.

Imbrie, J, Hays, J.D., Martinson, D.G., McIntyre, A., Mix, A.C., Morley, J.J., Pisias, N.G., Prell, W.L., and Shackleton, J.H., 1984, The orbital theory of Pleistocene climate: Support from a revised chronology of the marine $\delta^{18}O$ record, in: *Milankovitch and Climate, Part 1: NATO ASI Series, Series C*, Berger, A., Imbrie, J., Hays, J., Kukla, G., and Saltzman, B., eds., Mathematical and Physical Sciences, **126**, Reidel, Rotterdam, pp. 269-305.

Johnsen, S.J., Clausen, H.B., Dansgaard, W., Fuhrer, K., Gundestrup, N., Hammer, C.U., Iversen, P., Jouzel, J., Stauffer, B., and Steffensen, J.P., 1993, Greenland Ice Core Project Summit Core ^{18}O. IGBP PAGES/World Data Center-A for Paleoclimatology, Data Contribution Series 93-033.

Kaufman, A., and Broecker, W.S., 1965, Comparison of Th^{230} and C^{14} ages for carbonate materials from Lakes Lahontan and Bonneville, Journal of Geophysical Research, **70**: 4039-4054.

Kendall, A.C., and Broughton, P.L., 1978, Origin of fabrics in speleothems composed of columnar calcite crystals, Journal of Sedimentary Petrology, **48**: 519-538.

Lauritzen, S.-E., 1995, High-Resolution Paleotemperature Proxy Record for the Last Interglaciation Based on Norwegian Speleothems, Quaternary Research, **43**: 133-146.

Lauritzen, S.E., and Lundberg, J., in press, Isotope Stage 11, the "Super-Interglacial", from a North Norwegian Speleothem, in: *Studies of cave sediments*, Sasowsky, I., and Mylroie, J., eds., this volume.

Lauritzen, S.-E., and Lundberg, J., 1999a, Speleothems and climate: a special issue of *The Holocene*, The Holocene, **9**: 643-647.

Lauritzen, S.-E., and Lundberg, J., 1999b, Calibration of the speleothem delta function: an absolute temperature record for the Holocene in northern Norway, The Holocene, **9**: 659-669.

Linge, H., 1999, Isotopic studies of some northern Norwegian speleothems and calcareous algae from Svalbard, Ph.D. Thesis, University of Bergen, Bergen, Norway.

Lohmann, K.C., 1988, Geochemical patterns of meteoric diagenetic systems and their application to studies of paleokarst, in: *Paleokarst*, James, N.P. and Choquette, P.W., eds., Springer-Verlag, New York, pp. 58-80.

Lundberg, J., 1997, Paleoclimatic reconstruction and timing of sea level rise at the end of the Penultimate Glaciation, from detailed stable isotope study and TIMS dating of submerged Bahamian speleothem, in: Proceedings, International Congress of Speleology, 12th, Neuchâtel, Switzerland.

Lundberg, J., 1999. Uranium series dating on Finnigan-Mat (2^{nd} edition), University of Bergen, Geology Department, Internal report.

Martinson, D.G., Pisias, N.G., Hays, J.D., Imbrie, J., Moore, T.C., Jr. and Shackleton, N.J., 1987, Age dating and the orbital theory of the ice ages–Development of a high-resolution 0 to 300,000-year chronostratigraphy, Quaternary Research, **27**: 1-29.

Meese, D., Alley, R., Gow, T., Grootes, P.M., Mayewski, P., Ram, M., Taylor, K., Waddington, E., and Zielinski, G., 1994, Preliminary depth-age scale of the GISP2 ice core: CRREL Special Report 94-1.

Miotke, F.-D., 1974, Carbon dioxide and the soil atmosphere. Abhandlungen Karst-u. Hohlenkunde, A9, Munich, 52 p.

Plummer, L.N., Wigley, T.L.M., and Parkhurst, D.L., 1978, The kinetics of calcite dissolution on CO_2-water systems at 5°C to 60°C and 0.0 to 1.0 atm CO_2, American Journal of Science, **278**: 537-573.

Porter, S.C., 1977, Present and past glaciation threshold in the Cascade Range, Washington, U.S.A.–Topographic and climatic controls, and paleoclimatic implications, Journal of Glaciology, **18**: 101-116.

Porter, S.C., Pierce, K.L., and Hamilton, T.D., 1983, Late Wisconsin mountain glaciation in the western United States, in: *Late Quaternary environments of the United States, v. 1, The Late Pleistocene*, Porter, S.C., ed., University of Minnesota Press, Minneapolis, pp. 71-114.

Rightmire, C.T., 1978, Seasonal Variation in P_{CO_2} and ^{13}C Content of Soil Atmosphere, Water Resources Research, **14**: 691-692.

Shackleton, N.J., and Opdyke, N.D., 1973, Oxygen isotope and paleomagnetic stratigraphy of equatorial Pacific core V28-238: Oxygen isotope temperatures and ice volumes on a 10^5 year and 10^6 year scale, Quaternary Research, **3**: 39-55.

Stuiver, M., Grootes, P.M., and Braziunas, T.F., 1995, The GISP2 $\delta^{18}O$ climate record of the past 16,500 years and the role of the sun, ocean, and volcanoes, Quaternary Research, **44**: 341-354.

Turgeon, S., and Lundberg, J, in press, Chronology of discontinuities and petrology of speleothems as paleoclimatic indicators of the Klamath mountains, southwest Oregon, USA. Carbonates and Evaporites.

Vesely, M.M., 2000, Annual speleothem laminae width: a high-resolution indicator of paleoclimate in Ireland: M.A. Thesis, Department of Geography and Environmental Studies, Carleton University, 99 p.

Wells, R.E., and Heller, P.L., 1988, The relative contribution of accretion, shear, and extension to Cenozoic tectonic rotation in the Pacific Northwest, Geological Society of America Bulletin, **100**: 325-338.

Winograd, I.J., Coplen T.B., Landwehr, J.M., Riggs, A.C., Ludwig, K.R., Szabo, B.J., Kolesar, P.T., and Revesz, K.M., 1992, Continuous 500,000-year climate record from vein calcite in Devils Hole, Nevada, Science, **258**: 255-260.

SILICATES IN CARBONATE SPELEOTHEMS, GUADALUPE MOUNTAINS, NEW MEXICO, U.S.A.

Victor J. Polyak and Necip Güven*

1. ABSTRACT

Silicates such as amorphous silica, quartz, trioctahedral smectite (stevensite), and possibly kerolite have formed with carbonate minerals in carbonate speleothems from caves of the Guadalupe Mountains, New Mexico, U.S.A. The likely sources of Si were the disseminated silicate minerals *in situ* in the Permian dolostone units in which the caves have developed. Ca- and Mg-carbonate mineral precipitation from thin water-films on speleothems due to evaporation and CO_2 loss progressively increased the Si/(Ca+Mg) ratio, and concentrated the initially low percent of aqueous silica seeping into these caves. Amorphous silica precipitated with calcite and aragonite in stalagmites because the formation of these materials was rapid and the stalagmites are too young for the crystallization of quartz. The presence of organic material in the stalagmites hints that the amorphous silica may have an organic-related origin. Quartz and trioctahedral smectite formed with the Mg-carbonate minerals such as dolomite, huntite, and hydromagnesite. The authigenesis of quartz at the low temperature (15-25°C) of these caves, like that of well-ordered dolomite, required extensive periods of time (i.e., >>1 ka) in a stable environment conducive for silicate precipitation. Kerolite-like silicates, in aragonite crusts, seemed to be intermediate precipitates between amorphous silicates and trioctahedral smectite.

* Victor J. Polyak, Earth and Planetary Sciences, University of New Mexico, Albuquerque, New Mexico 87131. Necip Güven, Department of Geocsciences, Texas Tech University, Lubbock, Texas 87109-1053.

2. INTRODUCTION

There are relatively few reports of the authigenesis of silicates in carbonate speleothems (stalagmites, stalactites, and crusts). Mills (1965) noted interbanded opal, calcite and aragonite layers in speleothems from Argentina. Accounts of cave-authigenic opal and other silicates such as quartz and clays are generally associated with volcanic caves, or non-carbonate settings (Hill and Forti, 1997). Authigenic quartz in carbonate speleothems has not been well documented. Polyak and Güven (2000) reported the authigenesis of trioctahedral smectite in magnesian-carbonate speleothems such as dolomite crusts and huntite moonmilk. Polyak *et al*. (2001) noted the presence of authigenic (euhedral) quartz in association with dolomite in crusts. The present study focuses on the authigenesis of silicates in carbonate speleothems from the caves of the Guadalupe Mountains, southeastern New Mexico. While not abundant, silicates do sometimes occur in these carbonate speleothems.

2.1 Depositional Setting nd Samples

Caves in the Guadalupe Mountains such as Carlsbad Cavern and Lechuguilla Cave contain some of the most spectacular and unique carbonate speleothems and mineral assemblages in the world (Fig. 1). With the exception of water seeping into the caves along joints in the limestone and dolostone, these caves, like the surrounding regions, are relatively dry. The relative humidities in these caves generally vary from 70 to 95%, and change due to the cave's elevation, size of entrance, and morphological character. Due to

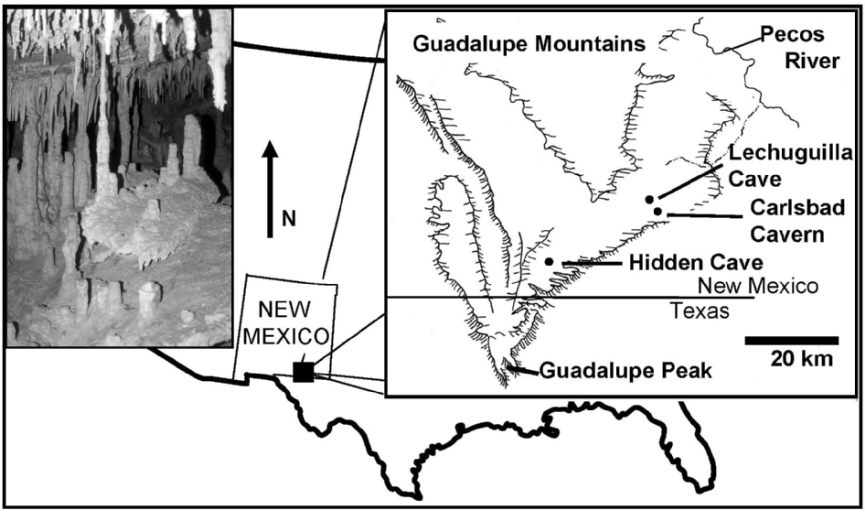

Figure 1. Map showing location of three caves in the Guadalupe Mountains, New Mexico pertinent to this study. The photograph shows typical carbonate speleothems.

the slightly evaporative conditions and Mg from the dolostone, Mg-carbonate minerals such as dolomite, huntite, and hydromagnesite are somewhat common (Hill, 1987). Thesilicate-bearing samples for this study were collected from seven caves: Carlsbad, Lechuguilla, Cottonwood, Hell Below, Lake, Hidden, and Gunsight caves. Samples included fragments of stalagmites, stalactites, rimstone dams, moonmilk, and crusts.

2.2 Methods

The silicates were extracted by removal of the carbonate fraction using the sodium acetate method of Jackson (1974), or by 5% hydrochloric acid digestion. Insoluble residues were dried, lightly ground, and the powders were analyzed using X-ray diffraction (XRD) and transmission electron microscopy (TEM). Oriented-clay mounts were dried at 25°C and 50% relative humidity. Clay samples were treated with ethylene glycol vapor for 24-48 hrs. Characteristic X-ray spectra were obtained on films and aggregates of the amorphous silicates and clays by an energy dispersive X-ray (EDX) microanalyzer interfaced to a JEOL JEM-100CX analytical electron microscope. Micrographs of clay particles were obtained in TEM mode. Small fragments of freshly fractured samples were mounted, coated with gold, and examined with scanning electron microscopy (SEM) on the same microscope. Thin sections for optical petrography were stained with alizarin red-S.

3. SILICATES IN CARBONATE SPELEOTHEMS

3.1 Amorphous Silicates

Amorphous silicates were found in stalagmites, stalactites, rimstones, and crusts near cave entrances or in cave zones where the relative humidity is lower (i.e., <95%). In optical thin sections of Holocene stalagmite samples, amorphous silica was observed along thin aragonite bands, and as a consequence, it appeared as sheets of insoluble residue when fragments of stalagmites were dissolved in 5% HCl. The insoluble material was gel-like when wet, and difficult to grind when dry. It formed molds of the aragonite needles (Fig. 2A) suggesting that its precipitation was soon after the aragonite. EDX microanalysis of preserved organic materials in these young stalagmites showed abundant Si incorporated in them. Amorphous silica also occurred as botryoidal opalline coatings on dolomite crusts with trioctahedral smectite and uranyl vanadates such as tyuyamunite. The botryoids of opal were usually associated with fine fibers of opal or Mg-silicates (Fig 2B).

3.2 Quartz

Quartz occurs in dolomite crusts in Carlsbad Cavern, Lechuguilla Cave, and probably other nearby caves, and within unusual iron oxide-rich stalactites (the "Rusticles") in Lechuguilla Cave. Most of the crystals of quartz were euhedral and 10-200 μm in diameter; however some exceeded 200 μm in diameter (Fig. 3). In the "Rusticles" of Lechuguilla Cave, quartz crystals, along with dolomite and calcite, formed cement in the central canal of these stalactites. Within the quartz were filaments of iron-

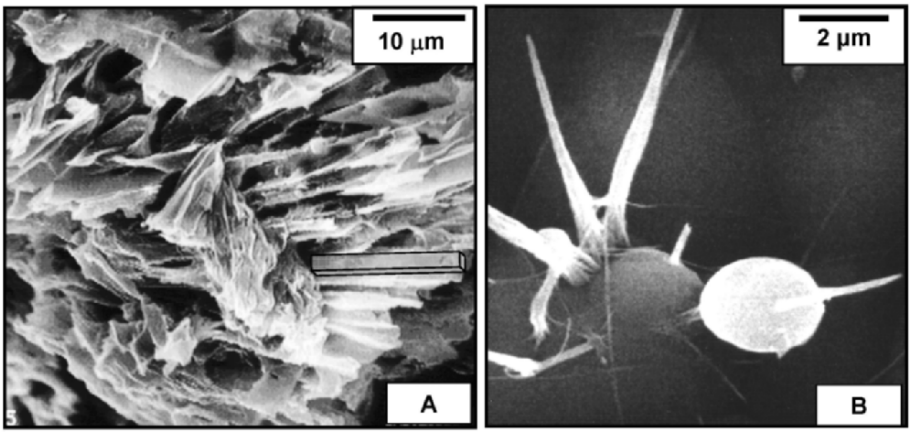

Figure 2. (A) SEM image of amorphous silica dissolved from a late Holocene stalagmite (Hidden Cave). Note the fibrous texture of the amorphous silica. These are molds of aragonite crystals. (B) SEM image of opal botyroids and filaments on an opalline coating on metatyuyamunite crystals (Spider Cave, from Polyak and Mosch 1995).

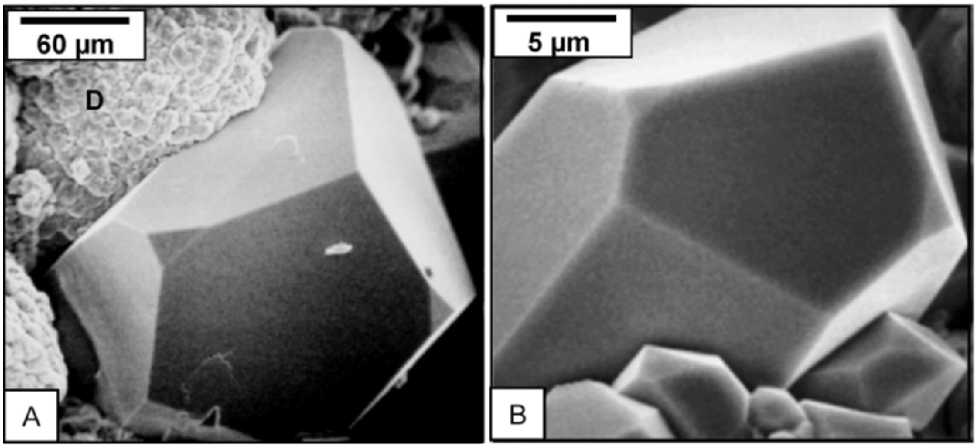

Figure 3. (A&B)SEM images of quartz crystals in dolomite crust, Carlsbad Cavern (D=dolomite).

oxide reported as fossil bacteria by Davis et al. (1990) and Provencio and Polyak (2001). In the dolomite crusts, quartz was associated with dolomite, trioctahedral smectite and other Mg-silicates, and sometimes tyuyamunite.

3.3 Trioctahedral Smectite

Trioctahedral smectite (stevensite) was common in Mg-carbonate crusts and moonmilk (Polyak and Güven, 2000). Most of the smectite appeared fibrous, or less commonly as films. The fibers and films formed filamentous aggregates that enveloped dolomite and huntite crystals (Fig 4).

3.4 Kerolite-like Silicates

Poorly formed Mg-silicate platelets made up the acid-insoluble residue of aragonite crusts. XRD and EDX microanalysis of this material by Polyak and Güven (2000) suggested that it was kerolite or kerolite-like. Kerolite is a non-expandable hydrous phyllosilicate with a chemical composition and X-ray diffraction pattern similar to talc and stevensite (Brindley et al., 1977). The clay fills spaces between aragonite needles in cave crusts.

3.5 Other Mg-Silicates

Fibers associated with dolomite crusts consisted of a mineral that we could not identify. These fibers appeared to protrude from pits in the dolomite crystals and extended outward from the surface of the crust (Fig. 5A). They were also associated with botryoidal opal (Fig. 5B). The morphology of these fibers inferred that they are not smectite. EDX microanalysis indicated that the fibers were a Mg-silicate mineral.

4. AUTHIGENESIS OF SILICATES

The sources of Si for cave-authigenic silicates were most likely the silicates disseminated in the dolostone units of the Permian Capitan reef complex. Silt-sized quartz and minor feldspar, and clays such as illite and dickite, made up approximately 1-5% of the dolostones.

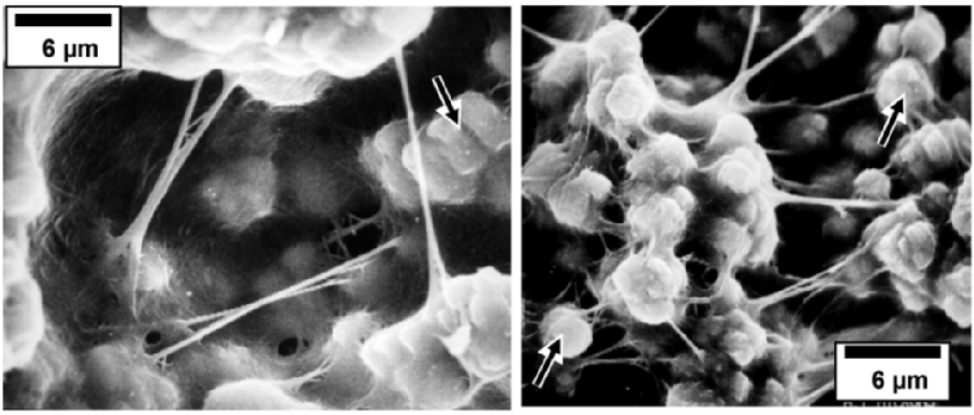

Figure 4. SEM images of filamentous aggregates of trioctahedral smectite enveloping dolomite crystals in dolomite crust (Carlsbad Cavern). Image on the right was modified from Polyak and Güven (2000). Arrows point to coated dolomite rhombs.

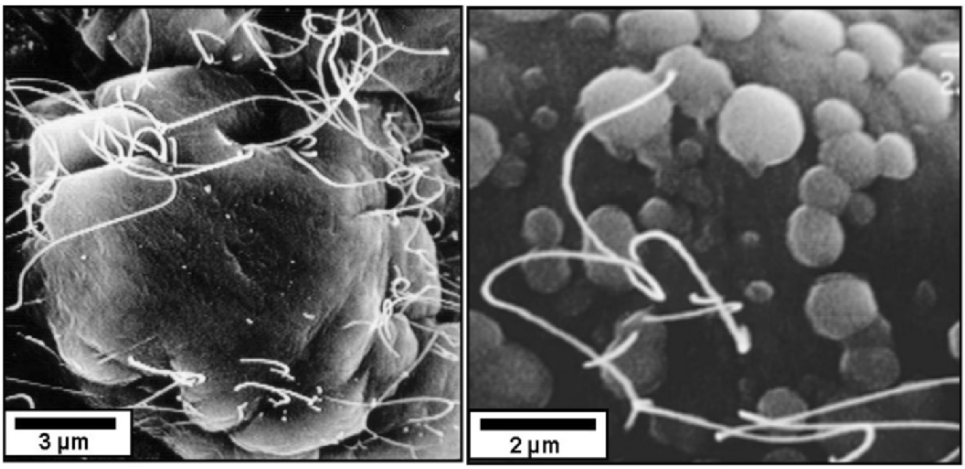

Figure 5. SEM images of Mg-silicate fibers associated with dolomite and opal (Spider Cave). (A) Mg-silicate fibers appear to grow from pits on the dolomite crystal. (B) Mg-silicate fibers extend from botryoidal opal.

Partial dissolution either in the soil zone, or along the paths of seeping water through the dolostone most likely provided the necessary concentrations of aqueous silica. Excess silica generated by sulfuric acid-influenced speleogenesis of these caves (Hill, 1987) may be another possible source of Si. Interbands of amorphous silica with calcite and aragonite in the Holocene stalagmites formed rapidly (1–5 years based on the number of annual bands), and were quickly coated by the next band of calcite or aragonite. For this reason, the silica is structurally immature. The silica can transform to opal A, opal CT, or quartz by diagenesis given ample time. Poorly crystalline kerolite-like silicates were associated with aragonite crusts, while moderately well-crystallized phases such as quartz and trioctahedral smectite were associated with dolomite and huntite crusts. Polyak and Güven (2000) documented this sequence of silicate precipitation that coexisted with the expected sequence of carbonate mineral precipitation in these caves. The expected and observed sequence of anhydrous speleothemic carbonate deposition in the thin water-film environment is Mg-calcite → aragonite → dolomite → huntite. To obtain dolomite crusts, the source water must loose much of its original Ca by calcite and aragonite precipitation. Likewise, the thin water-film, after deposition of calcite and aragonite, experiences an increase in Si/(Ca+Mg). The Si concentration increases by evaporation. The formation of dolomite further depletes the source water of Ca and Mg, which further increases the Si/(Ca+Mg). The microenvironment eventually becomes conducive to the formation of silicates such as opal, quartz, and trioctahedral smectite. This sequence of silicate precipitation in these caves is illustrated in Figure 6.

Origin of the amorphous silica in stalagmites may be related to organic materials. The incorporation of silica in fragments of invertebrate parts seems to support an organic-related origin. Amorphous silicate deposition associated with plants (Jones et al., 1998)

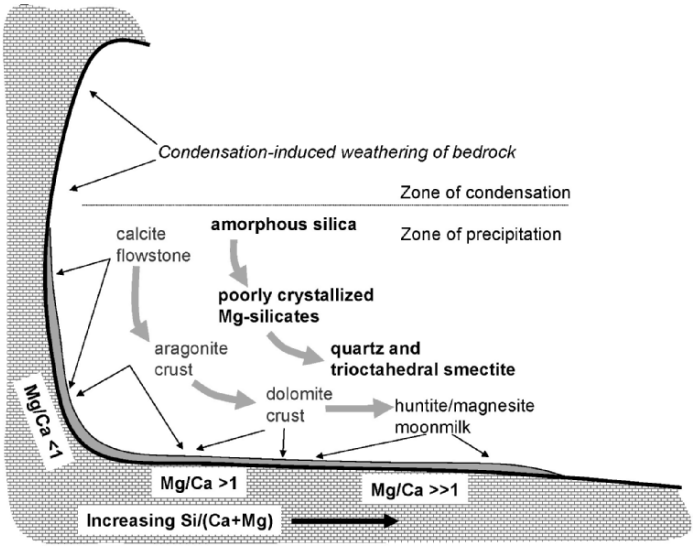

Figure 6. An example of a setting ideal for silicate precipitation in these caves. Modeled after a setting in Hell Below Cave where trioctahedral smectite formed with huntite moonmilk.

and microorganisms (Fortin and Beveridge, 1997; Fortin and Ferris, 1998; Westall, 1999) has been well documented. Also, organic gels have been used as templates for the synthesis of silica gels (Bujanowski, et al. 1994; Ono et al., 1998). Presence of organic substances, which were relatively abundant in the Holocene stalagmites from Hidden Cave, probably promoted and accelerated the formation of amorphous silica in carbonate speleothems.

The origin of euhedral quartz in carbonate speleothems is more difficult to explain. The quartz formed with dolomite, trioctahedral smectite, and in some settings, tyuyamunite. The origin of the dolomite may help explain how the quartz precipitated at such low temperature in the cave environment. Polyak et al. (2001) reported the formation of moderately well-ordered dolomite from these caves. They showed that the dolomite matured with time in a very stable depositional environment. At 30°C, Usdowski (1994) determined from laboratory experiments that it would take several hundred years (>600 years) to synthesize well-ordered dolomite. Polyak *et al*. (1998) demonstrated that these caves containing authigenic dolomite and quartz are in excess of 4 Ma in age. Therefore, if the cave environment has been relatively stable over that period of time, then there has been ample time for the development of well-ordered dolomite. By the same reasoning, quartz has probably formed in association with the dolomite in this environment over similarly long periods of time. Hervig et al. (1995) reported the precipitation of quartz overgrowths in sandstone at low temperature (15-35°C) over an extensive period of time (≤130 Ma). Chavetz and Zhang (1998) reported the authigenesis of euhedral quartz in marine dolomite at low temperature and shallow burial over a relatively short time (<1 Ma). We suggest that a long period of time in a stable environment conducive to quartz precipitation results in the maturation of poorly crystallized silicate to euhedral quartz at low temperature.

5. CONCLUSION

Silicates such as amorphous silica, trioctahedral smectite, and quartz, form in carbonate speleothems such as stalagmites, moonmilks, and crusts in the Guadalupe Mountains, New Mexico. In areas of relatively rapid carbonate mineral precipitation, amorphous silica was the common phase. In contrast, trioctahedral smectite and quartz formed where carbonate mineral precipitation was very slow and depositional conditions remained nearly constant for long periods of time. Other Mg-silicates such as kerolite formed in depositional environments between these two extremes.

6. ACKNOWLEDGMENTS

We are grateful to R. Turner and the Lincoln National Forest, D. Pate and J. Richards and Carlsbad Caverns National Park, and J. Goodbar and the Carlsbad District Bureau of Land Management for field assistance and permissions to collect samples. We also thank Carol A. Hill and Annabelle M. Foos for their constructive reviews of our manuscript.

7. REFERENCES

Brindley, G.W., Bish, D.L. and Wan, H., 1977, The nature of kerolite, its relation to talc and stevensite, *Mineral Mag*, **41**:443-452.

Bujanowski, V.J., Katsoulis, D.E., and Ziemelis, M.J. 1994, Gelation of silicone fluids using cholestryl esters as gelators, *Journal of Material Chemistry*, **4**:1181-1187.

Chafetz, H.S. and Zhang, J. 1998, Authigenic euhedral megaquartz crystals in a Quaternary dolomite, *J Sediment Res*, **68**:994-1000.

Davis, D.G., Palmer, M.V., and Palmer, A.N., 1990, Extraordinary subaqueous speleothems in Lechuguilla Cave, New Mexico, *Nat Speleol Soc Bull*, **52**:70-86.

Fortin, D. and Beveridge, T.J., 1997, Role of the bacterium *Thiobacillus* in the formation of silicates in acidic mine tailings, *Chem Geol*, **141**:235-250.

Fortin, D. and Ferris, F.G. 1998, Precipitation of iron, silica, and sulfate on bacterial cell surfaces, *Geomicrobiol J*, **15**:309-324.

Hervig, R.L., Williams, L.B., Kirkland, I.K., and Longstaffe, F.J. 1995, Oxygen isotope microanalyses of diagenetic quartz: possible low temperature occlusion of pores, *Geochim Cosmochim Acta*, **59**:2537-2543.

Hill, C.A., 1987, Geology of Carlsbad Cavern and other caves in the Guadalupe Mountains, New Mexico and Texas, *New Mexico Bureau of Mines and Mineral Resources, Bulletin*, **117**:150p.

Hill, C.A. and Forti, P., 1997, *Cave Minerals of the World*, National Speleological Society, Huntsville, Alabama, 238p.

Jackson, M.L., 1974, *Soil chemical analysis---Advanced course*, 2nd edition, published by author, University of Wisconsin, Madison, Wisconsin, 895p.

Jones, B., Renault, R.W., Rosen, M.R. and Klyen, L., 1998, Primary siliceous rhizoliths from Loop Road Hot Springs, North Island, New Zealand, *J Sediment Res*, **68**:115-123.

Mills, J.P., 1965, Petrography of selected speleothems of carbonate caverns, unpublished M.S. Thesis, University of Kansas, 47p.

Ono, Y., Nakashima, K., Sano, M, Kanekiyo, Y., Inoue, K., Hojo, J. and Shinkai, S., 1998, Organic gels are useful as a template for the preparation of hollow fiber silica, *Chemical Communications*, **1998**:1477-1478.

Polyak, V.J. and Güven, N., 2000, Authigenesis of trioctahedral smectite in magnesium carbonate speleothems in Carlsbad Cavern and other caves of the Guadalupe Mountains, New Mexico, *Clays Clay Miner*, **48**:317-321.

Polyak, V.J., Karlsson, H.R., and Provencio, P., 2001, Cave-authigenic dolomite in the Guadalupe Mountains, New Mexico, unpublished manuscript, Carlsbad Caverns National Park, 25p.

Polyak, V.J., McIntosh, W.C., Güven, N., and Provencio, P. 1998, Age and origin of Carlsbad Cavern and related caves from $^{40}Ar/^{39}Ar$ of alunite, *Science*, **279**:1919-1922.

Polyak, V.J. and Mosch, C.J., 1995, Metatyuyamunite from Spider Cave, Carlsbad Caverns National Park, New Mexico, *Natl Speleol Soc Bull*, **57**:85-90.

Provencio, P.P. and Polyak, V.J. 2001, Iron Oxide Rich Filaments: Possible Fossil Bacteria in Lechuguilla Cave, New Mexico, *Geomicrobiol J,* in press.

Usdowski, E., 1994, Synthesis of dolomite and geochemical implications, in: *Dolomites*, B. Purser, M. Tucker, and D. Zenger, eds., Blackwell Scientific Publications, Boston, pp.345-360.

Westall, F., 1999, The nature of fossil bacteria. A guide to the search for extraterrestrial life, *J Geophys Res*, **104 (E7)**:16437-16451.

RELIQUIAE DILUVIANAE ALTER: LAST INTERGLACIAL FLOOD DEPOSITS IN THE CAVES OF THE WEST INDIES

Donald A. McFarlane, and Joyce Lundberg*

1. ABSTRACT

Recent efforts to extend the terrestrial vertebrate record of the West Indies have resulted in the discovery of distinctive last-interglacial (Sangamonian) cave deposits on the islands of Jamaica, Puerto Rico, Hispaniola, and Anguilla. Each of these deposits apparently represents debris (including vertebrate bone) emplaced by catastrophic flooding during last-interglacial time. These are currently the only dated West Indian Late Quaternary vertebrate fossil-bearing cave deposits that are older than late Pleistocene (i.e., older than 35 ka). Moreover, no site from the time interval 35 – 100 ka has been found, suggesting that the conditions which resulted in the formation of these flood deposits have been rare or absent in post-Sangamonian time. We interpret this pattern as indicative of an episode of severe climate (perhaps increased hurricane frequency or severity) that may have occurred during oxygen isotope substage 5e.

2. INTRODUCTION

Vertebrate paleontological remains in caves have long been recognized as a vital and insightful source of paleoenvironmental information; as early as 1823, Buckland produced the beautifully illustrated volume *Reliquiae Diluvianae* documenting many cave paleontological sites in Europe as evidence of a paleo-flood, in this case interpreted as the biblical flood. In tropical environments, caves are often the only terrestrial environments in which vertebrate remains are commonly preserved, save for unusual exceptions such as the famed Dominican amber deposits (Poinar and Cannatella, 1987), and asphalt seeps in Trinidad and Cuba (Akersten, 1980). In the West Indies, the presence of a largely-exterminated and very unusual Late Quaternary mammalian fauna has inspired a 130-year history of paleontological investigation in the abundant karst of

* Donald A. McFarlane, W. M. Keck Science Center, Claremont,CA 91711, USA. Joyce Lundberg, Dept. of Geography and Environmental Studies, Carleton University,.Ottawa, K1S 5B6, Canada.

these islands. The earliest efforts by E. D. Cope in the late 19th century (based on field collections by van Rijgersma; McFarlane and MacPhee, 1989; 1993) led to early speculation concerning sea-level and sundered land bridges, and is embodied in Cope's specific epithet for the giant extinct rodent of Anguilla, *Amblyrhiza inundata*. More than a century later, patterns of West Indian fossil vertebrate distributions were used to infer an episode of later Pleistocene aridity (Pregill and Olson, 1981).

In view of the fact that paleoclimatic interpretations of the fossil record must depend on a good radiometric framework, it is surprising that radiometric studies of the West Indian vertebrate record were slow to begin. As late as 1981, only a single radiometrically-supported study was in print (Pregill, 1981). In the late 1980s this began to change, and there are now more than 60 published radiometric dates on late Quaternary West Indian vertebrates or vertebrate-bearing sites.

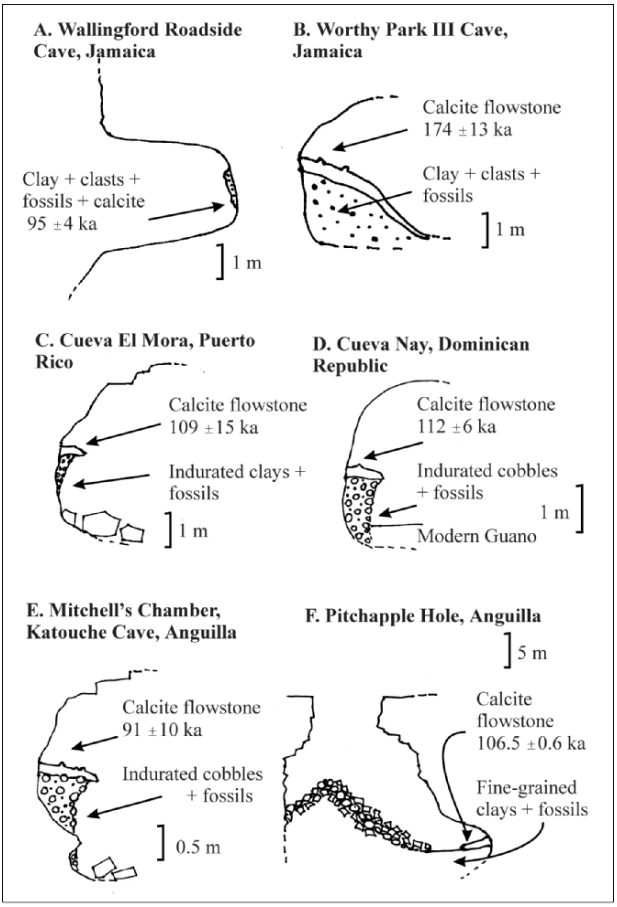

Figure 1. Diagrammatic cross sections of flood deposit sites with dates. All dates are U/Th alpha count dates, except for 1F, which is a TIMS date.

The West Indian terrestrial mammal fauna has had a long tenure on the islands, which is reflected in its high degree of phylogenetic distinctiveness. The earliest known mammalian specimen is from Eocene lagoonal deposits of Jamaica (Domming et al., 1997). However, the bulk of the mammalian record is preserved in cave deposits which do not extend back to such times because caves are relatively ephemeral over geological timescales. The oldest West Indian cave vertebrate-bearing deposits currently known are clastic dikes exposed in Cueva del Aleman, Isla de Mona, that have been dated to the earliest Pleistocene by paleomagnetic methods (Panuska et al., 1998).

Here we present a new synthesis of scattered paleontological data from the West Indies dating from the Late Quaternary, in particular, marine isotope stage (MIS) 5, and an interpretation of the paleoenvironmental significance of their temporal distribution and of the characteristics of the sediments in which they occur.

3. RESULTS

3.1 Last Interglacial Paleontological Records From West Indies Cave Deposits

Only a few sites in the West Indies have been found with paleontological remains from the Last Interglacial. These include sites from Jamaica, Puerto Rico, Dominican Republic, and Anguilla. The dates discussed below are all U-Th dates (the raw data are already published in the relevant publications). In this discussion, all errors are 1σ.

The first of the West Indian Last Interglacial cave sites to be identified was Wallingford Roadside Cave, Jamaica (Fig 1a). It contains a 'bone breccia' consisting of a vuggy clay indurated with calcite stringers and containing abundant vertebrate remains and a few small clasts. The extinct rodent(s) *Clidomys*, together with turtle and crocodile remains have been recovered. A suite of U/Th dates provide an age of 95 ± 4 ka for the calcite indurations and a maximum age of 130-180 ka for the fossils (MacPhee et al., 1989) placing them within MIS 5, the Last Interglacial.

Worthy Park I Cave, Jamaica (Fig 1b), is very similar to Wallingford Roadside Cave. The fossil-bearing deposit is an indurated clay plastered onto the walls of the entrance chamber, containing bones of *Clidomys* together with remains of freshwater turtle and frogs. The deposit is partially overlain with a flowstone that has yielded a U/Th age of 174 +13, -12 ka, which places it in marine isotope stage 6 (McFarlane et al., 1998).

The site from Puerto Rico, Cueva El Mora (Fig 1c), consists of remnants of a cave clay with clasts and bones of the extinct rodent *Elasmodontomys*, indurated and capped with flowstone. A U/Th date on the flowstone capping yielded an age of 108.9 +15.4, -13.3 ka, again placing the fossiliferous deposit most likely within MIS 5 (McFarlane et al., in press).

The Cueva Nay site, Dominican Republic (Fig 1d), is an abandoned trunk passage which preserves an incised bank of indurated stream cobbles, containing sparse vertebrate remains of the ground sloth cf. *Parocnus,* and capped with flowstone. A U/Th date on this flowstone gave an age of 112 ± 6 ka (McFarlane et al, 2000).

Mitchell's Chamber, in Katouche Cave, Anguilla, is a remnant of an abandoned cave stream passage with a thick deposit of stream gravels and cobbles (Fig 1e). This deposit preserves remains of the giant rodent, *A. inundata.* The whole deposit is capped with flowstone and penetrated by calcite stringers. Multiple dates on this flowstone and calcite

are statistically indistinguishable at 91 ± 10 ka (McFarlane et al., 1998). The stream deposits and associated fossils must thus have been emplaced before the end of marine isotope stage 5, and most likely within the Last Interglacial. For various reasons, discussed in McFarlane et al. (1998), *A. inundata* is believed to have become extinct during the Last Interglacial.

Pitchapple Hole, in Anguilla, is a 20 m deep, open pit cave (Fig. 1f) which contains an accumulation of lateritic cave earth containing abundant remains of *A. inundata*. A minimum age for the fossiliferous deposit of 106.5 ± 0.6 ka was obtained by U/Th dating of an overlying flowstone shelf (McFarlane et al., 1998). Specimens of *Amblyrhiza*

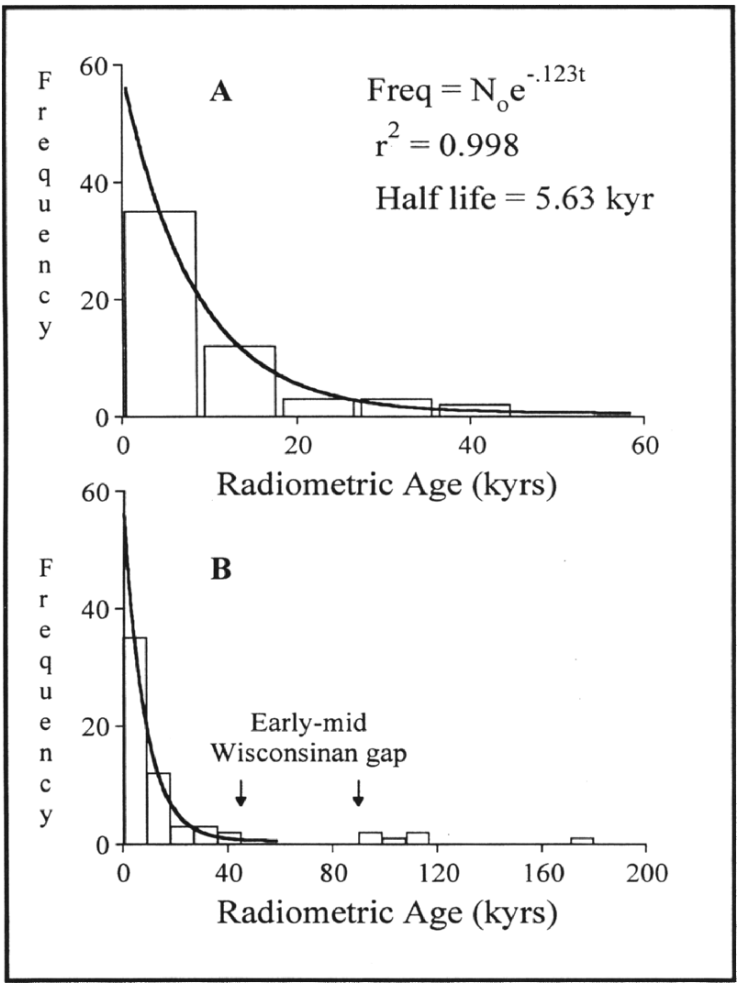

Figure 2. A: Age distribution of West Indian vertebrate sites over the past 50,000 years. B: Age distribution of all Quaternary West Indian vertebrate sites.

occur to within a few centimeters of the surface of the cave earth, indicating that little if any sediment accumulation has occurred here since Last Interglacial time.

All these sites, except for the Worthy Park site, date to MIS 5, the Sangamonian Interglacial. The distribution of these ages is discussed below as part of a general model of fossil distribution patterns.

3.2 Temporal Distribution of Paleontological Data from West Indies

Caves are often relatively short-lived phenomena on geological timescales, and fossil-bearing deposits even more so as they are eroded away or rendered inaccessible (and hence undiscovered) by collapse or infilling. Because these processes are either progressive (erosion) or essentially random (collapse), the probability of a fossil-bearing deposit surviving decreases with its age. If the probability of a fossil-bearing deposit being lost is approximately constant through time, then the age-frequency distribution of surviving deposits should show exponential decay. Taking all of the published West Indian radiocarbon data and plotting them against time (Fig 2A, n = 55) shows that they fit this pattern throughout the last 50,000 years. The approximate 'half-life' of the exponential decay curve is ~ 6 ^{14}C kyr. This therefore confirms the hypothesis of exponentially decreasing probability of preservation; the implication of this model is that the expected number of fossils for any age can be predicted.

However, if the six dates discussed above are added to the data set (making up the total published radiometric dataset for West Indian Late Quaternary vertebrate fossils) the graph (Fig 2B) reveals a somewhat different pattern. Five of the dates are centered on, or overlap, the last interglacial (Sangamonian), and one pre-dates it. Each of these dates was the result of attempts to interpret interesting paleontological assemblages irrespective of age, and are not artifacts of special efforts to locate old deposits. If the half-life for West Indian cave vertebrate sites in the Late Quaternary is ~6 ^{14}C kyr, and if one assumes a constant probability of deposition and/or preservation, then the probability of finding 5 of 61 dates dating from the Last Interglacial is vanishingly small ($p << 10^{-6}$). Clearly, we can have a high degree of statistical confidence in concluding that the probability of deposition and/or preservation has not been constant throughout the past 200 kyr, but in fact was many times higher during the Last Interglacial than at any time in the succeeding Wisconsinan.

3.3 Characteristics of Sediments

The second feature of interest in these six sites is the nature of the deposits in which the fossils are found.

The Wallingford Roadside Cave and the Worthy Park sediments are calcite-capped fluvial remnants, in the case of Wallingford plastered against the walls of the caves, and in the case of Worthy Park forming a sediment bank at the side of the passage. They have no signs of stratification. The sediments contain rounded clasts 1 – 2 cm in diameter. The Hjullstrom diagram of flow velocity required to entrain and transport clastic grains indicates water velocities of 1 to 1.5 ms^{-1}. The sediments are poorly packed, with many gaps between clasts, as if rapidly deposited, perhaps with organic debris that has now decayed. The nature of some of the fossil remains (turtle, frog, and crocodile) suggests

transportation by river flow rather than by vectors such as owls. Both of the Jamaican caves are in a similar situation; both today have large modern rivers sinking into base of a cliff. The caves, now ~40 meters above the modern river level, represent former sinks and are now closed or almost closed off with cave fill (McFarlane and Gledhill, 1985). The active cave walls are completely clean of sediment. The preservation of the sediment on the sides of the higher level caves implies no significant flood since emplacement. They may have been put in place during a very high water level event long after the abandonment of the passage as the normal sink.

The sediments in Cueva El Mora are as much as 3 m above the modern floor, and consist of clay with clasts and fossils but again with no indication of stratification. The clasts, of the order of 1-2 cm in diameter, are rounded to sub-rounded cobbles. The clay is also is full of holes, and contains turtle plastron fragments. The sediment beside the wall is somewhat indurated and has remained in place while the rest of the floor has since been removed. Stream flow is presumed to occur during extreme events such as hurricanes but no flow is observed in the cave today and no stream deposits have been emplaced since this Last Interglacial remnant.

The Cueva Nay sediments are in a very similar situation, although the clasts, at 5-10 cm diameter, are larger and the indurated sediment now plastered to the wall has less clay. These cobbles look like typical coarse-grained, bed-load alluvial deposits (but with no stratification) and suggest velocities of ~2 – 3 ms^{-1}. However, the presence of sloth vertebrae with undamaged vertebral processes suggest that the clasts were not transported for long distances during the particular episode that emplaced this deposit. The rounded allogenic clasts (many of volcanic lithologies) probably attained their roundness outside of the cave. The cave is situated east of a large intermittently-flooded polje whose only drainage is via another cave hydrologically connected to Cueva Nay (but now blocked). It is likely that the rounded clasts and the sloth bones were carried in from polje in a brief, high energy event.

The deposit in Mitchell's Chamber consists of sub-rounded gravel and cobbles (Fig 3). They range in size from 2 to 15 cm in longest axis and again look like standard bed-load deposits and indicate water velocities of ~ 3.5 ms^{-1}. They are clearly distinct from the other sediments in the cave, which are generally rare, and consist of fine-grained muds deposited in standing water, typical slack-water deposits. There appear to be no active stream deposits today, flow has not been observed in the cave, and, indeed, no surface streams are known on Anguilla. The Mitchell's Chamber deposit has been exposed by intermittent stream erosion and Katouche cave therefore presumably still carries an intermittent stream during extreme wet weather, but none of these flows have been energetic enough to have flushed significant surface debris, clasts, or vertebrate remains into the cave and the stream passage has not accumulated any kind of comparable clastic deposit since Last-Interglacial time. The flowstone capping is also distinct in that no other flowstone of comparable thickness occurs anywhere else in the cave; the rare, modern calcite deposits are in the form of thin and broken films.

Figure 3. Gravel and cobble sediment capped by calcite flowstone, in Mitchell's Chamber, Katouche Cave, Anguilla.

The fossil-bearing sediments in Pitchapple Hole are somewhat different from the other five deposits in that they are not obvious stream deposits. The sediments consist of fine-grained red clays accumulated at the foot of the breakdown talus filling the center of the pit. It is likely that they represent the flushing of fines out of the talus, but they have no evidence of any kind of stratification, no hardgrounds, no lenses of coarse-grained lags or anything that might suggest accumulation over a long time period. The feature that cannot easily be explained by slow flushing out of fines over time is the size of the vertebrate remains that are distributed throughout the red clay. These range up to 10 cm in longest dimension (Fig. 4). The standard Hjullstrom diagram is not designed for non-rock clasts and so cannot be used to indicate probable flow velocities; it can only be noted that the flow required to carry these bones must have been of sufficient velocity and discharge to entrain and transport relatively large clasts. Sedimentation stopped at the end of the Last Interglacial with the calcite capping. No comparable deposit from any more recent age can be found in the cave, and once again, stream flow is never observed in this cave or on the surface today.

4. PALEOENVIRONMENTAL INTERPRETATION

These six sites have several distinct features that must be explained: the unusual nature of the fossil assemblage; the unusual nature of the sediments; and the unexpectedly high rate of preservation.

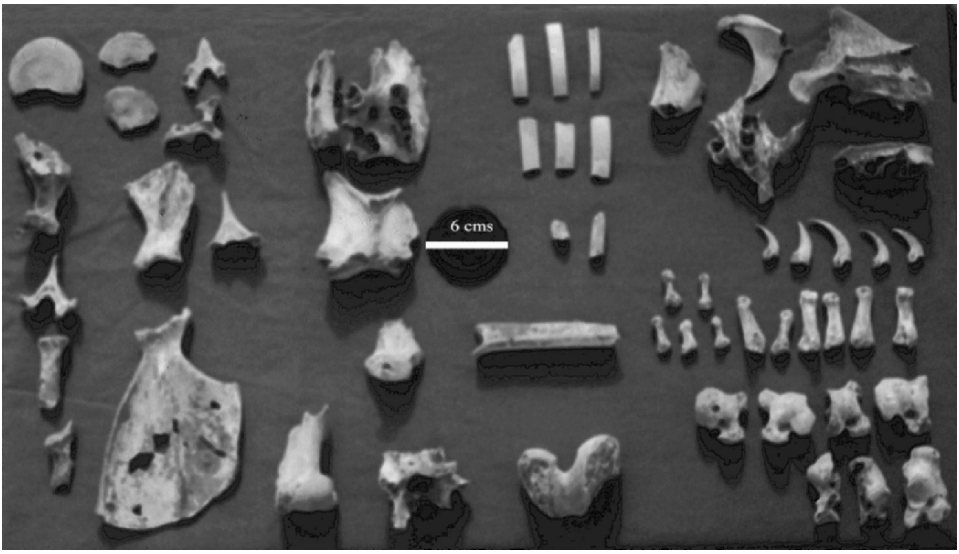

Figure 4. Amblyrhiza bone remains from Pitchapple Hole, Anguilla.

4.1 The Unusual Nature of the Fossil Assemblage

Vertebrate bone deposits accumulate in West Indian caves through several distinct processes. Most commonly, rich deposits of small vertebrates accumulate below owl roosts. These deposits are readily recognized by their lack of vertebrates with living body masses greater than 1–2 kgs, and by their high proportion of bird remains. Vertebrates also accumulate in caves through accidental falls into pits. These deposits over-represent larger vertebrates, and are deficient in birds and small reptiles.

The six sites lack either of these signatures, suggesting an alternative mode of transportation and deposition. Each of the known Last Interglacial vertebrate cave sites, with the exception of Pitchapple Hole, Anguilla (a pit-fall site), exhibits a taphonomy best interpreted as the result of storm-emplacement. We interpret each of these deposits as death assemblages emplaced by major floods backing up from the local river or stream sink, Wallingford Roadside cave, Jamaica, being a classic example where the fossil deposits are emplaced in a cave 40 m above the modern river sink

4.2 The Unusual Nature of the Sediments

The six deposits have many characteristics in common. The fossil remains include a mixture of large and small mammals, small birds, small reptiles, and aquatic vertebrates. The bones and teeth of megavertebrates deposited amongst stream cobbles are relatively unworn, suggesting little transportation. Most of the sediments are an inhomogeneous mixture of large and small vertebrate remains, stream cobbles, clays, and cavities. None are stratified and yet all seem to be fluvial deposits. Most are poorly packed with inter-

clast cavities. Most have relatively big clasts but at the same time preserve fossil remnants in a comparatively undamaged state. All are distinct from any subsequent deposits. All seem to have been deposited within a fairly short time interval and are not complicated by any subsequent deposition. Taking all this evidence together the most parsimonious explanation we have is that the sediments represent catastrophically emplaced flood deposits.

4.3 The Unexpectedly High Rate of Preservation

The unusually high number of preserved MIS 5 sites (several orders of magnitude higher than expected) requires unusual conditions of preservation. In view of the fossil assemblage and the nature of the sediments we suggest that the catastrophic floods created extraordinary conditions for preservation of fossil remains and that they have not been destroyed because no comparable floods have occurred since last interglacial times in these caves.

5. DISCUSSION

We suggest that the evidence indicates that the last interglacial may have experienced extreme, although probably rare, flood events. Given that similar cave deposits are not known from the West Indian Wisconsinan or Holocene record, we interpret this to mean that the West Indies were subject to more intense storm activity during the Last Interglacial.

If our interpretation is correct, we would expect to find other evidence of enhanced storm or hurricane activity in the geological record of the West Indies. While there are no other published records of storm events at inland sites, there is some evidence of increased wave activity on coastal sites, presumably indicating enhanced storm activity. Hearty et al. (1998) interpret a series of coastal sand ridges on the windward margin of several of the Bahama Islands as originating from extreme storms during the last interglacial. 'Megaboulder' (boulders of ~ 10^6 kg) deposits on Eleuthra (Hearty, 1997), suggest unusually intense wave activity at some stage during the last interglacial, which has been attributed to tsunamis or extreme hurricanes.

In view of these rather limited examples it seems that the evidence for catastrophic storms in the West Indies during MIS 5 is not yet very well supported. However, evidence for MIS 5 climatic instability in global climatic proxies such as ice and ocean cores is quite common (although currently under review, c.f. Kukla 2000). Adkins et al 1997 observe a rapid shift in oceanic circulation patterns around 118 ka, although their impact on storm patterns is unresolved. Ice cores show evidence of the strikingly difference nature of the Holocene and the Sangamonian Interglacials. For example, the GRIP ice core shows the Holocene as relatively stable but the Sangamon as fluctuating (Dansgaard et al., 1993).

In conclusion, the existence of karst 'hyper-flood' sedimentary facies in the last interglacial cave deposits of at least four West Indian islands suggests that additional efforts should be made to identify the signature of extreme events in MIS 5e deposits elsewhere in the Caribbean

6. REFERENCES

Adkins, J. F., E. A. Boyle, L. Keigwin, and E. Cortijo. 1997. Variability of the North Atlantic thermohaline circulation during the last interglacial period. *Nature* 390: 154-156.

Akersten, W. A. 1980. Fossils in asphalt. *Science* 248: 552.

Buckland, W. 1823. *Reliquiae Diluvianae; or, observations on the organic remains contained in caves, fissures, and diluvial gravel, and on other geological phenomena, attesting to the action of an universal deluge.* Murray, London.

Dansgaard, W., S. J. Johnsen, H. B. Clausen, D. Dahl-Jensen, N. S. Gundestrup, C. U. Hammer, C. S. Hvidberg, J. P. Steffensen, A. E. Sveinbjornsdottir, J. Jouzel, and G. Bond. 1993. Evidence for general instability of past climate from a 250-kyr ice-core record. *Nature* 364: 218-220.

Domning, D. P., R. J. Emry, R. W. Portell, S. K. Donovan, and K. S. Schindler. 1997. Oldest West Indian land mammal: rhinocerotoid ungulate from the Eocene of Jamaica. *Journal of Vertebrate Paleontology* 17: 638-641.

Hearty, P. J. 1997. Boulder deposits from large waves during the Last Interglaciation at North Eleuthera, Bahamas. *Quaternary Research* 48: 326-338.

Hearty, P. J., A. C. Neumann, and D. S. Kaufman. 1998. Chevron ridges and runup deposits in the Bahamas from storms late in oxygen-isotope substage 5e. *Quaternary Research* 50: 309-322.

Kukla, G. J. 2000. The Last Interglacial. *Science* 287: 987-988.

MacPhee, R. D. E., D. C. Ford, and D. A. McFarlane. 1989. Pre-Wisconsinan mammals from Jamaica and models of late Quaternary extinction in the Greater Antilles. *Quaternary Research* 31: 94-106.

McFarlane, D. A., and R. E. Gledhill. 1985. The Quaternary bone caves at Wallingford, Jamaica. *Cave Science* 12: 127-128.

McFarlane, D. A., J. Lundberg, A. Vale, and S. E. Lauritzen. *in press*. New specimens of the giant extinct rodent *Elasmodontomys obliquus* (Rodentia; Heptaxodontidae) from Puerto Rico, West Indies. *Caribbean Journal of Science*.

McFarlane, D. A., and R. D. E. MacPhee. 1989. Amblyrhiza and the Quaternary bone caves of Anguilla, British West Indies. *Cave Science* 16: 31-34.

—. 1993. *Amblyrhiza* and the vertebrate paleontology of Anguillan caves. *Boletin de la Sociedad Venezolana de Espeleologia* 27: 33-38.

McFarlane, D. A., R. D. E. MacPhee, and D. C. Ford. 1998. Body size variability and a Sangamonian extinction model for *Amblyrhiza*, a West Indian megafuanal rodent. *Quaternary Research* 50: 80-89.

McFarlane, D. A., A. Vale, K. Christenson, J. Lundberg, G. Atilles, and S. E. Lauritzen. 2000. New specimens of Late Quaternary extinct mammals from caves in Sanchez Ramirez Province, Dominican Republic. *Caribbean Journal of Science* 36: 163-166.

Panuska, B. C., J. M. Mylroie, D. Armentrout, and D. McFarlane. 1998. Magnetostratigraphy of Cueva del Aleman, Isla de Mona, Puerto Rico and the species duration of Audubon's Shearwater. *Journal of Cave and Karst Studies* 60: 96-100.

Poinar, G. O., and D. C. Cannatella. 1987. An upper Eocene frog from the Dominican Republic and its implication for Caribbean biogeography. *Science* 237: 1215-1216.

Pregill, G. K. 1981. Late Pleistocene herpetofaunas from Puerto Rico. *Miscellaneous Publications, University of Kansas Museum of Natural History* 71: 1-72.

Pregill, G. K., and S. L. Olson. 1981. Zoogeography of West Indian vertebrates in relation to Pleistocene climatic cycles. Annual Rev. Ecol. Syst. 12:75-98. *Annual Review of Ecology and Systematics* 12: 75-98.

Index